Advances in Science, Technology & Innovation
IEREK Interdisciplinary Series for Sustainable Development

Attila Çiner · Md Firoz Khan · Amjad Kallel ·
Jesús Rodrigo-Comino · Mario Parise · Rahim Barzegar ·
Zeynal Abiddin Ergüler · Nabil Khelifi · Imran Ali *Editors*

Recent Research on Environmental Earth Sciences, Geomorphology, Soil Science, Paleoclimate, and Karst

Proceedings of the 1st MedGU, Istanbul 2021 (Volume 4)

IEREK RESEARCH & KNOWLEDGE ENRICHMENT

Springer

Advances in Science, Technology & Innovation

IEREK Interdisciplinary Series for Sustainable Development

Advances in Science, Technology & Innovation (ASTI) is a series of peer-reviewed books based on important emerging research that redefines the current disciplinary boundaries in science, technology and innovation (STI) in order to develop integrated concepts for sustainable development. It not only discusses the progress made towards securing more resources, allocating smarter solutions, and rebalancing the relationship between nature and people, but also provides in-depth insights from comprehensive research that addresses the **17 sustainable development goals (SDGs)** as set out by the UN for 2030.

The series draws on the best research papers from various IEREK and other international conferences to promote the creation and development of viable solutions for a **sustainable future and a positive societal** transformation with the help of integrated and innovative science-based approaches. Including interdisciplinary contributions, it presents innovative approaches and highlights how they can best support both economic and sustainable development, through better use of data, more effective institutions, and global, local and individual action, for the welfare of all societies.

The series particularly features conceptual and empirical contributions from various interrelated fields of science, technology and innovation, with an emphasis on digital transformation, that focus on providing practical solutions to **ensure food, water and energy security to achieve the SDGs.** It also presents new case studies offering concrete examples of how to resolve sustainable urbanization and environmental issues in different regions of the world.

The series is intended for professionals in research and teaching, consultancies and industry, and government and international organizations. Published in collaboration with IEREK, the Springer ASTI series will acquaint readers with essential new studies in STI for sustainable development.

ASTI series has now been accepted for Scopus (September 2020). All content published in this series will start appearing on the Scopus site in early 2021.

Attila Çiner · Md Firoz Khan · Amjad Kallel ·
Jesús Rodrigo-Comino · Mario Parise ·
Rahim Barzegar · Zeynal Abiddin Ergüler ·
Nabil Khelifi · Imran Ali
Editors

Recent Research on Environmental Earth Sciences, Geomorphology, Soil Science, Paleoclimate, and Karst

Proceedings of the 1st MedGU, Istanbul 2021 (Volume 4)

Springer

Editors
Attila Çiner
Eurasia Institute of Earth Sciences
Istanbul Technical University
Istanbul, Türkiye

Amjad Kallel
Sfax National School of Engineering
University of Sfax
SFax, Tunisia

Mario Parise
University Aldo Moro
Bari, Italy

Zeynal Abiddin Ergüler
Kütahya Dumlupınar University
Kütahya, Türkiye

Imran Ali
Jamia Millia Islamia University
New Delhi, India

Md Firoz Khan
North South University
Dhaka, Bangladesh

Jesús Rodrigo-Comino
University of Granada
Granada, Spain

Rahim Barzegar
Groundwater Research Group (GRES)
Research Institute on Mines and Environment
(RIME)
Université du Québec
en Abitibi-Témiscamingue (UQAT)
Amos, QC, Canada

Nabil Khelifi
DAAD Alumni Researcher
Heidelberg, Germany

ISSN 2522-8714 ISSN 2522-8722 (electronic)
Advances in Science, Technology & Innovation
ISBN 978-3-031-42916-3 ISBN 978-3-031-42917-0 (eBook)
IEREK Interdisciplinary Series for Sustainable Development
https://doi.org/10.1007/978-3-031-42917-0

This Springer imprint is published by the registered company Springer Nature Switzerland AG
The registered company address is: Gewerbestrasse 11, 6330 Cham, Switzerland

Paper in this product is recyclable.

About MedGU

Steps toward the creation of a Mediterranean Geosciences Union (MedGU)

Mediterranean Geosciences Union (MedGU) aims to create a unique federation that brings together and represents the Mediterranean geoscience community specializing in the areas of Earth, planetary, and space sciences.

MedGU will be structured along the lines of American Geophysical Union (AGU) and European Geosciences Union (EGU).

The plan is to establish a large organization for the Mediterranean region that is more influential than any one local geoscience society with the objective of fostering fundamental geoscience research, as well as applied research that addresses key societal and environmental challenges.

MedGU's overarching vision is to contribute to the realization of a sustainable future for humanity and for the planet.

The creation of this union will give the Earth sciences more influence in policy-making and in the implementation of solutions to preserve the natural environment and to create more sustainable societies for the people living in the Mediterranean region. It is hoped that the union will also provide opportunities to Mediterranean geoscientists to undertake interdisciplinary collaborative research. MedGU plans to recognize the work of the most active geoscientists with a number of awards and medals.

Although MedGU has not yet been officially inaugurated, its first annual meeting is planned for November 2021 in Istanbul. This will provide a forum to achieve a consensus for the formation of this non-profit international union of geoscientists. Membership will be open to individuals who have a professional engagement with the Earth, planetary, and space sciences, and related studies, including students and retired seniors.

Nabil Khélifi and Attila Çiner have taken an ambitious approach to the launch of the first MedGU Annual Meeting 2021 and hope to develop it in the near future into the largest international geoscience event in the Mediterranean and the broader MENA region. Its mission is to support geoscientists based in this region by establishing a Global Geoscience Congress.

It is expected that hundreds of participants from all over the world will attend this first MedGU Annual Meeting 2021, making it one of the largest and most prominent geosciences events in the region. So far, over 1300 abstracts have been submitted from 95 countries. The meeting's sessions will cover a wide range of topics with more details available on the Conference Tracks.

This first 2021 Annual Meeting will have a "hybrid" format, with both in-person and virtual participation. Springer, its official partner, will publish the proceedings in a book series (indexed in Scopus) as well as a number of special issues in diverse scientific journals (for more details, see Publications). The official journal of MedGU is Mediterranean Geoscience Reviews (Springer).

Conference Tracks

The scientific committee of the MedGU invites research papers on all cross-cutting themes of Earth sciences, with the main focus on the following 16 conference tracks:

- Track 1. Atmospheric Sciences, Meteorology, Climatology, Oceanography
- Track 2. Biogeochemistry, Geobiology, Geoecology, Geoagronomy
- Track 3. Earthquake Seismology and Geodesy
- Track 4. Environmental Earth Sciences
- Track 5. Applied and Theoretical Geophysics
- Track 6. Geo-Informatics and Remote Sensing
- Track 7. Geochemistry, Mineralogy, Petrology, Volcanology
- Track 8. Geological Engineering, Geotechnical Engineering
- Track 9. Geomorphology, Geography, Soil Science, Glaciology, Geoarcheology, Geoheritage
- Track 10. Hydrology, Hydrogeology, Hydrochemistry
- Track 11. Marine Geosciences, Historical Geology, Paleoceanography, Paleoclimatology
- Track 12. Numerical and Analytical Methods in Mining Sciences and Geomechanics
- Track 13. Petroleum and Energy Engineering, Petroleum Geochemistry
- Track 14. Sedimentology, Stratigraphy, Paleontology, Geochronology
- Track 15. Structural Geology, Tectonics and Geodynamics, Petroleum Geology
- Track 16. Caves and Karst, a special session on the occasion of International Year of Caves and Karst

About the Conference Steering Committee

Executive Committee

Honorary Chair

A. M. Celâl Sengör

Associate Editor, Mediterranean Geosciences Reviews (Springer)
Eurasia Institute of Earth Sciences, Istanbul Technical University Istanbul, Turkey

Organizing Chair

Attila Çiner

MedGU (Interim) President
Founding Editor-in-Chief, Mediterranean Geosciences Reviews (Springer)
Chief Editor—Tracks 11 and 14, *Arabian Journal of Geosciences* (Springer)
Eurasia Institute of Earth Sciences, Istanbul Technical University, Turkey

Conference Manager

Mohamed Sahbi Moalla
Performer—The Leading Conference Organizer, Tunisia
Journal Coordinator, *Euro-Mediterranean Journal for Environmental Integration* (Springer)
ISET, University of Sfax, Tunisia

Conference Support

Mourad Amer
Founder and CEO of IEREK
Editor of ASTI Series (Springer/IEREK)
IEREK, Alexandria, Egypt

Conference Supervisor

Nabil Khélifi

Senior Publishing Editor, MENA program
MedGU-21 Supervisor
Springer, a part of Springer Nature, Germany

Local Organizing Team

Attila Çiner: Eurasia Institute of Earth Sciences, Istanbul Technical University, Turkey
Cengiz Yildirim: Eurasia Institute of Earth Sciences, Istanbul Technical University, Turkey
M. Akif Sarikaya: Eurasia Institute of Earth Sciences, Istanbul Technical University, Turkey
Tolga Gorum: Eurasia Institute of Earth Sciences, Istanbul Technical University, Turkey
Ömer Yetemen: Eurasia Institute of Earth Sciences, Istanbul Technical University, Turkey
Mustafa Üstüner: Artvin Çoruh University, Artvin, Turkey

Online Organizing Team

M. Sahbi Moalla: Performer—The Leading Conference Organizer, Tunisia
Melek Rebai: Performer—The Leading Conference Organizer, Tunisia
M. Bassem Abdelhedi: Performer—The Leading Conference Organizer, Tunisia
Oumayma Abidi: Performer—The Leading Conference Organizer, Tunisia
Toka M. Amer: IEREK—International Experts for Research Enrichment and Knowledge Exchange, Egypt

Advisory Committee

Hans Thybo

President of International Lithosphere Program (ILP)
Editor-in-Chief of *Earth and Planetary Science Letters* (EPSL)
Professor at:

- Eurasia Institute of Earth Sciences, Istanbul Technical University Turkey
- Center for Earth Evolution and Dynamics, University of Oslo, Norway

A. M. Celâl Sengör

Associate Editor, Mediterranean Geosciences Reviews (Springer)
Eurasia Institute of Earth Sciences, Istanbul Technical University Istanbul, Turkey

François Roure

Chief Editor—Track 15
Arabian Journal of Geosciences (Springer)
IFP—Energies Nouvelles, France

Giovanni Bertotti

Associate Editor, Mediterranean Geosciences Reviews (Springer)
Geoscience and Engineering, Delft University of Technology, The Netherlands

Abdullah Al-Amri

Founder and Editor-in-Chief
Arabian Journal of Geosciences (Springer)
King Saud University, Saudi Arabia

Akiça Bahri

Director for Africa at the International Water Management Institute (IWMI), Ghana (2005–2010)
Coordinator of the African Water Facility (AWF) at the African Development Bank (2010–2015)
Director of Research at the National Research Institute for Agricultural Engineering, Water, and Forestry (INRGREF), Tunisia (since 2016)
Professor at the National Agricultural Institute of Tunisia (INAT), Tunisia (since 2017)
Awardee of the International Water Association (IWA) Women in Water Prize (2018)
Associate Editor, *Euro-Mediterranean Journal for Environmental Integration* (Springer) (since 2019)
Minister of Agriculture, Water Resources and Fisheries in Tunisia (2019–2020)

Program Committee

Mustapha Meghraoui

Editorial Board Member, *Mediterranean Geosciences Reviews* (Springer)
Editor of *Arabian Journal of Geosciences* (Springer)
IPG Strasbourg, France

Sami Khomsi

University Tunis El-Manar, Tunis, Tunisia and King Abdulaziz University, Jeddah, Saudi Arabia

Scientific Committee

François Roure

Chief Editor—Track 15
Arabian Journal of Geosciences (Springer)
IFP—Energies Nouvelles, France

Anastasia Kiratzi

Professor of Seismology
Faculty of Sciences, Aristotle University of Thessaloniki, Greece

Broder Merkel

Chief Editor—Track 10
Arabian Journal of Geosciences (Springer)
Associate Editor of Environmental Earth Science (Springer)
Publisher of Freiberg Online Geoscience (FOG)
Institute of Geology, Technische Universität Bergakademie Freiberg, Germany

Elena Xoplaki

Chief Editor, *Euro-Mediterranean Journal for Environmental Integration* (Springer) Justus-Liebig-University Giessen, Germany

Publications Committee

Chair

Attila Çiner

MedGU (Interim) President
Founding Editor-in-Chief, Mediterranean Geosciences Reviews (Springer)
Chief Editor—Tracks 11 and 14, *Arabian Journal of Geosciences* (Springer)
Eurasia Institute of Earth Sciences, Istanbul Technical University, Turkey

Zeynal Abiddin Erguler

Chief Editor—Track 8
Arabian Journal of Geosciences (Springer)
Dumlupinar University, Kutahya, Turkey

Alina Polonia

The National Research Council (CNR)
Institute of Marine Sciences (ISMAR)
Bologna, Italy

Amjad Kallel

Chief Editor—Track 4
Arabian Journal of Geosciences (Springer)
Managing and Development Editor, *Euro-Mediterranean Journal for Environmental Integration* (Springer)
ENIS, University of Sfax, Tunisia

Mourad Bezzeghoud

School of Sciences and Technology (ECT)
Insititut of Earth Sciences (IIFA)
University of Évora, Portugal

Hesham El-Askary

Professor of Remote Sensing and Earth Systems Science
Editor of *Arabian Journal of Geosciences* (Springer)

Director Computational and Data Sciences Graduate Programs
Center of Excellence in Earth Systems Modeling and Observations
Schmid College of Science and Technology, Chapman University, USA

Zakaria Hamimi

President of ArabGU
IAGETH VP for Africa and IAGETH National Chapter for Egypt
Editor of *Arabian Journal of Geosciences* (Springer)
Professor, Benha University, Benha, Egypt

Outreach Committee

Hasnaa Chennaoui Aoudjehane

Member of the nomenclature committee of the Meteoritical Society
Laureate, "Prix Paul Doistau–Émile Blutet" from the French Academy of Sciences
Editor of *Arabian Journal of Geosciences* (Springer)
Professor, Hassan II University of Casablanca, Morocco

Catherine Kuzucuoglu

Associate Editor, Mediterranean Geosciences Reviews (Springer)
Research Director Emeritus
CNRS, Laboratoire de Géographie Physique
UMR 8591, Meudon, France

Preface

This proceedings volume is based on 57 papers accepted and presented during the 1st Mediterranean Geosciences Union (MedGU-21) Conference organized in Istanbul, Turkey, in 2021 under the auspices of Springer Nature. Although more than half of the contributions come from the Mediterranean region, many other countries around the globe also actively participated in developing this volume. In detail, almost half of this volume's papers (29) are related to the Environmental Earth Sciences. In the second part, a total of 19 articles contain works from Geomorphology, Soil Science, Landslides, Paleoclimate, Geoarcheology, and Geoheritage.

Last but not the least, the third part includes nine papers dealing with karst research. These were submitted to the special session on the occasion of the International Year of Caves and Karst (IYCK), declared for 2021 by the International Union of Speleology (UIS) under the auspices of UNESCO. Following the main goals of IYCK, the focus was on all spheres related to the fragile karst environment, especially regarding important issues such as the protection of caves and their natural resources and sustainability.

The book is relevant to all researchers and students on the topics mentioned above, presenting an updated view on field studies, laboratory analyses, and modeling in earth sciences.

İstanbul, Turkey — Attila Çiner
Kuala Lumpur, Malaysia — Md Firoz Khan
Sfax, Tunisia — Amjad Kallel
Granada, Spain — Jesús Rodrigo-Comino
Bari, Italy — Mario Parise
Montréal, Canada — Rahim Barzegar
Kütahya, Türkiye — Zeynal Abiddin Ergüler
Heidelberg, Germany — Nabil Khelifi
New Delhi, India — Imran Ali
June 2022

Contents

About the Editors

Attila Çiner is a Sedimentology and Quaternary Geology Professor at the Eurasia Institute of Earth Sciences at Istanbul Technical University, Turkey. After graduating from the Middle East Technical University in Ankara (1985), he obtained his M.Sc. degree at the University of Toledo, USA (1988), and his Ph.D. at the University of Strasbourg, France (1992). He works on the tectono-sedimentary evolution of basins and Quaternary depositional systems such as moraines, fluvial terraces, alluvial fans, and deltas. He uses cosmogenic nuclides to date these deposits. He primarily focuses on the glacial deposits and landscapes and tries to understand paleoclimatic and paleoenvironmental changes since the Last Glacial Maximum. Lastly, he was part of the Turkish Antarctic Expedition. He spent two months working on the site recognition and decision of the future Turkish scientific research station to be implemented on the continent. He is Editor-in-Chief of *Mediterranean Geoscience Reviews* and Chief editor of *Arabian Journal of Geosciences*, both published by Springer. He has published more than 100 peer-reviewed articles and book chapters.

Dr. Md Firoz Khan is an Associate Professor at the Department of Environmental Science and Management, North South University, since 2022 and a Leader of the AEROSOL LAB (pollutAnts-hEalth inteRactiOn eStimatiOn Lab). Before that, he taught Environmental Science and Geoinformatics for eight years in multiple countries, including Malaysia and China. His fields of expertise include but are not limited to air pollution/causes and effects, atmospheric chemistry, environmental chemistry, air pollution modeling, environmental toxicology, etc. He received his education in Japan (Ph.D.), the UK (M.Sc.), and Bangladesh (B.Sc.). He is an author or co-author of >110 peer-reviewed research articles published in many top-tiering journals. He engages with >20 research grants as a PI or CoPI received from national and international funding bodies in environmental research. Dr. Firoz is a lead lecturer and developer of a micro-credential online course titled “Chemometrics in Air Pollution” under the Future Learn Website. He evaluates research grants from the SWISS National Science Foundation (SNSF) and the Qatar National Research Fund (QNRF). Under his supervision (main and co-supervision), around 30 research students have received undergrad, postgrad, and Ph.D. degrees in air

pollution-health interaction. With immense experience in air pollution research, Dr. Firoz plays a vital role as an Associate Editor in several journals, i.e., *Observation and Modeling of Air Pollution* (a special issue of Sustainability, MDPI, Impact Factor: 3.889); *Elementa: Science of the Anthropocene* (Impact Factor 6.053, California University Press); *Frontiers in Environmental Engineering—Air Pollution Management* and *Arabian Journal of Geosciences* (Springer, Impact Factor: 1.827); and also serves as an expert member to Atmospheric Environmental Remote Sensing Society (AERSS) (Working Group-8: Air Quality, Climate, and Health).

Dr. Amjad Kallel is currently an Associate Professor of Environmental Geology in the Sfax National School of Engineers at the University of Sfax, Tunisia. He holds a B.Eng. in Georesources and Environment (1998) from the University of Sfax (Tunisia) and an M.Sc. degree and a Ph.D. degree in Georesources and Environment (2004) from Hokkaido University (Japan). He joined Venture Business Laboratory (VBL) at Akita University, Japan (2005–2006), as a researcher focusing on refining and recycling technologies for the recovery of rare elements from natural and secondary sources. On his return to Tunisia, he worked at the University of Gabes from 2006 to 2011, where he contributed to the elaboration of teaching programs at the Higher Institute of Water Sciences and Technologies of Gabes. Since 2011, he has joined the Sfax National School of Engineers. There, he has also been involved in various research projects related to Environmental Geology and Environmental Geotechnics. Dr. Kallel has co-organized many prestigious workshops, seminars, and international conferences. In 2016, Dr. Kallel joined the *Arabian Journal of Geosciences* (Springer) and the *Euro-Mediterranean Journal for Environmental Integration* (Springer) as Chief Editor and Managing Editor, respectively.

Jesús Rodrigo-Comino a graduate in Geography, currently works as an Assistant Professor at the University of Granada and was included for the second time in the World's Top 2% Scientists ranking by Stanford University. He got a Master in Territorial Planning and Geographic Information Systems (2013) at the University of Málaga/Granada, whose final work was divided into three national publications and a monograph. During his predoc stage, he obtained three scholarships for doctoral studies: DAAD (German Academic Exchange Service), La Caixa Foundation, and FPU (Ministry of Education, Spain). During this period, he completed his first doctoral thesis in Geography between the University of Trier (Germany—2 years) and Malaga (2 years) in 2018: "Actual Geomorphological Processes in Sloping Vineyards. A Comparison Between Ruwer-Mosel Valley (Trier, Germany) and Montes de Málaga (Málaga, Spain)". In 2023, he defended his second doctorate in engineering in Geomatics and Topography at the Polytechnic University of Valencia. His research career consists of four complete monographs (Nova, Springer, etc.) and some edited books (Elsevier, CRC, Nova),

>200 indexed publications in Scopus and WoS, leading international collaborations with research teams over the world. He is a regular reviewer in more than 150 indexed international journals, a member of two doctoral theses committees, and an evaluator of projects for the Ministries of Science of Chile, Peru, the United States, Serbia, Switzerland, Kazakhstan or Poland, and postgraduate scholarships for DAAD. He has organized several international scientific meetings and congresses (for example COST Actions, Biohydrology, and Fire in the Earth), sessions at international conferences (EGU, TerraEnvision, Conference of the Arabian Journal of Geosciences, etc.), oral presentations, and conference master classes (Germany, Bulgaria, Norway, Algeria, etc.). He is Editor-in-chief of the indexed journal (Scopus and ESCI; Q2) *Air Soil and Water Research* (SAGE) and *Euro-Mediterranean Journal for Environmental Integration* (Springer). In addition, he was Associate Editor at *Scientific Reports* (Nature) and *Hydrological Science Journal* (Taylor & Francis) and continues in the *Arabian Journal of Geosciences* (Springer), and *Journal of Mountain Science* (Springer). He has participated as a researcher in R+D+I projects on social issues related to housing or the census, or transfer and knowledge at a European level, such as the INTERREG Smart-Light HUB project (light pollution) or COST FIRElinks (fires). He has been invited to give lectures on agriculture, sustainable management, and erosion. He has supervised five final degree projects and three master's degrees. He has taught regulated and certified teaching at the Universities of Granada, Valencia, Málaga, León, Oviedo, Trier (in German), Quito (Ecuador), and La Habana (Cuba) on geopolitics, geomorphology, Geographic Information Systems, remote sensing, and statistical techniques. He managed some international (FIRElinks COST Action), national (BBVA Foundation), and regional projects and supervised two Ph.D. theses.

Mario Parise Graduated with honors in Geology at the Faculty of Sciences of the University Federico II, Naples, Italy. Since 1990, he has developed research mainly into the geological and geomorphological analysis of slope movements, namely with the identification of the areas susceptible to different types of slope movement (from debris flows, to deep-seated gravitational slope deformations, to general mass wasting processes) by means of stereoscopic interpretations of aerial photographs and field surveys. Particular focus is given to multi-temporal analysis, aimed at understanding the likely evolution of slopes, even in relationship with anthropogenic activities, and/or as a consequence of specific triggering events (rainfall, earthquakes, etc.). For several sites in southern Italy, he has outlined a framework of the influence of weathering in the predisposition of slope movements. He has also contributed to the analysis of rapid landslides (debris avalanches, rock avalanches) in different geological settings in Italy and abroad, and to studying the occurrence of debris flows and erosional processes in areas recently affected by wildfires. He has

studied various landslides in Italy and the USA, and within this research activity he has developed an expertise in the recognition and investigation of slope failures, production of thematic maps, and also collaborating in the interpretation of monitoring data and in slope stability analyses. In addition, since 2002 he is working in the field of karst research, focusing on the evaluation of the natural and anthropogenic hazards occurring in karst territories, with particular regard to sinkholes and to underground instability and failures. This research is carried out also thanks to the caving activity in which he is active since 1998. He is the author of over one hundred papers published on international journals and proceedings of international conferences. He has given several presentations in international symposium and workshops. He has acted as Guest Editor in 10 special issues for ISI international journals, and has published three books with the Geological Society of London. He is a Member of the Editorial Board of *Natural Hazards and Earth System Sciences*, *Journal of Mountain Sciences*, *Carbonates and Evaporites*, *Natural Hazards*, *Bulletin of Engineering Geology and the Environment*, *Opera Ipogea*, and *Journal of Cave and Karst Studies*.

Dr. Rahim Barzegar is a Postdoctoral Fellow in the Department of Bioresource Engineering at McGill University in Canada. Before joining McGill in 2019, he obtained a Ph.D. and M.Sc. in Hydrogeology and a B.Sc. in Geology from the University of Tabriz, Iran. He has worked as a postdoctoral researcher in joint projects at the University of Tabriz in Iran and Wilfrid Laurier University in Canada. His main research focuses on the exploration of new methods in machine learning- and deep learning-based hydrological modeling. His other research activities also revolve around time series analysis, water quality assessment, water resources management, and climate change impacts on water resources. Dr. Barzegar also acts as an Associate Editor for the *Arabian Journal of Geosciences* (Springer publication), *Earth Science Informatics Journal* (Springer publication), *Communications Earth and Environment* (Nature publication), and Topic Editor for *Water Journal* (MDPI).

Prof. Dr. Zeynal Abiddin Ergüler is a Full Professor at the Geological Engineering department at Kutahya Dumlupinar University (Turkey). Dr. Erguler holds a B.Sc. (1998), an M.Sc. (2001), and a Ph.D. degree (2007) in Geological Engineering from Hacettepe University (Turkey). His research interests mainly focus on rock mechanics, engineering geology, environmental geology, and soil mechanics. His current investigation is to understand and model the thermo-hydro-mechanical behavior of shale rocks in the area of shale gas production. In addition to performing many types of research and industry-funded projects, he has also taught and supervised undergraduate and graduate students. In 2017, Dr. Erguler joined the *Arabian Journal of Geosciences* (AJGS) as an Editor responsible for evaluating submissions in the fields of rock mechanics, engineering geology, environmental geology, and soil mechanics.

Nabil Khelifi undertook fellowships at the System for Analysis, Research and Training (START) in 2005 and the German Academic Exchange Service (DAAD), as part of my Ph.D. studies in Marine Geosciences at the University of Kiel in Germany (2006–2010). After my Ph.D., I received a research grant from the German Science Foundation (DFG) to conduct research projects at the GEOMAR Ocean Research Centre in Kiel on oceanography and climate reconstructions in the North Atlantic and the Mediterranean (2010–2013). My research findings have been presented at international conferences and published in esteemed journals. From 2009 to 2013, I co-organized with my Kiel colleagues two workshops on the Pliocene climate at the University of Bordeaux, France (2009), and the University of Bristol, UK (2013), funded by the European Science Foundation (ESF). In late 2013, I received the Swiss Government Excellence Scholarship to pursue my postdoctoral research career. In 2014, I joined Springer (now Springer Nature) in Heidelberg, Germany, as an Editor, and was promoted to Senior Editor in 2017 responsible for developing their publishing program in the Middle East and Africa, which consists of managing 20 journals and two book series. From 2015 to 2022, I was active in educational seminars for authors, reviewers, and editors to help improve publication output and quality. In 2015, I was also a visiting lecturer at King Saud University, KSA, and University of Sfax, Tunisia, where I gave lectures on publishing techniques. Recently, I launched two international conferences (more details at www.emcei.net and www.medgu.org) aiming at promoting two journals that I was managing at Springer. In 2016, I was awarded the Africa Green Future Leadership Award for my promotion of publications from Africa. In 2020, I received the Saudi Society for Geosciences Award.

Prof. Imran Ali is a world-recognized academician and researcher. He completed his Ph.D. at the Indian Institute of Technology Roorkee, Roorkee, India. Professor Ali is known globally due to his great contribution to pharmaceutical analysis by chromatography and capillary electrophoresis, the development of anticancer drugs, nanotechnology for water treatment, and water splitting for hydrogen green fuel generation. He has published more than 500 papers in reputed journals including papers in Nature and Chemical Reviews of more than 72 impact factors. He has also written six books published by Marcel Dekker, Inc., USA; Taylor & Francis, USA; John Wiley and Sons, USA; John Wiley and Sons, UK; Elsevier, The Netherlands; and Springer, Germany. His total citation is 35,500 with an h-index of 102 and an i10-index of 323. He is a member of various scientific societies globally. He is Editor-in-Chief of 02, Editor of 03, Associate Editor of 06 journals, and is on the editorial board of 40 journals.

Evaluation of the Radiation Doses and Excess Lifetime Cancer Risks Due to Natural Radioactivity in Drinking Groundwater in the United Arab Emirates

Rahaf Ajaj, Samar El-Sayed, and Mohammed A. Salem Al Yafei

Abstract

Groundwater encompasses varying natural radionuclides due to their interaction with the rock and soil that differ in geochemical, mineralogical, and chemical compositions. Exposure to these radionuclides can cause significant risks to human health. Thus, this study aims to estimate the annual effective dose equivalents (D_w) and the excess lifetime cancer risks (LCRs) for adults (>17 yr) living in the United Arab Emirates based on the water consumption rate of 285 (L/yr), and the activity concentrations for forty groundwater samples were calculated in a previous study. The annual effective dose equivalents (D_w) of ^{226}Ra, ^{232}Th, and ^{40}K were $2.69 \times 10^{+1} \pm 5.64 \times 10^{-1}$ (μSv/yr), $1.47 \times 10^{+1} \pm 4.53 \times 10^{-1}$ (μSv/yr), and $8.83 \pm 1.63 \times 10^{-1}$ (μSv/yr), respectively, with the total annual effective dose of $5.04 \times 10^{+1} \pm 0.74$ (μSv/yr). Consequently, the yearly radionuclide intake (D_a) was lower than the WHO-specified average limit. The total values of the excess (LCRs) for the ^{226}Ra, ^{232}Th, and ^{40}K were 9.95×10^{-5}. Accordingly, the excess LCR values for groundwater were found below the acceptable limit of 10^{-3} for radiological risk.

Keywords

Groundwater · Gamma-ray spectrometry · Primordial radioactivity levels · Effective dose equivalents · Lifetime cancer risks · United Arab Emirates

R. Ajaj (✉)
Abu Dhabi University, Abu Dhabi, UAE
e-mail: rahaf.ajaj@adu.ac.ae

S. El-Sayed
University of Sharjah, Sharjah, UAE

M. A. Salem Al Yafei
United Arab Emirates University, Al Ain, UAE

1 Introduction

Uranium-238, K-40, and Thorium-232 are the significant origins of naturally occurring radionuclides in different environments. Plants, animals, rocks, soil, air, and even water contain various concentrations of radionuclides (Vesterbacka et al., 2006). Groundwater contains varying amounts of radionuclides due to their interaction with the rock and soil, differing in geochemical, mineralogical, and chemical compositions. The World Health Organization and the Environmental Protection Agency have enforced limits on the amount of radium in drinking water due to its various health risks. Since radon-222 has a short half-life (3.82 days), it can damage lung tissue and increase the risk of lung cancer due to its alpha emission during decay. Furthermore, long-lasting radionuclides like lead-210, radium-226, uranium-238, and polonium-210 can impact the kidney, bladder, bone marrow, liver, and bone surfaces (Vesterbacka, 2005). Regional aquifer's groundwater movement, water, rock analysis, and submarine groundwater discharge can all be monitored by the isotopes of radium. Previous studies engrossed the high activity of radium-226 (U-23 8) and radium-228 (Th- 232), which is linked to parent isotopic sources (Grundl et al., 2006).

2005. Hence, this study aims to evaluate the radiation doses and excess lifetime cancer risks due to the natural radioactivity in the drinking groundwater in the United Arab Emirates.

2 Methods

2.1 Sampling and Analytical Method

Forty groundwater samples were collected in the United Arab Emirates. The water samples are gathered from different wells used for irrigation purposes. The locations of the sampling points were recorded using a GPS tracking

A. Çiner et al. (eds.), *Recent Research on Environmental Earth Sciences, Geomorphology, Soil Science, Paleoclimate, and Karst*, Advances in Science, Technology & Innovation, https://doi.org/10.1007/978-3-031-42917-0_1

Table 1 Annual effective dose equivalents (D_w)

^{226}Ra	^{232}Th	^{40}K	Total
D_w (μSv/yr) ± σ 2.69E+01 ± 5.64E−01	D_w (μSv/yr) ± σ 1.47E+01 ± 4.53E−01	D_w (μSv/yr) ± σ 8.83E+00 ± 1.63E−01	D_w (μSv/yr) ± σ 5.04E+01 ± 0.74

system. The water samples were placed in 1L Marinelli beakers and stored for one month to achieve secular equilibrium between the radium isotopes and progeny (Hamidalddin, 2014). The samples were measured using an Ortec Gamma-X (GMX) N-type High Purity Germanium (HPGe) Coaxial Radiation Detectors model GMX-40-P, with 30% relative photopeak efficiency and 3 keV resolution at 10 meV.

2.2 Theoretical Calculations

2.2.1 Annual Effective Dose Equivalents (D_w)

The annual effective dose equivalents from the consumption of drinking groundwater due to ^{226}Ra, ^{232}Th, and ^{40}K are mathematically calculated as follows (UNSCEAR, 2000):

$$D_w = A_w \, x \, C_w \, x \, F_w \tag{1}$$

The mean activity concentration (A_w) of ^{226}Ra, ^{232}Th, and ^{40}K was calculated in the previous study (Ajaj et al., 2021). The annual consumption rate (C_w) of water is 285 L/yr in the UAE, according to the EcoMENA website. According to WHO (2004), and ICRP (2012), the effective dose coefficient (F_w) for adults >17 was estimated to be 2.80E−07 Sv/Bq (^{226}Ra), 2.30E−07 Sv/Bq (^{232}Th), and 6.20E–09 Sv/Bq (^{40}K).

2.2.2 Lifetime Cancer Risk (LCR) for the Adult (>17 yr)

LCR was estimated using the following equation (EPA, 1999):

$$\mathrm{LCR} = D_a \left(\frac{\mathrm{Bq}}{\mathrm{yr}}\right) x D_l(\mathrm{yr}) x R_f \left(\frac{1}{\mathrm{Bq}}\right) \tag{2}$$

$$D_a = A_w \left(\frac{\mathrm{Bq}}{\mathrm{yr}}\right) x C_w \left(\frac{L}{\mathrm{yr}}\right) \left(\frac{\mathrm{Bq}}{\mathrm{yr}}\right) \tag{3}$$

where D_a is the annual radionuclide intake (Bq/yr), D_L is the lifetime duration assumed to be 70 years. According to Federal Guidance Report No. 13 (EPA 402-R-99-001), the mortality risk coefficient (R_F) values for ingestion of water are 7.17E−09 Bq^{-1} (^{226}Ra), 1.87E−09 Bq^{-1} (^{232}Th), and 4.30E−10 Bq^{-1} (^{40}K) (EPA, 1999).

3 Results

3.1 The Annual Effective Dose Equivalents (D_w)

The annual effective doses equivalents (D_w) of ^{226}Ra, ^{232}Th, and ^{40}K were $2.69 \times 10^{+1} \pm 5.64 \times 10^{-1}$ (μSv/yr), $1.47 \times 10^{+1} \pm 4.53 \times 10^{-1}$ (μSv/yr), and $8.83 \pm 1.63 \times 10^{-1}$(μSv/yr), respectively, with the total annual effective dose of $5.04 \times 10^{+1} \pm 0.74$ (μSv/yr). Table 1 shows the calculated annual effective dose equivalents (D_w).

3.2 The Lifetime Cancer Risk (LCR)

The total values of the excess (LCRs) for ^{226}Ra, ^{232}Th, and ^{40}K were 9.95×10^{-5}. Table 2 shows the calculated Lifetime Cancer Risks (LCRs).

4 Discussion

According to ICRP, only the risk to the population category >17 years (adults) can be estimated. The acceptable Cancer Risk Level is 7E−4 (National Research Council, 2004). The excess LCR values for groundwater were found below the allowable limit of 10^{-3} for radiological risk. Also, the ingestion dose (annual equivalent effective dose) and the cancer risk level are much lower than the ICRP recommended ingestion dose and cancer risk (1000 μSv/yr and 3.50E−3, respectively (ICRP, 2012)).

5 Conclusions

The annual radionuclide intake (D_a) was lower than the WHO-specified average limit. The excess LCR values for groundwater were found below the acceptable limit for radiological risk. Thus, the results obtained here can be used for tracing potential future fluctuations.

Table 2 The lifetime cancer risk (LCR) for the adult (>17 yr)

^{226}Ra	^{232}Th	^{40}K	Total
4.82E−05	8.35E−06	4.29E−05	9.95E−05

References

Ajaj, R., Shubyar, N., Alashban, Y., El-Sayed, S, Salah, T., & Al Yafei, S. (2021). Determination of primordial radionuclide concentrations in UAE groundwater using high-resolution gamma-ray spectrometry. *Journal of Radioanalytical and Nuclear Chemistry*. https://doi.org/10.1007/s10967-021-08021-2.JRNC-D-21-00586R1

Eckerman, K., et al. (2012). ICRP publication 119: Compendium of dose coefficients based on ICRP publication 60. *Annals of the ICRP, 41*, 1–130.

EcoMENA Homepage, https://www.ecomena.org/water-management-uae/

EPA, US. (1999). Environmental Protection Agency: Cancer Risk Coefficients for Environmental Exposure to Radionuclides, Federal Guidance Report N 13. EPA 402-R-99-001, Office of Radiation and Indoor Air.

Grundl, T., et al. (2006). A combined hydrologic/geochemical investigation of groundwater conditions in the Waukesha county area, WI. *Final Report Submitted to Wisconsin Groundwater Research Program*.

Hamidalddin, S. H. Q. (2014). Determination of agriculture soil primordial radionuclide concentrations in Um Hablayn, north Jeddah west of Saudi Arabia. *International Journal of Current Microbiology and Applied Sciences, 3*(6), 623–633.

National Research Council. (2004). *Review the army's technical guides on assessing and managing chemical hazards to deployed personnel*. National Academies Press.

UNSCEAR. (2006). UNSCEAR 2000 Report to the General Assembly with Scientific Annexes.

Vesterbacka, P. (2005). ^{238}U–series radionuclides in Finnish groundwater-based drinking water and effective doses.

Vesterbacka, P., et al. (2006). Activity concentrations of ^{226}Ra and ^{228}Ra in drilled well water in Finland. *Radiation Protection Dosimetry, 121*(4), 406–412.

WHO. (2004). *Guidelines for drinking–water quality* (2nd ed., Vol. 1). Recommendations, Geneva.

Indicators of Complex Urban Geochemical Transformation in Russian Metropolises

A. Ryanskaya, A. Seleznev, I. Yarmoshenko, and G. Malinovsky

Abstract

This study aimed to identify indicators of complex geochemical changes in urban landscapes in the context of contemporary sedimentation processes. The study was conducted in Russian cities with high anthropogenic pressure, in different climatic and economic zones, and in areas with different geological structures: Nizhny Novgorod, Rostov-on-Don, Murmansk, Tyumen, and Chelyabinsk. The study was based on the hypothesis that recent urban surface-deposited sediments (USDS) reflect changes in geochemical conditions occurring in the urban environment. Therefore, the sampling of environmental compartments participating in the formation of the USDS was conducted in multi-story residential quarters of each city: soil/ground from lawns; dust from sidewalks, driveways, and roads; sediments of local surface-depressed areas of microrelief. The combined analysis of the data on the chemical, mineral, and granulometric composition of the collected samples allowed identifying the following indicators of urban geochemical transformation: the petrogenic and anthropogenic geochemical associations of elements, the granulometric composition, the distribution of elements on granulometric fractions, and the mineral composition.

Keywords

Urban surface-deposited sediments · Geochemical transformation · Urban environment · Mineral composition · Granulometry · Chemical analysis · Heavy metals · Pollution

1 Introduction

Urbanization, increasing the number of cars, and an intensive anthropogenic impact accompany industrial production on the environment of the cities. As a result, the urban environment's components are subjected to geochemical changes throughout its existence. Under the geochemical changes of the landscape and its components, there is a problem associated with assessing the impact of contemporary geochemical processes on human health. The urban geochemical transformation is expressed in changes in the content of elements and forms of their presence in environmental components, changes in mineral and elemental composition, physical and chemical properties of soils, formation of artificial soil objects, changes in migration paths of pollutants in the functional zones of an urban landscape, and formation of a specific contemporary urban surface-deposited sediments (USDS) (Chin et al., 2017; Waters et al., 2016).

70% of the Earth's population lives in cities. Under the increasing anthropogenic load in urban areas, it is significant to develop new environmental assessment methods to consider the degree of geochemical changes in the urban environment and its compartments (Gerten et al., 2019). One of the crucial issues for urban areas is the intake of pollutants from diffuse sources. Various types of contemporary surface sediments (urban surface dirt) deposit the matter that comes from diffuse sources of pollution. Therefore, studying this object in the urban environment is relevant

A. Ryanskaya (✉)
The Zavaritsky Institute of Geology and Geochemistry, Ural Branch of the Russian Academy of Sciences, 15 Akademika Vonsovskogo Str., 620016 Ekaterinburg, Russia
e-mail: sandrian@rambler.ru

A. Seleznev · I. Yarmoshenko · G. Malinovsky
Institute of Industrial Ecology UB RAS, 20, S. Kovalevskoy Str., 620990 Ekaterinburg, Russia

A. Seleznev
Ural Federal University Named After the First President of Russia B.N. Yeltsin, 19, Mira Str., Ekaterinburg 620002, Russia

A. Çiner et al. (eds.), *Recent Research on Environmental Earth Sciences, Geomorphology, Soil Science, Paleoclimate, and Karst*, Advances in Science, Technology & Innovation, https://doi.org/10.1007/978-3-031-42917-0_2

and promising for obtaining geochemical and environmental information (Berger, 1997; Chambers et al., 2016; Poeppl et al., 2017).

The study aimed to identify the indicators of complex geochemical changes in urban areas under increasing anthropogenic pressure. The study was based on the hypothesis that contemporary surface-deposited sediments in the urban landscape reflect the changes in the geochemical conditions of the environment.

2 Materials and Methods

The USDS represents the upper part of the geological strata in the urban environment. The sediments are formed as a result of contemporary natural and anthropogenic processes. Natural factors of sedimentation include weathering of building construction materials, road surfaces and sidewalks, erosion of soils, and dust deposition from the atmosphere. Anthropogenic processes include excavation works, and ground and road surfaces being destroyed by passing and parking cars. Accumulation of sediments increases with insufficient cleaning and bad landscaping of city territories.

The urban geochemical study was conducted in Russian cities with high anthropogenic (mainly transport) pressure, located in different climatic and economic zones, in areas with various geological structures: Nizhny Novgorod (56°19′37″ N, 44°00′27″ E), Rostov-on-Don (47°14′26″ N, 39°42′38″ E), Murmansk (68°58′00″ N, 33°05′00″ E), Tyumen (57°09′ N, 65°32′ E), and Chelyabinsk (55°09′44″ N, 61°24′11″ E).

The samples of material of the environmental components forming USDS were collected in residential areas of multi-story apartment buildings of the cities in the warm and cold seasons: soil, surface-deposited sediments, road dust, snow-dirt sludge, and snow (Seleznev et al., 2019; Yarmoshenko et al., 1320). The samples were collected in functional landscape zones of the quarter: lawn, sidewalk, playground, driveway, and road. The field landscape survey describing the functional landscape condition segment was conducted for the selected quarters of the city (Yarmoshenko et al., 1320). In total, 200 samples of USDS were collected. Granulometric and mineral compositions and elements' content were determined in the collected samples. The elemental analysis of granulometric subsamples includes the determination of total concentrations of metals by mass spectrometry with inductively coupled plasma on mass spectrometer ELAN 9000 by Perkin Elmer (USA) in the chemical-analytical center of IIE UB RAS. The mineral composition of granulometric subsamples is determined by X-ray diffraction, and thermal analyses in the «Geoanalitik» shared research facilities of the IGG UB RAS. Thermal analysis of samples is carried out on a Diamond TG/DTA derivatograph; X-ray phase analysis—on X-ray diffractometer XRD-7000. Figure 1 shows examples of functional zones of a landscape where the environmental compartments were collected.

3 Results and Discussion

Comprehensive analysis of the results of granulometric, chemical, and mineral studies of samples of components involved in the formation of surface sediment revealed the correlation between the geochemical parameters of the urban environment and the cascade structure of the urban residential landscape. In addition, the number of indicators characterizing the geochemical changes of urban landscape was suggested.

1. Petrogenic geochemical association including Al, Fe, Ti, Mn, V, Th, and U. The cities differ in the concentrations of typomorphic elements in the studied environmental objects. In the association, the elements are arranged mainly in the following order: Al > Fe > Ti > Mn (in decreasing concentration). The content of typomorphic elements in the cities differs from 7 to 13 times. The association of the contents of typomorphic elements is unique for each city. In Nizhny Novgorod, Rostov-on-Don, and Tyumen, a decrease in the concentrations of iron and aluminum is observed in the following series of environmental objects: soil-sediment-road dust-snow-dirt sludge on sidewalks and driveways-snow-dirt sludge on the road. The variability of the concentrations of elements of the typomorphic association correlates with the mineral composition of the sampled environmental objects.
2. Anthropogenic association of elements (the most significant are Zn, Cu, and Pb). In most cities, the following patterns were observed: concentrations of Zn, Cu, and Pb decrease in a series of components: soil-sediment-road dust-snow-dirt sludge on the sidewalk and driveway-snow-dirt sludge on the road. High content of Ni in snow-dirt sludge in Tyumen (20–30 times higher than in other cities) was found. As shown by further mineral analysis, the increased content of Ni and Fe in Tyumen was associated with the use of crushed stone from serpentinite (containing minerals Ni) as an anti-icing agent in the winter period. Soil represents the main depot of metals of anthropogenic origin, which accumulate pollution over a long period. Surface sediment accumulated in yards and streets usually contains lower concentrations of heavy metals. In Nizhny Novgorod and Rostov-on-Don, the decrease of concentrations of the most significant heavy metals in the transition from soil to snow-dirt sludge on the road was found: for Zn 7–9 times, for Cu

Fig. 1 Examples of functional zones of landscapes where the samples were collected: **a** parking spaces in a courtyard area; **b** lawn

2–5 times, and for Pb 6–9 times. This ratio may indicate the absence of significant contemporary Zn, Cu, and Pb intake. At the same time, in Chelyabinsk, the inflow of metals at present occurs in quite substantial quantities.

3. Granulometric composition. The generally observed pattern for the cities was the order of environmental components distributed by the content of dust fraction <100 μm—from 26 to 57% in soil, from 16 to 38% in surface sediment, up to 53% in snow-dirt sludge, and up to 100% in solid materials in snow. The fine dust fraction (2–10 μm) contributes 1.6–12% to the total mass of the dust and surface dirt in the urban environment. In the composition of snow-dirt sludge, the fine fraction of 2–10 μm may reach 26%.
4. Distribution of anthropogenic metals by particle size fractions. The highest concentrations of Zn, Cu, and Pb were found in the dust fractions of 2–100 μm. The minimum Zn concentrations in samples of snow-dirt sludge in fractions (10–100 μm) are 5–10 mg/kg in Nizhny Novgorod, which corresponds to the insignificant level of contemporary Zn intake in the environment in this city. The maximum Zn content in snow-dirt sludge samples was found in Chelyabinsk. In Chelyabinsk, the copper content in different size fractions of surface sediments is not below 40 mg/kg and in the snow-dirt sludge reaches 86 mg/kg in the fraction (10–100 μm). The metals of the anthropogenic association are characterized by the higher accumulation in the fine fraction of the soil compared to the corresponding size fractions of surface sediment and road dust. At the same time, the fractions >100 μm did not show the stable elements' concentration dependence on the type of environmental

component. The heavy metals accumulated in the dust fraction of urban soils may represent the secondary source of pollution during erosion and weathering of the surface layer of soil.

5. Mineral composition. The surveyed cities differ in the mineral composition of the environmental components. In Nizhny Novgorod, Rostov-on-Don, and Tyumen, quartz and quartz-feldspar sand make a predominant contribution. At the same time, in Nizhny Novgorod and Rostov-on-Don, the second mineral component is the minerals belonging to the acid rocks and the basic rocks in Tyumen. In Chelyabinsk and Murmansk, the mineral composition of the elements is mainly related to acid rocks. The mineral composition of the surveyed environmental components is primarily associated with the geological conditions of the corresponding region. In most cities (Nizhny Novgorod, Rostov-on-Don, Tyumen), the mineral composition of the components of the environment is significantly contributed by the products of the destruction of construction materials. At the same time, in the cities of Chelyabinsk and Murmansk, the contribution of construction materials to mineral composition is insignificant.

4 Conclusions

The combined analysis of the data on the chemical, mineral, and granulometric composition of the collected samples allowed identifying the indicators of urban geochemical transformation. Those indicators confirm the influence of the factors determining the geochemical change of the urban landscape: erosion and weathering of artificially created surfaces; the negative impact of vehicles transporting the loose sediment between; low efficiency of environmental quality management; redistribution of pollution between the segments of the urban landscape.

Funding Russian Science Foundation, project number 18-77-10024, funded the reported study. Mineral analysis was conducted in the «Geoanalitik» shared research facilities of the IGG UB RAS. The re-equipment and comprehensive development of the «Geoanalitik» shared research facilities of the IGG UB RAS is financially supported by the grant of the Ministry of Science and Higher Education of the Russian Federation for 2021–2023 (Agreement No. 075-15-2021-680).

References

Berger, A. R. (1997). Assessing rapid environmental change using geoindicators. *Environmental Geology, 32*(1), 36–44.

Chambers, L. G., Chin, Y.-P., Filippelli, G. M., Gardner, C. B., Herndon, E. M., Long, D. T., Lyons, W. B., MacPherson, G. L., McElmurry, S. P., McLean, C. E., et al. (2016). Developing the scientific framework for urban geochemistry. *Applied Geochemistry, 67*, 1–20.

Chin, A., Beach, T., Luzzadder-Beach, S., & Solecki, W. D. (2017). Challenges of the "Anthropocene." *Anthropocene, 20*, 1–3.

Gerten, C., Fina, S., & Rusche, K. (2019). The sprawling planet: Simplifying the measurement of global urbanization trends. *Frontiers in Environmental Science, 7*, 140.

Poeppl, R. E., Keesstra, S. D., & Maroulis, J. (2017). A conceptual connectivity framework for understanding geomorphic change in human-impacted fluvial systems. *Geomorphology, 277*, 237–250.

Seleznev, A., Yarmoshenko, I., Malinovsky, G., Ilgasheva, E., Baglaeva, E., Ryanskaya, A., Kiseleva, D., & Gulyaeva, T. (2019). Snow-dirt sludge as an indicator of environmental and sedimentation processes in the urban environment. *Scientific Reports*, *9*(1), 17241.

Waters, C. N., Zalasiewicz, J., Summerhayes, C., Barnosky, A. D., Poirier, C., Galuszka, A., Cearreta, A., Edgeworth, M., Ellis, E. C., Ellis, M., et al. (2016). The Anthropocene is functionally and stratigraphically distinct from the Holocene. *Science*, *351*, aad2622.

Yarmoshenko, I., Malinovsky, G., Baglaeva, E., & Seleznev, A. (2020). A landscape study of sediment formation and transport in the urban environment. *Atmosphere*, *11*, 1320.

Study of Zn Pollution of a Large City Based on Analysis of Stable Zinc Isotope Ratios in Urban Surface-Deposited Sediments

Tatiana Okuneva, Andrian Seleznev, Darya Kiseleva, and Natalia Soloshenko

Abstract

The current work aimed to discriminate urban pollution sources using the zinc isotope ratio as a tracer. The study was conducted on the example of the large industrial city of Ekaterinburg, Russia. The urban surface-deposited sediment (USDS) collected in the multistory residential areas was analyzed as a geoindicator. The USDS represents a geochemical trap in an urban environment and reflects an area's contemporary urban geochemical conditions and their changes over time. USDS samples were collected from an irregular grid in the city during 2007–2010. Sample decomposition was conducted using a mixture of acids (HF, HNO_3, and HCl). Zn isotope ratios were measured using MC-ICP-MS Neptune Plus (Thermo Fischer, Germany). The isotope ratios were reported as δ^{66}Zn relative to the JMC-Lyon certified isotopic standard. Zinc isotope ratios in USDS samples varied from −1.00 to +0.49‰. 84% of investigated USDS samples in Ekaterinburg have a zinc isotope ratio, corresponding to road traffic and non-exhaust emissions (−0.50 to +0.49‰). The δ^{66}Zn values in the residential districts near the city's railway were −1.0 to −0.6‰; the value near the Railway Station was −0.29‰; next to highways were from −0.5 to −0.3‰.

Keywords

Urban environment · Urban surface-deposited sediments · Zn isotope ratios · Initial geochemical baseline · Pollution

1 Introduction

Environmental pollution is one of the most significant issues affecting the population's health. Therefore, one of the most critical tasks is studying pollutant sources' distribution. The δ^{66}Zn isotope ratio is of exceptional interest because zinc is an integral component of various artificial materials and technological devices. Moreover, anthropogenic activities have mainly altered its geochemical cycle (Mattielli et al., 2009; Ochoa & Weiss, 2016). Therefore, the zinc isotope ratio is used to identify pollution and metal migration sources in the anthroposphere (Gioia et al., 2008; Souto-Oliveira et al., 2019).

The current work aimed to discriminate urban pollution sources using the zinc isotope ratio as a tracer. The study was conducted on the example of the large industrial city Ekaterinburg, Russia. The city's urban surface-deposited sediment (USDS) was analyzed as a geoindicator.

2 Materials and Methods

The USDS accumulated in local depressed relief zones represents a geochemical trap (Seleznev & Yarmoshenko, 2014) reflecting the contemporary geochemical conditions and their changes in urban environments. The trap accumulates pollutants over space and time, characterizing the pollutant migration processes. The sedimentary material of USDS is represented by soil erosion material and particles transported from urban functional landscape zones, roofs,

T. Okuneva (✉) · D. Kiseleva · N. Soloshenko
The Zavaritsky Institute of Geology and Geochemistry, Ural Branch of the Russian Academy of Sciences, 15 Akademika Vonsovskogo Str., 620016 Ekaterinburg, Russia
e-mail: sandrian@rambler.ru

A. Seleznev · D. Kiseleva
Ural Federal University Named After the First President of Russia B.N. Yeltsin, 19, Mira Str., Ekaterinburg 620002, Russia

A. Çiner et al. (eds.), *Recent Research on Environmental Earth Sciences, Geomorphology, Soil Science, Paleoclimate, and Karst*, Advances in Science, Technology & Innovation, https://doi.org/10.1007/978-3-031-42917-0_3

pavement, local roads, and other surfaces. USDS samples were collected from an irregular grid in Ekaterinburg between 2007 and 2010. The data on elements' content in the USDS sample population obtained in the previous studies (Seleznev & Yarmoshenko, 2014, 2018; Seleznev et al., 2015) were used in the current analysis.

The Zn isotope measurements were conducted for USDS samples. The stage of sample decomposition included sequential dissolution in a mixture of acids HF: $HNO_3 = 1{:}3$; HCl: $HNO_3 = 3{:}1$; and HCl. The AG MP-1 ion-exchange resin (Bio-Rad Inc., USA) was used for chromatographic isolation of pure fractions of Zn. The Zn isotope ratios were measured on a Neptune Plus MC-ICP-MS spectrometer (Thermo Fisher) with an ASX 110 FR automatic sample introduction system (Teledyne CETACEAN, USA). The accuracy and long-term reproducibility of the measurement procedure were estimated using JMC-Lyon zinc reference material.

The initial geochemical baseline (IGB) relationship between the concentrations of Zn and Fe in USDS was reconstructed according to the approach (Seleznev & Yarmoshenko, 2018). The IGB reconstruction divided the USDS sample population into the "polluted" with Zn samples, in which the Zn concentration significantly deviates from IGB, and the "unpolluted" group.

3 Results and Discussion

In total, 213 samples of USDS were collected; element concentrations were measured in all the samples (Seleznev & Yarmoshenko, 2014, 2018; Seleznev et al., 2015). The δ^{66}Zn percentage was determined in 51 samples. Figure 1 represents the distribution of Zn concentrations in USDS samples in groups of "polluted" and "unpolluted" samples (Seleznev & Yarmoshenko, 2018), depending on the year of surface formation (Seleznev et al., 2015). The year of surface formation was calculated based on data on the content of anthropogenic radionuclide ^{137}Cs in USDS samples (Seleznev et al., 2015). The 173 mg/kg zinc concentration represents the IGB level for zinc in USDS in Ekaterinburg city. Zinc pollution in the city decreases depending on the year of landscape construction. Consequently, newer landscapes and soils have lower zinc content.

Zn isotope ratios in USDS vary in the range −1.00 to +0.49‰, mean −0.13, median −0.09, and standard deviation 0.25. Figure 2 shows the distribution of δ^{66}Zn in the groups of "polluted" and "unpolluted" with Zn samples depending on the urban landscape's formation year. In the group of "polluted" samples, there is a tendency to increase δ^{66}Zn by decreasing the age of the urban landscape; older USDS samples have a lower Zn isotope ratio. On the other

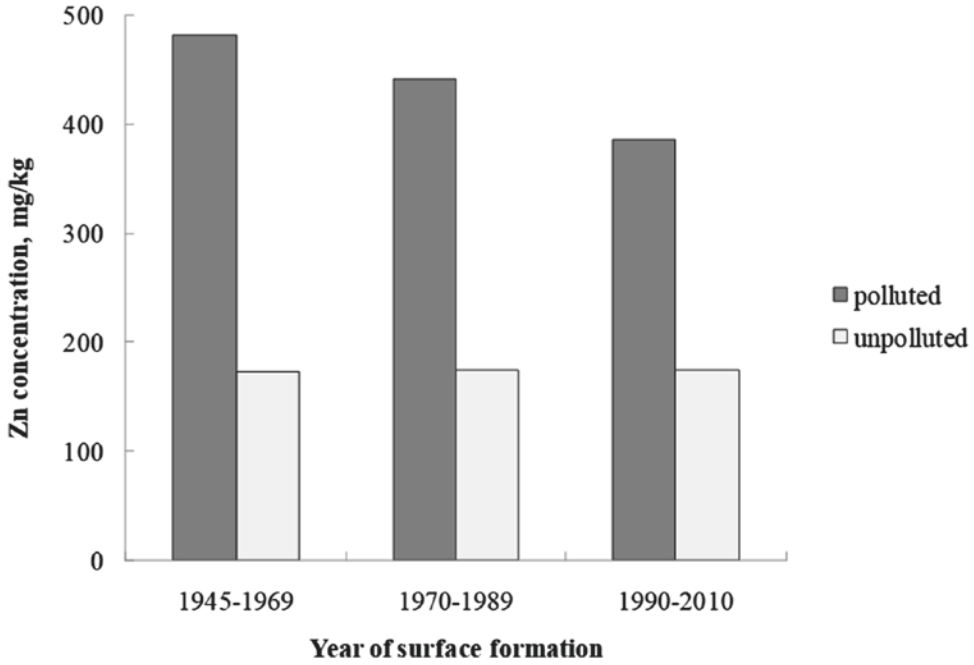

Fig. 1 Distribution of Zn concentration between the groups of "polluted" and "unpolluted" with Zn samples in dependence of year of surface formation in Ekaterinburg (Seleznev & Yarmoshenko, 2018; Seleznev et al., 2015)

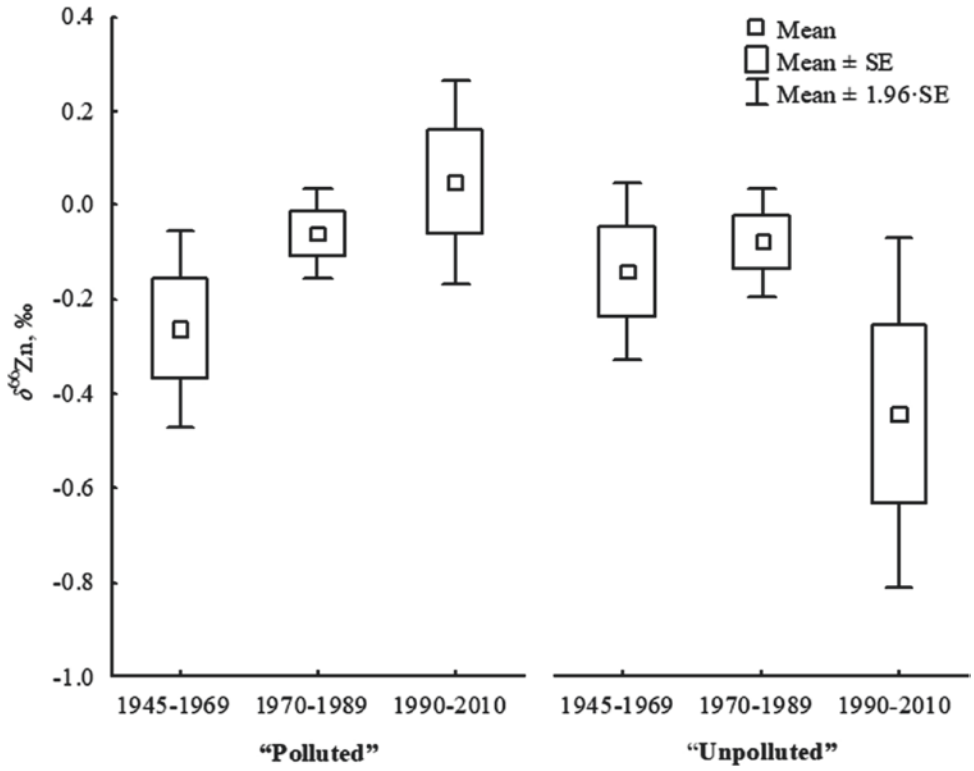

Fig. 2 The distribution of δ^{66}Zn in Zn-"polluted" and "unpolluted" samples depending on the year of formation of the urban landscape in Ekaterinburg (Seleznev & Yarmoshenko, 2018; Seleznev et al., 2015)

hand, the group of "unpolluted" samples in landscapes formed between 1990 and 2010 shows the lowest δ^{66}Zn values. These values may correspond to IGB for δ^{66}Zn in the urban landscape of Ekaterinburg before 1945.

The 84% of investigated USDS samples in Ekaterinburg have a zinc isotope ratio, corresponding to road traffic and non-exhaust emissions (−0.50 to +0.49‰) according to literature data (Souto-Oliveira et al., 2019). At the same time, more recent unpolluted with Zn samples have in their composition zinc from industrial emissions (δ^{66}Zn < −0.6) (Souto-Oliveira et al., 2019). The δ^{66}Zn values in the residential districts near the city's railway were −1.0 to −0.6‰; the value near the Railway Station was −0.29‰; next to highways were from −0.5 to −0.3‰.

4 Conclusions

The use of isotope tracing methods significantly expands the possibility of discrimination of urban pollution sources. Analysis of Zn isotope ratios shows the tendencies in pollution with Zn in Ekaterinburg over the last 70 years. The urban surface-deposited sediments show great potential as a geoindicating environmental compartment in a metropolitan area. A more detailed analysis of Zn isotope composition in combination with Pb and Cu will give more information about USDS composition and pollution sources in an urban environment.

Acknowledgements This work was carried out at the UB RAS "Geoanalitik" Center for Collective Use and supported by the Russian Foundation for Basic Research (RFBR), grant No. 19-35-60011. The equipment and comprehensive development of the "Geoanalitik" shared research facilities of the IGG UB RAS is financially supported by the grant of the Ministry of Science and Higher Education of the Russian Federation for 2021–2023 (Agreement No. 075-15-2021-680).

References

Gioia, S. M. C. L., Weiss, D., Coles, B., Arnold, T., & Babinski, M. (2008). Accurate and precise zinc isotope ratio measurements in urban aerosols. *Analytical Chemistry, 80*, 9776–9780.

Mattielli, N., Petit, J. C. J., Deboudt, K., Flament, P., Perdrix, E., Taillez, A., Rimetz-Planchon, J., & Weis, D. (2009). Zn isotope study of atmospheric emissions and dry depositions within a 5 km radius of a Pb–Zn refinery. *Atmospheric Environment, 43*, 1265–1272.

Ochoa, G. R., & Weiss, D. (2016). Zinc isotope variability in three coal-fired power plants: A predictive model for determining isotopic fractionation during combustion. *Environmental Science and Technology, 49*, 12560–12567.

Seleznev, A. A., Yarmoshenko, I. V., & Sergeev, A. P. (2015). ^{137}Cs in puddle sediments as timescale tracer in urban environment. *Journal of Environmental Radioactivity, 142*, 9–13.

Seleznev, A. A., & Yarmoshenko, I. V. (2014). Study of urban puddle sediments for understanding heavy metal pollution in an urban environment. In *Environmental technology & innovation* (Vol. 1–2, pp. 1–7).

Seleznev, A. A., Yarmoshenko, I. V., & Sergeev, A. P. (2018). Method for reconstructing the initial baseline relationship between potentially harmful element and conservative element concentrations in urban puddle sediment. *Geoderma*, *326*, 1–8.

Souto-Oliveira, C. E., Babinski, M., Araújo, D. F., Weiss, D. J., & Ruiza, I. R. (2019). Multi-isotope approach of Pb, Cu and Zn in urban aerosols and anthropogenic sources improves tracing of the atmospheric pollutant sources in megacities. *Atmospheric Environment, 198*, 427–437.

Lead Fluxes in Suspended Particulate Matter from a Tropical Estuary to the Atlantic Ocean

Lyndyanne Dias Martins, Vinícius Pereira Bacurau, Jorge Marcell Coelho Menezes, Francisca Denise Pereira Almeida, Rômulo De Araujo Soares, Francisco José Da Silva Dias, Kassandra Kelen Borges, Felipe Dos Santos Gonçalves, Willian Avelino Lopes, Raimundo Nonato Pereira Teixeira, and Francisco José De Paula Filho

Abstract

The primary purpose of this study was to estimate the discharges of lead (Pb) associated with suspended particulate matter (SPM) from the waters of the Parnaíba River Estuary (PRE) to the Atlantic Ocean. The sampling campaign, conducted at the neap tide, included a Lagrangian evaluation of six sampling points (P1–P6) and a Eurelian evaluation at two points (P2 and P5) during the tidal cycle (ebb/flood tides). The determination of SPM concentrations was performed by gravimetry. After acid extraction from sample extracts, particulate Pb was determined by flame atomic absorption spectrophotometry. The SPM concentrations varied between 20 and 920 mg L^{-1}, higher at ebb tide, and in those points under the more significant fluvial influence. Pb concentrations ranged 8–80 mg kg^{-1} and were higher at ebb tide and P3. The net balance resulting from the retained SPM and the total exported was equal to 82 tons day^{-1}. For lead, the net balance was 0.01 kg day^{-1} exported. The mass balances showed a higher export capacity for SPM, meaning that the estuary is a source of these materials for the adjacent Atlantic coast. The calculated loads were lower than those reported for other tropical estuaries, telling us that the Parnaíba River Delta is a conserved natural environment with a low anthropic impact.

Keywords

Metal fluxes · Mass balance · SPM · Trace metals · Parnaíba river delta

1 Introduction

Estuarine systems are zones of interaction between riverine and marine waters. Their areas depend on tidal oscillation, and their dynamics are intrinsically related to the biogeochemical cycles in these environments (Dias et al., 2013). In estuarine waters, suspended particulate matter (SPM) is the leading carrier of trace metals to the ocean. The latter can be released into the water through resuspension, adsorption, reduction or oxidation reactions of sediments, and degradation of organic tissues (Duan et al., 2014). SPM may have a significant capacity to adsorb pollutants, among them lead. Lead concentrations are strongly linked to anthropogenic sources such as domestic and industrial effluents, in addition to the atmospheric deposition of emissions related to the burning of fossil fuels, which have increased worldwide in recent years (Molisani & Esteves, 2013).

The Parnaíba River Estuary (PRE), located in northeastern Brazil, serves as a breeding area for several marine species, provides essential ecosystem services, and is protected by federal law (Ministério do Meio Ambiente 2006). Considering its environmental importance, the main objectives of this study were (i) to determine the concentrations, distribution, fluxes, and loads of Pb associated with SPM; and (ii) to infer whether the estuary acts as a sink or source of these materials to the adjacent Atlantic coast. Therefore, this study contributes to the global effort to increase the existing knowledge in the field of ocean sciences, contributing to the implementation of the 2030 Agenda for Sustainable Development.

L. D. Martins · V. P. Bacurau · J. M. C. Menezes · F. D. P. Almeida · W. A. Lopes · F. J. De Paula Filho (✉)
Federal University of Cariri, Ceará, Brazil
e-mail: francisco.filho@ufca.edu.br

R. De Araujo Soares · F. J. Da Silva Dias · K. K. Borges · F. Dos Santos Gonçalves
Federal University of Maranhão, Maranhão, Brazil

R. N. P. Teixeira
Regional University of Cariri, Ceará, Brazil

A. Çiner et al. (eds.), *Recent Research on Environmental Earth Sciences, Geomorphology, Soil Science, Paleoclimate, and Karst*, Advances in Science, Technology & Innovation, https://doi.org/10.1007/978-3-031-42917-0_4

2 Materials and Methods

Sampling was carried out in September 2019 (dry season) at neap tide, considering both the Lagrangian (spatial) and Eulerian (temporal) approaches. The instantaneous outflows in the estuary were measured using an Acoustic Doppler Current Profiler/SONTEK/YSI (ADCP) current meter with an acoustic frequency sensor of 1.5 MHz. The spatial distribution of Pb associated with the SPM was obtained in different sectors of the estuary (Lagrangian approach). In the Eurelian approach, we evaluated Pb and SPM fluxes from the drainage basin to the delta and from the latter to the adjacent Atlantic coast. The samples were collected during a 12-h tidal cycle (flood/ebb tides) from a sampling grid composed of 6 points (P1–P6). Water samples were collected in duplicate with a Van Dorn sampler and stored in 5-L polyethylene bottles. At the laboratory, the samples were filtered using Millipore AP 040 filters to obtain the SPM (Strickland & Parsons, 1972). Lead on the SPM was determined by atomic absorption spectrophotometry (Varian SpectraA 55B). Mass balance calculations were performed using data generated by the Eulerian approach (P2 and P5). The mass balance was calculated from flux variations (inflow and outflow) and according to the tidal regime.

3 Results

In September 2019, the PRE was strongly controlled by tidal forcing during the dry period. In this hydrodynamic condition, the SPM was up to an order of magnitude lower than other tropical estuaries on the northeastern coast of Brazil (Dias et al., 2013). Table 1 shows the flows (Q) and the SPM and Pb concentrations obtained under the two approaches used in this study (Lagrangian and Eulerian). Pb concentrations in the SPM are in the same order of magnitude as reported for Baisha Bay on the Guangdong coast of China (Gu et al., 2017). The instantaneous SPM fluxes at P2 13–513 g s^{-1} (flood tide) and 75–709 g s^{-1} (ebb tide) and P5 (23–102 g s^{-1} (flood tide) and 9–47 g s^{-1} (ebb tide) were calculated. The Pb fluxes for P2 were 33–404 g day^{-1} (flood tide) and 56–697 g day^{-1} (ebb tide), while at P5, they were 4–53 g day^{-1} (flood tide) and 5–24 g day^{-1} (ebb tide).

From the fluxes, we estimated the SPM and Pb loads for the PRE under the hydrodynamic conditions of the region´s dry season (Fig. 1). The net balance resulting from the retained SPM and the total exported was equal to 82 ton day^{-1}. For lead, the net balance was 0.01 kg day^{-1} exported.

4 Discussion

SPM concentrations were higher in the ebb tide waters at same order of magnitude as the reported for the tropical estuary of Arraial/São José (20 and 189.9 mg L^{-1}) (Azevedo et al., 2008). Pb concentrations were higher at the sampling sites under the greater marine influence, i.e., those closer to the river mouth (P2 and P3). Concentrations of the metal associated with the SPM decreased at the changing tides, a phenomenon probably related to the influence of the Maximum Turbidity Zone (Dias et al., 2013). In general, concentrations of particulate Pb in the PRE waters were lower than those of other estuaries of the Brazilian coast under different levels of anthropogenic influence (Dias et al., 2013; Molisani & Esteves, 2013).

The estimated SPM load (Fig. 1a) shows a similar contributions from the drainage basin to the estuary at the flood and ebb tides. The SPM balance indicates an outflow greater than the inflow to the estuary. Under the hydrodynamic conditions of the dry season, the estuary behaves as an exporter of materials carried in suspension. The Pb balance (Fig. 1b) shows that, during the dry season, the estuary is a Pb exporter to the adjacent Atlantic coast.

Table 1 Ranges, means, and standard deviations of Q, SPM, and Pb in the dry season

Approach	Q (m^3 s^{-1})		SPM (mg L^{-1})		Pb (mg kg^{-1})[a]	
	Flood	Ebb	Flood	Ebb	Flood	Ebb
Lagrangian	161–1005	512–1209	20–910	20–920	21–80	11–71
	821 ± 382	854 ± 270	410 ± 270	410 ± 230	40 ± 17	39 ± 19
Eulerian	133–1575	441–1669	120–450	20–320	8–75	8–72
	694 ± 302	804 ± 313	250 ± 100	130 ± 70	29 ± 31	45 ± 26

[a] Dry weight

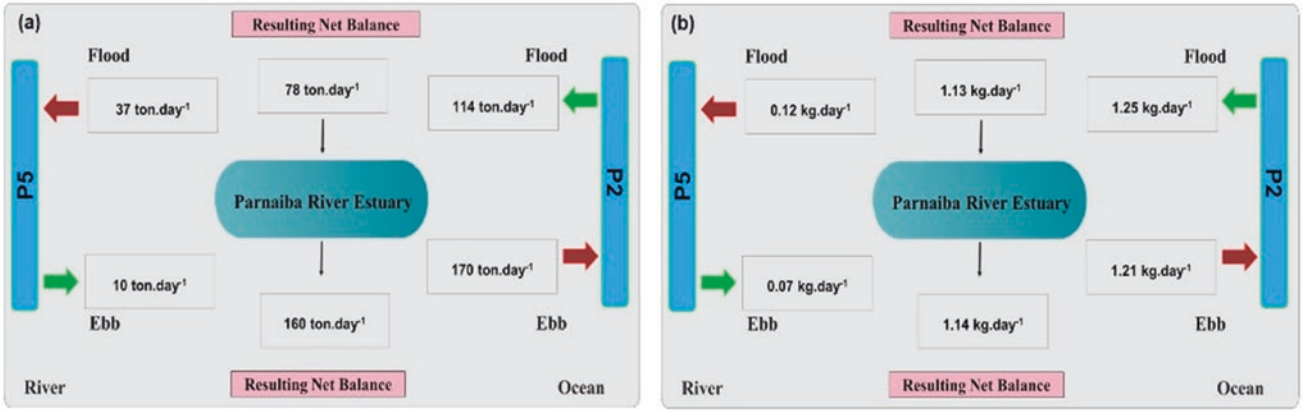

Fig. 1 Estimated balances of SPM (ton yr^{-1}) (**a**) and Pb (kg day^{-1}) (**b**) in the PRE during the dry season

5 Conclusions

Marine waters predominate in the PRE during the dry season, damming the fluvial outflow at flood tide. At ebb tide, the larger outflows destabilize the sediments and resuspend materials in the water column, increasing SPM concentrations. Therefore, by estimating the Pb inputs from the drainage basin to the PRE, we could see that the estuary is an exporter of Pb according to the resulting net balance.

It is essential to point out that these balances are only estimates and that instantaneous flows are extrapolated to a 24-h period or any other time. Thus, they must be interpreted cautiously, as it is impossible to ascertain whether these values remain constant over time. Therefore, more sampling campaigns are needed, especially during other seasons, to acquire data complementary to those obtained in this study.

Acknowledgements This study was supported by the Fundação Cearense de Apoio ao Desenvolvimento Científico e Tecnológico—FUNCAP (Grant No. BP4-00172-00080.01.00/2) and Conselho Nacional de Desenvolvimento Científico e Tecnológico—CNPq (Grant No. 408363/2018-5).

References

Azevedo, A. C. G., Feitosa, F. A. N., & Koening, M. L. (2008). Spatial and temporal distribution of the phytoplanktonic biomass and environmental variables in the Maranhense Gulf, Brazil. *Acta Botânica Brasílica, 22*(3), 870–877.

Dias, F. J. S., Marins, R. V., & Maia, L. P. (2013). Impact of drainage basin changes on suspended matter and particulate copper and zinc discharges to the ocean from the Jaguaribe river in the semiarid NE Brazilian coast. *Journal of Coastal Research, 29*(5), 1137–1145.

Duan, L. Q., Song, J. M., Yuan, H. M., Li, X. G., Li, N., & Ma, J. K. (2014). Distribution, chemical speciation and source of trace elements in surface sediments of the Changjiang Estuary. *Environmental Earth Sciences*, *72*, 3193–3204.

Molisani, M. M., & Esteves, F. A. (2013). Natural and anthropogenic emissions of nitrogen, phosphorous and metals into the Macaé river basin (Macaé, RJ, Brazil) influenced by oil and gas exploration in Campos Basin. *Química Nova, 36*(1), 1–7.

Ministério do Meio Ambiente. (2006). *Caderno da Região Hidrográfica do Parnaíba. Secretaria de Recursos Hídricos*. MMA.

Strickland, J. D., & Parsons, T. R. (1972). *A practical handbook of seawater analysis* (No. 167, 310p.). Bulletin Fisheries Research Board of Canada.

Gu, Y. G., Ouyanga, J., An, H., Jiang, S. J., & Tang, H. Q. (2017). Risk assessment and seasonal variation of heavy metals in settling particulate matter (SPM) from a typical southern Chinese mariculture base. *Marine Pollution Bulletin, 123*(1–2), 404–409.

Geochemical Transformation of Water Bodies in an Urban Environment Under Contemporary Surface Sedimentation in the Catchment

Andrian Seleznev, Tatiana Okuneva, Ilia Yarmoshenko, and Georgy Malinovsky

Abstract

The work aimed to study the geochemical transformation of the lake under sediment transport from the catchment. The study used a catenary complex approach based on the basin principle. The selected urban catchments had different functional landscape areas where contemporary sedimentation processes occur: carriageway, sidewalk, lawn, park/forest edge, beach, playground or sports ground, and parking lot. A sampling of environmental compartments was carried out in different functional landscape zones of catchments and on lakes in warm and cold periods of the year. In total, 28 samples of environmental compartments were collected from two catchments in warm and cold seasons, 18 samples of ice, water, and snow were collected on the lakes in the winter season, and 15 cores of bottom sediments. The cation and anion composition, pH, Eh, elements' concentrations, mineral composition, Pb isotopes, and concentration of technogenic radioactive isotope Cs-137 were determined in the collected samples. The connected functional landscape areas in the catchment supply the sedimentary material to the bottom sediments of the lakes. The decreasing order of concentrations of the elements in soils, surface-deposited sediments, and bottom sediments of water bodies was similar: Ti–Mn–Cr–Zn–V–Ni–Cu–Pb–Co–As–Sn. Such association confirms a similar genesis of metals in the lake and its catchment. Furthermore, the abnormally high salinity of snow-dirt sludge taken from the road is associated with the presence of an anti-ice mixture.

Keywords

Contemporary sedimentation · Urban surface-deposited sediments · Road dust · Snow-dirt sludge · Surface water bodies · Bottom deposits · Water · Urban environment · Geochemical transformation

1 Introduction

The processes of changes in the geochemical conditions of surface water bodies directly depend on the geochemical conditions of the catchment (Liu et al., 2013; Lundy et al., 2012). Therefore, one of the significant issues in an urban area is the pollutants' supply into water bodies from non-point sources in addition to runoff from the stationary pollution sources: spring meltwater runoff, rainwater and irrigation wash water, and in-soil and groundwater runoff (https://www.epa.gov/nps/basic-information-about-nonpoint-source-nps-pollution; https://www.epa.gov/nps; Lundy et al., 2012; Müller et al., 2020).

Sediment material for geochemical evaluation is important information such as the type of lake and lake surroundings. The urban sedimentary system produces significant global waste and pollution (Froger et al., 2018; Owens et al., 2016). This sediment, together with pollutants resulting from the urban sedimentation cascade, is transported to the surface water bodies (Chin, 2006). The part of the surface sediments reaching a water body becomes the bottom sediments and may tend to eutrophicate it and harm the inhabitants of water bodies.

A. Seleznev (✉)
Ural Federal University Named After the First President of Russia, B.N. Yeltsin, 19, Mira Str., Ekaterinburg 620002, Russia
e-mail: sandrian@rambler.ru

A. Seleznev · I. Yarmoshenko · G. Malinovsky
Institute of Industrial Ecology UB RAS, 20, S. Kovalevskoy Str., 620990 Ekaterinburg, Russia

T. Okuneva
The Zavaritsky Institute of Geology and Geochemistry, Ural Branch of the Russian Academy of Sciences, 15 Akademika Vonsovskogo Str., 620016 Ekaterinburg, Russia

A. Çiner et al. (eds.), *Recent Research on Environmental Earth Sciences, Geomorphology, Soil Science, Paleoclimate, and Karst*, Advances in Science, Technology & Innovation, https://doi.org/10.1007/978-3-031-42917-0_5

Soil, surface sediment, bottom sediments of the small water reservoirs, and snow are essential indicators of the urban environmental state. The work aimed to study the geochemical transformation of the lake under sediment transport from the catchment. The study was conducted on the example of two shallow lakes selected in the urban area of Ekaterinburg (Russia).

2 Materials and Methods

The study was carried out using a catenary complex approach. The catenary complex represents a catchment area together with a water body. The selected urban catchments had different functional landscape areas where contemporary sedimentation processes occur: carriageway, sidewalk, lawn, park, beach, sports ground, and parking lot.

Two small stagnant shallow water reservoirs were selected in Ekaterinburg (Russia): Chemodanchik (56.802092 N/60.538809 E) and the pond in Kharitonovsky Garden (56.846963 N/60.613751 E). Sampling was carried out in functional landscape zones of catchments and on lakes in warm and cold periods of the year. The samples of soil, surface-deposited sediments, and road dust were collected in the warm season in the catchments. In the winter-spring season, samples of undisturbed snow and snow-dirt sludge were collected in the catchments. In addition, the sampling of snow, ice, water, and bottom sediments was carried out on the lakes. The schematic maps of the location of sampling points in catchments are presented in Fig. 1. The cation and anion composition, pH, Eh, elements' concentrations, mineral composition, stable Pb isotopes, and Cs-137 were determined in the collected samples.

3 Results and Discussion

In total, 28 samples of environmental compartments were collected in warm and cold seasons, 18 samples of ice, water, and snow were collected on the lakes in the winter season, and 15 cores of bottom sediments. The decreasing order of concentrations of the elements in soils, surface-deposited sediments, and bottom sediments of water bodies was similar: Ti–Mn–Cr–Zn–V–Ni–Cu–Pb–Co–As–Sn. The association of elements confirms the similar genesis of elements and the connection of environmental compartments in the urban landscape of the lake and its catchment. Ti represents Typomorphic association, V, Co, Cr, Ni, and Mn, and technogenic—Pb, Cd, Cu, Zn, Mo, Sn, As, Sb, and Sn. The highest concentrations of Pb were found in green areas, lawns, parks, and forest parks. The source of Pb in landscape components is the combustion products of leaded gasoline, which are still present in soils since its use. The accumulation of Zn and Cu in roadside soils and road dust may indicate motor transport as the primary source of these elements. The concentrations of Cs-137 in bottom sediments are high (up to 380 Bq/kg). Vertical profiles of Cs-137 in bottom sediments show the Chernobyl fallout in the reservoir of the Kharitonovsky Garden at a depth of 16–20 cm (312 Bq/kg) and the Chemodanchik

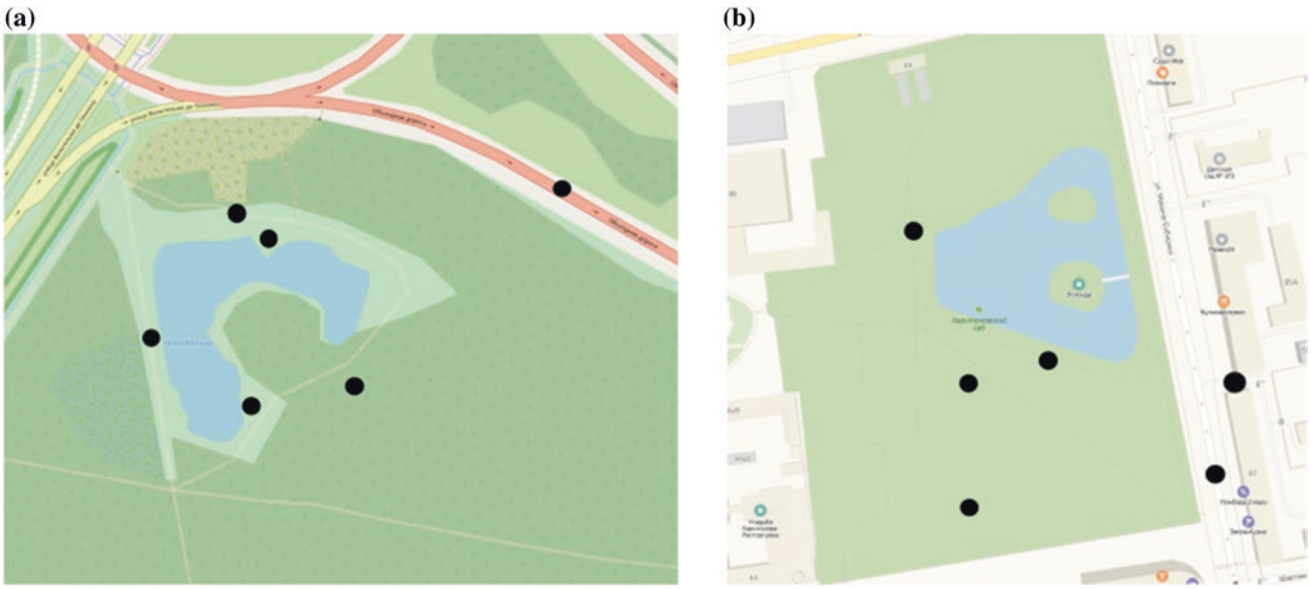

Fig. 1 The schematic maps of the location of sampling points in catchments of Chemodanchik (**a**) and pond in Kharitonovsky Garden (**b**) in Ekaterinburg

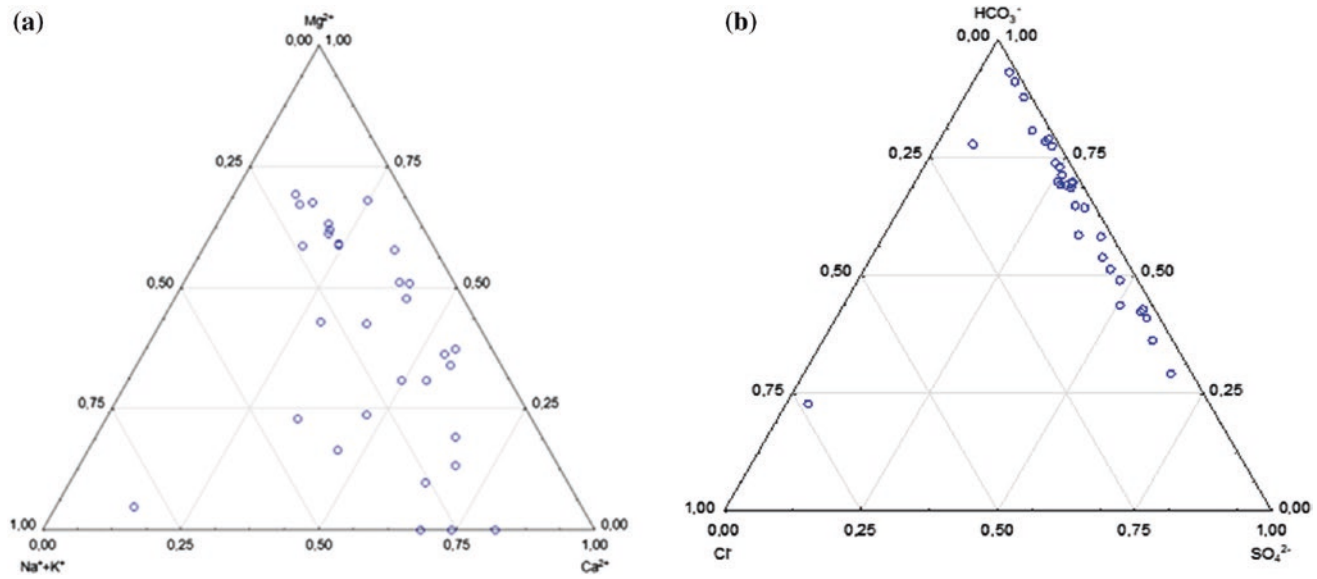

Fig. 2 Cation (**a**) and anion (**b**) composition of samples taken during the winter-spring season

reservoir—102 Bq/kg in the horizon of 12–16 cm. There is leaching of Cs-137 from the slope areas of the landscape due to contemporary sedimentation processes and surface washout of particles from the catchment. Cesium, in the form of atmospheric fallout, enters sediment material throughout the soil erosion. The winter samples are hydrocarbonate and sulfate; a sample of snow-dirt sludge from the road is chloride (due to anti-ice agents). The composition of surface waters determines the geochemical conditions of the surveyed water bodies. In spring, the melted snow, containing the elements accumulated during the winter, is transferred from the catchments into the reservoir. The analysis of physicochemical and hydrochemical parameters of snow from catchments showed shallow mineralization; ice and water have low and medium mineralization (Fig. 2). The abnormally high salinity of the snow-dirt sludge, up to 4000 mg/dm^3, taken from the road, is associated with the presence of anti-ice mixture.

4 Conclusions

The obtained results allowed identifying the geochemical processes determining the quality of water bodies in the urban environment. The connected functional landscape areas in the catchment supply the sedimentary material to the bottom sediments of the lakes. The composition of surface snow and snow-dirt sludge contributes to the geochemical conditions of the surveyed water bodies. The melting, polluted snow is transferred from the catchments into the lake in spring.

Funding The study was funded by RFBR (Grant No. 19-35-60011). Chemical analyses are performed at the "Geoanalitik" Shared Research Facilities of the IGG UB RAS. The re-equipment and comprehensive development of the "Geoanalitik" Shared Research Facilities of the IGG UB RAS are financially supported by the grant of the Ministry of Science and Higher Education of the Russian Federation (Agreement 075-15-2021-680).

References

Chin, A. (2006). Urban transformation of river landscapes in a global context. *Geomorphology, 79*, 460–487.

Froger, C., Ayrault, S., Evrard, O., Monvoisin, G., Bordier, L., Lefèvre, I., & Quantin, C. (2018). Tracing the sources of suspended sediment and particle-bound trace metal elements in an urban catchment coupling elemental and isotopic geochemistry, and fallout radionuclides. *Environmental Science and Pollution Research, 25*, 28667–28681.

https://www.epa.gov/nps/basic-information-about-nonpoint-source-nps-pollution

https://www.epa.gov/nps

Liu, A., Egodawatta, P., Guan, Y., & Goonetilleke, A. (2013). Influence of rainfall and catchment characteristics on urban stormwater quality. *Science of the Total Environment, 444*, 255–262.

Lundy, L., Ellis, J. B., & Revitt, D. M. (2012). Risk prioritisation of stormwater pollutant sources. *Water Research, 46*(20), 6589–6600.

Müller, A., Österlund, H., Marsalek, J., & Viklander, M. (2020). The pollution conveyed by urban runoff: A review of sources. *Science of the Total Environment, 709*, 136125.

Owens, P. N., Blake, W. H., Gaspar, L., Gateuille, D., Koiter, A. J., Lobb, D. A., Petticrew, E. L., Reiffarth, D. G., Smith, H. G., & Woodward, J. C. (2016). Fingerprinting and tracing the sources of soils and sediments: Earth and ocean science, geoarchaeological, forensic, and human health applications. *Earth-Science Reviews, 162*, 1–23.

Liquid Digester from Urban Wastewater Treatment Plants for *Chlorella vulgaris'* Growth and Nutrient Recirculation

Gassan Hodaifa and Amani Belaiba

Abstract

Wastewater treatment is an important issue because it directly impacts the environment and is directly related to climatic change. However, urban wastewater treatment plants just now cannot complete the treatment from the viewpoint of the circular economy. This work uses the digested liquid generated from the anaerobic digester as culture media to grow the green microalga *Chlorella vulgaris*. Different culture media at different effluent concentrations are prepared with tap water (5, 10, 25, 35, and 50%, v/v). The experiments were performed in stirred photobioreactors in batch mode with 1L capacity. The common operating conditions used were pH of the culture media = 8, mechanical agitation = 200 rpm, air supply rate = 0.5 L/min, and continuous artificial light at illumination intensity = 359 $\mu E\ m^{-2}\ s^{-1}$. The experimental results show that the kinetic growth parameters maximum specific growth rate ($0.0204\ h^{-1}$) and volumetric biomass productivity ($0.00860\ g\ L^{-1}\ h^{-1}$) values were determined in the culture at 25% (v/v) of digested liquid. Furthermore, the wastewater treated quality in terms of removal chemical oxygen demand percentage (26.6%) and total nitrogen removal percentage (94.7%) were determined in the cultures with 50 and 10% (v/v) of liquid digester from wastewater treatment plant (LD-WWTP). The highest net harvest biomass concentration ($x–x_o = 2.54 \pm 0.0155$ g/L), total lipid content (13.1%), and $\%CO_2$ removal (72.2%) at the end of the cultures were registered in culture operated at 25% (v/v) of LD-WWTP. These results show the possible recovery and recirculation of nutrients from LD-WWTP.

Keywords

Urban wastewater · Anaerobic digester · *Chlorella vulgaris* · Kinetic growth · Treatment

1 Introduction

Nowadays, nutrient recirculation is one of the most critical challenges in achieving a circular economy to ensure the environment's protection of the globe. Today's wastewater treatment plants (WWTPs) are essential in controlling and handling wastewater treatment. Still, the new climate change challenge requires more transformation and recirculation to achieve sustainability, which means this function is insufficient. Therefore, more nutrient control and recirculation capacity are needed to realize a correct life cycle of raw materials.

Currently, urban sludge generated in the WWTPs is treated through the anaerobic digester to produce biogas. Biogas is normally used for energy generation (as electric energy) and the digester liquid is concentrated for discharge or post-treatment and used as fertilizer or soil conditioner. Then, the liquid obtained is recirculated to the head of the WWTP. The anaerobic digestion process is based on the complex hydrolyzation of organic matter into soluble monomers, such as amino acids, fatty acids, sugars, and glycerol (Volschan-Junior et al., 2021). Then, this residue is rich in many organic and inorganic compounds, which could be used for microalgal growth.

This research aims to study the viability of liquid digester from WWTPs (LD-WWTPs) to use as a substrate for forming culture media for *Chlorella vulgaris* growth. This use allows the recovery of nutrients and the generation of algal biomass with high added value, especially for biofuel production, in addition to the liquid digester treatment.

G. Hodaifa (✉) · A. Belaiba
Molecular Biology and Biochemical Engineering Department, Chemical Engineering Area, University of Pablo de Olavide, Carretera de Utrera Km 1, ES-41013 Seville, Spain
e-mail: ghodaifa@upo.es

A. Çiner et al. (eds.), *Recent Research on Environmental Earth Sciences, Geomorphology, Soil Science, Paleoclimate, and Karst*, Advances in Science, Technology & Innovation, https://doi.org/10.1007/978-3-031-42917-0_6

2 Methods

A green microalga *Chlorella vulgaris* strain SAG 9.88 was grown in a liquid digester from urban wastewater treatment at different concentrations prepared with tap water (5, 10, 25, 35, and 50%, v/v) as culture media. The cultures have been carried out under natural conditions without prior sterilization of the culture media.

The common operating conditions used were pH of the culture media = 8, mechanical agitation = 200 rpm, air supply rate = 0.5 L/min, and continuous artificial illumination intensity = 359 $\mu E\ m^{-2}\ s^{-1}$. All experiments were carried out in stirred photobioreactors with 1 L capacity.

Biomass was generated, and biomass biochemical composition was determined. For biomass concentration (x, g/L), 5 ml of microalgal suspension was centrifuged at 4000 rpm for 10 min. The obtained biomass was washed three times with ultrapure water and measured at 600 nm in a UV–visible spectrophotometer. A linear calibration curve between absorbance and dry biomass was used to determine the biomass dry weight-cell concentration (g/L).

Total pigments (chlorophyll a, b, and carotenoids) were determined by a photo-colorimetric method after extraction with acetone at 90%, as described by Ritchie (2008). The total chlorophylls and total carotenoid contents were calculated according to the equations described by Jeffrey and Humphrey (1975) and Strickland and Parsons (1972), respectively.

At the end of each culture, biomass was separated and dried at 105 °C. Then, the total lipids content was determined. Next, the total lipid content of the biomass was extracted by a micro-Soxhlet extractor using n-hexane as a solvent for 24 h. Finally, the percentage of total proteins was determined as total nitrogen percentage ×6.25 (Becker, 1994).

The following parameters (Hodaifa et al., 2020) were determined for the liquid residue from the urban anaerobic digester (crude, filtered, and treated): pH value, electric conductivity (EC), and turbidity were directly measured by using a pH-meter Crison model GLP 22C, Conductimeter Crison, model GLP31, and Turbidimeter Hanna, model HI93703, respectively. Chemical oxygen demand (COD) was determined photometrically at 620 nm according to German Standard Methods. Total phenolic compounds (TPCs) were performed by making them react with a derivative thiazol, giving a purple azo dye, determined photometrically at 475 nm according to the standard methods. Total carbon (TC), total organic carbon (TOC), total nitrogen (TN), and inorganic carbon (IC) were determined using a Total Carbon and Nitrogen Analyzer provided by Skalar Company, model Formacs^{HT} and Formacs^{TN}. Total iron determination was performed by reducing all iron ions to iron (II) ions in a thioglycolate medium with a triazine derivative. According to the standard methods, this reaction results in a reddish-purple complex that was photometrically determined at 565 nm. Chloride, sulfate, and orthophosphate were determined photometrically at 450 nm, 420 nm, and 690 nm, respectively, according to the standard methods. Sodium, calcium, and potassium were directly determined by using a selective ion electrode for each ion (Crison, mod. GLP 22).

3 Results and Discussion

3.1 Characterization of the Liquid Digester from Urban Wastewater Treatment Plant (LD-WWTP)

Table 1 shows the characterization of tap water (as a control experiment) and filtered liquid digestor from the urban wastewater treatment plant, in addition to characterize this filtered LD-WWTP at different concentrations prepared with tap water (5, 10, 25, 35, and 50%, v/v) before treatment by *Chlorella vulgaris*. The comparison between tap water and LD-WWTP indicated the high turbidity, COD, TPCs, TC, TOC, IC, TN, NH_4, NH_3, total-P, Na, K, SO_4, Cl, and Fe of LD-WWTP. This high concentration of nutrients could be recovered using this residue for microalgal growth. However, the direct use of LD-WWTP as a culture medium is impossible due to the high osmotic pressure (high nutrient concentration), enabling microalgal cell growth. For this reason, different LD-WWTP concentrations were prepared to study the *C. vulgaris* growth since the nutrient distribution on the culture media depends on the dilution applied in each case (Table 1).

3.2 *C. vulgaris* Growth, Bioremediation, and Biochemical Composition

Figure 1 shows the net biomass generation in the different cultures developed from LD-WWTP. In all experiments, approximately a Lag phase with a 100 h duration was observed before the exponential growth phase. Only in the culture at 5% of LD-WWTP, no Lag phase was detected. This may be due to the presence of total phenolic compounds in the culture media that are considered growth inhibitors (Hodaifa et al., 2020).

The highest biomass generation was detected in the culture operated at 25% LD-WWTP with algal biomass concentration up to 2.5 g/L after 358 h. In this sense, ANOVA one-way analysis of variance shows that at the 0.05 level,

Table 1 Characterization of liquid digester from urban wastewater treatment before treatment by *Chlorella vulgaris* and control experiment

Parameter	Tap water	Filtered LD-WWTP	LD-WWTP before treatment				
			5%	10%	25%	35%	50%
pH	6.85	8.24	8.03	8.20	8.05	8.32	8.17
Conductivity, µS/cm	0.00256	1410	908	1330	2084	3088	5032
Turbidity, FTU	1.19	325	13.8	23.7	48.3	83.0	134
COD, mgO_2/L	0.00	976	39.3	89.4	315	329	550
Disolved O_2, mg O_2/L	8.2	7.74	7.83	7.94	7.08	7.57	5.73
Total solid, %	0.020	0.32	0.02	0.03	0.06	0.11	0.15
Organic matter, %	0.006	0.09	0.004	0.008	0.02	0.04	0.04
Ash, %	0.013	0.23	0.02	0.03	0.05	0.07	0.11
TPCs, mg/L	0.00	19.0	2.05	2.67	5.62	7.33	7.30
TC, mg/L	24.0	153	89.6	149	317	406	637
TOC, mg/L	1.85	31.2	13.8	24.5	52.3	86.3	124
IC, mg/L	22.1	122	75.8	125	265	320	513
TN, mg/L	0.51	115	62.4	112	212	253	360
NN, mg/L	0.15	0.40	0.25	0.27	0.00	0.26	0.26
NH_4, mg/L	0.42	1367	686	129	310	433	628
NH_3, mg/L	0.20	18,300	399	1149	3961	5846	9150
NO_3, mg/L	0.29	5.25	1.45	1.59	4.47	3.34	5.97
Total-P, mg/L	0.00	161	34.2	57.7	122	175	240
PO_4, mg/L	0.42	63.9	4.72	6.49	9.18	11.0	11.6
Na, mg/L	13.0	268	29.3	56.7	105	157	218
K, mg/L	0.95	64.2	2.50	3.20	5.10	7.70	10.2
Ca, mg/L	2.94	3.80	0.10	0.21	0.24	0.28	0.52
SO_4, mg/L	219	1408	335	386	406	511	606
Cl, mg/L	0.00	303	75.9	95.3	227	236	249
Fe, mg/L	0.00	5.05	0.50	0.61	1.21	1.74	2.28

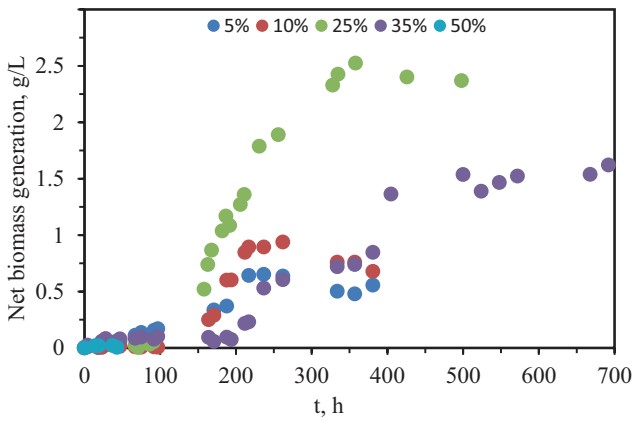

Fig. 1 Net *Chlorella vulgaris* biomass generation in LD-WWTP at different concentrations

the population means are significantly different (final biomass concentration mean = 1.18 g/L, F-value = 8.38, and P-value = 0.02004 < 0.05).

The net biomass generation increases by increasing LD-WWTP concentration in the culture media up to 25% (v/v). Then, this concentration is decreased to depreciable concentration at cultures with 50% (v/v) of LD-WWTP (Fig. 1). In Table 2, it can be seen the quality of the LD-WWTP after *C. vulgaris* growth. A notable improvement in their values was observed for all quality parameters. Cultures at 5 and 10% of the treated LD-WWTP could be discharged directly to the waterways since COD < 125 mg/L, TN, and Total-P < 10 mg/L (Directive 91/271/EEC on Urban Wastewater Treatment).

The final biomass obtained is rich in energetic compounds (carbohydrates + lipids), registering an average value of 66.1 ± 3.15%. The highest total lipid was 13.1% and registered in the culture at 25% of LD-WWTP.

Table 2 Characterization of liquid digester from urban wastewater treatment plant (LD-WWTP) after *Chlorella vulgaris*

Parameter	Control experiments	LD-WWTP after treatment by *Chlorella vulgaris*				
	Tap water	5%	10%	25%	35%	50%
pH	6.85	8.38	7.74	8.21	8.64	8.38
Conductivity, µS/cm	0.00256	817	917	2074	2045	3076
Turbidity, FTU	1.19	6.34	8.08	21.4	18.4	76.0
COD, mg O_2/L	0.00	35.7	71.5	286	243	404
Disolved O_2, mg O_2/L	8.20	7.00	6.83	2.55	7.14	6.61
Total solid, %	0.020	0.08	0.07	0.17	0.18	0.22
Organic matter, %	0.006	0.03	0.01	0.05	0.03	0.09
Ash, %	0.013	0.05	0.06	0.12	0.15	0.13
TPCs, mg/L	0.00	0.81	0.87	2.97	0.89	6.96
TC, mg/L	24.0	63.6	50.7	122	110	174
TOC, mg/L	1.85	38.0	37.5	114	85.5	142
IC, mg/L	22.1	25.3	13.2	8.42	24.1	31.0
TN, mg/L	0.51	7.12	5.91	98.6	15.6	213
NN, mg/L	0.15	0.00	0.00	0.00	0.00	0.14
NH_4, mg/L	0.42	2.86	8.33	123	13.1	284
NH_3, mg/L	0.20	1.61	9.21	236	8.30	540
NO_3, mg/L	0.29	0.43	0.72	3.96	1.79	3.70
Total-P, mg/L	0.00	6.60	5.90	18.4	23.0	47.0
PO_4, mg/L	0.42	3.30	4.51	8.06	5.86	6.52
Na, mg/L	13.0	173	599	173	469	356
K, mg/L	0.95	0.20	0.33	0.50	0.70	9.50
Ca, mg/L	2.94	0.08	0.18	0.20	0.25	0.50
SO_4, mg/L	219	298	285	186	195	531
Cl, mg/L	0.00	42.0	77.0	216	181	183
Fe, mg/L	0.00	0.03	0.07	0.58	0.13	2.27

4 Conclusions

The study of using LD-WWTP as a substrate to formulate culture media of *Chlorella vulgaris* demonstrated the viability of the recovery of nutrients and the possible bioremediation of LD-WWTP before its recirculation to the head of the WWTP. Higher net biomass generation and energetic compounds were obtained up to 3.5 g/L and 66.1 ± 3.15%, respectively. Total lipids up to 13.1% were obtained in the culture with 25% LD-WWTP, which can separate and convert into biodiesel. The carbohydrate fraction could be used for biofuel production. As a bad option, the whole biomass could be introduced to the anaerobic digester for major biogas yield.

Acknowledgements The Junta of Andalusia and the University of Pablo de Olavide are acknowledged for financial support through Project Ref.: UPO-1260312 "Revaluation and reuse of gaseous effluents (gaseous combustion 'CO_2') and liquids (urban and industrial wastewaters) through the use of advanced oxidation technologies and production of high added-value algal biomass". The authors also thank the University of Pablo de Olavide for its support through the Bridging Grants for the competition of the State R&D Plan under the Own Research and Transfer Plan 2018–2020, Ref.: RTI2018-101875-B-C22.

References

Becker, E. W. (1994). *Microalgae: Biotechnology and microbiology*. Cambridge University Press.

Directive 91/271/EEC on Urban Wastewater Treatment.

Hodaifa, G., Malvis, A., Maaitah, M., & Sánchez, S. (2020). Combination of physicochemical operations and algal culture as a new bioprocess for olive mill wastewater treatment. *Biomass and Bioenergy, 138*, 105603.

Jeffrey, S. W., & Humphrey, G. F. (1975). New spectrophotometric equations for determining chlorophylls a, b, c1 and c2 in higher plants, algae and natural phytoplankton. *Biochemie Und Physiologie Der Pflanzen (BPP), 167*, 191–194.

Ritchie, R. J. (2008). Universal chlorophyll equations for estimating chlorophylls a, b, c, and d and total chlorophylls in natural assemblages of photosynthetic organisms using acetone, methanol, or ethanol solvents. *Photosynthetic, 46*, 115–126.

Strickland, J. D. H., & Parson, T. R. (1972) A practical handbook of seawater analysis. *Fisheries Research Board of Canada, Bulletin*, 167–310.

Volschan-Junior, I., de Almeida, R., & Christe-Cammarota, M. (2021). A review of sludge pretreatment methods and co-digestion to boost biogas production and energy self-sufficiency in wastewater treatment plants. *Journal of Water Process Engineering, 40*, 101857.

Wastewater Treatment in the Skikda District: Current Situation and Interactions of the New Treatment Plant Project

Nabil Bougherira, Dounia Nechem, Hicham Chaffai, Sara Badach, Mohammed Bendjerad, Azzedine Hani, and Larbi Djabri

Abstract

In Algeria, among the measures developed are the treatment devices installed throughout the national territory. However, this reflection required colossal. In this work, we have tried to assess the environmental impact compared to the current situation, where no treatment is carried out (total flow of wastewater from the population of the municipalities of Larbi Ben Mhidi and Filfila estimated at 14,741 m^3/day), with all the adverse consequences of pollution (discharges into the sea), the impact on the population (the agglomeration of Larbi Ben Mhidi covers an area of 157.9 ha). To address this situation, the country is engaged in improving citizens' living conditions, increasing wastewater treatment capacity, and building more than 100 new units across the national territory. That of the grouping of Filfila will be the second treatment plant (in the city of Skikda); to rationalize the water demand and ensure better wastewater recovery for possible reuse in the agricultural, tourism, and industrial sectors. This research was conducted before the treatment plant's commissioning, or a set of analyses was conducted (April 2019) on the water to assess the quality of untreated discharge water (R1) and groundwater P1, P2, and P3. This analysis campaign includes physico-chemical parameters: temperature, pH, dissolved O_2, electrical conductivity, turbidity, nitrites, nitrates, BOD5, COD, suspended solids (SS), PO4, and SO4. The R1 wastewater analyses indicate high values that exceed the standard for BOD5-P-Nitrates and IPO, while the groundwater is below the norms.

Keywords

Projection of the treatment plant · Wastewater · Treatment · The purification power

1 Introduction

This study aims at the feasibility of a future treatment device and to characterize the different types of pollutants caused before the realization of the wastewater treatment plant project received from Filfila and Larbi Ben M'hidi (Skikda). The good purification performance of this future project will undoubtedly improve the quality of producing an acceptable quality of wastewater (purified) and attenuate environmental problems.

2 Materials and Methods

The study area is mountainous between several sub-catchment basins, including a set of gravity flow collectors.

The sewerage networks within the study area are located as follows:

- Network of Filfila,
- Network of Oued K'Sob, and
- Network of Larbi Ben M'Hidi.

To evaluate the pollution load of the wastewater from the different discharges that will feed the future sewage treatment plant (see Table 1), it is necessary to conduct a sampling and

N. Bougherira (✉) · H. Chaffai · S. Badach · M. Bendjerad · A. Hani · L. Djabri
Water Resource and Sustainable Development Research Laboratory (REDD) Faculty of Earth Sciences, Badji Mokhtar - Annaba University, P.O. Box 12, Annaba, Algeria
e-mail: nabil.bougherira@univ-annaba.dz

D. Nechem
Geology Research Laboratory (LRG), Faculty of Earth Sciences, Badji Mokhtar - Annaba University, P.O. Box 12, Annaba, Algeria

A. Çiner et al. (eds.), *Recent Research on Environmental Earth Sciences, Geomorphology, Soil Science, Paleoclimate, and Karst*, Advances in Science, Technology & Innovation, https://doi.org/10.1007/978-3-031-42917-0_7

Table 1 Summary of wastewater flows for the urban population (source: National sanitation office)

Horizons	2013	2015	2020	2030	2040
Filfila wastewater flow (m^3/d)	4.006	11.055	13.235	15.330	17.756
Larbi Ben M'hidi wastewater flow (m^3/d)	1.166	1.362	1.506	1.732	1.990
Total flow of wastewater from urban population (m^3/d)	5.172	12.417	14.741	17.062	19.746

analysis campaign of the various pollution parameters Labar (2009). The composition of these wastewaters gives us the results and the interpretation while considering the most critical parameters of pollution (see Table 3).

The samples were collected in April 2019. A discharge point (R1) and three (P1-P2-P3) wells were identified for water sampling of the urban grouping of Larbi Ben M'hidi and Filfila. During each sample selection, various physical measurements were made using a digital multi-parameter instrument. It is portable equipment of WTW type multi-3420 with a graphic screen and several digital electrodes "IDS". The measured parameters are

- Temperature;
- pH;
- Dissolved oxygen;
- Conductivity;
- Turbidity.

3 Results

3.1 In Situ Physical Measurements (Table 2)

The temperature of the water of the four samples is between 24 and 26.8 °C as minimum and maximum average values. These values conform with the Algerian standard of rejection.

The average pH values of the waters of the different sampling points are between 7.3 and 8, included in the range of values generally observed for urban wastewater of domestic character (Sakaa 2015).

Table 2 Physical measurements

Parameters	Min/Max	Results (R1)	P1	P2	P3
Temperature (°C)	24–26.8	24.7	24	26.8	24
pH	7.3–8	8	7.3	7.4	7.7
Dissolved O_2 (%)	0.31–9.34	0.31	7.46	8.08	9.34
Conductivity at 25 °C (µS/cm)	300–1000	1000	400	300	300
Turbidity	2.61–114	114	45.2	2.61	2.73

The results obtained for the analyzed samples show low dissolved oxygen contents for R1, however, exceeding the Algerian standard for P1, P2, and P3 with 9.34 mg/L.

The electrical conductivity of the water higher than 1500 µs/cm leads to excessive mineralization. The R1 is 1400 µs/cm.

The average turbidity levels measured for the four sampling points are between 2.61 and 114 mg/L. Therefore, R1 is turbid water, and P2 and P3 are clear water.

3.2 Analysis Results and Interpretations

The analyses of the samples was carried out by the laboratory of analyses of the complex GNL. K Sonatrach Skikda (Fig. 1).

The nitrite levels observed during sampling are trace amounts for the four sampling points.

The nitrate content observed for points P1 and P2 are very high, and that of the discharge is (6 mg/L).

The PO_4 value retained for the discharge is 13.14 mg/L. This content comes from household water.

The SO_4 values of samples are for R1 180.07 mg/L and for P1 428.47 mg/L. These values are above the standard. Contrarily, the ammonium value for the discharge point is 6.03 mg/L for groundwater P2 and P3; the contents are lower than the range values (12–60 mg/L).

The average suspended solid values (MES) recorded for the four sampling points are 163, 157, 137, and 142 mg/L, respectively.

3.3 Organic Pollution Index/Biodegradability Standard of the Discharges

The analysis in the various points was the subject of data processing by the establishment of classes of organic pollution of natural waters (03 wells) in the grouping of Larbi Ben M'hidi and Filfila (Skikda), which informs us on the influence of the discharges and the quality of water through an organic pollution index. This last one is calculated according to the method of Leclercq and Maquet (1987), whose principle is to distribute the values of the polluting

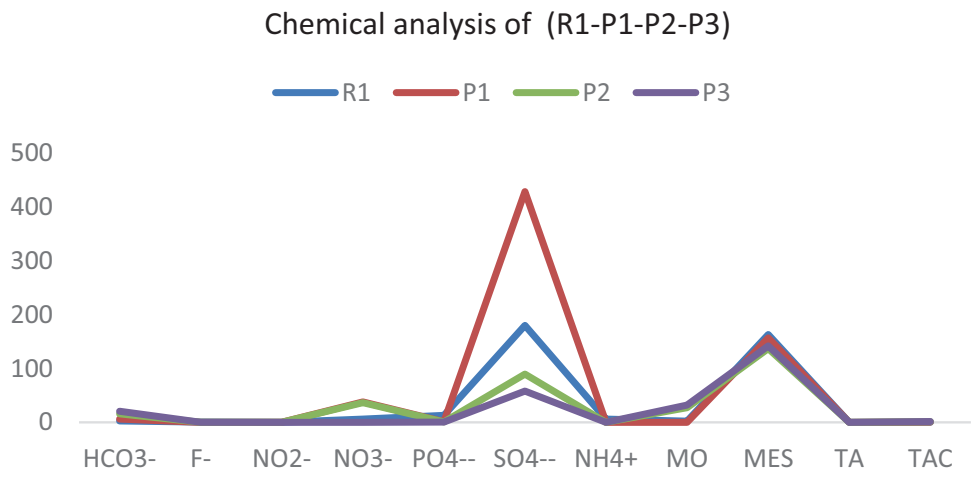

Fig. 1 Chemical analysis of water of the urban grouping of Larbi Ben M'hidi and Filfila

Table 3 Organic pollution index

The sampling point	COD	BOD5	Organic pollution	Type of pollution
R1	554	110	1.5	Very strong organic pollution
P1	0	5	3.5	Moderate organic pollution
P2	0	5	3.75	Moderate organic pollution
P3	0	5	4.5	Low organic pollution

elements in 05 classes, to determine from its measurements the number of corresponding classes for each parameter to make the average of it.

4 Discussion

The K ratio gives a first estimate of the biodegradability of the organic matter of a given effluent:

$$K = COD/BOD5 \quad (1)$$

The following limits are generally agreed upon: The biodegradability of water is expressed by the coefficient K. If

- $K < 1.5$: the effluent is readily biodegradable, and biological treatment is recommended.
- $1.5 < K < 2.5$: the effluent is moderately biodegradable; a biological treatment with the adaptation of strains is the most adequate in this case.
- $K > 2.5$: the effluent is not biodegradable; a physico-chemical treatment is recommended.

The average ratio (COD/BOD5) for the three wells is less than 1.5, but the average percentage (COD/BOD5) for the R1 discharge point is more significant than 2.5. This shows that we are in the presence of non-biodegradable urban wastewater. However, this is invalidated by the fact that a polluting industry discharges into the network.

5 Conclusions

By 2040, the wastewater treatment plant (Boutin et al. 1998) for the Filfila urban group will be able to handle 153,000 InhabitantEquivalent, which is an asset for a healthy environment, contributing enormously to the concept of sustainable development.

The impact of such a project is threefold; it will result in the following:

- The protection of the receiving environment (the sea); indeed, after purification, the purified water will have a composition per the standards of rejection in force in Algeria.
- The preservation of underground and surface resources.
- The reuse of purified wastewater for agricultural, tourist, and industrial purposes.

However, the negative impact deserves particular attention at the time of realization and the exploitation of the station.

Concerning the character of the wastewater, the campaigns of sampling and analysis carried out at the level of the three points of wastewater discharge of the grouping allowed us to note that

- The COD/BOD ratio is lower than 1.5 for the groundwater, contrary to the biodegradability criterion of the wastewater.

– The presence of some metallic trace elements and weak toxicity.
– The amount of phosphorus input on average is less than what is needed to begin the purifying process. When too little phosphorus is present in the effluent, additional input is necessary to reach the optimum performance.
– The discharge presents excessive mineralization in the case of possible reuse of the treated water in irrigation; it would be preferable to use the water for the crops less sensitive to salts and to adapt appropriate irrigation technics to the pre-defined crops.

References

Boutin, C., Duchène, P., & Liénard, A. (1998). Filières d'épuration adaptées aux petites collectivités. Document technique FNDAE 22.

Labar, S. (2009). Evaluation de la pollution des eaux souterraines dans un milieu industriel (Cas de la zone industrielle de Skikda, N.E. Algérien). Thèse de doctorat, Université d'Annaba, 168p.

Leclercq, L., & Maquet, B. (1987). Deux nouveaux indices chimique et diatomique de qualité d'eau courante. Application au Samson et à ses affluents (Bassin de la Meuse Belge). Comparaison avec d'autres indices chimiques, biocénotiques et diatomiques. *Documents de travail de l'Institut Royal des Sciences naturelles de Belgique*, *38*, 1–113.

Sakaa, B. (2015). Développement Durable, Vers un Modèle de GIRE dans le Bassin Versant de Saf-Saf; Thèses de doctorat, Université de Annaba; 143p.

Lead Removal from Water Solutions Using Alginate-Immobilized Peach Stone Particles

Zorica Lopičić, Jelena Milojković, Tatjana Šoštarić, Anja Antanasković, Marija Koprivica, Vladimir Adamović, and Linda Mitić

Abstract

Fruit processing industries generate millions of tons of organic waste annually, often improperly disposed of at open landfills. Based on the circular economy and waste management concepts, reusing these bio-waste materials is one of the future sustainable demands. Furthermore, recent investigations have shown that this material type can be reused as high-quality sorbents, with certain modifications that should be applied. Considering this, we have investigated the possible application of lignocellulosic waste-peach stones (*Prunus Persica* L.), immobilized in sodium alginate, as heavy metals sorbent. The immobilized particles (IPS) were utilized to remove metals from synthetic water solutions. Among all metals (Pb, Cu, Cd, and Zn), IPS has shown superior performance in Pb removal, governing further investigations. Dried IPS spheres were characterized by FTIR, SEM/EDX, and TG techniques. The batch reaction system investigated the effects of the contact time, initial Pb concentration, and mass-to-volume ratio. Optimized operational parameters were used in kinetic and isotherm studies. Obtained data were modeled using a nonlinear form of pseudo-first, pseudo-second, Elovich, Freundlich, and Langmuir equations. The results showed pseudo-second-order kinetics with Freundlich isotherm fitting Pb removal, indicating a heterogeneous IPS surface with the multilayer adsorption and adsorbed molecule interaction. As obtained from Langmuir isotherm, IPS particles have removed Pb by saturation capacity of 80.40 mg Pb/g. These preliminary results indicate that IPS can be applied to purify waters contaminated with lead metal.

Keywords

Waste biomass · Immobilization · SEM/EDX · Lead removal

1 Introduction

The growth of industrial activity and uncontrolled or improper release of pollutants into the environment induced the need for new methods and materials that might be used to solve environmental pollution issues. Many techniques have been developed for different pollutant removal. Still, most of them are often ineffective, economically or technically demanded, especially if the pollutant concentration (e.g., metals) falls below 100 mg/L (Abdolali et al., 2014). Sorption techniques using low-cost, abundant lignocellulosic waste (LCW) material might be applied for that purpose. Although LCWs pose some disadvantages concerning their direct applications as purification agents (Abdi & Kazemi, 2015; Abdolali et al., 2014), their properties might be improved by different modifications and immobilization in various polymer matrices (Chatterjee & Schiewer, 2014).

This paper investigates the possibility of lead (Pb) removal by immobilized LCW peach stone particles. Lead was chosen as a high-toxicity heavy metal, resistant to chemical or biological degradation, presenting a hazard to living and non-living environments (Check & Marteel-Parrish, 2013). On the other hand, recent investigations have shown that LCW generated by the fruit processing industry represents a stable matrix that might be efficiently used in wastewater purification (Lopičić et al., 2017). Therefore, to improve the sorption properties of the raw

Z. Lopičić (✉) · J. Milojković · T. Šoštarić · A. Antanasković · M. Koprivica · V. Adamović
Institute for Technology of Nuclear and Other Mineral Raw Materials, 11000 Belgrade, Serbia
e-mail: z.lopicic@itnms.ac.rs

L. Mitić
Faculty for Environmental Protection, Educons University, 21208 Sremska Kamenica, Serbia

A. Çiner et al. (eds.), *Recent Research on Environmental Earth Sciences, Geomorphology, Soil Science, Paleoclimate, and Karst*, Advances in Science, Technology & Innovation, https://doi.org/10.1007/978-3-031-42917-0_8

material as well as the overall separation process, we have immobilized mechanically treated peach stones (*Prunus Persica* L.) in the sodium alginate and applied it as an efficient sorbent in lead removal.

2 Materials and Methods

All the chemicals used in this study were of high purity. Peach stones (PS) were obtained as waste from a local juice factory. After washing, grinding, and sieving (to a diameter less than 0.1 mm), mechanically treated PS particles were immobilized in Na-alginate according to the method described by Yuan and Viraraghavan (2001). Formed alginate beads (IPS) were further used for the characterization and sorption experiments.

Dried IPS spheres were characterized by FTIR (Thermo Fisher Scientific Nicolet IS-50 spectrophotometer, ATR mode), SEM/EDX (model JEOL JSM-6610LV), and TG (Netzsch STA 409 EP) technique.

Sorption experiments were done in triplicate in a batch reactor with mixing (200 rpm) at constant temperature (25 °C) with optimization of operational parameters. Obtained values were further used in kinetic and isothermal studies. The analytical Pb(II) measurements were done using AAS (Perking Elmer AAS Analyst 300). The percent of Pb(II) removal, R (%), as well as the amount of Pb(II), sorbed per unit mass of IPS, q (mg/g), was calculated as described in Lopičić et al. (2017).

3 Results

3.1 IPS Sorbent Characterization

Figure 1a, b shows SEM images of the IPS sphere. IPS represents a regular sphere of 5 mm average diameter, with PS evenly entrapped within the matrix, regularly exposed to a highly developed surface. Opposite to native material (Lopičić et al., 2019), the presence of macro pores is not evident. EDX analyses showed typical LCW composition (Lopičić et al., 2019) with higher Ca picks than in native material, while after Pb(II) sorption, reduced peaks of Ca, as well as a new peak of Pb(II), are observed in the EDX spectrum (image not shown). Figure 1c presents a TG/DTA analysis of the IPS sample. The first negative peak at 86 °C on the DTA curve is assigned to the loss of free water and water linked through hydrogen bonds. The second mass loss corresponds to the thermal decomposition of IPS composite with the fracture of glycosidic bonds and release of H_2O, with a degradation peak moved from lower (pure alginate) to a higher temperature (333 °C). This result suggests the composite sorbent poses high thermal stability than the alginate itself. The final step of mass loss with a peak at 443 °C may be attributed to the carbonate formation, partial lignin, and cellulose degradation.

All bands' characteristics for raw PS have been seen on the FTIR spectrum of IPS (not shown), but due to the presence of the alginate with reduced intensity. The identified chemically active IPS groups were characterized as polysaccharides, cellulose, hemicellulose, and lignin, all present in composite material.

3.2 Batch Sorption Results

The immobilized particles of *Prunus Persica* L. waste biomass (IPS) were utilized to remove heavy metals from the synthetic water solutions. Among all metals (Pb, Cu, Cd, and Zn), IPS has shown superior performance in Pb(II) removal, so further sorption experiments were performed only with this pollutant. According to the literature review, the initial pH was set to 5.00 and was not adjusted during the sorption process. A significant decrease in pH (up to 3.98) is observed by the end of the process, owing to the presence of carboxylic groups as the main cation exchangers. The effect of the sorbent dose on the amount of Pb(II) sorbed by IPS and its corresponding removal percentage was investigated in the range 0.25–20 g/L. The results have shown an increase in percentage in Pb(II) removal (from 27.4 up to 90.8%) with an increase in IPS dose from 0.25 to 2.0 g/L. Further, an increase in sorbent dose increased R but significantly decreased Pb(II) sorbed. The influence of contact time revealed slow kinetics (equilibrium up to 24 h), which was the best fit by the pseudo-second-order model (Fig. 2a). Isotherm data showed the best correlation with the Freundlich model (Fig. 2b), indicating a multilayer sorption mechanism onto complex IPS surfaces.

4 Discussion

IPS characterization revealed a spherical sorbent shape with a high surface area and plenty of functional groups suitable for lead removal. This sorbent type posed higher thermal stability than the alginate itself and higher ash content than the raw PS, owing to crosslinked Ca in its matrix. Lead removal was superior to other sorbates investigated (thanks to ion exchange Ca–Pb). The typical overall adsorption efficiency (R(%)) was between 27% (for 0.25 mg/L of 1 M Pb solution) and 99% for the final value of 20 g of IPS/L. This removal efficiency did not appreciably increase with an increase in the mass-to-volume ratio higher than 2 g/L, and this operating parameter was selected for kinetic and isothermal investigations. Investigating the influence of contact

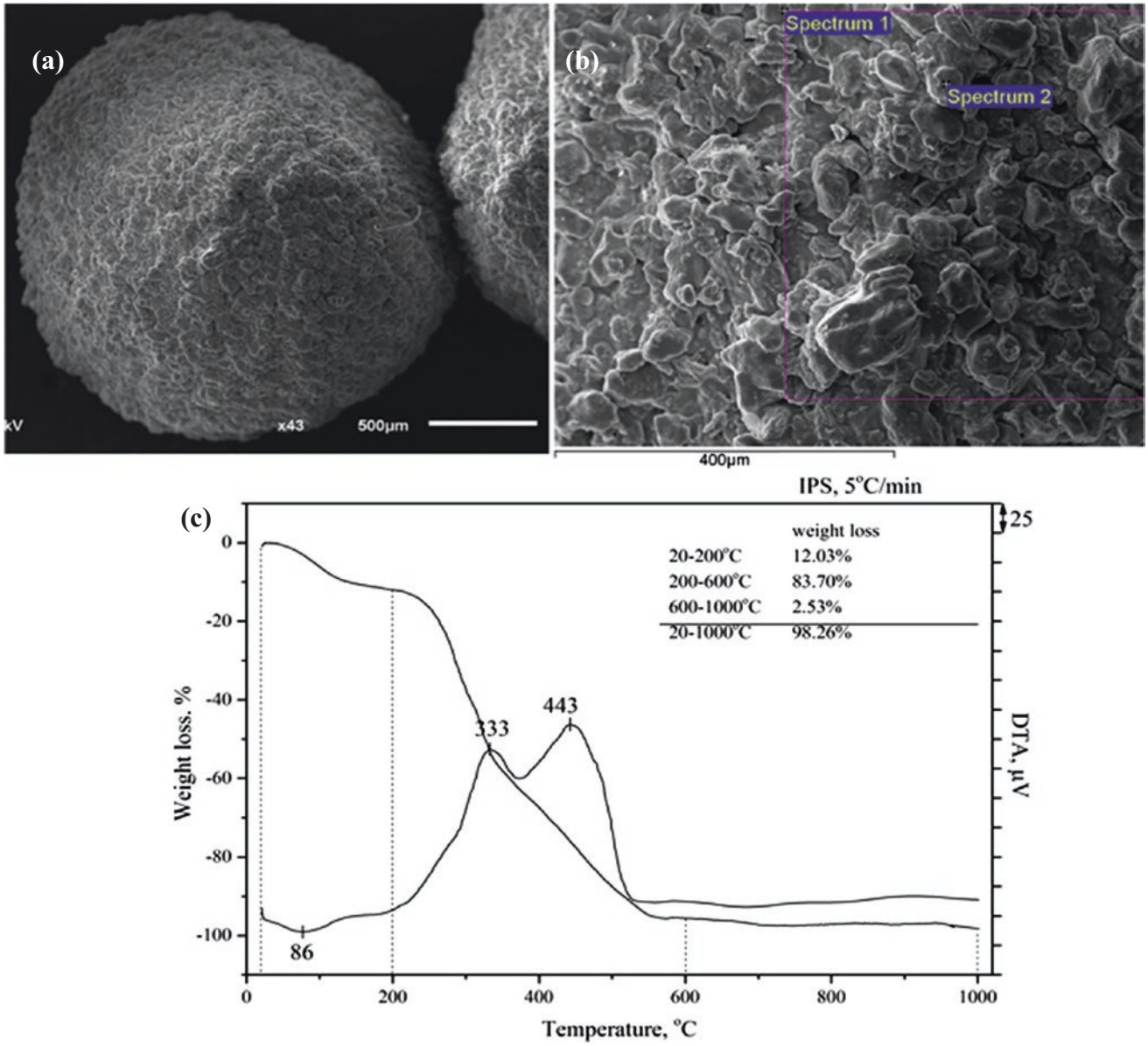

Fig. 1 **a** and **b** SEM micrographs of IPS at different magnitudes and **c** TG/DTA analysis of IPS sample

time showed slow kinetics best fitted by a pseudo-second-order equation. The results of isotherm investigations have demonstrated that the Freundlich isotherm fits better with the removal of Pb, indicating a heterogeneous IPS surface with multilayer adsorption and interaction between adsorbed molecules. Calcium alginate-immobilized PS particles have removed Pb by a saturation capacity of 80.40 mg Pb/g, as obtained from Langmuir isotherm. This value is much higher than the one for raw PS, which was calculated as 28.64 mg Pb/g under the same operational conditions. During the sorption process, calcium, added as a crosslinking agent, was exchanged with lead due to the affinity of the weak acid cation exchanger, the carboxyl group, which has a higher selectivity toward the lead.

5 Conclusions

Although LCW often has limited sorption capacity compared to current commercial sorbents, a good sorbent selection with a proper modification can considerably improve its sorption properties. Furthermore, based on the circular economy and waste management concepts, the reuse of LCW materials is one of the future demands in achieving economic and environmental sustainability. Preliminary results presented in this paper indicate that IPS can be applied to purify waters contaminated with lead metal. Thus, further investigations into the IPS application should be conducted.

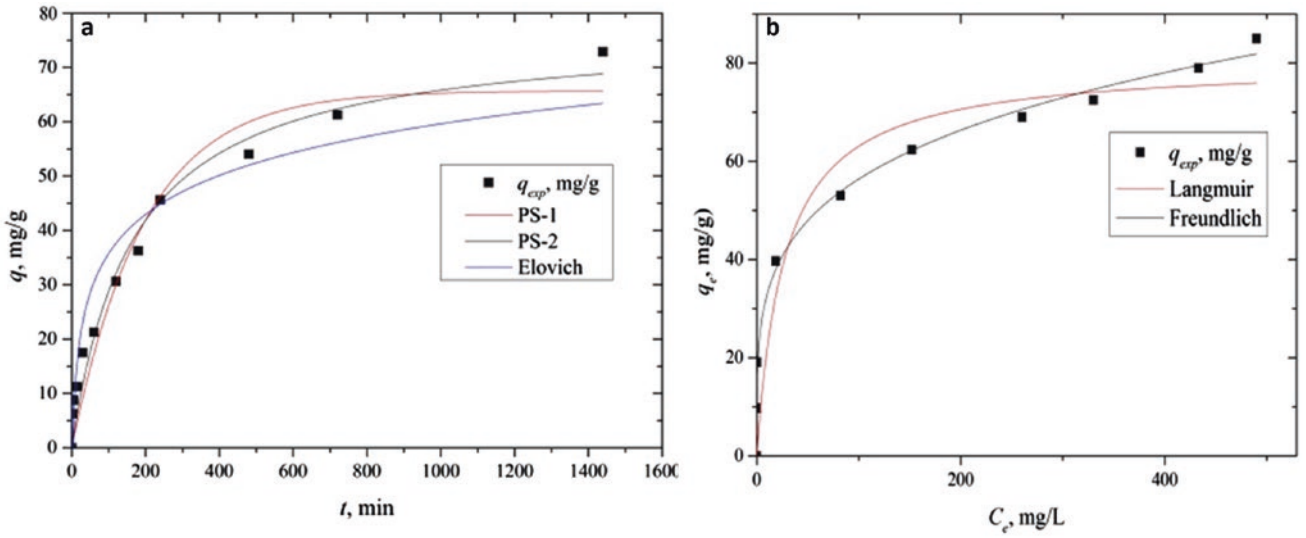

Fig. 2 **a** Kinetics and **b** equilibrium of Pb(II) uptake by IPS

Acknowledgements These results are part of the investigations supported by the Ministry of Education and Science of the Republic of Serbia (Grant number 451-03-9/2021-14/200023).

References

Abdi, O., & Kazemi, M. A. (2015). Review study of biosorption of heavy metals and comparison between different biosorbents. *Journal of Materials and Environmental Science, 6*(5), 1386–1399.

Abdolali, A., Guo, W. S., Ngo, H. H., Chen, S. S., Nguyen, N. C., & Tung, K. L. (2014). Typical lignocellulosic wastes and by-products for biosorption process in water and wastewater treatment: A critical review. *Bioresource Technology*, *160*, 57–66.

Chatterjee, A., & Schiewer, S. (2014). Multi-resistance kinetic models for biosorption of Cd by raw and immobilized citrus peels in batch and packed-bed columns. *Chemical Engineering Journal, 244*, 105–116.

Check, L., & Marteel-Parrish, A. (2013). The fate and behavior of persistent, bioaccumulative, and toxic (PBT) chemicals: Examining lead (Pb) as a PBT metal. *Reviews on Environmental Health, 28*(2–3), 85–96.

Lopičić, Z., Stojanović, M., Kaluđerović Radoičić, T., Milojković, J., Petrović, M., Mihajlović, M., & Kijevčanin, M. (2017). Optimization of the process of Cu(II) sorption by mechanically treated *Prunus persica* L.—contribution to sustainability in food processing industry. *Journal of Cleaner Production*, *156*, 95–105.

Lopičić, Z., Stojanović, M., Marković, S., Milojković, J., Mihajlović, M., Kaluđerović Radoičić, T., & Kijevčanin, M. (2019). Effects of different mechanical treatments on structural changes of lignocellulosic waste biomass and subsequent Cu(II) removal kinetics. *Arabian Journal of Chemistry*, *12*(8), 4091–4103.

Yan, G., & Viraraghavan, T. (2001). Heavy metal removal in a biosorption column by immobilized *M. rouxii* biomass. *Bioresource Technology*, *78*, 243–249.

Characterization of Natural and Modified Clay Used for a Filtration System Aiming at the Removal of Contaminants from Surface Water

Laura Scrano, Mauro Pallara, Roberto Buccioni, Giovanni Mongelli, Sabino Aurelio Bufo, and Rocco Laviano

Abstract

The scientific community has focused many research efforts on finding natural materials suitable for the most efficient wastewater purification. Our contribution is removing organic contaminants by exploiting the natural properties of clay and organo-clay materials. Two raw clayey materials (MIC and NC) were collected from the Basilicata region (South Italy), and another one was a Wyoming Na-montmorillonite (MMT) supplied by the Clay Minerals Society. Octadecyl-trimethyl-ammonium (Br) (ODTMA) was the organic cation used for modifying the clay surface to micelle-clay status. Unfortunately, MIC and NC could not retain a sufficient amount of surfactant. The MMT-ODTMA system, prepared using a concentration of the organic cation higher than the critical micelle concentration (CMC), was very effective in removing from water the herbicide atrazine, selected as the model contaminant for this study. This result encourages us to continue investigations to offer a low-cost and straightforward system to purify water even at home or small settlement levels.

Keywords

Wastewater · Purification · Clay minerals · Micelle-clay · Surfactant

L. Scrano (✉) · R. Buccioni · G. Mongelli · S. A. Bufo
University of Basilicata, Via dell'Ateneo Lucano10, 85100 Potenza, Italy
e-mail: laura.scrano@unibas.it

M. Pallara · R. Laviano
University of Bari "Aldo Moro", Via Orabona, 70126 Bari, Italy

S. A. Bufo
University of Johannesburg, Johannesburg 2092, South Africa

1 Introduction

Clay minerals, the colloidal fraction of soils and sediments, are characterized by a large specific surface, chemical and mechanical stability, layered structure, and high cation exchange capacity (CEC). As a result, they are excellent adsorbent materials and play an essential role in different fields, from research to industries, such as removing various contaminants present in surface water, groundwater, and wastewater (Murray, 2000; Neeraj & Chandra, 2021).

However, researchers aim to modify the adsorbent capacity of these natural materials by changing their surface properties from hydrophilic to hydrophobic. In addition, an increase in the basal spacing of the clayey layers is gained, allowing an adsorption zone to intercept contaminants that can remediate contaminated water from different kinds of organic pollutants (Carrizosa et al., 2001; Rodriguez-Cruz et al., 2007; Wang & Wang, 2008; Wang et al., 2010).

The mechanisms that control the adsorption of compounds into the modified clays depend on the type of organic cations used for their realization (Andrunik & Bajda, 2019). Therefore, the scientific community has focused many research efforts on methods for the purification of contaminated water based on the exploitation of the natural properties of clay materials (Ghafar et al., 2020; Sarkar et al., 2019; Xi et al., 2007).

Having this in mind, we characterized and modified several natural clayey materials. Some of them were collected from the Basilicata region (South Italy), and another was clay supplied by the Clay Minerals Society.

The organic cation used for modifying the clay surface was the octadecyl-trimethyl-ammonium-bromide (ODTMA-Br in Fig. 1), a surfactant synthesized at the University of Basilicata (98.8%). In addition, the organo-clays obtained were used in sorption experiments to remove a model contaminant from water.

A. Çiner et al. (eds.), *Recent Research on Environmental Earth Sciences, Geomorphology, Soil Science, Paleoclimate, and Karst*, Advances in Science, Technology & Innovation, https://doi.org/10.1007/978-3-031-42917-0_9

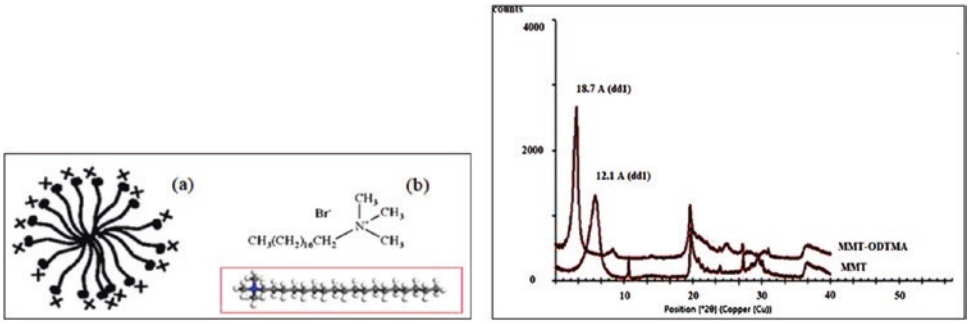

Fig. 1 Structure of micelle (**a**); structure of ODTMA (**b**); superimposed X-ray diffraction of natural and modified MMT (**c**)

2 Materials and Methods

The natural clayey materials collected from the Basilicata region were

- A multicolored clay (MIC) sampled near the town of Campomaggiore;
- A natural clay (NC) sampled near the town of Tursi;
- A montmorillonite (MMT) supplied by the Clay Minerals Society as source clay SWy-2-Na-montmorillonite (Wyoming).

The method adopted to prepare the organo-modified clays was similar to those described in the literature for a clay-micelle complex (Andrunik & Bajda, 2019; Wang & Wang, 2008; Xi et al., 2007).

The critical micelle concentration (CMC) value for ODTMA-Br is 0.3 mM. Therefore, the clay mineral was introduced into a solution of 12 mM of the surfactant at a rate of 10 g $L-^{1}$, and then stirred for 72 h. Finally, the complex was filtered and dried (by lyophilizing). The clay micelle can bind negatively charged organic molecules under its positive charge with the hydrophobic region (Fig. 1a).

MIC, NC, and MMT were analyzed by X-ray powder diffraction (XRD) before and after the inclusion of the surfactant. Thermogravimetric (TGA) and Fourier transform infrared spectroscopy (FTIR) analyses were also applied. The organo-modified clay samples were observed by Scanning Electronic Microscopy (SEM).

The ability of the organo-modified clay to remove contaminants was tested through a batch system using an aqueous solution of atrazine as an adsorption model. This compound was chosen because it is a hazardous herbicide belonging to the triazine family, used in the past to control the seasonal weeds in various crops but still present as a residue in many ground and surface waters ("Public Health Statement for Atrazine" 2003). The retention by surfactant-modified MMT was measured by liquid chromatography-tandem high-resolution mass spectrometry (LC/HRMS).

3 Results

The diffractometric analyses evidenced that

- MIC contains modest quantities of phyllosilicates, with the prevalent presence of kaolinite, chlorite, and smectite, scarce and poorly crystallized. The silico-clastic portion consists of quartz, predominant in feldspar. After treatment with the surfactant, no changes in the basal distance between the layers were evidenced.
- NC encloses an abundant amount of clay minerals. In particular, illite and smectite prevail over kaolinite and chlorite. The silico-clastic portion includes a significant amount of quartz, very subordinate feldspar, and calcite. After treatment with the surfactant, no changes in the basal distance between the layers were observed.
- After the treatment with ODTMA, MMT exhibits a variation of the basal spacing (d001) from 12.2 to 18.7 Å; besides, there are no significant differences between their outlines (Fig. 1c).

The FTIR spectra (Fig. 2a) show three signals at 1460, 2980, and 2850 cm^{-1} in the case of MMT-ODTMA transmittance, which are absent in the MMT outline.

Figure 2b depicts the thermal behavior of the clay mineral and the modified clay. The weight reduction of MMT was limited to 7%. Starting from 400 °C, the MMT-ODTMA complex shows high weight reduction (about 50%) due to the burning of the surfactant.

The SEM images did not add any information of interest about the changes in the morphology of MMT upon intercalation of ODTMA (data not shown).

On the other hand, the modified clay (MMT-ODTMA) was experienced to verify the effectiveness of removing the contaminant atrazine (used as a case study). The herbicide (MW = 215.68 g/mol) was tested as a sorption model at a rate of 0.35 mmol/g (75.5 mg/g).

Table 1 refers to the isotherm values obtained for the natural MMT and the micelle-clay MMT-ODTMA.

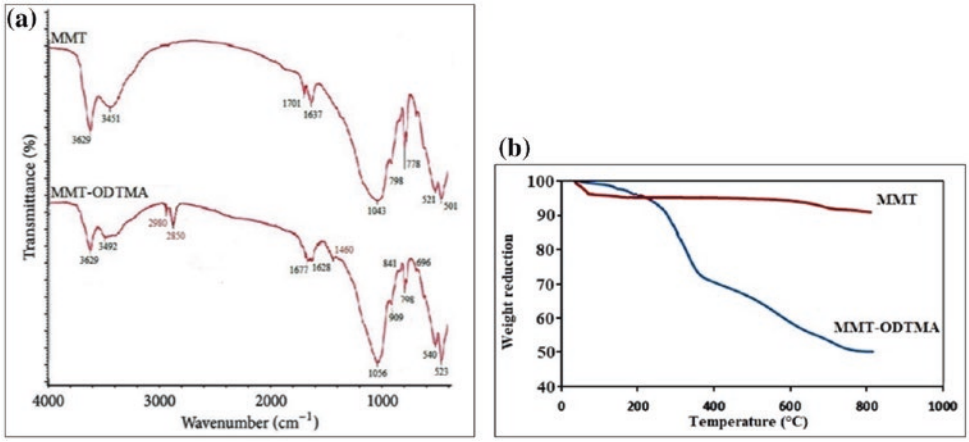

Fig. 2 FTIR spectra (a) and thermogravimetric curves (b) of natural and modified MMT

Table 1 Isotherm parameters of atrazine adsorption into MMT and MMT-ODTMA

Adsorbent	Langmuir			Freundlich		
	C_m (mg/g)	K (L/mg)	R^2	K_f (mg/g)	n_f	R^2
MMT	4.53	3.98	0.9994	3.76	3.7	0.8852
MMT-ODTMA	57.7	5.96	0.9985	29.7	1.9	0.8233

4 Discussion

The samples MIC and NC, collected in the regional territory of Basilicata, were not suitable for forming stable organo-clays due to their poor mineralogical structure. On the contrary, the Na-montmorillonite seems well intercalated by ODTMA without degrading the MMT basic structure. On the other hand, the FTIR spectra evidenced new signals due to CH vibrations, proving ODTMA intercalation into the clay layers.

The organo-mineral complex is stable below 400 °C, confirming that ODTMA moieties are enclosed in the interlayer space of the clay.

From the determination coefficients (R^2) in Table 1, the Langmuir model fits data better than the Freundlich equation. The MMT-ODTM can adsorb atrazine following simple classic mechanisms described by the Langmuir model, typically related to monolayer adsorption.

At the end of the batch filtration, the disappearance of the herbicide from the treatment solution was 76.5% of the initial amount. This quantity was considered as retained by the organo-clay. After the sorption, the atrazine recovery by water flowing from the air-dried organo-clay returned 20.1% of the retained chemical. The release of the herbicide was controlled again after six months of equilibration in water, giving 29.5% of the retained atrazine. Therefore, the organo-clay could strongly retain more than 50% of the atrazine used in the treatment.

5 Conclusions

The obtained results confirmed that, thanks to a sorption process, the micelle-clay, based on the modified MMT, can efficiently remove the organic chemical used as a model pollutant. Furthermore, the desorption test proved a high retention rate of the organic material within the MMT-ODTMA adsorption sites. Only by using an organic solvent was it possible to recover the retained substance completely. However, the organo-clay modified using a quaternary ammonium salt is undoubtedly suitable for industrial wastewater recycling but could be toxic if released in drinking water. For this reason, we are experimenting with new natural polymers for water filtration that are effective and safe forhuman and animal health and for the environment.

References

"Public Health Statement for Atrazine". (2003, September). *Toxic substances portal-atrazine*. Center for Disease Control, Agency for Toxic Substances and Disease Registry, Division of Toxicology and Human Health Sciences. Retrieved from, May 2, 2015.

Andrunik, M., & Bajda, T.: Modification of bentonite with cationic and nonionic surfactants: Structural and textural features. *Materials*, *12*(22), 3772 (2019). https://doi.org/10.3390/ma12223772

Carrizosa, J., Koskinen, W. C., Hermosin, M. C., & Cornejo, J. (2001). Dicamba adsorption–desorption on organoclays. *Applied Clay Science, 18*(5–6), 223–231.

Ghafar, A. H., Radwan, E. K., & El-Wakeel, S. T. (2020). Removal of hazardous contaminants from water by natural and zwitterionic surfactant-modified clay. *ACS Omega, 5*, 6834–6845.

Murray, H. H. (2000). Traditional and new applications for kaolin, smectite, and palygorskite: A general overview. *Applied Clay Science, 17*(5–6), 207–221.

Neeraj, K., & Chandra, M. (2021). Basics of clay minerals and their characteristic properties. IntechOpen Book Series. https://doi.org/10.5772/intechopen.97672, https://www.intechopen.com/online-first/76780

Rodriguez-Cruz, M. S., Sanchez-Martin, M. J., Andrades, M. S., & Sanchez-Camazano, M. (2007). Modification of clay barriers with a cationic surfactant to improve the retention of pesticides in soils. *Journal of Hazardous Materials, 139*, 363–372.

Sarkar, B., Rusmin, R., Ugochukwu, U. C., Mukhopadhyay, R., & Manjaiah, K. M. (2019). Chapter 5—modified clay minerals for environmental applications. In M. Mercurio, B. Sarkar, & A. Langella (Eds.), *Modified clay and zeolite nanocomposite materials* (pp. 113–127), Elsevier, NY.

Wang, T., Zhu, J. X., Zhu, R. L., Ge, F., Yuan, P., & He, H. P. (2010). Enhancing the sorption capacity of CTMA-bentonite by simultaneous intercalation of cationic polyacrylamide. *Journal of Hazardous Materials*, *178*, 1078–1084.

Wang, L., & Wang, A. (2008). Adsorption properties of Congo red from aqueous solution onto surfactant modified montmorillonite. *Journal of Hazardous Materials, 160*, 173–180.

Xi, Y., Frost Ray, L., & He Hongping, J. (2007). Modification of the surfaces of Wyoming montmorillonite by the cationic surfactants alkyl trimethyl, dialkyl dimethyl, and trialkyl methyl ammonium bromides. *Journal of Colloid and Interface Science*, *305*(1), 150–158. https://doi.org/10.1016/j.jcis.2006.09.033

Heavy Metal Pollution in the Core Sediment of Strait of Malacca

Wan Nur Izwani Mior Baharudin, Lavannia Ravikumar, Vishalini B. Maran, Dorinda Anthony Anthony Dass, Nur Aliah Syakirah Rosli, Najah Karimah Mustaffa, Noor Fazreen Dzulkafli, and Meng-Chuan Ong

Abstract

The Strait of Malacca receives heavy metal from the mainland into the marine environment. Therefore, five sediment core samples were collected by gravity core sampler during the 2019 Malacca Straits Scientific Expedition to assess the concentration of selected heavy metals, namely copper (Cu), zinc (Zn), cadmium (Cd), lead (Pb), arsenic (As), and mercury (Hg). The concentration of metals in sediments was determined by Inductively Coupled Plasma Mass Spectrometry (ICP-MS) after the Teflon Bomb digestion method with mixed acid. The accuracy test for the procedure was examined by analysis of Standard References Materials (SRM) NIST 1646a. The mean concentrations of metals in the sediment cores ranged 8.96–15.6 μg/g dry weight (Cu), 34.8–97.9 μg/g dry weight (Zn), 0.07–0.15 μg/g dry weight (Cd), 20.6–47.9 μg/g dry weight (Pb), 3.15–9.50 μg/g dry weight (As), and 0.03–0.11 μg/g dry weight (Hg). The results also revealed that the average heavy metal concentration in the core collected in the northern region of the Strait of Malacca is highly concentrated with Zn and Pb compared to the southern part. The index of geoaccumulation (Igeo) was applied to distinguish the pollution status and conclude that the area that was not polluted with studied metals except slightly contaminated by Pb and As. In addition, this metal deposition can influence other factors, such as naturally influenced process input and other anthropogenic factors. In a nutshell, this study can evaluate the risk of metal pollution and the effect of anthropogenic activities on the aquatic environment because most heavy metals become toxic in the environment, especially when it is highly concentrated in sediments.

Keywords

Strait of Malacca · Core sediment · Heavy metals · ICP-MS · Pollution

1 Introduction

The Strait of Malacca, embodying the West Coast of Peninsular Malaysia, is about 1,111 km long, one of the areas affected by heavy metal pollution (Saion et al., 2007). As the strait becomes the most important and busiest waterways for maritime activities, it brings the channel to accommodate more sewage discharge as the human population is also higher in the nearby coastal area. It has been recorded that 900 tankers and commercial vessels pass through the strait daily, with 70,000 ships annually (Amin et al., 2009).

The metals that enter the marine environment can accumulate in the bottoms of the sea, as the surface sediment receives contaminants from the urban sewage discharge and industrial, especially near the coastal area. The pollutants can easily be identified through metal spatial variations in the sediment (Dauvalter & Rognerud, 2001). The tremendous impact on land use and industrialization has led to the proliferation of heavy metal waste. The contamination with toxic compounds has increased pressure on coastal or estuarine ecosystems over the past decades due to human activity enhancement (Jiao et al., 2018).

W. N. I. M. Baharudin · L. Ravikumar · V. B. Maran · D. A. A. Dass · N. A. S. Rosli · N. K. Mustaffa · M.-C. Ong (✉)
Ocean Pollution and Ecotoxicology (OPEC) Research Group, Faculty of Science and Marine Environment, Universiti Malaysia Terengganu, Kuala Nerus, 21030 Terengganu, Malaysia
e-mail: ong@umt.edu.my

N. F. Dzulkafli
Faculty of Engineering and Life Sciences, Department of Science and Biotechnology, Universiti Selangor, Bestari Jaya, Malaysia

M.-C. Ong
Institute of Oceanography and Environment, Universiti Malaysia Terengganu, Kuala Nerus, 21030 Terengganu, Malaysia

A. Çiner et al. (eds.), *Recent Research on Environmental Earth Sciences, Geomorphology, Soil Science, Paleoclimate, and Karst*, Advances in Science, Technology & Innovation, https://doi.org/10.1007/978-3-031-42917-0_10

Down core sediment study has been used to trace the human activities that started with the founding and detection of phosphorus contamination in early 1960 (Livingstone & Boykin, 1962). In this case, the sediment core can help trace a record of changes in the concentration of chemical indicators in the environment (Kamaruzzaman & Ong, 2008). Hence, the development of the sediment core study can reflect variations in metal inputs over a long period (Robbins & Edgington, 1975). Therefore, studying heavy metal pollution in the Strait of Malacca core sediments is essential, as it can provide useful information on marine pollution from the past to current.

2 Materials and Methods

Five sediment cores along the Strait of Malacca, lengths from 120 to 180 cm, were collected during the Strait of Malacca Scientific Cruise Expedition using the RV Discovery vessel in 2019 (Fig. 1). The coordinates of the sampling locations were recorded by Global Positioning System (GPS). All the core samples were labeled, capped tightly, and stored in the freezer at low temperatures before the laboratory dissection (Abrahim & Parker, 2008).

The core was cut into 1 cm intervals and transferred to the petri dish accordingly. Then, the samples were dried in an oven at 60 °C for 5–7 days until they dried. Next, these dried samples were ground manually until the sediment sample turned to powder form and stored for analysis. Next, the samples were digested using the Teflon Bomb digestion method with mixed acid (HNO_3, HCl, and HF) and measured using Inductively Coupled Plasma Mass Spectrometry (ICP-MS) for the concentration of heavy metals (Kamaruzzaman et al., 2010).

3 Results

Figure 2 and Table 1 show the concentration of heavy metals in the five sediment cores (W1, W8, W19, W33, and W39) collected in this study. Generally, the highest concentration value was Zn, and the lowest was Hg. Compared to the past studies of the Strait of Malacca by Saion et al. (2007), only Cu concentration remains lower, while other metals, Zn, Cd, Pb, and As, were higher than the past studies. Besides, the concentration of Zn in the southern part of the Strait of Malacca (W1) is higher than in Sungai Buloh, Singapore (Cuong et al., 2005), while the northern part of the Strait of Malacca in this study also resulted in a higher concentration than the finding by Razak et al. (2018)'s studies.

4 Discussion

The information about the pollution status was obtained by calculation using the index of the geoaccumulation (Igeo) approach. These assessments used a background element's upper continental crust (UCC) values (Wedepohl, 1995) as a reference. The Igeo calculated following the formula by Ong et al. (2015):

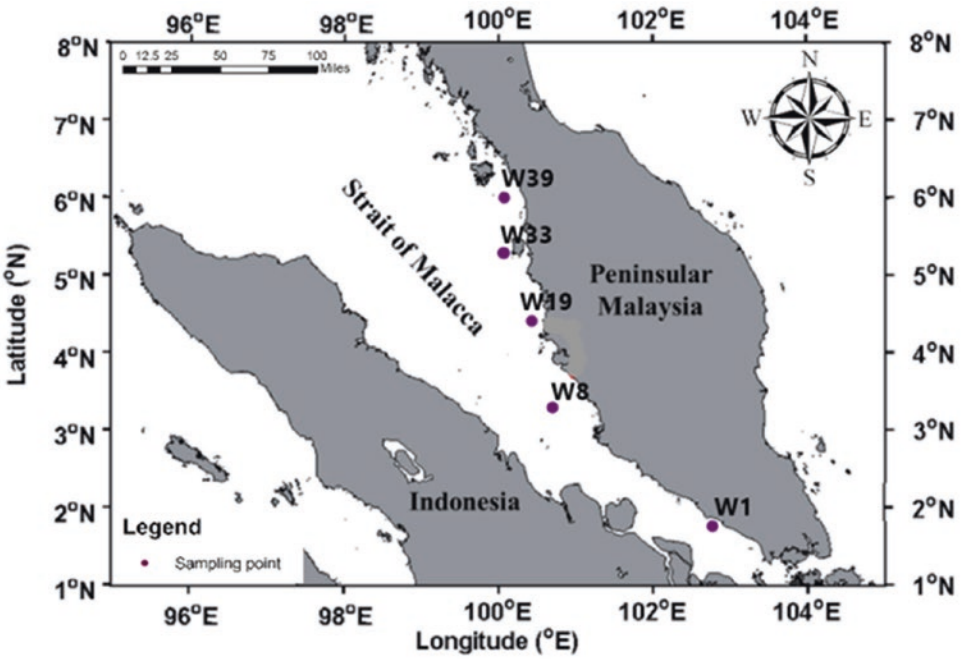

Fig. 1 The sampling sites of the sediment core

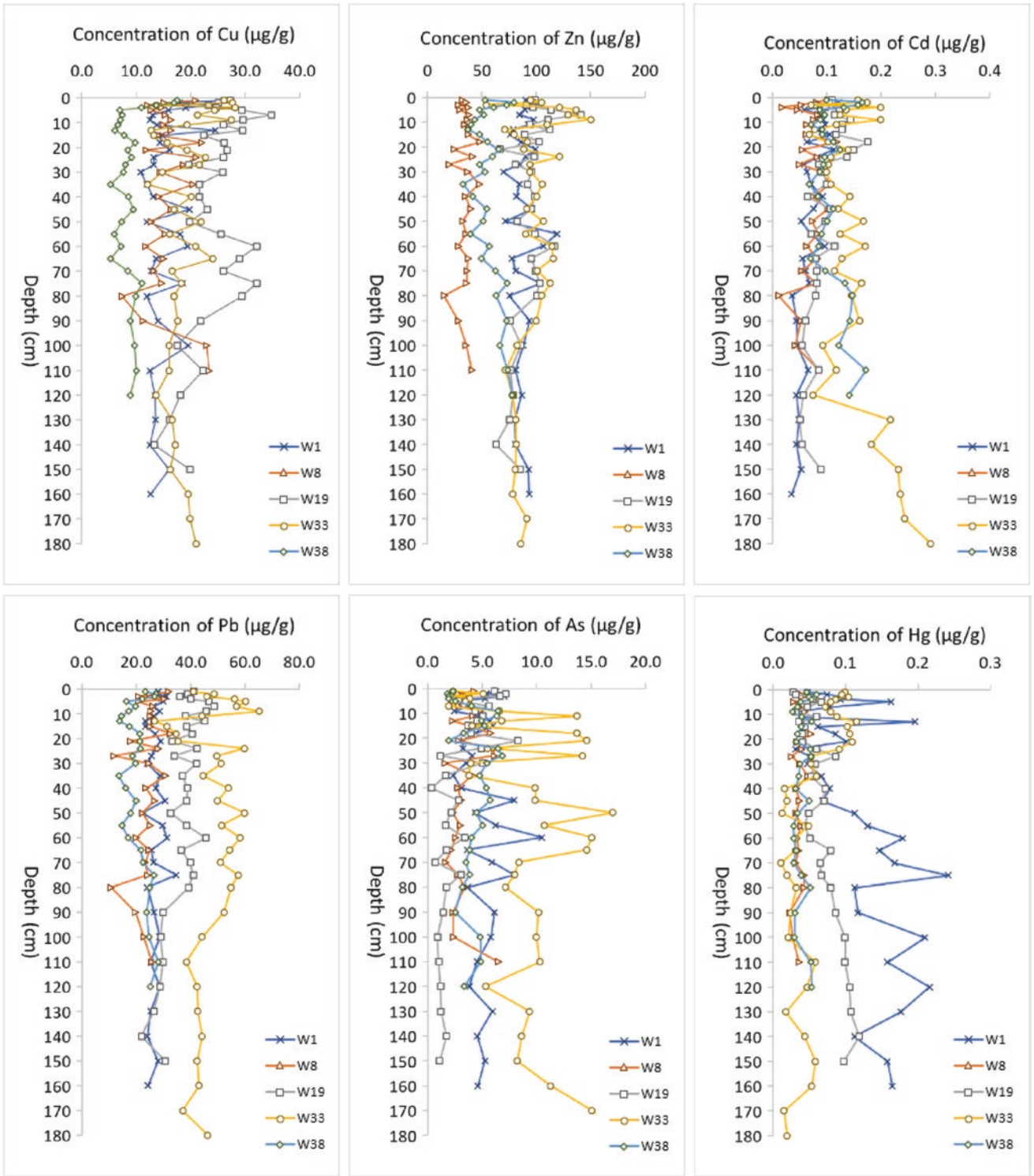

Fig. 2 Depth profile of metals of sediments in each core collected from Strait of Malacca

Table 1 The mean of heavy metal concentration in each core (μg/g dry weight)

Heavy metal	W1	W8	W19	W33	W39
Cu	15.6 ± 3.96	15.7 ± 3.87	24.5 ± 4.9	19.0 ± 4.36	8.96 ± 2.93
Zn	88.8 ± 10.7	34.8 ± 7.11	94.4 ± 15.5	97.9 ± 19.9	56.5 ± 12.9
Cd	0.07 ± 0.02	0.07 ± 0.025	0.10 ± 0.03	0.15 ± 0.05	0.11 ± 0.03
Pb	27.2 ± 2.73	24.0 ± 5.1	37.4 ± 6.3	47.9 ± 8.99	20.6 ± 4.25
As	5.01 ± 1.75	3.40 ± 1.37	3.15 ± 2.11	9.52 ± 5.55	4.17 ± 1.51
Hg	0.11 ± 0.06	0.03 ± 0.01	0.07 ± 0.025	0.06 ± 0.03	0.04 ± 0.01

Table 2 The value of Igeo, on average, for each core sediment

Station	Igeo values					
	Cu	Zn	Cd	Pb	As	Hg
W1	−0.498	0.179	−1.146	0.088	0.654	0.235
W8	−0.494	−1.172	−1.238	−0.124	0.095	−1.186
W19	0.164	0.256	−0.722	0.529	−0.296	−0.469
W33	−0.209	0.299	−0.159	0.882	1.349	−0.883
W39	−1.323	−0.504	−0.535	−0.338	0.369	−1.091

$$\text{Igeo} = \log_2\left[\frac{Cn}{1.5Bn}\right]$$

Cn was the element of heavy metal concentration, Bn was the background value, and 1.5 was the background matrix correction due to lithogenic effects. The classification of the calculated Igeo was referred to the Müller (1969) that indicates the sediment quality from uncontaminated to extremely contaminated; Igeo <0, practically uncontaminated; 0–1, slightly contaminated; 1–2, moderately contaminated; 2–3, moderately to heavily contaminated; 3–4, heavily contaminated; 4–5, heavily to extremely contaminated; lastly >5, extremely contaminated (Muller, 1969).

By referring to the classification of Igeo values in Table 2, all of the heavy metals Cu, Zn, Cd, Pb, As, and Hg fell between classes 0 and 1 except for core W33. Core W33 has high average Igeo values of As (1.349) that classify it in classes 1–2. From this finding, the Strait of Malacca can be categorized as uncontaminated or moderately contaminated of studied heavy metals.

5 Conclusions

In a nutshell, metal concentration in the Strait of Malacca was higher than that in other studies. Besides, Pb and Zn correlate with each other and conquer the Malacca Strait with a high concentration value in all cores. These metals were the main elements used mainly in human activities such as industrial, agriculture, mining, shipping, transportation, and construction both in West Peninsula Malaysia and Sumatra, Indonedia regions. Moreover, the geoaccumulation index (Igeo) indicates that the Strait of Malacca area was slightly polluted with Pb and As.

Acknowledgements This research was conducted from the Ministry of Higher Education funding under the Talent and Publication Enhancement Research Grant, TAPE-RG 55188. First, the authors wish to acknowledge their gratitude to the anonymous reviewers who gave free time and effort to make constructive recommendations that enhanced the value of this manuscript. The authors also wish to thank the Centre of Research and Field Services (CRAFS) for providing the RV Discovery vessel for the sampling activities.

References

Abrahim, G. M. S., & Parker, R. J. (2008). Assessment of heavy metal enrichment factors and the degree of contamination in marine sediments from Tamaki Estuary, Auckland, New Zealand. *Environmental Monitoring and Assessment, 136*(1–3), 227–238.

Amin, B., Ismail, A., Arshad, A., Yap, C. K., & Kamarudin, M. S. (2009). Anthropogenic impacts on heavy metal concentrations in the coastal sediments of Dumai, Indonesia. *Environmental Monitoring and Assessment, 148*(1–4), 291–305.

Cuong, D. T., Bayen, S., Wurl, O., Subramanian, K., Wong, K. K. S., Sivasothi, N., & Obbard, J. P. (2005). Heavy metal contamination in mangrove habitats of Singapore. *Marine Pollution Bulletin, 50*(12), 1732–1738.

Dauvalter, V., & Rognerud, S. (2001). Heavy metal pollution in sediments of the Pasvik River drainage. *Chemosphere, 42*(1), 9–18.

Jiao, Z., Li, H., Song, M., & Wang, L. (2018). Ecological risk assessment of heavy metals in water and sediment of the Pearl River Estuary, China. *Materials Science and Engineering, 394*, 1–13.

Kamaruzzaman, B. Y., & Ong, M. C. (2008). Recent sedimentation rate and sediment ages determination of Kemaman-Chukai mangrove forest, Terengganu, Malaysia. *American Journal of Agricultural and Biological Science, 3*(3), 522–525.

Kamaruzzaman, B. Y., Siti, W. A., Ong, M. C., & Joseph, B. (2010). Spatial distribution of lead and copper in the bottom sediments of Pahang river estuary, Pahang, Malaysia. *Sains Malaysia, 39*(4), 543–547.

Livingstone, D. A., & Boykin, J. C. (1962). Vertical distribution of phosphorus in Linsley Pond mud. *Limnology and Oceanography, 7*(1), 57–62.

Muller, G. (1969). Index of geoaccumulation in sediments of the Rhine River. *GeoJournal, 2*, 108–118.

Ong, M. C., Joseph, B., Shazili, N. A. M., Ghazali, A., & Mohamad, M. N. (2015). Heavy metals concentration in surficial sediments of Bidong Island, South China sea off the East coast of Peninsular Malaysia. *Estuarine, Asian Journal of Earth Sciences, 8*(3), 74–82.

Razak, A., Sakinah, N., Khalik, W. M. A. W. M., Shaari, H., Shazili, N. A. M., & Bidai, J. (2018). Spatial distribution of heavy metals in tropical coastal sediment of the Northern Malacca Strait, Malaysia. *Nature Environment & Pollution Technology*, *17*(4), 1115–1123.

Robbins, J. A., & Edgington, D. N. (1975). Determination of recent sedimentation rates in Lake Michigan using Pb-210 and Cs-137. *Geochimica et Cosmochimica acta*, *39*(3), 285–304.

Saion, E. B., Wood, A. K. H., Sulaiman, Z. A., Alzahrany, A. A., Elias, M. S., & Siong, W. B. (2007). Determination of heavy metal pollution in depth profile of marine sediment samples from the Strait of Malacca. *Fresenius Environmental Bulletin*, *16*(10), 1279–1287.

Wedepohl, K. H. (1995). The composition of the continental crust. *Geochimica et Cosmochimica Acta*, *59*(7), 1217–1232.

Removal of Pb(II), Cu(II), and Cd(II) from Aqueous Solution by Alginate-Immobilized Aquatic Weed *M. spicatum*

Jelena Milojković, Zorica Lopičić, Marija Mihajlović, Milan Kragović, Biljana Gligorijević, Tatjana Vojvodić, and Jelena Avdalović

Abstract

Biosorption is evolving as a potential alternative to the existing conventional technologies for the removal and/or recovery of pollutants from aqueous solutions. The present work investigates the possible application of waste biomass *Myriophyllum spicatum* (Ms) in removing contaminants, evaluating equilibrium through isotherms of selected heavy metals: lead, copper, and cadmium. As a heavy metal biosorbent, Ms was immobilized in alginate beads (Ms: Alginate 2:1). Applied biosorbent, MsA, was characterized by scanning electron microscopy with energy dispersive X-ray spectroscopy (SEM–EDX) and Fourier transform infrared spectroscopy (FT-IR). Experimental results were fitted (nonlinear) by six isotherm models: Langmuir, Freundlich, Sips, Redlich and Peterson, Toth, and Temkin. For lead(II) ion removal, fitting follows the following sequence, F ≈ R-P>S>To>L>Te, while for copper(II) and cadmium(II) ions are as follows: R-P>To ≈ Te ≈ L>S>F and R-P>L>To>S>F>Te, respectively. TOC analyses revealed that *M. spicatum* releases 35.04 mg/L of total organic content while immobilized sample, MsA, only 6.81 mg/L. Finally, this biosorbent was tested on a sample of real wastewater from a coal-fired thermal power plant complex TPP Kostolac (operated by PE "Electric Power Industry of Serbia"). The results indicate that using immobilized aquatic weed *M. spicatum* as a biosorbent has a high potential for heavy metal wastewater treatment applications.

Keywords

Biosorption · Heavy metals · Aquatic weed · Immobilization · Wastewater

1 Introduction

Myriophyllum spicatum L. is a submerged aquatic weed found in at least 57 countries. Therefore, this weed is native to Europe, Asia, and North Africa but is also a major aquatic invader across most of North America (Couch et al., 1985). This weed has been classified as a Category 1 weed due to its widespread negative effects on the environment around the world (Martin & Coetzee, 2014). *M. spicatum* fits the criteria for a prospective biosorbent because of its natural abundance, high availability, and non-toxic nature (Milojković et al., 2019). In our earlier investigations, we also showed good performance of *M. spicatum* immobilized in alginate beads (MsA) for the removal of Pb (Milojković et al., 2019), Cu (Milojkovic et al., 2019), and Cd (Milojković et al., 2016) ions from single-component aqueous solutions.

This study aims to continue previous research and investigate the possible application of alginate-immobilized aquatic weed M. spicatum in removing Pb, Cu, and Cd ions from multimetal aqueous solutions.

J. Milojković (✉) · Z. Lopičić · M. Mihajlović
Institute for Technology of Nuclear and Other Mineral Raw Materials, 86 Franchet d'Esperey, Belgrade, Serbia
e-mail: j.milojkovic@itnms.ac.rs

M. Kragović
"Vinča" Institute of Nuclear Sciences, National Institute of the Republic of Serbia, University of Belgrade, 22-24 Mike Petrovića Alasa, 11351 Belgrade, Serbia

B. Gligorijević · T. Vojvodić
PE "Electric Power Industry of Serbia", Branch TE-KO Kostolac, Nikole Tesle 5-7, Kostolac, Serbia

J. Avdalović
Institute of Chemistry, Technology and Metallurgy, Department of Chemistry, University of Belgrade, Studentski Trg 14-16, Belgrade, Serbia

A. Çiner et al. (eds.), *Recent Research on Environmental Earth Sciences, Geomorphology, Soil Science, Paleoclimate, and Karst*, Advances in Science, Technology & Innovation, https://doi.org/10.1007/978-3-031-42917-0_11

2 Materials and Methods

M. spicatum used to prepare beads MsA originates from Sava Lake (Belgrade, Serbia). *M. spicatum* was immobilized in alginate beads (Ms: Alginate = 2:1), and beads were made according to the method (Yan & Viraraghavan, 2001).

Scanning Electron Microscopy—Energy Dispersive X-Ray Spectroscopy (SEM–EDX) analysis was performed on MsA before and after the biosorption of heavy metals using JEOL JSM 6460 model. The release of organic carbon was determined by measuring the TOC by Analytik Jena, TOC/TN Analyzer (Multi N/C 2100S). In addition, infrared spectroscopy analysis (FT-IR) was performed on a Thermo Scientific Nicolet iS50 FT-IR spectrometer in transmission mode with 256 scans over a range 4000–400 cm^{-1}.

The adsorption of the Pb(II), Cu(II), and Cd(II) was studied at pH 5.0 in the concentration range 0.2–6 mmol/L (for each heavy metal) as batch biosorption tests with two g/L MsA. After 24 h, heavy metal concentrations were determined on an atomic absorption spectrometer Perking Elmer Analyst 300. In addition, Langmuir, Freundich, Sips, Redlich and Peterson, Toth, and Temkin adsorption isotherms were used to fit experimental results. Evaluation of isotherm was made using OriginPro 2021 software.

To determine the effectiveness of the MsA in real wastewater samples, this biosorbent was tested on wastewater samples from the coal-fired thermal power plant complex-TPP Kostolac (PE "Electric Power Industry of Serbia", Branch TE-KO Kostolac).

3 Results and Discussion

3.1 MsA Characterization

The presence of calcium in studied samples could explain the white areas visible on micrographs (Dibdiakova et al., 2015). Granule MsA is ovoid and spherical with rough, uneven edges (Fig. 1a, b). Different porosity is visibly stratified. Macro pores are made up of complex layers, and tiny balls are bonded to the surface of MsA. After biosorption of heavy metals, porosity exists (Fig. 1b) but is not as plain as in granules. EDX confirmed the infiltration of examined heavy metals. After sorption, reduced peaks of Ca, as well as new peaks of Pb(II) Cu(II), and Cd(II), are observed (Fig. 1g) compared to the starting MsA material (Fig. 1f).

TOC analysis showed that MsA releases only 6.81 mg/L of total organic content.

FT-IR showed that carbonyl, carboxyl, and hydroxyl groups are likely involved in the biosorption of detected heavy metals by MsA. Identified chemically active groups are components of polysaccharides, cellulose, hemicellulose, lignin, and proteins, which can be found in aquatic weed *M. spicatum* (Dibdiakova et al., 2015).

3.2 Heavy Metal Adsorption Study

During the biosorption process, the highest removal was obtained for lead ions with a maximum capacity of 0.530 mmol/g, while for copper 0.255 mmol/g, and the

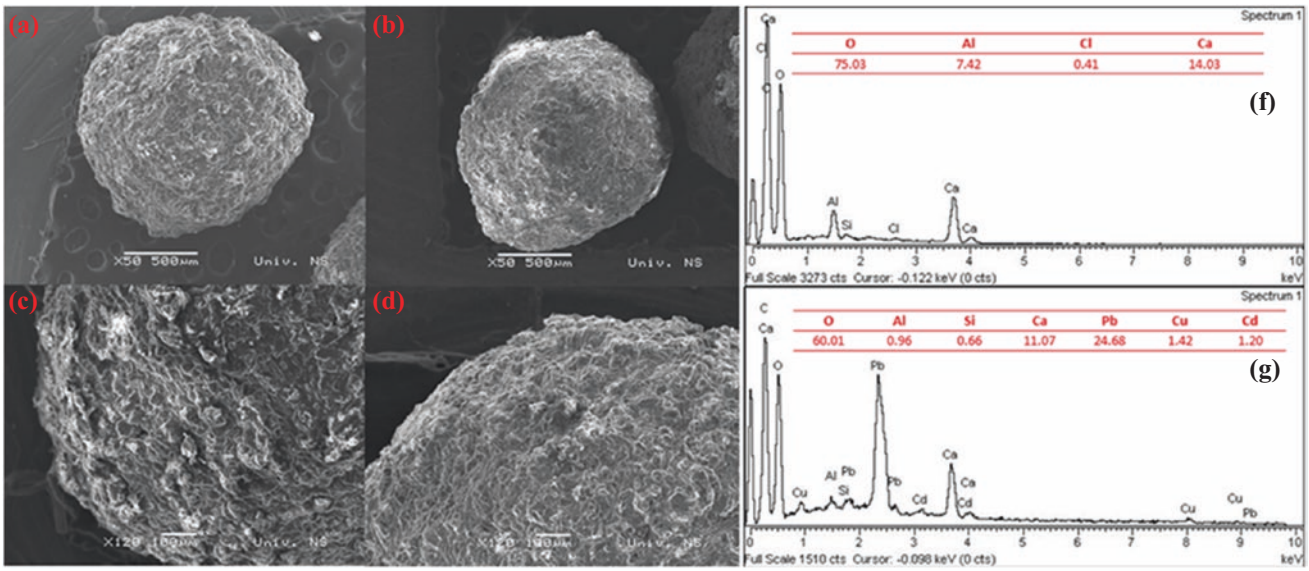

Fig. 1 SEM micrographs of MsA: before biosorption 50× **a** and **c** 120× magnification; after biosorption 50× **b** and **d** 120× magnification; **f** EDX before biosorption and **g** EDX after biosorption

Table 1 Parameters of isotherms obtained for heavy metal ion removal by MsA

Isotherm	Parameters	Pb(II)	Cu(II)	Cd(II)
Langmuir (L)	q_m (mmol/g) K_L/L/mg R^2	0.479 32.166 0.89641	0.251 21.739 **0.97392**	0.130 121.559 **0.86253**
Freundlich (F)	K_f n R^2	0.618 3.337 **0.97939**	0.268 2.354 0.90042	0.134 8.308 0.52145
Sips (S)	q_m K_S (L/g) n_S R^2	5.470 0.144 0.368 0.96457	0.666 0.681 0.426 0.94488	0.078 3.909 0.332 0.79875
Redlich and Peterson (R-P)	k_{RP} (L/g) a_{RP} (L/mg) b_{RP} q_m (mmol/g) R^2	105.235 174.659 0.736 0.602 **0.97790**	7.512 29.165 0.918 0.258 **0.98053**	10.825 87.716 1.081 0.123 **0.88843**
Toth (To)	q_m (mmol/g) K_T (mg/L)Th T_h R^2	1.620 0.234 0.208 0.95469	0.278 0.087 0.697 **0.97661**	0.127 8.125 1.674 0.85988
Temkin (Te)	b_T (J/mol) A_T (L/mg) R^2	89,265.475 921,277.849 0.56652	57,675.715 405.437 **0.97495**	477,630.489 6.386 0.43264

lowest for cadmium, 0.144 mmol/g. For lower initial heavy metal concentrations (2.5 mM), the removal efficiency was 90–100%, while for the highest concentrations (6 mM), MsA adsorbed 72% of lead, 39% of copper, and 14% of cadmium.

To get more information about the removal mechanism, Langmuir, Freundlich, Sips, Redlich and Peterson, and Toth and Temkin models were used to fit experimental results, and characteristic parameters are given in Table 1.

The affinity of MsA for binding heavy metal ions changes in the following order Pb>Cu>Cd. It is common for all three heavy metals that Redlich and Peterson isotherm is one of the best-describing models for their removal from solutions. According to this model, the maximal adsorption capacities of the MsA for lead, copper, and cadmium ions were 0.602, 0.258, and 0.123 mmol/g, respectively, which is in good agreement with ex12%). Lead ions removal was best described by Redlich and Peterson and Freundlich, while copper and cadmium ions removal were best described by Redlich and Peterson and Langmuir model. This suggests that for active centers in internal channels and cavities of MsA materials that are more difficult to access, there was direct competition between these heavy metals. Due to the higher affinity of the biosorbent for lead, copper and cadmium ions were displaced from these hard-to-reach places, so they were mainly bound only to surface-active centers. In contrast, lead ions were bound to the surface and in larger quantities to harder-to-reach centers.

The advantages of immobilization of *M. spicatum* were proven through TOC analysis because it was shown that immobilized biomass releases (6.81 mg/L) 5 times less organic matter compared to the biomass of this water weed (35.04 mg/L) during the treatment of water with the tested heavy metals.

MsA beads showed an excellent percentage of heavy metal removal from an actual sample of wastewater (TPP Kostolac). Chromium was removed in the highest percentage 75%, copper and zinc were released in the same amount 50%, Cd 30.8%, and then other heavy metals: Ni (20%), Pb (7.14%), Fe (5.12%), and Mn (4.45%).

4 Conclusions

Subsequent conversion of plant biomasses into animal feed, biochar, adsorbent, fertilizer, and bioenergy production materials may support a circular economy approach (Kurniawan et al., 2021). It is demonstrated that this water weed can be applied sustainably as alginate granules because it is easy to cut and collect, with no need for additional energy for drying, solving some potential ecological problems and low cost (Milojković et al., 2018).

The application of aquatic weed *M. spicatum* may support a circular economy approach because it is something that would be discarded as waste, and that would have to be

removed, disposed on landfills, and/or burnt; by its application described in this study, it is re-valued as biosorbent for Pb(II), Cu(II), and Cd(II) removal.

Acknowledgements These results are part of the projects supported by the Ministry of Education, Science and Technological Development (contract number 451-03-9/2021-14/200023) and Innovation Fund (project PoC5099) of the Republic of Serbia. Jelena Milojković is grateful to the public company "Ada Ciganlija" (Belgrade, Serbia) for providing samples of the aquatic weed *M. spicatum*. In addition, the authors are grateful to TE-KO Kostolac (TPP Kostolac) for making and enabling research on real wastewater samples.

References

Couch, R., & Nelson, E. (1985). *Myriophyllum spicatum* in North America. In L. W. J. Anderson (Ed.), *Proceedings, first international symposium on watermilfoil and related Haloragaceae species* (pp. 43–45). Aquatic Plant Management Society.

Dibdiakova, J., Wang, L., & Li, H. (2015). Characterization of Ashes from Pinus Sylvestris forest Biomass. *Energy Procedia, 75*, 186–191.

Kurniawan, S. B., Ahmad, A., Said, N. S. M., Imron, M. F., Rozaimah, S., Abdullah, S., Othman, A. R., Purwanti, I. F., & Hasan, H. A. (2021). Macrophytes as wastewater treatment agents: Nutrient uptake and potential of produced biomass utilization toward circular economy initiatives. *Science of the Total Environment, 790*, 148219.

Martin, G. D., & Coetzee, J. A. (2014). Competition between two aquatic macrophytes, Lagarosiphon major (Ridley) Moss (Hydrocharitaceae) and *Myriophyllum spicatum* Linnaeus (*Haloragaceae*) as influenced by substrate sediment and nutrients. *Aquatic Botany, 114*, 1–11.

Milojković, J., Popović-Djordjević, J., Pezo, L., Brčeski, I., Kostić, A., Milošević, V., & Stojanović, M. (2018). Applying multi-criteria analysis for preliminary assessment of the properties of alginate immobilized *Myriophyllum spicatum* in lake water samples. *Water Research, 141*, 163–171.

Milojković, J. V., Lopičić, Z. R., Anastopoulos, I. P., Petrović, J. T., Milićević, S. Z., Petrović, M. S., & Stojanović, M. D. (2019). Performance of aquatic weed—waste *Myriophyllum spicatum* immobilized in alginate beads for the removal of Pb(II). *Journal of Environmental Management, 232*, 97–109.

Milojkovic, J. V., Lopicic, Z. R., Sostaric, T. D., & Avdalovic, J. S. (2019). Biosorption of copper by immobilized Myriophyllum spicatum. *International Journal of Advances in Mechanical and Civil Engineering (IJAMCE), 6*(6), 7–11.

Milojković, J., Lopičić, Z., Kojić, M., & Petrović, M. (2016). Removal cadmium ions from aqueous solution by biosorbent—immobilized aquatic weed *M. spicatum*. EGU General. 2(5), 99–110.

Yan, G., & Viraraghavan, T. (2001). Heavy metal removal in a biosorption column by immobilized M. rouxii biomass. *Bioresource Technology*, *78*, 243–249.

Physico-chemical and Geotechnical Properties of Moroccan Phosphate Mining By-Products for the Application of Compacted Earth Bricks

M. Dadda, L. Saadi, K. Abdelouhadi, Y. Daafi, and M. Waqif

Abstract

This work aims to evaluate the potential use of phosphate mine waste rock as a base material for compacted earth brick (CEB) production. Thus, a by-product generated in significant quantities by exploiting deposits in El Youssoufia in Morocco was the subject of the present investigations. First, it was necessary to proceed to the mineralogical analysis of our samples by XRD, FTIR, and X-ray fluorescence. Then, other types of analysis were performed, such as DTA/TGA and morphological analysis by SEM–EDX. Finally, geotechnical characterization was performed by standard tests. The physico-chemical and geotechnical characterization results showed that the by-product consists mainly of quartz, limestone, and a small percentage of clay minerals. The specimens were prepared from a mixture of 70% of the by-product, 30% crushed sand, 1% Filasse fiber, and 8% cement. Mechanical and physical characterization tests were performed after 7 and 28 days of curing. The results of the mechanical compression tests revealed that the adopted mix achieved optimal mechanical properties. In addition, water absorption tests by capillary action showed a reduction in water absorption by increasing the percentage of cement.

Keywords

Waste rock · Phosphate mines · Compacted earth bricks · Compressive strength · Capillarity · Geotechnical characterization · Filasse

M. Dadda (✉) · L. Saadi · K. Abdelouhadi · M. Waqif
IMED-Lab, Faculty of Sciences and Techniques, Cadi Ayyad University (UCA), 40000 Marrakech, Morocco
e-mail: dadda.mohamed.b@gmail.com

Y. Daafi
UMP6, 43150 Benguerir, Morocco

1 Introduction

Morocco's building sector is the second most energy-intensive sector, accounting for 33.6% of total final energy consumption (AMEE), resulting in the depletion of natural resources and major environmental problems like global climate change. Therefore, interest in alternative building materials like the earth has increased to satisfy environmental and economic demands. Earthen construction can take many forms like adobes, cob, CEB (Hubert Guillaud, 2015)… However, the disadvantage of earthen constructions is the low resistance to humidity, which is the subject of several researches (Abid et al., 2021).

Several pieces of research have focused on utilizing the waste mining generated by the phosphate (El Machi, 2020) industry. The present work is aimed at the valorization of the phosphate waste mine on manufacturing compacted earth blocks (CEB). The specimens were prepared from a mixture of waste rock, crushed sand, the filasse fiber. This later allows CEB to be prepared with high mechanical and physical characteristics and reduce the water absorption ratio.

2 Materials and Technical Methods

2.1 Identification of Materials

The materials used are waste rock, crushed sand, and filasse fiber. The properties of these starting materials were performed according to the characterization methods detailed by Ajouguim et al. (2020). The properties are shown in Tables 1, 2, 3 and 4.

A. Çiner et al. (eds.), *Recent Research on Environmental Earth Sciences, Geomorphology, Soil Science, Paleoclimate, and Karst*, Advances in Science, Technology & Innovation, https://doi.org/10.1007/978-3-031-42917-0_12

Table 1 Compositions of the different formulations prepared

Code	Earth%	Sand%	Cement%	Fiber%
Ar	100	–	–	–
ArSa	70	30	–	–
ArSaF	70	30	–	–
ArSaC8%	70	30	8	–
ArSaCF8%	70	30	8	1
ArSaC6%	70	30	6	–
ArSaCF6%	70	30	6	1
ArSaC4%	70	30	4	–
ArSaCF4%	70	30	4	1

Sample codifications: Ar (earth), ArSa (earth + sand), ArSaF (earth + sand + filasse fiber), ArSaC (earth + sand + cement), and ArSaCF (earth + sand + cement + filasse fiber)

Table 2 Physical characteristics of the earth

Grain size distribution	Atterberg limits	The methylene blue test
Clay <2 µm: 32.8% Silt 2–20 Cµm: 19.62% Sand 20–0.2 µm: 47.58%	Liquid limit, WL = 70 The plastic limit, WP = 48 Plasticity index IP = 22	VBS = 4.21

Table 3 Chemical composition of the earth

Elements	Values%
SiO_2%	58.64
CaO%	20.34
Al_2O_3%	9.709
MgO%	7.728
Fe_2O_3%, MnO%, K_2O%, Na_2O%, TiO_2%, P_2O_5%	3.58

Table 4 Characteristics of the sand crashed

Characterization	Values
Apparent density (kg/m^3)	1.49
Specific density (kg/m^3)	2.67
Fines model (%)	9.29
Sand equivalent (%)	60.22

The soil is intercalated clays generated in significant quantities by exploiting deposits located in El Youssoufia in Morocco, Fig. 1.

The sand used to prepare specimens is crushed sand (0/5). The physical characteristics are grouped in Table 3.

2.2 Preparation of the Specimens

Based on the specimen preparation methodology proposed by Ajouguim et al. (2020), mass percentages of filasse fiber and cement were used in the earth and crushed sand mixture to prepare CEB blocks. The compositions of the different formulations of CEB are shown in Table 1.

3 Results and Discussions

The mechanical and physical properties of the CEB blocks were performed according to the characterization methods detailed by Ajouguim et al. (2020). The mechanical and physical characterization of the CEB bricks prepared are shown in Table 5.

The addition of the fibers led to an increase in compressive strength. This is due to the incorporation of the fibers in the composites, which will prevent the propagation of cracks.

The stabilization of the specimens by cement decreased the moisture content, Bruno et al. (2017) as well as an improvement in the behavior of the specimens with respect to capillarity, Fig. 2. which is a normal result because cement increases moisture resistance.

4 Conclusions

This work has shown the possibility of manufacturing CEB blocks using phosphate waste stabilized by cement and reinforced by filasse fibers. The obtained results allowed for getting interesting mechanical properties. However, the behavior of the porosity remains weak, which leads us to other studies to enhance the behavior of the CEB blocks in the presence of moisture and porosity.

Fig. 1 Visual aspect of the earth studied

Table 5 Mechanical and physical characterization of CEB bricks

Specimens	Mechanical properties				Physical properties
	Compressive strength at 7 days (Mpa)	Compressive strength at 28 days (Mpa)	Young's modulus (Mpa) at 7 days	Young's modulus (Mpa) at 28 days	Absorption test (%)
Ar	3,25	10,57	621,83	590,72	10
ArSa	5,25	9.32	404,9	504,1	5
ArSaF	7,55	19,55	239,37	761,84	4
ArSaC4%	7,06	12,66	487,06	570,6	3
ArSaCF4%	9,50	22,30	301,34	969,19	3,2
ArSaC6%	10,11	12,14	635,41	646,98	4
ArSaCF6%	8,67	27,16	261,15	1108,68	4
ArSaC8%	11,43	13,41	505,6	723,95	3
ArSaCF8%	11,50	31,90	386,61	1241,09	3.1

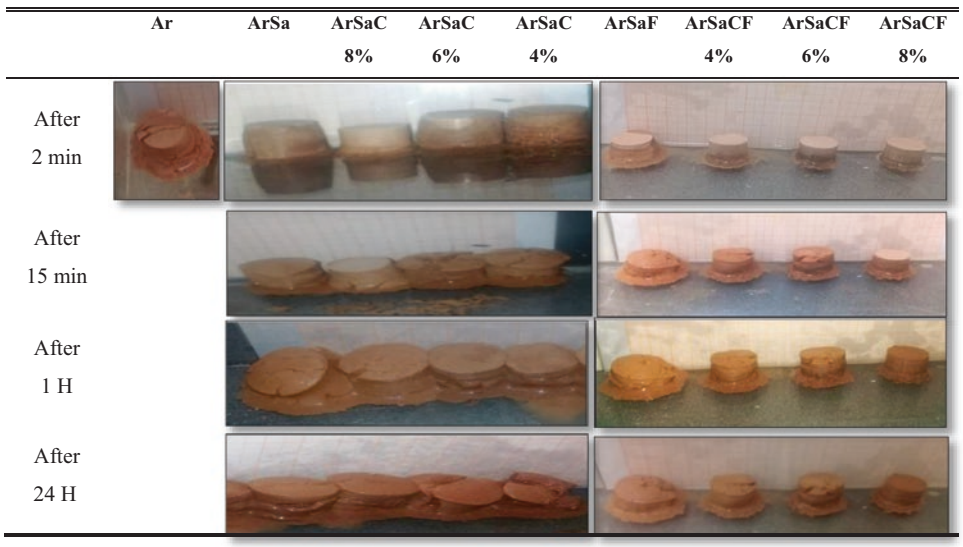

Fig. 2 Results of water absorption by capillarity

References

Abid, R., Kamoun, N., Jamoussi, F., & El Feki, H. (2021). Fabrication and properties of compressed earth brick from local Tunisian raw materials. *Bol la Soc Esp Ceram y Vidr*, 1–11. Published online.

Ajouguim, S., Talibi, S., Djelal-Dantec, C., et al. (2020). Effect of Alfa fibers on the mechanical and thermal properties of compacted earth bricks. Materials Today: Proceedings. Published online.

AMEE Homepage. Retrived from, Jul 30, 2021, http://www.amee.ma

Bruno, A. W., Gallipoli, D., Perlot, C., & Mendes, J. (2017). Effect of stabilisation on mechanical properties, moisture buffering and water durability of hypercompacted earth. *Construction and Building Materials, 149*(September), 733–740.

El Machi, A., Mabroum, S., Taha, Y., Tagnit-Hamou, A., Benzaazoua, M., & Hakkou, R. (2020). Valorization of phosphate mine waste rocks as aggregates for concrete. *Materials Today: Proceedings, 37*, 3840–3846.

Hubert Guillaud, H. H. (2015). Traité de construction en terre. *J des Africanistes*, *60*(1), 165–167.

Transport Process of Microplastics from Terrestrial to Aquatic Environment: Evaluation of the Current Knowledge

Hande Mahide Okutan, Philippe Le Coustumer, Bedri Kurtuluş, and Moumtaz Razack

Abstract

Since the first plastic production at an industrial scale in the 1950s, the importance of plastics in our lives and their production have continued to increase daily. Most of the studies focused on plastic debris accumulation in the marine environment. However, terrestrial environments significantly contribute to the plastic waste abundance of marine and freshwater environments. While investigating the accumulation in these environments, the land-based contamination sources, pathways, and transport mechanisms of plastic debris need to be accounted for to clarify the budget for global plastic contamination. Evaluation of the studies based on the mobility of microplastics (<5 mm) from terrestrial to the aquatic environment is the main concern of this review. Understanding the transport process into soil and soil to the surface and underground freshwater environments is important to emphasize the scale of plastic pollution. Microplastic contamination in the water directly bounds the organism and human health. The importance of microplastic contamination was highlighted by the experimental results of studies in the literature modeling microplastic transport from soil to aquatic environments using different methods. The results showed that salinity has effects on transportation. The maximum penetration depth was found to be ~7.5 cm. At last, the retention and aggregation effects on transport were revealed.

H. M. Okutan (✉) · P. Le Coustumer
Université Bordeaux Montaigne, 33607 Pessac, France
e-mail: hande-mahide.okutan@etu.u-bordeaux-montaigne.fr

H. M. Okutan · B. Kurtuluş
Muğla Sıtkı Koçman University, 48000 Muğla, Türkiye

P. Le Coustumer
Université de Bordeaux, Bordeaux Imaging Center, 33076, Bordeaux, France

M. Razack
University of Poitiers, IC2MP, 86073 Poitiers Cedex, France

Keywords

Microplastic · Terrestrial · Freshwater · Transport

1 Introduction

Plastics have become indispensable daily with their easy accessibility and long-term use. At the same time, this abundant usage and long life caused them to be encountered frequently as a pollutant in the environment. Plastics are lightweight, durable, and relatively resistant to decay, making them not only low-cost and preferable to use but also difficult to recover and recycle in the environment (Corcoran et al., 2017; O'Connor et al., 2019).

Microplastics (MPLs) result from the fragmentation of large pieces of plastics or are produced as pellets of size inferior to 5 mm. Primary MPLs are directly manufactured to be integrated with many daily life products. They are commonly used in personal care, detergents, and hygiene products. Secondary MPLs are fragmented from a larger plastic source. This fragmentation and gradual deterioration can be due to ultraviolet radiation-based photodegradation, mechanical abrasion, and biological effects (Sul & Costa, 2014; Wu et al., 2019). Primary MPLs generally exist as Polyethylene (PE), Polystyrene (PS), and Polypropylene (PP) type of polymers. Secondary MPLs can be found in kinds of many polymers (Birch et al., 2020). The size definition of MPLs is the plastic particles in the millimeter size to sub-millimeter size range and can be referred to as smaller than 5 mm (GESAMP, 2015; Maharana et al., 2020).

The source of plastic contaminations can be caused directly being pollutants in oceans like abandoned or loss of fishing gear (Barboza et al., 2019), or they can be transported from terrestrial sources. Most plastic litter sources are inland and introduced into oceans by rivers and used waters. Therefore, their pathways from the terrestrial environment have vital importance (Hurley & Nizzetto, 2018).

A. Çiner et al. (eds.), *Recent Research on Environmental Earth Sciences, Geomorphology, Soil Science, Paleoclimate, and Karst*, Advances in Science, Technology & Innovation, https://doi.org/10.1007/978-3-031-42917-0_13

Recent studies pointed out the presence of the MPLs in terrestrial, surface, and underground freshwater environments (Horton et al., 2017; Hurley & Nizzetto, 2018). Therefore, understanding the soil to surface and subterranean water transport mechanisms and their properties of terrestrial source-based plastic pollutants is important to emphasize the scale of the plastic pollution in the water and its effects.

This study aims to create a short report assessing the current studies, which know the MPL transport, based on terrestrial sources to aquatic environments.

2 Transport Processes of Microplastic Particles

The total plastic production from 1950 to 2015 was estimated to be 8300 million tons, and it is thought that approximately 60% of this production was discharged as plastic waste (Geyer et al., 2017). Although terrestrial systems are the source of the MPL contaminants, fluvial systems are the pathways for transporting contaminants to marine environments (Frei et al., 2019).

The effect of different salinities in transporting different sizes of MPL particles was experimented with in column tests in saturated porous media collected from the seafloor. Salinity levels were important to show the behavior of the MPLs in the estuarine regions with various salinity gradients. The preferred MPL type is PE; the used sizes were 0.1–2 μm—the effect of the salinity strongly bonded with the size of the MPLs. As a result, the particles' mobility increased while decreasing the salinity and particle size (Dong et al., 2018).

There is a study based on vertical MPL penetration in a saturated–unsaturated porous medium and models the effect of the precipitation in column experiments. The porous media consisted of sand (<2 mm). Different densities and sizes of PE and PP particles were used. The particle size changes between 535 and 21 μm. The experiment was implemented with a wet-dry cycle, and the precipitation, resampled as low ionic strength rainwater, was simulated with 1000 mm annual rainfall with 12 infiltration events. The results showed that the traveling depth of PP, which was 29 μm, was ~1.5 cm, which penetrated less depth than PE, depending on the major difference between them, which is density. The maximum penetration level of larger PE particles (349 μm, 181 μm, 535 μm) was ~3.5 cm. The smallest size of PE, which was 21 μm, was detected as the most mobile particle with ~7.5 cm travel depth. Forecasting historical weather data adapted the laboratory penetration results to 347 cities across China. The vertical penetration depth of the MPLs was estimated at 5.24 m in 100 years, depending on the groundwater level. The results showed that exposing MPLs from soil to groundwater is inevitable (O'Connor et al., 2019).

In transport modeling on rivers, the fate of the micro- and nano plastic particles was analyzed. Attachment efficiency between microplastic, nano plastic, and clays was determined in an aggregation-sedimentation experiment in the laboratory environment. Obtained attachment efficiency was used to model the hydrodynamic behavior of particles accounting for the parameters of advective transport, particle aggregation, sedimentation, resuspension, polymer degradation, and burial. Nearly spherical polymer particles sized 100 nm to 10 mm were used, and biofilm formation was considered. The results showed that rivers were the transport pathway of the micro and nano plastics and accumulation zones. 1–800 μm range of particles can be divided into classes depending on different achieved mobility results. The lower end of the range is more mobile than the higher end, which can be found in the river sediments depending on the effect of retention and low mobility. Nanometer- and millimeter-sized particles are more prone to retention than micro-sized particles exposed to marine and coastal areas and transported by rivers. The study also showed that the effects of biofilm formation are low on particle fate (Besseling et al., 2017).

3 Conclusion

Understanding the influencing properties of transport mechanisms of the behavior of microplastics in the environment is crucial for identifying potential microplastic fate-transport pathways from source to accumulation. Managing the reduction of the MPL pollution and their risks is also crucial. This progress can be performed efficiently by identifying the behaviors of MPL pollutions and their transport mechanism from soil to water bodies. The studies modeled the movement of various MPLs, concentration, size, flow rate, and salinity to understand the environmental impact of the MPL pollutants (Dong et al., 2018; Goeppert & Goldscheider, 2021; O'Connor et al., 2019).

This study emphasizes the recent findings of the transport behavior of MPLs into the soil and possible movements to water, which were modeled with laboratory experiments and predicted the results with field measurements. There is a possibility of vertical transportation of plastic contamination into groundwater, the largest freshwater source (O'Connor et al., 2019). The experiments pointed out that the movement of particles in low-salinity waters is faster than in high-salinity waters (Dong et al., 2018). The fluvial systems are both accumulation zones and agents (Besseling et al., 2017).

References

Barboza, L. G. A., Cózar, A., Gimenez, B. C. G., Barros, T. L., Kershaw, P. J., & Guilhermino, L. (2019). Macroplastics pollution in the marine environment. In C. Sheppard (Ed.), *World seas: An environmental evaluation*. (pp. 305–328). Academic Press.

Besseling, E., Quik, J. T. K., Sun, M., & Koelmans, A. A. (2017). Fate of nano- and microplastic in freshwater systems: A modeling study. *Environmental Pollution, 220*, 540–548. https://doi.org/10.1016/j.envpol.2016.10.001

Birch, Q. T., Potter, P. M., Pinto, P. X., Dionysiou, D. D., & Al-Abed, S. R. (2020). Sources, transport, measurement and impact of nano and microplastics in urban watersheds. *Reviews in Environmental Science and Bio/Technology, 19*, 275–336. https://doi.org/10.1007/s11157-020-09529-x

Corcoran, P. L., Jazvac, K., & Ballent, A. (2017). *Plastics and the anthropocene*. Elsevier Inc.

Dong, Z., Qiu, Y., Zhang, W., Yang, Z., & Wei, L. (2018). Size-dependent transport and retention of micron-sized plastic spheres in natural sand saturated with seawater. *Water Research, 143*, 518–526. https://doi.org/10.1016/j.watres.2018.07.007

Frei, S., Piehl, S., Gilfedder, B. S., Löder, M. G. J., Krutzke, J., Wilhelm, L., & Laforsch, C. (2019). Occurence of microplastics in the hyporheic zone of rivers. *Science and Reports, 9*, 15256. https://doi.org/10.1038/s41598-019-51741-5

GESAMP. (2015). Sources, fate and effects of microplastics in the marine environment: A global assessment.

Geyer, R., Jambeck, J. R., & Law, K. L. (2017). Production, use, and fate of all plastics ever made. *Science Advances*, *3*, 25–29 (2017). https://doi.org/10.1126/sciadv.1700782

Goeppert, N., & Goldscheider, N. (2021). Experimental field evidence for transport of microplastic tracers over large distances in an alluvial aquifer. *Journal of Hazardous Materials, 408*, 124844. https://doi.org/10.1016/j.jhazmat.2020.124844

Horton, A. A., Walton, A., Spurgeon, D. J., Lahive, E., & Svendsen, C. (2017). Microplastics in freshwater and terrestrial environments: Evaluating the current understanding to identify the knowledge gaps and future research priorities. *Science of the Total Environment, 586*, 127–141. https://doi.org/10.1016/j.scitotenv.2017.01.190

Hurley, R. R., & Nizzetto, L. (2018). Fate and occurrence of micro(nano)plastics in soils: Knowledge gaps and possible risks. *Current Opinion in Environmental Science & Health, 1*, 6–11. https://doi.org/10.1016/j.coesh.2017.10.006

Maharana, D., Saha, M., Dar, J. Y., Rathore, C., Sreepada, R. A., Xu, X. R., Koongolla, J. B., & Li, H. X. (2020). Assessment of micro and macroplastics along the west coast of India: Abundance, distribution, polymer type and toxicity. *Chemosphere*, *246*, 125708. https://doi.org/10.1016/j.chemosphere.2019.125708

O'Connor, D., Pan, S., Shen, Z., Song, Y., Jin, Y., Wu, W., & Hou, D. (2019). Microplastics undergo accelerated vertical migration in sand soil due to small size and wet-dry cycles. *Environmental Pollution, 249*, 527–534. https://doi.org/10.1016/j.envpol.2019.03.092

Do Sul, J. A. I., & Costa, M. F. (2014). The present and future of microplastic pollution in the marine environment. *Environmental Pollution*, *185*, 352–364. https://doi.org/10.1016/j.envpol.2013.10.036

Wu, P., Huang, J., Zheng, Y., Yang, Y., Zhang, Y., He, F., Chen, H., Quan, G., Yan, J., Li, T., & Gao, B. (2019). Environmental occurrences, fate, and impacts of microplastics. *Ecotoxicology and Environmental Safety, 184*, 109612. https://doi.org/10.1016/j.ecoenv.2019.109612

Quantification and Identification of Marine Litter on Five Beaches of the North-Central Algerian Coast

Yousra Ghezali, Boualem Hamdi, Shernai Safia, and Setiti Skander

Abstract

Plastics are primary marine pollutants that significantly threaten the environment, contaminating every part of the globe. As a result, litter is abandoned alongside the Algeria coastline. The most common litter includes plastic fragments, fishing gear, and packaging. About 90% of recorded items are plastic. The impacts of this pollution are still unknown, especially from microplastic levels. In this study, macro- and microplastics were sampled on several beaches on the Algerian coast to estimate their concentration. The orientation, degree of use, and slope of each beach and the distance from the large urban area were all measured to state their contribution to the accumulation of marine litter. Plastic litter along the coast was studied using a monitoring approach for identifying, collecting, and quantifying plastic debris. We used attenuated total reflection Fourier transformed (ATR-FTIR) spectroscopy to identify our samples. Two thousand two hundred and thirty-seven plastic particles were collected from different sampling points on the five beaches studied. Our samples contain 698 pieces >5 mm, 920 pieces are 4–5 mm, 532 pieces are 3–4 mm, 68 pieces are 2–3 mm, and 19 pieces are 1–2 mm were the most abandoned types of polymer. Polyethylene (PE), polypropylene (PP), polystyrene (PS), polyethylene terephthalate (PET), PVC, and NYLON accounted for 67%, 21%, 5%, 4%, and 3%, respectively.

Keywords

Microplastic · Pollution · Sediment · FT-IR · Algiers Bay

1 Introduction

Plastic pollution is one of the world's most pressing environmental issues. However, over the past decade, approximately 12 metric tons have been leaking into our oceans annually, and there has been significant attention to macro-litter (Microplastic Pollution: The Policy Context - Background Paper). As a result, scientists believe microplastics (plastics < 5 mm) are a considerable concern and consider them hazardous substances. Of the nearly 300 recognized impacts on wildlife from marine litter, over 70% can be attributed to microplastics (Plastic Strategy, 2018). They are especially dangerous as they can move through the food chain, creating compounded effects of their dangers (Plastic Strategy, 2018). Yet, little is known about microplastic levels or their impacts in Algeria.

Algeria is a transforming country and not a producer of plastic. The recovery activity represents only 7% of the plastic consumed. In 2019, Algeria became the world's fifth largest consumer of plastic bags after the United States of America, Morocco, France, and Italy, with 6.5 to 7 billion plastic bags per year (Pollution in the Middle East & North Africa; The plastic in the Mediterranean Sea, 2018). The estimation of plastic litter per year is 17332 tons, and due to a failing recycling industry, 60–80% of waste is dumped into the marine environment (The plastic in the Mediterranean Sea, 2018).

Microplastic pollution is considered an emergency crisis. Therefore, the main objective of this study is to conduct primary research on microplastics on several beaches and validate the hypothesis that there is a positive correlation between microplastic concentrations and particle size along the beach profile.

Y. Ghezali (✉) · B. Hamdi · S. Safia · S. Skander
Laboratory of the Conservation and Development of Marine Resources, ENSSMAL, B919 Campus Universitaire, 16320 Dely Ibrahim, Algiers, Algeria
e-mail: g.yousra92@gmail.com

A. Çiner et al. (eds.), *Recent Research on Environmental Earth Sciences, Geomorphology, Soil Science, Paleoclimate, and Karst*, Advances in Science, Technology & Innovation, https://doi.org/10.1007/978-3-031-42917-0_14

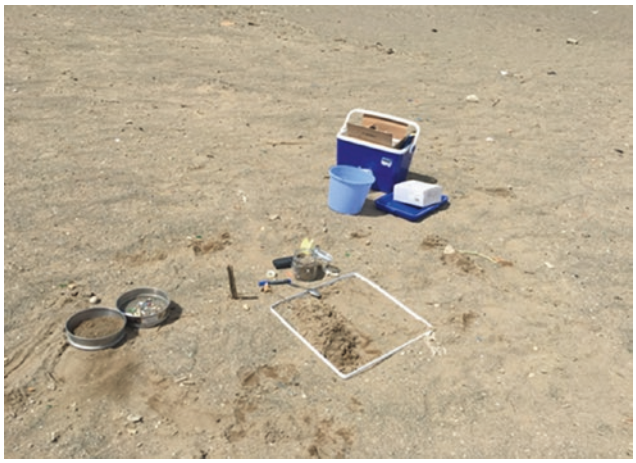

Fig. 1 Sampling images in sites

Fig. 2 FT-IR spectroscopy in use

2 Materials and Methods

Several field trips were made during January, March, April, June, and July 2019 to carry out sampling campaigns on the beach sediments using the Transect-Quadrat method (www.arocha.org/wp-content/uploads/2018/01/Microplasticsbibliography.pdf). This method consists of a uniform distribution of 10 lines perpendicular to the shore (transect), separated by a minimum of 10 m (Fig. 1).

2.1 Study Area

Five different areas were selected from the Algerian coastline as follows:

1. Beach with intense fishing activity
2. Beach with low fishing pressure
3. Beach with touristic activity
4. Beach near a disposal site
5. High biodiversity beach.

We had chosen one day before and one day after a storm and then used a quadrat of 50/50 cm for field trips. We collected the upper 2 cm surface layer and used sieves, which retain all that is <5 mm microplastic. The samples were kept at −4 °C. We used a binocular magnifier and NaCl for density separation for the quantification. Finally, FT-IR spectroscopy is used to identify the polymer type (Fig. 2).

3 Results

3.1 Analyzing Microplastic from Sediment

Using the data collected from the 25 samples of coastal sediments, the preliminary results state that all microplastics identified were from a "secondary" origin.

Fragments and fibers constitute most of the samples (71–81%), preceded by films (5–23%) (Fig. 3).

We enumerated 2237 pieces of plastic from various sampling points on the surveyed beaches: 698 pieces >5 mm, 920 pieces 4–5 mm, 532 pieces 3–4 mm, 68 pieces 2–3 mm, and 19 pieces 1–2 mm.

3.2 Microplastics Identification

- We used the FT-IR spectrometer to identify and document the chemical classification of plastics we found.
- The microplastic samples are placed under the FT-IR instrument, which uses infrared radiation to determine the types of polymer present in the samples.
- The most abandoned types of polymers detected were polyethylene (PE), polypropylene (PP), polystyrene (PS), polyethylene terephthalate (PET), PVC, and NYLON accounting for 67%, 21%, 5%, 4%, and 3%, respectively.
- The identification of polymer types was determined by comparing resulting spectra samples with a reference

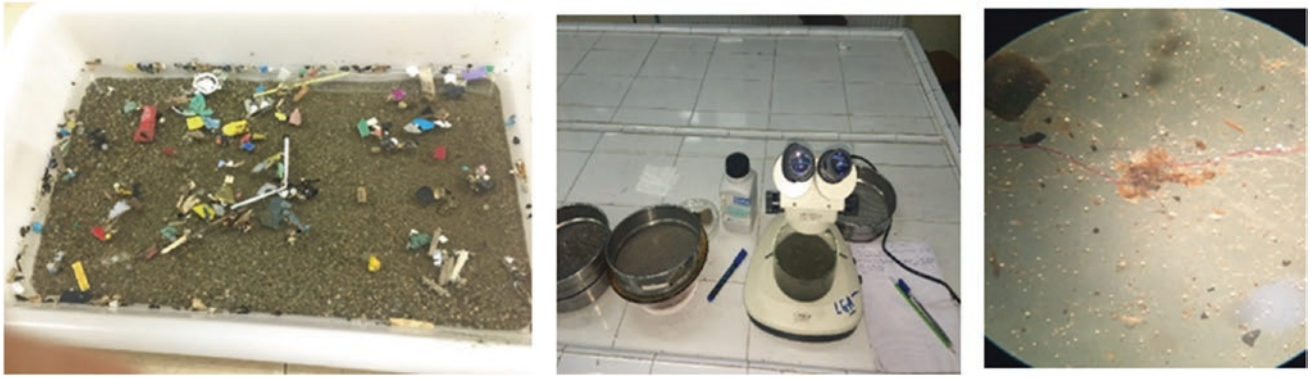

Fig. 3 Images showing the lab work to separate MPs from sediment and quantify them using a binocular magnifier

database, which helped us select the origin of our samples and identify the potential sources of these microplastics. This research study collaborates with oceanographers who study the currents so we can identify where the plastics may have come from.

4 Discussion

The preliminary results of our study show that microplastics are pervasive in beach sediments along the Algerian coast. The primary sources of plastic debris found on Algiers coastal beaches were land-based activities (such as commercial practices, agricultural and manufacturing practices, and tourist' litter and waste disposal). On the other hand, we also have sea-based fishing activities. Fragments were the most common shape type of microplastics (in terms of number), followed by Pellets and Fibers. PE, PP, PVC, and PS are recognized as fragments. PE or PP is used to manufacture pellets. PE, PP, and Nylon are confirmed as fibers. FT-IR spectroscopy analysis indicated that most plastics were polyolefins, which are plastic resins with a specific gravity of less than one, permitting them to be positively buoyant and quickly deposited on beaches (Andrady, 2011). This is not surprising because PE, with a global annual production of about 80 million tonnes, is predominantly used in packaging (plastic films, containers including bottles, and plastic bags).

Furthermore, with a total global production of around 55 million tonnes, PP is primarily used for food packaging, in the textiles industry, rope manufacturing, and reusable containers. In the beach sediments, the plastic debris is due to continuous degradation regarding deposition and weathering. Beaches are better settings than other natural environments for the breakdown of plastic waste (Andrady, 2011). Hence, the plastic debris found on the five beaches will continue to fragment into smaller ones, making it easier for those tiny particles to disperse due to wind and tide movement, entering the food chain into the big ocean.

5 Conclusions

- The samples taken from five beaches on the Algerian coast revealed a high microplastic content above the high tide line, located on shores that are not periodically cleaned and suffer from intense microplastic debris episodes.
- The microplastic content of those different beaches is comparable, or even higher, to those found in previous studies all along the Mediterranean Sea. This suggests a prominent need to develop periodical monitoring programs for further studies.
- Most microplastics obtained were fragments of PP, PE, PET, and PS (FT-IR was used for microplastic characterization) which is also in accordance with global plastic production.
- Plastic pollution knows no border. Instead, plastics travel from one country to another with **marine currents**, highlighting the need for a **regional and collaborative approach**.

References

Andrady, A. L. (2011). Microplastics in the marine environment. *Marine Pollution Bulletin, 62*(8), 1596–1605. https://doi.org/10.1016/j.marpolbul.2011.05.030

Microplastic Pollution: The Policy Context - Background Paper, *The scientific advice mechanism unit of the European commission*, 68 p. web version.

Plastic Strategy. (2018). A European strategy for plastics in a circular economy. In *Communication from the commission to the European parliament, the council, the European economic and social committee and the committee of the regions*. Brussels, January 16th 2018 COM. Available online: https://www.ec.europa.eu/environment/circular-economy/pdf/plastics-strategy.pdf

Pollution in the Middle east and north Africa: Pollution in Algeria April 9th, 2019.

The plastic in the Mediterranean Sea. (2018). Report. www.arocha.org/wp-content/uploads/2018/01/Microplasticsbibliography.pdf

Determination of Critical Self-Ignition Temperature of Tropical Peat Land: A Case Study from Indonesia

Krison V. Manulu, Ferian Anggara, Kyuro Sasaki, and S. S. Rita Susilawati

Abstract

Peat is a combustible material, and peat fire may be initiated by self-heating that triggers spontaneous combustion in some conditions. Therefore, peat type and volume are expected to correlate with the Critical Self-Ignition Temperature (CSIT) value. Eight samples used in this experiment represent hemic and sapric peats. This study uses a 5 cm wire-mesh basket to examine the CSIT value for each sample. Peat was heated at a constant ambient temperature (T_E) using a designated oven. Different T_E values were used to find the subcritical and supercritical conditions. Once these two conditions are obtained, the CSIT value is interpolated from the value between these two T_E. The results of the experiments show all of the samples start to self-ignite at 170 °C, and we can conclude that there is no significant correlation between the type of peat and its CSIT value. To up-scale the calculation into the larger peat volume, a trend on the book versus CSIT diagram was used to interpolate the CSIT value for thicker peat layers and conclude that 8 m of peat thickness with 10% of inorganic content and<50% of moisture may be ignited at a temperature less than 50 °C. The result of this study could be used as preliminary data on the surface temperature that may induce spontaneous combustion.

Keywords

Peat · Spontaneous combustion · CSIT

1 Introduction

Peat is defined as soils deposited in mires with>17% of organic content and>40 cm of thickness (Wüst et al., 2003), and then peatlands all over the topic and sub-tropic areas known as tropical peatlands (Andriesse, 1988). Indonesia is an attractive peat-related study area, with the most significant low peatland area in the world (21 of 44 million ha), and also has the largest share of tropical peatland carbon pool (57 of 89 Gt) (Osaki & Tsuji, 2018; Page et al., 2011). When peatland degradations occur, much CO_2 is released into the atmosphere. From 2000 until 2018, peatland fires in Indonesia produced 4.3 Gt CO_2, which became the second most significant contributor of greenhouse gases after the combustion of fossil fuel (KLHK, 2019). Since peat is a combustible material, some peat fire cases were caused by spontaneous combustion phenomenon (Kim et al., 2014; Onifade & Genc, 2018, 2019; Ramadhan et al., 2017; Restuccia et al., 2017).

Furthermore, spontaneous combustion was related to the CSIT, the minimum ambient temperature (T_E) to trigger the ignition (Wang et al., 2017). A lot of studies on CSIT were conducted to determine the key factors affecting the CSIT using coal and peat, i.e., volume, moisture, inorganic material, H/C ratio, and others (Frandsen, 1997; Huang et al., 2015; Kaymakçi & Didari, 2002; Küçük et al., 2003; Moroeng et al., 2017; Onifade & Genc, 2020; Restuccia et al., 2017; Rifella, 2019; Wang et al., 2017, 2019). However, no data on CSIT value in Indonesian tropical peatlands is available. Furthermore, the correlation between peat type to their CSIT value will be examined in this study.

K. V. Manulu
Undergraduate Program, Department of Geological Engineering, Universitas Gadjah Mada, Yogyakarta, Indonesia

F. Anggara (✉)
Department of Geological Engineering, Universitas Gadjah Mada, Yogyakarta, Indonesia
e-mail: ferian@ugm.ac.id

Unconventional Geo-Resources Research Group, Universitas Gadjah Mada, Yogyakarta, Indonesia

K. Sasaki
Department of Earth Resources, Kyushu University, Fukuoka, Japan

S. S. R. Susilawati
Center for Mineral, Coal, and Geothermal Resources, Geological Agency, Bandung, Indonesia

A. Çiner et al. (eds.), *Recent Research on Environmental Earth Sciences, Geomorphology, Soil Science, Paleoclimate, and Karst*, Advances in Science, Technology & Innovation, https://doi.org/10.1007/978-3-031-42917-0_15

2 Materials and Methods

Peat samples used in this study are from Sungai Punggurbesar—Sungai Kapuas Peatland Hydrological Unit (PHU), West Kalimantan, Indonesia. Samples are collected by the Center for Mineral, Coal, and Geothermal Resources, Geological Agency, and the proximate and ultimate analysis. Samples were classified by their decomposition degree to examine the correlation between peat type and their composition with the CSIT value. The moisture content from each model was recalculated before the experiments, and the samples were stored in the freezer to maintain their moisture.

The experiments to determine the CSIT were conducted on a $5 \times 5 \times 5$ cm wire-mesh basket that was put in the designated oven with a thermocouple attached to monitor the temperature, as shown in Fig. 1a. The samples were placed in the basket inside the oven and heated with a constant T_E value. When the samples' temperature was increasing and approaching the ambient temperature, there were two possibilities regarding the trend between temperature versus time; it would stay close to the ambient temperature, known as the subcritical condition, or it would be accelerated and overshoot the ambient temperature, known as the supercritical condition (see Fig. 1d, e). Different T_E values would result in other trends. CSIT was projected as the temperature between two T_E values that satisfied subcritical and supercritical conditions. The smaller the gap between those two temperatures, the CSIT value would be more accurate.

3 Results

After getting T_E values for each condition at each sample, CSIT values were obtained. As shown in Table 1, there is no significant variation in CSIT values.

Peat types were classified by running the squeeze test to get the decomposition degree referred to as von Post scale. The result of the peat type classification is also presented in Table 1.

4 Discussion

The CSIT value shows identical results on different peat types and their properties from the studied area. It may be due to the small number of samples during the experiments or the exact composition of the models.

Thus, up-scaling was conducted to mimic the natural condition, mainly focusing on the peat thickness. The term up-scaling is limited to the peat thickness without

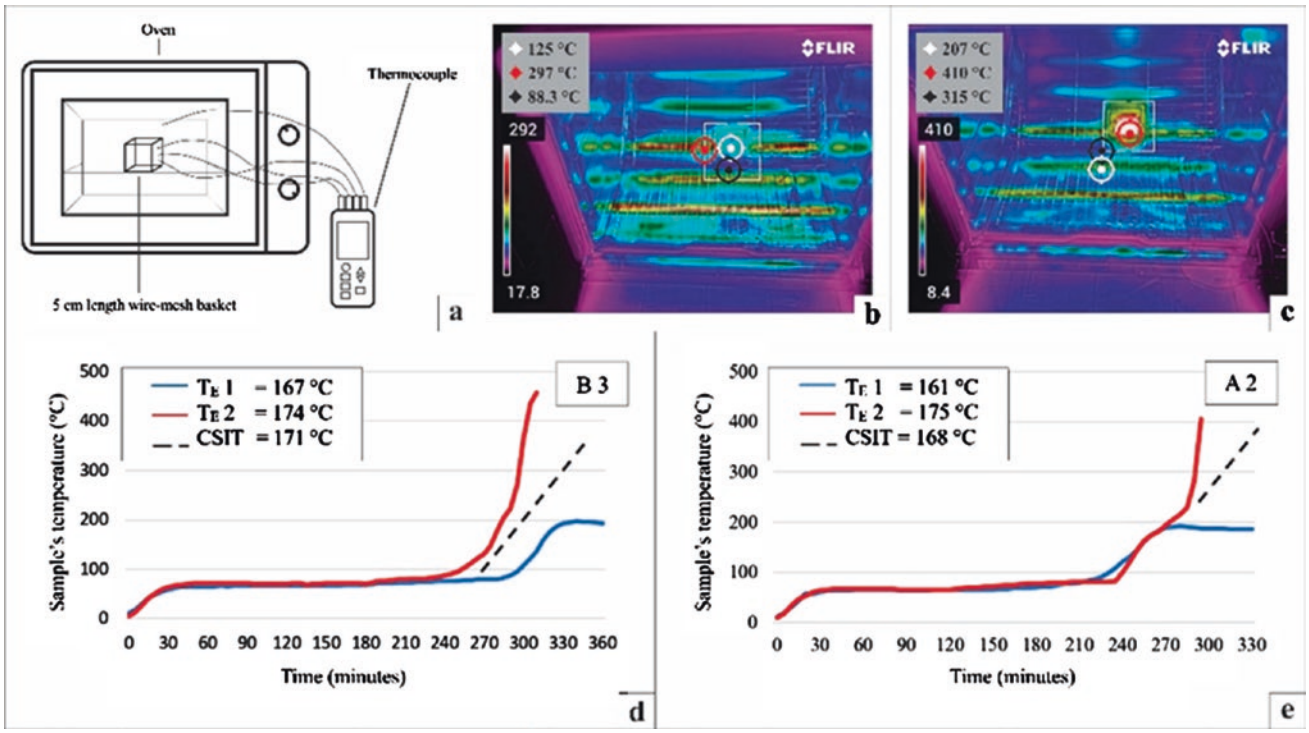

Fig. 1 **a** Experimental apparatus used to determine CSIT value, **b** sample on heat generation stage, **c** sample on supercritical condition, **d** determination of CSIT on sample B 3, and **e** determination of CSIT on sample A 2

Table 1 CSIT value for each sample in 5 cm length cubic

Sample's code	Peat type	von post scale	Moisture content (%)	Inorganic content (%)	CSIT value (±5 °C) (°C)
A1	Hemic	H5	44	17	169
A2	Sapric	H8	50	3	168
B1	Hemic	H7	52	2	169
B2	Hemic	H6	44	1	171
B3	Hemic	H6	48	11	171

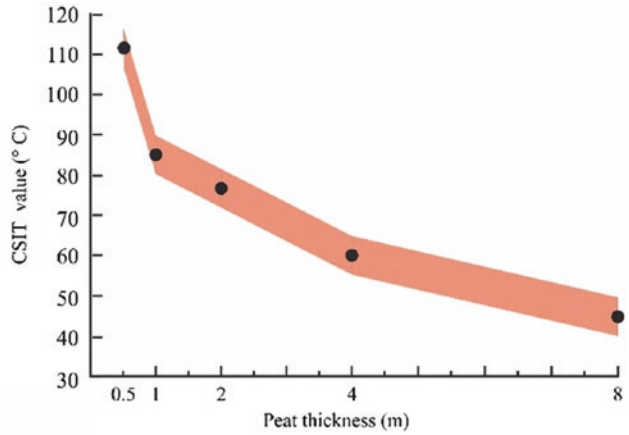

Fig. 2 CSIT values on larger peat thickness

considering a lot of complex factors that exist in nature. This study adopts the trendline from Restuccia et al. (2017), who run CSIT experiments on peat samples with varied volumes (Restuccia et al., 2017). Assuming that models were always cube-shaped, then the book was converted to thickness. Figure 2 shows the result of CSIT values on some larger peat thicknesses.

Based on Frandsen (Frandsen, 1997) and Huang et al. (2015), moisture and inorganic content are the main controlling factors on spontaneous combustion aside from ambient temperature. Combustion will occur if the peat's moisture and inorganic content don't exceed the threshold. Otherwise, there is no spontaneous combustion. Peat with less than 10% IC can be combusted in under 50% moisture content.

5 Conclusions

Based on the result of experiments, peat with 5 cm of thickness starts to self-ignite at 163–175 °C. This range applies to both hemic and sapric since there is no strong correlation between those decomposition degrees with CSIT values. Therefore, the projection on peat thickness and CSIT value estimate that a peat 8 m thick or more has a CSIT value of less than 50 °C.

Moisture and inorganic content have an essential role in ensuring that spontaneous combustion can happen or not. For example, peat with less than 10% inorganic content may self-ignite if its moisture value is under 50%.

References

Andriesse, J. P. (1988). Nature and management of tropical peat soils. *FAO Soils Bulletin*.

Frandsen, W. H. (1997). Ignition probability of organic soils. *Canadian Journal of Forest Research, 27*(9), 1471–1477. https://doi.org/10.1139/x97-106

Huang, X., Rein, G., & Chen, H. (2015). Computational smoldering combustion: Predicting the roles of moisture and inert contents in peat wildfires. *Proceedings of the Combustion Institute, 35*(3), 2673–2681. https://doi.org/10.1016/j.proci.2014.05.048

Kaymakçi, E., & Didari, V. (2002). Relations between coal properties and spontaneous combustion parameters. *Turkish Journal of Engineering and Environmental Sciences, 26*(1), 59–64. https://doi.org/10.1016/s0140-6701(03)90480-2

Kim, J. K., Lee, H. D., Kim, H. S., Park, H. Y., & Kim, S. C. (2014). Combustion possibility of low rank Russian peat as a blended fuel of pulverized coal fired power plant. *Journal of Industrial and Engineering Chemistry, 20*(4), 1752–1760. https://doi.org/10.1016/j.jiec.2013.08.027

KLHK. (2020). *Inventarisasi gas Rumah Kaca (GRK) dan monitoring, Pelaporan*, Verifikasi (MPV) 2019.

Küçük, A., Kadioğlu, Y., & Gülaboğlu, M. Ş. (2003). A study of spontaneous combustion characteristics of a Turkish lignite: Particle size, moisture of coal, humidity of air. *Combustion and Flame, 133*(3), 255–261. https://doi.org/10.1016/S0010-2180(02)00553-9

Moroeng, O. M., James Roberts, R., Bussio, J. P., & Dixon, R. D. (2017). Self-heating potential of coal inferred from elemental data: A case study of the witbank coalfield of South Africa. *Energy and Fuels*, *31*(11), 11811–11817. https://doi.org/10.1021/acs.energyfuels.7b02109

Onifade, M., & Genc, B. (2020). A review of research on spontaneous combustion of coal. *International Journal of Mining Science and Technology*, 1–9. https://doi.org/10.1016/j.ijmst.2020.03.001

Onifade, M., & Genc, B. (2018). Spontaneous combustion of coals and coal-shales. *International Journal of Mining Science and Technology*. https://doi.org/10.1016/j.ijmst.2018.05.013

Onifade, M., & Genc, B. (2019). Spontaneous combustion liability of coal and coal-shale : A review of prediction methods. *International Journal of Coal Science & Technology, 6*(2), 151–168. https://doi.org/10.1007/s40789-019-0242-9

Osaki, M., & Tsuji, N. (2015). *Tropical peatland ecosystems* (pp. 1–651). https://doi.org/10.1007/978-4-431-55681-7

Page, S. E., Rieley, J. O., & Banks, C. J. (2011). Global and regional importance of the tropical peatland carbon pool. *Global Change Biology, 17*(2), 798–818. https://doi.org/10.1111/j.1365-2486.2010.02279.x

Ramadhan, M. L., Palamba, P., Imran, F. A., Kosasih, E. A., & Nugroho, Y. S. (2017). Experimental study of the effect of water spray on the spread of smoldering in Indonesian peat fires. *Fire Safety Journal, 91*, 671–679. https://doi.org/10.1016/j.firesaf.2017.04.012

Restuccia, F., Huang, X., & Rein, G. (2017). Self-ignition of natural fuels: Can wildfires of carbon-rich soil start by self-heating? *Fire Safety Journal, 91*(March), 828–834. https://doi.org/10.1016/j.firesaf.2017.03.052

Rifella, A. (2019). The effects of coal particle size on spontaneous combustion characteristics. *International Journal of Coal Preparation and Utilization*, 1–25. https://doi.org/10.1080/19392699.2019.1622529

Wang, Y., Zhang, X., Sugai, Y., & Sasaki, K. (2017). Determination of critical self-ignition temperature of low-rank coal using a 1 m wire-mesh basket and extrapolation to industrial coal piles. *Energy and Fuels, 31*(7), 6700–6710. https://doi.org/10.1021/acs.energyfuels.7b00409

Wang, Y., Zhang, X., Zhang, H., & Sasaki, K. (2019). Effects of temperature gradient and particle size on self-ignition temperature of low-rank coal excavated from inner Mongolia, China. *Royal Society of Open Science*, *6*(9). https://doi.org/10.1098/rsos.190374

Wüst, R. A. J., Bustin, R. M., & Lavkulich, L. M. (2003). New classification systems for low organic-rich deposits based on studies of the Tasek Bera Basin, Malaysia. *Catena, 53*(2), 133–163. https://doi.org/10.1016/S0341-8162(03)00022-5

Impact of Lockdown on Air Pollutant Variation in Metropolitan Cities

Pallavi Pradeep Khobragade and Ajay Vikram Ahirwar

Abstract

In early 2020, the COVID-19 pandemic swept the globe. In many countries, the complete lockdown resulting from the COVID-19 outbreak helped improve air quality, particularly in developing countries such as India. The main aim of the study is to assess the variation in AOD and various atmospheric pollutants such as $PM_{2.5}$, PM_{10}, NO_2, SO2, and O_3 before and after the lockdown. The data source used for the current study includes MODIS-Aqua, OMI, and ground-based monitoring data gathered from Central Pollution Control Board (CPCB). Time-averaged maps of Aerosol Optical Depth (AOD) at 500 nm, daily 1° [OMI OMAERUVd v003], and at 550 nm (Deep Blue, Land-only) daily 1° [MODIS-Aqua MYD08_D3 v6.1] were plotted on NASA's Giovanni during 2010–2020. The data was extracted during the lockdown phases in India from March 25, 2020, to May 17, 2020. During the same period, changes in mean AOD were assessed during 2010–2019. Significant reductions were observed in mean AODs. Similarly, changes in the concentration of other pollutants were observed in the study areas during COVID. Fluctuations in the contaminants have also resulted from changes in meteorological conditions; hence, the impact of wind speed, temperature, and humidity are also studied on changing pollutant concentrations. This is owing to a reduction in local emissions resulting from anthropogenic activities due to the pandemic-control lockdown procedures. This work aids in visualizing pollutant responses in metropolitan cities as a result of reduced anthropogenic emissions, which can aid in developing atmospheric governance strategies.

Keywords

AOD · COVID-19 · Air pollutants · Metropolitan cities

1 Introduction

COVID-19, a novel coronavirus, was initially discovered in December 2019 and has since spread around the globe (Prakash et al., 2021; Verma & Kamyotra, 2021). Public isolation and lockdown resulted in a considerable reduction in global air pollution emissions (Bao & Zhang, 2020; Pal et al., 2021; Yadav et al., 2020).

This research looks at how air pollutant levels changed in India's six megacities based on ground and space-derived data during the COVID-19 shutdown compared to the previous years under typical conditions.

2 Research Area and Data Sources

The study area counts six megacities of India and time-averaged maps of Aerosol Optical Depth (AOD) at 500 nm, daily 1° [OMI OMAERUVd v003], and at 55 nm (Deep Blue, Land-only) daily 1° [MODIS-Aqua MYD08_D3 v6.1] were plotted on NASA's Giovanni during 2010–2020. A dataset spanning five primary types of air contaminants, including $PM_{2.5}$, PM_{10}, NO_2, SO_2, and O_3, makes up the air quality data obtained from Central Pollution Control Board (CPCB). Meteorological data were obtained from www.worldweatheronline.com.

P. P. Khobragade (✉) · A. V. Ahirwar
National Institute of Technology, Raipur, Chhattisgarh, India
e-mail: khobragadepallavi19@gmail.com

A. Çiner et al. (eds.), *Recent Research on Environmental Earth Sciences, Geomorphology, Soil Science, Paleoclimate, and Karst*, Advances in Science, Technology & Innovation, https://doi.org/10.1007/978-3-031-42917-0_16

3 Results

3.1 Differences in the Concentrations of Aerosols and Trace Gases

Table 1 shows the difference in AOD concentrations in the megacities, and estimates from the OMI satellite and the MODIS model revealed a considerable decrease in column AOD. A mean reduction in AOD in all the megacities is −0.42%, as estimated by OMI and −0.06% by MODIS. The alteration in pollutants in lockdown was compared to the mean daily pollutants of earlier accessible years to present a comparative measurement of relative improvement in comparison to pre-lockdown circumstances (2018–2019, all through megacities).

Pollutant emissions in the atmosphere such as $PM_{2.5}$, PM_{10}, NO_2, SO_2, and O_3 changed during the lockdown phase up to −71%, NA, −66%, −35%, −13% in Ahmedabad, −40%, −51%, −72%, 52%, 32% in Bangalore, −56%, −65%, −79%, −34%, 59% in Delhi, −48%, −46%, −44%, 78%, 100% in Hyderabad, −41%, NA, −69%, −28%, 9% in Kanpur, and 28%, −18%, −51%, 51%, −20% in Mumbai, respectively. Figure 1 shows the plots of mean pollutant concentration data during the pandemic year (March 25–May 17) in 2020 and during the same period in 2018–2019. $PM_{2.5}$ and PM_{10} showed a reduction in all the megacities except in Mumbai, where $PM_{2.5}$ levels increased up to 28%.

3.2 Influence of Meteorology

An overall 7.2% temperature decrease is observed in megacities during lockdown, which may be due to the minimization of human activities and vehicular movement (Pal et al., 2021). A slight increase in wind speed of up to 6% is noticed in the cities except in Kanpur, and in other towns where wind speed is increased during the lockdown period, which might have helped in the improved scattering of pollutants. The 4% increase in RH in the cities, except Kanpur, is the reason behind the pollutant concentrations' decrease (Fig. 2).

4 Discussion

The key atmospheric pollutants AOD, $PM_{2.5}$, PM_{10}, NO_2, SO_2, and O_3 declined during the lockdown phase in the selected megacities compared to previous years' data.

Table 1 Difference in AOD concentrations in six megacities of India during lockdown (March 25, 2020–May 17, 2020) and before lockdown during the same period from 2010 to 2019

Cities	OMI (mean) 2010–2019	2020	Difference	% reduction	MODIS (mean) 2010–2019	2020	Difference	% reduction
Ahmedabad	0.30	0.21	−0.28	−27.84	0.27	0.21	−0.02	−1.85
Bangalore	0.44	0.21	−0.51	−50.69	0.30	0.10	−0.06	−6.15
Delhi	0.46	0.21	−0.53	−53.09	0.56	0.41	−0.08	−8.11
Hyderabad	0.39	0.30	−0.23	−23.08	0.50	0.50	0.00	0.10
Kanpur	0.48	0.21	−0.55	−55.45	0.65	0.41	−0.15	−14.97
Mumbai	0.36	0.21	−0.42	−42.29	0.38	0.21	−0.06	−6.30

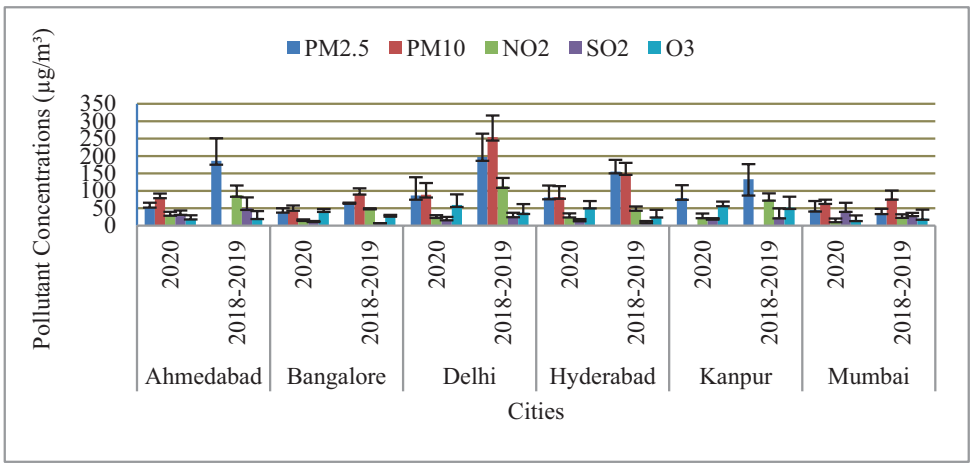

Fig. 1 Impact of lockdown on air pollution levels during two situations, i.e., during lockdown (March 25, 2020–May 17, 2020) and mean concentrations before lockdown during the same period in 2018–2019

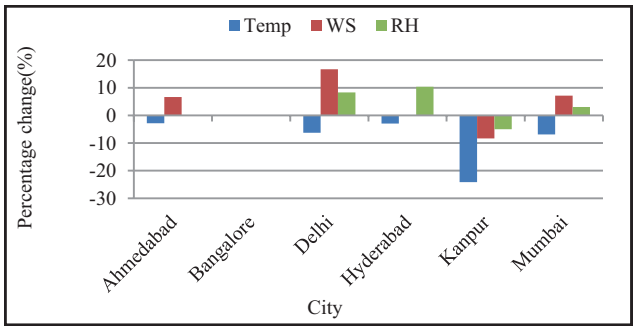

Fig. 2 Percentage changes in meteorological parameters, including temperature, wind speed, and relative humidity in the selected megacities of India

Overall change in mean pollutant concentrations including $PM_{2.5}$, PM_{10}, NO_2, SO_2, and O_3 including all the cities is −38%, −45%, −64%, 14%, and 35%, respectively. In cities like Delhi, vehicular emissions are one of the emitters of $PM_{2.5}$; hence, lockdown minimizes the $PM_{2.5}$ levels (Shrestha et al., 2020). NO_2 concentrations were reduced in all the areas, which may be due to a pause in vehicular and transportation activities (Pal et al., 2021). SO_2 concentrations increased in Bangalore, Hyderabad, and Mumbai from biomass burning and industrial emissions that may not have been turned down (Bar et al., 2021; Shrestha et al., 2020). O_3 emissions often follow the reverse trend as the other trace gases in all regions except in Ahmedabad and Mumbai. The established tight controls have resulted in a significant reduction in vehicle movement and the closure of certain industries, resulting in an improvement in air quality. Such a significant drop in pollution levels is expected to improve public health and prevent health issues and mortality rates linked to air pollution.

5 Conclusions

The research examined six key air contaminants to see how air quality changed after the COVID-19 pandemic curtailed human activity in 6 Indian megacities from March 25, 2020–May 17, 2020, and the same period during 2010–2019. Almost all the contaminants, excluding SO_2 and O_3, were reduced during the lockdown period. Spatial and ground-based data affirm that general air pollution levels have been greatly influenced following the pandemic. Reduced pollution levels have occurred due to the closure of industrial activities and a decline in vehicular movement during the lockdown phase. According to the study, strict enforcement of air pollution regulations could be an alternate tool for pollution control in industrial and transportation-dominated areas.

References

Bao, R., & Zhang, A. (2020). Does lockdown reduce air pollution? Evidence from 44 cities in northern China. *Science of the Total Environment, 731*, 139052.

Bar, S. et al. (2021). Impacts of partial to complete COVID-19 lockdown on NO_2 and $PM_{2.5}$ levels in major urban cities of Europe and USA. *Cities,* 117, 103308.

Pal, S. C., et al. (2021). Improvement in ambient-air-quality reduced temperature during the COVID-19 lockdown period in India. *Environment, Development and Sustainability, 23*, 9581–9608.

Prakash, S., Goswami, M., Khan, Y. D. I., & Nautiyal, S. (2021). Environmental impact of COVID-19 led lockdown: A satellite data-based assessment of air quality in Indian megacities. *Urban Climate, 38*, 100900.

Shrestha, A. et al. (2020). Lockdown caused by COVID-19 pandemic reduces air pollution in cities worldwide. https://eartharxiv.org/repository/view/304. https://doi.org/10.31223/OSF.IO/EDT4J

Verma, R. L., & Kamyotra, J. S. (2021). Impacts of COVID-19 on air quality in India. *Aerosol and Air Quality Research, 21*, 200482.

Yadav, R., et al. (2020). COVID-19 lockdown and air quality of SAFAR-India metro cities. *Urban Climate, 34*, 100729.

Evaluation of Background Concentrations of Tropospheric Ozone Using Dynamic Phase Portrait Methodology

Aleksandr Khaustov and Margarita Redina

Abstract

The study aims to estimate the applicability and precision of a methodology for identifying the background concentration of ozone. These values are necessary to estimate a maximum permissible emission value, understand the population's health risk level, and evaluate the activity of ozone sources (first of all man-made). Currently applied state-approved methods have some limitations; thus, applying a new methodology based on the time variations of impurity concentration is of research and practical interest. Research objects are concentrations of tropospheric ozone in Moscow (anthropogenic polluted atmospheric air, mostly because of the transport activity) and in the settlement with relatively low pollution levels. Initial data are the results of the continuous records of concentrations of ozone, its precursors, and meteorological parameters from the ozone monitoring network. The methodology tested in this study to identify a background ozone concentration is the dynamic phase portrait method, considering variations of changes in concentration during the time. The value obtained presents the concentration of tropospheric ozone most characteristic of the studied location. The background concentration value obtained using the tested methodology is more consistent with the values calculated using the state-approved methodology the longer the observation period is. Furthermore, the values identified make it possible to consider the peculiarities of the distribution of pollutants and the complex meteorological factors in a particular territory and to abandon the standard values assigned.

A. Khaustov (✉) · M. Redina
Peoples' Friendship University of Russia (RUDN University), Moscow 117198, Russia
e-mail: khaustov-ap@rudn.com

Keywords

Ozone · Background concentration · Tropospheric · Monitoring · Phase portrait

1 Introduction

Tropospheric ozone is one of the strongest toxicants, causing significant negative effects on human health and ecosystems. Its sources in the troposphere are natural and anthropogenic; a complex set of factors causes the concentrations.

The purpose of the study was to determine background concentrations of tropospheric ozone. This is a basis for assessing the well-being of territories and establishing norms for acceptable emissions of pollutants that are precursors of ozone or potential sources of dangerous pollutants during oxidation processes with the participation of ozone. A currently applied state-approved method has a set of limitations (size of a data set, averaging algorithm). For the locations where the monitoring system is not developed enough, some prescribed values are to be applied for the environmental regulation. Thus, a new approach will be suggested and tested for this particular task.

2 Objects of the Study

The objects of the study are the characteristics of atmospheric air of urban areas in the European part of Russiawith different levels and sources of pollution—concentrations of tropospheric ozone. Two locations are considered: Moscow (mainly emissions of precursor substances by transport) and the district center Krasnye Polyany (emissions of precursors by industrial and municipal facilities). The data were obtained from the continuous measurements by the ozone monitoring network stations (every 20 min, records of concentrations of ozone, nitrogen oxide, PM_1, PM_4, PM_{10}, hydrocarbons total, methane, and meteorological

A. Çiner et al. (eds.), *Recent Research on Environmental Earth Sciences, Geomorphology, Soil Science, Paleoclimate, and Karst*, Advances in Science, Technology & Innovation, https://doi.org/10.1007/978-3-031-42917-0_17

parameters, as presented in the study (Andreev et al., 2020)) for November 1–30, 2021. Thus, the total data sets counted 2160 measurements for each parameter for each location. Such a data set size allows us to obtain reliable statistical estimations.

3 Methods of the Study

The background ozone concentration in our study is determined using the method of dynamic phase portraits (Trofimchuk, 2018): the trajectory of changes in the O_3 concentration C and the speed of this process dC/dt is analyzed. This allows us to identify stable and unstable states of the system (the distribution of O_3 in the troposphere), time characteristics, critical points (indicators of the system's transition from one stable state to another), and attractors on the O_3 changes trajectory. The method of phase portraits is common in the study of natural systems. The essence of this method is to estimate the dynamics of the analyzed value over time: a spline function is constructed that reflects the ratio of the concentration increment per unit of time (Y-axis) and the actual concentration (X-axis). In addition, the attractor points to which the O_3 concentration tends are identified; the intersection point of the approximation line for the constructed phase portrait with the abscissa axis corresponds (in our case) to the desired value of the background concentration.

To build the dynamic phase portrait, the initial data sets were processed, and the median values of the ozone concentration were calculated:

- the daily to identify the monthly background concentration, and
- the hour medians—to identify the daily background concentration.

The daily background concentrations for both the studied locations were calculated for the typical date. A cluster analysis (single linkage method, Euclidean distances) was applied to determine such a date. These are representative days, during which variations in meteorological parameters and measured concentrations of substances reflect the changes in these values for each of the 30 days (November 1–30, 2020) considered. For Moscow and Krasnye Polyany, a typical day was selected for November 30. On the cluster dendrograms, this day is in the center of the group of considered dates.

The obtained value presents a *local background*: this is the most typical value of the O_3 concentration for the vicinity of the control point (and not the value formed on the "background, that is, clean territory").

4 Results

As a result of the data processing, patterns of daily and monthly dynamics of ozone concentrations for both cities were identified. The reasons for their differences from the dynamics of other regions were evaluated. A slight dependence of the concentration variations on the solar radiation intake in both cities was revealed.

The values of the average monthly (median) background O_3 concentrations were obtained. They were relatively close (about 0.015 mg/m^3 in Moscow and Krasnye Polyany), despite the differences in the volume of anthropogenic loads in both urban areas (Fig. 1a, b). The data processing operations can probably explain such a matching: in this case, we analyze the daily median concentrations.

Similar estimations were obtained for "typical days" (Fig. 1c, d), November 30.

As can be seen from the graphs, the values of the background ozone concentration for the technogenically loaded territory (Moscow; Fig. 1c) was 0.029 mg/m^3, and for the "background" one, 0.024 mg/m^3 (Krasnye Polyany; Fig. 1d).

5 Discussion

In all the considered cases, the values of background concentrations in both settlements do not exceed the national values of the maximum permissible concentration for residential areas (0.030 mg/m^3).

Estimations of the correlation of O_3 concentrations with meteorological parameters and concentrations of other controlled substances showed significant and strong relationships: negative—with NO, CO, dust particles, and air humidity (probably, O_3 is consumed for the oxidation of gaseous, dissolved, and sorbed on the PM impurities); positive—with wind speed (probably due to the intensification of gas exchange and the influx of new precursor substances).

At the same time, the dependence of the ozone concentration on the magnitude of the arrival of solar radiation was not revealed. One of the possible reasons is the generally low solar activity during the study period for both points. Also, the analysis of the daily dynamics showed clear peaks of concentrations in the morning for both monitoring points. On the other hand, some studies show morning lows, especially in Asian regions (Arshinov et al., 2015; Héroux et al., 2013; Zhamsueva et al., 2013). Therefore, a possible explanation is the differences in the receipt of solar radiation in the European and Asian territories.

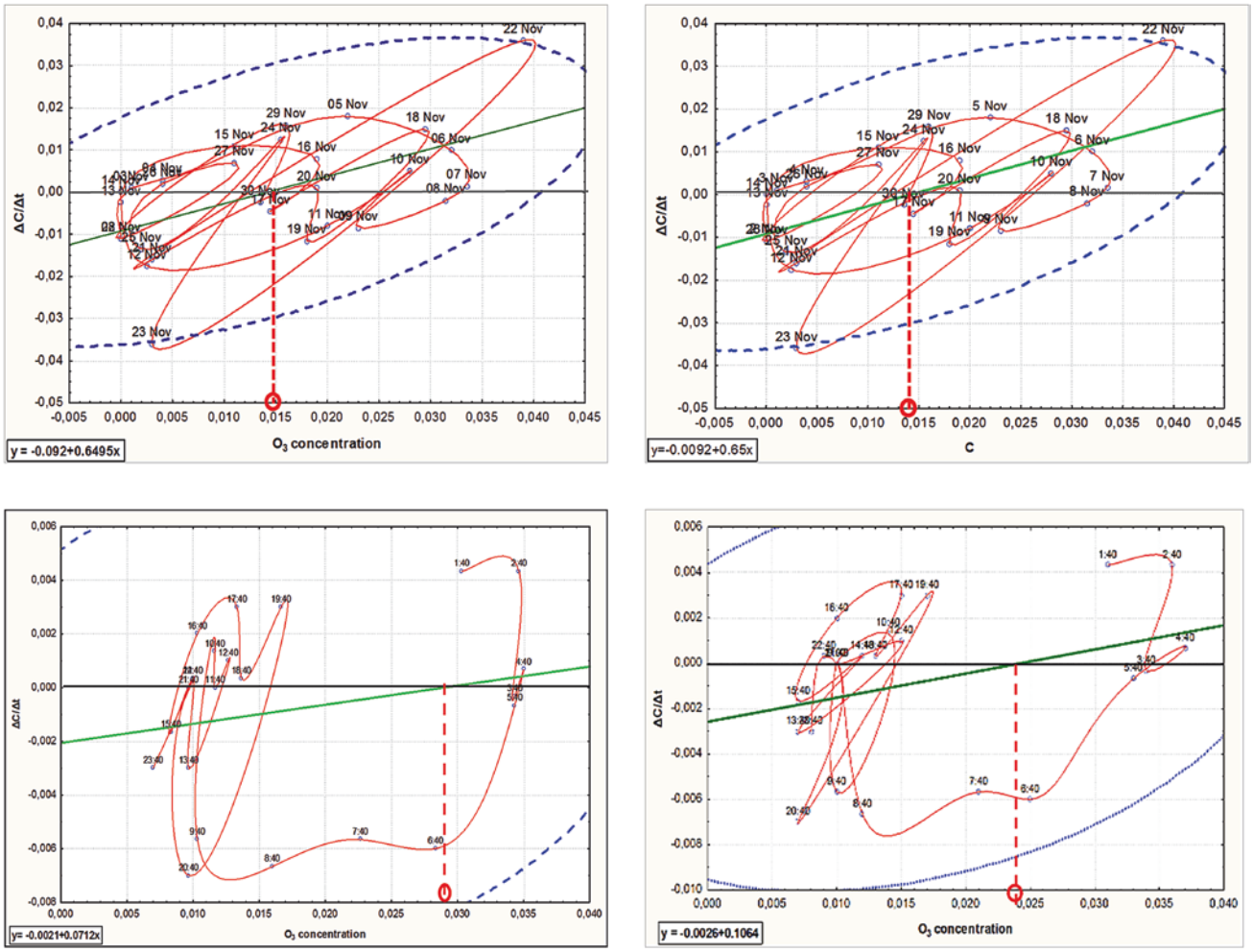

Fig. 1 Phase portrait of ozone concentrations by median values: for November 1–30, 2020, for a technogenically loaded (**a**) and relatively safe (**b**) territory and for a typical day (November 30, 2020) for a technogenically loaded (**c**) and relatively safe (**d**) territory

6 Conclusions

No excess of background values over the MPC was established for both considered locations. However, in the conditions of a large city, the concentrations are higher due to the presence of precursor substances (mainly nitrogen oxides and hydrocarbons) coming from anthropogenic sources (transport), which is proved by the complexity of the phase portraits.

This leads to the need for more detailed studies and monitoring of tropospheric ozone to understand the chemical processes of atmospheric transformation, especially under anthropogenic influences on air quality.

The results obtained in this study present a state of atmospheric pollution for only one month and for one typical day as "test periods". Nevertheless, the study shows this method's applicability for identifying the most typical atmospheric situations—forming local background concentrations of substances.

The phase portrait method demonstrates its effectiveness for these purposes based on continuous observations. Furthermore, it can be used in practice to regulate local anthropogenic loads. This allows us to consider the peculiarities of the distribution of pollutants and the complex meteorological factors in a particular territory and to refuse the assigned regulatory values. This can be a new flexible air quality regulation approach depending on local conditions.

References

Andreev, V. V., Arshinov, M. Y., Belan, B. D., Davydov, D. K., et al. (2020). Surface ozone concentration over the Russian territory in the first half of 2020. *Optica Atmosfery i Okeana, 33*(9), 710–721.

Arshinov, M. Y., Belan, B. D., Davydov, D. K., Savkin, D. E., Sklyadneva, T. K., Tolmachev, G. N., & Fofonov, A. V. (2015). Mesoscale differences in ozone concentration in the surface air in the Tomsk region (2010–2012). *Trudy IOFAN, 71*, 106–117.

Héroux, M. E., Braubach, M., Korol, N., Krzyzanowski, M., Paunovic, E., & Zastenskaya, I. (2013). The main conclusions about the medical aspects of air pollution: The projects REVIHAAP and HRAPIE WHO/EC. *Gigiena i sanitariya*, *6*, 9–14.

Khaustov, A., Redina, M., & Khaustova, N. (2021). Determination of background concentrations of tropospheric ozone in natural and anthropogenically changed conditions using the phase portraits approach. In *E3S web of conferences* (vol. 265, p. 02004). EDP Sciences.

Trofimchuk, M. M. (2018). On the possibility to assess the ecological state of aquatic ecosystems based on entropy. *Meteorologiya i Gidrologiya, 7*, 80–86.

Zhamsueva, G. S., Zayakhanov, A. S., Tsydypov, V. V., Balzhanov, T. S., Azzayaa, D., & Oyunchimeg, D., Bull. of the buryat scientific center of the Siberian branch of the Russian academy of sciences. *2*, 229–246.

Contribution of Google Earth and Images from the Sentinel-2 Satellite to the Monitoring of the Silting of Cap Djinet Harbor (Algeria)

Nour el islam Bachari, Hocine Dahmani, Nacef Lamri, Mohamed Mazouzi, Bilel Bensari, and Fouzia Houma

Abstract

In this study, we integrate remote sensing in oceanographic studies and coastal engineering projects by using satellite images to extract the values of suspended matter in the water and track sediment transport along the coastline. We used Sentinel-2 products and Case 2 Regional Coastcolor (C2RCC) plugin to extract Total Suspended Matter (TSM) values on the Algerian coast for the last six years to construct a database for future studies. We then used the processed products to assess sediment transport in the region of Cap Djinet, where the fishing port suffers from a notably high sedimentation phenomenon. In the last part of the study, we tried to find a correlation between TSM-extracted values and measured depths. Remote sensing was also combined with in situ depth measurements, which we used to construct a bathymetric map of the port. Using satellite imagery, we could assess the damage done to the port throughout the years. We were also able to understand better the causes of this problem, which helped us determine why the solutions implemented by the authorities did not work.

Keywords

Sentinelle C2RCC. TSM · Line coast · Google · Bathymetry

1 Introduction

Algeria has a coastline of almost 1600 km. The Algerian government has built numerous fishing ports along the coastline to exploit the country's halieutic resources better. Numerical methods are used to quantify sediment transport for the choice of port site. The results of MIKE21 gave us a favorable opinion for selecting the location of the port of Cap Djanet. In 2006 the port was constructed. After a few years, the sedimentation problem started, mainly in the southern region of the port. The problem became evident in 2011. In 2009, a study was carried out to solve the problem by modifying the port's design. Also, dredging of the port was carried out, but the problem persists. It is interesting to follow the results of sediment transport from space by remote sensing (Cherif et al., 2019).

2 Materials and Methods

2.1 Study Area

The Cap Djinet harbor is located about 75 km east of Algiers, protected by two jetties and groynes. The main one is about 580 m to the north. The second is in the entrance pass in the south with a length of 340 m. The groynes to the north are 160 m, and the other to the south 120 m. Along the coastline is a long beach, extending from the mouth of Wadi Isser in the west to the mouth of Wadi Sebaou in the east. For monitoring the coastline, we used Google Images taken over several dates.

N. e. i. Bachari (✉) · N. Lamri · M. Mazouzi · B. Bensari
Laboratory of Biological Oceanography and the Marine Environment (LOBEM), University of Science and Technology of Houari Boumedien (USTHB), El Alia, PO Box 32, 16111 Bab Ezzouar, Algiers, Algeria
e-mail: bacharinour@gmail.com

H. Dahmani · F. Houma
Marine and Coastal Ecosystems Laboratory (ECOSYSMarL), National Higher School of Marine Sciences and Coastal Management (ENSSMAL), Campus Dely Ibrahim Bois Des Cars, Dely Ibrahim, Algiers, Algeria

A. Çiner et al. (eds.), *Recent Research on Environmental Earth Sciences, Geomorphology, Soil Science, Paleoclimate, and Karst*, Advances in Science, Technology & Innovation, https://doi.org/10.1007/978-3-031-42917-0_18

2.2 Processing Sentinel Data

The processing of images from the Sentinel satellite is presented in the following Fig. 1.

Finally, the resulting products were processed using the C2RCC plugin, which gives a product containing both TSM values (Sent et al., 2021). We can then extract TSM values from any point we want using the Pin manager tool. The extracted values are then loaded into Excel for further manipulation.

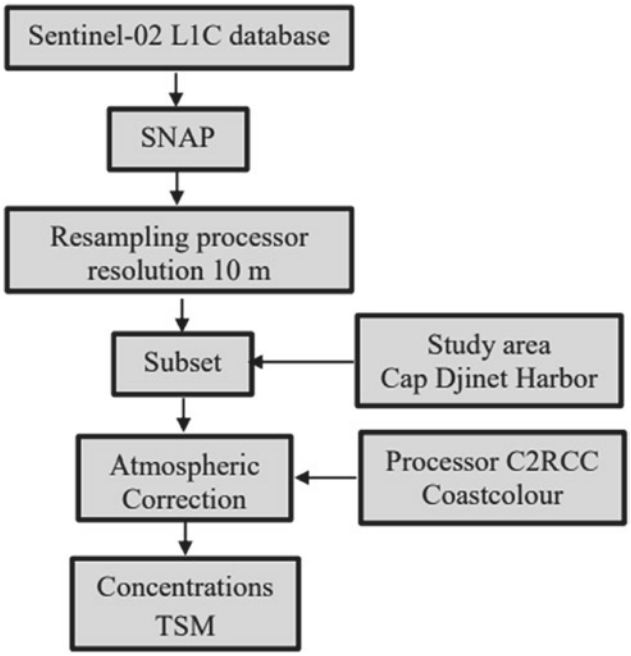

Fig. 1 Processing chain of Sentinel-2 L1C products

2.3 In Situ Measurement

To calibrate the models used, we need to make in situ bathymetry measurements and the concentration of suspended matter (TSM). As for the depth measurements, we used a Plastimo Echotest II depth sounder and measured the TSM using a multiparameter's HANNA. We took depth measurements from 329 different points.

3 Results

From the shoreline changes, we can see that the sedimentation levels have increased, especially in the southern and eastern parts. The region under the northern spur has also been subjected to the same phenomenon. From the coasts extracted from the satellite images, we can conclude that the changes made in 2011 and 2014 failed to resolve the problem and that sedimentation continued (Islam et al., 2017) (Fig. 2).

From the images, we can see that the shoreline drift current prevents the sediment coming from Wadi Sebaou from moving toward the west. It also prevents it from leaving the coast into deep waters, forcing some sediment to move along the coastline toward the west and directly into the northern part of the harbor (Fig. 3).

As for the western region, we can see that the sediment is being directly transported toward the harbor (Filipponi, 2018). Finally, we are interested in looking for a correlation between the TSM and the Z bathymetry. The correlation between TSM and Z is essential and reaches 0.91, provided that the depth is between 0.8 and 25 m. The bathymetric

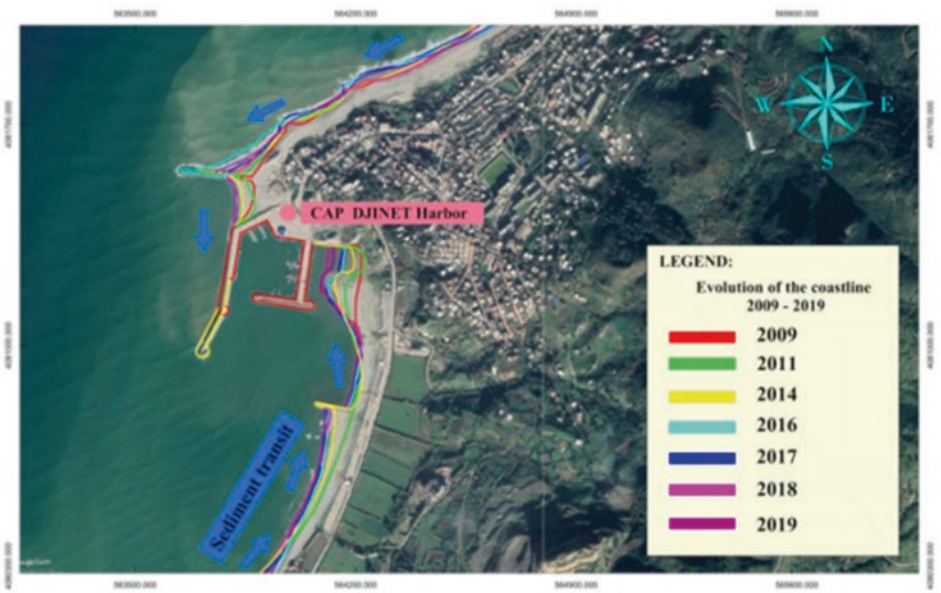

Fig. 2 Changes in the coastline between 2009 and 2019

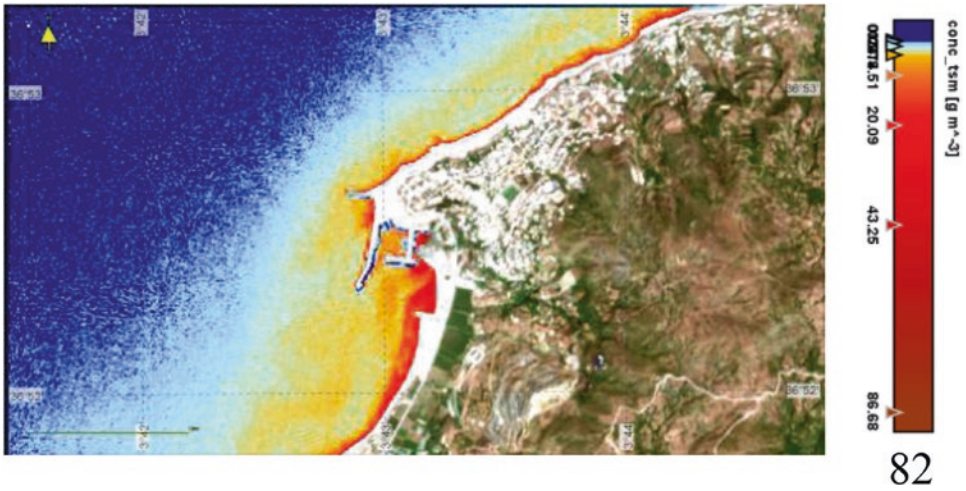

Fig. 3 Satellite-derived TSM concentrations for 07/08/2020

map produced is injected into the MIKE-21 model. After several configurations, we propose the optimal solution is to extend the groyne further into the water. In this case, the sedimentation takes place in front of the port in the area with high bathymetry. The silting time of the port is long if it takes place.

4 Conclusions

This work has allowed us to conclude an essential aspect of coastal engineering in the feasibility studies on the site choice for a harbor project. The numerical and reduced models must integrate remote sensing before starting the modeling phase. It is necessary to add the satellite image before and after the floods to decide on the feasibility of the harbor structure.

References

Cherif, Y. S., Mezouar, K., Guerfi, M., & Sallaye, M. (2019). Nearshore hydrodynamics and sediment transport processes along the sandy coast of Boumerdes, Algeria. *Arabian Journal of Geosciences, 12*(24), 1–17. https://doi.org/10.1007/s12517-019-4981-0

El Islam, B. N., Fouzia, H., & Khalid, A. (2017). Combination of satellite images and numerical model for the state followed the coast of the bay of BejaiaJijel. *International Journal of Environment and Geoinformatics, 4*(1), 1–7. https://doi.org/10.30897/ijegeo.306486

Filipponi, F. (2018). River color monitoring using optical satellite data. *Proceedings*, *2*(10), 569. https://doi.org/10.3390/iecg_2018-05336

Sent, G., Biguino, B., Favareto, L., Cruz, J., Sá, C., Dogliotti, A. I., Palma, C., Brotas, V., & Brito, A. C. (2021). Deriving water quality parameters using Sentinel-2 imagery: A case study in the Sado Estuary, Portugal. *Remote Sensing*, *13*, 1043. https://doi.org/10.3390/rs13051043

Bio-based Materials: Composite and Paper Productions from Tunisian *Opuntia Ficus-Indica* (Cactaceae) Feedstock

Faten Mannai and Younes Moussaoui

Abstract

Natural lignocellulosic fibers are the most effective alternatives for synthetic materials for select applications. Among these lignocellulose fibers, Tunisian *Opuntia ficus-indica* (Cactaceae) fibers have been considered non-woody raw materials for manufacturing sustainable and ecological products. This paper reports the exploitation of Tunisian *Opuntia ficus-indica* (Cactaceae) as a potential feedstock for value-added applications such as reinforcement in bio-based material and raw material for pulp and paper manufacturing. As reinforcement in composite material, layers of fibrous networks were isolated and incorporated into biodegradable thermoplastic polymers. Their properties toward thermomechanical enhancement, swelling, and biodegradability have been investigated. As raw material for pulp and paper manufacturing, two green processes of delignification were tested: mi-chemical and chemical methods. The first green methods are based on the mi-chemical treatment using a soft operation of chemical delignification of raw material in a soda-hydrogen peroxide mixture, followed by mechanical grinding for fiber individualization, which gives a high pulp yield (80.8%). The second green procedure is a chemical treatment of raw material with a soda-anthraquinone mixture with a pulp yield close to 41.4%. Pulps were used for hand-made sheet production, and normed methods and standards characterized the obtained samples. The obtained papers have good mechanical and structural properties. Finally, the studied bio-based crops showed the suitability of Tunisian *Opuntia ficus-indica* fibers as a new trend in sustainable and eco-friendly green materials.

Keywords

Green · Composite · Product · Paper · *Opuntia*

1 Introduction

With the rising industry demand for bio-based material, the researcher's attention is drawn toward recognizing the alternative novel source of natural fibers for its distinctive features like cost-effectiveness, biodegradability, and abundant availability. Various industries have shifted toward commercialized material with the potential use of natural fibers as a reinforcement element in composites to replace synthetic material and as raw material for paper manufacturing using green processes to reduce the environmental impact. Natural fibers from Tunisian *Opuntia ficus-indica* were considered one of the strongest and stiffest available lignocellulose fibers from renewable plant biomass (Bouakba, 2013; Mannai, 2020a).

This research provides a brief study of the feasibility of *Opuntia ficus-indica* fibers to (i) develop a natural fiber-reinforced polymer composite using two thermoplastic polymers, which are polyvinyl alcohol (PVOH) and styrene butadiene rubber (SBR); and (ii) produce pulp and paper using two green methods which are mi-chemical treatment using a soft operation of chemical delignification of raw material in soda-hydrogen peroxide mixture, followed by mechanical grinding for fiber individualization, and chemical treatment of raw material with the soda-anthraquinone mixture. It is interesting to point out there are a few reports on the use of Tunisian *Opuntia ficus-indica* fibers as

F. Mannai (✉) · Y. Moussaoui
Laboratory for the Application of Materials to the Environment, Water and Energy (LR21ES15), Faculty of Sciences of Gafsa, University of Gafsa, 2112 Gafsa, Tunisia
e-mail: mannai_faten@yahoo.com

Y. Moussaoui
Organic Chemistry Laboratory (LR17ES08), Faculty of Sciences of Sfax, University of Sfax, 3029 Sfax, Tunisia

F. Mannai · Y. Moussaoui
Faculty of Sciences of Sfax, University of Gafsa, 2112 Gafsa, Tunisia

A. Çiner et al. (eds.), *Recent Research on Environmental Earth Sciences, Geomorphology, Soil Science, Paleoclimate, and Karst*, Advances in Science, Technology & Innovation, https://doi.org/10.1007/978-3-031-42917-0_19

raw material for paper manufacturing and as a natural filler in reinforced polymer composite sectors, and they are the most interesting and discerning materials.

2 Materials and Methods

Composites were prepared by a simple hand lay-up method, without using any coupling agents and dried at room temperature for 72 h (Mannai, 2018a). Fibrous networks were isolated from *Opuntia ficus-indica* trunk and used as a reinforcing agent (Mannai, 2020b). Polyvinyl alcohol (PVOH) and styrene-butadiene rubber (SBR) latex were used as two thermoplastic polymers. The obtained composites were characterized by several methods, such as Dynamic Mechanical Analysis "DMA" to characterize the thermomechanical behaviors, and the detailed analysis protocol was described by Mannai (2020b), swelling rate (soaking materials in water) and biodegradability of specimens in soil burial (Mannai, 2020b). In addition, pulping of raw material (dried chips: 2–3 × 1–2 × 1.5–2 cm^3) was performed with (i) mi-chemical treatment using soda-hydrogen peroxide mixture [6 g sodium hydroxide: 13 g hydrogen peroxide; temperature: 80 °C and time: 4 h] followed by mechanical grinding for fiber individualization (Mannai, 2016, 2020a); (ii) and the second procedure is a chemical treatment with the soda-anthraquinone mixture [alkaline charge: 20%; anthraquinone concentration: 0.1%; temperature: 170 °C; time: 2 h; temperature ramping rate 2.4 °C min^{-1}] (Mannai, 2018b, 2020a). The obtained pulps were used for hand-made sheet preparation, and the obtained specimens were characterized by applying TAPPI standards which were described in detail by Mannai (2016, 2018b, 2020a).

3 Results

3.1 *Opuntia Ficus-Indica* Fibrous Network-Reinforced Polymer Composites

The thermomechanical, dimensional stability (swilling rate) and biodegradability of produced composite materials are investigated and summarized in Table 1. The loss factor [tan δ] is higher for SBR-based composites than PVOH-based materials. This result suggests the amorphous aspect of SBR-based materials (Mannai, 2018a). The relaxation temperature [Tα] is higher for PVOH-based composites than SBR-based materials. This confirms the effectiveness of the fiber as a reinforcing agent with a high polymer-filler interaction. The temperature offset of the storage tensile modulus [log E'] shows that at 20 °C, PVOH-based materials are stiffer than SBR latex-based materials, in which the latest are the strongest at a low temperature of 0 °C. The swelling rate of the PVOH composite is very high (80%) compared to the SBR-based material (18.1%). The weight loss of PVOH and SBR-based materials after soil burial during the 210 days tends to be 93 and 86.6%, respectively (Mannai, 2020a, 2020b).

Table 1 Thermomechanical, swelling, and biodegradability behaviors of composites reinforced with fibrous networks (F-N) of Tunisian *Opuntia ficus-indica* (Mannai, 2020b)

Properties of composites	PVOH-FN	SBR-FN
Loss factor [Tan δ]	0.18	0.58
Relaxation temperature [Tα] (°C)	36	25.5
Temperature offset of the storage tensile modulus [log E'] (°C)	20	0
Swelling rate (%)	80	18.1
Soil weight loss (%)	93	86.6

3.2 Pulp and Paper Production

The given data on the morphological and physical properties of pulp and hand-made papers are displayed in Table 2. The pulp yield of mi-chemical pulps is higher than that of chemical pulp. The fiber length (and width) of the *Opuntia ficus-indica* mi-chemical and chemical pulps were 764 µm (38 µm) and 737 µm (45.6 µm), respectively (Mannai, 2016, 2018b). The data relating to the physical and mechanical properties of hand-made papers confirm that the studied raw material has the potential for use in paper manufacturing using the soft delignification by applying the mi-chemical procedure, which can affect the paper properties by increasing the fiber flexibility and strength (Mannai, 2016, 2020a).

Table 2 Fiber and hand-made paper produced from Tunisan *Opuntia ficus-indica* pulps (Mannai, 2016, 2018b, 2020a)

Pulp and paper properties	Mi-chemical (Mannai, 2016)	Chemical (Mannai, 2018b)
Yield (%)	80.8	41.4
Fiber length (µm)	764	737
Fiber width (µm)	38	45.6
Bases weight (g/m^2)	38.4	65.2
Thickness (µm)	149	135
Burst index (kPa m^2 $g-^1$)	0.67	5.8
Tear index (mNm2 g^{-1})	19.2	12
Young's modulus (GPa)	1.7	1.83
Breaking length (km)	1.9	1.57

4 Discussion

The viscoelastic (thermomechanical) properties for both PVOH and SBR-based composites mainly depend on both the matrix and the kind of fiber orientation on the fibrous network by adhesion bending (interaction) between fibers (Mannai, 2020b). From the study of produced composites, eco-friendly *Opuntia*-derived fiber-reinforced polymer (thermoplastic) composites would be the materials for the near future not only as a solution to the growing environmental threat but also as a solution to alleviating the uncertainty of the petroleum supply (Mannai, 2020a, 2020b). In addition, the fiber length and width (morphological properties) results of produced chemical and mi-chemical pulps confirmed the high quality of individual cellulosic fibers. These parameters have been influenced by the types of fiber treatment (Mannai, 2016, 2018b, 2020a). Furthermore, the results of hand-made papers indicate that the paper fabricated from Tunisian *Opuntia ficus-indica* fibers has satisfactory mechanical and structural properties (Mannai, 2018b, 2020a).

5 Conclusions

The natural fibers derived from Tunisian *Opuntia ficus-indica* (Cactaceae) plants prove their greatest potential for use: (i) as a sound reinforcement candidate for high-performance biodegradable thermoplastic composites because of their excellent characteristics and eco-friendliness; and (ii) as raw material in pulp and paper production by applying two different delignification methods which affect the pulp properties and paper characteristics. Thus, these researches suggest that Tunisian *Opuntia ficus-indica* fibers can produce paper from non-woody plants with various qualities (strength) and for future green-based products for selective applications.

References

Bouakba, M. (2013). Cactus fiber/polyester biocomposites: Manufacturing, quasistatic mechanical and fatigue characterization. *Composites Science and Technology, 74*, 150–159.

Mannai, F. (2016). Cellulose fiber from Tunisian Barbary fig "*Opuntia ficus-indica*" for papermaking. *Cellulose, 23*(3), 2061–2072.

Mannai, F. (2018a). Green process for fibrous networks extraction from *Opuntia* (Cactaceae): Morphological design, thermal and mechanical studies. *Industrial Crops and Products, 126*, 347–356.

Mannai, F. (2018b). Alkaline delignification of cactus fibers for pulp and papermaking applications. *Journal of Polymer and the Environment, 2*(6), 798–806.

Mannai, F. (2020b). *Opuntia* (Cactaceae) fibrous network-reinforced composites: Thermal, viscoelastic, interfacial adhesion and biodegradation behavior. *Fibers and Polymers, 21*(10), 2353–2363.

Mannai, F. (2020a). Novel trend in the use of *Opuntia* (Cactaceae) fibers as potential feedstock for material science applications. In E. S. Hamadttu (Ed.), (pp. 143–158). IntechOpen.

Sediment Type and Their Relation to the Presence of Seagrass *Posidonia oceanica* in the Mediterranean Lagoon

Karim Ben Mustapha, Abderraouf Hzami, Oula Amrouni, Aya Hammami, Chrystelle Montigny, Gil Mahé, and Hechmi Missaoui

Abstract

This study aims to determine the sediment pattern changes and seagrass response to natural and anthropogenic factors in urbanized coastal lagoons in Ghar El Melah, Tunisia, in the central Mediterranean. We explore seagrass metrics over 37 radials and 106 spatial lagoon stations and sediment characteristics in 21 stations in December 2020 and April 2021. Floristical assessment is based on structural and functional metrics and seagrass distribution. The result reveals the presence of *Cymodocea nodosa*, *Zostera marina*, *Z. nolti*, *Ruppia maritima*, and *R. cirrhosa*, while *P. oceanica* is reported for the first time in lagoon systems of northern Tunisia, which cover ~70 ha, showing a density ranging from 56 shots/m^2 to 2111 shots/m^2. Grain-size analysis of marine lagoon sediment revealed a predominance of very fine sand (D50 goes from 0.063 to 0.120 mm) and mud distribution (D50 ranges from 0.001 to 0.063 mm) inside the lagoon except in the lagoon channel when it dropped by coarser sand (Median equal to 0.2 mm). The sediment and seagrass distribution variability is controlled by the historical deltaic deposits inside the lagoon and the neighboring marine processes. The lagoon's center and urban sides are marked by the absence of seagrass meadows where sediment is composed of clay fractions. The ecological quality of the lagoon is strongly affected by urban activities and coastal management.

Keywords

Seagrass · *Posidonia oceanica* · Coastal lagoon · Sediment · Mediterranean · LMI COSYS-Med 2 · Tunisia

1 Introduction

The seagrass *Posidonia oceanica* is one of the most significant components in shallow water in the Mediterranean basin (Mazzella et al., 1993). The linkage between *P. oceanica* and the sediment pattern is largely studied in the extended coastal areas of the Mediterranean (Falco et al., 2000). Interaction between coastal geomorphology, hydrodynamics processes, and meadows' presence and distribution was demonstrated (Jeudy de Grissac & Bourderesque, 1985). For the last decades, seagrass species have undergone the effect of global warming (Marba & Duarte, 1997), accentuated by intense anthropogenic stressors in marine and coastal habitats (Cavazza et al., 2000). This study aims to use Sediment Type distribution to study kinetic sediment and the affinities of fine-grained particles and macrophyte distribution and its metrics in the coastal lagoon system in the context of human and climate stressors.

2 Materials and Methods

2.1 Study Area

The Ghar El Melah lagoon lies on the eastern Mediterranean coast (Fig. 1a) at the North limit by Jebel Nadhour and in the southwestern is limited by the Medjerda basin plain (37°11′26.73″ N and 9°51′5.27″ E). The coastal lagoon covers a total of 3000 ha and is 6.45 km in width and 10.6 km in length. The maximum depth of the water level in Ghar El Melah lagoon is approximately 3 m, and it is connected to the Mediterranean Sea by the Boughaz

K. B. Mustapha · A. Hzami · O. Amrouni (✉) · A. Hammami · H. Missaoui
University of Carthage, National Institute of Marine Sciences and Technologies, 2025 Tunis, Carthage, Tunisia
e-mail: Oula.amrouni@instm.rnrt.tn

C. Montigny · G. Mahé
HydroSciences Montpellier, CNRS, IMT, IRD, Université de Montpellier, 34095 Montpellier, France

A. Çiner et al. (eds.), *Recent Research on Environmental Earth Sciences, Geomorphology, Soil Science, Paleoclimate, and Karst*, Advances in Science, Technology & Innovation, https://doi.org/10.1007/978-3-031-42917-0_20

channel, which is 75 m wide and 6 m deep. The site is characterized by the Mediterranean and semi-arid climate within a medium rainfall range (540 mm/yr) when the evapotranspiration rate is about 1450 mm/yr. The study area climate is characterized by seasonal air temperature variability with a medium value range of ~12 °C to ~27 °C in winter and summer, respectively (INM, 2020).

2.2 Sedimentological Survey and Data Analysis

A total of 21 subsurface samples were collected by Van Veen grab in December 2020 in the lagoon area (Fig. 1b). Surficial samples are sieved under the AFNOR column for the >0.063 sizes. The sediment-particle distribution is determined by the calculation of the grain-size parameters (Modal value Mo, average mean size Md, and Mz, standard deviation σ, skewness Ski and Kurtosis Ku), according to Folk and Ward (1957). The mud particles (silt and clay) ranging from 0.063 to 0.001 were measured by *Malvern Mastersizer* 2000 to determine their median grain-size index (D50) and frequency distribution according to Barusseau 1973 schema (Barusseau, 1973).

2.3 Macrophyte Sampling

In the Ghar El Melah coastal lagoon, macrophyte identification and metrics were undertaken over six radials and 106 spatial lagoon stations (Fig. 1b) in December 2020 and April 2021. Macrophytes were sampled every 250 m over the radial varying from 1400 to 5700 m longer at a depth of −1 to −3.5 m. During the campaign of April 2021, we sampled 21 stations, a square of 0.09 m^2, for the coverage and phenology characteristics (Khsiba et al., 2020).

3 Results

3.1 Sediment Type Distribution

We subdivided the lagoon area into three compartments: Sector 1—the Channel area, Sector 2—the southeastern ridge, and Sector 3—the center of the lagoon. Table 1 illustrates the granulometric parameters of the subsurface sediment of the lagoon of Ghar El Melah. Sedimentological analysis reveals that 35% of the collected samples are composed of fine and medium-sandy fractions with a median particle size

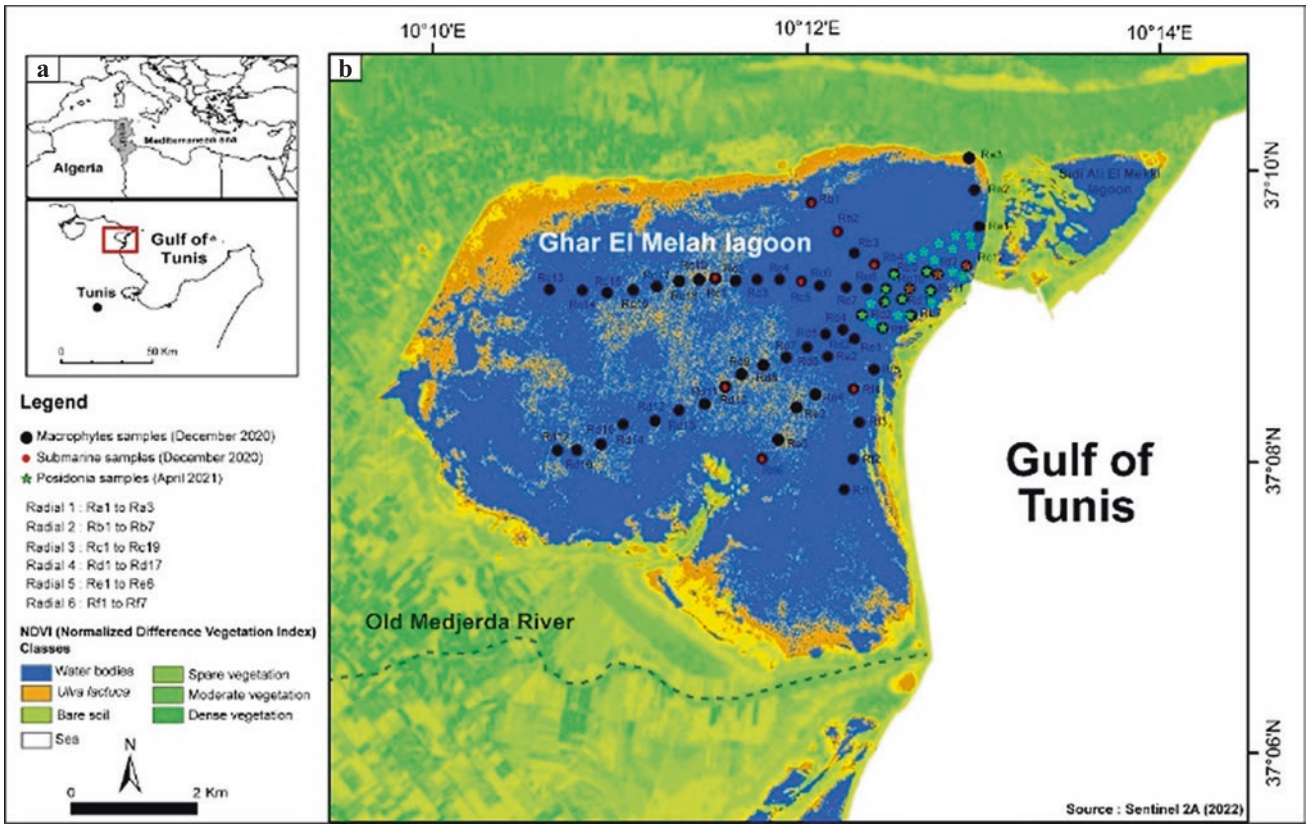

Fig. 1 **a** Location of the study site, the lagoon of Ghar El Melah, Gulf of Tunis. **b** Position of marine macrophytes and bottom sediments sampling in the lagoon

Table 1 Grain size parameters of surface sediment in Ghar El Melah lagoon (December 2020)

Zone	Samples	% Clay	% Silt	% Sand	Mo	Md	Mz	σ	SKI	Ku	D50
Sector I	Ra1	–	0	100	0.25	0.21	2.27	0.41	0.06	0.73	–
	Rd1	–	0	100	0.25	0.2	2.27	0.59	0.15	0.97	–
	Ra2		0	100	0.315	0.2	2.21	0.42	0.22	0.84	–
	Rc12	100	0	0	–	–	–	–	–	–	6
	Rb4	96	4	0	–	–	–	–	–	–	4.3
	Rc10	87	12	0	–	–	–	–	–	–	8
Sector II	RF3	–	0	100	0.16	0.18	2.4	0.69	0.53	1.65	–
	RF6	–	0	100	0.16	0.16	2.54	0.35	0.6	2.02	–
	RF4	98	2	0	–	–	–	–	–	–	5
Sector III	Re2	–	0	100	0.315	0.35	1.48	0.34	0.21	1.19	–
	Rd6	–	0	100	0.16	0.17	2.4	0.84	0.33	2.17	–
	Rc1	95	5	0	–	–	–	–	–	–	6
	Rb2	100	0	0	–	–	–	–	–	–	6.6
	Rb1	93.6	6.4	0	–	–	–	–	–	–	5
	Rc5	95	5	0	–	–	–	–	–	–	5
	Re4	84	16	0	–	–	–	–	–	–	8
	Rd10	100	0	0	–	–	–	–	–	–	5.7
	Re6	92	8	0	–	–	–	–	–	–	8.7

Silt: particle size < 0.063 mm; Sand: particle size > 0.063 mm; Mo: Modal value (mm); Md (Median in mm scale); Mean (Mz phi scale), standard deviation (σ, sorting), skewness (SKI) and kurtosis (Ku). D50 is the mean value of the silty-clay fractions (<0.063 mm). Sector I: Channel; Sector II: Sandy barrier; and Sector III: Center of lagoon

Md of 0.16–0.315 mm, mainly localized in the channel area and the southeastern ridge of the lagoon. The modal value reveals that the sediments are unimodal for 100% of cases with a Mo range from 0.16 to 0.315 mm. Sediments are moderately well-sorted (Ra1, Ra2, RF6) to poorly sorted (Rd1, RF3) and asymmetric to very asymmetric to a fine fraction (+0.1 < SKI < +1 Φ). The center of the lagoon is composed of muddy facies (65%) within 20% of silt (D50 > 0.04 mm) and 80% of clay components (D50 ranging from 4 to 9 μm).

3.2 Seagrass Identification and Distribution

Figure 2 illustrates the seagrass species identification and the three main algae and their distribution in the lagoon of Ghar El Melah. Metric investigation reveals the presence of five seagrass species (*Cymodocea nodosa*, *Zostera marina*, *Zostera nolti*, *Ruppia* spp, and *Posidonia oceanica*) and two nitrophilous algae (*Chaetomorph asp* and *Ulva lactica*). At the same time, *Caulerpa prolifera* was not as present as it would be. *Cymodocea nodosa* is present in nearly 20% of the stations in the three sectors, while *Zostera* spp, although present in the three sectors, has a weak occurrence in sector II (14%). *Ruppia* spp is absent in sector I and is weakly present in the other two sectors. *Caulerpa prolifera* is well represented in the three sectors. In contrast, *Chaetomorpha* spp is present everywhere, which is not the case for *Ulva lactuca* as it is only weakly present in sector I. Seagrass *P. Oceanica* was only found in the northeastern ridge of the lagoon, which covers ~70 ha, showing a density ranging from 56 to 2111 shots/m^2; and coverage varying from 8 to 100% per m^2 in the channel and sandy barrier border.

4 Discussion

Sedimentological analysis of the submarine lagoon sediment shows the predominant distribution of the muddy type over the lagoon bedforms. At the same time, the sandy type fine-grained sedimentation covers the barrier island lagoon. Habitat's investigation through the lagoon reveals the omnipresence of *Cymodocea nodosa* and *Zostera* spp in the muddy seabed of the lagoon. While the intermittent distribution of *Rupia* spp meadows is probably related to the new sandy deposit near the channel corridor and the higher turbidity of the lagoon water (Verhoeven, 1979; Kantrud et al., 1991). The presence of the two nitrophilous algae species indicates the enrichment of the muddy sediment and/or water by organic matter (OM). This high-level OM enrichment is mainly caused by the surrounding urban and harbor wastes (Bancon-Montigny & Amrouni, 2021). *Cymodocea nodosa*, *Zostera spp,* and *Caulerpa prolifera*

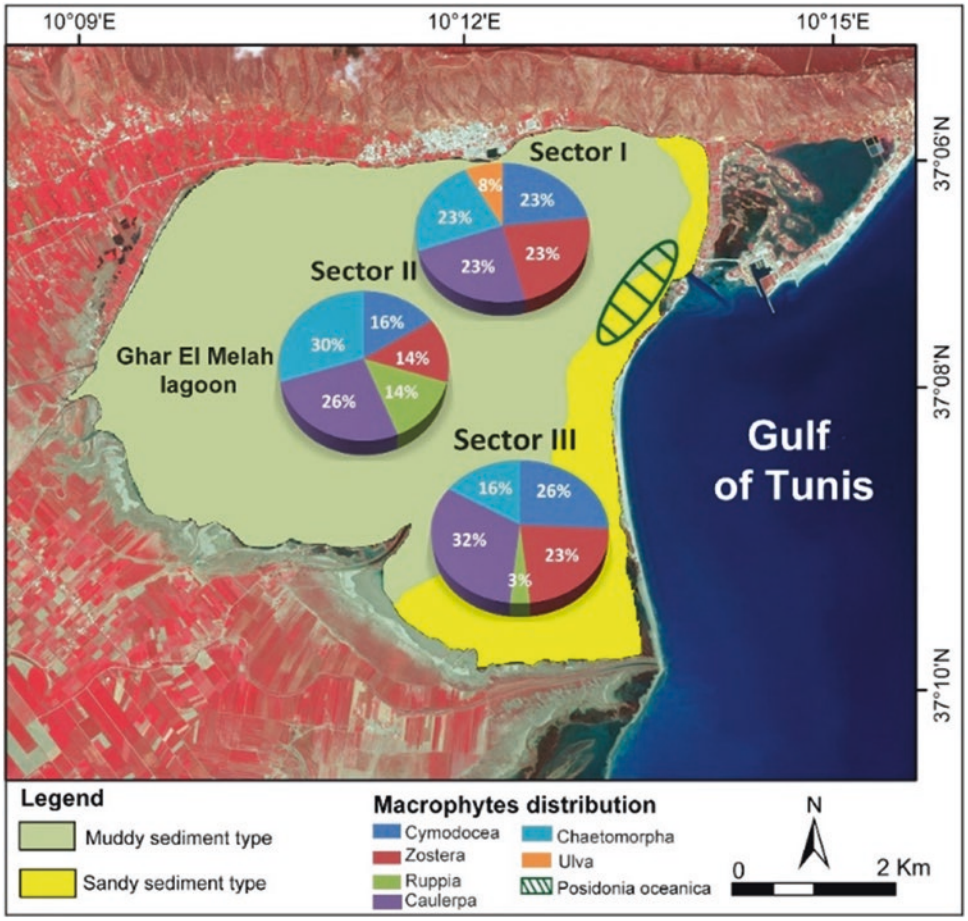

Fig. 2 Sediment type and macrophytes distribution in the coastal lagoon of Ghar El Melah, Gulf of Tunis, Tunisia (December 2020 and April 2021)

present dominant facies of the 'Calm Mode Superficial Muddy Sand Biocenosis' (SVMC) type (Muséum, 2020) of lagoon environments. Sandy Type distribution in the sand barrier island is positively correlated with the new first presence of patches/meadows of seagrass *P. oceanica* in the northeastern Tunisian lagoon. The lagoon of Ghar El Melah is controlled by wave-induced processes and suffers from rapid sedimentation inside the lagoon driven by continental yields, longshore current, and human management (dam, dikes, etc.) (Amrouni et al., 2020). The response of the ecosystem habitats to these drivers is expressed by the newly implemented *P. oceanica* and by the variability of the distribution of macrophyte species with an increasing pattern of nitrophilous algae species occurrence.

5 Conclusions

The ecosystem study of the Ghar El Melah lagoon occurred according to sedimentological and ecological approaches. Sediment distribution of the sea bedforms reveals the predominance of the muddy facies over the lagoon. At the same time, the fine-grained sedimentation is located surrounding the Boughaz channel and the barrier island areas. Floristical identification and metric show the presence of a variable macrophytes species with a significative presence of *Cymodocea nodosa* and *Zostera* spp in the muddy seabed. Nitrophilous algal species are noted and indicate the Organic matter enrichment level of the water and or sediment bodies of the lagoon. *P. oceanica* is reported for the first time in lagoon systems of northern Tunisia, covering ~70 ha, showing a density ranging from 56 shots/m^2 to 2111 shots/m^2. The observed variability of the sediment and seagrass distribution is probably controlled by the historical deltaic deposits inside the lagoon and the neighboring marine processes. The lagoon's center and urban sides are marked by the absence of seagrass meadows where sediment is composed of clay fraction (D50 < 0.04 mm). The ecological quality of the lagoon is strongly affected by urban activities and coastal management.

References

Amrouni, O., Beji, Y., Heggy, E., & Sánchez, A. (2020). Coastal sedimentary dynamic of wetland ecosystem of semi-arid areas in north Africa. In *3rd conference of the Arabian journal of geosciences* (pp. 2–5).

Bancon-Montigny, C., & Amrouni, O. (2021). Study of the Dispersion of contaminants from the Medjerda river basin to the marine ecosystem of the Gulf of Tunis, Mediterranean. In *3rd EMCEI, euro mediterranean conference for environmental integration* (pp 10–13).

Barusseau, J. P. (1973). Evolution du plateau continental rochelais (golfe de Gascogne) au cours du Pléistocène terminal et de l'Holocène. Les processus actuels de la sédimentation. Thèse d'Etat, Bordeaux I.

Cavazza, W., Immordino, F., Moretti, L., Peirano, A., Pironi, A., & Ruggiero, F. (2000). Sedimentological parameters and seagrasses distribution as indicators of anthropogenic coastal degradation at Monterosso Bay (Ligurian Sea, NW Italy). *Journal of Coastal Research, 16*(29), 295–305.

De Falco, G., Ferrari, S., Cancemi, G., & Baroli, M. (2000). Relationship between sediment distribution and Posidonia oceanica seagrass. *Geo-Marine Letters, 20*, 50–57.

Folk, R. L., & Ward, W. C. (1957). Brazos River bar, a study in the significance of grain size parameters. *Journal of Sedimentary Petrology*, *27*, 514.

INM.: Institut National de Météorologie. (2020). Données climatiques de la région de Bizerte.

Jeudy de Grissac, A., & Bourderesque, C. F. (1985). Roles des herbiers de phanerogames marines dans les mouvements des sedimentscôtiers: les herbiers a Posidoniaoceanica. *Coll Franco-JaponaisOceanogr* (vol. 1, pp. 143–151).

Kantrud, H. A., & Wigeongrass, L. (1991). (*Ruppia maritima*): A literature review. [Online.] http://www.npwrc.usgs.gov/resource/literatr/ruppia/ruppia.htm

Khsiba, S. Amrouni, O., Ben Mustapha, K., Gaaloul, N., Bancon Montigny, C., & Chouba, L. (2020). Grain-size trend and ecological state of southern Mediterranean coastal lagoons: Case of the Gulf of Tunis. *Journal of African Earth Sciences*, *174*.

Marba, N., & Duarte, C. M. (1997). Interannual changes in seagrass (*Posidonia oceanica*) growth and environmental change in the Spanish Mediterranean littoral zone. *Limnology and Oceanogra-Phy, 42*, 800–810.

Mazzella, L., Scipione, M. B., Gambi, M.C., Buia, M. C., Lorenti, M., Zupo, V., & Cancemi, G. (1993). The Mediterranean seagrass Posidonia oceanica and *Cymodocea nodosa*: A comparative overview. In *1st international conference on mediterranean coastal environment, MEDCOAST 93*, (pp. 103–116).

M.N.H.N. Muséum National d'Histoire Naturelle, Paris (2020). https://dcsmm.milieumarinfrance.fr/Le-Plan-d-Action-pour-le-Milieu-Marin/Cycle-1-2012-2018/Consultation-des-documents-du-Cycle-1/Biocenoses-des-fonds-meubles-de-l-infralittoral-Mediterranee-occidentale

Verhoeven, J. T. A. (1979). The ecology of Ruppia-dominated communities in western Europe. I. Distribution of Ruppia representatives in relation to their autecology. *Aquatic Botany*, *6*, 197–268.

Planning Ecological Corridors to Integrate into a Regional Green Infrastructure

Rocío Losada-Iglesias, Andrés M. García, and David Miranda

Abstract

Ecological corridors are fundamental to mitigating the impacts of climate change on biodiversity by promoting species migration and avoiding genetic isolation. However, these elements of green infrastructure present more challenges for their delimitation. This is because its effectiveness in connecting habitats depends on the mobility habits of different species. Generally, this information is scarce and costly to obtain, even more so when it comes to the delimitation of corridors at the regional level, which must ensure the mobility of many species. This work proposes a methodology of delimitation of corridors that seeks a compromise solution between the high demand for data of methods based on species mobility habits and the generalization of methods based on structural connectivity. To do this, umbrella species' distribution probability maps are inferred from species inventory data and used as a proxy of landscape resistance to species mobility. This information is inserted in a least cost path model based on graph theory to determine the ecological corridors of the green infrastructure in the region of Galicia (northwestern Spain). The obtained corridors are compared with those delimited by expert knowledge in the green infrastructure strategy of the region. The results show that the methodology complements methods based on structural connectivity and allows non-expert planners to gain insights into the factors that influence species mobility.

Keywords

Ecological corridor · Planning · Green infrastructure · Delimitation · Umbrella species

R. Losada-Iglesias (✉) · A. M. García · D. Miranda
University of Santiago de Compostela, 27002 Lugo, Spain
e-mail: rocio.losada@rai.usc.es

1 Introduction

The current Climate Change scenario is expected to promote changes in species distribution and a reduction of biodiversity. The existing nature protection areas are not big enough to grant species adaptation to these changes (Alagador et al., 2016). Green Infrastructures (GI) are proposed as a possible solution since one of their objectives is favoring nature protection areas' ecological connectivity. Creating integrated Ecological Corridors (EC) as elements of the GI will make it possible to avoid species isolation and increase their habitat range, making them more resilient to changes (European Commission Communication of the Commission to the European Parliament).

The delineation of EC is complex and raises a continuous debate that results in many methods and models. Connectivity is, in turn, divided into structural and functional connectivity. The first measures the landscape structure's connection without considering the species' behavior (Taylor et al., 1993). The second measures the degree to which the landscape avoids or facilitates the movement of a species or a group of species (Bélisle, 2005). Methods for delineating EC that only consider structural connectivity are easy to implement but do not account for all the landscape connectivity. At the same time, models based on functional connectivity are based on species mobility empirical data that are costly to obtain for many species (Reed et al., 2017). These costs can be reduced by considering a few umbrella species (Fleishman et al., 2001). Another alternative to overcome the data burden is using expert opinion, but these methods are often subjective (Zeller et al., 2012).

The present study presents a methodology to reduce empirical data needs when delimiting EC considering functional connectivity. The resulting corridors are compared with those delimited with expert knowledge that considers structural connectivity to analyze whether the proposed methodology complements these methods.

A. Çiner et al. (eds.), *Recent Research on Environmental Earth Sciences, Geomorphology, Soil Science, Paleoclimate, and Karst*, Advances in Science, Technology & Innovation, https://doi.org/10.1007/978-3-031-42917-0_21

2 Materials and Methods

2.1 Study Area

The study focuses on the region of Galicia (NW of Spain), with an approximate area of 2.9 million hectares. The regional government is currently developing a GI strategy where a proposal of EC has been made. This proposal was based on expert knowledge methods that consider structural connectivity. A delimitation proposal of the EC makes this study area interesting for comparing both methodologies.

2.2 Methodology

The proposed method considers a few umbrella species for delineating the EC. These species were chosen to reference the methodology proposed in the Methodological Guide for identifying the Spanish GI (Ministerio para la Transición Ecológica y el reto demográfico (MITECO), 2020). It tried to select species from all taxa representing diverse habitats (Fleishman et al., 2001). Species with a wide distribution or presence in areas far from one another were discarded. The finally selected species were: *Alytes obstetricans, Hyla arborea, Rana temporaria, Felis silvestris, Galemys pyrenaicus, Genetta genetta, Mustela putorius,* and *Lacerta schreiberi.*

The methodology uses a logistic regression model to obtain the presence probability maps of the selected species. These maps could be used as a proxy for the territory's resistance to the species movement (Fattebert et al., 2015). The model relates the species' absence and present data from the Spanish Inventory of Terrestrial Species (Ministerio para la Transición Ecológica y el reto demográfico (MITECO), 2012) with biophysical variables, namely: altitude, slope, topographic wetness index, average annual temperature, average precipitation, solar irradiation, land cover percentage, land cover edge density, distance to rivers, distance to roads, and distance to population settlements. Species for which the model obtained a low AUC were discarded.

Using a stepwise method, the logistic regression model was calibrated with data at a 10×10 km resolution of the grid used in the species inventory (Ministerio para la Transición Ecológica y el reto demográfico (MITECO), 2012). The calibrated model was then run considering variables at a 1×1 km resolution to obtain probability of presence maps at a finer resolution. The maps were subtracted to 1 to invert the values and obtain the mobility resistance maps. These resistance maps were combined with other maps considering the slope resistance, population density, and road network to obtain a cost map for each umbrella species.

The resistance maps were inputted in the ArcGIS "cost connectivity" tool to obtain the least cost paths between the species presence areas. The species presence areas were determined by selecting the biggest land cover patches—obtained from SIOSE, the Spanish land cover database (2014)—with a high species presence probability in the GI core areas. The core areas of the GI correspond with sites included in the European Union Natura 2000 Network of the region. Those areas crossed by more than one least cost path separated by less than 200 m were considered as an EC.

3 Results

Figure 1 shows the EC delimited with this methodology, which was based on functional connectivity, and those proposed for the Galician GI strategy, which was based on structural connectivity, especially the latter, considering the river network.

4 Discussion

The results show that the proposed methodology helps to find EC that complement those of the Galician GI strategy, which were delimited by expert knowledge, considering mainly the river network and the structural connectivity. For example, in certain areas, the EC obtained overlaps the corridors of the Galician GI strategy proposal. This may be explained by the influence of structural connectivity on functional connectivity (Doerr et al., 2011). However, in most cases, the delimited EC shortcuts the river network to connect the GI core areas. This is more in line with the mobility habits of species that are less dependent on wetlands and can move through a wide range of habitats, allowing them to find a shorter path. In addition, some GI core areas are not linked by river courses, the main landscape elements considered corridors in the Galician GI strategy.

Therefore, the results show that the proposed method complements the ones based on structural connectivity well, finding complementary routes for concrete species.

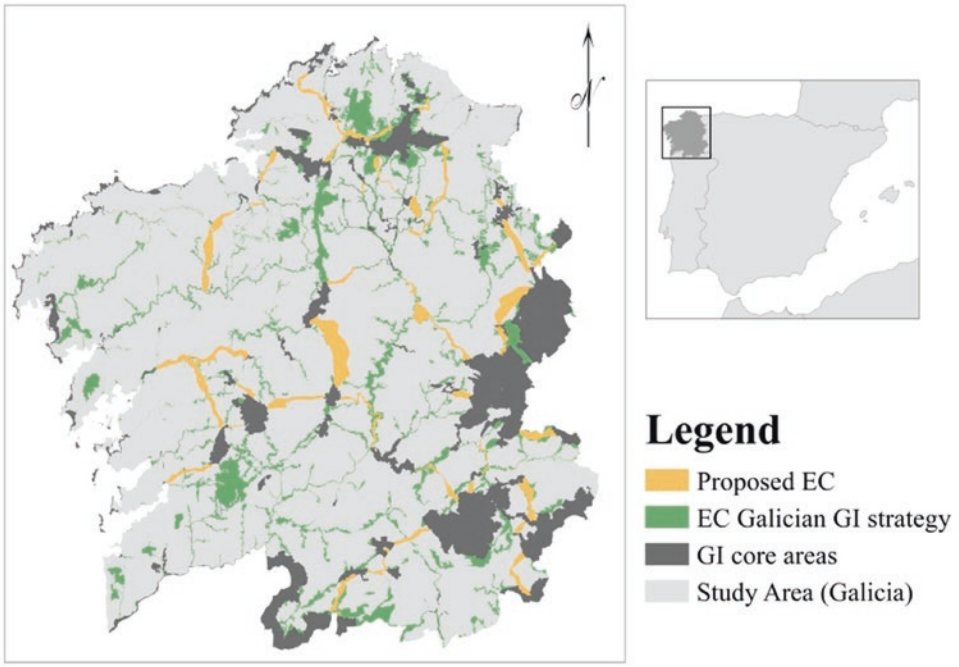

Fig. 1 The EC proposed for the Galician GI strategy (green) and those EC proposed with this methodology (orange)

5 Conclusions

Promising results are obtained with the proposed methodology, which uses public easy-to-obtain data to infer resistance maps using a regression model. This could reduce the costs of obtaining information to delineate EC considering functional connectivity, which would allow considering a wider number of species and thus planning EC that favors the mobility of many of them. In addition, the model could explore the influence of the variables on species mobility, allowing non-expert planners to gain a deeper knowledge of landscape resistance to species mobility.

Furthermore, the proposed methodology can complement methods based on structural connectivity, which would provide greater connectivity of the territory, increasing species resilience to the impacts of climate change.

Acknowledgements This research was funded by Fundación Biodiversidad of the Spanish Ministry of Ecological Transition, project title "INVERCLIMA—Infraestructura Verde para la adaptación de la ordenación territorial al cambio climático".

References

Alagador, D., Cerdeira, J. O., & Araújo, M. B. (2016). Climate change, species range shifts and dispersal corridors: An evaluation of spatial conservation models. *Methods in Ecology and Evolution*, *7*(7), 853–866. https://doi.org/10.1111/2041-210X.12524

Bélisle, M. (2005). Measuring landscape connectivity: the challenge of behavioral landscape ecology. *Ecology*, *86*(8). https://doi.org/10.1890/04-0923

Doerr, V. A. J., Barrett, T., & Doerr, E. D. (2011). Connectivity, dispersal behaviour and conservation under climate change: A response to Hodgson et al. *Journal of Applied Ecology*, *48*(1), 143–147. https://doi.org/10.1111/j.1365-2664.2010.01899.x

European Commission Communication of the Commission to the European Parliament, the Council, the European Economic and Social Committee and the Committee of the Regions. *EU biodiversity strategy for 2030: Bringing nature back into our lives*, COM/2020/380 final.

Fattebert, J., Robinson, H. S., Balme, G., Slotow, R., & Hunter, L. (2015). Structural habitat predicts functional dispersal habitat of a large carnivore: How leopards change spots. *Ecological Applications*, *25*(7), 1911–1921. https://doi.org/10.1890/14-1631.1

Fleishman, E., Murphy, D. D., & Blair, R. B. (2001). Selecting effective umbrella species. *Conservation in Practice*, *2*(2). https://doi.org/10.1111/j.1526-4629.2001.tb00007.x

Ministerio para la Transición Ecológica y el reto demográfico (MITECO). (2012). Inventario Español de Especies Terrestres.

Ministerio para la Transición Ecológica y el reto demográfico (MITECO). (2020). Estrategia Nacional de Infraestructura Verde y de la Conectividad y Restauración Ecológicas.

Reed, G. C., Litvaitis, J. A., Callahan, C., Carroll, R. P., Litvaitis, M. K., & Broman, D. J. A. (2017). Modeling landscape connectivity for bobcats using expert-opinion and empirically derived models: how well do they work?. *Animal Conservation*, *20*(4). https://doi.org/10.1111/acv.12325

Taylor, P. D., Fahrig, L., Henein, K., & Merriam, G. (1993). Connectivity is a vital element of landscape structure. *Oikos*, *68*(3), 571. https://doi.org/10.2307/3544927

Zeller, K. A., McGarigal, K., & Whiteley, A. R. (2012). Estimating landscape resistance to movement: a review. *Landscape Ecology*, *27*(6). https://doi.org/10.1007/s10980-012-9737-0

Toxicological Evaluation of Intermediate Products of Tetracycline Photocatalytic Treatment Using Brine Shrimp (*Artemia salina*) Model System

Nassima Belhouchet, Boualem Hamdi, Omar Bouras, Leila Korichi, Ouahiba Lazzouni, and Haroun Chenchouni

Abstract

Photocatalysis is an eco-friendly technique used to oxidize various organic contaminants in polluted waters. Previous research has shown that the photocatalytic process effectively degrades persistent organic pollutants such as dyes and pharmaceuticals. However, partial photocatalytic degradation always generates various intermediate products that are sometimes more toxic than the original molecules. These intermediates are highly toxic to aquatic life and must be treated and disposed of before being released into the environment. This study aims to evaluate the toxicity of tetracycline (TC) and its intermediate compounds using the Brine Shrimp (*Artemia salina*) model system. Toxicity was assessed using the "Lethality Assay" on Brine Shrimp samples. The number of dead nauplii was counted after 24 and 48 h of exposure to TC samples before and after photocatalytic treatment. The first part of the experiment concerned the determination of the 50% lethal concentration (LC50) of TC, at 24 and 48 h, before photocatalytic treatment. The corresponding results showed that the LC50 of TC before treatment was 2.8 g L^{-1} and 1.9 g L^{-1} at 24 and 48 h, respectively. The second experiment concerned the comparison of the toxicity of TC intermediates between the samples treated by solar irradiation and UV irradiation (24W). Toxicity tests revealed mortality kinetics in all samples treated with either solar or UV irradiation. Larval mortality began within the first hour of solar irradiation. Conversely, samples treated for 5 h with UV irradiation recorded the highest mortality.

Keywords

Photocatalysis process · Toxicity testing · Tetracycline (TC) · Brine shrimp *Artemia salina* · LC (24 h) · LC (48 h)

1 Introduction

During heterogeneous photocatalysis, the degradation mechanisms of pollutants lead to the formation of various intermediate products (Belhouchet et al., 2019). Through their biodegradability or effect on living organisms, the environmental impact of these intermediates may vary from that caused by the original pollutant molecules. Antibiotics are one of the essential classes of emerging contaminants that are widely and increasingly used in human and veterinary medicine (Scaria et al., 2021). Worldwide, antibiotics are commonly used in aquaculture farming environments where many diseases occur due to the scarcity of adaptive immune systems in aquatic species. For this reason, it seems essential to combine the assessment of the potential impacts of reaction intermediates with studies conducted to compare the

N. Belhouchet · B. Hamdi
National Center for Research and Development of Fisheries and Aquaculture (CNDRPA), Boulevard Front de Mer, 42415 Bou-Ismaïl, Tipaza, Algeria

N. Belhouchet (✉)
Laboratory of Conservation and Valorization of Marine Resources, National School of Marine Science and Coastal Management (ENSSMAL), University Campus of Dely Ibrahim, Bois Des Cars, 16320 Cheraga, Algiers, Algeria
e-mail: belhouchet.n@gmail.com

O. Bouras · L. Korichi · O. Lazzouni
Laboratoire Eau Environnement Et Développement Durable, Faculté de Technologie, Université Saad Dahlab-Blida1, 09000 Blida, Algeria

H. Chenchouni
Department of Nature and Life Sciences, Faculty of Exact Sciences and Nature and Life Sciences, University of Tebessa, 12002 Tebessa, Algeria

Laboratory of Natural Resources and Management of Sensitive Environments 'RNAMS', University of Oum-El-Bouaghi, 04000 Oum-El-Bouaghi, Algeria

A. Çiner et al. (eds.), *Recent Research on Environmental Earth Sciences, Geomorphology, Soil Science, Paleoclimate, and Karst*, Advances in Science, Technology & Innovation, https://doi.org/10.1007/978-3-031-42917-0_22

degradation efficiencies of catalysts (Mboula et al., 2012). This study aims to evaluate the toxicity of TC before and after photocatalytic treatment using the "Lethality Assay" on the Brine Shrimp (*Artemia salina*) model.

2 Materials and Methods

2.1 Hatching and Preparation of the Nauplii of *A. salina*

The crustacean Artemia salina (Brine Shrimp) is an aquatic arthropod that lives in lake and ponds under specific salinity, oxygen, temperature, and pH conditions and is very sensitive to environmental changes. *A. salina* is preferred in bioassay studies due to its ease of culture, availability, low cost, and adaptation to adverse conditions in marine ecotoxicology studies (Madhav et al., 2017). In this test, we used cysts available at the CNRDPA Laboratory (National Center for Research and Development of Fisheries and Aquaculture, Bou-Ismaïl, Tipaza, Algeria) to feed fish.

Artemia Brine Shrimp cysts were obtained from INVE Aquaculture Nutrition (Salt Lake City, USA). Natural seawater (NSW), filtered and sterilized before testing, was used to hatch *Artemia salina* cysts and perform the toxicity tests. The preparation of hatched Nauplii (24 h) for toxicological tests was carried out according to the protocols of Shaala et al. (2015) and Kim et al. (2020). These larval stages are known to be the most sensitive to external stimuli such as chemicals (Manfra et al., 2015).

2.2 Toxicity Test

This study included two experiments. First, we studied the 50% lethal concentration (LC50) of TC at 24 and 48 h before photocatalytic treatment. The tetracycline (TC) ($C_{22}H_{24}O_8N_2$) was obtained from Sigma-Aldrich, with a Purity of 98%. We conducted these tests to determine the LC50 (24 h) and LC50 (48 h) by varying the initial concentration of untreated TC from 50 to 5000 mg L^{-1}, including the following concentrations: 50, 100, 200, 400, 800, 1000, 1500, 2000, and 5000 mg L^{-1}. The corresponding tests were performed according to standard protocols used by (Shaala et al., 2015). The tested nauplii were not fed. The number of dead (completely immobile) larvae was counted under the OPTIKA stereo microscopy, and the mortality was calculated using the equation (Eq. 1).

The second experiment was oriented toward comparing the toxicity of TC intermediates between samples treated by solar irradiation and those treated by ultraviolet (UV) irradiation (24W). The TC intermediate samples were obtained from the photocatalytic degradation of TC (Belhouchet et al., 2019). Toxicity determination of TC by-products on *A. salina* nauplius samples was performed at t = 1 h, 2 h, and 5 h under UV (24 W) irradiation and at t = 1, 2, 3, 4, and 5 h under solar irradiation.

Determination of the LC50 (24 h) and LC50 (48 h) was carried out by plotting the recorded mortality rates against the decimal logarithms of the concentrations tested.

2.3 Determination of % Mortality

Determination of the percent mortality was performed after 24 h of treatment using the following formula (Sahgal et al., 2010):

$$\%\text{Mortality} = \frac{(\text{Total nauplii-alive nauplii})}{\text{The total amounts of larves}} \times 100 \quad (1)$$

3 Results

3.1 Lethal Concentration (LC50) of Tetracycline Before Photocatalytic Treatment

Toxicity tests on *Artemia* nauplii before photocatalytic treatment with TC showed that the percent mortality of *A. salina* increased with increasing TC concentration. The mortality of the nauplii increased in the same direction as the exposure time. The TC concentration that killed 50% of the nauplii after 48 h was lower than that of 24 h. Therefore, the lethal LC_{50} (24h) and LC_{50} (48h) concentrations are 2.8 and 1.9 g L^{-1}.

3.2 Nauplius Mortality Caused by By-Products of TC Photocatalysis Treatment

Figure 1 shows the percentage of Nauplius mortality recorded based on TC samples treated with UV irradiation (24 W). The highest mortality rate was recorded in samples exposed for 5 h of photocatalytic treatment by UV irradiation. At this exposure time, mortality exceeded 50%. However, the sample exposed to TC by-products resulting from 1 h of UV photocatalytic treatment did not record any mortality after 24 h. In contrast, the 48 h samples showed low mortality compared to samples of 5 h.

In contrast to samples treated with UV irradiation, Nauplius samples exposed to TC by-products resulting from 1 and 2 h under solar irradiation catalysis recorded

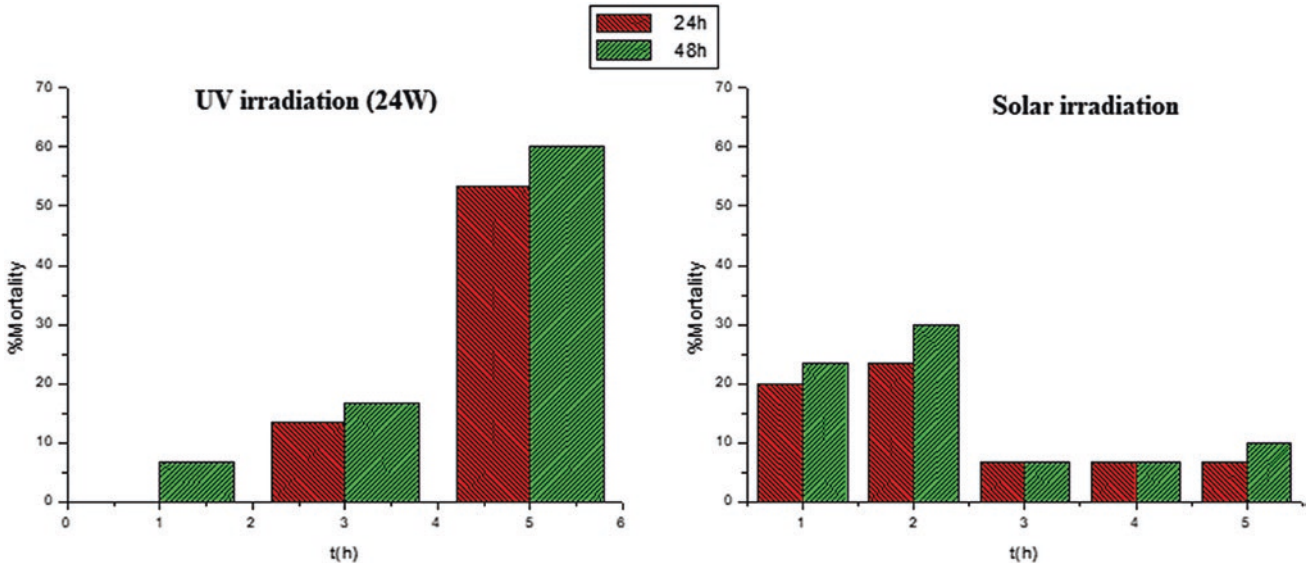

Fig. 1 Mortality rate of *Artemia salina* nauplii recorded based on TC samples treated as a function of treated TC samples by **a** UV irradiation (24 W) after 1, 3, and 5 h of exposure and **b** with solar irradiation for 1, 2, 3, 4, and 5 h of exposure

a higher mortality rate (20–30%) compared to those from 3, 4, and 5 h, where the mortality was between 7 and 10% (Fig. 1). This is probably related to the nature and toxicity of the molecules released during photodegradation in the first two hours of photocatalytic treatment. On the contrary, after 2 h of photocatalytic treatment by solar irradiation, the mortality rate was lower and remained almost constant. This is probably explained by the toxic nature of the molecules released in the first two hours, then degraded and transformed into less toxic molecules. Therefore, the mortality rate is probably caused by TC by-products and the CO_2 produced during the total mineralization of the TC.

4 Discussion

Antibiotics are considered potential emerging environmental contaminants. They are widely and increasingly used in human and veterinary medicine, including growth promotion and prophylaxis in livestock and aquaculture (Kovalakova et al., 2020; Scaria et al., 2021). In addition, antibiotics can increase antibiotic resistance in pathogenic bacteria, which is of particular concern. Therefore, there is a need to study and evaluate the negative effects of antibiotic contamination on the ecosystem and, ultimately, on human health (Liu et al., 2017). Based on the results obtained for LC_{50} (24h) = 2.8 and LD_{50} (48h) = 1.9 g L^{-1}. Results show that TC is not toxic to Artemia ((LC50 (µg mL^{-1}) > 1000), not toxic (Achmad et al., 2019)).

Similar studies using zoological groups related to *Artemia* are available in the literature. The acute toxicity of another antibiotic of the Nitrofuran family (Furazolidone) was evaluated in vivo on two crustacean species: *A. salina* and *Daphnia magna*. The results indicate significant toxicity of the compound on *D. magna*, while *A. salina* is found to be much less sensitive (Macri et al., 1988). The differences in sensitivity observed between *A. salina* and *D. magna* may be due to several reasons. The first assumption is based on the possibility of a slowing down of the ingestion rate caused by the toxic substance (Nasri et al., 2013). The second explanation proposed is based on differences in the filtration patterns of the species considered. Some species do not make any selection of the particles and swallow those useful for nutrition and the useless or even dangerous particles which leads to a concentration of toxic substances in the digestive tract.

On the contrary, *D. magna* filters the particles to be ingested according to their size (Kořínek et al., 1986; Nasri et al., 2013). Furthermore, the study of oxytetracycline (OTC) toxicity on *Artemia parthenogenetica* (Ferreira et al., 2007) shows that *Artemia* was significantly resistant to OTC, with LC_{50} values (24 and 48 h) for *A. parthenogenetica* of 871 and 806 mg L^{-1}, respectively. In addition, toxicity tests on samples treated by the photocatalytic process (solar and UV irradiation) showed different toxicity levels. The results show that the TC by-products are more toxic than the initial TC molecule. This toxicity may be related to the toxic nature of the molecules released during the photocatalytic process.

5 Conclusion

The LC50 for TC was identified as 2.8g L^{-1} and 1.9 g L^{-1} after 24 and 48 h of exposure, respectively. Toxicity tests conducted on first-generation *Artemia salina* larvae exposed to TC and TC photocatalytic intermediate products revealed mortality kinetics for samples treated with solar and UV irradiation. This study indicates that larval mortality begins within the first hour of incubation (24 h) for samples treated with solar irradiation. On the other hand, samples treated with UV irradiation showed high mortality of nauplii for samples of 5 h under photocatalytic treatment. This mortality may be related to the toxic nature of the molecules released during the photocatalytic process.

References

Achmad, R. S., Aditya, L. A., & Cahyariza, N. I. (2019). Acute toxicity test of black pomegranate peel extract (*Granati fructus* Cortex) against larvae of shrimp (*Artemia salina* Leach). *Medical Laboratory Technology Journal, 5*, 62–69.

Belhouchet, N., Hamdi, B., Chenchouni, H., & Bessekhouad, Y. (2019). Photocatalytic degradation of tetracycline antibiotic using new calcite/titania nanocomposites. *Journal of Photochemistry and Photobiology, A: Chemistry, 372*, 196–205. https://doi.org/10.1016/j.jphotochem.2018.12.016

Ferreira, C. S. G., Nunes, B. A., De Melo Henriques-Almeida, J. M., & Guilhermino, L. (2007). Acute toxicity of oxytetracycline and florfenicol to the microalgae *Tetraselmis chuii* and to the crustacean *Artemia parthenogenetica*. *Ecotoxicology and Environmental Safety*, *67*, 452–458 (2007). https://doi.org/10.1016/j.ecoenv.2006.10.006

Kim, M., Lee, W., Park, J., Kim, W., Jo, S., Kim, W., Kim, C., Park, H., Lee, G., & Park, J. (2020). Advanced tracking system of multiple *Artemia* and various behavioral endpoints for ecotoxicological analysis. *Ecological Indicators, 116*, 106503. https://doi.org/10.1016/j.ecolind.2020.106503

Kořínek, V., Křepelová-Macháčková, B., & Macháček, J. (1986). Filtering structures of Cladocera and their ecological significance. II: Relation between the concentration of the seston and the size of filtering combs in some species of the genera *Daphnia* and *Ceriodaphnia*. *Vestn Cesk Spol Zool*, *50*, 255–258.

Kovalakova, P., Cizmas, L., Mcdonald, T. J., Marsalek, B., Feng, M., & Sharma, V. K. (2020). Occurrence and toxicity of antibiotics in the aquatic environment: A review. *Chemosphere, 251*, 126351. https://doi.org/10.1016/j.chemosphere.2020.126351

Liu, S., Zhao, H., Lehmler, H.-J., Cai, X., & Chen, J. (2017). Antibiotic pollution in marine food webs in Laizhou Bay, North China: Trophodynamics and human exposure implication. *Environmental Science & Technology, 51*, 2392–2400. https://doi.org/10.1021/acs.est.6b04556

Macri, A., Stazi, A., & Di Delupis, G. D. (1988). Acute toxicity of furazolidone on *Artemia salina*, *Daphnia magna*, and *Culex pipiens molestus* larvae. *Ecotoxicology and Environmental Safety, 16*, 90–94. https://doi.org/10.1016/0147-6513(88)90021-8

Madhav, M., David, S. E. M., Kumar, R. S., Swathy, J., Bhuvaneshwari, M., Mukherjee, A., & Chandrasekaran, N. (2017). Toxicity and accumulation of Copper oxide (CuO) nanoparticles in different life stages of *Artemia salina*. *Environmental Toxicology and Pharmacology, 52*, 227–238. https://doi.org/10.1016/j.etap.2017.03.013

Manfra, L., Savorelli, F., Di Lorenzo, B., Libralato, G., Comin, S., Conti, D., Floris, B., Francese, M., Gallo, M., & Gartner, I. (2015). Intercalibration of ecotoxicity testing protocols with *Artemia franciscana*. *Ecological Indicators, 57*, 41–47. https://doi.org/10.1016/j.ecolind.2015.04.021

Mboula, V. M., Hequet, V., Gru, Y., Colin, R., & Andres, Y. (2012). Assessment of the efficiency of photocatalysis on tetracycline biodegradation. *Journal of Hazardous Materials*, *209*, 355–364. https://doi.org/10.1016/j.jhazmat.2012.01.032

Nasri, A., Boufahja, F., Hedfi, A., Mahmoudi, E., Aissa, P., & Essid, N. (2013). Réponse des différents taxons méiofaunistiques à la contamination par un antibiotique (la Penicilline G): étude microcosmique.

Sahgal, G., Ramanathan, S., Sreenivasan Sasidharan, M., Mordi, N., Ismail, S., & Mansor, S. M. (2010). Brine shrimp lethality and acute oral toxicity studies on *Swietenia mahagoni* (Linn.) Jacq. Seed methanolic extract. *Pharmacognosy Research*, *2*(4), 215–220. https://doi.org/10.4103/0974-8490.69107

Scaria, J., Anupama, K., & Nidheesh, P. (2021). Tetracyclines in the environment: An overview on the occurrence, fate, toxicity, detection, removal methods, and sludge management. *Science of the Total Environment, 771*, 145291. https://doi.org/10.1016/j.scitotenv.2021.145291

Shaala, N. M. A., Zulkifli, S. Z., Ismail, A., Azmai, M. N. A., & Mohamat-Yusuff, F. (2015). Lethal concentration 50 (LC50) and effects of Diuron on morphology of brine shrimp *Artemia salina* (Branchiopoda: Anostraca) Nauplii. *Procedia Environmental Sciences, 30*, 279–284. https://doi.org/10.1016/j.proenv.2015.10.050

GUIDE–Cell De-clustering Application: A Case Study on Groundwater Arsenic Contamination

Gunes Ertunc

Abstract

More intensive sampling in the areas of very high or very low values is usually done preferentially to understand the distribution of the regionalized variable better. However, this situation causes a biased difference with the actual distribution of this variable and is misleading. Therefore, samples should be collected at regular intervals or randomly to avoid biased mean differences due to preferential sampling. Alternatively, cell de-clustering can be applied to represent the statistical characteristics of the variable properly. This study applies cell de-clustering to groundwater arsenic measurements as a case study. The naïve statistics from the preferential sampling of high arsenic values and cell de-clustered statistics were compared in the case study. The original data arsenic concentration exceeds the allowable limits. However, the results show that the mean arsenic concentration for the de-clustered data is safe. The cell de-clustering application is a modular part of GUIDE (Geostatistical Utility in Domaining and Estimation), an executable computer application compiled by the author. Some of the critical features of this application are exploratory data analysis, estimation with ordinary kriging, and classification with support vector machines, which are also presented in this paper. This application is made available as a freeware tool for professional or educational use.

Keywords

Cell de-clustering · Arsenic · Contamination

G. Ertunc (✉)
Hacettepe University, Ankara 06800, Turkey
e-mail: gertunc@hacettepe.edu.tr

1 Introduction

Most of the time, decisions about a regional variable are made based on a statistical analysis of spatial data having non-uniform spatial distribution. Heterogeneity in the spatial setting in the field has a direct effect on the attribute value at interest. For example, mineralization can be attributed to underground geological environments, and domains or pollutant concentrations in groundwater can be attributed to the flow directions of the water. It is very common for the sample values to have abnormally high or low values in a part of the field. Collecting more sampling in regions with outliers is natural as it is to understand the structure of the attribute better. However, it should be considered that there will be a biased difference in the true distribution of this variable.

To account for the irregular sampling and bias caused by heterogeneous site-specific effects on the data, the cell de-clustering method has been presented by many researchers in the literature as an important geostatistical tool for analyzing spatial data (Deutsch & Journal, 1998; Deutsch et al., 1998; Pyrcz & Deutsch, 2002; Renard et al., 2020).

Random variable distributions or the ratios related to the categorical features are the basic input parameters in the uncertainty assessment analysis or geostatistical simulations. De-clustering techniques are frequently used to determine these distributions or ratios. In this technique, a weight ($w_i = 1, \ldots, n$) is assigned to each sample ($z_i = 1, \ldots, n$) based on its proximity to the surrounding data. Data that are closer together are given less weight, while data that are far apart gain more weight. The basic assumption here is that more frequently collected data is preferably collected from low or high-value locations. The clustering technique creates non-parametric distribution and summary statistics using assigned weights.

In this study, the de-clustering software application which the author compiles is presented. The applet is a modular part of the software GUIDE (Geostatistical Utility

A. Çiner et al. (eds.), *Recent Research on Environmental Earth Sciences, Geomorphology, Soil Science, Paleoclimate, and Karst*, Advances in Science, Technology & Innovation, https://doi.org/10.1007/978-3-031-42917-0_23

in Domaining and Estimation) containing solution tools for statistical analysis of spatial data, estimation by the kriging method, and determination of homogeneous geological regions has been compiled with MATLAB Compiler™. The de-clustering applet, which is the subject of the study, can be downloaded free of charge from http://yunus.hacettepe.edu.tr/~gertunc/GUIDE_declustering.rar.

2 Materials and Methods

The cell de-clustering method is based on a grid adapted to the data extent and weights attached to each sample according to the percentage of them falling into the cells forming this grid. The cells that make up this grid are completely different from the concept of block model cells used in geostatistical estimation or simulation. In this method, cell size depends on the distance between data in sparsely sampled regions. The following equation shows the calculation of the weight per sample:

$$w_i = \frac{\frac{1}{n_{dh}}}{n_{vs}} \quad (1)$$

where w_i: weight of sample at location i, n_{dh}: number of occupied cells, n_{vs}: number of samples falling into cells.

Weighted descriptive statistics are calculated with weights assigned to all samples. In this way, statistics calculated with weighted data, biased and misleading statistics are corrected caused by preferential sampling.

The grid location's lower left corner directly affects the samples' weights. The number of random origins provides an average weight for each sample. This randomization is described with the term "offset". Generally, the offset number is selected between 25 and 100.

Another important parameter of the cell de-clustering method is cell size. In the very small selected cell size, the weight assigned to each sample will equal one since the number of filled cells will equal the number of samples. On the other hand, in the case of a very large cell, all sample locations will be weighted equally. In both cases, the weighted average values are equal. Therefore, to select the optimum cell size, a series of calculations was made for each cell size ranging from small to large.

The optimum cell size is the range of data in the sparsely sampled location. However, this optimum size is not exactly known, and a range of cell sizes should be considered input parameters to help select the correct size. Therefore, the maximum cell size should not be set too large. The best approach to choosing the optimal cell size is to evaluate the de-clustered mean for various cell sizes and choose a value close to minimizing or maximizing this mean.

3 GUIDE-Cell De-clustering and Case Study

The Cell De-clustering applet consists of a total of 4 input screens. First, the user sets the working directory where the MS Office Excel file is located. After that, northing, easting, and attribute columns are matched. Finally, in the following application window (Fig. 1), the necessary input parameters for the cell de-clustering method are entered.

The dataset used in the study consists of a synthetic arsenic value of 153 groundwater samples dispersed in a

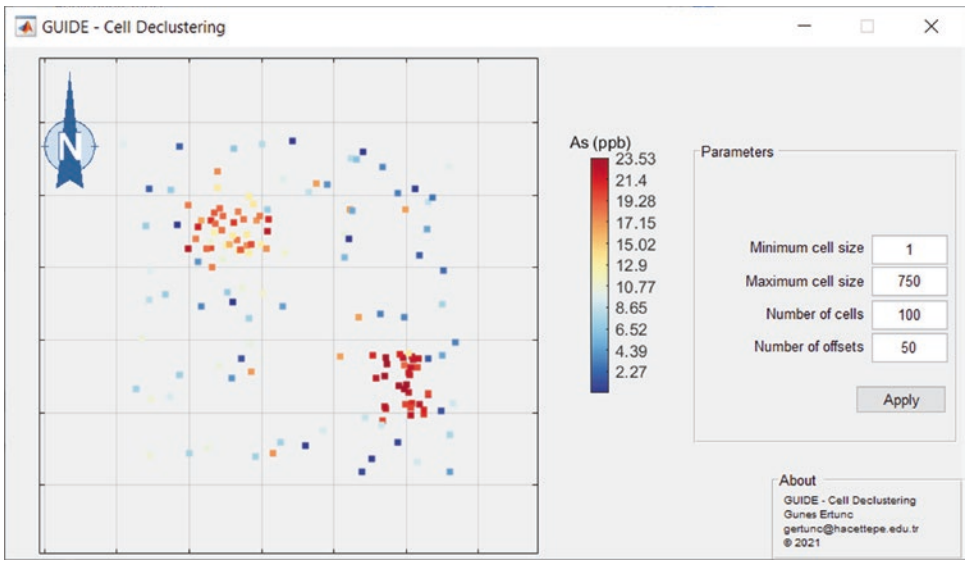

Fig. 1 Cell de-clustering parameters

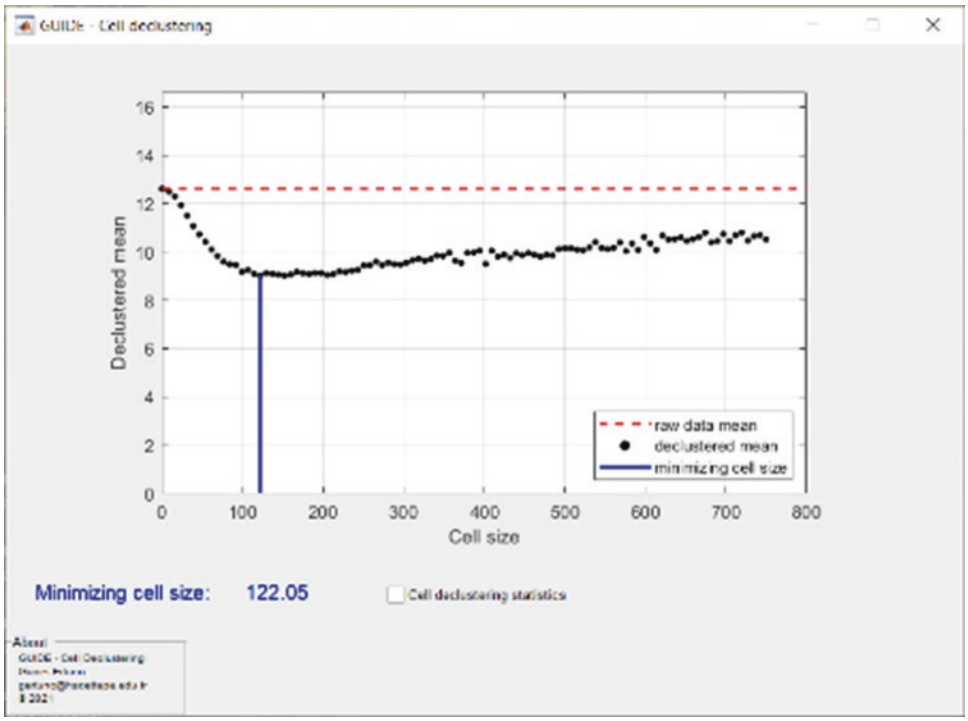

Fig. 2 Cell de-clustering results

two-dimensional space containing arsenic concentrations measured in μg/L. Minimum and maximum cell sizes are selected as 1 and 750 m, respectively. The number of offsets is 50, and de-clustered means are calculated for 100 different cell sizes.

The results (Fig. 2) show that the minimum de-clustered mean is obtained at cell size 122.05 m. De-clustered statistics are calculated based on this cell size, and the results screen is presented in Fig. 3.

4 Conclusion

The de-clustering method aims to eliminate biased statistics. This is done by weights assigned based on the proximity of sample values to each other. In cell de-clustering, sample values are not subjected to change (i.e., outlier values remain in the data set and de-clustered set.

In this case study, the arsenic average of the original data set is 12.60 μg/L, which is above the WHO provisional

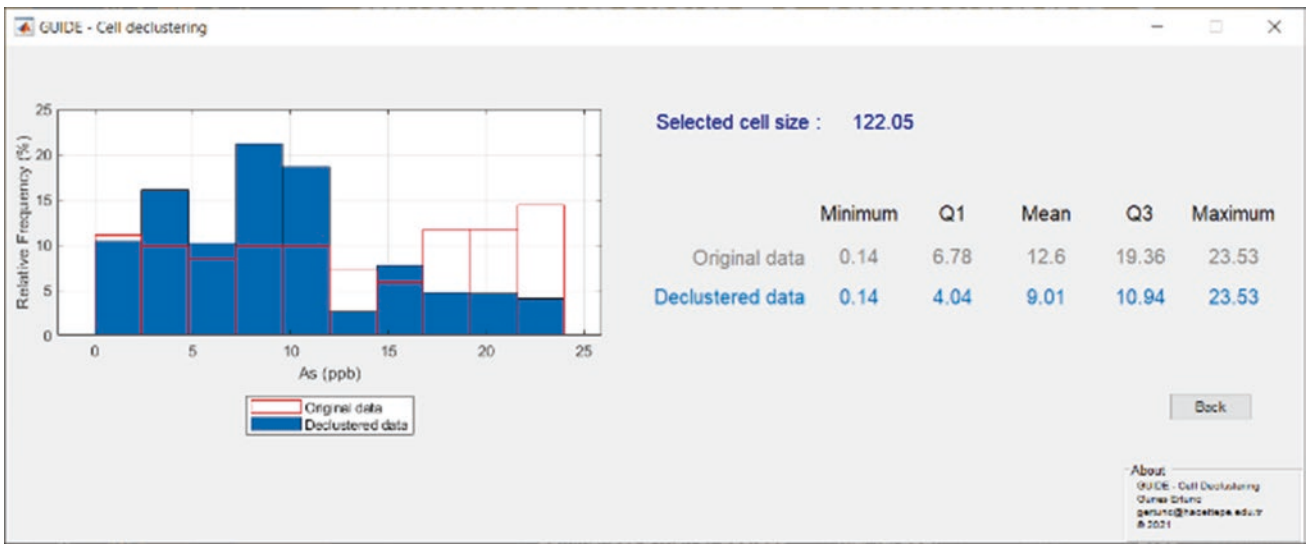

Fig. 3 Cell de-clustering statistics

guideline value of 10 μg/L (WHO, 2021). This result is due to the collection of more samples from the regions with high values. In other words, preferential sample collection is biased and misleading. When the histograms of the original and de-clustered data are compared (Fig. 3), it is seen that high values of the original data are more frequent. This is because high values are sampled more frequently, and the cell de-clustering method reduces the weights of these values and produces results that correct biased statistics. As a result of the de-clustered statistics, it was revealed that the average is 9.03 μg/L and remained within acceptable limits.

References

Deutsch, C. V., Frykman, P., & Xie, Y. L. (1999). *Declustering with Seismic or "soft" geologic data, centre for computational geostatistics report one 1998/1999*. University of Alberta.

Deutsch, C. V., & Journel, A. G. (1998). *GSLIB: Geostatistical software library: And user's guide* (2nd ed.). Oxford University Press.

Pyrcz, M. J., & Deutsch, C. V. (2002). De-clustering and debiasing. In *Centre for computational geostatistics*, Paper 62, Annual Report 4.

Renard, D., Bez, N., Desassis, N., Beucher, H., Ors, F., & Laporte, F. (2020). *RGeostats: The geostatistical package*. MINES ParisTech.

WHO. https://www.who.int/news-room/fact-sheets/detail/arsenic. Last accessed 25 Mar 2021.

Forecasting of Water Level Fluctuations with Periodic Fuzzy Logic Models for Two Shallow Eastern Mediterranean Lakes

Özlem Yağbasan and Vahdettin Demir

Abstract

In this study, forecasting of monthly water levels is investigated by using three different Adaptive Neuro-Fuzzy Inference Systems (ANFISs), ANFIS with Grid Partition (ANFIS-GP), ANFIS with Substructive Clustering (ANFIS-SC), and ANFIS with Fuzzy C Means (ANFIS-FCM) for forecasting 3-month ahead water level of Lakes Mogan and Eymir stations in Central Turkey with the periodic component analysis. The data sample comprises monthly monitoring records of average lake water levels from 1997 to 2020. While 90% of the whole data was used to train the three models, 10% was used for testing. The root means squared error (RMSE), mean absolute error (MAE), and the determination coefficient (R^2) were used as the evaluation criteria in the study. The results revealed that the ANFIS-SC method was slightly better at predicting lake water levels than the ANFIS-FCM and ANFIS-GP methods regarding RMSE values.

Keywords

Forecasting · Lake Water Level Fluctuation · ANFIS · Periodic Component

1 Introduction

Understanding the variation of lake water level fluctuations and the potential drivers might provide valuable insights into lake management and conservation (Gownaris et al., 2018). Water lake level fluctuations are crucial in different spatial and temporal scales under natural conditions. Furthermore, their impacts are expected to be enhanced within the global climate change projections with potential management problems (Leira & Cantonati, 2008). Therefore, Lake water level modeling and forecasting are very important for managing water resources, including regional flood and drought, groundwater, and environmental flow analysis.

In this study, the aims of the current research are (i) investigation of three different fuzzy logic models (ANFIS-FCM, ANFIS-GP, and ANFIS-SC) for modeling water levels forecasting, (ii) investigation of the influence of the periodicity component for water levels forecasting, and (iii) demonstration of the effectiveness. Lakes Mogan and Eymir in Central Turkey have been used to perform the proposed models.

2 Materials and Methods

Shallow Eastern Mediterranean Lakes Mogan and Eymir, 20 km south of Ankara in Central Turkey, are important scenic, recreational, and ecological resources for Ankara and Gölbaşı (Fig. 1). Lake Mogan has a drainage area of 926 km^2, while Lake Eymir has a drainage area of 42 km^2. Even though both lakes and the surrounding regions primarily serve urban housing and recreational purposes, the lakes have significant wildlife and ecological values (Yagbasan et al., 2017, 2020). Hydrologically connected lakes are designated as "Specially Protected Areas", and Lake Mogan

Ö. Yağbasan
Department of Geography Education, Gazi University, 06500 Ankara, Turkey

V. Demir (✉)
Department of Civil Engineering, Faculty of Engineering and Natural Sciences, KTO Karatay University, 42020 Karatay, Konya, Turkey
e-mail: vahdettin.demir@karatay.edu.tr

A. Çiner et al. (eds.), *Recent Research on Environmental Earth Sciences, Geomorphology, Soil Science, Paleoclimate, and Karst*, Advances in Science, Technology & Innovation, https://doi.org/10.1007/978-3-031-42917-0_24

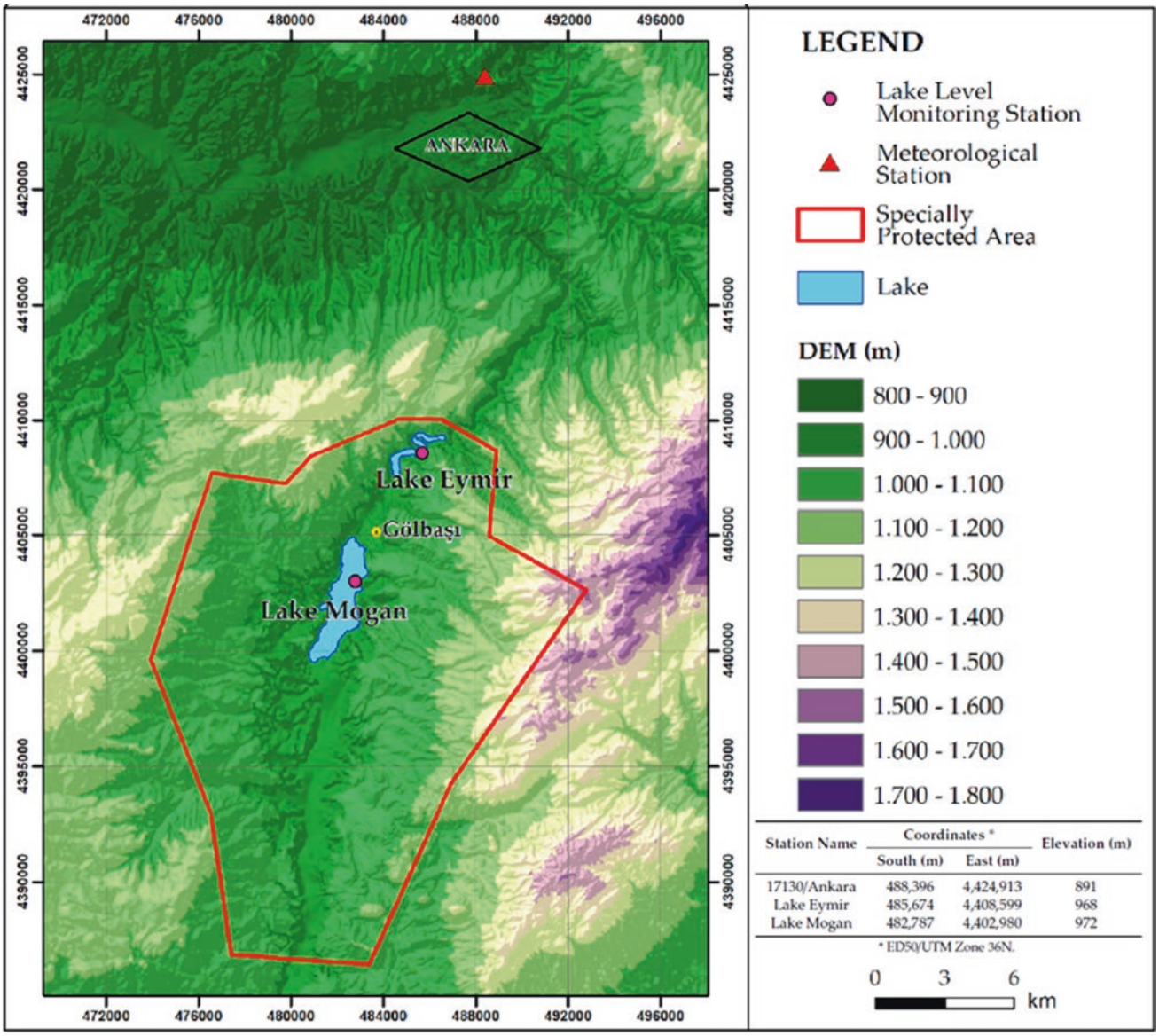

Fig. 1 Digital elevation map of the study area and location of the monitoring stations, modified from Yagbasan et al. (2020)

was declared as an "Important Bird Area" in 1990 by the Ministry of Environment and Urbanization (Yagbasan et al., 2020). The lake levels between 1997 and 2015 were obtained from State Hydraulic Works. Unfortunately, these lake levels have not been monitored post-2015. Dear Prof. Dr. Meryem Beklioğlu from Middle East Technical University provided the lake levels for 2015–2020.

2.1 ANFIS-FCM

In ANFIS-Fuzzy C Means Clustering (FCM), datasets are divided into groups, and datasets with the same characteristics belong to the same clusters. In contrast, datasets that are not similar belong to different clusters (Bezdek, 1973; Kurtulus & Razack 2010).

2.2 ANFIS-SC

The ANFIS subtractive clustering (ANFIS-SC) model combines ANFIS with the subtractive clustering (SC) approach. Every data point set in SC is regarded as a possible cluster center (Kisi et al., 2017).

2.3 ANFIS-GP

The ANFIS Grid partitioning (GP) method is one of the input partitioning methods frequently used in fuzzy logic methods (Jang, 1993; Silarbi et al., 2014). In this method, each variable is partitioned independently, characterizing the membership functions of the previous variable.

3 Results

The study divided the data into training and testing classes before modeling. The training data set accounts for 90% (238 months) of all data, while the testing data set accounts for 10% (26 months) (Chen et al., 2020; Müsevitoğlu et al., 2020). The study modeled water level fluctuations of the lakes using the ANFIS-FCM, ANFIS-SC, and ANFIS-GPC methods. In addition, 3 months ahead, water level data and periodicity component (month number of the year, e.g., 1, 2, 3,…12) were used as input data. The comparison of the models in the study included the Root Mean Square Error (RMSE), Mean Absolute Error (MAE), and coefficient of determination (R^2), as shown in Eqs. (1–3).

$$\mathrm{RMSE} = \sqrt{\frac{1}{N}\sum_{i=1}^{N}(L_e - L_o)^2} \tag{1}$$

$$\mathrm{MAE} = \frac{1}{N}\sum_{i=1}^{N}|L_e - L_o| \tag{2}$$

$$R^2 = \frac{\left[\sum_{i=1}^{N}(L_e - \overline{L}_e)(L_o - \overline{L}_o)\right]^2}{\sum_{i=1}^{N}(L_e - \overline{L}_e)^2 \sum_{i=1}^{N}(L_o - \overline{L}_o)^2} \tag{3}$$

Here, N is the number of data, and L_e and L_o indicate the forecasted and observed lake water levels. Table 1 shows the comparison criteria for the methods.

Figure 2 depicts the training and test results of the approaches as graphs. Figure 3 also includes the Taylor diagrams showing methodology and test results.

Table 1 Comparison criteria in training and test phases

Station name	METHODS	DATA SETS	RMSE	MAE	R^2
Lake Mogan	ANFIS-FCM	Training	0.130	0.088	0.918
		Test	0.186	0.148	0.812
	ANFIS-SC	Training	0.134	0.090	0.913
		Test	0.185	0.147	0.812
	ANFIS-GP	Training	0.141	0.010	0.903
		Test	0.203	0.017	0.796
Lake Eymir	ANFIS-FCM	Training	0.161	0.100	0.959
		Test	0.163	0.132	0.750
	ANFIS-SC	Training	0.160	0.101	0.959
		Test	0.155	0.130	0.722
	ANFIS-GP	Training	0.143	0.009	0.967
		Test	0.214	0.016	0.570

In Table 1 and Figs. 2 and 3, the ANFIS-SC method forecasts the lake water levels slightly better than ANFIS-FCM and ANFIS-GP regarding RMSE values.

4 Discussion

Furthering our understanding of the lake water levels to the hydrological drivers is of the utmost importance in contributing to their conservation with adequate mitigation and adaptation measures. Although various models contain hydrological and hydrometeorological variables such as precipitation, runoff, temperature, and evaporation, using a model that simulates level changes based on historical level records is more cost-effective and valuable (Şen et al., 2000). Based on RMSE and MAE (Table 1), the predictions of ANFIS-SC models are acceptable compared to previous studies. For example, Karimi et al. (2012) predicted water levels with RMSE values of 0.81 and 0.07 for the Urmia Lake in Northwestern Iran by using ANFIS (Karimi et al., 2012).

5 Conclusions

In the study, forecasting monthly water levels is investigated using three different ANFISs, for Lakes Mogan and Eymir. The results are as follows: in both lakes, the ANFIS-SC model gave the smallest RMSE value, while the ANFIS-GP model gave the highest RMSE value. Moreover, the periodic component increased the model performance by 5–20%.

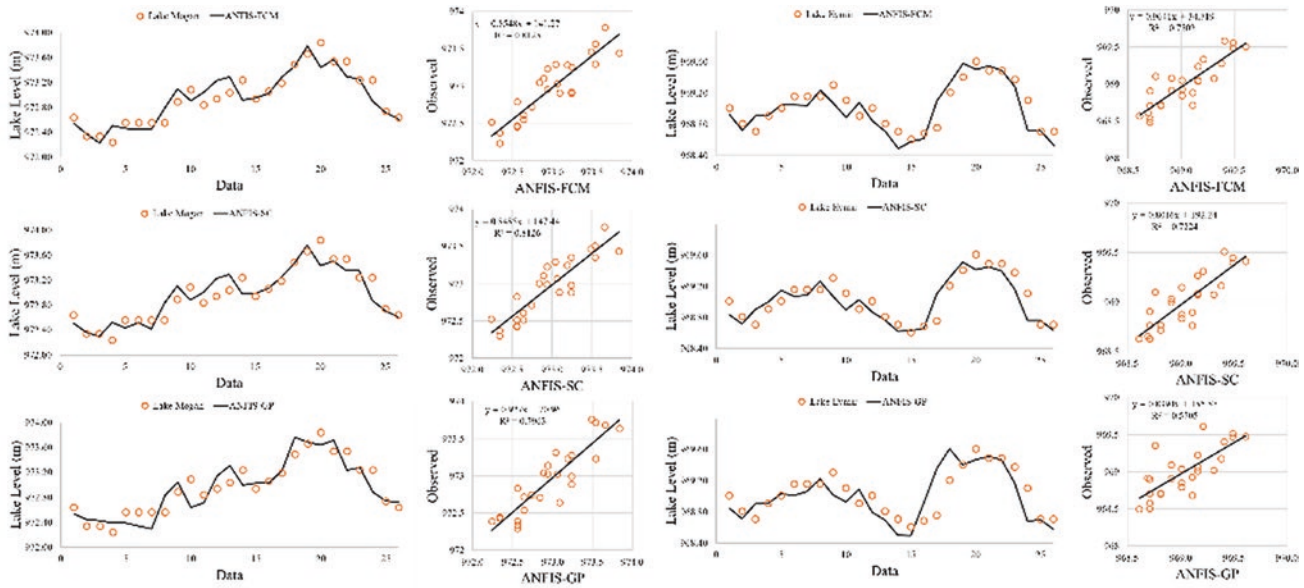

Fig. 2 The water level from the ANFIS's methods for Lakes Mogan and Eymir in the test phase, respectively

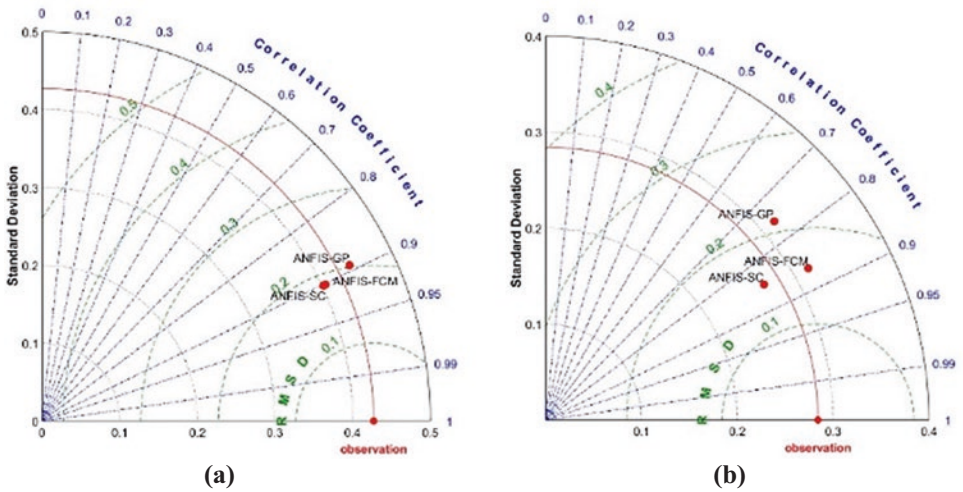

Fig. 3 Taylor diagram: for Lake Mogan (**a**), Lake Eymir (**b**)

References

Bezdek, J. C. (1973). Cluster validity with fuzzy sets. *Journal of Cybernetics, 3*, 58–73. https://doi.org/10.1080/01969727308546047

Chen, Y., Song, L., Liu, Y., Yang, L., & Li, D. (2020). A review of the artificial neural network models for water quality prediction. *Applied Sciences*, *10*. https://doi.org/10.3390/app10175776

Gownaris, N. J., Rountos, K. J., Kaufman, L., Kolding, J., Lwiza, K. M. M., & Pikitch, E. K. (2018). Water level fluctuations and the ecosystem functioning of lakes. *Journal of Great Lakes Research, 44*, 1154–1163. https://doi.org/10.1016/j.jglr.2018.08.005

Jang, J.-S.R. (1993). ANFIS: Adaptive-network-based fuzzy inference system. *IEEE Transactions on Systems, Man, and Cybernetics, 23*, 665–685. https://doi.org/10.1109/21.256541

Karimi, S., Shiri, J., Kisi, O., & Makarynskyy, O. (2012). Forecasting water level fluctuations of urmieh lake using gene expression programming and adaptive neuro-fuzzy inference system. *International Journal of Ocean and Climate Systems, 3*, 109–125.

Kisi, O., Demir, V., & Kim, S. (2017) Estimation of long-term monthly temperatures by three different adaptive neuro-fuzzy approaches using geographical inputs. *Journal of Irrigation and Drainage Engineering*, *143*. https://doi.org/10.1061/(ASCE)IR.1943-4774.0001242

Kurtulus, B., & Razack, M. (2010). Modeling daily discharge responses of a large karstic aquifer using soft computing methods: Artificial neural network and neuro-fuzzy. *Journal of Hydrology*, *381*, 101–111.

Leira, M., & Cantonati, M. (2008). Effects of water-level fluctuations on lakes: An annotated bibliography. *Hydrobiologia, 613*, 171–184.

Müsevitoğlu, A., Arslan, M. H., Aksoylu, C., & Özkış, A. (2020). Experimental and analytical investigation of chemical anchors's behaviour under axial tensile. *Measurements Journal of the International Measurement Confederation*, *158*. https://doi.org/10.1016/j.measurement.2020.107689

Şen, Z., Kadioğlu, M., & Batur, E. (2000). Stochastic modeling of the Van Lake monthly level fluctuations in Turkey. *Theoretical and Applied Climatology, 65*, 99–110. https://doi.org/10.1007/s007040050007

Silarbi, S., Abderrahmane, B., & Benyettou, A. (2014). Adaptive network based fuzzy inference system for speech recognition through subtractive clustering. *International Journal of Artificial Intelligence & Applications, 5*, 43–52. https://doi.org/10.5121/ijaia.2014.5604

Yagbasan, O., Demir, V., & Yazicigil, H. (2020). Trend analyses of meteorological variables and lake levels for two shallow lakes in central Turkey. *Water, 12*, 414. https://doi.org/10.3390/w12020414

Yagbasan, O., Yazicigil, H., & Demir, V. (2017). Impacts of climatic variables on water-level variations in two shallow Eastern Mediterranean lakes. *Environmental Earth Science*, *76*. https://doi.org/10.1007/s12665-017-6917-x

Simulation and Evaluation of Thermal Interference Between Ground Source Heat Pumps (GWHP) in Kutahya Residential Area (Western Anatolia, Turkey)

Ali Samet Ongen and Zeynal Abiddin Erguler

Abstract

Increasing global warming and environmental problems have led developed countries to renewable energy sources. In this context, Groundwater Heat Pumps (GWHP), a renewable, clean, and environmentally friendly energy system, have become very popular globally. Despite these advantages of GWHPs, unplanned use of the system may cause thermal interference between extraction and injection wells or adjacent GWHPs, and it threatens system performance and sustainability. As there would be more GWHP installations in urban areas, thermal interference is expected to occur, especially in densely urbanized areas. Therefore, it aimed to create thermal interaction models between GWHPs in the Kutahya (Turkey) residential area using the FEFLOW software in this study. Following this purpose, groundwater temperature and groundwater level were measured between January–December (2019) in 41 observation wells. Also, the thermal properties of soils were determined. To simulate thermal interference, 50 GWHPs were affected in the alluvial aquifer in the study area using the FEFLOW software, and thermal interference simulations between GWHPs for 50 years were created. According to simulations, the thermal effect increases over time. Also, it was observed that the hydraulic conductivity, extraction/injection flow rate, and distance between systems directly affect thermal interference. Considering that thermal interference negatively affects system performance, it can be concluded that the hydraulic conductivity, flow rate, and distance between systems should be considered in the design phase to avoid the thermal effect between extraction and injection wells and adjacent GWHPs.

Keywords

Groundwater heat pump · Shallow geothermal energy · Thermal interference

1 Introduction

Energy needs also increased due to population growth in cities. The growing energy demand has led to an increase in the consumption of fossil fuels. Fossil fuels cause many environmental problems, especially global warming, due to high CO_2 emissions. Because of these fuels' environmental impact and costs, countries have turned to renewable energy sources that can be an alternative to fossil fuels. In this direction, shallow geothermal energy systems are becoming increasingly common worldwide. One of the most critical factors in the performance and sustainability of external geothermal systems is the thermal interaction that develops within the system and/or between neighboring systems. Therefore, it is essential to create thermal interaction models in the design phase of shallow geothermal systems to predict thermal plume borders. Thermal interaction may occur within/between external geothermal systems depending on time, and this thermal interaction may adversely affect system performance.

2 Materials and Methods

To determine the groundwater temperature and groundwater level in the city center of Kütahya, 41 water wells from different residential areas (urban, rural, and industrial) were used. Groundwater level and groundwater temperature measurements were carried out periodically for 12 months,

A. S. Ongen (✉) · Z. A. Erguler
Department of Geological Engineering, Kutahya Dumlupinar University, 43270 Kutahya, Turkey
e-mail: alisamet.ongen@dpu.edu.tr

A. Çiner et al. (eds.), *Recent Research on Environmental Earth Sciences, Geomorphology, Soil Science, Paleoclimate, and Karst*, Advances in Science, Technology & Innovation, https://doi.org/10.1007/978-3-031-42917-0_25

from January to December 2019, at measurement wells distributed over an area of approximately 53 km^2.

Within the scope of the study, FEFLOW software was used to predict the thermal zone and groundwater flow that will occur underground over time due to heat transfer within shallow geothermal systems or between neighboring systems, and thermal interaction models were created in the study area. Furthermore, to observe the effect of hydraulic conductivity, flow, and distance parameters, different hydraulic conductivity, flow, and distance values were used in the models. All models created using the FEFLOW software were made in the laboratories of the Department of Environmental, Land, and Infrastructure Engineering of the Technical University of Turin (Politecnico di Torino).

3 Results

The heat transfer models created in the FEFLOW software are presented in Figs. 1, 2 and 3. Models were created under different hydraulic conductivity, flow, and system distance (between extraction and injection wells) conditions. In the scenario presented in Fig. 1, the hydraulic conductivity value was accepted as 5.1 m/day, 10 m/day, 25 m/day, and 44.42 m/day, respectively. In the model shown in Fig. 2, created to determine the effect of the distance between the extraction and the injection well on the thermal interaction, the distance between the wells was set as 100 m and 200 m, respectively. For the last model, created to see the effect of flow rate, extraction, and injection rates were

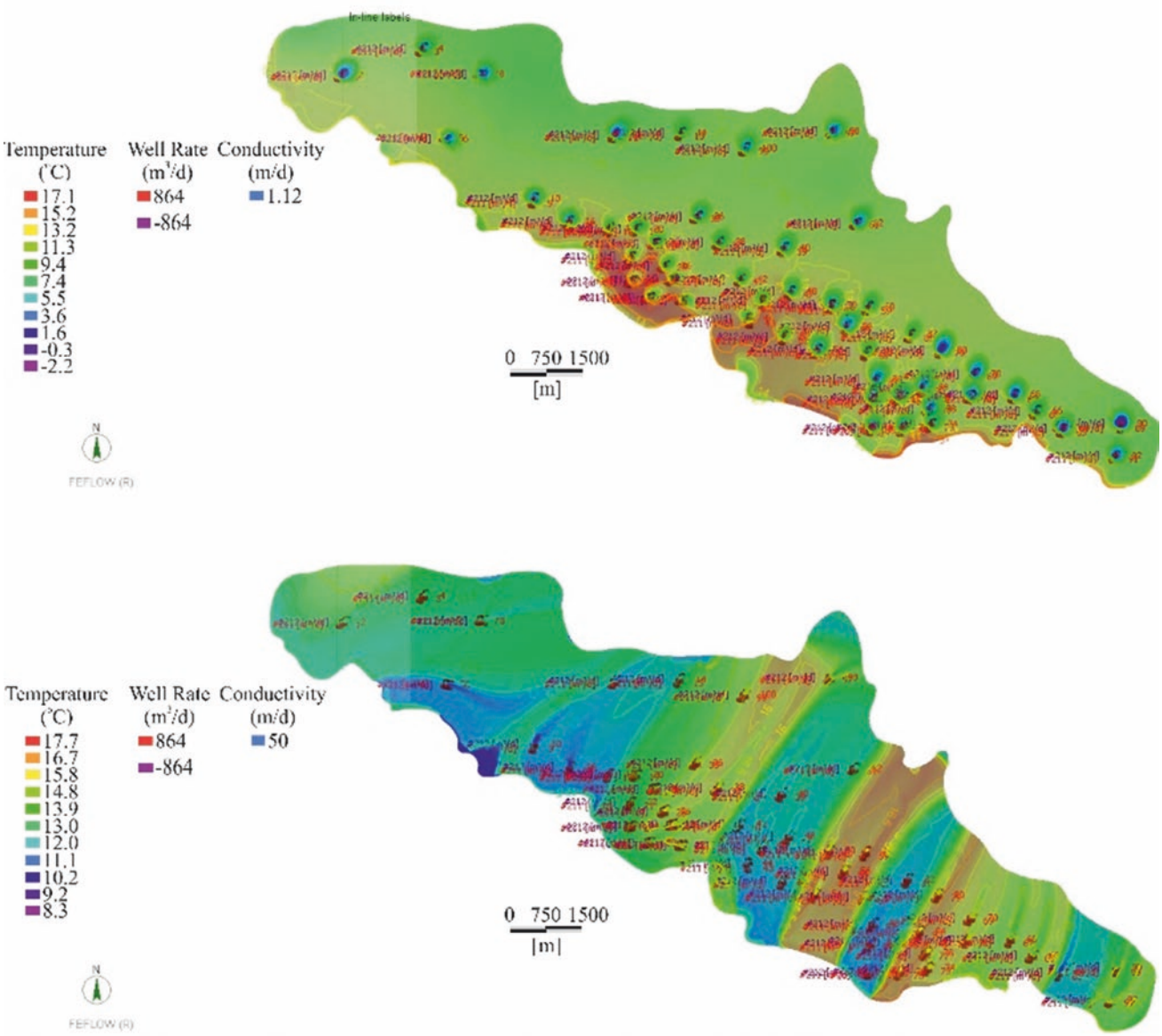

Fig. 1 Thermal plume observed at different hydraulic conductivity values (simulation time: 50 years)

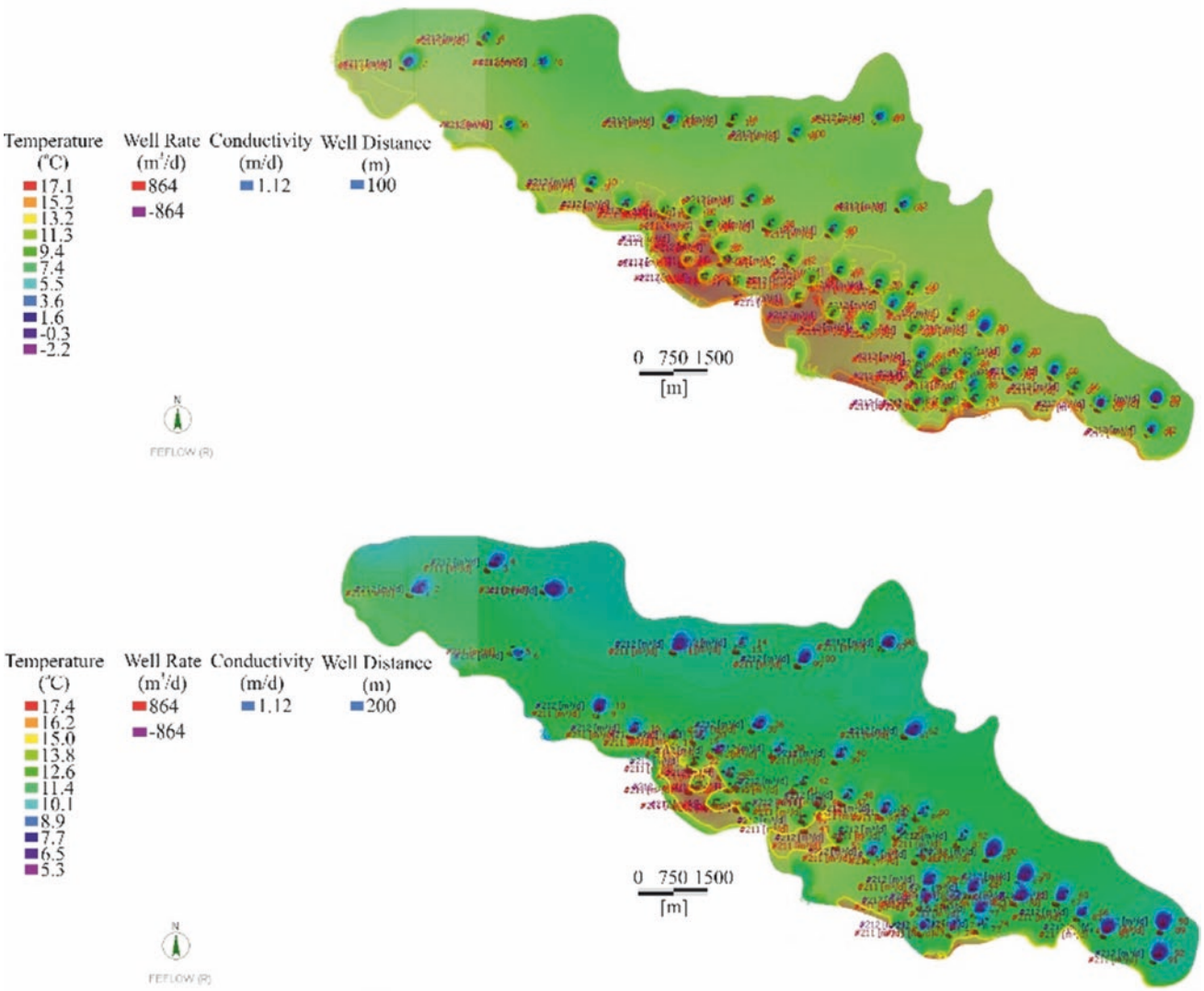

Fig. 2 Thermal plume observed at different distance values between systems (simulation time: 50 years)

accepted at 86.4 m^3/day and 864 m^3/day (see Fig. 3). The simulation period for each model was accepted as 50 years for Figs. 1 and 2, 1–10–25 and 50 years for Fig. 3.

4 Discussion

According to the thermal interaction models, hydraulic conductivity and distance between shallow geothermal systems are the most critical factors affecting the thermal plume wideness. However, a study conducted by Freedman (2012) found that the injection flow rate of the system is more effective on the thermal plume than hydraulic conductivity. However, according to the results obtained in this study, it was observed that the effect of flow rate on the thermal plume was less than the hydraulic conductivity and distance between systems.

5 Conclusions

As can be seen in the models created within the scope of the study, hydraulic conductivity, flow rate, and the distance between the extraction and injection well have a critical role in the thermal interaction between shallow geothermal systems. The thermal interaction decreases as the hydraulic conductivity coefficient, the flow rate, and the distances between the extraction and injection well increase. Therefore, these parameters should be considered for system efficiency and sustainability during the design phase.

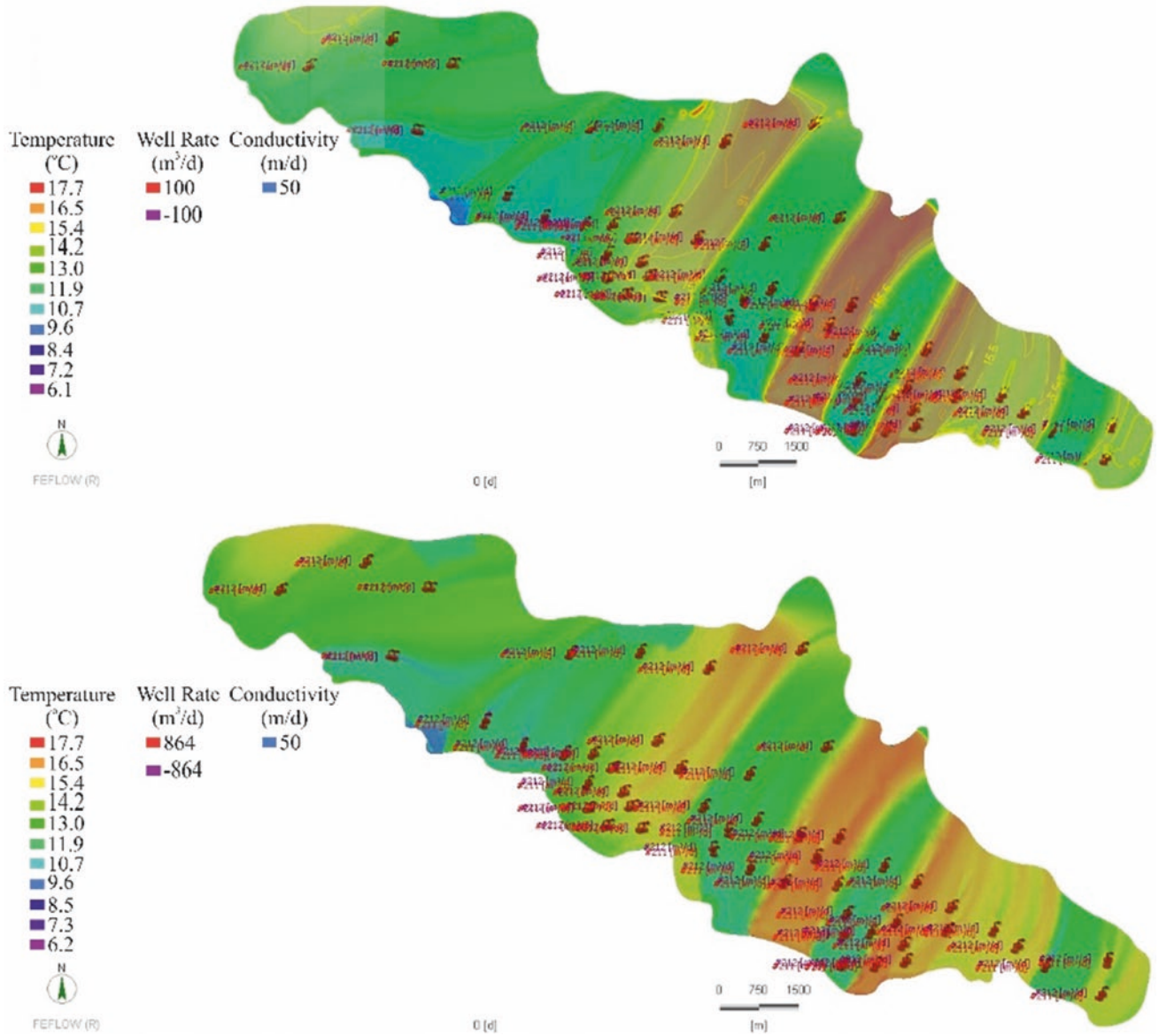

Fig. 3 Thermal plume observed in different extraction and injection flow rates (simulation time: 50 years)

Reference

Freedman, V. L., Waichler, S. R., Mackley, R. D., & Horner, J. A. (2012). Assessing the thermal environmental impacts of and groundwater heat pump in southeastern Washington State. *Geothermics, 42*.

Sensitive Space Changes Analytical Model: An Application in Prieto Diaz, Sorsogon, Philippines

Ana Marie R. Abante

Abstract

This paper presents the way of measuring the spatial clustering of host-built environment's variating situation, land conditions, and the multiple hazards impacting the study area using the Getis-Ord Gi* statistical tool. This tool analyzes the hotspot or coldspot spatial patterns based on the risk space parameters: safe, comfortable, and accessibility that optimized the hot spot or coldspot results in the ArcGIS platform. It aims to introduce a sensitive space changes analytical model to explore the ecosystem from ridge to reefs relative to the risk reality phenomenon based on the actual land and water utilization in Prieto Diaz. The sensitive space changes depending on the settlements. At the same time, the independent variations were attributed to the ecosystem through the ridge to reefs relative and risk reality phenomenon in the 5th-class municipality. The model revealed that only 8% of the entire land area falls within the no-build zone, which needs full recovery and prevention to advance preparedness, yet these areas are populated. In contrast, 38% of the territorial limits were calculated as resilient (coldspot) space meaning there is food security and sufficiency from the upland to the coastal areas. The remaining regions have insignificant Z scores. The study concluded that development is not just about sustaining it; it should reflect stability where risk influences sensitive space. The practical implication of examining the sensitive space variations in terms of processing the risk hotspot or coldspot information points to where a disaster could occur before it happens. Therefore, planners, engineers, decision-makers, and stakeholders must conversate with science-based sensitive space change information regarding variances of exposure and risk reality phenomena. They should also identify where the no-build zones are regarded as sensitive space that changes independently as the ridge-to-reef ecosystem relatively changes as climate changes.

Keywords

Sensitive space changes · Risk reality · Stability · Advanced preparedness · Risk hotspot

1 Introduction

Prieto Diaz is a 5th class municipality of Sorsogon, Philippines, where agriculture and fisheries industries significantly impact the environment where the farmers and fishermen live and work to produce food. This paper aims to introduce a sensitive space changes analytical model to explore the ecosystem from ridge to reefs relative to the risk reality phenomenon based on the actual land and water utilization in Prieto Diaz using the ArcGIS platform.

1.1 Related Literature

In the words of Abante (2021a, 2021b), the geophilosophical realness of risk in terms of risk hotspot and coldspot information brings insights into the stability or instability of resettlement sites as a host environment (Abante, 2021a, 2021b; Amano et al., 2021a, 2021b; Bankoff, 2020; Chainey, 2010). The paper of Bankoff's (2020) study suggests that to make societies more resilient to hazards, a better understanding of the relationship between resiliency and hazard is required to improve disaster risk reduction policies and even to inform everyday urban planning and civil engineering decisions (Amano et al., 2021a; Bankoff,

A. M. R. Abante (✉)
Bicol University, Legazpi City, Albay, Philippines
e-mail: anamarie.abante@bicol-u.edu.ph

A. Çiner et al. (eds.), *Recent Research on Environmental Earth Sciences, Geomorphology, Soil Science, Paleoclimate, and Karst*, Advances in Science, Technology & Innovation, https://doi.org/10.1007/978-3-031-42917-0_26

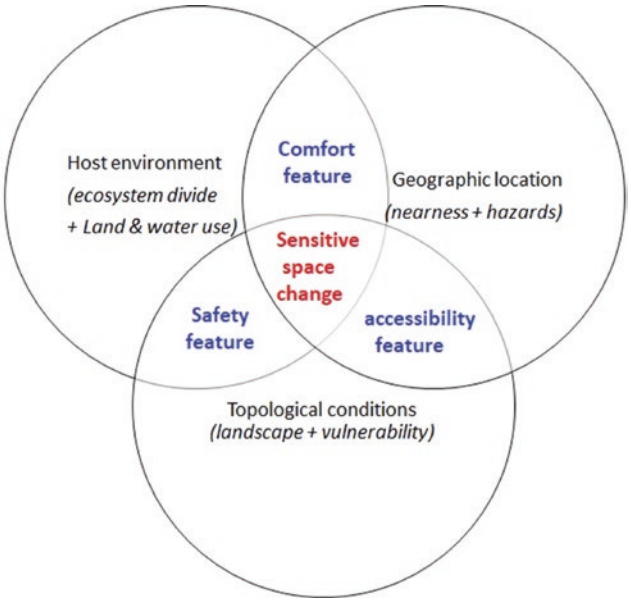

Fig. 1 Sensitive space changes in the analytical model

2020). Authors such as Amano et al. (2021b) highlighted the significance of the environmental change that primarily threatens populations by human-induced land use and environmental change as major threats of the twenty-first century (Amano et al., 2021a, 2021b).

1.2 Framework

The Sensitive space changes analytical model hints at a sensitive space that changes depending on its location relative to the topological conditions. Sensitive space changes result from how we measure risk vs. stability of the physical features of the host-built environment for urban use areas as climate changes with selection criteria.

The sensitive space changes, as shown in Fig. 1, is an analytical model that depicts the relationships of the resilient space selection criteria: safety, comfort, and accessibility relative to the variating situation of the host-built environment (land use), condition of the topography or landscape (vulnerability), and the nearness measurement of the host-built-environment with danger zones or hazard impact areas (ecosystem) (Abante, 2021a, 2021b; Amano et al., 2021a, 2021b; Bankoff, 2020; Chainey, 2010).

2 Methods

The approach to answer the research objectives are as follows: (i) assessing the land and water situation which according in 1900s to 1999 which affected the terrestrial and marine biodiversity; (ii) the ridge to reef divide information was integrated to the ecosystem information; (iii) building the GIS-based elements of risk: hazards, vulnerability, exposure and capability of the municipality; (iv) disaster risk assessment was carried out to analyze the risk hotspots and map where the disaster-prone areas are areas frequently experiencing weather disturbances and natural calamities; (v) the watershed and integrated ecosystem assessment extracted the ecosystem-based land and water use information; (vi) based on the land use policy area classification: protection, production, settlement and infrastructure which was paired or overlaid with the risk hotspot or coldspot information, the land and water conforming or non-conforming; (vii) all the six steps above disclosed where the sensitive areas that area variating depending on land and water utilization (Fig. 2).

Fig. 2 Sensitive space changes modeling approach

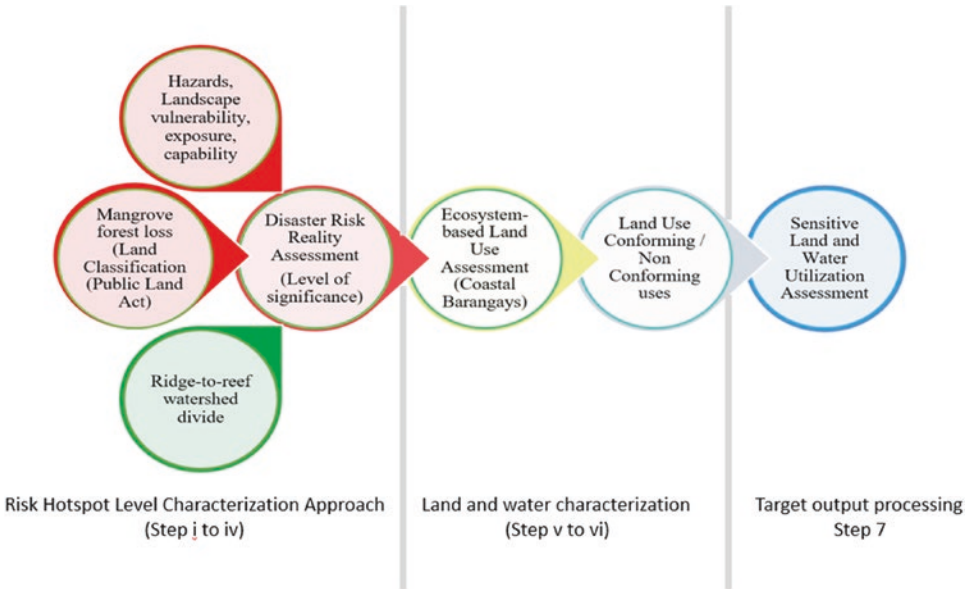

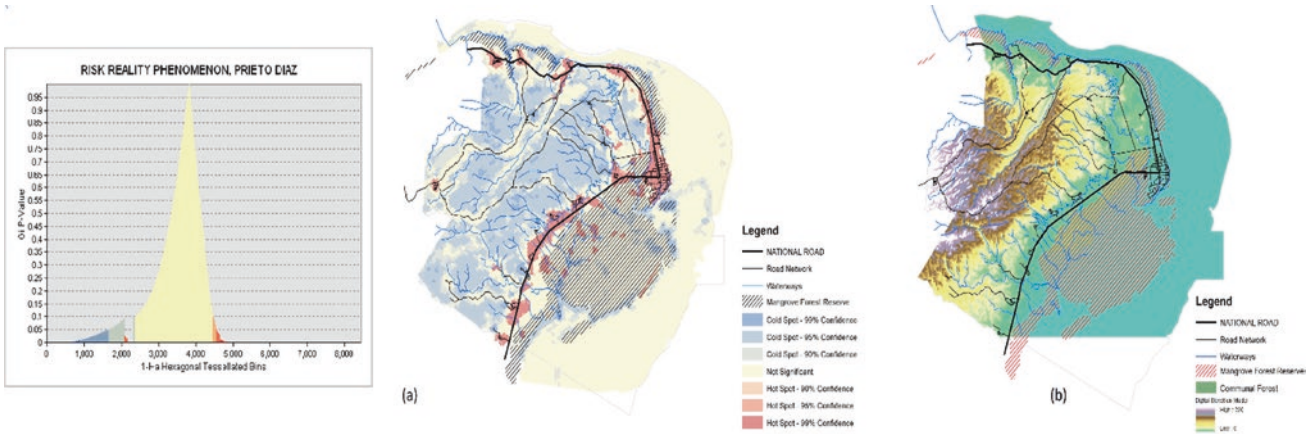

Fig. 3 **a** Risk reality phenomenon; **b** Digital elevation model, Prieto Diaz, Sorsogon

3 Results

Based on the Abante Risk Reality Mathematical Formula, only 8% of the entire municipality's land area (mostly urban use areas) falls within the no-build zone (sensitive space where risk falls between ≥64 and 125 risk quantities) which needs a full recovery and prevention to advance preparedness, yet these areas are populated. In contrast, 38% of the territorial limits were calculated as resilient space (hinting that risk is less than one unit), meaning there is food security and sufficiency from the upland to the coastal areas before and during the COVID-19 lockdown (Fig. 3).

4 Discussion

Although it may seem that the adaptive capacity of the municipality may not be comparable with the Sorsogon City or first-class municipalities of Sorsogon, it may appear to be one of the poorest local government units. Still, in terms of land's highest-best land and water utilization, the municipality continued its natural coastal resources conservation that provides a sustainable source of livelihood and income in the present time. A healthy environment and a promising economy can ensure the locals' quality of life and well-being. Visualizing the result by overlaying the map features of the actual land utilization with risk hotspot information with 95–99% significance and based on actual land use showed that preventive and mitigation measures were generally needed within 8% of the total land of the municipality. The urban and urban use with 95–99% risk hotspot significance level falls within the insignificant preparedness. It hints that proper land utilization can reduce risk, and mitigation measures can advance preparedness. Thus, the results indicated the correlation between risk reduction and stability and the correlation of advanced preparedness to sustainable development, considering that 92% of the total land area conforms with the highest-best-land use (generally agricultural and aquacultural uses), hinting at food sufficiency in the locality. The protected mangrove and seagrass bed areas and fish sanctuary, in addition to naturally irrigated rice land and coconut in the upland, answers the odd question of why a 5th class municipality like Prieto Diaz was slightly affected by high unemployment rates happening worldwide during the lockdown in March to June 2020.

5 Conclusions

The study concluded that development is not just about sustaining it. It should reflect stability where risk is equal to one in a sensitive space, advanced preparedness, and nullifying exposure happenstance should result from proper planning and the right decision in local governance. The practical implication of examining where the sensitive space variations in terms of processing hotspot or coldspot risk information indicate where a disaster could occur before it happens. The planners, engineers, decision-makers, and stakeholders must be conversant with science-based information on variances of exposure and risk reality phenomena and be able to identify where the no-build zones are regarded as sensitive space, which independently changes as the ridge to reef ecosystem relatively changes as climate changes.

Acknowledgements This research was conducted as part of the preparatory works for the extension services of Bicol University Faculty entitled "Technical and Training Assistance on the Formulation of the Prieto Diaz Comprehensive Land Use Plan, the Year 2021–2030". The author acknowledges the results of the joint undertaking of Bicol University and the Local Government Unit of Prieto Diaz, following the memorandum of agreement to enhance the academic and research programs of the university.

References

Abante, A. M. R. (2021a). Reintroducing the GeoNames that feature the land and water near the Montufar and Bingay Points in Prieto Diaz. *Sorsogon, Philippines International Journal of Computing Sciences Research* (in Press). https://doi.org/10.25147/ijcsr.2017.001.1.70

Abante, A. M. R. (2021b). Geophilosophical realness of risk: A case study in national housing authority resettlement sites in Albay, Philippines. *SN Applied Sciences, 3*(4).

Amano, N., Bankoff, G., Findley, D. M., Barretto-Tesoro, G., & Roberts, P. (2021a). Archaeological and historical insights into the ecological impacts of pre-colonial and colonial introductions into the Philippine Archipelago. *The Holocene, 31*(2), 313–330.

Amano, N., Wang, Y. V., Boivin, N., & Roberts, P. (2021b). 'Emptying forests?' Conservation implications of past human–primate interactions. *Trends in Ecology & Evolution*.

Bankoff, G. (2020). Under the Volcano: Mount Mayon and co-volcanic societies in the Philippines. *Environment and History, 26*(1), 7–29.

Chainey, S. (2010). *Advanced hotspot analysis: Spatial significance mapping using Gi**. University College London.

A Turbulent Hybrid Model to Simulate a Partially Pressurized Flow

Wahiba Mokrane

Abstract

People often experience unpleasant situations related to water supply or wastewater network dysfunction. For example, a wrong procedure of filling a discharge pipe or a sudden thunderstorm may modify the flow structure. Over or under pressures will induce overflows, cavitation phenomenon, or pipes bursting. In this background and through the present work, we initially attempt to simulate the transient pressure profile along a partially filled pipe. Flow is modeled by a turbulent hybrid model, including near and far from the wall domain. However, for calculus, the volume of fluid VOF method is used first, then coupled to level set one LSCVOF. Numerical results reveal that the pipe is fully pressurized when the VOF method is used and when the LSCVOF is applied. Furthermore, simulation results present a good correlation compared to the stationary state, which is more important as the level set is associated. Therefore, the most recommended method to simulate transient flow through the partially filled conduit is the LSVOF one.

Keywords

Hybrid model · Turbulent flow · Volume of fluid · Level set · Transient pressure

1 Introduction

To simulate the transition from free surface flow, investigators propose several models (Kerger et al., 2009; Konozsy, 2019). However, many factors influencing this phenomenon make mathematical modeling difficult (Mokrane, 2021). In the present work, we use a turbulent hybrid model that considers both near and far from the pipe wall zone. This consists of a combination between the K-omega and the K-epsilon models (Kerger et al., 2011).

2 Methods

A transient flow, through a partially filled pipe initially, may be governed by the Navier Stokes equations. We choose a turbulent hybrid model, said sstk-omega designing shear stress transport k-omega. This model comprises the K-omega one available in sub-layers near the pipe wall and the K-epsilon available away from the pipe walls. On the other hand, we first use the volume of fluid (VOF) as a computational method. Then Level set (LS) method is associated with the VOF one as a coupled level set—the volume of fluid method (CLSVOF).

Hence, the curvature problem generated when the interface is tracked using the VOF method may be eliminated thanks to the LS. Furthermore, numerical results are compared in each case to experimental data. Finally, the most appropriate procedure will be recommended.

3 Results

3.1 Results Issued from the VOF Method

In this case, the turbulent hybrid model sst k-omega is solved thanks to the volume of the fluid method. Numerical results and experimental ones are shown in Fig. 1, where P_{vof} indicates static pressure values obtained when the VOF technique is used, and P_{exp} designs the experimental result.

W. Mokrane (✉)
MVRE Laboratory, Higher National School for Hydraulics, Blida, Algeria
e-mail: mokranewah@yahoo.fr

A. Çiner et al. (eds.), *Recent Research on Environmental Earth Sciences, Geomorphology, Soil Science, Paleoclimate, and Karst*, Advances in Science, Technology & Innovation, https://doi.org/10.1007/978-3-031-42917-0_27

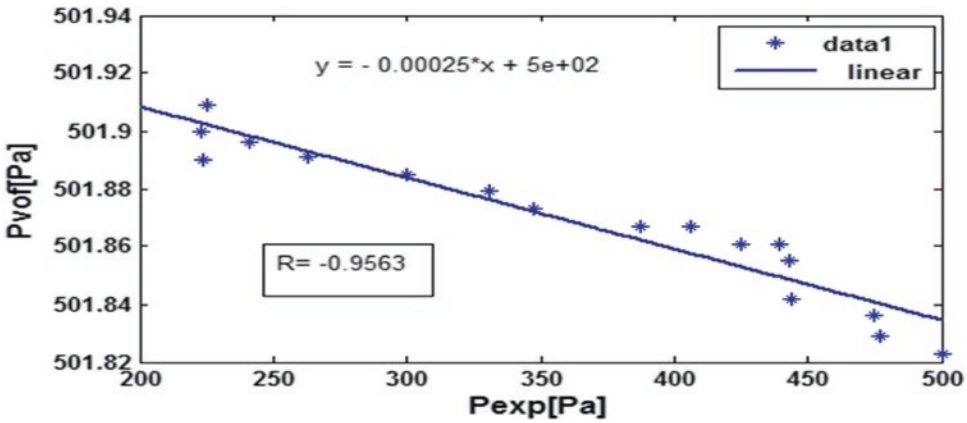

Fig. 1 Results of the volume of fluid computation (VOF)

3.2 Results Issued from CLSVOF Method

In the second step, the coupled method is used to compute the turbulent hybrid model solutions, and results are presented in Fig. 2, where P_{voflsm} indicates static pressure values obtained thanks to the CLSVOF method.

3.3 Results of Correlation Between VOF and CLSVOF Results

Here we present the correlation between the volume of fluid method and the coupled one to the Level set method. This is shown in Fig. 3.

4 Discussion

Numerical results and solutions of the turbulent hybrid model 'sst k-omega' are plotted on experimental results corresponding to a stationary state. This concerns static pressure values presented in Figs. 1 and 2.

Computed results 'P_{vof}' are issued from the volume of the fluid numerical method. Data presented in Fig. 1 illustrate a high negative correlation with experimental results. This reveals a linear monotone relationship between numerical and experimental results, which develop differently. This will be augmented by a numerical solution obtained through a lap of time and exceeds 500 Pascals. Hence, this means that the pipe is entirely pressurized.

When the CLSVOF method is used, numerical results of the static pressure plot, depending on those of the stationary state, show a high negative correlation value, according to Fig. 2. This reflects a linear monotone relationship between numerical and experimental results, which evolve in two different directions. Also, all numerical solution values express a completely pressurized flow.

To examine the convergence of the VOF and the CLSVOF techniques, results are plotted in Fig. 3, and a high positive correlation is detected. However, the CLSVOF method has displayed the highest correlation coefficient value with the experimental results and is the most recommended.

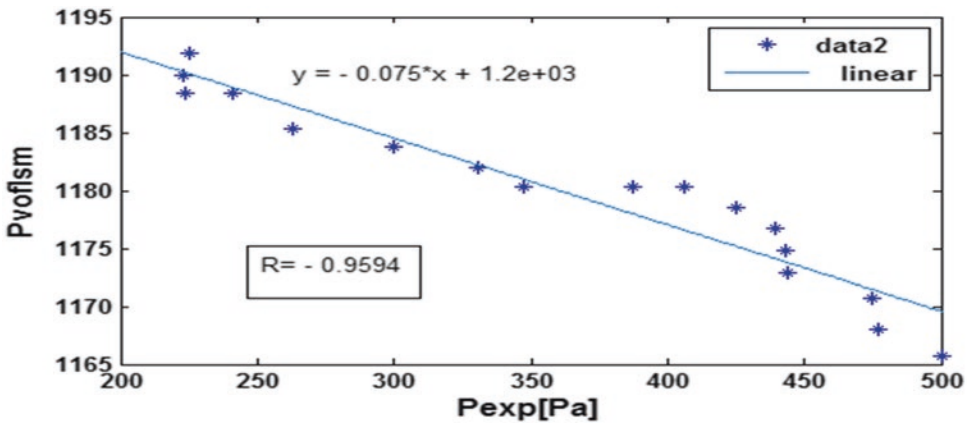

Fig. 2 Results of the CLSVOF method

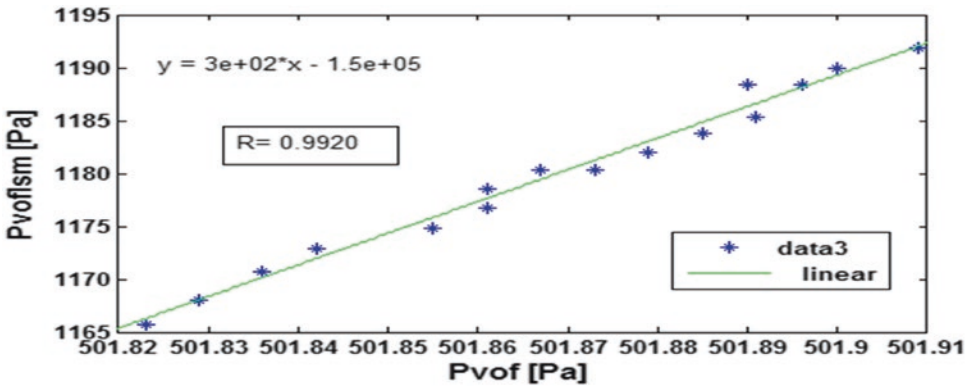

Fig. 3 Correlation between VOF and CLSVOF results

5 Conclusions

To simulate transient turbulent flow through a partially filled pipe, the hybrid model sst k-omega permits considering all flow zones near and away from the pipe wall. Hence, choosing an adequate procedure to solve this mathematical model is necessary. Therefore, the present work applied different numerical methods, the volume of fluid one, firstly, then coupled with the level set one.

Compared to experimental results, numerical solutions have revealed that the coupled method designed by CLSVOF is the most recommended. However, a high convergence is found between the two approved techniques through a high correlation between numerical solutions issued from the cited methods.

References

Kerger, F., Archambeau, P., Erpicum, S., Dewals, B., & Pirotton, M. (2009). Simulation numérique des écoulements mixtes hautement transitoires dans les conduites d'évacuation des eaux. *Houille Blanche, 5*, 01–08.

Kerger, F., Archambeau, P., Erpicum, S., Dewals, B., & Pirotton, M. (2011). An exact Riemann solver and a Godunov scheme for simulating highly transient mixed flows. *Journal of Computational and Applied Mathematics, 235*, 2030–2040.

Konozsy, L. (2019). *A new hypothesis on the anisotropic Reynolds stress tensor for turbulent flows* (1st ed.). Springer.

Mokrane, W. (2021). Effect of solid deposition on the risk of pressure surges in closed pipes. *Euro-Mediterranean Journal for Environmental Integration, 6*(28), 01–07.

Critical Evaluation of Methods for Calculating the Carbon Footprint: The Experience of RUDN University

Aleksandr Khaustov, Margarita Redina, and Zhandos Kenzhin

Abstract

A carbon footprint is currently one of the widely distributed methods for assessing an anthropogenic impact on environmental systems. Despite a long history of such estimations, there is no unified model for its calculation. Existing approaches include different components of artificial processes as sources of greenhouse gas emissions. On the example of RUDN University (Moscow, Russia), the article presents the results of applying different calculation methodologies. The use of these approaches gives a difference of up to 2.5 times. At the same time, greenhouse gas absorption is out of consideration. Thus, the relevance of the issues of carbon footprint assessment requires the development of detailed methods for assessing the role of urban ecosystems and the selection of good accounting algorithms for all activities of organizations considered as objects of analysis in terms of greenhouse gas emissions.

Keywords

Greenhouse gases · RUDN University · Algorithm · Carbon footprint

1 Introduction

Many economic entities face carbon footprint assessments as indicators of environmental pressures. Modern environmental and climate policy is primarily determined by quantitative estimations of greenhouse gas emissions and uptake and the prospects for their reduction or intensification.

Universities are particularly interested in this regard as educational and scientific centers. On the one hand, they can act as model objects for developing assessment methods and algorithms for reducing emissions. On the other hand, they act as centers for spreading information and forming the professional culture of future specialists. The RUDN University, as the Russian national coordinator of the global partnership UI GreenMetric World University Rankings Network, implements programs to improve environmental friendliness and decarbonization. In the international ranking of UI GreenMetric, the critical point of assessment is greenhouse gas emissions (UI-GreenMetric-Guideline, 2020). Thus, it is interesting to compare different models of GHG emissions and adsorption of the university, as well as approaches to their accounting following the currently existing schemes and limitations (Gallo et al., 2020; Harris et al., 2020; Marland et al., 2014; Mirabella & Allacker, 2021).

In the present article, different approaches to calculating GHG emissions and the university's carbon footprint are compared and the possible decisions for obtaining more detailed and accurate estimations are suggested.

2 Object and Methods of the Study

The objects of the study are the RUDN University campus (Moscow, Russia), with an area of 144 hectares, and components of the university's "everyday life" as sources of GHG emissions and, on the other hand, possible sinks of GHGs. The territory is affected by man-made (primarily transport) loads, which reduce vegetation and soil absorption capacity. The environmental monitoring program implemented by RUDN has allowed us to accumulate a

A. Khaustov (✉) · M. Redina · Z. Kenzhin
Peoples' Friendship University of Russia (RUDN University), Moscow 117198, Russia
e-mail: khaustov-ap@rudn.com

A. Çiner et al. (eds.), *Recent Research on Environmental Earth Sciences, Geomorphology, Soil Science, Paleoclimate, and Karst*, Advances in Science, Technology & Innovation, https://doi.org/10.1007/978-3-031-42917-0_28

significant amount of data on the state of the campus urban ecosystem, which helps us assess the territory's role in gas exchange and greenhouse gas absorption. In addition, in the framework of participation in the UI GreenMetric ranking, the university's carbon footprint is assessed annually. In this regard, it became possible to evaluate in detail the effectiveness of existing methods for the carbon footprint accounting for urban areas in the example of the RUDN campus.

The preliminary evaluations have been carried out using the UI GreenMetric calculation algorithm for the carbon footprint (UI-GreenMetric-Guideline, 2020). Also, the approaches to the carbon footprint evaluation can be based on the following models: the Process analysis (PAS2050 method) (BSI, 2008); Life Cycle Assessment method with a process model (Cooper & Fava, 2006); Environmental Input–Output (EIO) models (Pan & Kraines, 2001), and Hybrid EIO-LCA methods (Heijungs & Suh, 2006).

The models listed are oriented first on the production systems and allow us to obtain a rate of emissions calculated for the unit of the product as of CO_2 equivalent.

3 Results

The previously calculated carbon footprint caused by the use of electricity on the university campus based on the above-listed approaches reaches the following values:

- UI GreenMetric methodology: 21.0 tons of CO_2;
- the Carbon Footprint Calculator algorithms: 8.3 tons;
- the US EPA algorithms: 17.7 tons (Abdullina, 2020).

Fundamental differences in the calculation algorithms cause significant discrepancies.

It is to be emphasized that such an estimation is made for only one of the components of the environmental impact of the university–electricity consumption. Although the campus doesn't participate in any industrial activity and generally only uses energy and material flows produced outside, the variety of components to be evaluated for the complete assessment of GHG emissions is wide (Fig. 1).

Else one side of the full carbon footprint calculation underestimated in the listed models is GHG absorption. These values are currently not included in the final evaluation of carbon footprint. This can be due to the complexity of calculations and the absence of reliable standard calculation schemes.

4 Discussion

A university produces GHG emissions as a result of electricity and heat consumption, the realization of teaching and research itself (use of techniques and instruments in labs, including digital tools and networks, use of multimedia, etc.), establishing a set of "service" processes like cooking and cleaning, ensuring the dormitories, sports facilities, etc. Sure, the evaluation of electricity consumption only reflects a big part of GHG emitted on the campus but covers not all of these processes. Therefore, it is necessary to suggest a more flexible and comprehensive evaluation model that can reflect the most important carbon footprint components for such an object as a university (Fig. 1). Turning to the UI Green Metric ranking experience (UI-GreenMetric-Guideline, 2020), we can say that even these objects differ quite significantly, and it is necessary to use different approaches for the comparison of urban and suburb campuses. Thus, applying too generalized calculation schemes leads to the loss of accuracy of carbon footprint evaluations.

It is also crucial that the assessments do not consider the campus green areas' role in releasing and absorbing CO_2 and other greenhouse gases (Abdullina, 2020). Our preliminary experiment allowed us to estimate the daily dynamics of gas exchange of the soil and vegetation cover and its dependence on the weather conditions. In addition, there are substantial anthropogenic transformations of the

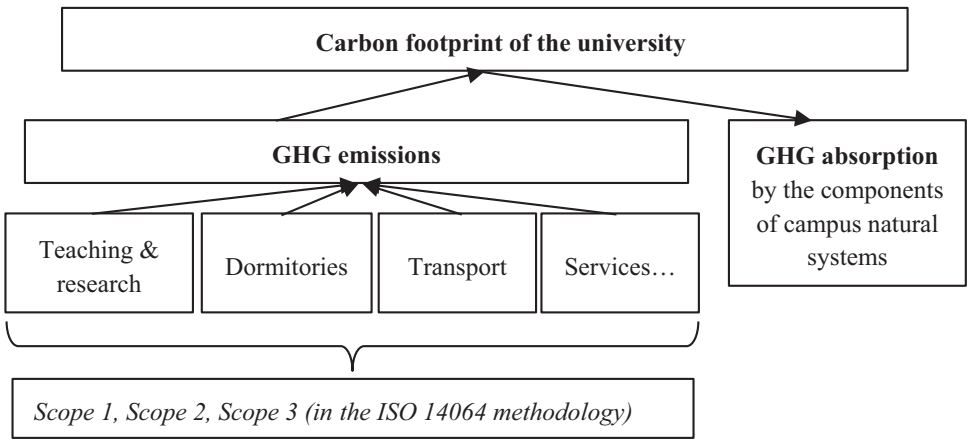

Fig. 1 Sources and sinks of GHG in a university campus

natural systems of the campus. Therefore, for the detailed evaluation of GHG absorption, a system of measurements of GHG, meteorological conditions, and concentrations of marker compounds reflecting the total pollution level is necessary.

5 Conclusion

Application of the widely distributed methodologies for the evaluation of the carbon footprint of the university (on the example of the RUDN University energy consumption) showed a difference of up to 2.5 times. This demonstrates significant uncertainties in the calculation methods and justifies the necessity of detailed individual plans for such a group of objects like universities. The relevance of the issues of carbon footprint assessment requires the development of precise methods for assessing the role of urban ecosystems and the selection of good accounting algorithms for all activities of organizations considered as objects of analysis in terms of greenhouse gas emissions.

References

Abdullina, L.R. (2020). Review and analysis of existing methods for calculation of the carbon foot. Calculation of the carbon trace on the example of RUDN University campus. In *Ecology and climate. All-Russian Scientific Conference with International Participation* (pp. 7–8).

BSI. (2008). Guide to PAS 2050: How to assess the carbon footprint of goods and services.

Cooper, J. S., & Fava, J. A. (2006). Life-cycle assessment practitioner survey: Summary of results. *Journal of Industrial Ecology, 10*(4), 12–14.

Gallo, M., Arcioni, L., Leonardi, D., et al. (2020). GHG accounting for sustainable mega-events: How lessons learnt during the Milan Expo 2015 world fair could lead to less carbon-intensive future mega-events. *Sustainable Production and Consumption, 22*, 88–109.

Harris, S., Weinzettel, J., Bigano, A., & Källmén, A. (2020). Low carbon cities in 2050? GHG emissions of European cities using production-based and consumption-based emission accounting methods. *Journal of Cleaner Production, 248*, 119206.

Heijungs, R., & Suh, S. (2006). Reformulation of matrix-based LCI: From product balance to process balance. *Journal of Cleaner Production, 14*(1), 47–51.

Marland, E., Cantrell, J., Kiser, K., Marland, G., & Shirley, K. (2014). Valuing uncertainty part I: The impact of uncertainty in GHG accounting. *Carbon Management, 5*(1), 35–42.

Mirabella, N., & Allacker, K. (2021). Urban GHG accounting: Discrepancies, constraints and opportunities. *Buildings and Cities, 2*(1).

Pan, X., & Kraines, S. (2001). Environmental input-output models for life-cycle analysis. *Environmental and Resource Economics, 20*(1), 61–72.

UI-GreenMetric-Guideline. (2020). Retrieved May 20, 2021, from https://docviewer.yandex.ru/?tm=1632723831&tld=ru&lang=ru&name=UI-GreenMetric-Guideline-2020-Rus-21.07.2020.pdf&text=UI-GreenMetric-Guideline-2020-Rus-21.07.2020.pdf&url=http%3A//greenmetric.ui.ac.id/wp-content/uploads/2015/07/UI-GreenMetric-Guideline-2020-Rus-21.07.2020.pdf&lr=213&mime=pdf&l10n=ru&sign=d4118ed58428fe594ecf5ea0452b2501&keyno=0

Wildfire Spreading Capacities of Vegetated Surfaces Within the Metropolitan Region of Northwestern Türkiye

Artan Hysa and Aqil Tariq

Abstract

The main objective of this study is to assess the wildfire spreading capacity of the vegetated surfaces within the inter-metropolitan area in northwestern Türkiye. The study utilizes the WSCI model recently adapted for the WUI scale. The model considers 16 criteria about the anthropogenic, geophysical, fuel, and hydro-meteorological factors. All analysis steps are performed in QGIS by utilizing various open-source geospatial data providing information about each criterion. The results highlight certain hotspots of significant wildfire spreading risk among the vegetated surfaces within the study area. Furthermore, there is a considerable amount of man-made structures within WUI that are potentially exposed to relatively high levels of wildfire risk. The results presented in this study could be of assistance to the institutions that are responsible for wildfire management within the inter-metropolitan area. As wildfire behavior ignores administrative boundaries, cross-boundary supervision by neighboring municipalities is crucial for effective wildfire management. The method presented here is reproducible in other inter-metropolitan regions in developing countries, where the intensification of urbanization in WUI generates high levels of wildfire exposure.

Keywords

Wildland urban interface · QGIS · Multi-criteria analysis · Istanbul · Fire risk

A. Hysa (✉)
Faculty of Architecture and Engineering, Epoka University, 1032 Tirana, Albania
e-mail: ahysa@epoka.edu.al

A. Tariq
Department of Wildlife, Fisheries and Aquaculture, College of Forest Resources, Mississippi State University, 39762-9690 Mississippi State, USA

1 Introduction

Northwestern Türkiye is home to highly dense metropolitan areas like Istanbul and Bursa. This inter-metropolitan zone stretches by including other urban centers like Izmit, Sakarya, and Duzce. The current population living within this area exceeds 20 million inhabitants. On the other hand, the site is exposed to natural hazards like earthquakes, flooding, and wildfires. The elongated hot seasons and the increase in maximum temperatures are expected to elevate the risk of wildfires across the Mediterranean region (Lozano et al., 2017). The zones expected to be affected the most are the wildland-urban interface (WUI), putting under risk valuable vegetation stock that envelops the urbanized lands and the man-made assets of social and economic value.

In this context, this study aims to reveal the wildfire spreading capacities of the vegetated surfaces within the metropolitan area of Northern Türkiye. Similar studies are rare for this region as the wildfire has not been a concern. But, considering the consequences of climate change, wildfire risk areas are projected to expand and put under risk areas like metropolitan Istanbul.

2 Materials and Methods

The study area consists of the metropolitan zone in the Northern part of Türkiye (see Fig. 1). The total surface area is 15,013 km^2, and vegetated surfaces cover about one-third of it. The study area includes important metropolitan cities like Istanbul and Bursa. The wildfire spreading capacities of the existing vegetated surfaces are worth investigating, considering that the area is home to 21,033,797 inhabitants, according to Urban Atlas (UA) records.

The method of this study relies on the wildfire spreading capacity index (WSCI), initially developed for national-scale studies (Hysa et al., 2021, 2021a). It counts

A. Çiner et al. (eds.), *Recent Research on Environmental Earth Sciences, Geomorphology, Soil Science, Paleoclimate, and Karst*, Advances in Science, Technology & Innovation, https://doi.org/10.1007/978-3-031-42917-0_29

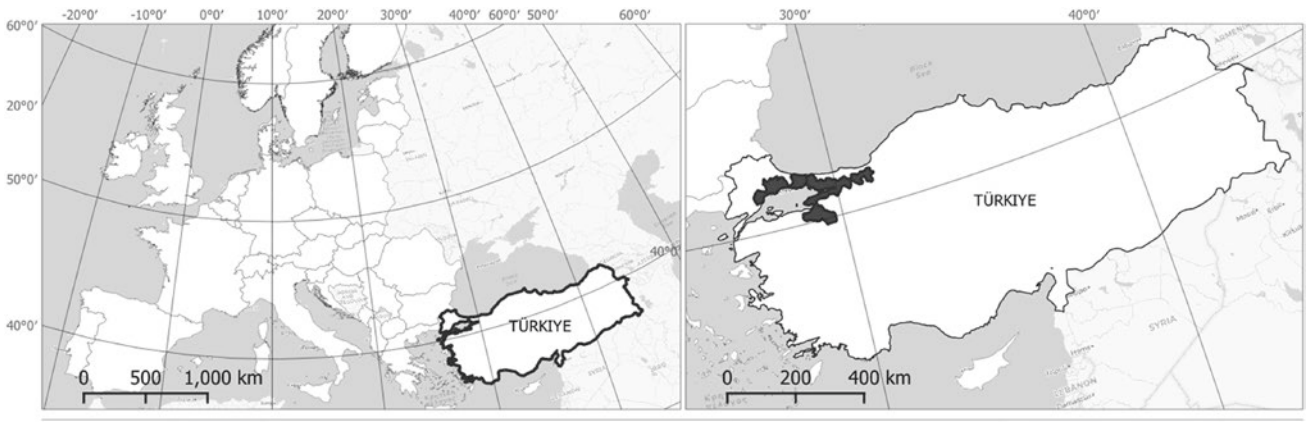

Fig. 1 Study area of the metropolitan area of Northern Türkiye

sixteen criteria that have a proven relationship with wildfire spreading behavior. Furthermore, the model is adapted to the metropolitan scale and has been successfully tested in developing metropolitan areas in the Western Balkans (Hysa, 2021). Referring to the following equation, the WSCI index value is calculated as the sum of the products between each criterion normalized inventory value (C_j) and its relevance impact factor (β_j).

$$\mathrm{WSCI} = \sum_{j=1}^{m} \beta_j C_j \tag{1}$$

This study utilizes various open-source datasets to supply the model with reliable geospatial information. For example, UA data define the vegetated surfaces as the main target of the indexing procedure. Open street map (OSM) data provided information for distance to settlements (S2), distance to any road (S3), distance to main roads (S4), and distance to water sources (P4). The digital elevation model supplied information about slope (P1), aspect (P2), and altitude (P3). CORINE Land Cover (CLC) enabled the fuel type (F1). Copernicus Climate Change Service enabled the Burned Area Fraction (BAF) maps. All climate criteria (E1, E2, E3, and E4) rely on WorldClim 2.0 (Fick & Hijmans, 2017).

3 Results and Discussion

The first set of results belongs to the inventory record per each criterion. Figure 2 shows the relative impact levels of each criterion on wildfire spreading capacity. The green-yellow–red color ramp highlights the critical areas (in red). We used Jenks' natural break classification method to make the value distribution more distinguishable. The inventory values are normalized before being used within the WSCI equation.

The WSCI mapping results in Fig. 3 show that the vegetated surfaces in the southern and eastern parts of the study area face higher wildfire spreading capacities. The main reason behind that remains on the collective contribution of some criteria like fuel type (Fig. 2e), solar radiation (Fig. 2a), precipitation (Fig. 2b), tree cover density (Fig. 2f), and distance to water sources (Fig. 2k). On the other hand, Fig. 2q shows that the wildfire activity has been recorded on the western part of the study area (based on the remotely sensed burned area fraction between 2015 and 2019).

At first glance, the non-alignment between the WSCI mapping and the recent wildfire activity may sound contradictory. However, the WSCI map is not proposed as a wildfire ignition predicting model. Instead, regardless of the ignition chances, it brings a weighting procedure among vegetated surfaces by their wildfire spreading capacities. We suggest that the highlighted reddish areas be studied further in detail. Future works can perform vulnerability and exposure analysis within the wildland-urban interface. The next steps of this study must consider the assessment of the building stock being exposed to the highest wildfire risk.

4 Conclusions

This study presented the indexing of vegetated surfaces within the metropolitan area of Istanbul by their wildfire spreading capacities. The method counts sixteen parameters

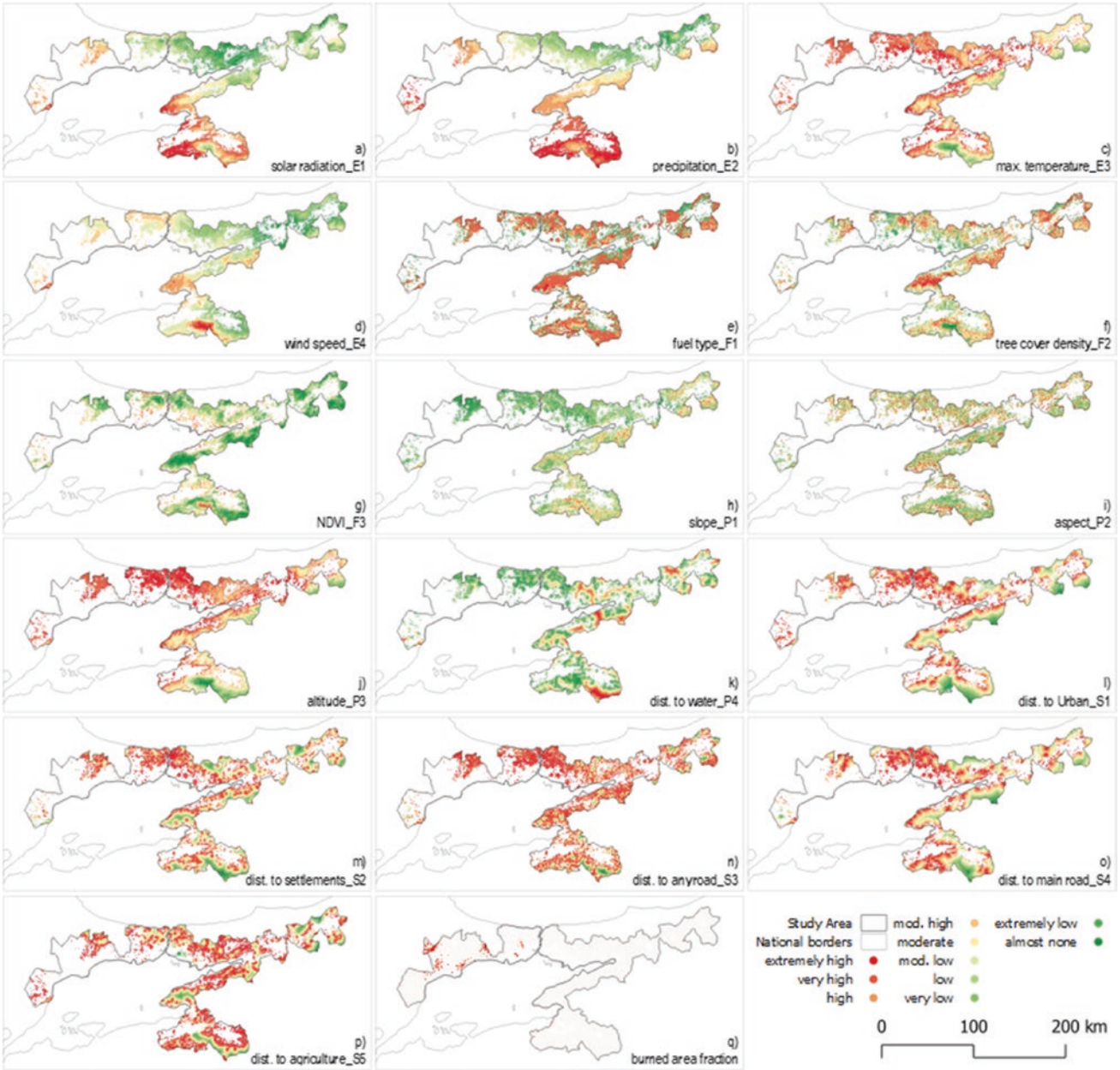

Fig. 2 The relative risk of each criterion (classified via Jenks natural break method)

based on the study area's social, geophysical, fuel, and hydro-meteorological properties. Our study's results visually show a significant wildfire spreading risk in remote areas and close to the wildland-urban interface (WUI). Future studies can rely on these results to perform vulnerability and/or exposure analysis for the human settlements within WUI.

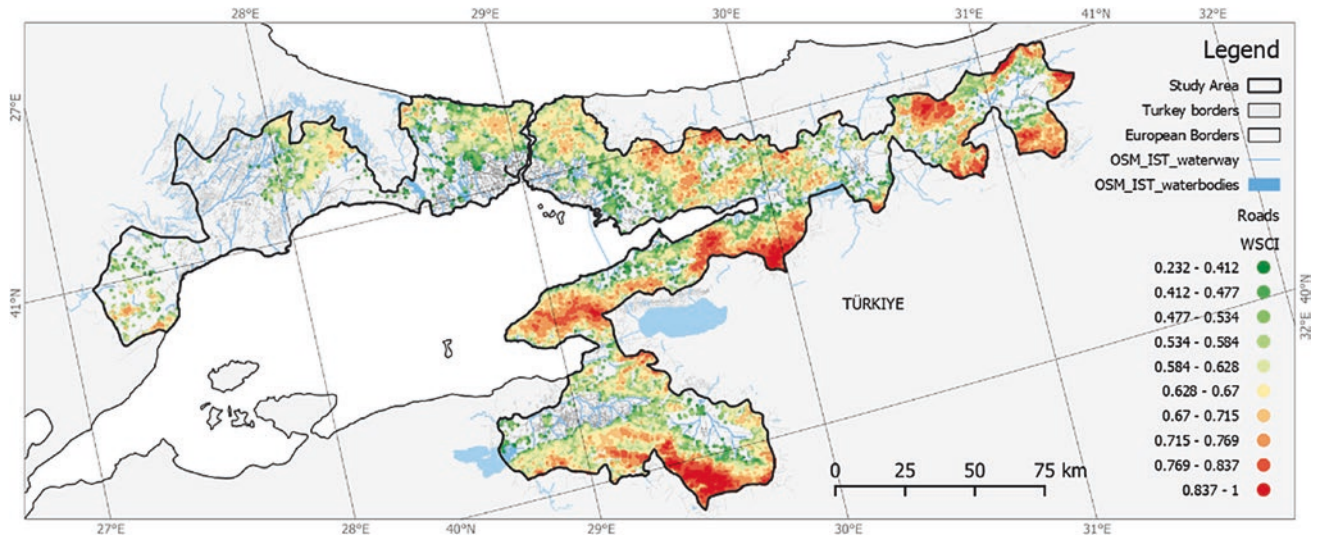

Fig. 3 Wildfire spreading capacity results for the metropolitan area in northwest Turkey

References

Fick, S. E., & Hijmans, R. J. (2017). WorldClim 2: New 1-km spatial resolution climate surfaces for global land areas. *International Journal of Climatology, 37*, 4302–4315.

Hysa, A. (2021). Indexing the vegetated surfaces within WUI by their wildfire ignition and spreading capacity, a comparative case from developing metropolitan areas. *International Journal of Disaster Risk Reduction, 63*, 102434.

Hysa, A., Spalevic, V., Dudic, B., Roşca, S., Kuriqi, A., Bilaşco, Ş, & Sestras, P. (2021). Utilizing the available open-source remotely sensed data in assessing the wildfire ignition and spread capacities of vegetated surfaces in Romania. *Remote Sensing, 13*(14), 2737.

Hysa, A., Yunitsyna, A., Manahasa, E., Naselli, F., Manahasa, O.D., Dervishi, S. (2021a) Current challenges in architecture and urbanism in Albania. An overview of wildfire prone forest surfaces within the metropolitan area of Tirana and Sarajevo. Springer International Publishing Cham 111–123.

Lozano, O. M., Salis, M., Ager, A. A., Arca, B., Alcasena, F. J., Monteiro, A. T., Finney, M. A., Del Guidice, L., Scoccimarro, E., & Spano, D. (2017). Assessing climate change impact on wildfire exposure in mediterranean areas. *Risk Analysis, 37*(10), 1898–1916.

Features of the Elenina Bank (Sea of Azov)

Viacheslav Krylenko and Marina Krylenko

Abstract

The Elenina Bank is an underwater accumulative form of the eastern part of the Sea of Azov. The analysis of the modern structure of the Elenina Bank is carried out using literary sources and remote sensing data. The digital elevation model of the underwater relief for the Elenina Bank was built based on Sentinel-2 satellite images using the mutual correlation between the brightness of the spectrum channels and depth. The Elenina Bank is composed of sand and shells. The length of the Elenina Bank is about 40 km, with a width of up to 5 km. At the western end of the bank, arc-shaped ridges up to 6 km long are found. The Elenina Bank accumulates most of the sediments transferred to the north-northeast since there is no shelly detritus in the modern bottom sediments to the north of the Elenina Bank. The Elenina Bank is an active accumulative form and affects the lithodynamic processes of the adjacent part of the Sea of Azov.

Keywords

Accumulative form · Underwater relief · Sea of Azov

1 Introduction

The Elenina Bank is an underwater accumulative form of the eastern part of the Sea of Azov. The Elenina Bank is generally regarded as an element of inherited relief not involved in modern lithodynamic processes. However, there is reason to believe that the Elenina Bank continues to influence the Dolgaya Spit and determines the sediment fluxes of the adjacent part of the Sea of Azov (Fig. 1). The given article analyses the present structure of the Elenina Bank. In addition, it provides an assessment of the landform's impact on the development of adjacent accumulative forms and the hydrological regime of the Sea of Azov.

2 Materials and Methods

The analysis of the modern structure of the Elenina Bank was performed using literature sources and remote sensing data. The first graphic image of the bank is available on the maps of Pieter Bergman (1701–1702). Information on the configuration and size of the bank was given in Budischev (1808) and half a century later in Sukhomlin (1854).

In 2018–2019, digital models of underwater relief for the Azov Sea water area near the Elenina Bank were built based on Sentinel-2 space data using the mutual correlation of spectrum channel brightness and depth (Krylenko et al., 2019).

3 Results and Discussion

The Elenina Bank was formed as a spit during the Phanagorian regression 2.5–1.7 thousand years ago when the sea level was 3–9 m lower than now (Matishov & Polshin, 2019). Assuming an average sea level fall of 5–6 m during the regression, there was a vast expanse of water to the NE of the Yeysk Peninsula with a wave fetch of at least 50 km. When the shoreline alignment was shifted, the bank's base found itself at the curve of the bedrock shore where the spit could form (Fig. 2). A sediment flow initiated by the NE swells and amplified by runoff currents of the Don contributed to the formation of an accumulative body directed to the WNW.

V. Krylenko (✉) · M. Krylenko
Shirshov Institute of Oceanology RAS, Moscow, Russia
e-mail: krylenko.slava@gmail.com

A. Çiner et al. (eds.), *Recent Research on Environmental Earth Sciences, Geomorphology, Soil Science, Paleoclimate, and Karst*, Advances in Science, Technology & Innovation, https://doi.org/10.1007/978-3-031-42917-0_30

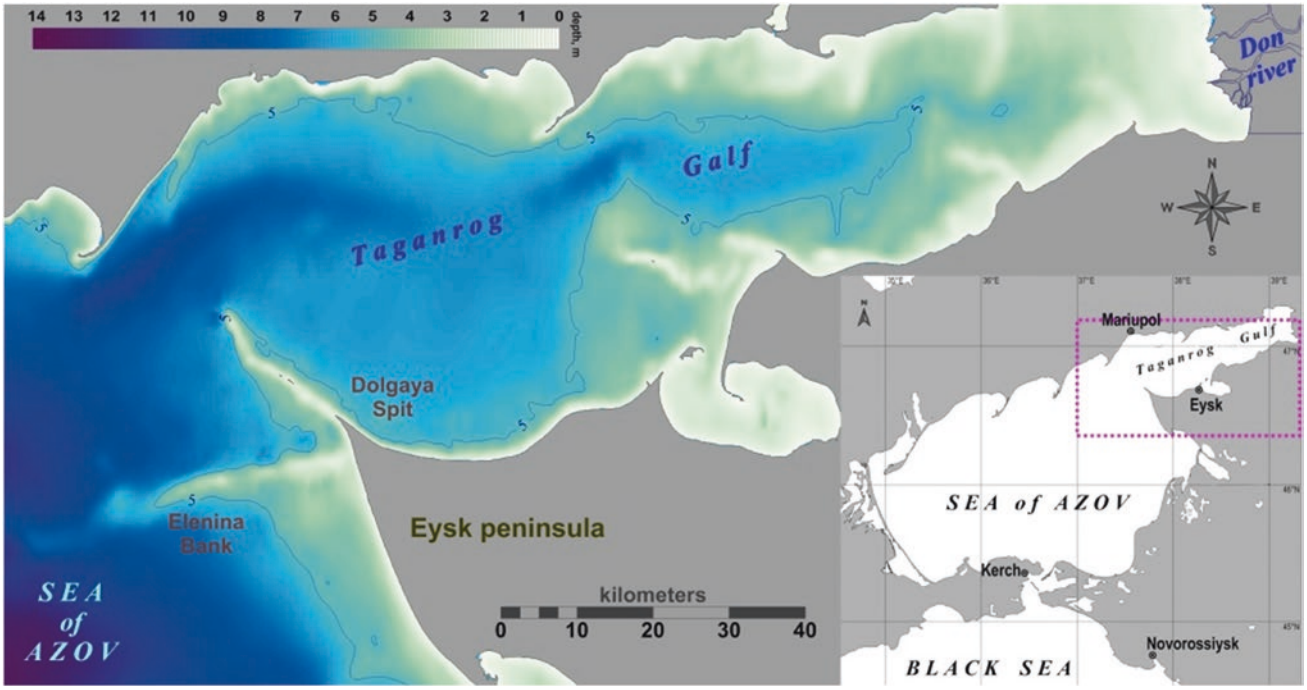

Fig. 1 The eastern part of the Sea of Azov

During the subsequent rise in sea level near the NW end of the Yeysk Peninsula, the influence of W and SW waves intensified, directing longshore drifts to the NW, where the present-day Dolgaya Spit began to form. The transgression cut off the Elenina Bank from the coastal sediment feeding zone, and sedimentation there acquired features characteristic of the open sea. The sea level rise was probably rapid, as the body of the Elenina Bank was not eroded. However, some of its material may have been shifted northwards and contributed to the growth of the Dolgaya Spit.

The primary source of sediment for the Elenina Bank is biogenic. The Elenina Bank is composed of detrital sand and shells of *Cerastoderma glaucum*. This mollusk, which is highly productive, plays a crucial role in the development of beach-forming sediments in the Sea of Azov. Large volumes of shell rock are produced in the vast expanse of seabed south of the Elenina Bank. The bottom slope and wave mode contribute to shells' active wave transport to N-NW (Matishov, 2011). The shell rock, carried by waves along the flat southern slope of the Elenina Bank, reaches the northern edge of the accumulative body. There is practically no further extension of the accumulative body northward because, as depths increase, more and more sediment is required. Contemporary deposits to the Elenina Bank's North contain no shell detritus.

The modern length of the Elenina Bank is about 40 km (Fig. 2), the width is up to 5 km, and the minimum depth is 1.5–2 m. In Burkatsky et al. (2016), the seabed to the north of the Elenina Bank is classified as an area dominated by fluvial lithodynamic conditions; to the south of it, there are mixed fluvial-wave conditions; along the shore–wave conditions. The revealed relief and configuration of the bank do not confirm the presence of wave-initiated longitudinal sediment movement at this time. The relief on profile E9 (Fig. 2) indicates the sediment movement along the northern slope of the accumulative form during periods of increasing currents directed from Taganrog Bay. The body of the Elenina bank probably contributes to the formation of strong currents to its north, driving sediment along the steep northern slope.

At the western end of the bank, in the area of profile E11 (Fig. 2), there are eight arc-shaped ridges up to 6 km long, with a distance of 0.3–0.5 km between adjacent ridges. The height of the ridges is about 0.5 m. These forms may be submerged relict distal tips, similar to those found on the modern spits of the Sea of Azov (Fig. 3). Another variant of the genesis of these forms may be the oscillatory movements of water arising from the flow around the Elenina Bank during storm surges or seiche phenomena. Similar forms were found at the tip of the Dolgaya Spit underwater shoal (Fig. 3) (Krylenko et al., 2019).

4 Conclusions

The data showed that the Elenina Bank is an active accumulative form—it accumulates shell rocks carried by waves from the south. In addition, at its present stage of

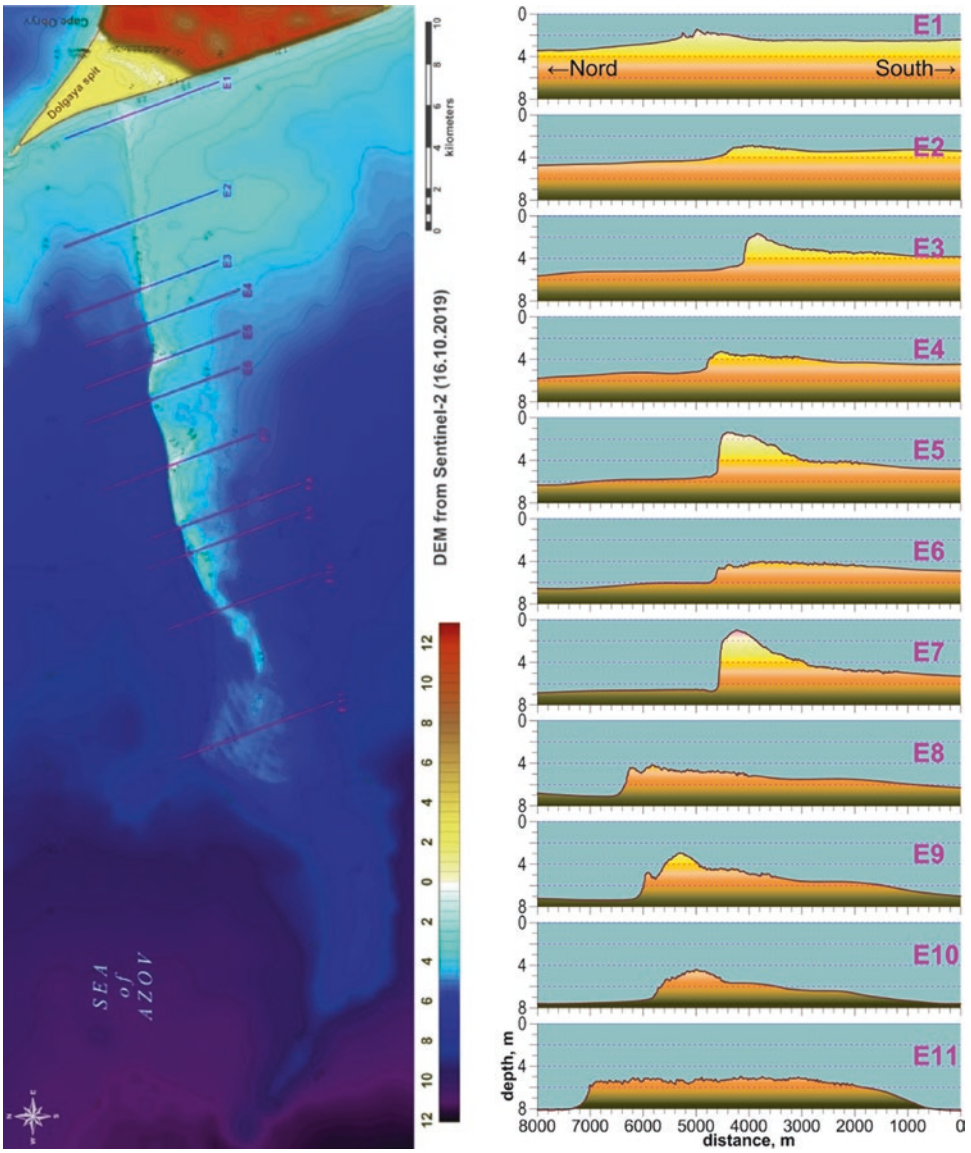

Fig. 2 Underwater relief of the Elenina Bank

Fig. 3 Relief forms near tips of the accumulative forms of the Sea of Azov: on the left is the Elenina Bank; in the center is Biryuchy Island; on the right is the bank of Dolgaya Spit

development, the accumulative body of the Elenina Bank continues to influence the sediment fluxes of the adjacent part of the Sea of Azov.

Russian Science Foundation grant 20-17-00060 funded this research

References

Budischev, I. M. (1808). *Sailing directions and the sea guide to the Sea of Azov*. Saint Petersburg.

Burkatsky, O. N., Aksenov, V. A., & Kuzmin, V. Yu. (2016). Landscape and ecological zoning of the south-eastern part of the Sea of Azov. In *Marine biological research: Achievements and prospects* (pp. 283–286).

Krylenko, V., Aleinikov, A., Krylenko, M., Beliaeva, N., & Moiseeva, N. (2019). Possibility of the underwater topography studying of large accumulative forms according to Sentinel-2 data. *Proceedings of SPIE, 11174*, 111741P.

Matishov, G., & Polshin, V. (2019). New result on the history of the Azov Sea in the Holocene. *Reports of the Academy of Sciences, 15*(1), 42–53.

Matishov, G. G. (Ed.) (2011). *Ecological Atlas of the Sea of Azov*. Rostov-o-Don Publishing house of the SSC RAS.

Sukhomlin, A. M. (1854). *Sailing directions of the Sea of Azov and the Kerch-Yenikalsky Strait*. Nikolaev.

Morphodynamic Approach of a Beach in Sedimentary Stability: Case of Beninese Coast from Djondji to Fidjrosse

Moussa Bio Djara, Raoul Adéniyi Laibi, Christophe Kaki, Tinonkiyè Sylvestre Yantikoua, Mamadou Sadio, Amadou Tahirou Diaw, and Lucien Marc Oyédé

Abstract

Benin's coast is subject to natural processes and human interventions that split it into three segments: the west cell drift, the middle cell drift, and the east cell drift. The coast from Djondji to Fidjrosse (middle cell drift) matches a transitional zone that should evolve in stable conditions. Analysis of the morphodynamic of this coast carried out by Remote Sensing, using Landsat satellite images and bathymetry of the seabed reveals heterogeneous reliefs of the inshore, consisting of bars and troughs interspersed with drainage channels and five erosion pockets on the beach. These are the critical points: (i) Flanho-Agouin (−0.32 m/yr), (ii) Avlékété (−0.37 m/yr), (iii) Adjahédji (−0.21 m/yr), (iv) Adounko-Togbin (−0.44 m/yr), and (v) Bah (−0.31 m/yr). These five persistent erosion pockets are successive huge crescent-shaped and related to the bathymetric configuration of the submarine shoreface and inverse coastal currents that control the horizontal movement of Beninese marine waters.

Keywords

Remote sensing · Bathymetry · Sediment cell · Littoral drift · Morphodynamics · Erosion pocket · Coastal currents

M. B. Djara (✉) · R. A. Laibi · C. Kaki · T. S. Yantikoua · L. M. Oyédé
Laboratory of Geology, Mines and Environment, Department of Earth Sciences, University of Abomey-Calavi, Abomey-Calavi, Benin
e-mail: moussabiodjara@yahoo.fr

M. B. Djara · T. S. Yantikoua
Multidisciplinary Doctoral School, University of Abomey-Calavi, Abomey-Calavi, Benin

M. Sadio · A. T. Diaw
Laboratory of Geoinformation (LERG), Ecole Supérieure Polytechnique, University Cheikh Anta Diop of Dakar, Dakar, Senegal

1 Introduction

Since the 1960s, Benin has made significant development infrastructures that negatively impact its coast today. This is mainly the port of Cotonou, built in 1962 to the immediate west of the Cotonou River estuary channel, and the hydroelectric dam of Nangbéto, built on the Mono River in Togo in 1987. These various infrastructures have significantly disturbed the stability of Benin's coast. Moreover, the Togolese rehabilitation projects of old infrastructures and new coastal defense infrastructures construction exacerbated the erosion which has already been observed in the sector of Hillacondji-Djondji since the 1990s. These disturbances led to the split of Benin's coast into three sectors or sedimentary cells (Fig. 1): the Hillacondji-Djondji sector or Western cell forming a part of the district of Grand-Popo, the Djondji-Fidjrosse sector or Central cell extending on the district of Ouidah, Abomey-Calavi, and Cotonou and the Akpakpa-Kraké sector or Eastern cell belonging to the district of Cotonou and Sèmè-Podji.

The beaches of the Djondji-Fidjrosse sector, the object of this study, present two scenarios. Some are experiencing accretion and others erosion. Therefore, this study aims to analyze the evolution of this sector's shore by examining the morphodynamic characteristics and bathymetric characteristics of the front beach.

2 Material and Methods

2.1 Acquisition, Processing, and Analysis of Satellite Images

Landsat satellite images constitute most of the iconographic material used to analyze the morphological evolution of the beaches and the shoreline of the coastal segment between Djondji and Fidjrosse. They come from archives images from instruments TM (Thematic Mapper), ETM+

A. Çiner et al. (eds.), *Recent Research on Environmental Earth Sciences, Geomorphology, Soil Science, Paleoclimate, and Karst*, Advances in Science, Technology & Innovation, https://doi.org/10.1007/978-3-031-42917-0_31

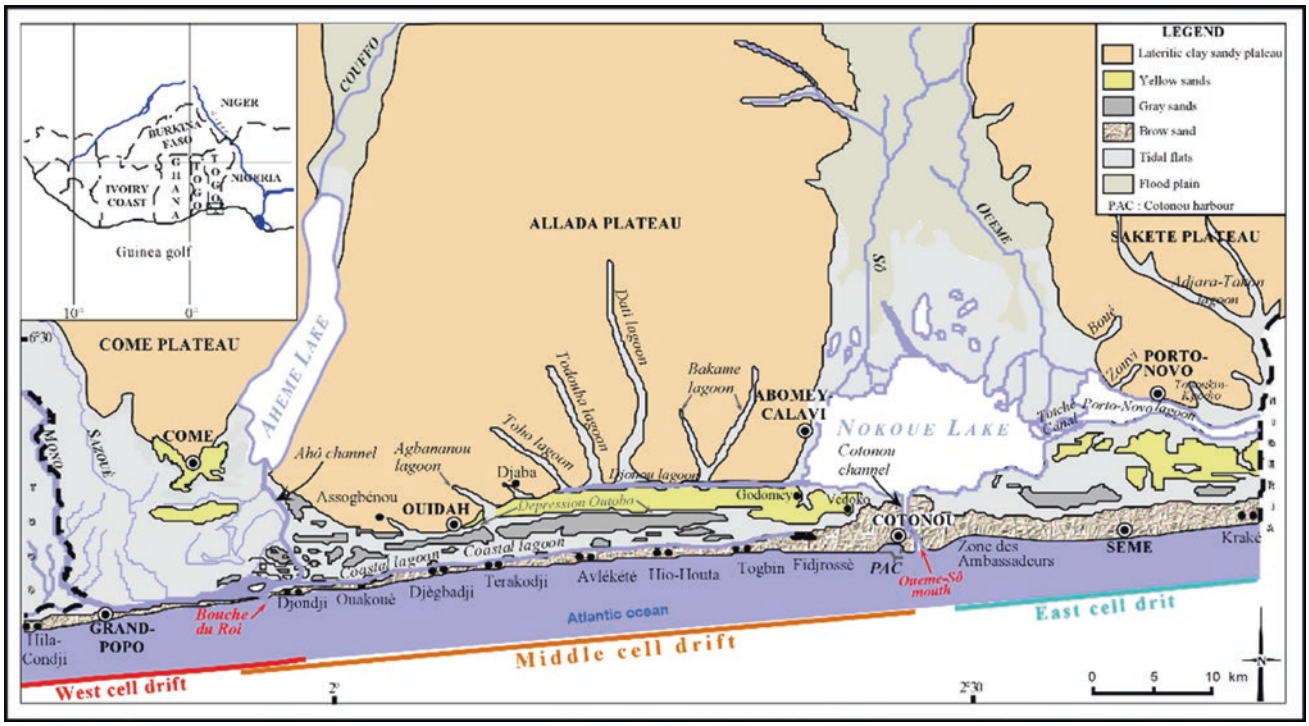

Fig. 1 Geomorphological map of the various sedimentary cells of the Benin coast

(Enhanced Thematic Mapper Plus) of satellites Landsat 4, 5, and 7 and LC8 (Continued Landsat). These images are already orthorectified and projected in the UTM/WGS84 projection system, and each is accompanied by metadata specifying the acquisition parameters, the type of sensor, the satellite type, and the date.

Before using the selected images Landsat, we assessed their quality by superimposing geometric linear elements as the river meanders, for example. The study area was then bounded on all scenes using the Erdas Imagine 8.5 software. In addition, to facilitate the photo interpretation, colored compositions, "false colors," have been developed by combining the views of 453 channels (RGB).

The Landsat images 7 ETM+ and LC8 retained were re-sampled to 15 m by multiresolution fusion from the views of channels 8 and 453 (Pan, RGB). The reference line selected for referencing the coastline is the instantaneous shoreline because it is more easily visible on Landsat images. In addition, the reference to this shoreline reduces the margins of error for a coastline like a coast Benin where the average tidal range is small, of the order of 1 m. The digitization of the selected reference line was performed by computer-aided photo interpretation with the Arc View 3.2 software.

The diachronic analysis from satellite images was traced back to the shore's historical changes (accretion and erosion). These changes were measured automatically using the Digital Shoreline Analysis System program (DSAS) version 2.2.1 (Thieler et al., 2004) following perpendicular transects to the shorelines to compare. These transects were generated from a baseline (Baseline). The DSAS works as an ArcView or ArcGIS addition. It measures the distance between the intersection transects and coastline points, calculates the rates of evolution along each transect and returns the results as attribute tables. Finally, the results are translated into a statistical graph in Excel and compared to the mapping of the study area.

2.2 Methods for Acquiring and Processing Bathymetric Data

Bathymetric surveys were made from a dual-frequency single-beam echo sounder type ECHOTRAC CV100 coupled to a GPS receiver to acquire the probe data. They were measured at a frequency of 33 kHz (opening 23°) and a frequency of 200 kHz (Opening 5°). The measuring range of depths is from 20 cm to 300 m with an accuracy: in theory, 1 cm ±0.1% prof (±3 cm for 20 m). The data acquisition is performed using the software eChart, HYPACK, which verifies the positioning quality with regard to the theoretical radials and especially synchronized positioning-sounder acquisitions. In addition, tide corrections are made to determine the real depth at each point.

Campaign in one survey was conducted in September 2017. It covered the segment from the mouth called "la

Fig. 2 Graphical representation of the three subsectors of bathymetric measurements on the Djondji-Fidjrosse segment

Bouche du Roy" of the river Mono to Fidjrosse up to a distance of fifty-five (55) kilometers (Fig. 2), about the contour line −20 m. These series of measures have been grouped by sector on the coast segment.

The laboratory methods relate to the processing of data for their practice performance. First, with Excel, we converted the gross data into exportable files that are projected later in the ArcGIS 10.1 software to materialize and assess the bathymetric path. Then, to complete the operation, bathymetric points sowings are treated with Surfer 11 software that allows 2D and 3D representation of a digital elevation model and the slope calculations and plotting profiles following points well identified.

3 Results

3.1 Coastline Morphodynamics

3.1.1 Coastline Evolution Analysis in Djègbadji West ("la Bouche du Roi"-Djègbadji)

The coast segment between Djondji and Djègbadji belongs to the central cell. The analysis of the kinematics of the coastline of this segment from Djondji up to Djègbadji South of Ouidah (Fig. 3) shows that it is evolving today, in a context of erosion between Djondji and Meko with speeds around −1 m/year (11 m in 13 years).

This development is to be linked to the instability of the estuary river "la bouche du Roi" since the bringing in service of the Nangbéto dam on the Mono river. On the other hand, the coastline between Meko and Djègbadji is experiencing general accretation at an average rate of 1 m/year (16 m in 13 years). This confirms that the Meko coast sector to the east belongs to the transition zone/accretion of the central cell.

3.1.2 Analysis of the Evolution of the Coastline Between Djègbadji and Fidjrosse (Up to the Port)

Three Landsat images from different dates were used to assess changes in the shore between Djègbadji and Fidjrosse using the Digital Shoreline Analysis System (DSAS) L71192056_05620001213 (13/12/2000), L71192056_05620021203 (03/12/2002), and LC81920562013279LGN00 (06/10/2013). The results of this analysis are presented in Fig. 3 in a map and graphical form.

The analysis of these results shows different evolutions of the coastline (Fig. 3):

- **the coast between Djègbadji and Flanho** changes in the same context of stability/accretion, which characterizes the coast of Meko-Djègbadji. The average accretion speed is of the same order for these two segments: 1–1.5 m/yr;
- **the coast between Flanho and Avlékété** is broadly affected by erosion, with an average speed of −0.32 m/

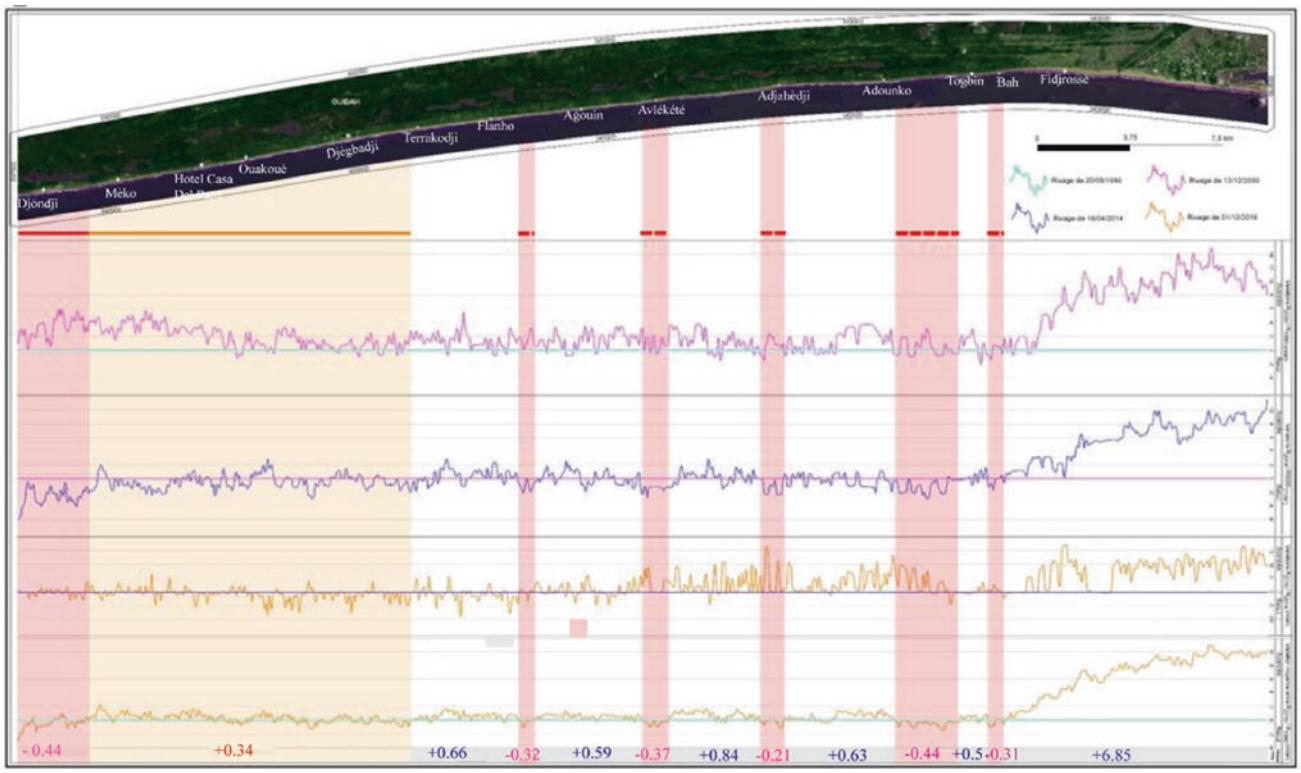

Fig. 3 Evolutions of the shoreline of the coastal sector Djondji-Fidjrosse (Ouidah) between 2000 and 2016

yr in the west of Avlékété and −0.37 m/yr at Avlékété. But in detail, this coast has two segments of erosion interspersed by an accretion segment;

- **the coast from Avlékété to Fidjrosse** is generally experiencing accretion with an average rate of 0.58 m/yr in the west of Adounko and erosive changes in trend, with an average speed of −0.21 m/yr at Adjahèdji, −0.44 m/yr between Adounko and Togbin and −0.31 m/yr at Bah. This evolution shows a detailed diagram comparable to that of the west coast of Avlékété: three erosion pockets inserted in an accretion segment;
- **the coast between Fidjrosse and the port of Cotonou** evolves in a sandy accumulation context with an average annual rate of 6.20 m/yr. This functioning scheme is imposed by the port facilities that work as a fixed side border. The coast between Fidjrosse and the port of Cotonou in accretion at the upstream side-drift of these port facilities and marks the end of the central cell, while the downstream side-drift defines the start of the east cell (Fig. 3).

3.2 Bathymetric Analysis of Beachfront Seabed

Bathymetric data have achieved maps and Numeric Terrain Models (MNT) in 3D followed by west–east and north–south sections. The central sector of the bathymetric map indicates depths varying between −3 and −21 m. The minimum depths are observed on the front beach, where curves-shaped morphologies appear, whereas the maximum depths are identified at the open sea (Fig. 4).

These curves stand across the front beach line. This morphology, characterized by irregularities on the front beach in the central part, shows two regular sub-segments, Djondji to Avlékété west and Fidjrosse to the port of Cotonou eastward (Fig. 4).

3.2.1 Analysis of MNT Between Djondji and Djègbadji

The bathymetric map shows depths from −4 to −20 m. The relief on the MNT shows on the front beach erosion pockets and a flat and decreasing surface toward the open sea. The west–east and north–south profiles obtained from the MNT indicate no particular disturbances (Fig. 5). However, some less expressive transverse drainage channels are observable.

The uniform relief of the front beach indicates the low sediment movement supported by the reverse currents (underflow or rip currents). The erosion pockets observed on the front beach and drainage channels result from the removal of currents, which return sediment washed to the front beach along a direction perpendicular to the shore.

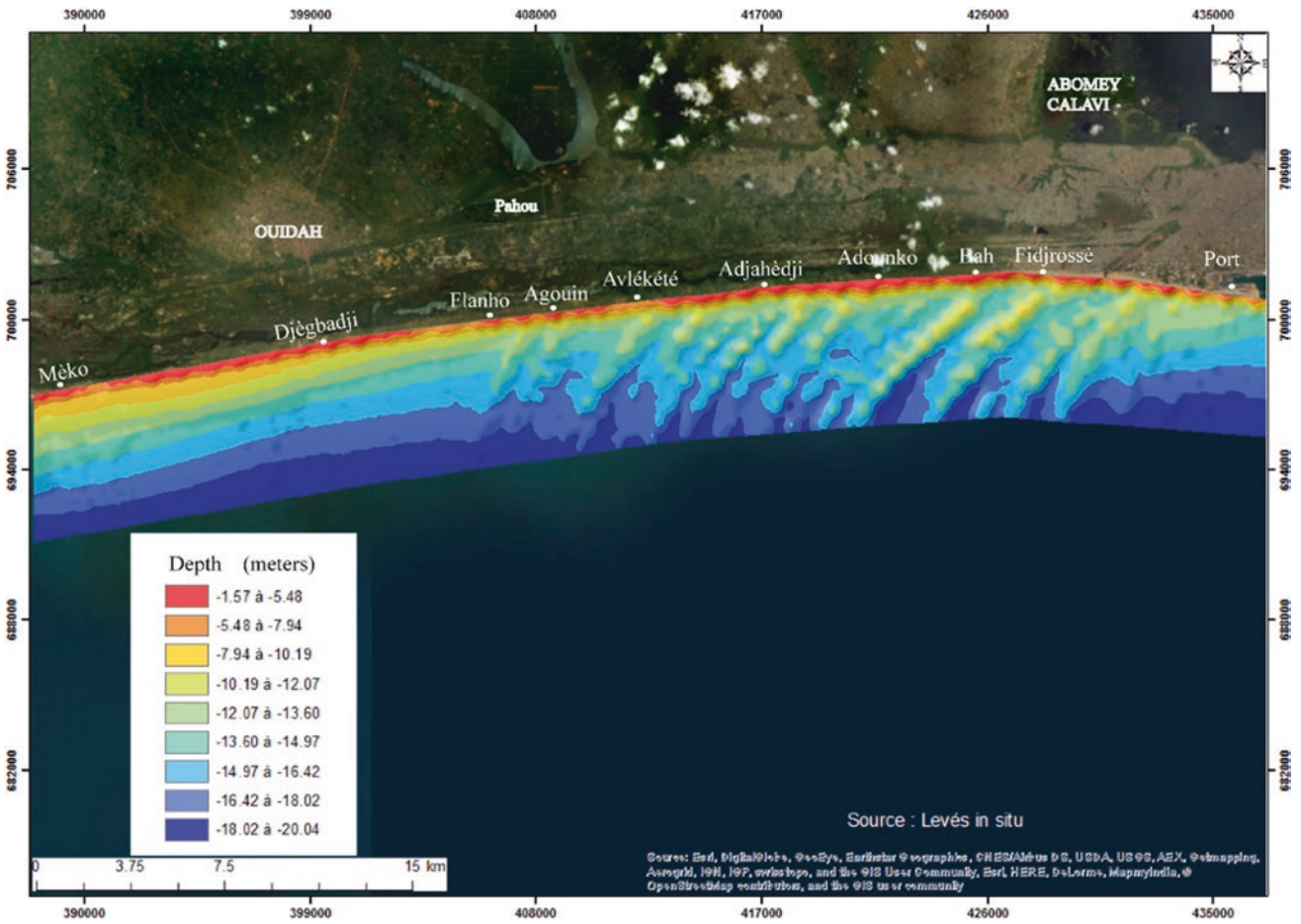

Fig. 4 Bathymetry of the coastal area of the Central segment (Djondji-Fidjrosse)

3.2.2 Analysis of MNT Between Flanho and Avlékété

The bathymetric maps show depths from −5 to −20 m and high reliefs of peaks separated by drainage channels. The west–east profiles have a complex morphology consisting of dunes and channels. However, the altitude decrease to the sea is remarkable. The structure of MNTs shows a relief of the front beach, highly heterogeneous, marked by a succession of bars and troughs, some being built on the west side and the other being destroyed on the east side (Fig. 6).

3.2.3 Analysis of MNT Between Avlékété and Fidjrosse

Bathymetric maps indicate depths from −5 to −20 m, and like the previous side, the relief remains heterogeneous, consisting of peaks separated by drainage channels (Fig. 7). The morphology, complex in nature, consists of dunes and South-West-oriented channels. This orientation is consistent with the sediment transport direction corresponding to the littoral drift.

3.2.4 Analysis of MNT Between Fidjrosse and the Port of Cotonou

The bathymetric maps show depths from −3 to −18 m. The relief of the seabed is characterized by a more or less flat and decreasing surface from the coast to the open sea (Fig. 8). This morphology reflects the availability of sediments in the immediate proximity of a blocking zone represented here by the sand stop headland from the port of Cotonou which promotes an upstream sedimentary excess.

In sum, the bathymetric maps and MNTs of the central sector show, from west to east, three subsectors: Djondji-Flanho, Flanho-Fidjrosse, and Fidjrosse-port of Cotonou. The first subsector (Djondji to Flanho), as the third subsector (Fidjrosse to the port of Cotonou), is characterized by a flat and decreasing seabed to the open sea with erosion pockets to the coast (Figs. 5 and 8). The second subsector between Flanho and Fidjrosse is characterized by a complex morphology consisting of dunes and channels (Figs. 6 and 7). The waves surge, and reverse currents shape these bars and South-West-oriented troughs. Reading the MNT of

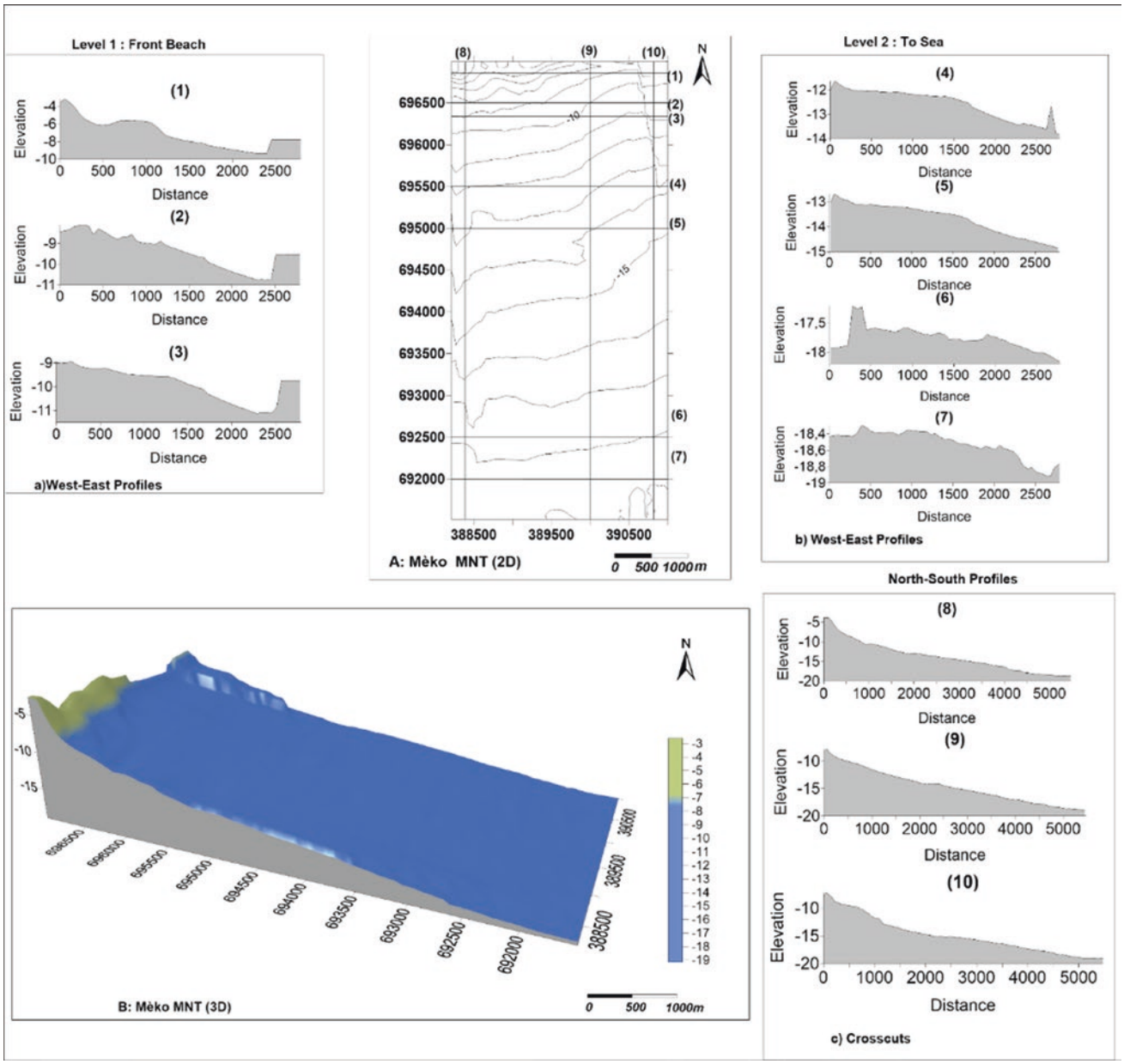

Fig. 5 MNT of Meko illustrating the profiles obtained following the directions: **a** west–east on the front beach, **b** on the west–east on the open sea, **c** north–south on MNTs (A: MNT 2D and B: MNT 3D)

the second subsector, we note a good correlation between beach changes and sedimentary availability. Similarly, these MNTs guide sediment transport directions highlight cross-sectional and longitudinal components of the beach and the influence of coastal currents.

The flat and inclined surface toward the South-East is characterized by leaching followed by a distribution of sediments by wave currents from the open sea and conjugated to the littoral drift. On the other hand, the presence of a highly differentiated relief made up of dunes and channels as the Flanho-Fidjrosse subsector showing successive constructions and destructions of submarine sedimentary dunes shows a great disturbance of sediment in transit in the subsector by tidal currents and multidirectional winds described above.

4 Discussion

Located on a side whose cause of the sedimentary dynamics is littoral drift, the estuary of a river called "la Bouche du Roi" works as a movable side border between the West sedimentary cell and that of the center (Figs. 5 and 6). A sedimentary or hydro sedimentary or morpho-sedimentary

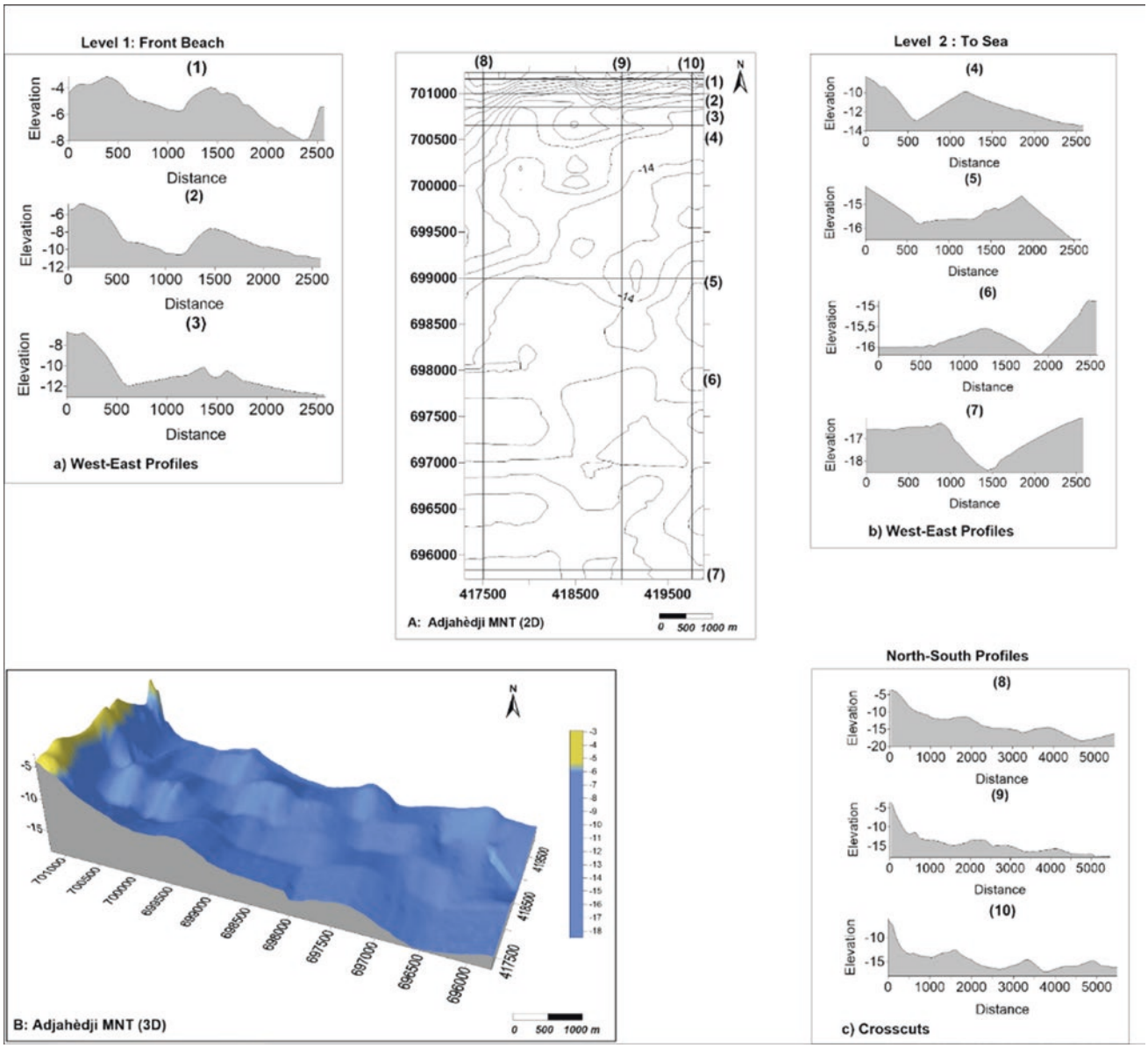

Fig. 6 MNT of Adjahèdji illustrating the profiles obtained following the directions: **a** west–east on the front beach, **b** on the west–east on the open sea, **c** north–south on MNTs (A: MNT 2D and B: MNT 3D)

cell or drift cell is defined as a coast section in a balanced overall sedimentary context along which the sediments flow (Cohen et al., 2002). It comprises four borders (Certain & Barusseau, 2002): the land border, closed, formed by dunes and emerged beach; the marine border, open; two fixed or mobile lateral boundaries more or less impermeable indicating, one, the start zone of littoral transit [source zone (a)], the other, the storage zone of sand that has transported [wells zone (c)]. The two regions (source and wells) are joined by a transition zone (b). In general, there is a close parallel between erosion and source zone, accretion and wells zone, while between the two, it prevails instead of stability (transition zone).

Based on the model of a sedimentary cell, we can say that the coastal sector between Djondji and Fidjrosse includes two coast segments in stability/accretion alternating with two other segments in erosion. Thus, we note special features by comparing this evolution context to that of the classical transition area of a drift cell. The coast segment between Djègbadji and Agouin (or more generally between Meko and Agouin) and that between east Avlékété and Adjahédji can be seen as developing in a context of stability/accretion following the pattern of change of a transition zone of a drift cell. On the other hand, the Agouin and Avlékété-Fidjrosse segments in erosion exhibit a pattern of change opposite to that of the transition region of a drift

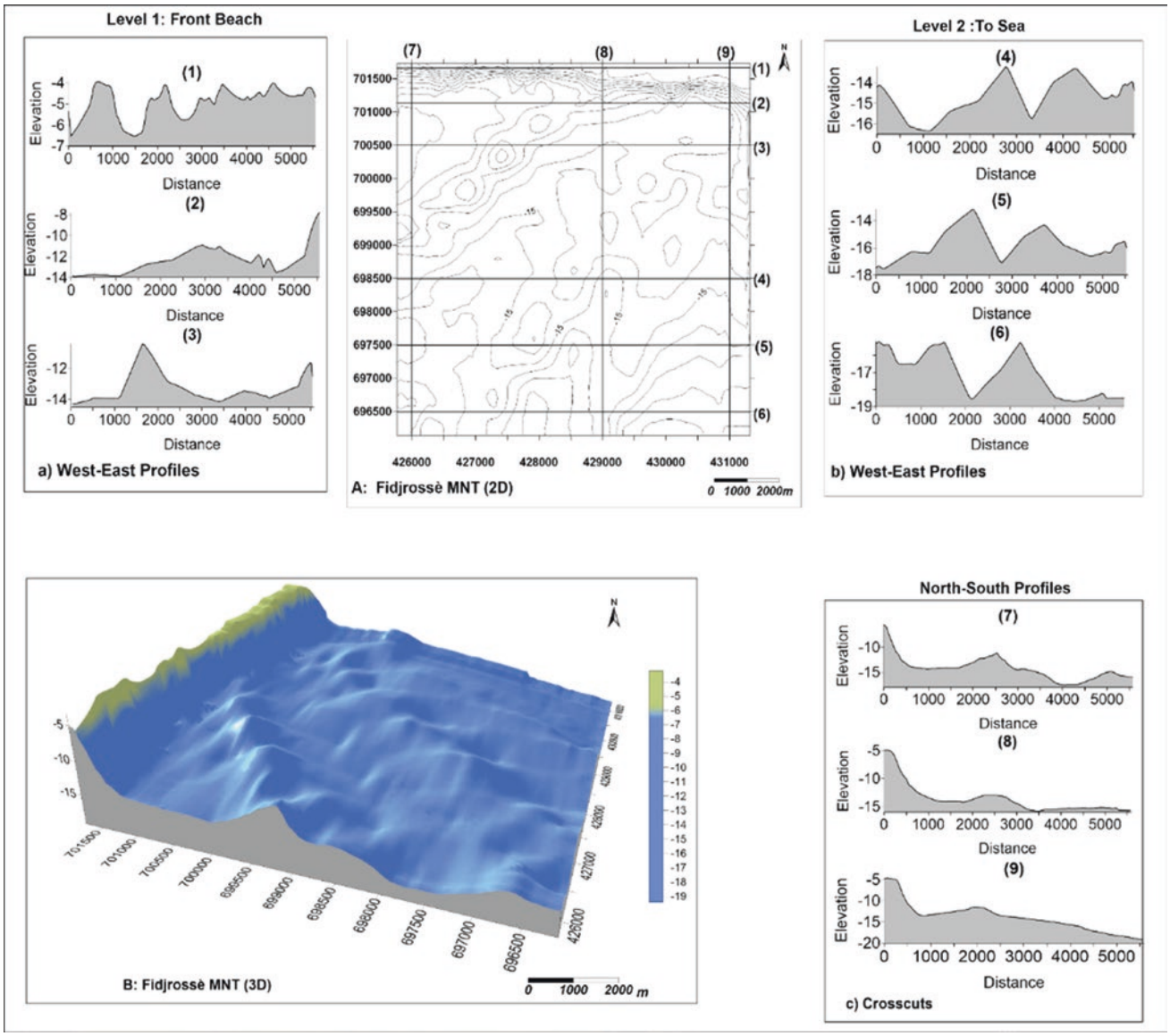

Fig. 7 MNT of Fidjrosse illustrating the profiles obtained following the directions: **a** west–east on the front beach, **b** on the west–east on the open sea, **c** north–south on MNTs (A: MNT 2D and B: MNT 3D)

cell. These special features introduced in this coast change can be explained by changes in the orientation of the coastline. Thus, the analysis of the geometry of the coast between Djondji and Fidjrosse reveals two major orientation changes. The first is located on the coast after Agouin-Houta, which then translates erosion observed at Avlékété. The second is located on the coast after Adjahèdji, thus causing erosion of the coastline at Togbin and Adounko.

Overall, in the functioning of the front beach, the currents are induced by waves modulated in time and space by the tidal cycle (Dehouck et al., 2006). When energy conditions happen, the reverse current and longitudinal drift are the two major agents of sediment transport, one exporting sediments seaward outside of the breaking zone, the other favoring an oriented longitudinal transport according to the incidence of waves. Observed bars forming rhythmic systems and channels intersecting them called troughs (on MNTs) result from the interaction between the reverse currents and tide. The oblique orientation of these forms over the coast and migration is induced by the waves' impact and the direction of the longitudinal drift (Apoluceno et al., 2002; Lafon et al., 2004). These intertidal bar systems are relatively stable, maintained at low energy conditions to moderate, destroyed during storms, and reformed in 5–9 days intervals (Lafon et al., 2005).

However, at the local level, the boundaries between the compartments and cells introduce important discontinuities in the littoral sedimentary drift. Ultimately, the

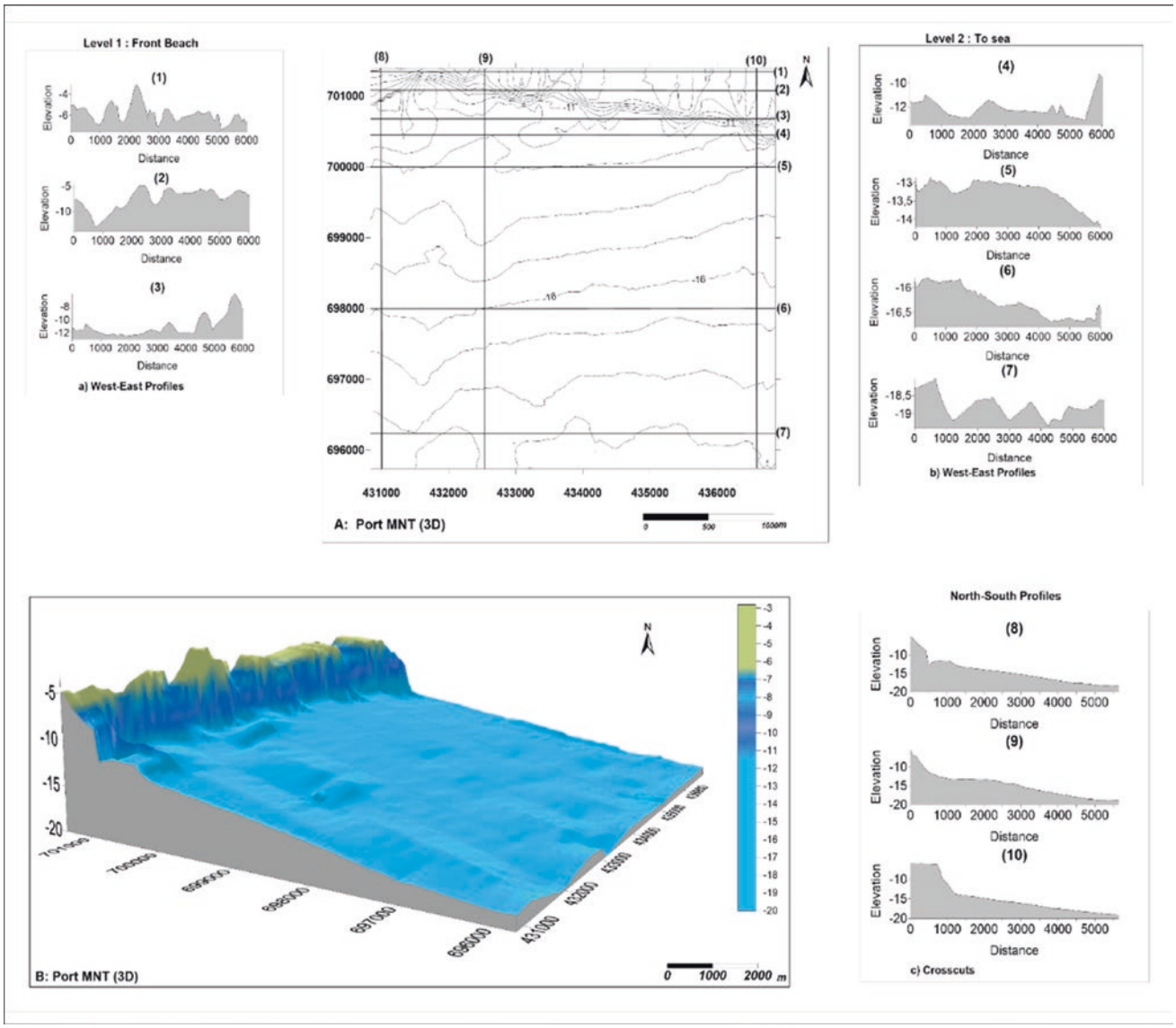

Fig. 8 MNT of the port of Cotonou illustrating the profiles obtained following the directions: **a** west–east on the front beach, **b** on the west–east on the open sea, **c** North–South on MNTs (A: MNT 2D and B: MNT 3D)

organization of the littoral drift in the west led to each scale, a redistribution scheme between the source zones, depleted of sediments (Djondji-Meko subsector), and wells zones (Fidjrosse-port of Cotonou subsector), where stocks are much more important. The volume of the sand reservoir of the front beach seems to correspond with the evolution of the beach. Wherever the reservoir is depleted, the beach's changing trend is negative; in contrast, the beaches associated with important reservoirs do not suffer from erosion.

A remarkable feature in the study area's sediment distribution, bathymetry, and hydrodynamic evolution lies in irregular shapes relating to oblique bars built on the subsegment between Flanho and Fidjrosse in the central part. This morphology with irregularities on the front beach concerns the area of the five persistent erosion pockets observable in the field and revealed by satellite images. It is probably related to periodic coastal reverse and vortex currents circulating for some in a sense south-east/north-west from Nigeria to Togo and other, very violent, from the coast toward the open sea with north-east/south-west component.

5 Conclusions

The appreciation of the geometry of the coastline of the Djondji-Fidjrosse sector is made possible by analyzing a series of Landsat satellite images and the bathymetric seabed of the front beach. It is learned from the analysis of these images that the central cell is characterized by erosion linked not only to the effect of the littoral drift, but also

by the migration of the estuary Mono River ("la Bouche du Roi"). The MNT, characterized by a flat relief and a few withdrawal current channels, shows this area's sediment deficit. Thus, the coast segment affected by erosion remains that of Mèko-Djondji close to the mouth. With the migration of the River estuary "Bouche du Roi", this segment at risk of erosion will also extend eastward toward Ouidah. As a result, many fishing villages will be ruined along the coast, hotels destroyed, and historical and cultural monuments demolition.

East of Djègbadji, sediments availability is increasingly noted by differentiated MNTs and a submarine organization in bars and troughs disrupted by coastal currents, which sporadically causes erosions on some points between Djègbadji and Fidjrosse as persistent pockets observed on site and highlighted by the Landsat images.

References

Apoluceno, D. M., et al. (2002). Morphodyamics of ridge and runnel systems during summer. *Journal of Coastal Research*. https://doi.org/10.2112/1551-5036-36sp1.222

Certain, R., & Barusseau, J.-P. (2002). Contrôles météo-marins et géologiques du bilan sédimentaire des prismes littoraux sableux—Conséquences en matière d'aménagement. In *érosion littorale en Méditerranée Occidentale. CIESM Workshop Series* (Vol. 18, pp. 25–29).

Cohen, O, Dolique, F., Anthony, E. J., & Hequette, A. (2002). L'approche morphodynamique en géomorphologie littorale. In Rue d'ULM (éd.) *Regards, pratiques et savoirs* (pp. 191–211).

Dehouck, et al. (2006). Morphodynamique des plages sableuses de la mer d'Iroise (Finistère). Océan, Atmosphère. Université de Bretagne occidentale-Brest.

Lafon, V., De Melo Apoluceno, D., Dupuis, H., Michel, D., Howa, H., & Froidefond, J. M. (2004). Morphodynamics of nearshore rhythmic sandbars in a mixed-energy environment (SW France): I. Mapping beach changes using visible satellite imagery. *Estuarine, Coastal and Shelf Science, 61*(2), 289–299.

Lafon, V., Dupuis, H., Butel, R., Castelle, B., Michel, D., Howa, H., & De Melo Apoluceno, D. (2005). Morphodynamics of nearshore rhythmic sandbars in a mixed-energy environment (SW France): 2. Physical forcing analysis. *Estuarine, Coastal and Shelf Science, 65*(3), 449–462.

Thieler, E. R., Ergul, A., Martin, D., & Thompson, M. (2004). Tutorial for the digital shoreline analysis system (DSAS) version 2.2.1. Extension for ArcView. USGS/PEROTSYSTEMS (30 pp.).

Evolution of the Tuzla Spit from Natural Geosystem to Natural-Technogenic One

Marina Krylenko and Viacheslav Krylenko

Abstract

Monitoring the coastline dynamics is necessary for successful coastal zone management. The Tuzla Spit (Russia) is located south of the Kerch Strait, which connects the Sea of Azov and the Black Sea. The analysis of the coastline dynamics of the Tuzla Spit is based on the study of modern and archival maps and remote sensing data. In general, the dynamics of Tuzla Spit are determined by a combination of two main factors: the volume of incoming sediment and the intensity of hydrodynamic processes in the strait. A significant part of the changes in the Tuzla Spit in the twenty-first century was initiated by anthropogenic impact. In 2003, part of the Tuzla Spit's coastline was stabilized technologically. In 2016–2020, bridges across the Kerch Strait were built along the Tuzla Spit and Tuzla Island dam. Despite a high dynamism and variability, the Tuzla Spit geosystem is stable, as there is a natural mechanism that limits both growth and complete erosion of the accumulative body. It has been established that both the increase and decline of this accumulative form were observed in the last century. The modern dynamics of the Tuzla Spit result from natural processes in the conditions of increased anthropogenic pressure.

Keywords

Sea coast · Geosystem · Azov-Black Sea region · Remote sensing

M. Krylenko (✉) · V. Krylenko
Shirshov Institute of Oceanology RAS, Moscow, Russia
e-mail: krylenko@mail.ru

1 Introduction

In recent decades economic activity on the Russian coasts of the Black Sea and the Sea of Azov has been characterized by the intensification of development. As a result, the human pressure on coastal geosystems increases, leading to the degradation of their components and disturbing the natural balance in coastal development processes. In addition, sea coasts, especially accumulative ones, are very dynamic, and the biological processes taking place in them can be unfavorable for economic use. Therefore, with changing natural conditions and increasing intensity of anthropogenic impact, it is necessary to monitor coastal processes (Aibulatov, 2005; Kosyan & Krylenko, 2019).

The Tuzla Spit is a typical accumulative coastal form. It is located south of the Kerch Strait, which connects the Sea of Azov and the Black Sea (Fig. 1). The modern Tuzla Spit was formed 1000–1500 years ago at a sea level 1.5–2.0 m below the modern one (Peshkov et al., 2005). The purpose of this paper is to study the features of the evolution of the Tuzla Spit, especially its coastline, using maps and remote data for 250 years.

2 Materials and Methods

The analysis of the dynamics of the Tuzla Spit is based on the study of modern and archival maps and remote sensing data. In 1771, a hydrographic survey was done, and a map of the Kerch Strait was drawn, which depicts the Tuzla Spit as a chain of islands. Until the 1960s, maps were the main and often the only source of data on the position of the coastline. Geometrical correction of cartographic images was made. Map referencing was done using Global Mapper software.

An essential source of information about the previous state of the Tuzla Spit is aerial and space survey materials. The oldest remote sensing materials available are space

A. Çiner et al. (eds.), *Recent Research on Environmental Earth Sciences, Geomorphology, Soil Science, Paleoclimate, and Karst*, Advances in Science, Technology & Innovation, https://doi.org/10.1007/978-3-031-42917-0_32

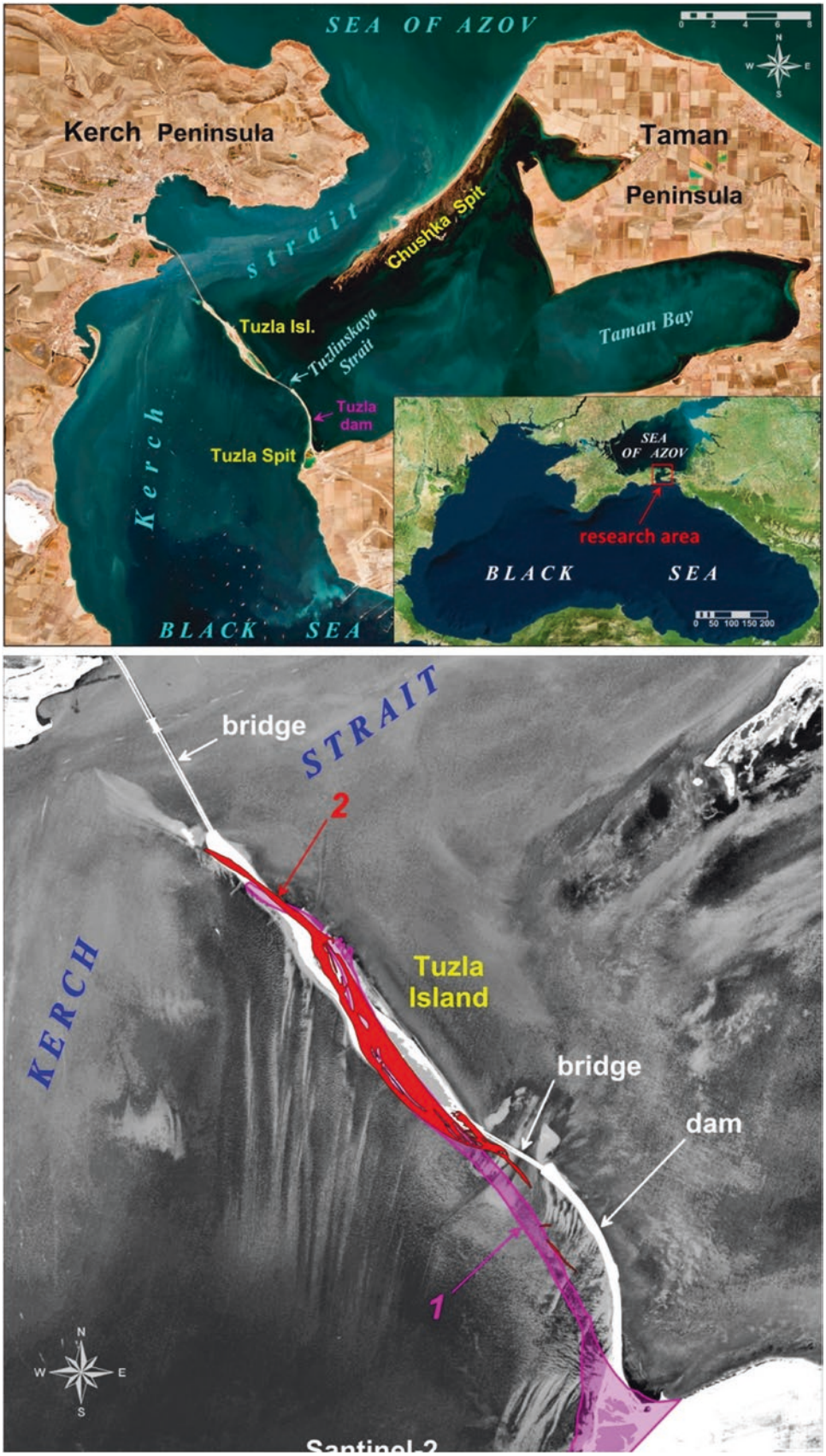

Fig. 1 Scheme of the Kerch Strait (at the top) and changes of the Tuzla Spit 1920–2019: 1—1920 year (pink); 2—1965 year (red); 3—2019 (gray)

images from the 1960s and 1970s, provided by the US Geological Survey (USGS, 2020). In addition, a series of images from satellite Sentinel-2 is used. The water surface mask was calculated using the NDWI index (Gao, 1996). Spatial data and space images were processed using Scanex Image Processor software (Krylenko et al., 2019). A raster or vector was transformed according to a polynomial model of the third degree. Further data processing and visualization were performed in Golden Software.

3 Results and Discussion

The configuration of the coastline and bottom of the Kerch Strait contributes to forming an accumulative barrier form (Fig. 1). On the contrary, water exchange through the Kerch Strait prevents the formation of the accumulative body. Three types of currents are characteristic: from the Sea of Azov, from the Black Sea, and the weak current variable in direction (Diakov et al., 2016). The frequency of occurrence on average per year is 40% for the Black Sea currents. The sediment feeding of the modern Tuzla Spit is carried out mainly from the Black Sea. Intensification of cyclonic activity and an increase in wave energy from the Black Sea led to a rise in the flow of sediment from the Black Sea and the thickness of the accumulative body.

As the analysis of maps of the eighteenth-nineteenth centuries shows, the Tuzla Spit consisted of separate islands during that period, and the process of growth and combining spit parts was observed. In the second half of the nineteenth century, the Tuzla Spit moved toward Kerch Peninsula. A narrowing of the strait accompanied this. Gradually, the sediment supply to the distal part was reduced, and its erosion began again. In the second decade of the twentieth century, the distal portion of the Tuzla Spit decreased by 1.5 km.

In 1925, during storm of the SW direction, the Tuzlinskaya Strait formed near the root of the Tuzla Spit, and Tuzla Island was the Tuzla Island separated. By 1953, the Tuzlinskaya Strait width increased to 4 km and the length of the Tuzla Island to 7 km. The axis of the accumulative body shifted 800–1000 m to the NE from 1925 to 2003. The shift between 1920 and 1965 was slower than between 1965 and 2003.

Before the manufactured transformation, the SW coast of Tuzla Island was represented by a high (2 m) beach ridge that gradually shifted to the NE. The formation of 1–2 submarine bars was observed along the shore. Long (up to 6 km) narrow tongues were followed to the south of the island. A network of ridges and hollows complicates their surface. On the NW side of the island, there was observed the formation of a series (up to 10) of underwater bars along with above-water forms.

In 2003, the southern part of the Tuzla Spit was restored by a limestone dam (volume of material 580,000 m^3). Its length is 3.8 km, and its width is 41–60 m. A beach (5–30 m) formed along the dam. As a result, there was an intensification of currents (until 100–180 cm/s) (Diakov et al., 2016) in Tuzlinskaya Strait and activation of the erosion of the Tuzla Island (200 m/year) (Fig. 1). As the width of the Tuzlinskaya Strait increased, current velocities in it decreased again (60 cm/s) (Diakov et al., 2016) and coastline stabilized.

In 2016–2020, the Tuzla Spit and the Tuzla Island were technologically stabilized, and a bridge across the Kerch Strait was built. It begins near the root of the Tuzla Spit and runs along the dam and Tuzla Island. It should be noted that the bridge's construction has led to a reduction in the cross-sectional area of the strait, which will result in more intensive currents (up to 120–200 cm/s). This can lead to erosion of the bottom, but the washout of the coasts is unlikely since they are protected.

4 Conclusions

Thus, both growth and erosion of the accumulative form of the Tuzla Spit are observed. The analysis of maps and satellite images has shown that part of the above-water accumulative body was never completely eroded. In general, the dynamics of the accumulative form are determined by the volume of incoming sediment and the intensity of hydrodynamic processes in the strait. Despite a high dynamism and variability, the geosystem of the Tuzla Spit as a whole is highly stable, as there is a natural mechanism that limits both growth and complete erosion. At the end of the twentieth and the beginning of the twenty-first centuries, a significant part of the Tuzla Spit's shoreline changes was directly or indirectly initiated by anthropogenic impacts. The modern dynamics of the Tuzla Spit result from natural processes that occur in conditions of increased anthropogenic pressure. The revealed patterns can be used in the integrated management of the coastal zone for similar accumulative coastal forms of the Azov region.

Russian Science Foundation funded this research, grant 20-17-00060.

References

Aibulatov, N. (2005). *Russia's activity in the coastal sea zone and environmental problems*. Nauka.

Diakov, N., Fomina, N., Timoshenko, T., & Polozok, A. (2016). Features of water exchange through the Kerch Strait according to

field observations. *Environmental Safety of the Coastal and Shelf Zone of the Sea, 1*, 62–67.

Gao, B. (1996). NDWI—a normalized difference water index for remote sensing of vegetation liquid water from space. *Remote Sensing of Environment, 58*, 257–266.

Kosyan, R., & Krylenko, M. (2019). Modern state and dynamics of the Sea of Azov coasts. *Estuarine, Coastal and Shelf Science, 224*, 314–323.

Krylenko, V., Krylenko, M., & Aleynikov, A. (2019). Revision of the coastline length of the Azov Sea according to remote sensing data. *Proceedings of SPIE, 11174*, 111741B.

Peshkov, V. M., Porotov, L. V., & Gusakov, I. N. (2005). On restoring the Tuzla spit. *Geology and Minerals of the World Ocean, 2*, 127–134.

USGS. (2020). Retrieved December 21, 2020, from http://earthexplorer.usgs.gov

Relative Sea-Level Changes in the Central Aegean from the Late Roman/Early Byzantine Period Onwards

Eleni Kolaiti, Nilhan Kızıldağ, Harun Özdaş, and Nikos Mourtzas

Abstract

Geoarchaeological data from the central and northern Cycladic plateau coasts, Peloponnese and Crete, and the western coast of Turkey shed light on the Late Roman/Early Byzantine period, for which little is known about the relative sea-level (RSL) changes. This study focuses mainly on ancient maritime installations and coastal structures (e.g., quays, breakwaters, fish tanks, protective rockfills, and buildings), all falling in the same chronological frame. A total of 34 locations throughout the central Aegean (eastern Peloponnese: 5 locations, Cycladic plateau: 6 sites, Crete: 10 locations, western coast of Turkey: 13 locations) were evaluated. Data suggest an RSL rise of 2.40 ± 0.20 m in the eastern Peloponnese and central/northern Cyclades, 1.25 ± 0.05 m in Crete, and a variable RSL rise from 1.50 ± 0.40 m to 4.20 ± 0.30 m on the coast of western Turkey since at least the sixth century AD onwards. The spatial distribution of the above sites in the backarc area of the Hellenic subduction zone implies that the complex tectonic regime of the central Aegean Sea reflects the differential rates of RSL rise over the reference period of about 1400 years.

Keywords

Aegean sea · Greek coast · Turkish coast · Relative sea-level rise · Late Roman/Early Byzantine period

1 Introduction

Recent geoarchaeological studies of relative sea-level (RSL) changes on both the Greek and Turkish coasts of the central Aegean Sea, mainly based on archaeological markers (ancient remains related to a former sea level) and geomorphological indicators (marine tidal notches, marine terraces, and beach rock generations), show a remarkable subsidence trend during the Late Holocene.

Since the early nineteenth century onwards, numerous studies have dealt with the Late Holocene RSL changes of the Aegean, covering a broad period of the last six millennia (e.g., Kolaiti & Mourtzas, 2020 and related references therein). Nevertheless, a few studies have focused on the RSL changes that happened in Late Antiquity, after the fourth century AD onwards, a period for which little is known to date (e.g., Bechor et al., 2019; Kolaiti, 2020; Kızıldağ & Özdaş, 2021; Kolaiti & Mourtzas, 2023). Therefore, to establish the rates of RSL changes in the central Aegean since the Late Roman/Early Byzantine period, we collected and evaluated geoarchaeological data from the Greek and the western Turkish coasts.

This study focuses on submerged ancient maritime installations and coastal structures (e.g., quays, breakwaters, fish tanks, protective rockfills, and buildings), all falling chronologically within the reference period. A total of 34 locations throughout the central Aegean area was evaluated: 5 sites on the eastern coast of the Peloponnese (Kolaiti, 2019), 6 spots on the islands of the central and northern Cycladic plateau (Kolaiti & Mourtzas, 2020; Kolaiti & Mourtzas, 2023), 10 locations on the coast of Crete (Mourtzas et al., 2016), and 13 locations on the coast of western Turkey (Kızıldağ, 2019; Kızıldağ & Özdaş, 2021) (Fig. 1).

E. Kolaiti (✉)
Institute of Historical Research, National Hellenic Research Foundation, Athens, Greece
e-mail: kolaitieleni@gmail.com; Eleni.Kolaiti@nottingham.ac.uk; info@aktes.gr

E. Kolaiti · N. Mourtzas
Department of Classics and Archaeology, University of Nottingham, UK, England

E. Kolaiti · N. Mourtzas
Society for the Study of Ancient Coastlines NPO - AKTES, Athens, Greece

N. Kızıldağ · H. Özdaş
Institute of Marine Sciences and Technology, Dokuz Eylül University, Izmir, Turkey

A. Çiner et al. (eds.), *Recent Research on Environmental Earth Sciences, Geomorphology, Soil Science, Paleoclimate, and Karst*, Advances in Science, Technology & Innovation, https://doi.org/10.1007/978-3-031-42917-0_33

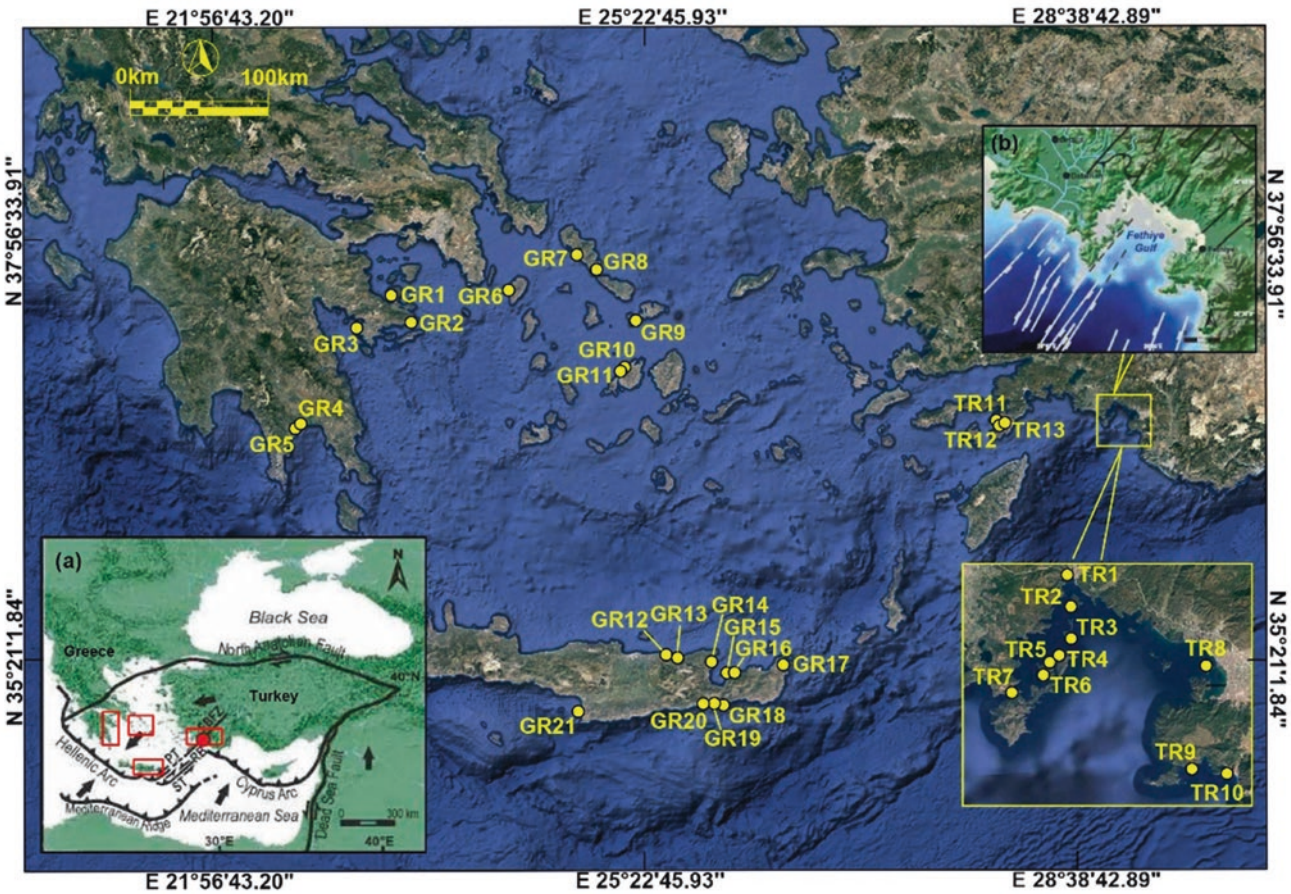

Fig. 1 Location map of the study areas along the Greek and Turkish coasts. Locations are indicated in yellow and are reported in Table 1 (columns A and B). **a** Geotectonic features of the Eastern Mediterranean Sea. FBFZ: Fethiye-Burdur Fault Zone, PT: Pliny Trench, ST: Strabo Trench, RB: Rhodes Basin. Red squares indicate the study areas. **b** Major faults around the Fethiye Gulf (from Kızıldağ and Özdaş (2021))

2 Seismotectonic Setting of the Central and South Aegean

The Aegean Sea and its surrounding coastal areas of Greece and western Turkey is one of the most seismically active and rapidly deforming regions (see Fig. 1a). The convergence rate between the Aegean region and the Nubian (African) plate (~35 mm/yr) is attributed to the rapid southwestward motion of the Aegean region (e.g., Reilinger et al., 2010). The northward subduction of the African plate beneath west Turkey and the Aegean region is causing the extension of the continental crust and volcanism in the overlying Aegean extensional province (e.g., Taymaz et al., 2007). Normal faulting predominates in the Greek mainland, along the eastern Aegean islands, and the western coast of Turkey, while thrust faulting predominates in the Hellenic Arc. As a result, the central Aegean appears aseismic, while E-W structures offshore the west Anatolia are delineated by seismic activity. The most significant part of seismicity is crustal, concentrated along major active seismic zones at less than 30 km focal depths. Focal mechanisms indicate transpressional tectonics along the Hellenic Arc and transtensional tectonics across the overriding Aegean plate (Kassaras et al., 2020).

3 Materials and Methods

All depths reported herein are corrected for tide and atmospheric pressure and correspond to depths below mean sea level (bmsl). The functional elevation of the operational features of the ancient coastal remains, directly related to a former sea level when they were in use and now submerged, with respect to mean sea level, provides not only a reasonable estimate of the RSL rise since the time they were in use, but also the dating of the sea-level stand during their use and a terminus *post quem* for the time that the sea-level change may have occurred. In this study, a mean elevation of the top surface of a quay or breakwater of 0.60 ± 0.30 m above mean sea level (amsl) during the period it was in use, 0.10 m amsl for a slipway, 0.30–0.50 m amsl for a protective rockfill, sea wall, and coastal building, and $\pm$ 0.05 m for a fish tank, which is the most precise sea-level marker, are assumed (e.g., Mourtzas et al., 2016; Kızıldağ, 2019 and related references therein).

4 Results

The location and archaeological age of the ancient maritime and coastal structures and the measured mean depths of their functional features for the 34 study areas are presented in Table 1 (columns A÷E). The submerged ancient remains along the Greek coastline are located between 1.60 and 2.20 m bmsl in the eastern Peloponnese, 1.10 and 2.60 m bmsl in the central/northern Cyclades, and 0.70 and 1.40 m bmsl in Crete. On the Turkish coastline, the submerged ancient remains were measured between 0.70 and 1.20 m bmsl at Bozburun Peninsula and 1.60 and 3.60 m bmsl in Fethiye Gulf.

5 Discussion

Based on the measured mean depths of the ancient coastal remains in reference to their functionality, and comparing these with the depths of available geomorphological sea-level indicators, the related sea-level stands when the ancient structures were in use can be inferred (Table 1, column F). To summarize, the results point to an RSL rise of 2.40 ± 0.20 m to 2.60 ± 0.30 m in the eastern Peloponnese, 2.40 ± 0.20 m in the central/northern Cyclades, 1.25 ± 0.05 m in Crete and an RSL rise ranging from 1.50 ± 0.40 m to 4.20 ± 0.30 m in the western coast of Turkey since at least the sixth century AD onwards.

The spatial distribution of the above sites in the backarc area of the Hellenic subduction zone implies that the complex tectonic regime of the central Aegean Sea reflects on the differential rates of the RSL rise during the reference period (about the last 1400 years): from 1.70–1.90 mm/yr in areas of seismic quiescence (Cyclades) or moderate seismicity (eastern Peloponnese) to 0.90–2.90 mm/yr in regions of intense seismotectonic deformation (Crete, western coast of Turkey). Furthermore, the comparative study of the submerged ancient remains from Greece and Turkey, all falling within the same historical period, has confirmed that the RSL rise varies in different geotectonic contexts due to the differential vertical tectonic movements of the crust and is locally affected by fault activations (see Fig. 1b). Further data processing will enable assessing the amount of vertical tectonic movements and the resulting subsidence rates of that period.

Table 1 Archaeological sea-level indicators along the coast of Greece and western Turkey evaluated in this study. **Column A**: Number of site as shown on Fig. 1. **Column B**: Location, P: Peloponnese, C: Cyclades, Cr: Crete, F: Fethiye Gulf, Bz: Bozburun Peninsula. **Column C**: Type of archaeological indicator, pr.w./w: protective wall/wall, rf: rockfill, br: breakwater, b/b.c.: building/building complex, sl: slipway, s.d.: sea defensive works, q: quay, f.t.: fish tank, c/ch: cistern/channel, m: masonry, ws: workshop, p: pavement. **Column D**: Archaeological age, R: Roman, LR: Late Roman, EB/LB/PB/: Early/Late/Post-Byzantine, u.s.: as above. V: Venetian. **Column E**: Measured mean depth (m, bmsl), **Column F**: Related sea-level stand at the time of use (m, bmsl)

A	B	C	D	E	F
GR1	Palaiokastro, Methana (P)	pr.w./rf	PB	1.65–2.20	2.40 ± 0.20
GR2	Agios Athanassios (P)	br	LB or PB	2.00	2.60 ± 0.30
GR3	Thini (P)	br	LR (end 6c. AD)	2.05	2.65 ± 0.30
GR4	Valtaki (P)	w	u.s.	1.60 ± 0.10	2.40 ± 0.20
GR5	Mandilou Bay (P)	b.c.	LR-EB (6c. AD)	1.60 ± 0.10	2.40 ± 0.20
GR6	Poises (Keos, C)	sl	R	2.55–2.60	2.40 ± 0.20
GR7	Palaiopolis (Andros, C)	br/rf	R/EB (41AD-5c.)	2.00–2.40	2.40 ± 0.20
GR8	Exo Steno (Andros, C)	w/rf	R/LR	1.10/2.45	2.40 ± 0.20
GR9	Ancient Delos (C)	s.d.	LR	2.00–2.50	2.40 ± 0.20
GR10	Krotiri (Paros, C)	br	R/LR	1.60	2.40 ± 0.20
GR11	Paroikia (Paros, C)	b.c./rf	u.s.	1.75–2.35	2.40 ± 0.20
GR12	Chersonissos (Cr)	q f.t.	R (67 BC-395 AD)	1.00 1.20	1.25 ± 0.05

Table 1 (continued)

A	B	C	D	E	F
GR13	Mylos bay (Cr)	c/ch	B or V (961 AD - 1669)	0.70	1.25 ± 0.05
GR14	Poros Eloundas (Cr)	br/b	EB (395–824 AD)	1.00–1.30	1.25 ± 0.05
GR15	Psira island (Cr)	m	R/LR (67 BC-395 AD)	1.00	1.25 ± 0.05
GR16	Mochlos (Cr)	w f.t.	R or B (67–824 AD) R (1–200 AD)	~1.00 1.10–1.40	1.25 ± 0.05
GR17	Kouremenos (Cr)	br	R/LR (69 BC-400 AD)	1.20 ± 0.10	1.25 ± 0.05
GR18	Ferma (Cr)	f.t.	R (1–200 AD)	1.30	1.25 ± 0.05
GR19	Ierapetra (Cr)	br	R/LR (67 BC-395 AD)	0.30–1.30	1.25 ± 0.05
GR20	Stomio Ierapetra (Cr)	b/ws	R (1–200 AD)	1.20	1.25 ± 0.05
GR21	Matala Bay (Cr)	11 f.t.	u.s.	1.25 ± 0.05	1.25 ± 0.05
TR1	Göcek Bay (F)	b.c	LR/EB (5–7 c.)	2.10 ± 0.20	2.70 ± 0.50
TR2	Göcek Isl. (F)	q	u.s.	2.50 ± 0.10	3.10 ± 0.30
TR3	Zeytinli-Şeytan Isl. (F)	q	u.s.	2.40 ± 0.10	3.00 ± 0.30
TR4	Tersane Isl. (F)	p	u.s.	2.40 ± 0.10	3.00 ± 0.30
TR5	Domuz Isl., N (F)	q	u.s.	3.40 ± 0.10	4.00 ± 0.30
TR6	Domuz Isl., W (F)	q	u.s.	3.60 ± 0.10	4.20 ± 0.30
TR7	Hamam Bay (F)	b	u.s.	3.40 ± 0.20	4.00 ± 0.30
TR8	Şövalye Isl. (F)	q	u.s.	1.60 ± 0.10	2.20 ± 0.30
TR9	Gemiler Isl. (F)	q	u.s.	2.30 ± 0.10	2.90 ± 0.30
TR10	Ölüdeniz Lagoon (F)	b.c.	LR/EB (6–7 c.)	2.50 ± 0.20	3.10 ± 0.50
TR11	Bozburun Bay (Bz)	br	LR/EB (5–7c.)	1.00 ± 0.20	1.80 ± 0.40
TR12	Söğüt Isl. (Bz)	b/ws	u.s.	1.20 ± 0.20	1.80 ± 0.50
TR13	Söğüt Bay (Bz)	br	u.s.	0.70 ± 0.20	1.50 ± 0.40

References

Bechor, B., Theodoulou, T., Spada, G., Dean, S., & Sivan, D. (2019). Medieval relative low sea-level indications from the Peloponnese and the Aegean Sea. *Quaternary International, 545*, 17–27.

Kassaras, I., Kapetanidis, V., Ganas, A., Tzanis, A., Kosma, C., Karakonstantis, A., Valkaniotis, S., Chailas, S., Kouskouna, V., & Papadimitriou, P. (2020). The new seismotectonic atlas of Greece (v1.0) and its implementation. *Geosciences, 10*, 447. https://doi.org/10.3390/geosciences10110447

Kızıldağ, N. (2019). Late Holocene sea-level change along the coast of Fethiye Gulf in Southwestern Turkey. *Geoarchaeology, 34*, 295–310.

Kızıldağ, N., & Özdaş, H. (2021). Relative sea-level changes along the Fethiye coast (SW Turkey) based on recent archaeological data. *Geoarchaeology, 36*, 474–489.

Kolaiti, E. (2019). *Changes in the anthropogenic environment along the eastern coast of the Peloponnese on the basis of archaeological and morphological indicators of the Late Holocene relative sea level changes. Proposing a geoarchaeological method of approach*. PhD Thesis, University of the Peloponnese, Kalamata.

Kolaiti, E. (2020). Palaeoshoreline reconstruction of Agios Vlassis Bay (Ancient Epidaurus, East Peloponnese, Greece). *Annuario della Scuola Archeologica di Atene e delle Missioni Italiane in Oriente, 98*, 511–522.

Kolaiti, E., & Mourtzas, N. (2020). New insights on the relative sea level changes during the Late Holocene along the coast of Paros Island and the northern Cyclades (Greece). *Annals of Geophysics 63*, OC669. https://doi.org/10.4401/ag-8504

Kolaiti, E., & Mourtzas, N. (2023). Late Holocene relative sea-level changes and coastal landscape readings in the island group of Mykonos, Delos, and Rheneia (Cyclades, Greece). *Mediterranean Geoscience Reviews, 5(3)*, 99-128. https://doi.org/10.1007/s42990-023-00104-4

Mourtzas, N., Kolaiti, E., & Anzidei, M. (2016). Vertical land movements and sea level changes along the coast of Crete (Greece) since Late Holocene. *Quaternary International, 401*, 43–70.

Reilinger, R., McClusky, S., Paradissis, D., Ergintav, S., & Vernant, P. (2010). Geodetic constraints on the tectonic evolution of the Aegean region and strain accumulation along the Hellenic subduction zone. *Tectonophysics, 488*, 22–30.

Taymaz, T., Yilmaz, Y., & Dilek, Y. (2007). The geodynamics of the Aegean and Anatolia: Introduction. In T. Taymaz, Y. Yilmaz, & Y. Dilek (Eds.), *The geodynamics of the Aegean and Anatolia* (Vol. 291, pp. 1–16). Geological Society. Special Publications.

Estimation of Glacial Lake Dynamics in the Sikkim Himalayas by the Inferential Statistical Techniques

Deepali Gaikwad, Supratim Guha, and Reet Kamal Tiwari

Abstract

Himalayan glaciers are retreating under the climate warming scenario, leading to the temporal variation in the expansion and formation of glacial lakes, which have been identified as highly susceptible to Glacial Lake outburst floods (GLOFs). Therefore, the present study intends to estimate the glacial lake area changes (RGLAC) rate for the entire Sikkim Himalaya by extracting twenty-four samples of glacial lakes using non-parametric inferential statistics. Results showed that the area of sample glacial lakes increased from 9.62 km^2 to 13.59 km^2 between 1988 and 2020; overall increased by 41.27%. The highest RGLAC was observed during 2008–2013; after that, it decreased continuously. Furthermore, the maximum volume change among all the large glacial lakes ($\geq$1 km^2) was observed in GL-18. Hence, this study suggests exploring the dynamics of glacial lakes, especially the larger ones, to make better plans to mitigate the damages and minimize the losses due to GLOFs.

Keywords

Glacial lake changes · Friedman test · Wilcoxon signed-rank test · Volume of glacial lakes · Sikkim Himalaya

1 Introduction

Climate warming leads to glacier-wastage, and causes the continuous formation and expansion of glacial lakes (Garg et al., 2017; Mitkari et al., 2017; Remya et al., 2019), more extensively in Sikkim Himalayas (Shukla et al., 2018). These rapidly expanding glacial lakes are the reason for catastrophic Glacial Lake outburst floods (GLOFs) events which have tremendous impacts on the downstream region. Due to this, the Himalayan region has the highest risk globally due to its past GLOF events (Harrison et al., 2018). Therefore, timely monitoring of glaciers and glacial lakes is essential which can help in mitigating the GLOF risk. The applicability of inferential statistics can become more manageable and less time-consuming in studying glacial lake dynamics since inferential statistics enable inferences about the whole population from observations of samples (Kalish & Thevenow-Harrison, 2014; Guha and Tiwari, 2022). Hence, the present study used statistics to generalize the changing behavior of glacial lakes for the entire Sikkim Himalaya, which helps to understand glacial lake variations to prepare better strategies against glacial-related hazards.

2 Method

Using multi-temporal Landsat images, twenty-four samples of glacial lakes of different sizes and shapes located at different elevations were selected. Landsat images were downloaded from (https://earthexplorer.usgs.gov/). To extract the glacial lake area, the boundaries of twenty-four sample glacial lakes were manually delineated by utilizing green, red, and near-infrared bands of Landsat images for the seven periods (1988, 2000, 2008, 2013, 2016, 2018, and 2020). Additionally, elevation information of these glacial lakes was obtained from Shuttle Radar Topography Mission Digital Elevation Model (SRTM DEM). Afterward, the rate of glacial lake area change (RGLAC) was estimated

D. Gaikwad · S. Guha · R. K. Tiwari (✉)
Geomatics Engineering Laboratory, Department of Civil Engineering, Indian Institute of Technology Ropar, Rupnagar 140001, India
e-mail: reetkamal@iitrpr.ac.in

A. Çiner et al. (eds.), *Recent Research on Environmental Earth Sciences, Geomorphology, Soil Science, Paleoclimate, and Karst*, Advances in Science, Technology & Innovation, https://doi.org/10.1007/978-3-031-42917-0_34

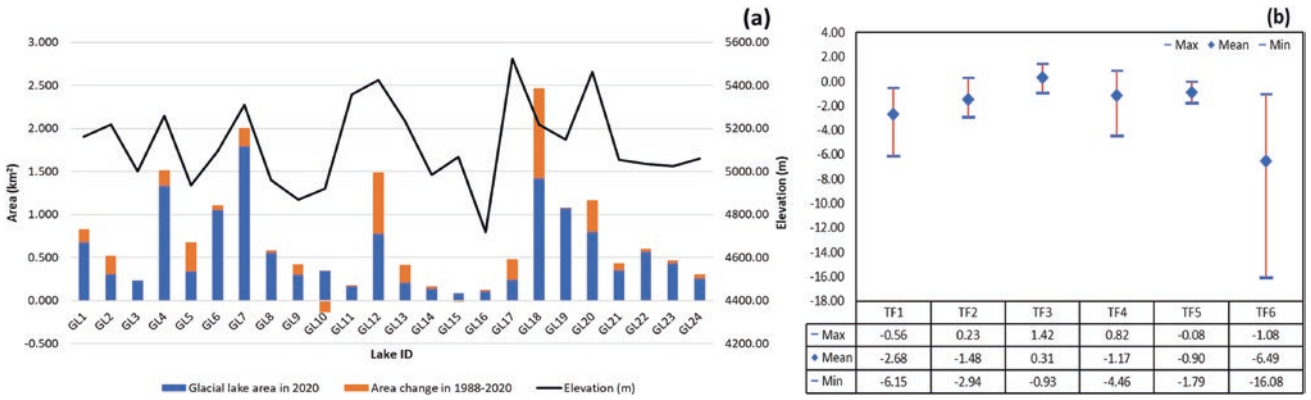

	TF1	TF2	TF3	TF4	TF5	TF6
Max	-0.56	0.23	1.42	0.82	-0.08	-1.08
Mean	-2.68	-1.48	0.31	-1.17	-0.90	-6.49
Min	-6.15	-2.94	-0.93	-4.46	-1.79	-16.08

Fig. 1 **a** Area change (km^2) of all selected glacial lakes from 1988 to 2020, along with elevation information **b** The confidence interval of RGLAC in all timeframes

between 1988–2000 (TF_1), 2000–2008 (TF_2), 2008–2013 (TF_3), 2013–2016 (TF_4), 2016–2018 (TF_5), and 2018–2020 (TF_6).

Finally, inferential statistics were applied to determine the RGLAC for the entire Sikkim Himalayas by utilizing the selected samples. For this purpose, a non-parametric Friedman test was carried out on the RGLAC to evaluate whether it is equal in all timeframes. If it is not similar in all timeframes, a Wilcoxon signed-rank test can be conducted on all comparisons individually to determine exactly where the difference exists. The null hypothesis (H_0) and the alternative hypothesis (H_a) of the statistical test have been mentioned below:

H_0: The rate of glacial lake area change is equal in all timeframes.

H_a: The rate of glacial lake area change is not equal in all timeframes.

Further, the volume of the large glacial lake (≥1 km^2) was estimated by multiplying the area and depth, where the depth was computed using an empirical relationship (Eq. 1) given by Fujita et al. (2013). Because this relationship has already been successfully applied in different regions of the Himalayas (Goswami & Goyal, 2021; Majeed et al., 2020).

$$D_M = 55 \times A^{0.25} \quad (1)$$

where D_M is the mean depth (m), A is the area (km^2), and V is the volume (Million m^3).

3 Results

Temporal change in the area of the selected glacial lake has a heterogeneous trend throughout the study period. Both expansion and contraction have been noted in all timeframes. However, growth has been observed in most of the glacial lakes (see Fig. 1a). The total area of all sample glacial lakes increased from 9.62 km^2 to 13.59 km^2 between 1988 and 2020, and an overall increase of 41.27%. In statistical assessment, the non-parametric Friedman test has rejected the null hypothesis, which indicated that the RGLAC was not equal in all timeframes. Afterward, the Wilcoxon signed-rank test was executed to determine which timeframes have different RGLAC. The results showed a significant difference in RGLAC between TF_1–TF_3, TF_2–TF_3, TF_2–TF_4, and TF_3–TF_6 timeframes and other remaining comparisons (TF_1–TF_2, TF_1–TF_4, TF_1–TF_5, TF_1–TF_6, TF_2–TF_5, TF_2–TF_6, TF_3–TF_4, TF_3–TF_5, TF_4–TF_5, TF_4–TF_6, TF_5–TF_6) have a considerable similarity.

Furthermore, the pairwise comparison revealed that the RGLAC was highest in TF_3, decreased consistently, and was noted to be lowest in TF_6. At the same time, it was observed to moderate during TF_1, which slightly raised during TF_2. Finally, we presented the confidence interval of RGLAC in all timeframes for the entire Sikkim Himalaya (see Fig. 1b).

The volume of large glacial lakes GL-04, GL-06, GL-07, GL-18, and GL-19 has changed from 65.96 Mm^3 to 79.07 Mm^3, 55.27 Mm^3 to 58.36 Mm^3, 96.72 Mm^3 to 113.75 Mm^3, 16.32 Mm^3 to 85.62 Mm^3, and 60.07 Mm^3 to 60.16 Mm^3, respectively, between 1988 and 2020. The most significant volume enlargement was observed in the fourth glacial lake (GL-18), which increased by 424.46%, while the lowest expansion of only 0.14% was seen in the last glacial lake (GL-19).

4 Discussion

The rapid expansion of glacial lakes represents the rate of deglaciation, which is very prominent in the Sikkim Himalayas. However, the presence of a large number of

these glacial lakes makes glacial-related studies on the regional level challenging and time-consuming. Therefore, using samples to infer about the whole population through inferential statistics was conducted in this study. Lake samples were methodically selected under different conditions and employed appropriate inferential statistical methods, significantly minimizing sampling error. Consequently, it is highly probable that the selection of different samples from the Sikkim Himalayan region will yield similar trend in the rate of glacial lake expansion (Guha and Tiwari, 2022).

Furthermore, the study comprises more recent years to understand the latest trend of RGLAC. However, the temporal change in the glacial lake area, which was selected as the sample in the present study, is heterogeneous. The highest RGLAC was observed during 2008–2013, which decreased continuously until 2018–2020. The probable reasons for decreasing RGLAC may be precipitation declination in the study area, disconnection of the lake from its mother glacier, and drain out of the larger lake, as suggested by the study (Shukla et al., 2018).

The regular and systematic real-time monitoring of glacial lakes, especially the larger ones, helps to make better mitigation plans, such as installing an early warning system, creating global and local awareness, and physical mitigation to lower the lake level. However, physical mitigation is impractical and expensive as these lakes exist primarily in remote places. However, it can be implemented in extreme risk conditions, such as Tsho-Rolpa, and Imja lakes levels were lowered by several meters by constructing a canal with local inhabitants' help. In addition, GLOF early warning systems were also installed to minimize the downstream GLOF risk in the Nepal Himalayas (Bajracharya, 2010).

5 Conclusions

The present study demonstrated the application of remote sensing techniques and inferential statistics for glacial lake change detection. Selected samples have been analyzed statistically to explore the variation of all glacial lakes in the Sikkim Himalayas. The observed trend of RGLAC was heterogeneous, showing a peak in 2008–2013, which decreased continuously and became lowest in 2018–2020. However, the total area of sample glacial lakes was constantly increasing throughout the study period, as most of the glacial lakes have been expanding.

References

Bajracharya, S.R. (2010). Glacial lake outburst flood disaster risk reduction activities in Nepal. *International Journal of Erosion Control Engineering, 3*(1).

Fujita, K., Sakai, A., Takenaka, S., Nuimura, T., Surazakov, A. B., Sawagaki, T., & Yamanokuchi, T. (2013). Potential flood volume of Himalayan glacial lakes. *Natural Hazards and Earth System Sciences, 13*, 1827–1839.

Garg, P. K., Shukla, A., Tiwari, R. K., & Jasrotia, A. S. (2017). Assessing the status of glaciers in part of the Chandra basin, Himachal Himalaya: A multiparametric approach. *Geomorphology, 284*, 99–114.

Goswami, U. P., & Goyal, M. K. (2021). Assessment of glacial lake development and downstream flood impacts of critical glacial lake. *Natural Hazards*.

Guha, S., & Tiwari, R. K. (2022). Analysis of differential glacier behaviour in Sikkim Himalayas in view of changing climate. *Geocarto International, 37*(27), 16020–16042.

Harrison, S., Kargel, J. S., Huggel, C., Reynolds, J., Shugar, D. H., Betts, R. A., Emmer, A., Glasser, N., Haritashya, U. K., Klimeš, J., Reinhardt, L., Schaub, Y., Wiltshire, A., Regmi, D., & Vilímek, V. (2018). Climate change and the global pattern of moraine-dammed glacial lake outburst floods. *The Cryosphere, 12*, 1195–1209.

Kalish, C. W., & Thevenow-Harrison, J. T. (2014). Chapter one–descriptive and inferential problems of induction: Toward a common framework. In Brian H. Ross (Ed.), *Psychology of learning and motivation* (Vol. 61, pp. 1–39). Academic Press.

Majeed, U., Rashid, I., Sattar, A., et al. (2020). Recession of Gya Glacier and the 2014 glacial lake outburst flood in the Trans-Himalayan region of Ladakh, India. *Science of the Total Environment*.

Mitkari, K. V., Arora, M. K., & Tiwari, R. K. (2017). Extraction of glacial lakes in Gangotri glacier using object-based image analysis. *IEEE Journal of Selected Topics in Applied Earth Observations and Remote Sensing, 10*(12), 5275–5283.

Remya, S. N., Kulkarni, A. V., Pradeep, S., & Shrestha, D. G. (2019). Volume estimation of existing and potential glacier lakes, Sikkim Himalaya, India. *Current Science, 116*(4), 620–627.

Shukla, A., Garg, P. K., & Srivastava, S. (2018). Evolution of glacial and high-altitude lakes in the Sikkim, Eastern Himalaya over the past four decades (1975–2017). *Frontiers in Environmental Science, 6*.

Morphostructure of Landslides: Characterization Through Electrical Resistivity Tomography (ERT)

Javiera Fuenzalida, Pierre-Yves Descote, Gustavo Gatica, Luis F. Robledo, Diego Villalobos, Sergio Carvajal, Xaviera Palma, Cristóbal Ramírez, Ivo Fustos, Mauricio Calderon, Wen Nie, and Wei Xie

Abstract

Rotational landslide has generally been characterized through shallow geophysics methods and satellite analysis to study potential hazards to the population. At present, the recognition of landslides by their morphostructure considers the combination of multiple sources of information and precision levels acquired through geomorphological, geophysical, and geotechnical methods. Our landslide case study is in San José de Maipo, Central Chile. We present a methodology for morphostructural characterization through electrical resistivity tomography. The validation of this methodology considers data acquisition through the ARES II resistivity system, data processing using RES2DINV inversion software, and the electric profile interpretation. The Wenner-Schlumberger geometric arrangement was used for the ERT data acquisition, with two contrasts in the resistivity values. Therefore, we interpret that the morphostructures are limited by sharp contrasts in resistivity values between horizontal and vertical layers (resistivity values) along the unstable slope. These values show high resistivity values in the upper zone of the landslide and low values in the lower zone. We delimited the rupture surface at 20 m in the middle of the profile. The depth decreases laterally, reaching 5 m. Finally, the proposed morphostructural model allowed the sliding to be characterized geometrically as a concave upward recognizable rupture surface of known depth and extension. We presented the mosphostructural model to determine the landslide geometrically to obtain data on the rotational landslide's depth, extension, and morphology.

Keywords

Morphostructure · Landslide · Electrical resistivity tomography

J. Fuenzalida · P.-Y. Descote (✉) · G. Gatica · L. F. Robledo · D. Villalobos · S. Carvajal · X. Palma · C. Ramírez
Facultad de Ingeniería, Universidad Andrés Bello, Santiago, Chile
e-mail: pierre.descote@unab.cl

I. Fustos
Departamento de Ingeniería en Obras Civiles, Universidad de La Frontera, Temuco, Chile

M. Calderon
Centro de Investigación en Sustentabilidad y Gestión Estratégica de Recursos, Facultad de Ingeniería, Universidad del Desarrollo, Santiago, Chile

W. Nie
School of Resources and Environmental Engineering, Jiangxi University, Ganzhou, China

Spatial Information Technology and Big Data Mining Research, Chengdu, China

W. Xie
Quanzhou Institute of Equipment Manufacturing, Haixi Institutes, Quanzhou, China

1 Introduction

Slide-type landslides are a latent danger for surrounding communities, particularly in areas of high slopes with adverse climatic conditions. Therefore, it is necessary to apply minimally invasive techniques to obtain subsurface information and delimit morphostructures of this type of deposit. Therefore, using new technologies and generating an information network is fundamental to identifying possible landslide risks (Cruden & Varnes, 1996). Survey methods such as satellite imagery allow for obtaining superficial terrain information. However, they do not provide subsurface information, particularly electrical resistive tomography, which allows for calculating the electrical resistivity of materials. Thus, generates a two-dimensional image of the subsoil distribution by indicating gradations and contrasts in the resistivity values. Therefore, it is possible to delimit

A. Çiner et al. (eds.), *Recent Research on Environmental Earth Sciences, Geomorphology, Soil Science, Paleoclimate, and Karst*, Advances in Science, Technology & Innovation, https://doi.org/10.1007/978-3-031-42917-0_35

morpho-structurally deposits of landslide type, to suggest a sliding or rupture plane that allows determining the depth and thickness of the detachment zone.

2 Geological Settings

The intervention is in San José de Maipo (Fig. 1a, b), Central Andes, Chile (33°38′S). Here converge different geological, tectonic, and climatic factors that constitute a potential area for geological hazards, likely to trigger landslides (Fig. 1c). The rock units present in the region corresponding to a succession of volcanic, volcanoclastic, and continental sedimentary rocks corresponding to the Abanico Fm. (Eocene Sup) and Farrellones Fm. (Miocene), underlain by discordant unconsolidated modern sediments. (Holocene) (Aguirre, 1960; Klohn, 1960; Ormeño, 2007).

3 Methodology

Data acquisition was carried out by applying the Electrical Resistivity Tomography profiling method, using GF Instruments ARES II model resistivity meter, with a Wenner-Schlumberger electrode configuration and an electrode spacing of 5 m. The data was then processed with RES2DINV software (Software, 2010), which automatically determines a subsurface's two-dimensional resistivity model from the measurements' data. Subsequently, they were processed with the RES2DINV software (Software, 2010), which automatically determines a two-dimensional resistivity model of the subsurface from the data obtained from the electrical image measurements. This method uses the inverse problem to obtain the model of real resistivities of the subsurface from the apparent resistivities obtained in the field (Loke, 2003).

4 Results

4.1 Block Model

A total of 332 apparent resistivity values were taken, which are distributed as shown in (Fig. 2). As the measurement depth increases, the resulting data taken laterally decreases; however, it increases in depth.

4.2 Pseudosections

To generate a model of resistivity distribution, which represents the geometry of the body in which the resistivity values are distributed in the subsurface, an inversion routine based on the least-squares method with smoothness constraint (DeGroot-Hedlin & Constable, 1990; Loke, 2003; Sasaki, 1992; Thiele, 1980) is used (Fig. 3), based on the grid method Eq. (1), we have:

$$(J^T J + \lambda F)\Delta q_k = J^T g - \lambda F q_k \tag{1}$$

4.3 Study Profile

The profile study with N-S orientation and an extension of 195 m is in the lower zone of the landslide with the Wenner-Schlumberger method, an arrangement moderately sensitive to vertical and horizontal structures (Loke, 1999). With an electrode spacing of 5 m, a depth of investigation

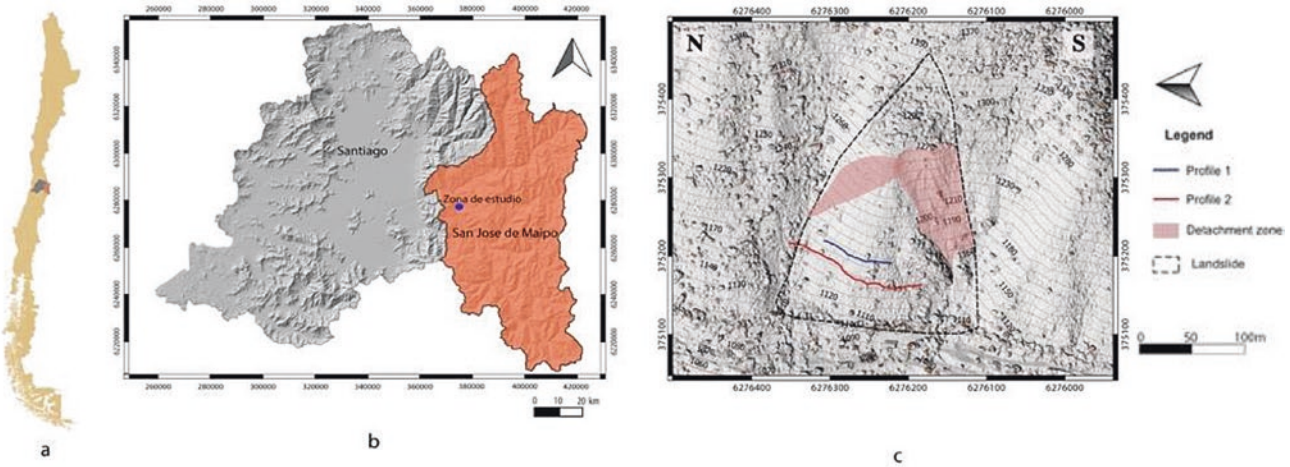

Fig. 1 **a** Location of the study area in Chile, **b** Location map of San José de Maipo town, Central Chile (33°38′S), **c** Location map of the landslide case. Redline 2 shows Profile 2 of the electrical resistivity tomography

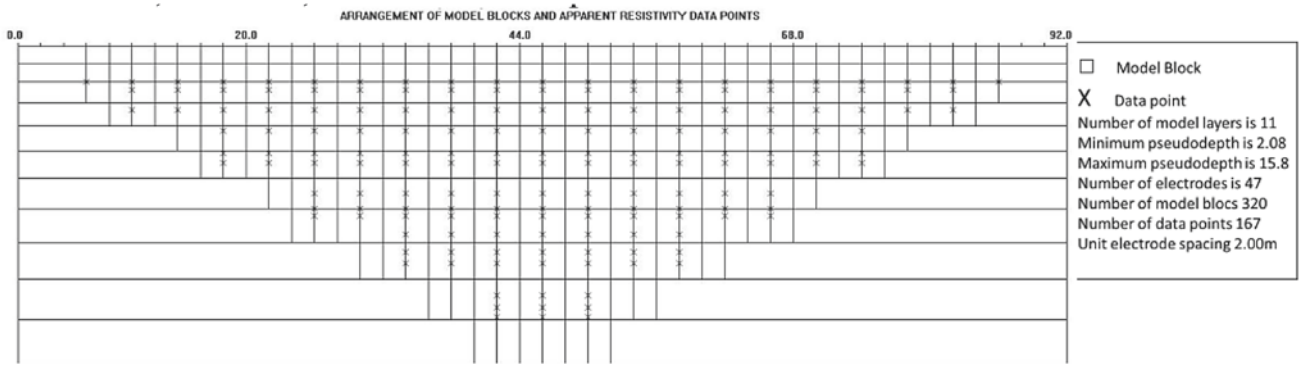

Fig. 2 The Block model of profile number 2 (shown in Fig. 1c) shows the spatial distribution of the data processing through RES2DINV inversion software of the landslide case San José

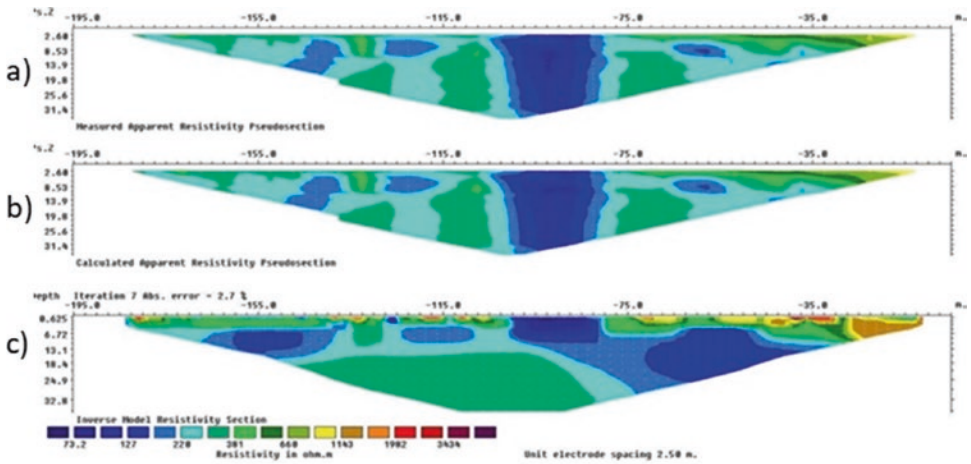

Fig. 3 Measured (**a**) and calculated (**b**) apparent resistivity pseudosections. **c** Real resistivity model for the Profile n°2 performed after seven iterations and RMS error is at 2%

of 45 m was achieved. The resistivity values in the landslide show a range of 73.2–3.434 Ω m. Two levels are assumed, an upper one as the sliding mass and a lower one interpreted as the possible rocky substrate, the sliding surface (Fig. 4) is postulated at a depth of 20 m for the central zone of the landslide. This depth decreases toward the ends of the landslide, obtaining depths of 5 m, indicating a concave shape upwards. The southern side of the profile shows a greater depth for the sliding zone, which agrees with the accumulation zone of the landslide under the southern collapse zone. The zones with low resistivity values, represented in blue, are similar to saturated zones (Fig. 4).

5 Discussion

Values above 1000 Ω m are associated with weathered igneous rocks (Palacky, 1987). On the other hand, lower values (48–1000 Ω m) can be related to the presence of clay within the sliding block (or sliding mass). The maximum depth obtained was 22 m. The average sliding surface of 20 m inferred by the change of distribution and value of resistivities with a gradual increase in resistivity values from 165 to 300 Ω m, values greater than 300 Ω m would correspond to a possible rocky substrate, given the difference in resistivity values for the sliding surface it is inferred that this does not maintain a constant depth along the profile. The sliding mass is composed of rock, soil, and vegetation. From the (TER) data, the thickness of the sliding block was estimated to be approximately $20 + -0.54$ m in the middle zones, decreasing to $5 + -0.14$ m on the sides. The concave upward shape of the slide surface suggests a rotational type slide as defined in landslide types and processes (Cruden & Varnes, 1996). Another critical factor was the topographic correction of the profile, and because the topography of the landslide presented varied heights, the final model may have suffered inaccuracies. Finally, it is essential to discuss the effectiveness of the method. First, a strength of the technique used is its speed at the time of data collection, allowing it to obtain a large amount of resistivity data in short periods. It is a minimally invasive method. However, a disadvantage would be the weight of the equipment, as it would make its execution difficult in terrain with limited access.

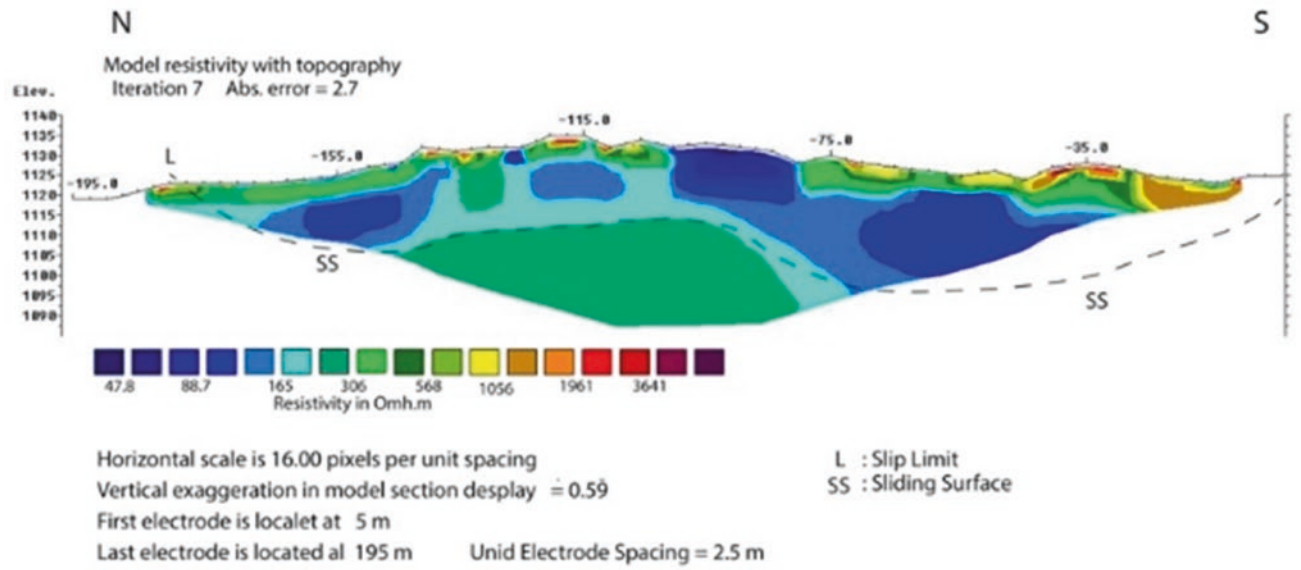

Fig. 4 Identification of the sliding surface from Profile n°2 and definition of landslide shape

6 Conclusions

Finally, it can be concluded that an electrical tomography method is an adequate tool for the characterization of subsoil resistivities, specifically in landslide-type mass removals. The proposed morphostructural model allowed for characterizing the landslide geometrically, obtaining depth, extension, and morphology of the landslide, and identifying unstable areas of the rotational landslide. Therefore, it is recommended to use the technique in landslides in pre-elimination phases to evaluate the risk of possible landslides or in later stages to estimate the stability conditions, subsoil variations such as moisture content within the landslide mass, stratigraphic distribution, and effect of structures, facilitating the study for subsequent mitigation measures.

This research was done under the project ANID PII180007.

References

Aguirre, L. (1960). Geología de los Andes de Chile Central, provincia de Aconcagua. *Instituto de Investigaciones Geológicas, Santiago, Chile, 9*, 70.

Cruden, D., & Varnes, D. (1996). Landslide types and processes. In A.K. Turner & R.L. Schuster (Eds.), *Landslides: Investigation and mitigation* (675 pp.). Special Report 247. Transportation research board, National Research. National Academy Press.

DeGroot-Hedlin, C., & Constable, S. (1990). Occam's inversion to generate smooth, two-dimensional models form magnetotelluric data. *Geophysics, 55*, 1613–1624.

Geotomo Software. (2010). RES2DINV, Rapid 2-D resistivity and IP inversion using the least-squares method. Geoelectrical imaging 2D & 3D: Malaysia, Geotomo Software (151 pp.).

Klohn, C. (1960). Geología de la Cordillera de los Andes de Chile Central, Provincia de Santiago, Colchagua y Curicó. *Instituto Investigaciones Geológicas, Santiago, Boletín, 8*, 95.

Loke, M. H. (1999). Electrical imaging surveys for environmental and engineering studies. A practical guide to 2-D and 3-D surveys (66 pp.).

Loke, M. H. (2003). Rapid 2D Resistivity & IP inversion using the least-squares method. Geotomo Software, Manual (122 pp.).

Ormeño, A. (2007). Geodinámica de la hoya hidrográfica del río Maipo en la zona cordillerana de la Región Metropolitana: Implicancias neotectónicas. Tesis (Magister en Ciencias, mención geología). Santiago. Universidad de Chile, Departamento de Geología (177 pp.).

Palacky, G. (1987). Resistivity characteristics of geological targets. In M. Nabighian (Ed.), *Electromagnetic methods in applied geophysics* (Vol. 1, 55 pp.). Society of Exploration Geophysicists.

Sasaki, Y. (1992). Resolution of resistivity tomography inferred from numerical simulation. *Geophysical Prospecting, 40*, 453–464.

Thiele, R. (1980). Hoja Santiago, Región Metropolitana. Santiago: Servicio Nacional de Geología y Minería. Carta Geológica No. 39.

Landslide Susceptibility Analysis Using 3D Modeling: A Case Study in San José de Maipo, Chile (33°38′S)

Diego Villalobos, Pierre-Yves Descote, Cristóbal Ramírez, Mauricio Calderon, Luis F. Robledo, Gustavo Gatica, Javiera Fuenzalida, Sergio Carvajal, Xaviera Palma, David Ruete, Wen Nie, and Wenbin Jian

Abstract

Massive landslides are rock and soil movement processes that have social, economic, and environmental impacts. Their study contributes to the balance of human settlements with the ecosystem and dynamics to mitigate and prevent risk. The intervention zone's geomorphology, geology, precipitation, and geometry must be quantitatively considered to establish a susceptibility model. A methodology is proposed to analyze the susceptibility of mass removal with a 3D model built from aerial photogrammetry. The first step considers planning and executing a photogrammetric flight. Then, the photographic and topographic data are processed to generate a 3D model. At the same time, a map overlay is made from ortho mosaics, Digital Elevation Models, and layers. Finally, a model of transverse slope profiles is generated to determine the safety factor in San José de Maipo, Chile (33°38′S). The site presents traces and evidence of a landslide. Surface measurements of constructions, vegetation, and tension cracks were obtained. The main structural trends and depth of contact between bedrock and surface deposits detected are described. The generated models contribute to the susceptibility analysis by characterizing the landslide morphologies. Currently, it is possible to characterize undetectable removals only with Landsat imagery. The methodology is scalable to other geographic zones with geological evidence of rockslides, thus reducing uncertainty.

Keywords

Photogrammetry · Landslide · Geological modeling · Geological hazard · Risk

1 Introduction

Integrating risks associated with geologic hazards in land-use planning can contribute to the proper design and construction of mitigation infrastructure for the community. For this, the characteristics of the mass removal processes and their impact on the ecosystem must be studied in depth. In addition, monitoring and prediction are required to determine the risk and avoid disasters that may impact human life, ecology, or economic losses (UNISDR, 2012).

The difficulty in predicting the occurrence of landslides today requires more information on areas prone to movement. Usually, these areas are often inaccessible, and conventional mapping can only record limited areas, whereas with Landsat imagery, the spatial resolution is much lower. The use of UAVs for photogrammetry allows capturing the terrain's morphological characteristics and specific measurements of the parts that contribute to landslides.

D. Villalobos · P.-Y. Descote (✉) · C. Ramírez · L. F. Robledo · G. Gatica · J. Fuenzalida · S. Carvajal · X. Palma · D. Ruete
Facultad de Ingeniería, Universidad Andrés Bello, Santiago, Chile
e-mail: pierre.descote@unab.cl

M. Calderon
Centro de Investigación en Sustentabilidad y Gestión Estratégica de Recursos, Facultad de Ingeniería, Universidad del Desarrollo, Santiago, Chile

W. Nie
School of Resources and Environmental Engineering, Jiangxi University, Ganzhou, PR China

Spatial Information Technology and Big Data Mining Research Center, Chengdu, PR China

W. Jian
Department of Geotechnical Geological Engineering, Fuzhou University, Fuzhou, PR China

A. Çiner et al. (eds.), *Recent Research on Environmental Earth Sciences, Geomorphology, Soil Science, Paleoclimate, and Karst*, Advances in Science, Technology & Innovation, https://doi.org/10.1007/978-3-031-42917-0_36

2 Local Geological Settings

The area is in San José de Maipo in the mountain range of central Chile (33°38′S), with high slope and rainfall conditions, evidence, and susceptibility to landslides. The western slope of Divisadero hill was analyzed at the foot of which sanitary facilities and houses were exposed to this phenomenon. The slope has fluvial-alluvial deposits, volcanic rock units of the Abanico and Farellones formations, and a kilometer anticlinal fold with an NNW-NS orientation (Fock et al., 2006) (Fig. 1).

In particular, the western slope of Divisadero hill presents unstable material conditions (Sepúlveda et al., 2009, 2012), where the geometry of the landslide and the flow deposits of intense rainfall (1997 and 1999) caused severe damage to houses nearby. Due to this population's high exposure and the health center at the foot of the slope, containment pits were built to mitigate the flow toward the settlement (Carrasco, 2000). A geomorphological map of the locality was built, which infers a reverse fault along the Cerro Divisadero, landslide scarps, and dejection cones in the area selected for this study (Alvarez Arriagada, 2006) determined the depth of the slope slip surface through electrical resistivity profiles.

A photogrammetric flight is proposed based on geomorphological evidence to measure escarpments, tension cracks, and other structures. In addition, we offered a susceptibility map using GIS map algebra based on susceptibility assessment (Mora Chinchilla, 2004), along with 2D and 3D analysis of geological and geometric characteristics to determine the level of slope stability.

3 Methodology

The literature describes the geological materials that make up the slope and their predominant geomorphological features. The way of acquiring the data and analyzing the 3D models and maps produced is shown in Fig. 2 and has 5 phases.

3.1 Flight Planning and Execution

The area delimited for the flight of the west slope of Divisadero Hill is represented by the yellow rectangular polygon in Fig. 2. The site is approximately 14 ha, with populated areas on an old river terrace to the west and

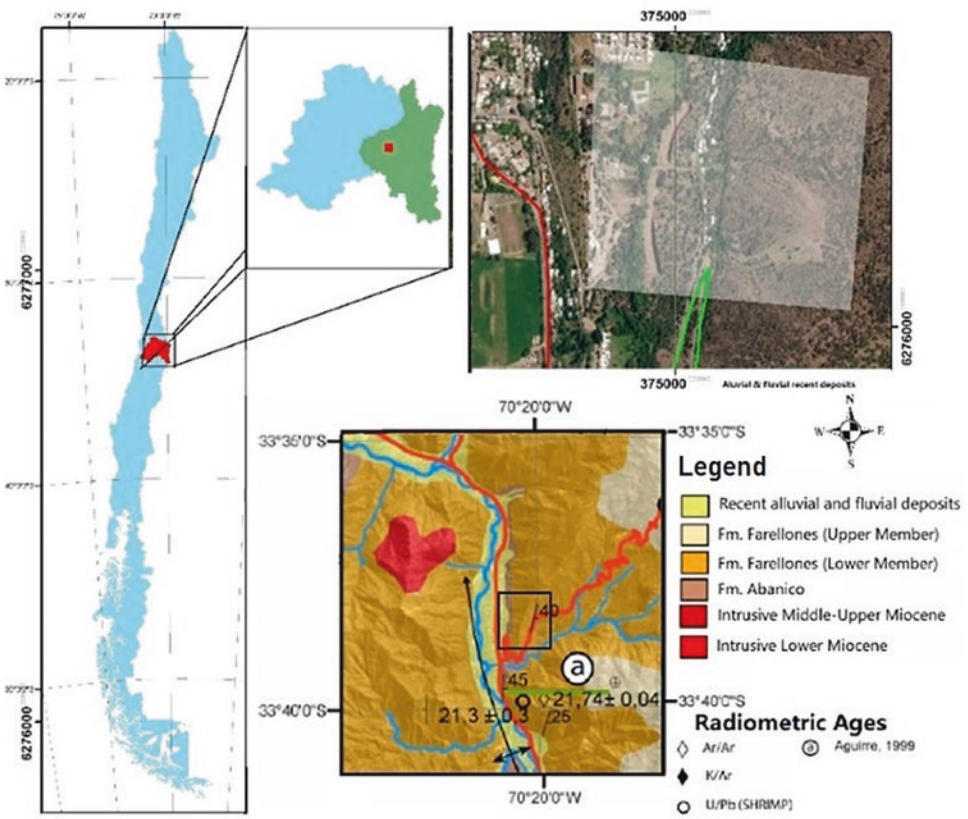

Fig. 1 Location of the west slope of Cerro Divisadero next to the local geologic map. The white box in the satellite image corresponds to the flight polygon

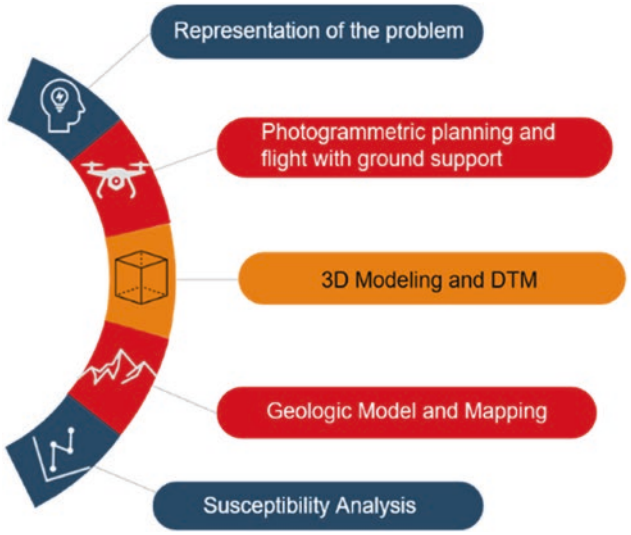

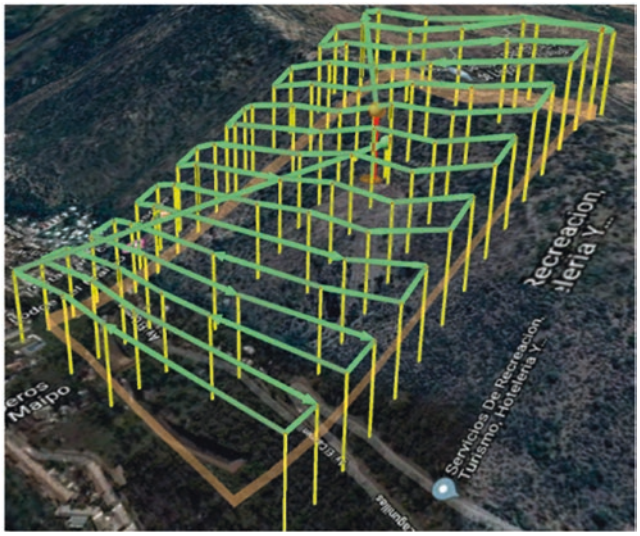

Fig. 2 Methodological schema and flight plan with UgCS planner

Divisadero hill to the east. The aircraft used for photography is a *DJI–Phantom 4*. In addition, high-precision GNSS equipment is used to georeference the terrain by ground control points (GCP) with GNSS from Emlid–Reach RS+ as a base station and a second mobile antenna to capture a set of points within the flight area to deliver centimeter accuracy in three dimensions.

3.2 Process, Modeling and Analysis

Using Agisoft Metashape 1.5.1, photos and control points are loaded to generate the dense point cloud, digital terrain models (DTM), orthomosaics, and contour lines, with the USGS (2017) workflow. Then, with Leapfrog GEO 4.0, a geological model is generated with the modeled 3D data based on information from geological, geomorphological (Carrasco, 2000; Fock et al., 2006), photointerpretation, and geophysical (Alvarez Arriagada, 2006) maps to quantify the volume of the deposits associated with the main landslide. Subsequently, with Arcmap 10.5 software, the susceptibility maps are generated based on those developed by Mora-Vahrson (1994), considering the geomorphological factor to obtain the susceptibility. Once the geological model is generated in Leapfrog, cross sections of the relief in detail and the contacts of the rocks and deposits are exported and analyzed in Slope/W software considering the safety factor modeling of material and Bishop, Morgenstern-Price and Fellenius analysis for static and pseudo-static cases (Bishop, 1955).

4 Results

Map Analysis shows high susceptibility in the high slope areas, with flow marks and escarpments. In addition, moderate susceptibility of the rotational landslide area. From the 3D model of the deposits and stratified rocks, an approximate volume of material susceptible to movement of 53,000 m^3 and containment volumes of 27,000 and 80,000 for the north and south containment pits, respectively, are obtained (Fig. 3).

5 Conclusions

The photogrammetric survey of Divisadero Hill achieved sufficient resolution and spatial accuracy to identify the essential morphological features of the main landslide, flow marks, and rockfall deposits. In addition, approximate structural features of the rock outcrops are distinguished. The integration of data with a resolution of fewer than 10 cm into a GIS results in a higher level of detail in the susceptibility map compared to one with satellite data. The analysis of the maps generated to determine susceptibility corroborates that geoforms such as scarps, tension cracks, and flow and rockfall deposits negatively affect the equilibrium on the slope, making it prone to landslides of different types.

The analysis of the slope profiles with 2D pseudo-static equilibrium modeling allowed the determination of a factor of safety (FS) in agreement with the in situ observations. On the other hand, the analysis of the 3D mesh associated

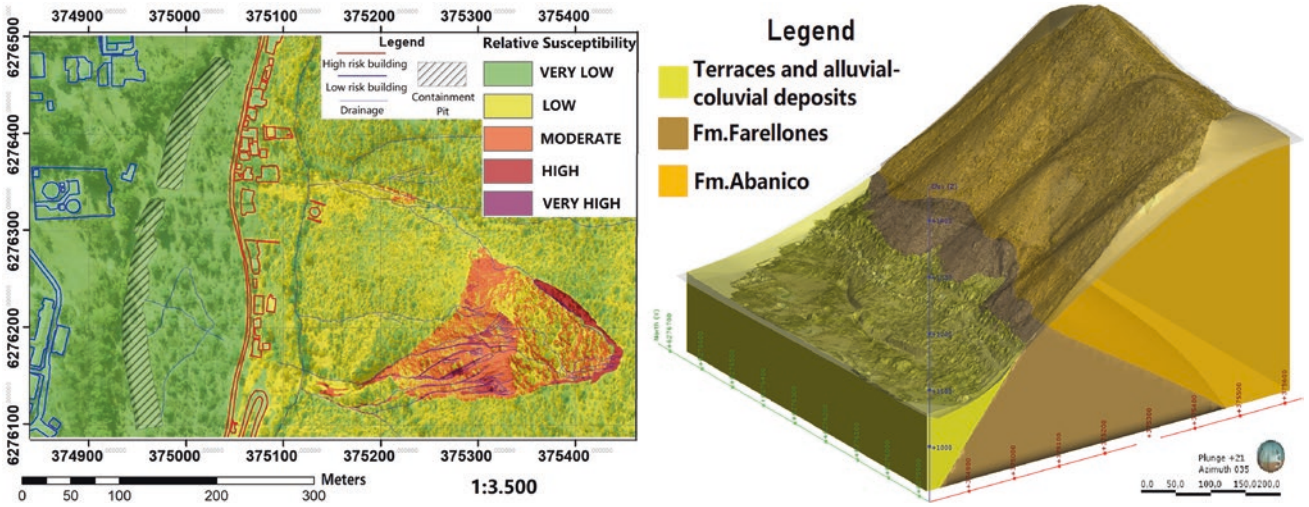

Fig. 3 (Left) Map of relative susceptibility to landslides on Orthomosaic, color scale indicates the probability of occurrence of MR. Blue and red lines correspond to houses and other civil infrastructure at risk. (Right) 3D geologic model for volume calculation

with the geological model of the slope allowed the dimensioning of the existing deposits to estimate volumes prone to movement. Finally, the method can be applied to large areas and is therefore scalable to regional problems, providing greater detail with respect to the satellite photo interpretation method.

Acknowledgements This research was made under the project ANID PII180007 from the Chilean National Research Agency (ANID).

References

Alvarez Arriagada, M. A. (2006). Factibilidad de utilización de técnicas geofísicas en estudios de fenómenos de remoción en masa. Universidad de Chile.

Bishop, A. W. (1955). The use of the slip circle in the stability analysis of slopes. Geotechnique*, 5*, 7–17.

Carrasco, N. (2000). Peligro de remoción en masa en el sector de San José de Maipo. Departamento de Geología, Universidad de Chile.

Fock, A., Charrier, R., Maksaev, V., Farías, M., & Alvarez, P. (2006). Evolucion cenozoica de los Andes de Chile central (33°–34°S) (Vol. 2, pp. 205–207). XI Congreso Geológico Chileno.

Mora, S. Y., Vahrson, W. (1994). Macrozonation methodology for landslide hazard determination. Bulleting of the Association of Engineering and Geologist, *31*(1), 49–58.

Sepúlveda, S. A., Rebolledo, S., Petley, D. N., Alvarez, M. & Schachter, P. (2009). Deslizamiento de San José de Maipo: Nuevos antecedents e implicancias en el peligro geológico (pp. 1–4). XII Congreso Geológico Chileno.

Sepúlveda, S. A., Rebolledo, S., Alfaro, A., Lara, M., Moffat, R., & Petley, D. (2012). Evaluación del peligro de remoción en masa en el deslizamiento de San José de Maipo, Chile central. SEREMI Metropolitana, Santiago.

UNISDR. (2012). Towards a Post-2015 framework for disaster risk reduction.

USGS National UAS Project Office: Agisoft Photoscan Workflow (2017).

The Red-Colored Weathering Crusts of the Lagonaki Highland (Adygea Republic, Russia)

Anna Revunova and Olga Khokhlova

Abstract

The paper describes red-colored weathering crusts from four sections in the Kurdzhip region of the Lagonaki Highland (1800 m). Currently, there are no conditions for developing such formations because of decreasing average annual temperatures up to 4 °C. Favorable conditions for forming red-colored deposits were formed in the Upper Pliocene. Since such soil formations can retain inherited characteristics for a long time, we were able to restore their development conditions. This study is essential for basic science—the study of the mountainous regions' paleoclimate, and for nature protection since most karst areas of the highland are offered as a geosite. It is a UNESCO natural heritage site. Micromorphological thin sections, particle size distribution, and gross analysis were studied in selected samples. In thin sections, grains of hematite, pseudomorphs of clay over dissolved limestones, outbursts of mesofauna, repeatedly recrystallized grains of sparite, and signs of loamy mass movement were found. Differences in the particle size distribution of the samples are analyzed. The high values of geochemical coefficients and the high TiO_2 and Rb content confirm the ancient age of the weathering crust. A geochemical barrier was identified in the sections based on the difference in the content of trace elements (vanadium, cobalt, nickel, and strontium). The growth of relict plants in this area indirectly confirms the Upper Pliocene age of the deposits. In parallel, increased content of heavy metals in the weathering crusts (nickel, cobalt) was established,

Keywords

Paleosols · Upper pliocene · Weathering crust · Paleoclimatic reconstruction · Red-colored soils

1 Introduction

Paleosols carry information about the conditions of their formation. After the lapse of time from the moment of burial and conservation, only the most stable signs remain. The signs of soil formation persist for the longest time in the lower horizons (Targulian & Goryachkin, 2008).

The four sections studied in this work reveal the red-colored weathering crusts. Now in the Lagonaki Highlands, there are no conditions for developing such formations since the average annual temperatures (~4 °C) do not allow the leaching and decarbonization of limestones, which are necessary for red-colored soil formation (Valkov et al., 2007). According to the remains of the hyena and roe deer found in the Sukhaya cave (N 44.143056, E 40.031944, northwest slope of the Azishtau ridge) (Lozovoy, 2011), in the Upper Pleistocene, a subtropical climate prevailed on the territory of the highlands (Abdurakhmanov & Batkhiev, 2013), and the absolute heights were less. The territory's location in the past in warmer weather is also emphasized by relict plants—representatives of the Colchis thermophilic flora (Litvinskaya, et al. 2017).

2 Materials and Methods

Lagonaki is a relict of peneplained Upper Miocene or Pliocene relief (Milanovsky, 1968), which, in turn, is the result of fold-thrust deformation of bottom sediments of the Mesotethis ocean (Trifonov et al., 2020). In the Quaternary period, the general oscillatory uplift of the mountain zone

A. Revunova (✉)
St. Petersburg State University, Universitetskaya Emb., 7-9, St. Petersburg 199034, Russia
e-mail: reina_abc@mail.ru

O. Khokhlova
Institute of Physicochemical and Biological Problems of Soil Science RAS, Moscow Region, St. Institutskaya, 26, Pushchino 142290, Russia

A. Çiner et al. (eds.), *Recent Research on Environmental Earth Sciences, Geomorphology, Soil Science, Paleoclimate, and Karst*, Advances in Science, Technology & Innovation, https://doi.org/10.1007/978-3-031-42917-0_37

prevailed against the background of which local uplifts occurred, highlighted by block faults. As a result, the highland has a gentle structural northern slope and steep structural slopes. Its preservation in the relief is ensured by the resistance of Jurassic limestones composing the highland surface to denudation and by the extensive development of karst and the absence of surface runoff (Trihunkov, 2009).

We have studied four sections of red-colored weathering crusts in the northwestern region of the highland at an altitude of ~1800 m. They are overlain by modern residual calcareous subalpine soils 10–20 cm thick. In the first section, 60 cm of red-brown clay with the inclusion of weathered limestone fragments lies under the modern soil, and the lower layer is an interlayer of yellow and red clays with spots and gray lenses. In the second section, a gleyed horizon of brown–red clay with fragments of limestone lies under the modern soil. In the third section, a monomeric 80 cm layer of red-colored loam with limestone inclusions, the degree of weathering that decreases from top to bottom, lies under the modern soil. Finally, in the fourth section, the weathering crust is stratified. The upper 30 cm horizon is light red. The lower one is red. In both horizons, inclusions of weathered limestones are noted. Finally, all sections are underlain by a gray–yellow, strongly weathered limestone layer. Placer samples were taken from the red-colored horizons for gross analysis and particle size distribution. To study micromorphological thin sections, undisturbed samples were taken too.

3 Results

In a micromorphological thin section made from a sample from the upper red-colored layer of the first section, a grain of hematite, pseudomorphs of clay along the voids from under dissolved limestones, plant remains, and outbursts of mesofauna, sparite grains, and ring clay structures were found. The underlying layer is more carbonic and contains recrystallized grains of sparite. Traces of waterlogging and strongly weathered quartz grains are noticeable. The micromorphological study of the second section revealed the superposition of a loamy mass on recrystallized limestones, mesofauna outbursts, and the presence of structured dark red clay. Micromorphological study of the third section showed the presence of spots of iron oxides, secondary carbonate grains, and hematite grains. In the thin section from the fourth section, grains of iron oxides were also found. However, the loamy mass is mostly brown here. Traces of the restructuring of soil aggregates are visible. This section is entirely carbonate-free. Only in the underlying layer, separate grains of sparite have been preserved. There are both ferruginous nodules and completely deferred clayey remnants. In all sections, pore cracks were found in the clay mass.

The particle size distribution of the studied samples is similar. Sand predominates only in the second section. The maximum colloidal particles are 52% (1st and 4th sections). In other cases, their number is about 40%.

The analysis of the gross composition showed a great contrast in the chemical composition of the deposits of the third and fourth layers of the first section. Thus, the amount of SiO_2 differs almost five times—47 and 10%, respectively. There is also a large difference in Al_2O_3 (20 and 4.8%, respectively), CaO (4.5 and 43%), TiO (1 and 0.2%), K_2O (3.3 and 0.6%), and MgO (3.2 and 1.8%). The indicators of the amount of Fe_2O_3 are approximately equal to 7.4 and 5%. The second section has average values of SiO_2 (38%), Al_2O_3 (16.3%), CaO (14%), Fe_2O_3 (6.3%), TiO (0.83%), and K_2O (2.4%). It has a maximum amount of MgO (5.2%). The third and both horizons of the fourth section contain the maximum amount of SiO_2, more than half the mass—from 51 to 55.5%. They also approximately coincide in other indicators: 18–23% Al_2O_3, 0.8–0.9% CaO, 6.7–9.7% Fe_2O_3, ~1% TiO_2, and 4–5.5% K_2O. The amount of Na_2O in all sections is low—0.06–0.16%.

The results of the analysis of trace elements are shown in Table 1.

The weathering coefficient $Al_2O_3/(CaO+Na_2O+K_2O+MgO)$ is high in the third layer of the first Section (1.8), in the third (2.2), and fourth (2.5) sections. In the fourth layer of the first section, the indicator, on the contrary, is low (0.1). In the second section, the indicator is average (0.8). The third section also has the maximum leaching ratio (Ba/Sr), 5.2. In other sections, the coefficient is lower: 2.1–3.5.

Table 1 The content of trace elements in the studied soils, ppm

Sample	V	Co	Ni	Rb	Sr	Zr	Ba	Pb
Section 1, Layer 3	89	<10	101	113	71	244	216	63
Section 1, Layer 4	14	12	39	21	27	12	57	10
Section 2	40	<10	72	81	104	124	276	20
Section 3	100	13	102	172	72	269	374	63
Section 4, Layer 2	267	24	118	234	181	258	523	80
Section 4, Layer 3	114	12	86	144	115	326	405	60

4 Discussion

The ferruginous color of the loamy mass and grains of hematite found in the first, third, and fourth sections indicate the development of the studied soil formations in a subtropical climate since hematite does not form in a temperate climate (Zonn, 1982). Clay pseudomorphs along the voids from under dissolved limestones in the first section, zones of carbonate-free red-brown loamy mass in the second, and repeatedly recrystallized carbonates in the first, second, and third sections indicate a long and intense limestone leaching. Ring microstructures indicate the soil character of the sediments, pseudomorphs of clay, also colored with iron in yellow–brown and red colors, by plant remains and discharges of mesofauna in the first and second sections and aggregation of soil from the fourth section. Pores-cracks in the clay mass are formed due to the variable water regime.

The clayey particle size distribution is typical for the lower horizons of red-colored soils. The introduction of modern carbonates can explain the sandy composition of the sample from the second section.

Al_2O_3 is associated with secondary minerals. Its high content in almost all samples, even in the sandy second section, indicates a powerful eluvial process. The exception is the 4th layer of the 1st section, where carbonates (43% CaO) prevail. This also underlines the low content of Na_2O, which is associated with primary minerals. Fe_2O_3 is one of the most stable substances in red-colored soils (Zonn, 1982). It is high and approximately the same in all samples (5–9.7%).

Interestingly high TiO_2 content. In sedimentary rocks, the titanium content is small. In limestones, its amount is 0.03–0.04% (Sheudzhen et al., 2015). Increased content of TiO_2, which accumulates in the residual way (Kovda & Rozanov, 1988), is a consequence of the high degree of weathering of the material in question. Moreover, in the first section, the amount of TiO_2 in the underlying horizon is significantly less than in the overlying one (0.23 and 1.10%, respectively). This contrast may be due to the turbulent movement of soil material and the introduction of fresh material.

The ratio SiO_2: Al_2O_3 >2 allows us to call these crust ferciallite except for layer 4 of Sect. 1, which belongs to the siallitic saturated due to the predominance of CaO (Kovda & Rozanov, 1988). Ferrallitization of eluvium of carbonate rocks is possible at temperatures of the active period over 30 °C, with constant optimal soil moisture (Valkov et al., 2007). As a result, coagulation of iron and aluminum hydroxide sols occurs during the migration of solutions of silicic acid sols. Now such temperatures are set extremely rarely in the highlands (Lozovoy, 1984).

The revealed patterns can be traced in the distribution of microelements. In Sects. 3 and 4, the content of vanadium is increased, confined to primary minerals, and accumulates in a residual way due to the long-term weathering of limestone. Also, in all samples except the second one, rubidium content increased, the source of which is alkaline igneous rocks, which have not been found within the region. It also accumulates residually during the weathering of limestones, like zirconium and barium. Cobalt and nickel content are classified as pollution (Orlov, 1985).

The coefficients of weathering and leaching confirm the strong and prolonged weathering of the studied sections. The only exception is the lower horizon of the first section, which has already been discussed.

5 Conclusions

Thus, we have studied four sections of the lower soil horizons. It was revealed that they belong to the red-colored weathering crusts, which could have formed on this territory no later than the early Pliocene. The ratio SiO_2: Al_2O_3 >2 allows us to call these CMs ferciallite. The pores-cracks found during the micromorphological study of thin sections suggest vertical properties except for layer 4 of Sect. 1, which is classified as saturated siallite due to the predominance of CaO. The contrasting distribution of elements in Sects. 1 and 4 revealed a geochemical barrier. At the same time, the contamination of the studied CM with heavy metals, cobalt and nickel, was revealed.

References

Abdurakhmanov, G. M., & Batkhiev, A. M. (2013). Historical-faunistic and zoogeographic characteristics of the Caucasian mammals. *South of Russia: Ecology, Development., 8*(3), 34–52.

Lozovoy, S.P. (2011). Karst landscapes are an argument for the creation of the Mezmay natural park. In: Pogorelov A. V. (Ed.), *Geographical research of the Krasnodar region. Collection of scientific papers* (pp. 21–31). Krasnodar: Kuban State University (Krasnodar).

Lozovoy, S. P. (1984). *Lagonaki highland* (p. 160). Book Publishing House.

Milanovsky, E. E. (1968). *The latest tectonics of the Caucasus* (483 p.). M: Nedra.

Orlov, D. S. (1985). *Soil chemistry. Textbook* (376 p.). Publishing House of Moscow University.

Red data book of the krasnodar territory. In: Litvinskaya, S. A. [and others] (Ed.), *Plants and Mushrooms/Adm. Krasnodar. Edges* (3rd edn, 850 p.). Krasnodar, 2017

Sheudzhen, A. Kh., Korsunova, M. I., Bondareva, T. N., Osipov, M. A., & Esipenko, S. V. (2015). *Titanium in leached chernozem of western Ciscaucasia* (No. 112, p. 10). Krasnodar: KubSAU.

Soil Science. Part 1. Soil and soil formation. In: Kovda, V. A., & Rozanov, B. G. (Eds.), *Textbook. for high school*. In 2 parts. Part 1. M.: Higher. Sch (400 p.).

Targulian, V. O., Goryachkin S.V. Soil memory. Soil as a memory of biosphere-geosphere-anthropospheric interactions. Moscow. URSS. 2008.692 p.

Trifonov, V. G., Sokolov, S. Y., Sokolov, S. A., & Khesami, Kh. (2020). Mesozoic-Cenozoic structure of the Black Sea-Caucasian-Caspian region and its relationship with the structure of the upper mantle. *Geotectonics, 3*, 55–81.

Trihunkov, Y. I. (2009). *Morphostructure and dangerous geomorphological processes of the Northwest Caucasus: Diss. Candidate of Geographical Sciences: 25.00.25.* Moscow: Place of defense: Institute of Geography RAS.

Valkov, V. F., Kazeev, K. Sh., Kolesnikov, S. I., Kutrovsky, M. A. (2007). *Soil formation on limestones and marls* (198 p.). Rostov-on-Don: JSC "Rostizdat"

Zonn, S. V. (1982). *Iron in soils* (p. 208). Nauka.

Impact of Secondary Salinization in Alluvial Soils on Organic Carbon Stock: A Case of the Lower Medjerda Valley in Northern Tunisia

Nadhem Brahim, Hatem Ibrahim, Jamel Jaouadi, and Roland Bol

Abstract

The irrigated public plots developed since the 1960s on the lands of the Lower Medjerda Valley, specifically those of the governorate of Manouba, very fertile at the start, have shown several problems since the 2000s, where yields are reduced to half or more. Soil salinization is a severe problem that constitutes a significant constraint in developing irrigated plots. Several irrigated plots, such as Chouigui and Jedaida's, have experienced great agricultural interest due to their good yields and the variety of their products. However, the nature of the clay soils and the quality of the waters of the Medjerda River accelerated the appearance of salinity traits until they were severely degraded in some plots. For soil sampling, a grid at the level of the plots was carried out. In each plot, a soil pit was carried out, and for each sample taken, three replicates were carried out, knowing that each plot has an area of one hectare for each. The objective is to study the state of salinity and assess its impact on the stock of organic carbon. The soils will be collected at different depths according to a systematic division of 20 cm to a depth of one meter. The results show that the different samples have a basic pH greater than 7.5 and can reach 8.1 with high $CaCO_3$ contents, which sometimes exceed 50% because of the lithological nature of the carbonate rocks that gave rise to these soils. The soils have increasing salinity depending on the depth; the electrical conductivity is 1.1 mS/cm at the surface and can reach 6.8 mS/cm at depth (80–100 cm). Regarding the soil organic carbon stock, the stock varies from 5.65 to 7.52 kg C m^{-2} at the surface (0–20 cm) to 22.59 and 29.57 kg C m^{-2} at one-meter depth. Despite the existing salinity, the soils still have a good stock comparable to healthy soils; the exogenous organic input explains this by farmers and the use of adequate vegetation tolerant to salt stress.

Keywords

Alluvial soil · Irrigated perimeter · Salinization · Organic carbon stock · Tunisia

1 Introduction

Today, soil salinization is the primary constraint on agriculture worldwide. Indeed, 20% of cultivated soils are affected by salinization, and the figure increases, especially with irrigated plots where almost 50% of the land is saline. The formation of saline or sodic soil generally results from the accumulation of salts in the surface horizons (Brady & Weil, 2002; Essington, 2004). These soils' genesis is essentially conditioned by climatic conditions, the texture of the soils, the water regime of the soil, and the abundance of salts in the water. The origin of this salinization is due to the accumulation of salts in the soils, namely sodium (Na^+), generally the most common, calcium (Ca^{2+}), magnesium (Mg^{2+}), and potassium (K^+), particularly in the form of chlorides (Cl^-), but also sulfates (SO_4^{2-}). The risks of secondary salinization are more significant in arid and

N. Brahim (✉) · J. Jaouadi
Faculty of Sciences of Tunis, Laboratoire Plantes, Sols et Environnement LR21ES01, El Manar II, University of Tunis El Manar, El Manar II, 2092 Tunis, Tunisia
e-mail: nadhem.brahim@fst.utm.tn

H. Ibrahim
Department of Earth Science, Faculty of Sciences of Bizerte, University of Carthage, Jarzouna, 7021 Bizerte, Tunisia

R. Bol
Institute of Bio-Geoscience, Agrosphere Institute (IBG-3), Juelich Research Center, Jarzouna, 52428 Jülich, Germany

School of Natural Sciences, Environment Centre Wales, Bangor University, Deiniol Road, Bangor LL57 2UW, Gwynedd, UK

A. Çiner et al. (eds.), *Recent Research on Environmental Earth Sciences, Geomorphology, Soil Science, Paleoclimate, and Karst*, Advances in Science, Technology & Innovation, https://doi.org/10.1007/978-3-031-42917-0_38

semi-arid areas such as Tunisia where irrigation water is often mineralized. The development of agriculture irrigated with mineralized water and without efficient drainage often results in secondary saline manifestations (FAO, 2007; Weil and Brady, 2016).

This salinization has undesirable effects on the properties of the soil, mainly, on the destruction of the soil structure and the dispersion of minerals, on the decrease in permeability, on the pH of the soil, the reduction in fertility, and the disappearance of initial vegetation and the appearance of new salt-tolerant vegetation.

In Tunisia, soils affected by salts cover about 1.5 million hectares, or roughly 10% of the country's surface (Hachicha, 2007). They are found throughout the country. However, their abundance is especially in the center and the south of the country under climatic aridity.

The deltaic plain of Medjerda is characterized by alluvial soils rich in fine particles of clay and silt, very hydromorphic in poorly drained areas. To all this is added the semi-arid climate characterized by a deficient water balance throughout the year round which promotes intense evaporation of irrigation water. This work aims to study the behavior of the alluvial soil of two agricultural plots in Jedaida-Manouba, which are irrigated by the waters of the Medjerda and Chafrou rivers.

2 Materials and Methods

2.1 Study Area

The three study plots, each with an area of one hectare, are administratively attached to the governorate of Manouba and the delegation of Tebourba for plot one and the delegation of Jedaida for the two plots 2 and 3. Figure 1 shows their locations on Google Earth.

Plot no. 1 is located in Chouigui-Tebourba (36° 53′ 59.40″ N 9° 47′ 40.28″ E) with an altitude of 143 m above sea level. The plot is located on a slope of 5°, and it is irrigated using a saltwater borehole and cultivated with barley.

Plot no. 2 is located in Jedeida (36° 50′ 05.9″ N 9° 56′ 55.7″ E) with an altitude of 18 m above sea level. The plot is cultivated in Artichoke, adjacent to the Chafrou river, a tributary of the Medjerda river, whose waters irrigate it.

Plot n° 3 is located in Jedeida (36° 50′ 44.0″ N 9° 57′ 31.8″ E) with an altitude of 18 m above sea level. It is 450 m from Oued Medjerda. The plot is cultivated with onions. The waters of Oued Medjerda irrigate the plot.

Using a soil auger, three profiles are made in each plot. From each profile, we sample six levels to a depth of one

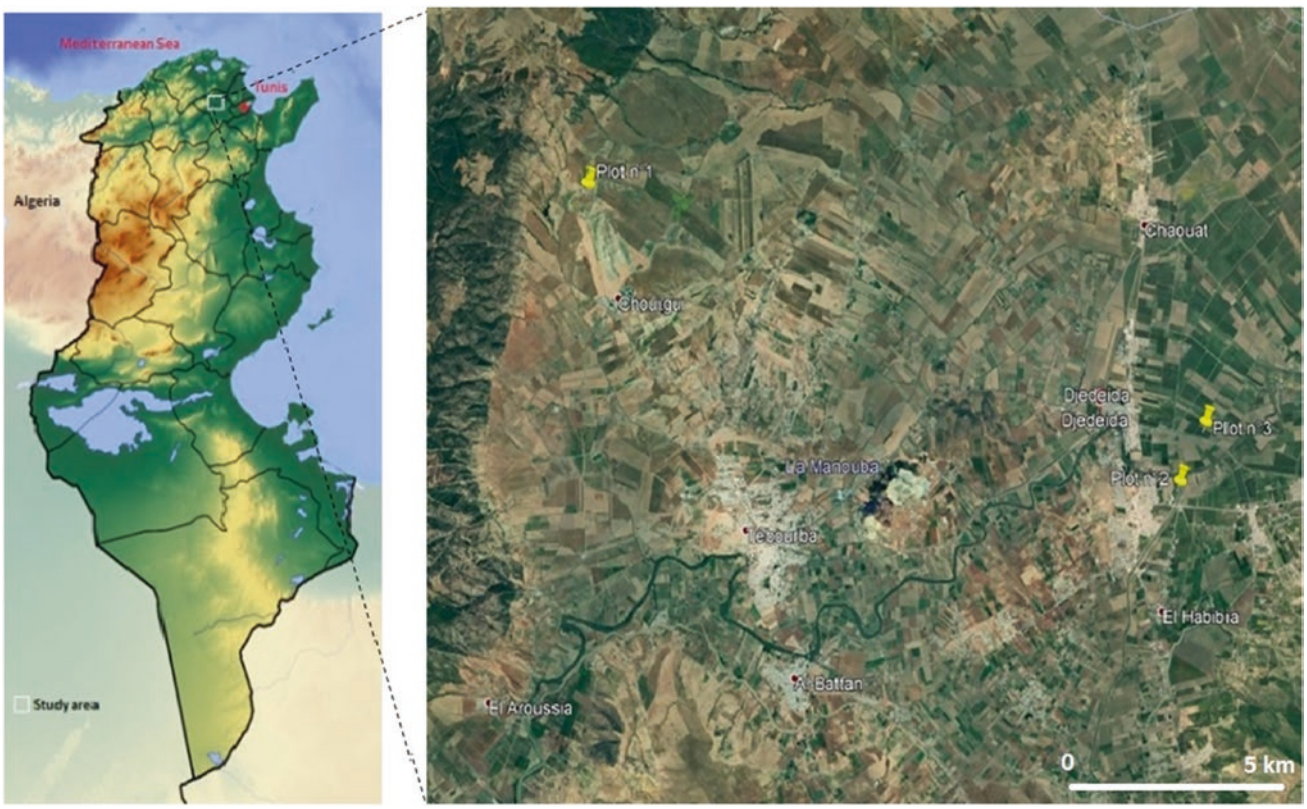

Fig. 1 Location of the study area on the map of Tunisia and location of the three study plots on Google Earth 2021

meter. These levels are as follows: 0–10, 10–20, 20–40, 40–60, 60–80, and 80–100 cm.

2.2 The Climate of the Study Area

The climate of the governorate of Manouba is Mediterranean belonging to the upper semi-arid bioclimatic stage, with mild and humid winters and dry and hot summers. The minimum temperature is 6 °C, and the maximum can reach 45 °C. The average rainfall is 450 mm.

The distribution of rainfall in the area is characterized by the following:

- a rainy autumn period that accumulates about 36% of the annual rainfall. These rains are often in the form of heavy thunderstorms.
- A rainy winter accounts for about 37% of the annual rainfall.
- A spring period with moderate rainfall, which accumulates about 21% of the annual rainfall.
- A dry summer period lasting three months (June, July, and August) which accumulates less than 5% of the annual rainfall.

2.3 Pedological Data of the Study Area

The soils in the study area can be categorized into two categories:

– Lithosols accumulate on the foothills, sometimes crusted and generally shallow and well drained. These soils are suitable for arboriculture.
– Cambisol, calcisol, and regosol occupy the lower part of the topography. These soils have a clayey texture favoring hydromorphy in the event of excess water P1 is a Cambisol, P2 is a Calcisol, and P3 a Regosol.

2.4 Soil and Water Analysis

In the field, we identified the color of each horizon from the Munsell code. We also determined the structure and texture of different samples. Then we did an HCl test for each sample while noting the presence and absence of effervescence caused by calcium carbonates, hydromorphic traits, and the presence and absence of plant roots and rootlets.

In the laboratory, we carried out the analyzes on the soil samples: the particle size fraction; pH; electrical conductivity; salinity; organic carbon; bulk density, and on water (irrigation water and soil water) the Analysis of the geochemical elements.

2.5 Water Irrigation Analysis

The three types of water used in the irrigation plots show poor quality. Table 1 summarizes the main characteristics.

2.6 Statistical Analysis

Data were analyzed using the statistical analysis software (IBM SPSS Statistics Version 20).

3 Results and Discussion

The particle size analysis of the soils of the three plots shows that they all have a silty clay texture. For P1, the clay content is between 26 and 31%, silts between 53 and 56%, and sand between 16 and 19%. For P2, the clay content is much higher than for P1 and P3. It is between 34 and 44%. P3 looks a lot like P1 in terms of particle size. The common point of these three soils is the richness in clay and silt, making them heavy soils naturally exposed to hydromorphy in case the topography is flat, which is almost the case for these three soils. For the three soils, the pH is slightly alkaline. It is between 7.4 and 8.1. The highest values are found at a depth of around 1 m.

The water saturation (WS) shows very well the effect of the fine mineral matter of these soils in the percolation of water. These waters in heavy rains are submerged. The infiltration is very low and requires time to be carried out. The values vary between 47.7 and 70.3%. The electrical conductivity is also close in the three soils; it goes from 1.2 to 6.9 mS/cm.

The three soils are well-carbonated, and a strong effervescence with the HCl test is present throughout the profile. The Analysis shows that P1 is more carbonated than P2 and P3, with the content always greater than 46%.

Table 1 Water quality in the three study sites

	pH	CE (mS/cm)	SAR
Water irrigation P1 (Sounding 160 m deep)	7.4	14.9	7
Water irrigation P2 (Chafrou river)	8.8	7.3	13
Water irrigation P3 (Medjerda river)	8.6	4.6	7

Table 2 Soil organic carbon stocks ($n=3$; ±: St. E.)

Depth (cm)	SOC stock (kg C m^{-2})		
	P1 (Cambisol)	P2 (Calcisol)	P3 (Regosol)
0–20	6.01 ± 0.99	7.52 ± 0.81	5.65 ± 0.06
20–40	6.32 ± 0.32	7.05 ± 0.34	5.09 ± 0.84
40–60	5.03 ± 0.18	5.76 ± 0.49	4.04 ± 0.27
60–80	4.16 ± 0.38	4.88 ± 0.25	3.87 ± 0.05
80–100	2.75 ± 0.11	4.37 ± 0.13	3.93 ± 0.45
Total	*24.25 ± 1.98*	*29.57 ± 2.02*	*22.59 ± 1.67*

Regarding the richness in organic carbon, the three soils have a good content; they are of the order of 2% or more on the surface and of the order of 1% in depth. Indeed, the plots are generally well amended by manure and are located under a climate favoring the annual input of organic matter from seasonal crops.

The bulk density values vary from 1.36 at the surface to 1.53 g/cm^3 at depth.

Table 2 summarizes the carbon stocks in the three plots. The results show that the stocks over a depth of one meter are 24.25 for P1, 29.57 for P2, and 22.59 kg C m-2 for P3. By examining the stock as a function of depth, we notice that the surface layers are the richest in organic carbon. This stock of C in these soils, which are in the process of losing their fertility as a result of secondary salinization and the accumulation of salts due to irrigation, is nevertheless very comparable to those that are "healthy" and do not show salinity signs.

These values are relatively high compared to these same types of soil in Tunisia, where Brahim et al. (2014) calculated an average stock for all Tunisian Regosols of 8.39 kg C $m-^2$, for Cambisols 10.18 kg C m^{-2}, in another more recent study for Regosols under olive trees or pasture Znaidi et al. (2020) showed that the stock under Regosols shows a good capacity to sequester C by going from the desert bioclimate where the stock ranging from 5.76 to 8.22 kg C $m-^2$ in and under a lower semi-arid bioclimate the stock ranging from 10.52 and 12 kg C m^{-2}, and in our study under a higher semi-arid bioclimate in addition to irrigation, the stocks are comparable to forest soils. Comparing these stocks with those obtained from the global database Batjes (1996) developed, these soils have a stock much higher than the normal, which is of the order of 6 kg $Cm-^2$ for Calcisols, 9.6 kg C m^{-2} for Cambisols, and 5 kg C $m-^2$ for Regosols. By comparing these soils with solonchaks whose stocks do not exceed 4.2 kg Cm^{-2} in the world (Batjes, 1996) and 7.5 kg C $m-^2$ in Tunisia (Brahim et al., 2014), these soils seem to be a sink of C to preserve by trying to solve the irrigation with this poor-quality water.

4 Conclusion

The secondary salinity in different soils in the Medjerda plain had no significant effect on C storage. It is advantageous to see the impact of calcium carbonates on organic matter and the effect of salts on organic carbon. However, heavy clay-rich soils must be used with great care. The secondary salinization that has appeared in these soils is the best example.

References

Batjes, N. (1996). Total carbon and nitrogen in the soils of the world. *European Journal of Soil Science, 47*, 151–163.

Brady, N. C., & Weil, R. R. (2002). *The nature and properties of soils* (13th ed.). Prentice Hall.

Brahim, N., Ibrahim, H., & Hatira, A. (2014). Tunisian soil organic carbon stock: Spatial and vertical variation. *Procedia Engineering, 69*, 1549–1555.

Essington, M. E. (2004). *Soil and water chemistry, an integrative approach*. CRC Press.

FAO. (2007). Extent and causes of salt-affected soils in participating countries. In: AGL: Global network on integrated soil management for sustainable use of salt affected soils.

Hachicha, M. (2007). Les sols salés et leur mise en valeur en Tunisie. *Secheresse, 18*(1), 45–50.

Weil, R. R, & Brady, N. C. (2016). *The nature and properties of soils* (15th ed). Prentice-Hall Inc. ISBN-13: 978-0-13-325448-8.

Znaidi, A., Brahim, N., Ibrahim, H., et al. (2020). Comparison of organic carbon stock of Regosols under two different climates and land use in Tunisia. *Arabian Journal of Geosciences, 13*, 1011. https://doi.org/10.1007/s12517-020-06011-4.

Salinity Load and Ion Transport in Clay Soils: A Case Study in a Salt Production Area, Sakon Nakhon Province, Thailand

Sarunya Promkotra, Thidarat Cotanont, Pitchaporn Intamol, and Tawiwan Kangsadan

Abstract

Salinity load and ion transports in clay soils are operated in a salt production area in Ban Muang District, Sakon Nakhon Province, Thailand. The salinity distribution of the study area covering 10×15 m and nine sampling points are considered by the topographic map and the elevation area. The diagonal line of the study area is obtained by the cross-sectional line with the series of 1–3, where the high, middle, and low elevations are indicated in series 1, 2, and 3, respectively. The solid bedrock beneath this region is a delineation of laterite deposits. Besides, in the top soils, clay compositions, mica group, chlorite, kaolinite, and montmorillonite differ from the bottom soils. Clay minerals of the topsoil are more than the bottom soil, varying in the range of 11–18 and 10–17%, respectively. Chemical species of water-extraction solutions from clay soils appear to be the NaCl type. NaCl salt continuously dissolves until it reaches the equilibrium condition. Numerical parameters entirely depend on observation in the field and corresponding to ion concentrations of Na^+ and Cl^- ions. Their transports are related to the diffusion flow in high-concentration areas diffusing from higher to lower ones. Different movements are affected by the surface water flow and also the elevation.

Keywords

Salinity load · Ion transport · Clay soils · Ban Muang district · Sakon Nakhon

1 Introduction

Halite weathering processes can release Na^+ ions into environments and accumulate in soils and streams. Almost weathered soils can absorb some ions, especially soils containing clay minerals, such as montmorillonite, chlorite, or smectite. The source of salinity in Sakon Nakhon Province comes from rock salts in the Maha Sarakham Formation (DMR, 2020). Tectonic affected the Maha Sarakham Formation gradually uplifted, and seawater is intruded from the east into the Khorat Basin during Cretaceous (Sattayarak, 1983). Therefore, many areas in northeastern Thailand are influenced by saline soils that originated from the dissolution of NaCl from the deep accommodated rock salt. Even though Na^+ and Cl− ions are normally dissolved salts, many other ions, such as K^+, SO_4^{2-}, and HCO_3^-, are also found (Promkotra, 2013; Promkotra & Kangsadan, 2013). This study intends to investigate the effect of salt transport on the soil surface. The study area is located in Ban Muang District, Sakon Nakhon Province, Thailand, which is close to a salt farm near Bo Daeng Subdistrict. White salt sprawling across the surface area is noticed from the far-sighted view because of pumping flaws and brine leakage covering the surface area.

2 Materials and Methods

2.1 Area Design

The research is designed to study ion transport in soils. The boundary of the study area in Ban Muang District

S. Promkotra (✉) · T. Cotanont · P. Intamol
Department of Geotechnology, Faculty of Technology, Khon Kaen University, Khon Kaen, Thailand
e-mail: sarunya@kku.ac.th

T. Kangsadan
Chemical and Process Engineering Program, The Sirindhorn International Thai-German Graduate School of Engineering (TGGS), King Mongkut's University of Technology North Bangkok (KMUTNB), Bangsue, Bangkok, Thailand

A. Çiner et al. (eds.), *Recent Research on Environmental Earth Sciences, Geomorphology, Soil Science, Paleoclimate, and Karst*, Advances in Science, Technology & Innovation, https://doi.org/10.1007/978-3-031-42917-0_39

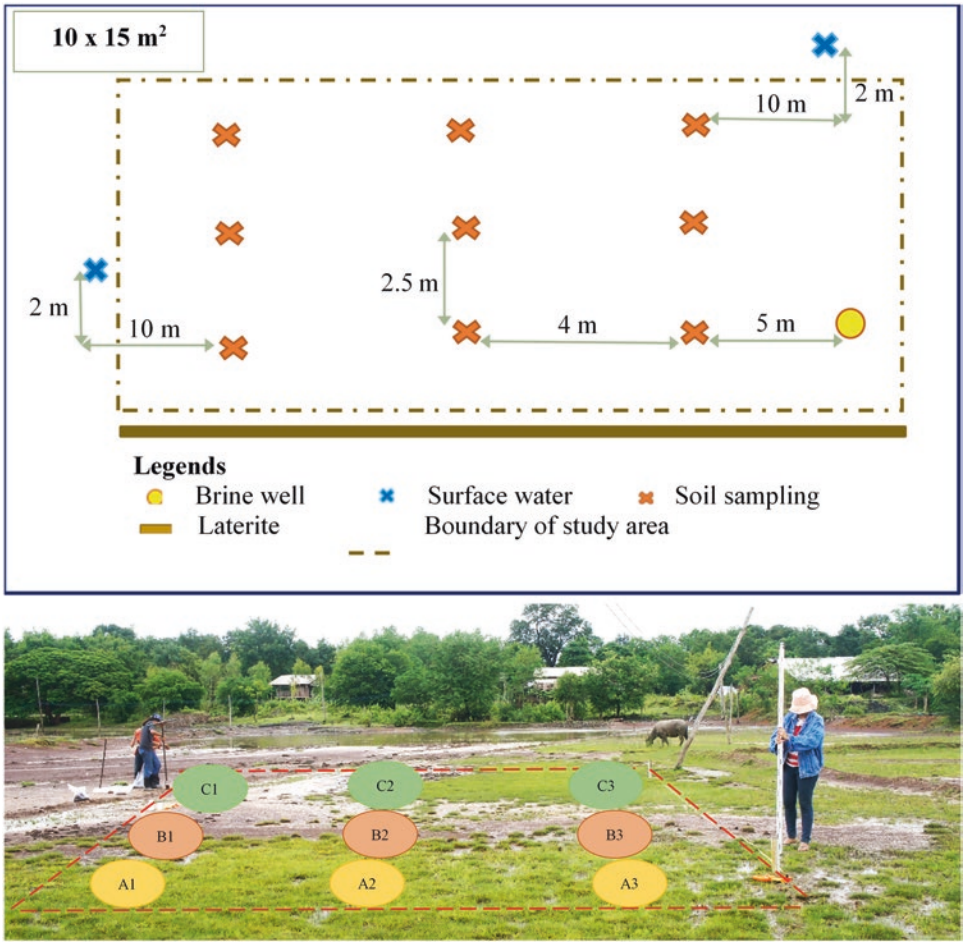

Fig. 1 Area design with elevation (AMSL) as a function of sampling points

based on the UTM Grid Reference System is situated in 48Q 0341874E–0341888E, 0341877E–0341888E, 1969996N–1970010N, and 1969995N–1970010N, covering the area of 10 × 15 m (Fig. 1). Diagonal line of the study area is obtained by the cross-sectional line with the series of 1–3, where the high, middle, and low elevations are indicated in the series 1, 2 and 3, respectively. Underground brine is brought to boiling on the evaporating pan.

2.2 Soils and Water-Extraction Solution from Soils

The topographic map considers nine sampling points depending on the topography (elevation) of the theodolite in the rainy season. First, specific areas of the sampling point are drilled by hand auger to obtain soil cores. Then, soils from the drilled hole are collected. Soil levels in each soil core are mainly separated into two strata (top and bottom levels) based on colors or grain sizes. Finally, top and bottom soils are tested for soil texture according to ASTM D 422 (Standard Test Method for Particle-Size Analysis of Soils) and for mineral compositions by X-ray Diffractometry (XRD).

Water-extraction solution from soils is carried out at room temperature by stirring 20 g of dried soils for 1 h with 20 mL of de-ionized water in an Erlenmeyer flask. This extracted solution is separated from the solid residue by filtration through a 0.45 µm filter membrane and kept in a 4 °C refrigerator. Major cations and anions in this extracted solution are determined by spectroscopy technique.

3 Results and Discussions

3.1 Soils and Water-Extraction Solution from Soils

Soil textures based on the grain size can be determined depending on the quantity of sand, silt, and clay according to the USDA soil classification system (USDA, 2020). The soil type of all soil samples is signified as sandy loam. Mineral compositions associated with soil samples in each location are identified into six groups, including quartz

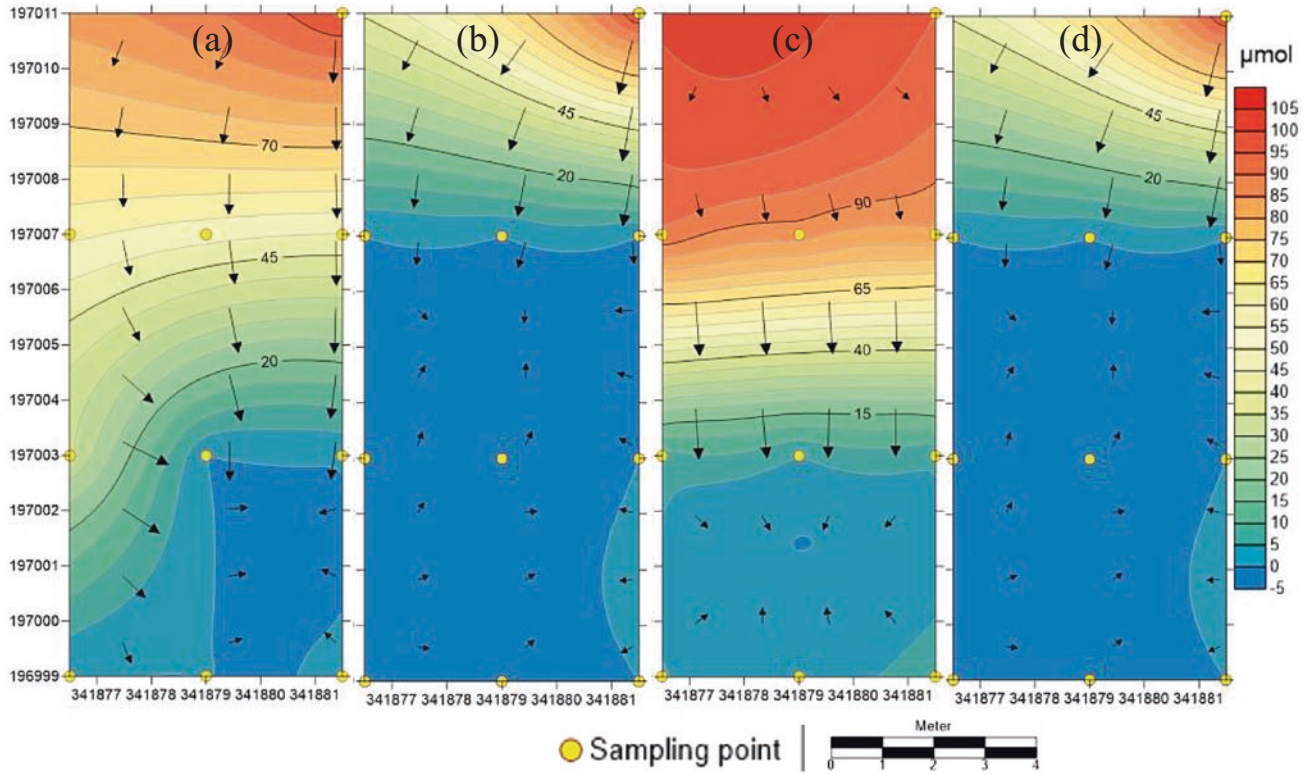

Fig. 2 Diffusive transport of Na^+ and Cl− related to study area as a function of sampling points **a** Na^+ at top soils, **b** Na^+ at bottom soils, **c** Cl^- at top soils, and **d** Cl− at bottom soils

(69–72%), clay (13–18%), feldspar (4–6%), hematite (1–2%), sulfate (5–7%), and halite (0.5–1%). Besides, clay compositions, mica, chlorite, kaolinite, and montmorillonite are found in top soils with a range of 11–18%, while bottom soils have 10–17%. As for water-extraction solutions from soils, Na^+ and Cl^- ions are mostly found.

3.2 Mass Transport

Diffusion flow of mass transport depends on observations in the field corresponding to Na^+ and Cl^- ions concentrations and compares between top and bottom soils, especially salt load (NaCl). Ion transport of Na^+ and Cl^- in mol is evaluated for ion distribution by using the Surfer software program. Transport phenomena of Na^+ and Cl^- in top and bottom soils have similar behavior in which the high concentration flows from the upper to the lower area. However, Cl− transport at bottom soils indicates the influence of runoff surface water (Fig. 2). Therefore, halite (NaCl) exhibiting similar behavior in both top and bottom soils accumulates in the almost middle area.

4 Conclusions

Salinity distribution of the study area in Ban Muang District, Sakon Nakhon Province, is performed in nine soil samples. Soils are contaminated by brine from the storage tank. Water-extraction solutions from clay soils exist to be the NaCl type. The NaCl salt always dissolves until it reaches an equilibrium state. Ion transport of Na^+ and Cl− are associated with the diffusion flow in high concentration depending on the elevation of the study area.

References

DMR Homepage. Retrieved July 2, 2020 from http://www.dmr.go.th/.

Promkotra, S. (2013). Chemical kinetics between brine and rock salt transitions. *Defect and Diffusion Forum, 334–335*, 43–48.

Promkotra, S., & Kangsadan, K. (2013). Geochemical speciation associated to brine and groundwater. *Applied Mechanics and Materials, 423–426*, 1422–1426.

Sattayarak, N. (1983). *Review of the continental Mesozoic stratigraphy of Thailand*. Hai Yai.

USDA Homepage. Retrieved January 4, 2020 from https://www.nrcs.usda.gov/wps/portal/nrcs/detail/soils/survey/.

A Case Study to Present Test Results and a Possible Framework for the Determination of the Anisotropy of Tropical Residual Soils in Mauritius

Reshma Rughooputh and Adityam Koomar

Abstract

Soil properties are not isotropic but anisotropic in nature. The associated properties include compressibility, shear strength, and stress–strain behavior. This paper highlights a case study in Mauritius on the test results and recommendations of a possible framework to capture the presence of anisotropy on a tropical residual. Tests include classification and index properties tests and consolidated undrained triaxial testing on undisturbed specimens sampled in the vertical and horizontal directions from adjacent sections. The soil exhibited slight anisotropic behavior. Anisotropy ratios of 0.87 and 0.94 were observed in c_u and ϕ', respectively. At higher confining stresses, stress–strain characteristics, effective principle stress ratio σ_1'/σ_3', pore pressure responses, and stress paths all tended toward isotropy. The methodology adopted in this research serves as a valid framework for assessing anisotropy for other types of tropical soils.

Keywords

Tropical residual
soils · Properties · Anisotropy · Framework

1 Introduction

Powrie (2014) reported the axisymmetry of structural anisotropy and stress anisotropy for a horizontally- and vertically-cored specimen in a triaxial cell. These symmetry conditions are maintained for a vertically-cored sample because the horizontal stresses imposed during the triaxial test align with the actual in-situ horizontal direction. However, with a horizontally-cored specimen, horizontal stresses during the triaxial test align with the in-situ vertical direction. Complete symmetry is then lost, and the specimen will deform in a non-cylindrical manner. Ladd and Lambe (1964) and Duncan and Seed (1966) are notable authors investigating this feature. Two essential features were determined: 1. In-situ anisotropic stresses are released during sampling. 2. When weathered soil specimens are extruded from their tubes during sample preparation, they experience negative pore pressure, so the effective stresses become isotropic. Therefore, directional characteristics are absent due to anisotropy in principle stresses during the routine triaxial test. Other methods, such as consolidation under anisotropic conditions or collecting samples along different orientations, have been previously used to account for anisotropy. According to Leroueil and Hight (2002, cited by Bica et al., 2008), anisotropic behavior is commonly categorized as 1. 'Inherent' anisotropy in in-situ soils results from developments in the soil macro- and micro-structure as weathering and consolidation occur. It prevails when the micro-structure is preserved during loading, as soil particles arrange into specific modes. Casagrande and Carrilo (1944) define inherent anisotropy as a natural physical characteristic in the material formed due to its stress history and environmental conditions (Cited by Ispir M. E., 2011). 2. 'Induced' anisotropy is mainly derived from volumetric changes as the soil shears during anisotropic loading conditions. In addition to particle orientation, there is a directional distribution of particles as large-strain loading occurs (After Casagrande and Carrilo, 40 1944. Cited by Ispir M. E., 2011).

R. Rughooputh (✉) · A. Koomar
University of Mauritius, Reduit, Mauritius
e-mail: re.rughooputh@uom.ac.mu

A. Çiner et al. (eds.), *Recent Research on Environmental Earth Sciences, Geomorphology, Soil Science, Paleoclimate, and Karst*, Advances in Science, Technology & Innovation, https://doi.org/10.1007/978-3-031-42917-0_40

Table 1 Summarized initial specimen data of triaxial Samples

Initial specimen data	Sample orientation	Vertical			Horizontal		
	Sample reference	VER-60	VER-120	VER-240	HOR-60	HOR-120	HOR-240
	Length, L (mm)	100	100	100	100	103	100
	Diameter, D (mm)	50	50	50	50	43	50
	Initial Mass, m_o (g)	376.62	366.75	364.63	354.98	338.79	389.04
	Initial moisture Content, w_o (%)	42.61	43.75	41.03	46.23	41.06	39.62
	Initial density, ρ (Mg/m^3)	1.92	1.87	1.86	1.81	2.07	1.85
	Initial dry density ρ_D (Mg/m^3)	1.34	1.3	1.32	1.24	1.46	1.32
	Particle density (Known) ρ_S (Mg/m^3)	2.83	2.83	2.83	2.83	2.83	2.83
	Initial voids ratio e_o	0.49	0.53	0.51	0.59	0.37	0.51
Compression stage	Cell pressure (kPa)	220	360	400	220	360	400
	Initial pore pressure (kPa)	160	160	160	160	240	160
	Initial effective pressure (kPa)	60	120	240	60	120	240

2 Materials and Methodology

Triaxial compression tests were carried out on undisturbed specimens sampled at two different inclinations—vertical 141 and horizontal (50 mm diameter) to investigate the anisotropic stress–strain characteristic of in-situ soils. The testing program also comprised soil classification tests (142 BS 1377:1990). Soil classification tests included determining natural moisture content, Atterberg limits, particle density, and particle size distribution. To avoid irreversible changes to soil behavior due to drying, sample preparation for Atterberg limits was carried out following the wet preparation method prescribed in BS 1377: Part 2. In addition, the small pycnometer method, suitable for fine-grained soils, was carried out to determine the particle density. Sodium hexametaphosphate was used as a dispersing agent during the wet sieving procedure. Six consolidated undrained (CU) triaxial tests were carried out: three for each sample orientation (Table 1). Vertical samples: VER-60, 120, 240, and horizontal samples: HOR-60, 120, 240. Numbers indicate the effective confining stress in kPa.

3 Results

The particle density was 2.83 Mg/m^3. Figure 1 displays the plasticity chart for the soil samples. Particle size results indicated that the soil was well graded, comprising fine sand and clayey silt, with a coefficient of uniformity (C_u) of 160 and a coefficient of gradation (C_c) of 10.

Table 1 summarizes the initial specimen data for the CU tests. Figure 2 displays the stress paths based on CU test results, while Table 2 contains the shear strength parameters and calculated anisotropy ratios.

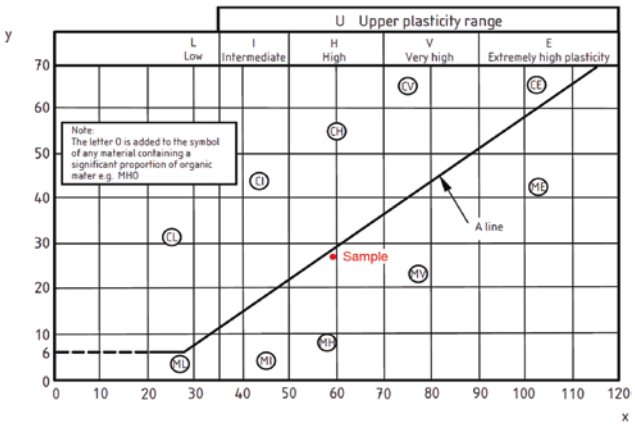

Fig. 1 Plasticity chart

4 Discussion

The findings are summarized as 1. Correlations from the Atterberg limits and pore pressure coefficient A_f suggest the specimens were lightly overconsolidated, more so in the horizontal direction. 2. In-situ soils from Ebène, Mauritius, are slightly anisotropic in undrained shear strength cu and effective friction angle ϕ'. Anisotropy ratios (HOR/VER) of 0.87 and 0.94 are observed in cu and ϕ', respectively. 3. At higher confining stresses (240 kPa), stress–strain characteristics, effective principle stress ratio σ_1'/σ_3', pore pressure response, and stress paths all were toward isotropy. The respective curves exhibited similar and almost overlapping shapes. Conversely, anisotropy is more significant at lower confining stresses (60 kPa and 120 kPa). 4. Normalized and non-normalized stress path characteristics for HOR and VER curves at the lowest confining stress (60 kPa) were the least stable. The possible cause is that soil fabric and the

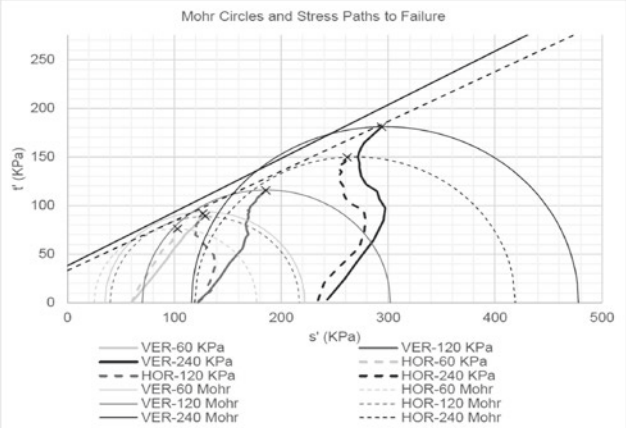

Fig. 2 Stress paths of VER and HOR samples

Table 2 Shear strength parameters

Shear strength parameter	HOR	VER	Anisotropy ratio (HOR/VER)
c_u (kPa)	33	38	0.87
ϕ' (°)	27.1	28.9	0.94

existence of weak planes or fissures can relax at lower confining stresses such that anisotropy is more pronounced. 5. When compared to past research, the sampled soil data fit within the typical range of values obtained from data gathered by Mayne (1985) on 42 different clays. Moreover, the data produced by Ispir (2011) on Ankara clay is somewhat similar to the sample soil data in terms of index properties and anisotropy ratios.

5 Conclusions

The findings and analysis suggest that a tentative correction factor of 0.87 may need to be applied to cu only to obtain a preliminary anisotropic strength during the safety assessment of soil behavior. The anisotropic soil behavior may not necessarily be considered at higher confining stresses since soil behavior tends toward isotropy. However, the recommended anisotropy ratio will not apply to soils in other geological settings, for example, in mountainous regions, where in-situ stresses differ from the sampled soil. Choosing appropriate strength parameters is critical in determining or assessing soil behavior safety. The findings show that the anisotropic soil strength should be accounted for at low confining stresses for soils in relatively leveled geological settings.

References

Bica, D., Bressani, L. A., Vendramin, D., Martins, F. B., Ferreira, P. V. M., & Gobbi, F. (2008). *Anisotropic shear strength of a residual soil of sandstone*. *Canadian Geotechnical Journal, 45*(3), 367–376. https://doi.org/10.1139/T07-098.

British Standards Institution. (1990). BS 1377:1990 Methods of test for soils for Civil 419 Engineering. Milton Keynes: BSI 420.

Casagrande, A., & Carrillo, N. (1944). Shear failure of anisotropic materials. In: *Proc. Boston* 423 *soc. civ. engineers* (vol. 31, pp. 74–87).

Duncan, J. M., & Seed, H. B. (1966). Anisotropy and stress reorientation in clay. *Journal of the Geotechnical Engineering Division, 92*(5), 21–50.

Ispir, M. E. (2011). A Laboratory study of anisotropy in engineering properties of ankara clay. In: *The graduate school of natural and applied sciences of middle east technical university*. 448

Ladd, C. C., & Lambe, T. W. (1964). *The strength of undisturbed clay determined from undrained tests*. Phaladephia STP: American Society for Testing and Material.

Leroueil, S., & Hight, D. W. (2002). *Behaviour and Properties of natural soils and soft rocks*. In: *The symposium of characterisation and engineering properties of natural soils*, Singapore. Swets Zeilinger, Lisse (vol. 1, pp. 29–254).

Mayne, P. W. (1985). Stress anisotropy effects on clay strength. *Journal of Geotechnical Engineering,* 464–465.

Powrie, W. (2014). *Soil mechanics concepts and applications* (3rd ed., p. 478). CRC Press.

Peat-Forest Fire Impact on the Soil Quality: Assessing the Chemodiversity of Organic Matter Extracted from Tropical Malaysian Peat Swamp Forest Soil

Noor Fazreen Dzulkafli, Norakma Mohd Nor, Norazlina Idris, Nurhafizah Ibrahim, Ainilhawa Sazali, and Noor Hidayah Pungot

Abstract

Peat fire incidents destroy the above-ground vegetation and penetrate the underlying peat, resulting in undesirable environmental impacts, including organic matter. In this study, the effects of the fires on the peat swamp forest of Raja Musa Peat Swamp Reserve Forest, Malaysia, were investigated through the characterization of dissolved organic matter extracted from the soil in burnt and unburnt sites. The organic matter composition was extracted by the alkaline extraction method. The elemental composition, UV-Visible spectrometer, fluorescence spectrofluorometer, analysis of amino acid and carbohydrate species performed the characterization of organic matter. The results showed soil physical and chemical properties variations among the two peat soil areas. The DOM of the burnt soil samples was found to be more aromatic and contained more carbon content than the unburnt soil. The total amino acid concentration (TAC) and total carbohydrate concentration (TCC) in DOM ranged from 3.1 to 6.8 and 10.8 to 28.3 mg/g. The biological index (BIX), which is related to the soil's biological activity, was higher in unburnt soil. The outcomes from this study will be of great use to further understand the biogeochemical processes in this unique ecosystem and can be used in peat swamp forest management.

Keywords

Peat fire · Soil organic matter · Chemical characterization · Amino acid · Carbohydrate

1 Introduction

The increased fire occurrences in the peat swamp forest have led to concern about the effects of forest fire on soil quality. It causes significant losses of soil C and N, which tend to decline further under continuous cultivation. Studies on the effects of fires on peat swamp forests have been conducted; including the examination of the impact of fire on the stand structure (Ainuddin & Goh, 2010), sources of anthropogenic fire ignitions (Cattau et al., 2016), and impacts of logging activity on fire (Franke et al., 2012). However, few studies explore the effect of peat-forest fire on soil quality. Therefore, this study aims to investigate the impact of fire on the characteristics of soil organic matter (SOM) of peat swamp forests.

2 Methodology

The study site of this study is Raja Musa Peat Swamp Forest Reserve, situated in Kuala Selangor, Malaysia. We collected soils from two sampling sites that represent soil with fire history (burnt soil-A1) and undisturbed (unburnt-A2) areas (Fig. 1).

The peat soil's physical properties, such as the pH, total organic carbon (TOC), moisture, and ash content, were determined. Extraction of organic matter (DOM) was performed with 10% NaOH solution in a ratio of 1:10 (w/v). The DOM fractions were then evaluated for dissolved organic carbon (DOC), elemental composition, UV-Visible spectroscopy, and fluorescence spectrofluorometer. The

N. F. Dzulkafli (✉) · N. M. Nor · N. Idris · N. Ibrahim · A. Sazali
Department of Science and Biotechnology, Faculty of Engineering and Life Sciences, Universiti Selangor, Jalan Timur Tambahan, 45600 Selangor, Malaysia
e-mail: fazreen@unisel.edu.my

N. H. Pungot
Faculty of Applied Sciences, Universiti Teknologi MARA (UiTM), Shah Alam, 40450 , Selangor, Malaysia

A. Çiner et al. (eds.), *Recent Research on Environmental Earth Sciences, Geomorphology, Soil Science, Paleoclimate, and Karst*, Advances in Science, Technology & Innovation, https://doi.org/10.1007/978-3-031-42917-0_41

total amino acid concentration (TAC) and total carbohydrate concentration (TCC) analyses were performed using the colorimetric method (Fischer et al., 2007). All analyses were performed in triplicate to minimize the error from the experimental procedure.

3 Results

The physical and chemical properties of the burnt and unburnt soil are shown in Table 1. The TOC value is higher in A1 (62%) than in A2 soil (55%). Both soil samples are in acidic condition, with the pH value higher in A1 than A2 as the combustion of SOM releases exchangeable cations (K^+, Na^+, Ca^{2+}, and Mg^{2+}) and H^+ ion attaches on negatively charged soil colloids.

Tables 2 and 3 show the characteristics of DOM-A1 and DOM-A2. There is a significant difference in the C/N ratio value between DOM-A1 and DOM-A2. The variation might be due to the heat-induced formation of large condensed structures, including heterocyclic nitrogen forms (Sazawa et al., 2018). TAC values are lower than TCC values in both DOM samples, with higher values in DOM-A1. BIX was found to be higher in DOM-A2 compared to DOM-A1. $SUVA_{254}$ values are 2.04 ± 0.55 and 1.06 ± 0.39 or DOM-A1 and DOM-A2, respectively. The value of HIX for DOM-A1 was 1.5 times higher than DOM-A2.

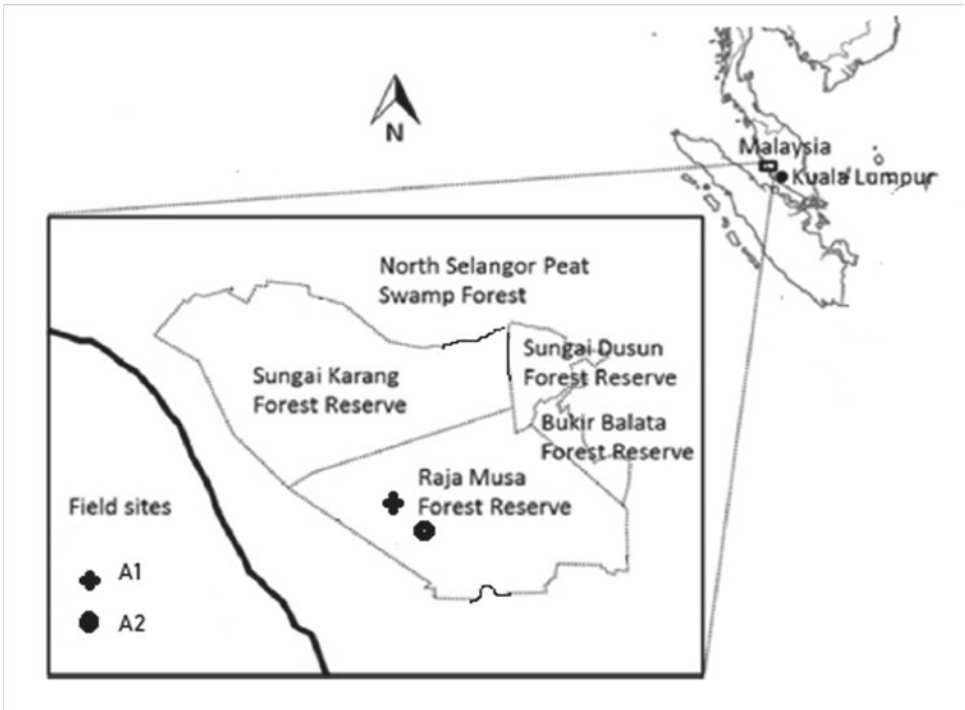

Fig. 1 Maps showing the study area with sampling points

Table 1 Physical and chemical properties of soils

Stations	Description	TOC (%)	Moisture content (%)	Ash content (%)	pH
A1	Burnt soil	62	85.73	99.25	3.91
A2	Unburnt soil	55	84.02	98.76	3.35

Table 2 Elemental atomic ratio, TAC, and TCC value of DOM

Sample	H/C	O/C	C/N	TAC (mg/g)	TCC (mg/g)
DOM-A1	0.12 ± 0.08	0.92 ± 0.01	37.18 ± 0.63	6.20 ± 2.08	10.98 ± 3.75
DOM-A2	0.12 ± 0.04	0.63 ± 0.04	50.19 ± 0.55	5.20 ± 1.90	18.57 ± 8.91

Results are presented as the mean ($n = 3$) ± SD

Table 3 DOC and DOM spectral indices derived from UV-Visible and fluorescent spectroscopy

Station	DOC (mg/L)	$SUVA_{254}$ (L/mg.C/m)	BIX	HIX
DOM-A1	8.57 ± 2.35	2.04 ± 0.55	1.08 ± 0.11	2.26 ± 0.89
DOM-A2	5.92 ± 1.58	1.06 ± 0.39	1.36 ± 0.02	1.46 ± 0.52

Results are presented as the mean ($n = 3$) ± SD

4 Discussion

The fire event not only affects the total amount of soil organic matter, but also exerts changes in its chemical composition, either by incorporating external material (charred and/or fresh) or by the chemical alteration of the existing SOM (Jiménez-Morillo et al., 2020). In this study, we observed differences in concentration and DOM composition between the two soil samples. A temperature of less than 350 °C can increase the organic matter solubility and higher proportions of aromatic structures in water-soluble organic matter, which is frequently attributed to a combination of physical and chemical factors in soils (Hermes et al., 2021). The alteration of carbohydrate compounds due to the temperature explains the lower TCC value in DOM-A1. In addition, the results indicated a higher ratio of O/C in DOM-A1, suggesting that the organic matter is more oxidized and attributed to carboxylic and phenolic compounds.

The greater $SUVA_{254}$, HIX, and lower H/C values in DOM-A1 soil samples compared to DOM-A2 soil samples appear to be related to a higher presence of condensed aromatic compounds in the former. The lower C/N ratio in burnt soil is due to the accumulation of recalcitrant organic N-forms in the charred material. BIX, which reflects the proportion of biological contribution to DOM with the value of BIX exceeding 1, indicates that the primary source of DOM-A2 is from the organisms, bacteria, and their metabolites in the soil (Li et al., 2015).

5 Conclusions

The results revealed that forest fire affects peat soil's organic matter properties. The samples with fire event history contain more aromatics and carbon content than the unburnt soil. Findings from this study will provide information on the biogeochemical processes in this unique ecosystem after the forest fire event and further be used in managing peat swamp forests.

References

Ainuddin, N. A., & Goh, K. (2010). Effect of forest fire on stand structure in Raja Musa peat swamp forest reserve, Selangor Malaysia. *International Journal of Environmental Science and Technology, 3*, 56–62.

Cattau, M. E., Harrison, M. E., Shinyo, I., Tungau, S., Uriarte, M., & DeFries, R. (2016). Sources of anthropogenic fire ignitions on the peat-swamp landscape in Kalimantan Indonesia. *Global Environmental Change, 39*, 205–219. https://doi.org/10.1016/j.gloenvcha.2016.05.005

Franke, J., Navratil, P., Keuck, V., Peterson, K., Siegert, F. (2012). Monitoring fire and selective logging activities in tropical peat swamp forests. *IEEE Journal of Selected Topics in Applied Earth Observations and Remote Sensing, 5*, 1811–1820, https://doi.org/10.1109/JSTARS.2012.2202638.

Fischer, H., Meyer, A., Fischer, K., & Kuzyakov, Y. (2007). Carbohydrate and amino acid composition of dissolved organic matter leached from soil. *Soil Biology & Biochemistry, 39*, 2926–2935. https://doi.org/10.1016/j.soilbio.2007.06.014

Hermes, A. L., Ebel, B. A., Murphy, S. F., & Hinckley, E. L. S. (2021). Fates and fingerprints of sulfur and carbon following wildfire in economically important croplands of California, U.S. *Science of the Total Environment*, *750*. https://doi.org/10.1016/j.scitotenv.2020.142179.

Jiménez-Morillo, N. T., Almendros, G., De la Rosa, J. M., Jordán, A., Zavala, L. M., Granged, A. J. P., & González-Pérez, J. A. (2020). Effect of a wildfire and of post-fire restoration actions in the organic matter structure in soil fractions. *Science of the Total Environment, 728*. https://doi.org/10.1016/j.scitotenv.2020.138715.

Li, Y., Wang, S., & Zhang, L. (2015). Composition, source characteristic and indication of eutrophication of dissolved organic matter in the sediments of Erhai Lake. *Environment and Earth Science, 74*, 3739–3751. https://doi.org/10.1007/s12665-014-3964-4

Sazawa, K., Wakimoto, T., Fukushima, M., Yustiawati, Y., Syawal, M. S., Hata, N., Taguchi, S., Tanaka, S., Tanaka, D., & Kuramitz, H. (2018). Impact of peat fire on the soil and export of dissolved organic carbon in tropical peat soil, Central Kalimantan Indonesia. *ACS Earth and Space Chemistry, 2*, 692–701. https://doi.org/10.1021/acsearthspacechem.8b00018

Classification Tests and Sensitivity Analysis of a Residual Tropical Soil

Reshma Rughooputh and Vedna Devi Gopal

Abstract

This paper presents test results on the influence of sample preparation on the geotechnical and compaction properties of tropical residual soils at a selected site in Mauritius. Sensitivity analysis was carried out, and it was observed that pre-drying markedly decreases the liquid limit, plasticity index, and clay content of the soil tested. This was due to the dehydration of clay particles and aggregation of particles. Re-wetting did not bring back the original properties of the soils, as observed in the varying results for compaction and California Bearing Ratio (CBR)—soaked and unsoaked tests. Sample test results include two sampling depths (0–1 m and 1–2 m, respectively). The findings revealed that increased pre-drying temperature significantly affects soil behavior. For instance, for a standard mixing time of 10 min, an oven-dried sample at a depth of 1–2 m reduced the liquid limit by 16.7%, linear shrinkage limit by 5.5%, and exhibited non-plasticity (NP). Further, oven-drying showed a decrease of 11.32% in particle density and a reduced clay fraction of 6% for particle size distribution. The maximum dry density and minimum optimum moisture content were obtained for the oven-dried samples. The highest CBR values and lowest swell potential were obtained for samples remolded using oven-dried soil. This was attributed to the dehydration of clay particles upon drying, which influenced the soil's natural properties. In addition, soaking had a marked effect in reducing the CBR value of the soil.

Keywords

Tropical residual soils · Pre-drying · Air-dried · Oven-dried · Natural conditions · Index properties · Compaction · California bearing ratio (CBR)

1 Introduction

The effect of sample preparation is markedly obvious for Atterberg limit values. Pre-drying the specimens instead of starting at natural moisture content is said to cause a reduction in liquid limit and plasticity index values (Terzaghi, 1958; Sunil & Krishnappa, 2012; Nayak & Preetham, 2020; Wesley & Matuschika, 1990). Iron and aluminum oxidize with drying and increase the cementing effect. Drying can also cause allophane and halloysite or sesquioxides to dehydrate, creating a stronger bond between particles which provides resistance to water. As a result, the soil becomes less plastic. This effect is irreversible even upon rewetting Oven-drying has a more significant effect on reducing the plasticity of tropical soils than air-drying (Fookes, 1997). This is confirmed by Muttaya and Huat's (1994) study on Malaysian soils: when the drying condition was changed from air-dried to oven-dried, the liquid limit decreased from 61 to 46%, and the plastic limit reduced from 40 to 33%. This trend was also reported for linear shrinkage values. Robinson and Thagesen (2004) revealed that intense remolding of the soil, which is proportional to the duration of mixing, tends to break down the coating surrounding individual soil particles and the aggregations present in tropical soils. This effect results from cementing agents such as sesquioxides. In its natural state, this coating lessens the clay mineral's ability to absorb water. With remolding, the coatings are destroyed, resulting in increased plasticity. Gidigasu (1974) demonstrated how sample preparation influenced the compaction characteristics of

R. Rughooputh (✉) · V. D. Gopal
University of Mauritius, Reduit, Mauritius
e-mail: re.rughooputh@uom.ac.mu

A. Çiner et al. (eds.), *Recent Research on Environmental Earth Sciences, Geomorphology, Soil Science, Paleoclimate, and Karst*, Advances in Science, Technology & Innovation, https://doi.org/10.1007/978-3-031-42917-0_42

a lateritic soil from Ghana. Air-drying and oven-drying decreased the optimum moisture content and increased the maximum dry density. Sunil and Krishnappa (2012) conducted studies on lithormargic clay and lateritic soil and associated the changes in compaction characteristics upon drying with the aggregation effect. When dried before testing, the clays cannot absorb all the water necessary to attain a moisture state during the mixing. Similarly, pre-test drying influenced the results of CBR. The works of Nayak and Preetham (2020) on marine clays showed higher soaked and unsoaked CBR values when the drying temperature increased.

2 Site and Methodology

The soil samples used for this study contained heavily weathered tropical clayey soil obtained from a construction site. In the geological map of Mauritius by Giorgi et al. (1999), the site is located on the Intermediate Lava Series, which consists of basalt rocks with olivine material. Sampling was conducted at two different depths, namely 0–1 m and 1–2 m, respectively, with soil type of Low Humic Ferruginous Latosols with brown to reddish brown silty clay loams with stones and boulders and few ironstone nodules (MSIRI, 1962). Laboratory tests were conducted using standard BS 1377 Part 1:1990, BS 1377 Part 2:1990, and BS 1377: Part 4:1990 and modified procedures for the sensitivity analysis. The tests were conducted on air-dried (AD), oven-dried (OD), and as-received (AR) soil samples to investigate the effect of pre-drying conditions on the results of the classification tests and the compaction characteristics of the soil. The investigations of interest were: moisture content, Atterberg limits, linear shrinkage, particle density, particle size distribution, Proctor tests, and California Bearing Ratio (CBR).

3 Results

The difference in moisture content was calculated by comparing the moisture content of the air-drying temperature at 20 °C to the moisture content resulting from standard oven-drying at 105 °C and 50 °C. A greater difference of 8.04% (0–1 m) and 8.69% (1–2 m) was obtained for oven-drying at 105 °C for the respective depths. All differences were greater than 4–6%, indicating that the soil contained structural water (Fookes, 1997). Further, air-drying for both samples resulted in the lowest moisture content, indicating that the structural water was not entirely lost for this technique. The particle density of the tropical soil studied ranged from 2.77 Mg/m^3 to 3.18 Mg/m^3. A decrease in particle density and loss of inter-particle water were noted with temperature. The highest liquid limit values of 52.35% and 55.86% are obtained for samples in their natural conditions, whereas the lowest values of 40.63% and 39.16% for oven-dried samples for the respective depths. This marked a decrease of 11.72% and 16.7% for corresponding depths. Linear shrinkage values decreased considerably from natural to air-dried and oven-dried samples. The plasticity chart showed that increased mixing on samples in natural and air-dried conditions causes the points to move upwards parallel to the A-line on the plasticity chart. However, it was observed that the highest peaks were obtained for oven-dried samples at both depths, with almost a parallel shift in trend for compaction tests (Fig. 1). CBR tests in both soaked and unsoaked conditions. Soaking reduced the CBR values significantly and is more pronounced for tests remolded using oven-dried specimens with an overall reduction of 71.6% and 43.5% for 0–1 m and 1–2 m, respectively, for bottom CBR values. The potential swell values were derived from the soaked CBR test and obtained as the maximum attainable expansion. The swell values were reduced from a maximum for air-drying to low values at 110 °C.

4 Discussion

This study investigates the effects of sample preparation, predominantly pre-drying, on tropical soil. The following observations were drawn:

(i) the large percentage difference in moisture content obtained from the different drying conditions indicated the presence of significant structural water driven off samples at elevated temperatures of 50 °C and 105 °C. Hence, the conventional drying temperature of 105 °C, as specified in British Standards for moisture content determination, should not be revised; (ii) the decrease in values of particle density as the drying condition was changed from a natural state to oven-dried revealed the loss of inter-particle water from the clay particles upon drying and a change in the structure; (iii) the particle size distribution altered significantly with oven-drying accompanied with a decrease in the clay and silt fraction and a predominant increase in sand fraction; (iv) pre-drying of soil samples had an enormous effect on the plasticity behavior of the soil at Cote-D'Or. There was a marked decrease in both the liquid limit and plasticity index values upon drying, which is associated with aggregations formed from the dehydration of clay particles; (v) the soil was a little sensitive to remolding, and therefore, the standard mixing time of 10 min was not enough to break the bonds to achieve complete remolding for tropical soils; (vi) the linear shrinkage also showed sensitivity to pre-drying since the measured values decreased with temperature; (vii) the soil was sensitive to crushing

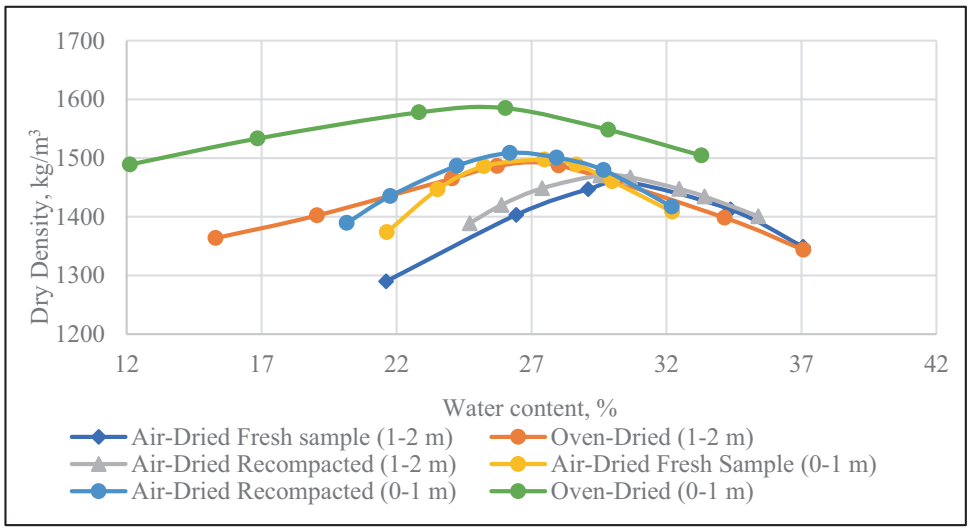

Fig. 1 Effect of drying on MDD and OMC

and resulted in de-structuration of the natural soil particles. Under the same compaction effort, oven-drying increased the maximum dry density and reduced the optimum moisture content and; (viii) the rise in pre-drying temperature caused a significant increase in CBR values for both soaked and unsoaked conditions. For soaked conditions, the swell potential of the soils was reduced with increasing drying temperature. This is linked with the aggregation effect that gave better strength for oven-dried samples.

5 Conclusions

The main problem identified with the tested soil was its sensitivity to drying, hence the loss of its natural structure during the process. Field compaction near the optimum moisture content to a specified density based on oven-dried soil compacted in the laboratory would be problematic due to the different OMCs of the soil in natural, air-dried, and oven-dried conditions. The same applies to CBR tests that are important for pavement design. Hence, misleading compaction values obtained from pre-dried samples should not be used as a reference value to determine the relative compaction percentage on site. Instead, the soil should be tested in the laboratory without pre-drying or minimum air-drying for design purposes.

References

British Standards Institution. (1990). *BS 1377: 1990 Methods of test for soils for Civil Engineering*. BSI.

Fookes, P. G., (1997). *Tropical residual soils.* A Geological Society engineering group working party revised report. London: The Geological Society.

Gidigasu, M. (1974). Degree of weathering in the identification of laterite materials for engineering purposes-a review. *Engineering Geology, 8*(3), 213–266.

Giorgi, L., Borchielini, S., & Delucchi, L. (1999). *Carte Géologique au 1:50000, Schema hydrogéologique*. Notice explicative. Project Franco-Mauricien "Appui à la gestion des resources en eau et à la preservation de leur qualité".

Mauritius Sugarcane Industry Research Institute. (1962). *Soil map of mauritius*. Directorate of overseas surveys.

Muttaya, P., & Huat, B. B. K. (1994). Effect of pre-test treatment on engineering properties of local residual soils. *Journal of Institution of Engineers. Malaysia, 55*, 29–41.

Nayak, S., & Preetham, H. K. (2020). *Effect of drying temperature and rewetting on the engineering properties of marine clay.* Transportation Infrastructure Geotechnology.

Robinson, R., & Thagesen, B. (2004). *Road engineering for development* (2nd ed.).

Sunil, B., & Krishnappa, H. (2012). Effect of drying on the index properties of lateritic soils. *Geotechnical and Geological Engineering, 30*(4), 869–879.

Terzaghi, K., 1958. Design and performance of Sasumua Dam. *Proc. I.C.E.* 9, 369–394

Wesley, L., & Matuschka, T. (1990). Geotechnical engineering in volcanic ash soils. *International Journal of Rock Mechanics and Mining Sciences & Geomechanics Abstracts, 1*, 333–342.

Controlling Sand and Dust Storms Hot Spots in the Mesopotamian Flood Plain

Ali Al Dousari, Mohamad Al Rawi, Peter Petrov, Modi Ahmed, Noor Al Dousari, Abeer Al Saleh, and Teena William

Abstract

Dust storms have important environmental consequences, including climate change, nutrient additions to the ocean and terrestrial ecosystems, ocean sedimentation, soil formation, and loess deposition. Two source areas (hot spots) for sand and dust storms (SDS) were identified in the Mesopotamian Flood Plain after monitoring the area for 25 years via satellite images. Both areas contribute around 21% of the total SDS and cover about 400 km2. The two hot spots affect the region's health and economy of approximately 40 million people. The objective is to complete a survey of the soil and dust samples and to develop a mitigation plan to establish a success story in controlling SDS to help enhance the air quality and help the community. Dust samples in the region consist majorly of quartz (42%), carbonates (45%), and other minerals, including (clay, feldspars, and heavy minerals) which are nearly similar to the silt and clay samples picked from both two hot spots. A detailed work plan was established for controlling these two hot spots using the establishment of channels from Euphrates River attributes and extensive plantation using native vegetation mainly (Tamarix sp.). Therefore, several agreements with Iraqi universities and the Ministry of Agricultural and Kuwait Institute for Scientific Research (KISR) for four years of monitoring air quality before, during, and after the stabilization project.

Keywords

Dust · Sand and dust storms · Kuwait · Iraq · Kuwait

1 Introduction

Sand and dust storms (SDS) are considered the most common meteorological phenomena in the Arabian Gulf region (Al-Dousari et al., 2016). The Arabian Gulf is surrounded by a desert ecosystem characterized by active aeolian conditions (Al-Dousari, 2009). The prolonged drought and land degradation periods are primary activators of SDS in deserts (Al-Dousari & Al-Hazza, 2013). Significant quantities of dust particles are blown thousands of kilometers from their source (Al-Dousari., 2005), and it has been estimated that windblown dust derived from soil erosion contributes approximately 500 million tons of particulate matter to the atmosphere each year (Al-Dousari et al., 2013). Up to two billion tons of dust blows into the atmosphere in a year within major SDS trajectories (Al-Dousari et al., 2004). Frequent occurrences of SDS in the Arabian Gulf cause an acute environmental problem that can affect the society's safety, health, and economic well-being (Al Awadhi et al., 2014). The SDS passing over the Arabian Gulf is a significant sediment source (Al-Dousari & Al-Awadhi, 2012). Al-Dousari and Al-Awadhi (Al et al., 2019) identified five major SDS trajectory areas in the northern Arabian Gulf: the Western Desert of Iraq, the Mesopotamian Flood Plain, the Nafud Desert, Ahwar, and Ahwaz (Al-Hemoud et al., 2020). Another interesting aspect is the possible effects of draining the Ahwar marshland, which acts later as a new source area for dust (Al Dousari & Al Dousari, 2021; Al-Dousari et al., 2020). Primary SDS sources are within the southern Arabian Gulf Regions Empty Quarter, Nafud (Al-Awadhi et al., 2000), and Baluchistan (Wahab et al., 2018) deserts. Therefore, this study aims to monitor hot spots for SDS trajectories and propose a regional control action plan.

A. Al Dousari (✉) · P. Petrov · M. Ahmed · N. Al Dousari · A. Al Saleh · T. William
Kuwait Institute for Scientific Research, Kuwait City, Kuwait
e-mail: adousari@kisr.edu.kw

M. Al Rawi
Geography Department, Aswan University, Aswan, Egypt

A. Çiner et al. (eds.), *Recent Research on Environmental Earth Sciences, Geomorphology, Soil Science, Paleoclimate, and Karst*, Advances in Science, Technology & Innovation, https://doi.org/10.1007/978-3-031-42917-0_43

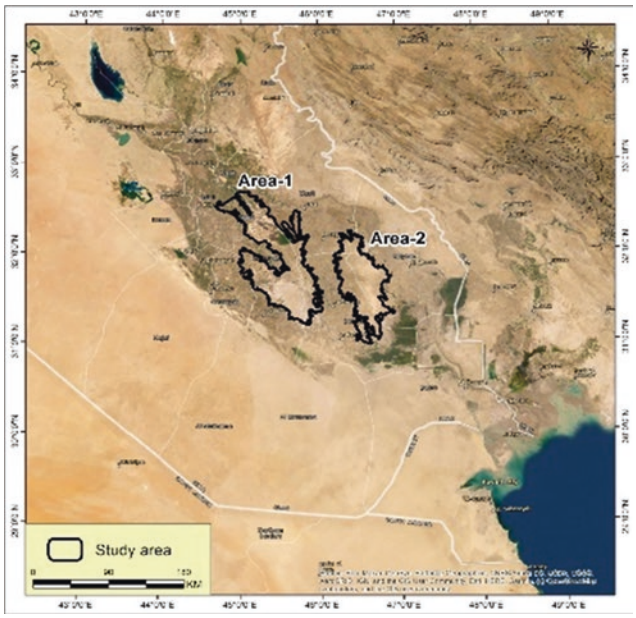

Fig. 1 Study area

2 Study Area

The studied area is South of Iraq and Northern Kuwait. Area 1 (11,491 km^2) is located between 31°11′51″N, 32°41′50″N Northern latitude and 44°41′10″E, 46°3′21″E Eastern longitude. The Area 2 (6512 km^2) is situated between 30°58′47″N, 32°15′57″N Northern latitude and 46°9′53″E, 46°58′19″E Eastern longitude (Fig. 1).

3 Materials and Methods

Several field visits for the study areas and around 50 soil samples were collected for physical and chemical properties. In addition, a round of 1560 samples of dust was assembled in Kuwait for two 24 months period. Also, several agreements with Iraqi universities and the Ministry of Agricultural and Kuwait Institute for Scientific Research (KISR) for four years of monitoring air quality during the stabilization project and after. The study aimed to assess changes in land cover and vegetation density (NDVI) between 1964 and 2020 using Landsat imagery, where remote sensing technology and geographic information systems (GIS) were used to detect changes quickly and accurately (Table 1). In addition, we used Corona Satellite imagery captured in 1968 to compare the past period with the present.

Table 1 The Satellite imagery data was collected from more sensor types and more sources

Sensor type	Date	Accuracy	Sources	Website
Corona satellite	5 May 1968	1 m	USA army	https://corona.cast.uark.edu/
Landsat TM	16 May 1984	30 m	USGS	https://eos.com/landviewer/
Landsat TM	4 May 1991	30 m	USGS	https://eos.com/landviewer/
Landsat ETM+	4 May 2000	30 m	USGS	https://eos.com/landviewer/
Landsat OLI	7 April 2013	30 m	USGS	https://eos.com/landviewer/
Landsat OLI	10 May 2020	30 m	USGS	https://eos.com/landviewer/
Topog Maps	1990	1:200,000	Soviet army	https://maps.vlasenko.net/

4 Results and Discussion

The research showed the following:

Comparing the areas' boundaries between (1968 and 1984), (1984 and 1991), (1991 and 2000), (2000 and 2013) and (2013 and 2020), it became clear that the area of bare lands increased at the expense of the area of water bodies and wetlands. Therefore there is receding water and an increase in soil desertification due to the drying up of ponds and swamps and their conversion to agricultural lands (Fig. 2). With comparing the boundaries of the bare land area between, there is a decrease in plain areas, it decreased to 3982.9 km in Area 1 and 1983.9 km^2 in Area 2, and the final location in 2020 is 6446.6 km^2 only in Area 1 and 2964.5 km^2 in Area 2 (Fig. 1).

Dust samples in the region consist majorly of quartz (42%), carbonates (45%), and other minerals, including (clay, feldspars, and heavy minerals) which are nearly similar to the silt and clay samples picked from both two hot spots. Therefore, a detailed work plan was established for controlling these two hot spots using the establishment of channels from Euphrates River attributes and extensive plantation using native vegetation mainly (*Tamarix* sp.). The mechanical and biological methods will be used to protect the third river from the creeping sands and turned

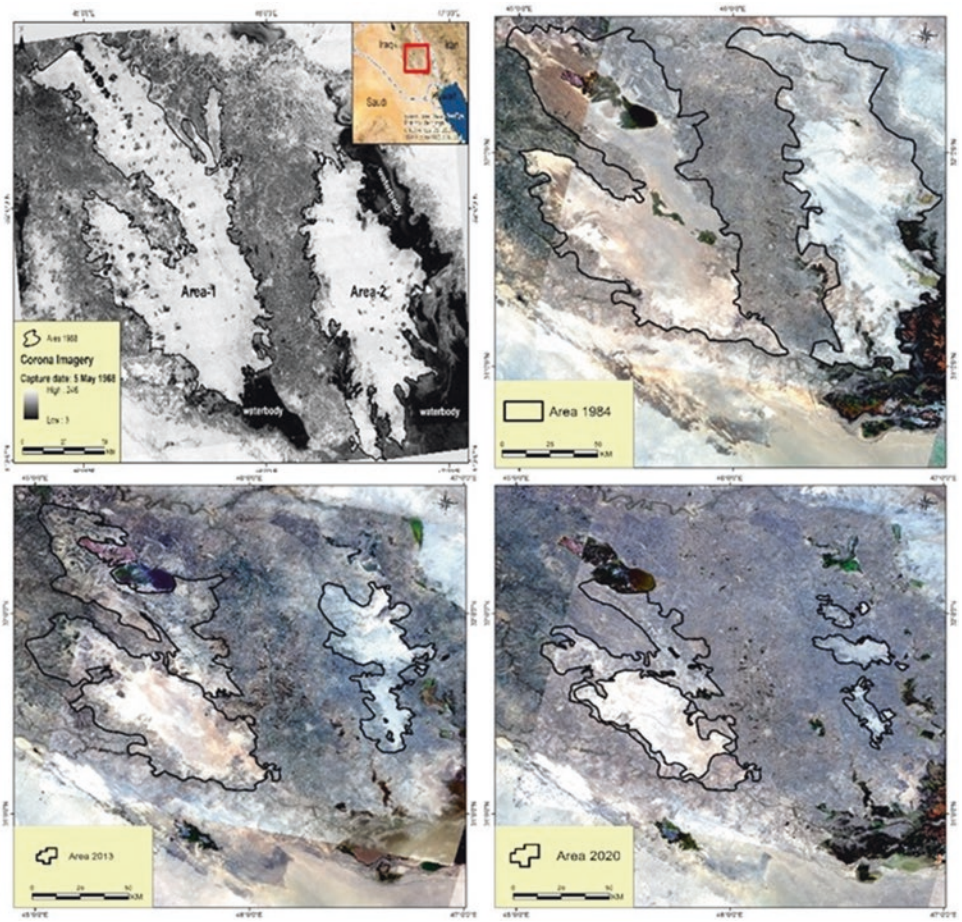

Fig. 2 Satellite images (1968, 1989, 1991, 2000, 2013, and 2020) show the reduction of the hot spots' total area by nearly 65%

into farmland after it was infested with creeping sands. The mechanical techniques will include Mud cover, Earthen mounds, and establishing water channels. The Biological method included the production of native and drought-resistant plants. The following species have been cultivated in this region and have yielded encouraging results: *Prosopis* sp., *Ethyl Tamarix Articulata*, *Rugby Atriplex* sp., and *Blink Tamarix passerinoides*. The shrubs that grow naturally in the region are *Shnan Slidizia* sp. and *Jabbagab Cornolaca* sp.

5 Conclusions

It was observed that the hot spot source areas for SDS were reduced in size since areas since 1968 by around 65%. However, the area is still an active source of SDS, affecting more than 45 million people in downwind regions, including southern Iraq, Ahwaz in Iran, Kuwait, the eastern side of Saudi, Qatar, Bahrain, and UAE. Therefore, stabilizing the area using mechanical and biological methods will cause the reduction of SDS by 20–30% in the affected areas.

References

Al-Dousari, A. M., Aba, A., Al-Awadhi, S., Ahmed, M., & Al-Dousari. N. (2016). Temporal and spatial assessment of pollen, radionuclides, minerals and trace elements in posited dust within Kuwait. *Arabian Journal of Geosciences, 9*, 95. https://doi.org/10.1007/s12517-015-2182-z.

Al-Dousari, A. M. (2009). Recent studies on dust fallout within preserved and open areas in Kuwait. In: Bhat, N., Al-Nasser, A., & Omar, S. (Eds.), *Desertification in Arid lands: Causes, consequences and mitigation* (pp. 137–147). Kuwait: Kuwait Institute for Scientific Research.

Al-Dousari, A. M., & Al-Hazza, A. (2013). Physical properties of aeolian sediments within major dune corridor in Kuwait. *Arabian Journal of Geosciences, 6*(2), 519–527.

Al-Dousari. (2005). Causes and indicators of land degradation in the north-western part of Kuwait. *Arabian Gulf of Scientific Research*, *23*(2), 69–79.

Al-Dousari, A. M., Al-Awadhi, J., & Ahmed, M. (2013). Dust fallout characteristics within global dust storms major trajectories. *Arabian Journal of Geosciences, 6*(10), 3877–3884.

Al-Dousari, A. M., et al. (2004). *Analysis of dustfallout data and sediments in Kuwait* (pp. 21–24). International conference on Atmospheric Pollution.

Al Awadhi, J., Al-Dousari, A., & Khalaf, F. I. (2014). Influence of land degradation on the local rate of dust fallout in Kuwait. *Atmosphere and Climate Sciences, 3*, 10.

Al-Dousari, A. M., & Al-Awadhi, J. (2012). Dust fallout in northern Kuwait, major sources and characteristics. *Kuwait Journal of Science and Engineering, 39*(2A), 171–187.

Al, D. A., et al. (2019). Off-road vehicle tracks and grazing points in relation to soil compaction and land degradation. *Earth Systems and Environment, 16*(5), 2415–2426.

Al-Hemoud, A., et al. (2020). Sand and dust storm trajectories from Iraq Mesopotamian flood plain to Kuwait. *Science of the Total Environment, 710*, 136–291.

Al Dousari, A., & Al Dousari, N. (2021). Deposited dust. In: *Atlas of fallen dust in Kuwait* (pp. 47–56). https://doi.org/10.1007/978-3-030-66977-5_2.

Al-Dousari, A., Ramadan, A., Al-Qattan, A., Al-Ateeqi, S., Dashti, H., & Ahmed, M. (2020). Cost and effect of native vegetation change on aeolian sand, dust, microclimate and sustainable energy in Kuwait. *Journal of Taibah University for Science, 14*, 628–639.

Al-Awadhi, J. M., Al-Dousari, A., & Al-Enezi, A. (2000). Barchan dunes in northern Kuwait. *Arab Gulf Journal of Scientific Reseach, 18*(1), 32–40.

El Wahab, R., Al-Rashed, A.R., & Al Dousari, A. (2018). Influence of physiographic factors, vegetation patterns and human impact on aeolian landforms in arid environment. *Arid Ecosystem, 8*(2).

Nutrient Dynamics in a Tropical Estuary Under a Semiarid Climate

Maria Aparecida Pereira Santos, Ana Celia Maia Meireles, Lyndyanne Dias Martins, Francisca Denise Pereira Almeida, Vinícius Pereira Bacurau, Willian Avelino Lopes, Felipe Dos Santos Gonçalves, Jorge Marcell Coelho Menezes, Francisco José Da Silva Dias, and Francisco José De Paula Filho

Abstract

This study aimed to analyze the temporal (Eurelian) and spatial (Lagrangian) distribution of hydrochemical parameters (pH, temperature (T), dissolved oxygen (DO), turbidity (NTU), salinity (S), total nitrogen (TN), and total phosphorus (TP) in the Parnaíba River Delta (PRD). The sampling campaign was conducted at neap tide in six sampling sites (P1 to P6) along the tidal cycle (ebb/flood) in September 2019. The physicochemical parameters were measured in situ with portable multi-parameter probes while the nutrient fractions (TN and TP) were quantified in the laboratory. Data were subjected to statistical analysis with the Past software (version 4.03). The hydrochemical parameters were similar at both tides. TN and TP had maximum values of 7.42 μmol/L and 1.08 μmol/L, respectively. The N:P ratio showed that the estuarine waters were nitrogen-limited. The PCA results showed that the tested parameters behaved similarly in the two approaches of the study. In both methods, TN, turbidity, and TP were positively correlated with each other and negatively correlated with pH, DO, and temperature. Estuarine biogeochemical processes of nutrient assimilation by primary producers lead to the conversion of such nutrients into organic matter, which can, in turn, lead to increased turbidity. Higher concentrations of TN and TP were observed in the innermost areas of the estuary. Studies and direct measurements of primary productivity inside the estuary are yet to be conducted and may contribute to clarifying nutrient dynamics in the water column. These patterns will guide and support the evaluation of nutrient intake at the continent-ocean interface in the estuary.

Keywords

Tropical Estuaries · Nutrients · Hydrogeochemistry · Hydrodynamic approach · Parnaíba River Delta

1 Introduction

Estuarine ecosystems are open systems with a constant flow of matter and energy. They are also responsible for a range of physical, chemical, and biological processes that are essential for the maintenance and balance of the environment. As a result, the United Nations (UN) established the Decade of Ocean Science between 2021 and 2030 (Brasil., 2021).

The continent-ocean interfaces are transport routes for materials between land and sea and include several processes that influence the natural dynamics of these systems. As open systems, estuaries have a constant flow of matter and energy, responsible for various physical, chemical, and biological processes essential for maintaining the environment. Estuarine systems stand out from others in the coastal zone because of their high biological productivity (Braga et al., 2000; Pereira-Filho et al., 2003). In these systems, we find a complexity of biogeochemical processes due to the variability of biotic-abiotic interactions between the water column and the sediment (De Paula Filho et al., 2020; Telesh & Khlebovich, 2010).

The Parnaíba River Delta, located in the semiarid Brazilian northeast, is a complex mosaic of ecosystems intersected by bays and estuaries flowing into the Atlantic Ocean through five main channels. It has a meso-tidal regime with a tidal height of up to 2.8 m (ANA - Agência Nacional de Águas, 2012). The Delta has a unique

M. A. P. Santos · A. C. M. Meireles · L. D. Martins · F. D. P. Almeida · V. P. Bacurau · W. A. Lopes · F. Dos Santos Gonçalves · J. M. C. Menezes · F. J. De Paula Filho (✉)
Federal University of Cariri, Ceará, Brazil
e-mail: francisco.filho@ufca.edu.br

F. J. Da Silva Dias
Federal University of Maranhão, Maranhão, Brazil

A. Çiner et al. (eds.), *Recent Research on Environmental Earth Sciences, Geomorphology, Soil Science, Paleoclimate, and Karst*, Advances in Science, Technology & Innovation, https://doi.org/10.1007/978-3-031-42917-0_44

environmental importance for the Brazilian coast, as it serves as a breeding area for several marine species and provides various ecosystem services such as coastal zone protection, water supply and purification, and climate regulation. For that reason, it is protected by law (De Paula Filho et al., 2020).

Anthropic actions interfere with natural estuarine dynamics, impacting them both by destroying the landscape and adding chemical species that can compromise the system's balance. Therefore, this study mainly evaluated nutrient dynamics (nitrogen and phosphorus) in the Parnaíba River Delta estuary using spatial and temporal approaches involving their total concentrations and hydrochemical parameters.

2 Materials and Methods

The instantaneous outflows were measured using an ADCP (Acoustic Doppler Current Profiler/SONTEK/YSI) current meter. Subsurface and bottom water samples were duplicated at six points (P1 to P6) from the mouth to the mainland. The Lagrangian and Eurelian approaches were adopted to evaluate the influence of the estuarine gradient on the behavior of nutrients and hydrochemical parameters in a tidal cycle. In this approach, it was possible to determine how the concentrations behaved along a complete tidal cycle (Dias et al., 2013). A Van Dorn bottle was used for bottom water sampling, and the samples were stored in polyethylene bottles. The physicochemical parameters were measured in situ with portable multi-parameter probes, while the nutrient fractions (TN and TP) were quantified according to Valderrama (1981). The relative molar concentrations of N and P have been used to estimate which of these nutrients is limiting the growth of algae in aquatic systems (Redfield, 1934).

3 Results

In general, the parameters monitored during the tidal cycle showed little variability. (Table 1). Values of zero salinity were found near the Delta's mouth (P1).

In the (spatial) Lagrangian approach, the results obtained by multivariate statistical principal component analysis (PCA) showed that TN, turbidity, and TP are positively correlated with each other (Fig. 1) and that dissolved oxygen concentrations are inversely correlated to said parameters. Their behavior was similar under the Eurelian approach, highlighting the strong association between nutrient concentrations and turbidity.

The dissolved oxygen content (DO) ranged from 4.8 to 12.1 mg $L-^{1}$, considering both the flood and ebb tides, showing good water oxygenation.

The pH readings were similar to those reported for tropical estuaries on the northeastern Brazilian coast. A salinity gradient was observed following the fluvial flow, where salinities higher than the oceanic average occurred only at P1 (37.3 mg kg^{-1}). In 60% of the analyzed samples, the N:P ratio showed nitrogen limitation.

4 Discussion

Higher concentrations of TN and TP were observed at the sampling sites located at the innermost areas of the estuary (P5 and P6), directly correlating with turbidity. It seems apparent that the sea dams the fluvial water masses inside the estuary during the dry season. The results obtained through the multivariate analysis show a correlation where waters with higher nutrient concentrations tend to present higher turbidity values. The excess of turbidity affects the aquatic biota, as it may affect the luminosity conditions in the water column, thus interfering with the metabolism of

Table 1 Descriptive statistics of the parameters evaluated in the Parnaíba River delta

Approach	pH	*T* (°C)	*S* (g $kg-^{1}$)	DO (mg L^{-1})	Turbidity (NTU)	TP (mg $L-^{1}$)	TN (mg L^{-1})
Lagrangian	7.1–8.4	27–29	0–33.1	6.4–7.8	0.4–19.6	n.d. – 0.7	n.d. – 2.9
	7.8 ± 0.5	29 ± 0.7	10.1 ± 14.3	7.0 ± 0.38	6.7 ± 6.4	0.1 ± 0.2	0.8 ± 0.7
Eulerian	7.0–8.6	27–29	0.03–37.4	4.8–12.1	5.92–21.3	n.d. – 0.1	n.d. – 3.23
	7.8 ± 0.5	28 ± 0.6	9.7 ± 13.7	7.3 ± 1.6	12.3 ± 3.29	0.01 ± 0.04	0.74 ± 0.57

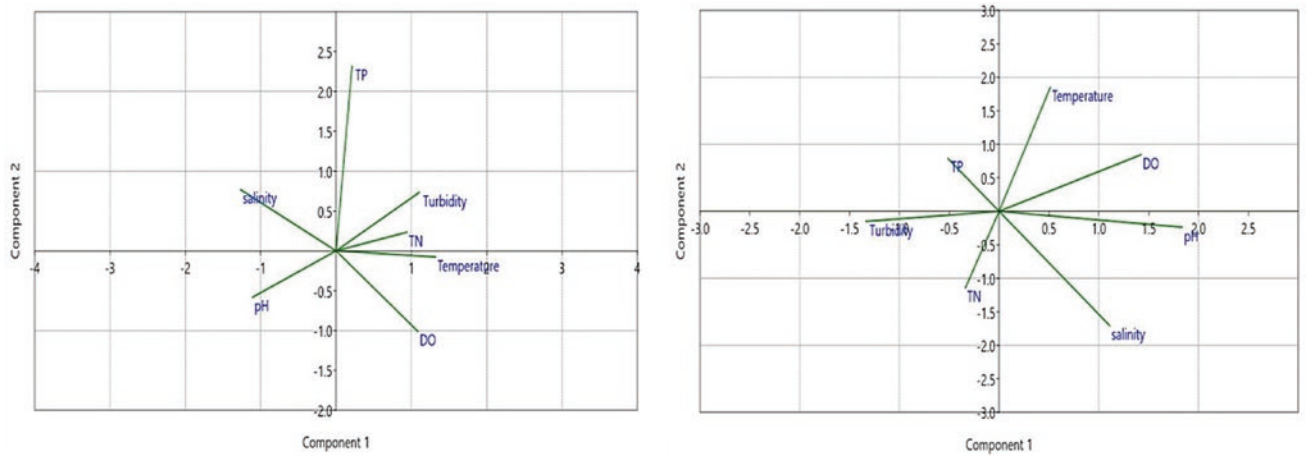

Fig. 1 Principal component analysis (PCA) of the parameters monitored under the Lagrangian (**a**) and Eurelian (**b**) approaches during a tidal cycle

underwater autotrophic organisms by hindering photosynthesis (De Paula Filho et al., 2020).

5 Conclusions

In general, the monitored hydrochemical variables did not show high variability, except for salinity, considering that during the dry season, there are lesser river discharges. TN, TP, and Turbidity showed a significant positive correlation with each other both spatially and temporally. On the other hand, DO is negatively correlated with higher nutrient concentrations in estuarine waters. The N:P results demonstrate the Parnaiba River Delta is a highly dynamic environment regarding nutrient availability.

Acknowledgements This study was supported by the Fundação Cearense de Apoio ao Desenvolvimento Científico e Tecnológico—FUNCAP (Grant No. BP4-00172-00080.01.00/2) and Conselho Nacional de Desenvolvimento Científico e Tecnológico—CNPq (Grant No. 408363/2018-5).

References

ANA - Agência Nacional de Águas. (2012). Panorama da qualidade das águas superficiais no Brasil, Brasília, https://www.ana.gov.br/textos-das-paginas-do-portal/publicacoes. 2021/05/21.

Brasil. Ministério da Ciência e Tecnologia, inovação e comunicação. Década da Ciência Oceânica. Retrieved April 21, 2021, from http://decada.ciencianomar.mctic.gov.br/.

Braga, E. S., Bonetti, C. V. D. H., Burone, L., & Bonetti Filho, J. (2000). Eutrophication and bacterial pollution caused by industrial and domestic wastes at Baixada Santista estuarine system – Brazil. *Marine Pollution Bulletin, 40*(2), 165–173.

De Paula Filho, F. J., Marins, R. V., Chicharo, L., Souza, R. B., Santos, G. V., & Braz, E. M. A. (2020). Evaluation of water quality and trophic state in the Parnaíba River Delta, northeast Brazil. *Regional Studies in Marine Science*, *34*

Dias, F. J. S., Marins, R. V., & Maia, L. P. (2013). Impact of drainage basin changes on suspended matter and particulate copper and zinc discharges to the ocean from the Jaguaribe River in the Semiarid NE Brazilian Coast. *Journal of Coastal Research, 29*(5), 1137–1145.

Pereira-Filho, J., Spillere, L. C., & Schettini, C. A. F. (2003). Nutrient dynamics in the region of Itajaí Harbour, SC. *Atlântica, Rio Grande, 25*(1), 11–20.

Redfield, A. C. (1934). On the Proportion of organic derivatives in sea water and their relation to the composition of plankton. *James Johnston Memorial Volume*. University Press of Liverpool, 26–77.

Telesh, I. V., & Khlebovich, V. V. (2010). Principal processes within the estuarine salinity gradient: A review. *Marine Pollution Bulletin, 61*, 149–155.

Valderrama, J. C. (1981). The simultaneous analysis of total nitrogen and total phosphorus in natural waters. *Marine Chemistry, 10*(2), 109–122.

A Model for Quantitative Recovery of Paleoclimate Evolution Using Pollen Assemblage: A Case Study of the Fourth Member of the Shahejie Formation in the Chezhen Depression

Tao Chen and Jinliang Zhang

Abstract

In this paper, a quantitative reconstruction model of paleoclimate evolution is proposed. The model combines the advantages of pollen climate analysis and coexistence analysis. It analyzes the evolution trend of paleoclimate and uses the climate parameters of extant nearest relative genera to reconstruct the paleoclimate during the geological time quantitatively. Based on this model, the climatic parameters and evolution of the fourth member of the Eocene Shahejie Formation in the Chezhen Depression of the Bohai Bay Basin were quantitatively analyzed. The results of pollen climate analysis showed that the fourth member of the Shahejie Formation was in a warm and humid evolutionary stage, accompanied by alternating dry and humid, warm and cold evolution. In addition, the paleoclimatic parameter values of the fourth member of the Shahejie Formation in the Chezhen Depression were recovered quantitatively. The quantitative reconstruction of climate parameters can provide a more intuitive understanding of the geological background of the study area and further guide oil and gas exploration and development.

Keywords

Pollen · Coexistence analysis · Quantitative reconstruction · Paleoclimate evolution

1 Introduction

Paleoclimate is the main depositional driver of stratigraphic formation in terrestrial basins, and it somewhat controls the lake basin sedimentation type. Hence, paleoclimate reconstruction has an irreplaceable indicative role in oil and gas exploration. Consequently, paleoclimate has been the focus of palaeosedimentary environmental analysis. The application of many research methods, such as petrological, geochemical, and micropaleontological methods, has led to the rapid development of paleoclimate-related studies (Alexandrine et al., 2019; Huth et al., 2020). In microsomal paleontology, pollen type composition and abundance are considered important and effective indicators of paleoclimate. In this study, a quantitative paleoclimate reconstruction model using pollen is proposed and applied to the fourth member of the Shahejie Formation (Es4) in the Chezhen Depression by combining the advantages of pollen climate analysis and coexistence analysis.

2 Model Principle and Establishment

The nearest relative genus approach (Mosbrugger & Utescher, 1997; Mosbrugger, 1999) is used here to determine the fossil pollen climatic parameters. The climatic significance of pollen can be illustrated by combining specific climatic parameters. For example, select climate parameters to establish temperature evolution index T and humidity evolution index H, respectively. The absolute dominant taxa were chosen to perform quantitative reconstruction through the superimposed coexistence interval method (Mosbrugger & Utescher, 1997), and the resulting climatic parameters are the paleoclimatic conditions during the survival of the fossil pollen.

T. Chen · J. Zhang (✉)
Faculty of Geographical Science, Beijing Normal University, Beijing 100875, China
e-mail: jinliang@bnu.edu.cn

A. Çiner et al. (eds.), *Recent Research on Environmental Earth Sciences, Geomorphology, Soil Science, Paleoclimate, and Karst*, Advances in Science, Technology & Innovation, https://doi.org/10.1007/978-3-031-42917-0_45

3 Model Case Application

The model was applied to the Es4 in the Chezhen Depression. The pollen types and groupings selected are shown in Table 1. The results of pollen climate analysis showed (Fig. 1) that the Es4 as a whole was in a warm and humid evolutionary stage, accompanied by alternating dry and humid, warm and cold evolution. The climatic evolution of the Es4 was finely divided: in terms of temperature evolution, the Es4 went through the evolutionary stages of alternating warm and hot, continuous hot, continuous warm, and continuous hot; in terms of humidity evolution, the Es4 went through the evolutionary stages of alternating dry and wet, continuous wet, alternating dry and wet, continuous wet, continuous dry, and continuous wet. After selecting the absolute dominant species superposition interval, the climatic parameters of the Es4 in the Chezhen Depression were obtained as follows: the mean annual temperature (MAT) from −9.2 to 21.6 °C, the mean monthly coldest temperature (CMT) from −22.7 to 13.2 °C, the mean monthly warmest temperature (WMT) from 13.7 to 28.3 °C, the mean annual precipitation (MAP) from 201 to 1741 mm, the monthly wettest precipitation (WMP) from 33 to 293 mm, the driest monthly precipitation (DMP) from 5 to 94 mm.

4 Discussion

Coexistence analysis methods have been widely used for paleoclimate reconstruction based on Eurasian fossil plant assemblages. Studies based on coexistence methods have significantly impacted the literature, with over 10,000 citations to date (Grimm & Potts, 2016). However, the coexistence analysis is controversial due to the violation of certain basic assumptions, but what can be agreed upon is that the method is better for reconstructing younger flora. Furthermore, the results are more reliable (Grimm & Denk, 2012). In addition, the results obtained from the coexistence analysis in this study will be validated by the pollen climate analysis, so it is considered that the model applies to the Eocene and younger flora, and the results are more accurate and reliable.

5 Conclusions

(1) Combining pollen climate analysis and coexistence analysis, a method of quantitative paleoclimate reconstruction using pollen is summarized and proposed, which is more applicable to Eocene and younger flora with accurate results.
(2) The climatic evolution of the Es4 in the Chezhen Depression was refined and analyzed based on the trends of temperature index T and humidity index H. As a result, the temperature evolution of the Es4 can be divided into four stages, and the humidity evolution into six stages.
(3) The climatic parameters of Es4 in the Chezhen Depression are the MAT (−9.2 to 21.6 °C), MCT (−22.7 to 13.2 °C), MWT (13.7 to 28.3 °C), MAP (201 to 1741 mm), WMP (33 to 293 mm), and DMP (5 to 94 mm).

Table 1 Quantitative classification of the climate indicator significance of pollen. The subscript med represents the median of the interval

Climate indicator type	Division basis	Fossil pollen
Hot climate group	$MAT_{med} > 15$ ℃, $CMT_{med} > 5$ ℃	*Liquidambarpollenites*, *Ephedripites*, *Taxodiaceaepollenites, Taxodiaceaepollenites hiatus*
Warm climate group	10 ℃ < MAT_{med} < 15 ℃, 0 ℃ < CMT_{med} < 5 ℃	*Quercoidites*, *Ulmipollenites*, *Juglanspollenites*
Cold climate group	$MAT_{med} < 10$ ℃, $CMT_{med} < 0$ ℃	*Alnipollenites*, *Piceapollis*, *Pinuspollenites*, *Abietineaepollenites*, *Betulaepollenites, Betulaceoipollenites*
Xerophytic group	$MAP_{med} < 1200$ mm, $DMP_{med} < 100$ mm	*Alnipollenites*, *Ephedripites*, *Pinuspollenites*, *Abietineaepollenites*, *Rutaceoipollenites*
Wet group	$MAP_{med} > 1200$ mm, $WMP_{med} > 200$ mm	*Liquidambarpollenites*, *Quercoidites*, *Juglanspollenites*, *Taxodiaceaepollenites, Taxodiaceaepollenites hiatus, Piceapollis*

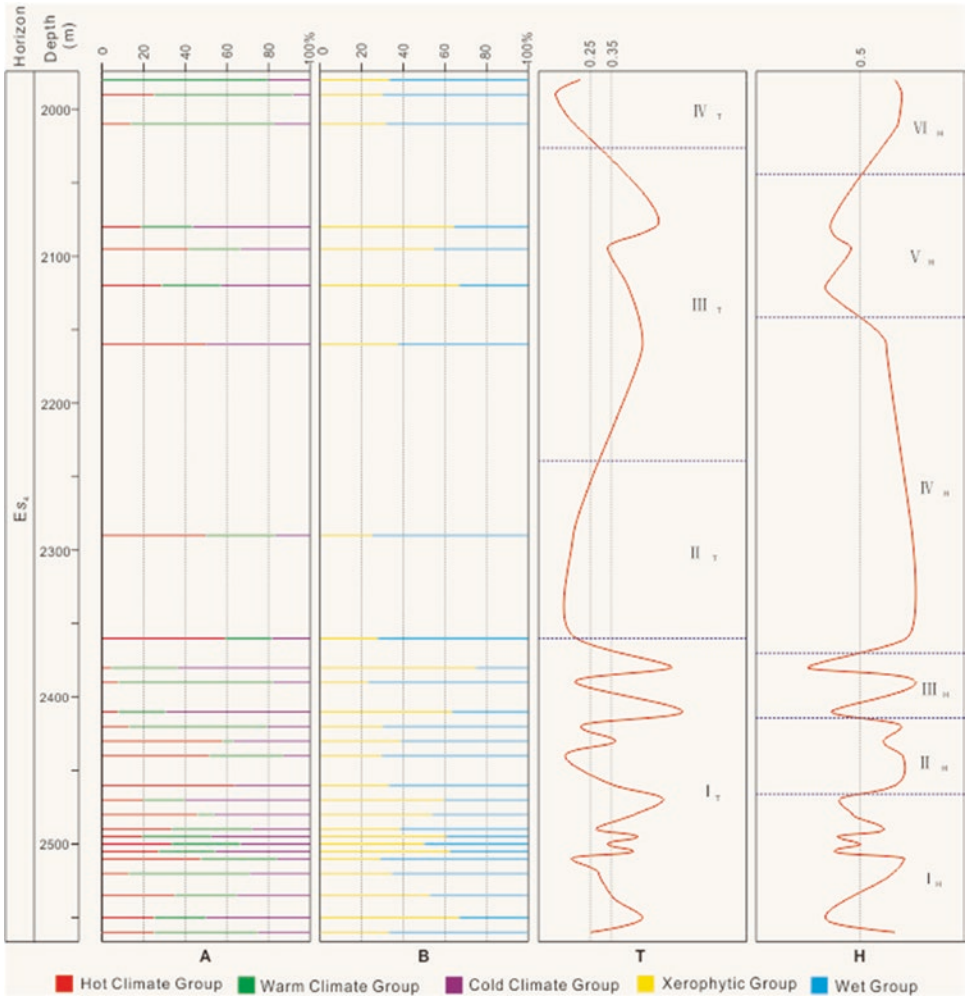

Fig. 1 Climate evolution map of the fourth member of Shahejie formation in Chezhen depression

References

Alexandrine, N., Simon, N., & Gabriel, N. (2019). The late Pleistocene – Holocene paleoclimate reconstruction in the Adamawa plateau (Central Cameroon) inferred from the geochemistry and mineralogy of the Lake Fonjak sediments. *Journal of African Earth Sciences, 150*, 23–36.

Grimm, G. W., & Denk, T. (2012). Reliability and resolution of the coexistence approach—A revalidation using modern-day data. *Review of Palaeobotany and Palynology, 172*, 33–47.

Grimm, G. W., & Potts, A. J. (2016). Fallacies and fantasies: The theoretical underpinnings of the Coexistence Approach for palaeoclimate reconstruction. *Climate of the past, 12*(3), 611–622.

Huth, T. E., Cerling, T. E., Marchetti, D. W., Bowling, D. R., Ellwein, A. L., Passey, B. H., Fernandez, D. P., Valley, J. W., & Orland, I. J. (2020). Laminated soil carbonate rinds as a paleoclimate archive of the Colorado Plateau. *Geochimica Et Cosmochimica Acta, 282*, 227–244.

Mosbrugger, V., & Utescher, T. (1997). The coexistence approach: A method for quantitative reconstructions of Tertiary terrestrial palaeoclimate data using plant fossils. *Palaeogeography, Palaeoclimatology, Palaeoecology, 134*(1/4), 61–86.

Mosbrugger, V. (1999). The nearest living relative method. In T. P. Jones & N. P. Rowe (Eds.), *Fossil plants and spores: Modern techniques* (pp. 261–265). Geological Society.

Meghalayen Climate and Environment Changes Inferred from Geochemical, Paleontological, and Sedimentological Proxies of Lagoonal Sediment Sequences of the Thapsus Coast (Eastern Tunisia)

Mohamed Kamoun, Martin R. Langer, Chahira Zaibi, Mohamed Ben Youssef, Amjad Kallel, and Fekri Kamoun

Abstract

This study presents paleoenvironmental results from three radiocarbon-dated lagoonal sedimentary sequences from the Thapsus lagoon in the southern Gulf of Monastir (Tunisia). Variations in major and trace element concentrations and foraminifera associations coupled with measurements of grain size, total nitrogen (TN), total organic carbon (TOC), total inorganic carbon (TIC), and atomic TOC/TN ratios (C/N) were conducted to reconstruct the climate since ~3900 cal yr BP. In addition to a regional drying trend in the late Holocene, five distinct climatic and environmental stages were recorded: (i) between 120.000 and 3993 cal yr BP, after the deposition of the marine carbonate sandstones in an open marine embayment (Upper Pleistocene, marine isotopic substage 5e), the Rass Dimasse coast continued to emerge as a result of reactivated border faults and tectonic uplift; (ii) Toward 3993 cal yr PB, a first marine transgression was detected across the emerged landscape as evidenced by the dominance of the marginal/marine (50%) and marine/brackish (40%) foraminifera. The presence of clastic materials and poorly sorted fine sands indicate high energy conditions and reduced values of the fluvial K/Al, Rb/Al, and Mg/Al elemental ratios mark a period of aridity; (iii) between 3993 and 2203 cal yr PB, the increase of brackish/marine foraminifera coupled with high abundance values (900 ind./2gr) indicate a closure of the lagoon and more restricted conditions. The elemental ratios of marine Cl/Al, Ca/Al, Na/Al, S/Al, and fluvial K/Al, Mg/Al, and Rb/Al, combined with the high Ba/Al productivity ratios, suggest a humid period and an inflow of oxygenated water through a tidal channel; iv) toward 1242 cal yr BP in age, the sediments reveal marked changes in element ratios indicative for substantial aeolian input (Ti/Al, Zr/Al, and Si/Al ratios). Also, proxies for Redox conditions (V/Al, Mn/Al, and Fe/Al ratios) suggest reducing fluvial input and decreasing the marine water circulation intensity. At 1242 cal yr BP, this stage led to the present-day semi-enclosed lagoon setting where coastal drift currents and the development of a sandspit started to control the lagoonal dynamics and water salinity. The lagoon was progressively filled with medium-sized sand. The lagoonal fauna at this stage is characterized by the dominance of marine/brackish foraminifera and a reduction of species richness and abundance values; v) Finally, during the Little Ice Age, the decrease of redox proxy ratios (V/Al, Mn/Al, and Fe/Al) suggests increasing bottom-water oxygenation conditions. A moderate rise of fluvial elemental ratios points to a humid period. The present-day Rass Dimasse lagoon is impacted by the rising sea level, exceptional tides, and intense storms, despite being positioned behind an extensive sandspit.

Keywords

Foraminifera · Thapsus · Sandspit · Sediment dynamics · Lagoon · Holocene · Sea-level

M. Kamoun (✉) · C. Zaibi · F. Kamoun
GEOGLOB Laboratory, Faculty of Sciences of Sfax, Sfax University, BP 1171, 3000 Sfax, Tunisia
e-mail: med23km@yahoo.fr

M. Langer
Institut Für Geowissenschaften, Paläontologie, Universität Bonn, Nussallee 8, 53115 Bonn, Germany

M. Ben Youssef
Water Researches and Technologies Center, Borj Cedria, Tunisia

A. Kallel
Sfax National School of Engineering, 3000 Sfax, Tunisia

A. Çiner et al. (eds.), *Recent Research on Environmental Earth Sciences, Geomorphology, Soil Science, Paleoclimate, and Karst*, Advances in Science, Technology & Innovation, https://doi.org/10.1007/978-3-031-42917-0_46

1 Introduction

Holocene sequences of coastal wetland sediments from Tunisia were shown to preserve a detailed record of sea level variations, climate change, the process of sedimentary dynamics, and anthropogenic forcings (Anzidei et al., 2011; Ben Khalifa et al., 2019; Jedoui et al., 1998; Kamoun et al., 2020; Khadraoui et al., 2019; Martinez-Ruiz et al., 2015; Zaïbi et al., 2016). The sedimentary deposits contain well-preserved and abundant benthic foraminifera, a group of organisms widely used to infer past palaeoenvironmental conditions in lakes, lagoons (Zaïbi et al., 2016), estuaries, and sebkhas from Tunisia (Ben Khalifa et al., 2019). The foraminiferal assemblages preserve a record of environmental change, and their analyses have provided new information on the impact of natural and anthropogenic forcings. Our objectives were to (1) trace the history of coastal environmental change at Thapsus, (2) reconstruct the shoreline evolution related to natural processes such as sedimentary dynamics, climate change, and eustatic variation, (3) correlate major events with those recognized at other sites along the Mediterranean coast.

2 Environmental Setting

Thapsus was a Roman harbor city on the eastern coast of Tunisia. It is located 10 km north of Mahdia city. The present-day Thapsus coast reveals (Fig. 1): (i) a coastal plain rich in archaeological sites, (ii) a coastline showing the outcrops of Upper Pleistocene marine sediment deposits, (iii) a shallow-water lagoon situated in front of the archeological Thapsus site, (iv) a 6 km long sandspit protecting the shallow lagoon; (v) the open sea which is characterized by dense seagrass meadows of *Posidonia oceanica*.

3 Material and Methods

For paleoenvironmental analysis, we have selected core RD8 due to its microfauna richness, total length, and radiocarbon-dated levels, and we describe its sediment types, grain size, and fossil content. For micropaleontological analysis, at least 300 specimens of foraminifera were picked from each sample. Grain sizes and geochemical characteristics, such as the concentration values of the marine elements Ca, Cl, and Sr and the terrigenous elements Fe, Ti, Al, Si, and K (Jedoui et al., 1998), are provided with relevant information on sources and detrital input variations. For the identification of foraminifera, we follow (Cimerman & Langer, 1991).

4 Results

Core RD8 has a total length of 130 cm long and consists of five lithological units (Figs. 2 and 3).

Unit U1: corresponds to white carbonate sandstones, is Upper Pleistocene in age, and is commonly referred to as the Tyrrhenian series, which outcrops at Thapsus and Chebba. Unit U2, ~3990 calyr BP in age, is deposited directly above the erosional contact on the white carbonate sandstone. Sediments of U2 are rich in molluscs and lithoclastes but marked by poorly sorted grain types (fine sands ~30% and medium sands ~20%). U2 is characterized by abundant benthic foraminifera, including shallow-water indicators such as *Ammonia* (30%) and *Elphidium* (30%). U2 also revealed reduced values of aeolian (Ti/Al, Zr/Al, and Si/Al) and fluvial (K/Al, Rb/Al) element ratios. The composition of the foraminiferal faunal assemblages and the element ratio values indicate the development of a nearshore shallow-water environment following a marine

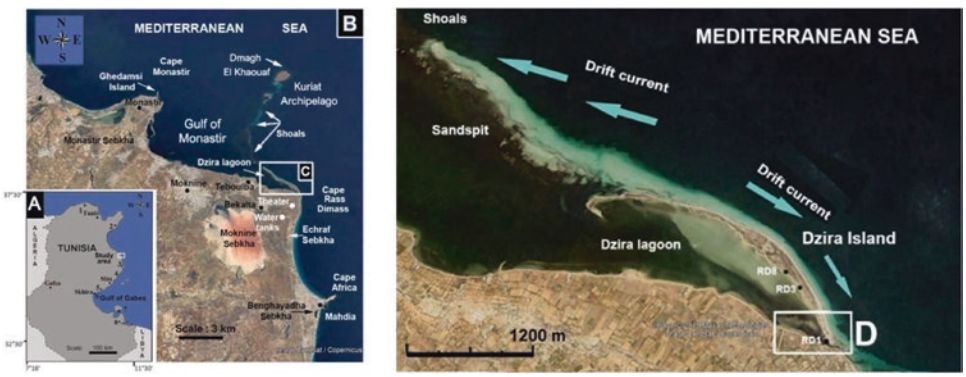

Fig. 1 **a** Location map of the study area along the coast of Tunisia; **b** coastal area between Monastir and Mahdia with the location of the Dzira lagoon north of Rass Dimass, **c** (rectangle). **d** Google Earth Image showing the sandspit protecting Dzira Lagoon, the location of Core RD8 and the shallow entrance of the tidal channel at the SE corner of the rectangle

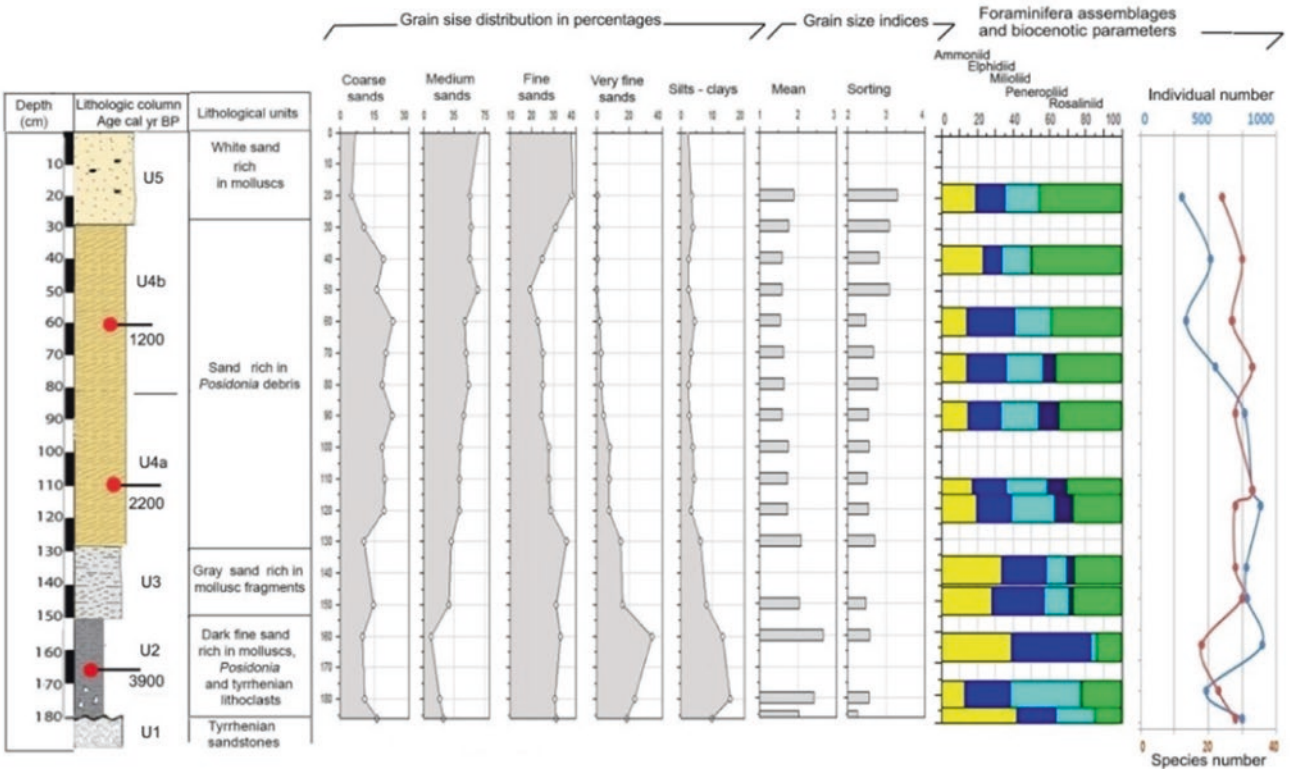

Fig. 2 Lithologic columns and lithological units of core RD 8

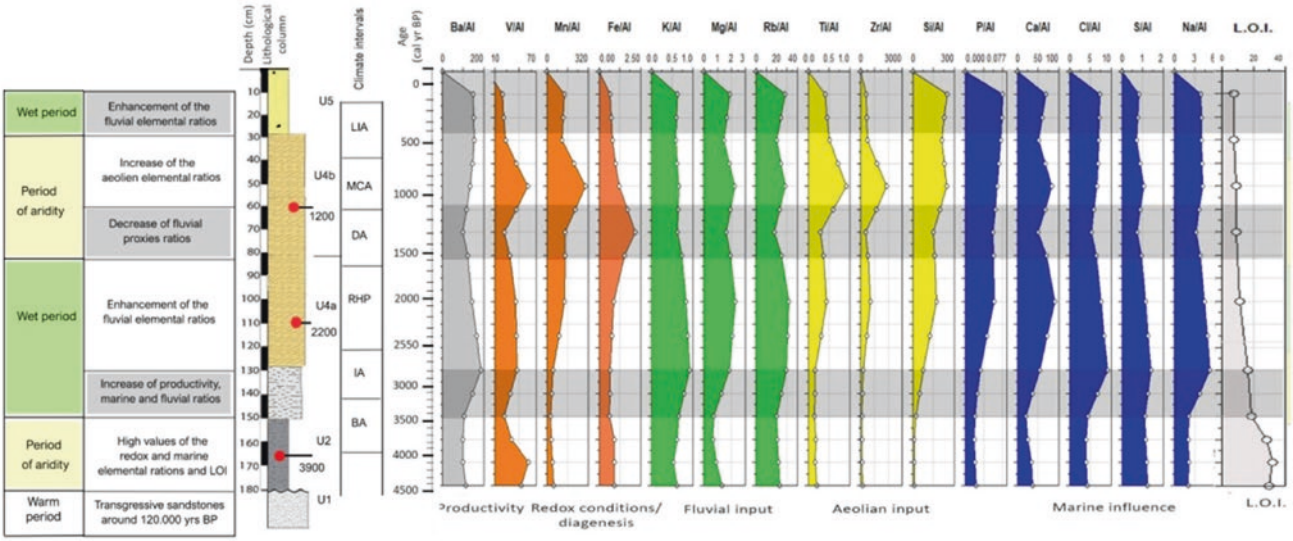

Fig. 3 Geochemical data for core RD8

transgression. According to Kamoun et al. (2020) and (Martinez-Ruiz et al., 2015), the Holocene marine transgression peaked at around 3550–4050 cal yr BP in southeastern Tunisia and other parts of the Mediterranean coast.

Unit U3 was rich in mollusc fragments, revealed decreasing percent values for silt, clay, and very fine sand, and fell into the very poorly sorted sediments category.

U3 shows progressively increasing marine (Cl/Al, Ca/Al, Na/Al) and fluvial (K/Al, Mg/Al, Rb/Al) element ratios.

These results, coupled with the high Ba/Al productivity ratio, suggest an inflow of oxygenated water.

Unit U4a, ~2200 cal yr BP in age, reveals enrichment of medium (45%) and coarse sands (20%) and shows the highest values for species richness and foraminiferal abundance. U4a is also characterized by increasing values in epiphytic peneroplids (10%) and by decreasing abundances of ammonia foraminifera. The interval between 130 and 80 cm records high K/Al, Mg/Al, and Rb/Al values.

Unit U4b, ~1200 cal yr BP in age, records increasing values for P/Al and Ca/Al ratios and higher numbers of ammonia foraminifera (20%). Symbiont-bearing epiphytic peneroplids are absent in this interval. The total number of species and individuals decreases, suggesting that the exchange of waters from the lagoon to the open sea became more restricted. An increase in the values of aeolian input proxies marks U4b. Along the 80 cm of U4b, K/Al, Mg/Al, and Rb/Al values decrease slightly, suggesting a reduction of fluvial input and/or variations in the intensity of circulating waters.

Unit U5 consists of sands rich in molluscs debris. It reveals a low number of species and individuals and is marked by the dominance of rosaliniid foraminifers (45%). Species of *Rosalina* are indicators for phytal substrates (Langer, 1993)). Percent abundances of ammoniid (20%), elphidid (15%), and miliolid foraminifera (20%) are 20%, 15%, and 20%, respectively, and their composition is indicative of shallow water and restricted conditions [11; 12] (Langer et al., 2013; Lipps & Langer, 1999). U5 is characterized by decreasing values for aeolian and redox conditions proxies, suggesting increasing rates of bottom-water oxygenation during this time interval. A moderate increase in fluvial elemental ratios has also been recorded.

5 Conclusions

This study allowed us to reconstruct the coastal evolution of the Thapsus coast. We dated and identified a first marine transgression at ~3900 cal yr BP, with sediments and marine biotas deposited on top of marine Tyrrhenian sandstones. Around 2200 cal yr BP, a second transgressive event was recorded, as indicated by abrupt changes in foraminifera assemblages. More restricted conditions followed the transgressive event at around 1200 cal yr BP. During the Iron age and the humid Roman Period, an increase in the elemental ratios K/Al, Mg/Al, and Rb/Al suggest a higher fluvial input through paleowadis and a wet period. Our results agree with previous findings corresponding to the Roman Humid Period (RHP). The results from core RD8 can also be correlated with data sets from other Tunisian locations (Ben Hamad et al., 2018), such as the wetlands of Lake Ichkeul, the Medjerda floodplain, and other study sites from central Tunisia. The results of our study also provide evidence for a phase of aridity as marked by increasing eolian proxy values (Ti/Al, Zr/Al, and Si/Al). The multiproxy analyses of the core sediments from Dzira lagoon thus document that the evolution of the coastal area around Thapsus was shaped by a sequence of concerted processes involving climate change and sediment dynamics, comparable to records that affected several Mediterranean regions during the Holocene.

References

Anzidei, M., Antonioli, F., Lambeck, K., Benini, A., Soussi, M., & Lakhdar, R. (2011). New insights on the relative sea level change during Holocene along the coasts of Tunisia and western Libya from archaeological and geomorphological markers. *Quaternary International, 232*, 5–12.

Ben Khalifa, K., Zaïbi, C., Bonnin, J., Carbonel, P., Zouari, K., Mnif, T. & Kamoun, F. (2019). Holocene environment changes in the Hachichina wetland (Gulf of Gabes, Tunisia) evidenced by foraminifera and ostracods, geochemical proxies and sedimentological analysis. *RivistaItaliana di Paleontologia e Stratigrafia, 125*, 517–549.

Ben Hamad, A., Viehberg, F., Khadraoui, A., Zaïbi, C., Trabelsi, Y., Mouanga, G. H., Langer, M. R, Abida, H., & Kamoun, F. (2018). Water level and atmospheric humidity history of lake Ichkeul (northern Tunisia) during the last 3000 years. *Arabian Journal Geosciences, 11*(12), 316

Cimerman, F. & Langer, M. R. (1991). *Mediterranean foraminifera—Academia Scientarium et Artium Slovenica, Dela, Opera 30, Classis IV: Historia Naturalis*(p. 1–119, pl. 1–93). Ljubljana.

Jedoui, Y., Kallel, N., Fontugne, M., Ben Ismail, M. H., M'Rabet, A., & Montacer, M. (1998). A high relative sea level stand in the middle Holocene of Southeastern Tunisia. *Marine Geology, 147*, 123–130.

Kamoun, M., Zaibi, C., Langer R. M., Khadraoui, A., Ben Hamad, A, & Ben Khalifa, K. (2020). Environmental evolution of the Acholla coast (Gulf of Gabes, Tunisia) during the past 2000 years as inferred from palaeontological and sedimentological proxies. *Neues Jahrbuch für Geologie und Paläontologie*, *296*(3).

Khadraoui, A., Zaïbi, C., Carbonel, P., Bonnin, J., & Kamoun, F. (2019). Ostracods and molluscs in northern Sfax coast: Reconstruction of Holocene paleoenvironmental changes and associated forcing. *Geo-Marine Letters*. https://doi.org/10.1007/s00367-019-00576-0

Langer, M. R. (1993). Epiphytic foraminifera. *Marine Micropaleontology, 20*, 235–265.

Langer, M. R., Thissen, J. M., Makled, W. A., & Weinmann, A. E. (2013). Foraminifera from the Bazaruto Archipelago (Mozambique). *Neues Jahrbuch Für Geologie Und Paläontologie, 267*(2), 155–170.

Lipps, J. H., & Langer, M. R. (1999). Benthic foraminifera from the meromitic, Mecherchar Jellyfish Lake, Palau (western Pacific). *Micropaleontology, 45*, 278–284.

Martinez-Ruiz, F., Kastner, M., Gallego-Torres, D., Rodrigo-Gamiz, M., Nieto-Moreno, V., & Ortega-Huertas, M. (2015). Paleoclimate and paleoceanography over the past 20,000 yr in the Mediterranean Sea Basins as indicated by sediment elemental proxies. *QuaternarySci. Rev., 107*, 25–46.

Zaïbi, C., Kamoun, F., Viehberg, F., Carbonel, P., Jedoui, Y., Abida, A., & Fontugny, M. (2016). Impact of relative sea level and extreme climate events on the Southern Skhira coastline (Gulf of Gabes, Tunisia) during Holocene times: Ostracodes and foraminifera associations response. *Journal of African Earth Sciences, 118*, 120–136.

Palaeoclimate and Dietary Niche of Family Cervidae from the Siwaliks (Pakistan): Does Coeval Occurrence of Species Leads to Niche Partitioning?

Muhammad Tahir Waseem, Abdul Majid Khan, Jay Quade, Abdul Ghaffar, and Ghulam Sarwar

Abstract

Biogeochemistry is crucial to reconstruct the climate, diet, and habitats of extinct animals. The Siwalik sediments of Pakistan exhibit an excellent record of faunal elements, providing an opportunity to explore palaeohabitats of diverse mammalian communities that existed in the Siwaliks. This study is the first to investigate the dietary niche and climatic context of the Siwalik cervids from ~5 Ma to ~2 Ma (early Pliocene to early Pleistocene). Tooth enamel of 25 fossil samples belonging to four different species (*R. simplicidens*, *C. sivalensis*, *C. triplidens*, and *C. rewati*) was subjected to carbon ($\delta^{13}C$) and oxygen ($\delta^{18}O$) isotope analysis. Family Cervidae shows significantly different average $\delta^{13}C$ values of −12.2‰, −9.9‰, and 1.0‰ for early Pliocene (~5 Ma), late Pliocene (~3 Ma), and early Pleistocene (~2.2 Ma) time spans, respectively. $\delta^{13}C_{enamel}$ values indicate that cervids preferred a close habitat and preferably browsed on C_3 vegetation in forested parts of the fan during the early Pliocene, with the gradual shift toward increasing C_4 vegetation in diet and more open habitat over time. By the early Pleistocene, Siwalik cervids fed entirely on C_4 vegetation in open grassland settings. Such change in the diet seems to be synchronous with increased complexity (increased enamel thickness and hypsodonty) in dentition over time. $\delta^{18}O_{enamel}$ reveals a significant shift through time with values of −10.0‰, −5.9‰, and 3.7‰ from the early Pliocene, late Pliocene, and early Pleistocene, respectively. Many species of the family Cervidae were coeval and diachronous, possibly justified by the niche partitioning hypothesis.

Keywords

Carbon isotopes · Oxygen isotopes · Cervids · Tatrot

1 Introduction

Family Cervidae is among the notable families of large herbivores which existed in the Siwaliks for a more extended period. Cervids in the Siwaliks exhibit a temporal range extending from the early Pliocene (~5 Ma) to thePleistocene (~2.0 Ma) period, and their record is comprehensively debated based on their morphological characters (Croitor, 2017). Eight species belonging to the family Cervidae have been reported from the Siwaliks of Pakistan, including *Cervus sivalensis*, *Cervus triplidens*, *Cervus colberti*, *Rucervus* sp. 1, *Rucervus simplicidens*, *Rucervus (?)* sp. 11, *Rucervus* sp. 111 and *Axis punjabiensis* (Ghaffar et al., 2017). Later on, another species *Cervus rewati* was also discovered in the Upper Siwaliks.

All the species exhibit extreme brachydonty, while *C. rewati* shows sub-hypsodont teeth with a comparative complexity in dental features (e.g., strong styles on the upper molars). The morphological features indicate a clear-cut browsing nature for this family, mainly feeding on lower branches of trees (Croitor, 2017). The species are also considered diachronous, thus, meaning niche specification within the different family species. However, no isotopic records are available for the Siwalik's cervids which may

M. T. Waseem (✉)
Zoological Science Division, Pakistan Museum of Natural History, Shakarparian, Islamabad 44000, Pakistan
e-mail: tahirmuhammad1213@gmail.com

A. M. Khan · G. Sarwar
Institute of Zoology, University of the Punjab, Lahore 54590, Pakistan

J. Quade
Department of Geosciences, University of Arizona, Tuscan 85721, USA

A. Ghaffar Department of Zoology, Cholistan University of Veterinary and Animal Sciences (CUVAS), Bahawalpur, Punjab, Pakistan

A. Çiner et al. (eds.), *Recent Research on Environmental Earth Sciences, Geomorphology, Soil Science, Paleoclimate, and Karst*, Advances in Science, Technology & Innovation, https://doi.org/10.1007/978-3-031-42917-0_47

attest to their feeding behavior and ecology. Therefore, we report here the first isotopic records of the family Cervidae from the Siwalik sub-Group of Pakistan.

1.1 Geologic Settings

Mangla-Samwal section (Fig. 1a) is present in the southwest of Mirpur, Azad Kashmir of the Siwaliks sub-Group of Pakistan (Fig. 1b). The 700 m thick section shows the Upper Siwalik depositional settings, which are highly fossiliferous and yield a variety of vertebrate fossils. The section contains alternating sandstone and mudstone. Like the Rohtas Anticline, Mangla-Samwal is also caped by conglomerates at the top of the section. The top of the section lies a little below Rohtas anticline and is at the top of Chron 2. In contrast, the bottom can be correlated to the C3n.1n. The upper part of the section can be related to *Elephas hysudricus* range zone biostratigraphically (Dennell et al., 2006).

Bhimber (Fig. 1a) is present in the southwest of Azad Kashmir and is comparatively a smaller section compared to Magla-Samwal Anticline. The section is represented by greyish mudstone and sandstone. The section can be ascribed to Pinjor Formation/Stage due to the occurrence of *Equus* above the Gauss/Matuyama boundary. The upper part of the section can be placed at the top of Chron 2, equivalent to the Mangla-Samwal section, whereas the lower part can be placed at C2r.2r (~2.47 Ma).

2 Materials and Methods

A sum of twenty-five fossil specimens (more preferably molars) belonging to Family Cervidae was selected for this study. After the initial cleaning, bulk samples were made from the lingual sides of each molar from root to crown direction, and enamel powder was collected in 5 mg Eppendorf tubes. All the pieces were subjected to pretreatment before the stable isotope analysis. A rotary foredoom dental drill is used to extract the enamel in powdered form. The powdered enamel sample was treated with hydrogen peroxide (H_2O_2) and acetic acid (CH_3COOH) to neutralize the effects of organic and inorganic impurities, as given by Koch et al. (Koch et al., 1997). After that, the enamel was additionally treated with 30% H_2O_2 overnight. It was then washed with de-ionized water (H_2O) and treated with 0.1 N CH_3COOH for 4 h. Samples were again washed. For drying out the samples, ethanol was added and left for 24 h. CO_2 production takes place by dissolving the enamel samples in 95% H_3PO_4. The CO_2 was examined with the help of Isotope Ratio Mass Spectrometry (IRMS) at PINSTECH, Islamabad. Statistical analysis was carried out using Statistical Package for the Social Sciences (SPSS) 21.0

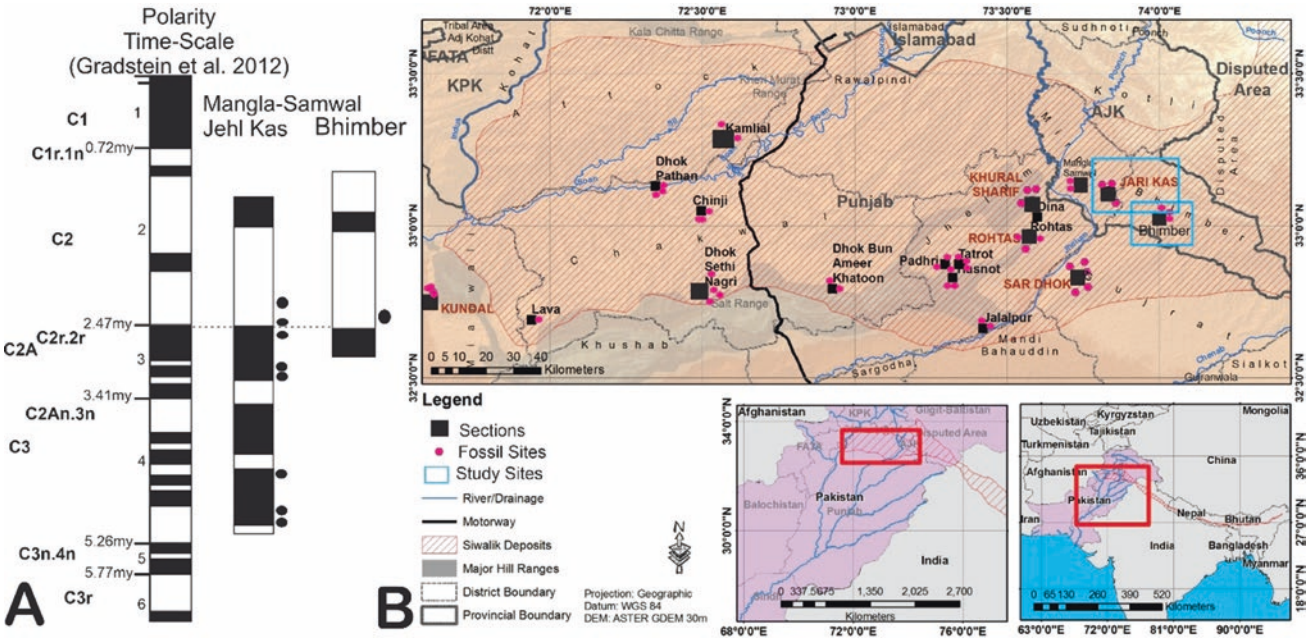

Fig. 1 Generalized map of the Siwaliks sub-Group of Pakistan. **a** Geological settings of studied sections based on Palaeomagnetic dating. **b** Studied sites along with other fossil localities

version. The normality of the data was checked by using the normality test, and then Student's *t*-test was used to analyze the results.

3 Results

A sum of 25 bulk samples was subjected to isotopic analysis. The average $\delta^{13}C_{enamel}$ and $\delta^{18}O_{enamel}$ values were found to be −9.1‰ and −5.8‰ respectively. The maximum and minimum values for stable isotopes of carbon were 1.1‰ and −13.5‰, respectively. The values for carbon and oxygen isotopes were non-normally distributed. Thus, a non-parametric test was run for the analysis. Inter-group analysis revealed no significant differences among the early Pliocene/late Pliocene and essential differences between the late Pliocene/early Pleistocene $\delta^{13}C$ values of Cervids.

Maximum and minimum $\delta^{18}O_{enamel}$ values of the family Cervidae were found to be −5.8‰ and −11.3‰, respectively. Furthermore, intergroup analysis (non-parametric) revealed significant differences among the early Pliocene and late Pliocene $\delta^{18}O$ values of Cervids ($p<0.05$). At the same time, no significant differences were found among late Pliocene/Pleistocene Cervids ($p=0.6$).

4 Discussion and Conclusion

The early Pliocene cervids depict an average value of $\delta^{13}C_{enamel}$ as −12.2‰ indicating that at ~5 Ma, cervids browsed exclusively (Fig. 2). The lower carbon isotope values suggest the dominance of browsing with no evidence of grazing in cervids during the early Pliocene. This finding aligns with the browsing hypothesis based on the dental characters (simple brachydont teeth). Cervids show the same dominant browsing trend throughout the early Pliocene (Fig. 2) but with few values indicating browsing to mixed feeding with a small amount of C_4 vegetation (average $\delta^{13}C_{enamel}=-10.9‰$). This shows a steady shift from forestlands to woodlands around ~4 Ma. The records of cervids from the Siwaliks exhibit their entire lineage, which was more persistent with a browsing nature (Croitor, 2017). However, no considerable records of cervids from the middle/late Miocene have been reported from contemporary faunas of other regions, including East Africa and Myanmar.

Toward the late Pliocene epoch, Cervids showed a dietary shift toward C_4 vegetation (average $\delta^{13}C_{enamel}=-3.3‰$, $n=11$), while in Indian Siwaliks, Cervids sustained a C_3 diet ($\delta^{13}C_{enamel}=-9.0‰$) by the end of Pliocene (Patnaik et al., 2019). Thus, it can be assumed that cervids shifted toward a C_4 dietary behavior early in the Siwaliks of Pakistan (Fig. 2) compared to the Siwaliks of India. Cervids from Indian Siwaliks indicate a grazing behavior on the C_4 diet in the Pleistocene ($\delta^{13}C_{enamel}=1.35‰$), attesting to the previous hypothesis.

The early Pliocene cervids are believed to endeavor a humid climate with year-round rainfall. The oxygen isotope values attest to this hypothesis by representing an average of −6.4‰ (Fig. 2), which indicates comparatively low evapotranspiration as in the late Pliocene, which is a result of higher humidity leading to low oxygen isotope values. Cervids have been categorized under evaporative sensitive clade based on their digestive physiology as they full

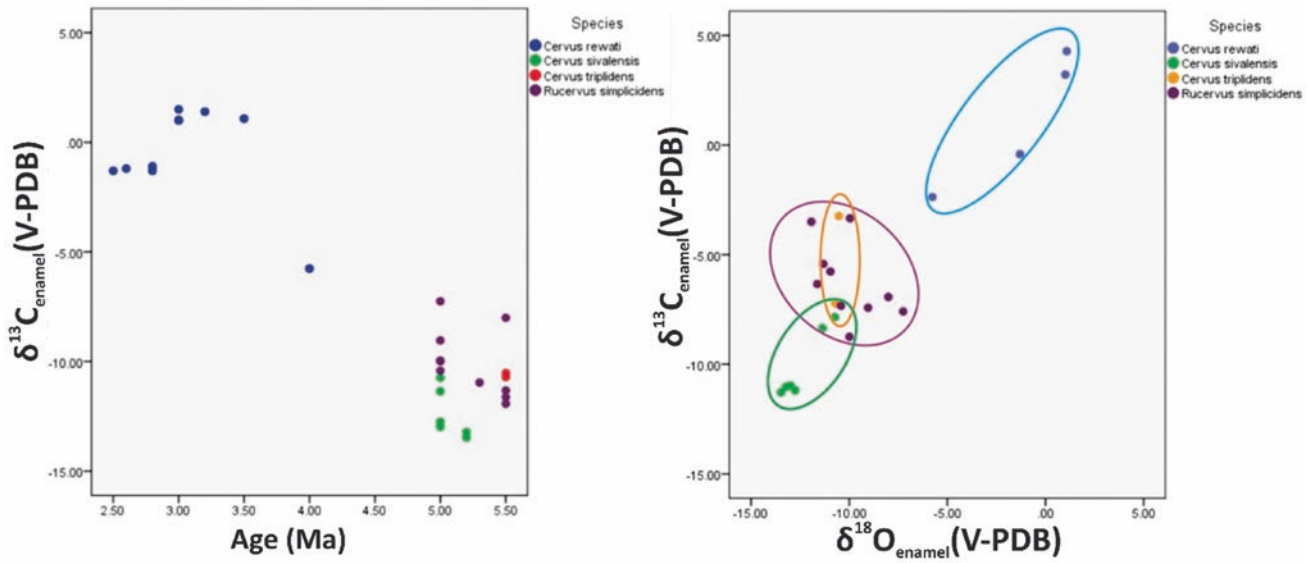

Fig. 2 $\delta^{13}C_{enamel}$ and $\delta^{18}O_{enamel}$ values of the studied samples showing the dietary change and niche overlap between the studied species of Family Cervidae

fill their water requirements from their food majorly (Faith, 2018). Thus, the more evapotranspiration, the higher the oxygen isotope values will be, and vice versa. Thus, the low oxygen isotope values of oxygen reveal that cervids were feeding on the shades during the early Pliocene.

The taxa, which chiefly rely upon the foliage for the water requirements, rarely drink actively from the water sources (e.g., bovids, cervids, giraffes, hippos, etc.). But, if their feeding does not fulfill their water intake requirements, they drink actively from water sources. The late Pliocene cervids show a marked and significant increase in oxygen isotope values ($\delta^{18}O_{enamel} = -2.2‰$). The considerable differences between the early Pliocene and the late Pliocene oxygen isotope values of cervids showed a sharp rise in aridity through time as the evapotranspiration increased considerably. The late Pliocene Cervids fed upon C_4 grasses with shallow water content. Thus it indicates that the late Pliocene cervids drank actively from open un-shaded evaporating water holes in a Savannah and Grassland-dominated ecosystem. Cervids continued to inhabit open lands dominated by C_4 grasses and few open water holes as the rivers shrank by the Pleistocene time (Khan et al., 2020).

Many species of the family Cervidae were coeval and diachronous, which can only be justified by the niche partitioning hypothesis. *R. simplicidens* and *C. sivalesnsis* existed for a longer time interval, and at some point, both were coeval. Former preferred semi-forestland to woodland settings and inhabited more open spaces ($\delta^{13}C_{enamel} = -10.0‰$, $\delta^{18}O_{enamel} = -6.2‰$), while the latter preferred dense forests and inhabited the shadier areas ($\delta^{13}C_{enamel} = -12.4‰$, $\delta^{18}O_{enamel} = -10.1‰$). *C. triplidens* and *C. rewati* appeared later in the Siwaliks of Pakistan (~5 Ma). The former species fed upon the C_3 diet dominantly and showed mixed feeding to some extent with the dominance of C_3 vegetation and inhabited open spaces ($\delta^{13}C_{enamel} = -10.6‰$, $\delta^{18}O_{enamel} = -5.2‰$). In contrast, the latter species inhabited most of the Plio-Pleistocene period, dominated by grasslands, and fed upon the C_4 grasses. Family Cervidae represents a classic case of niche portioning among the member of the same family. We can conclude that the family Cervidae was among those mammalian families which shifted toward C_4 vegetation by the late Pliocene in the Siwaliks of Pakistan (Fig. 2). The modern cervids in India have been reported to inhabit a comparative ecology and live in forests relying chiefly on C_3 diets. These are the regions that show a comparatively lower MAT and higher MAP.

Acknowledgements The authors are thankful to Roman Croitor (Senior Researcher, Institute of Zoology, Academy of Sciences of Moldova) for his constructive comments on the initial version of this work. This work is a part of the Ph.D. thesis of Muhammad Tahir Waseem and supported by the Higher Education Commission Pakistan vid grant no. 315-28107-2BS3-243.

References

Croitor, R. (2017). Description of a new deer species (Cervidae, Mammalia) from the Early Pliocene of Eastern Europe, with a review of early dispersals and palaeobiogeography of the subfamily Cervinae. *Neues Jahrbuch Für Geologie Und Paläontologie-Abhandlungen, 283*(1), 85–108.

Dennell, R. W., Coard, R., & Turner, A. (2006). The biostratigraphy and magnetic polarity zonation of the Pabbi Hills, northern Pakistan: An Upper Siwalik (Pinjor Stage) Upper Pliocene Lower Pleistocene fluvial sequence. *Palaeogeography, Palaeoclimatology and Palaeoecology, 234*, 168–185. https://doi.org/10.1016/j.palaeo.2005.10.008

Faith, J. T. (2018). Paleodietary change and its implications for aridity indices derived from $d^{18}O$ of herbivore tooth enamel. *Palaeogeography Palaeoclimatology Palaeoecology, 490*, 571–578.

Ghaffar, A., Siddiq, M. K., Akhtar, M., Khan, M. A., Khan, A. M., & Azeem, M. I. (2017). Antler remains (Cervidae, Artiodactyla, Mammalia) from a new locality in the Pinjor formation (1.6–0.8 Ma), Pakistan. *Revista Brasileira de Paleontologia, 20*(1), 23–30.

Khan, A. M., Iqbal, A., Waseem, M. T., Ahmad, R. M., & Ali, Z. (2020). Palaeodietary and Palaeoclimatic interpretations for herbivore fauna from late Pliocene to early Pleistocene Siwaliks of Pakistan. *Journal of Animal and Plant Sciences, 30*(2), 355–363.

Koch, P.L., Tuross, N., & Fogel, M. L. (1997). The effects of sample treatment and diagenesis on the isotopic integrity of carbonate in biogenic hydroxylapatite. *Journal of Archaeological Science*, *24*, 417–429.

Patnaik, R., Singh, N. P., Paul, D., & Sukumar, R. (2019). Dietary and habitat shifts in relation to climate of Neogene-Quaternary and associated mammals of Indian Subcontinent. *Quaternary Science Reviews, 224*, 105968.

Lasergrammetry and Photogrammetry for a Survey and 3D Representation of Caves and Its Interest in the Development of Loco-Regional Geo-Tourism: Case of Kef El Baroud Cave, Province of Benslimane, Morocco

Hicham Benani, Lalla Amina Ouzzaouit, Larbi Boudad, Sofia Hakdaoui, Ayoub Nehili, and Najib Bahi

Abstract

The underground world is a multi-faceted environment, caves are natural cavities shaped by water for millions of years, but their exploration for scientific and tourist purposes is late. It does not take shape until the second half of the nineteenth century. With karst explorations, we could develop knowledge of the underground world, a world to be explored and preserved. Underground tourism in Morocco remains largely under-exploited. The limestone surface in Morocco is 99,890 km^2, or 14% of the country's total surface for only three caves developed. This under-exploitation is explained by the lack of evaluation of karst heritage richness reflected by the lack or absence of archives of the caves. This is published in the only official document, "inventory of caves of Morocco 1981" (Ministère de l'équipement direction hydraulique, « Inventaire Spéléologique du Maroc». Ministère de l'équipement direction de l'hydraulique, 1981). Terrestrial laser scanning and 3D photogrammetry techniques using a LEICA RTC 345 scanner were used in the relatively small KEF EL BAROUD cave developed in Devonian limestone, located in the province of BEN SLIMANE. The site is situated, in the valley of Oued Cherrat, about 10 km east of the town of Ben Slimane. These measurements allowed the reconstruction of the stages of evolution of the paragenetic morphologies and their relationship with the local geomorphology, speleothems, and structural elements. Furthermore, the field measurements were integrated with the morphometric analyses of the numerical models, which allowed a much larger number of observations and the discernment of the different karstification processes and speleogenetic phases. The results are a clear example of the combination of 3D photogrammetric data where they need to correct and update the topographies of Moroccan caves for wide exploitation by the general public. The surveys were carried out to compare the outcomes of the two methods in mapping small-size caves (B. Lips, « Maroc Bilan des explorations 79/81». Groupe Spéléo Vulcain echo du vulcain N°41, 1981. [En ligne]. Disponible sur: https://www.sudoc.fr/146193989). The final rendering of the treatment shows the interest of 3D modeling in the exploitation of the KEF EL BAROUD cave, which represents a typical example of the exploitation of this heritage by developing an interactive visualization in the virtual space of the cave. This is the first Moroccan attempt to create a virtual 3D model of a cave.

Keywords

Karst · Caves · Underground topography · 3d modeling · Lasergrammetry · Photogrammetry

1 Introduction

When we talk about natural heritage, such as karst caves, digital reconstruction is an interesting resource for the preservation and enhancement of origin and scientific support.

The recent development of techniques linked to the contribution of data processing has made it possible. It provides local actors with an efficient and reliable tool that allows the cave to be valued.

H. Benani (✉) · L. A. Ouzzaouit · L. Boudad · S. Hakdaoui · N. Bahi
Faculty of Sciences Rabat, Department of Geology, Mohammed V University, Rabat, Morocco
e-mail: hicham.benani@um5r.ac.ma

A. Nehili · N. Bahi
Faculty of Letters and Human Sciences, Sultan Moulay Slimane University, Beni Mellal, Morocco

A. Çiner et al. (eds.), *Recent Research on Environmental Earth Sciences, Geomorphology, Soil Science, Paleoclimate, and Karst*, Advances in Science, Technology & Innovation, https://doi.org/10.1007/978-3-031-42917-0_48

Given the application of these two most used techniques, photogrammetry, and lasergrammetry, in the digital modeling of the KEF AL BAROUD cave, the restitution of the measurements and the virtual representation tangibly reflects the geo-morphological complexity of the site.

2 Materials and Methods

To carry out this project, we have provided several tools and databases summarized in the table below.

To define the entry point of the KEF AL BAROUD cave, we used a GARMIN GPS, which allows us to convert the coordinates into functions of the desired projection system.

For conventional topography, we used the LEICA DISTO-X 310, an accurate laser range finder equipped with 3-axis compass/clinometers with full tilt compensation that sends the results of distance and tilt data wirelessly to the PDA terminal. TRIMBLER JUNO SC, the stored data was then sent to visual topo for processing (Bussa et al., 1997).

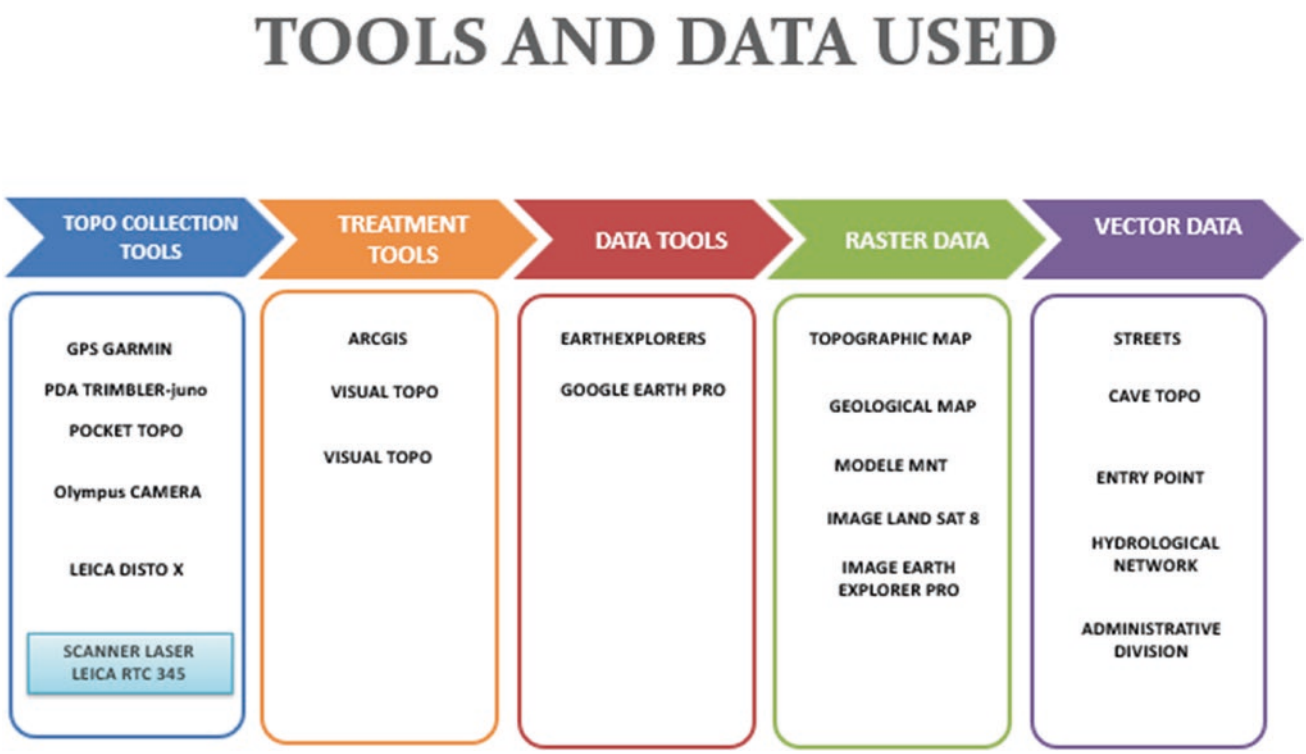

The lasergrammetry of the KEF AL BAROUD cave was provided by the RTC 345 terrestrial laser scanner from LEICA.

The point cloud obtained and the processing on the appropriate software allowed us to get a digital modelization of the cave which

The RTC 345 scanner has additional features that provide added value.

Indeed, it is ideally suited for applications that require short-range scanning while offering high-definition precision and the unique advantage of real-time on-site data logging with a scan range of up to 70 m and an accuracy of ± 1 mm.

The acquisition speed of about 2,000,000 points per second.

3 Results of Lasergrammetry and Photogrammetry

The final result, therefore, resulted in the representation of the space of the KEF EL BAROUD cave and the production of a geometrically correct document, satisfactory and consistent with the complexity of the cave. Furthermore, the 3D lasergrammetry approach and the photogrammetry images of the KEF EL BAROUD cave produce spectacular accuracy. Indeed, the graphical and metric information on the site and its environment and on the different structures which compose it allows ride first to highlight the geo-morphological complexity of the cave, and the precise data obtained give access to an analysis of the information received from different sources. The data capture technique by terrestrial laser scanning and close-up photogrammetry constitutes the most precise approach to generating high-resolution 3D models of a cave. The capture and processing of photogrammetric and lasergrammetry data used to create 3D models are to be proposed for a topography taking into account the complexity of the terrain and the infinite details that conventional techniques cannot provide since the recording is point-to-point spaced so that the information enters points are lost. Our results highlight the potential of these techniques to obtain photorealistic models that facilitate a complete analysis of the information available on the volume of the cave and on the speleothems that compose it (Fig. 1).

4 Topography of the Kef El Baroud Cave by DISTO-X

The topography of the cave by the conventional method, DISTO-X, although widely used in caving, does not give the details of the advanced technique of lasergrammetry and photogrammetry. The stations spaced from the outlets only provide an overview. The overall morphological aspect of the cave, obstacle zones, and difficult angles cannot be represented. This method cannot accurately visualize the complexity of the cave (Fig. 2).

5 Discussion

Lasergrammetry is a booming field; the performance of laser scanners allows surveys to be more precise in a minimum of time.

Even if laser scanners greatly facilitate the lifting of points by scanning, the treatment remains a complex step, especially when it comes to a complicated building which is the cave that constitutes a natural heritage to be preserved, exploited, and valued.

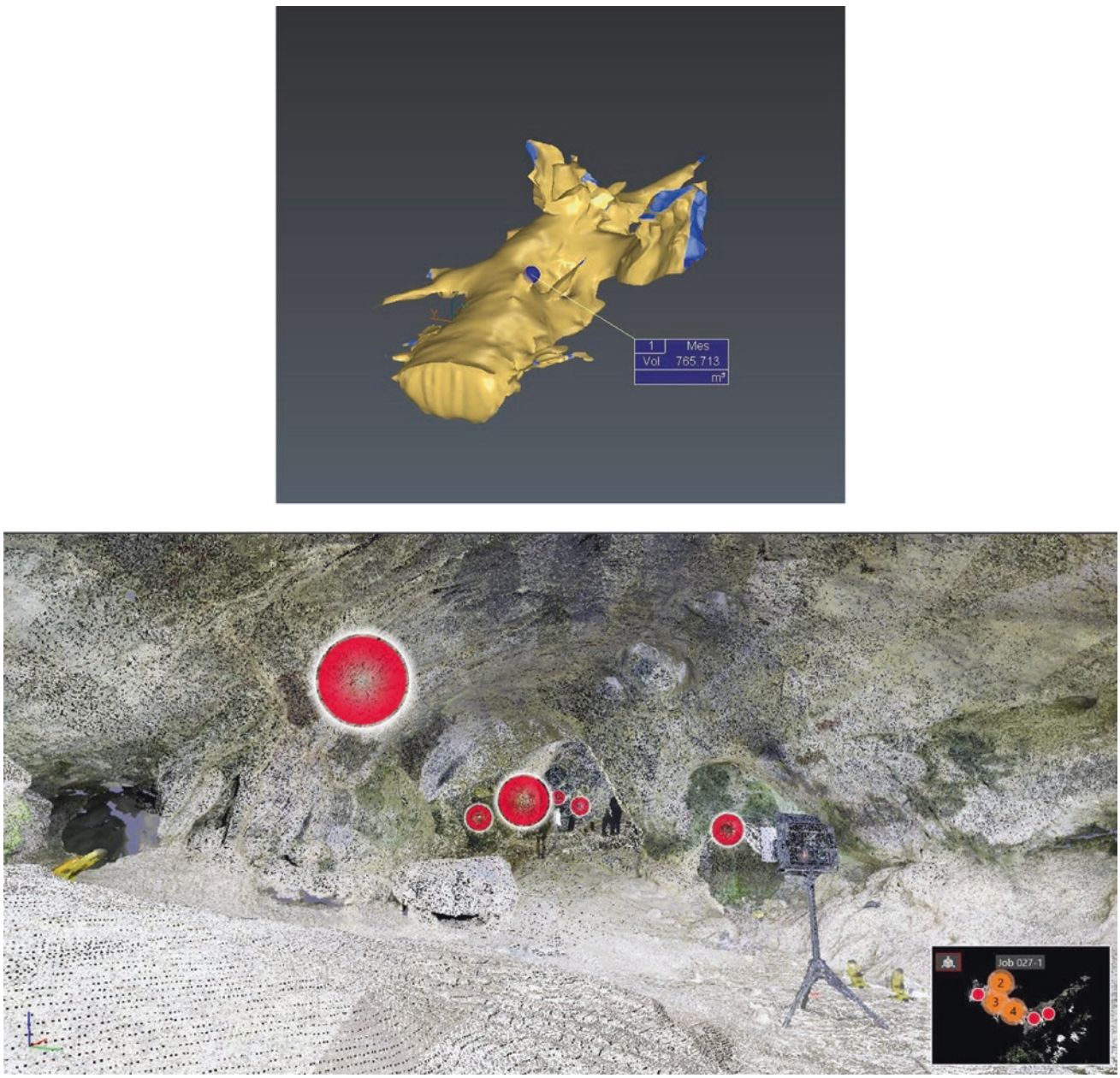

Fig. 1 Lasergrammetry of the Kef EL Baroud cave and its volumetry

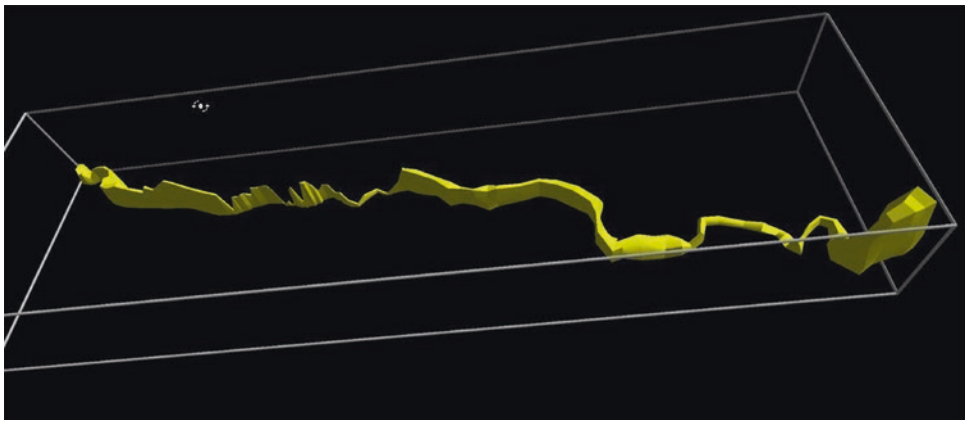

Fig. 2 Topography of the Kef El Baroud cave in the projected mode by DISTO-X method

6 Conclusions

The 3D modeling of the KEF EL BAROUD cave allowed us to achieve a precise morphological representation of the cave. The photogrammetric restitution also showed us the infinite details of the cave and the possibility of the virtual representation of the latter to set up a guided tour on the web for a cave heritage value.

Lasergrammetry and photogrammetry made it possible to produce a model more faithful to reality while respecting the geological complexity of the cave with a precision of the order of a millimeter over the entire model.

This precision is strongly requested in the volumetric measurements of the rooms for a possible development to the general public, but also georeferenced surveys in archeology. Lasergrammetry remains essential for its ease and relatively advanced mode of treatment nowadays.

References

Bussa et al., M. P. (1997). Application of a cellular automaton for recognition of straight tracks in the spectrometer DISTO. *Computational and Applied Mathematics, 34*(7–8), 695–701. https://doi.org/10.1016/S0898-1221(97)00170-3.

Lips, B. (1981). Maroc Bilan des explorations 79/81 ». Groupe Spéléo Vulcain echo du vulcain N°41. [En ligne]. Disponible sur: https://www.sudoc.fr/146193989.

Ministère de l'équipement direction hydraulique. (1981). Inventaire Spéléologique du Maroc. Ministère de l'équipement direction de l'hydraulique.

Karst Aquifers, a Strategic Tool for Mitigating the Impact of 100-Years Droughts

Bernard Collignon and Fouzia Bensaoula

Abstract

The Mounts of Tlemcen are a real water tower in western Algeria, a region with limited water resources and which is hit several times a century by intense multi-year droughts (more than three following years). To cope with these periods of drought, one of the region's best assets is the existence of large karst aquifers. Their renewable reserves (the flux) are significant but are already largely used. On the other hand, permanent reserves (the stock) are not subject to any strategic management, although they would cover water demand during multiannual drought episodes. We will show that more intensive exploitation of permanent reserves would make it possible to cover demand during 50-year and even 100-year droughts through the construction of additional borehole fields, which would not be exploited in a "usual" year (when dams are the most cost-effective water resource), but only during periods of severe rainfall deficit. This strategy enabled it to cope with the powerful 1979–1999 drought at an economic and environmental cost much lower than seawater desalination. In the longer term, the high storage capacity of these aquifers would also make it possible to store valuable resources presently lost at sea (the overflow of dams during rainy years and the outflow from wastewater treatment plants in winter).

Keywords

Mounts of Tlemcen · Karst · Strategic water resources · Managed aquifer recharge (MAR) · Algeria

1 Introduction: Karst Reservoirs and Their Management

The erosion of carbonate rocks leads to the formation of karst aquifers, which have specific properties: high heterogeneity, high permeability, and relatively limited storage (Collignon, 1986; Stevanovic, 2015). These properties make it possible to exploit them more intensively than porous aquifers, but this implies rigorous reserves management. We will illustrate this with the example of Tlemcen, where large karst aquifers have been mobilized to limit the impact of the exceptional drought during the 1979–1999 period.

2 Increasing Levels of Aquifer Exploitation

A karst aquifer behaves like a reservoir whose storage properties vary little with depth (each meter of drawdown releases an equivalent volume of water) (Collignon, 2018). The optimal management of such a reservoir implies the construction of a sufficient number of highly productive boreholes, some of which will be used to pump water during periods of rainfall deficit and others to reinject water during periods of water surplus.

The climate of Northern Algeria is Mediterranean, with hot and dry summers and rainy winters. The interannual rainfall variability is very high, and large dams have been built since the last century to store water and cover water needs during deficit years. The drought in Western Algeria

B. Collignon (✉)
Bottombillion, 198, Ch. d'Avignon, 84470 Châteauneuf-de-Gadagne, France
e-mail: collignon@bottombillion.fr

F. Bensaoula
Département d'Hydraulique, Université de Tlemcen (Algérie), Tlemcen, Algérie

A. Çiner et al. (eds.), *Recent Research on Environmental Earth Sciences, Geomorphology, Soil Science, Paleoclimate, and Karst*, Advances in Science, Technology & Innovation, https://doi.org/10.1007/978-3-031-42917-0_49

Table 1 Successive management strategies for karstic aquifers in the Tlemcen region

	Management model	Application
<1950	Karst spring gravity flow	Gravity-fed irrigation systems along oued chouly
1950–1975	Water reservoirs downstream of the springs	Beni Bahdel, Meffrouch, Sidi Abdelly and Sikkak dams (385 Mm^3 of storage)
1975−1983	Wells-abstraction rate<renewable reserves	50 wells (25 Mm^3/year)
1983−2000	Wells-abstraction rate>renewable reserves	200 wells (100 Mm^3/year)
>2000	Karst aquifers as strategic reserves	Adding 2 desalination plants (70 Mm^3/year) and slowing down 20 highly productive boreholes
>2030	Artificial recharge of karst aquifers	Underground storage of overflow from dams and wastewater treatment plants

is characterized by the recurrence of more than four successive deficit years (1915/1919−1939/1949−1981/1987−1992/2000). According to Hubert (2003), the 68-year evolution of river flows in western Algeria shows a break in the 1970s, with a sharp decrease in water inflows to dams (Fig. 2).

As a result of this drop in rainfall, the dams were no longer filling up sufficiently to cover the water needs (Assaba et al., 2013), which continued to grow (fourfold in 40 years). As a result, the government launched massive investments in other water resources: boreholes during the 1980s and 1990s and seawater desalination in the 2000s (Table 1).

3 Results

3.1 Boreholes to the Rescue of Oran's Drinking Water Supply

The 1981/88 drought showed the limits of the regulating capacity of existing dams. They were insufficient to compensate for the impact of a ten-year rainfall deficit. To urgently secure the water supply to the cities of western Algeria, about twenty deep boreholes were drilled in the karst along the Beni Bahdel dam's main pipeline to capture an additional 12 Mm^3/year of underground water, which was reinjected into the dam's penstock.

3.2 Overuse of Aquifers

The success of this operation encouraged the government to increase the number of boreholes in karstic aquifers (nearly 200 boreholes for the Tlemcen Mounts, Zaouia, and Chott el Gharbi) (Hubert, 2003). The cumulative production capacity of all these boreholes reaches 80 Mm^3/year, i.e., almost half of the renewable reserves of karstic aquifers, estimated at 200 Mm^3/year (Bensaoula et al., 2019; Collignon, 2018). The consequence was not long in coming: the first signs of overexploitation appeared in the 1990s. Six of the 81 boreholes operated by ADE (the water utility in the wilaya of Tlemcen) are now abandoned. Twenty-nine other boreholes have been put on standby because of the high drawdown of the water table (ADE, 2019).

3.3 Desalination of Seawater and Resting of Boreholes

To secure the water supply without compromising the sustainability of groundwater resources, the Algerian authorities have decided to develop water production capacities by desalinating seawater. Two desalination plants (Souk Tlata and Honaine) were commissioned between February 2011 and July 2012 in the wilaya of Tlemcen with a theoretical capacity of 70 Mm^3/year. This additional resource has enabled ADE to reduce groundwater abstraction on the northern slopes of the Tlemcen Mounts and to let the aquifer level rise again.

3.4 Interconnection of Various Water Resources

ADE (the water service utility) supplies drinking water to all its customers, mobilizing three main types of resources: seawater desalination, large dams, and boreholes in karstic aquifers. In addition, ADE organized integrated management of several water resources. This is possible because it has built an extended network of main pipes (nearly 1000 km of tubes with diameters ranging from 90 to 1500 mm) that interconnect all the water resources to all the major distribution points.

4 Discussion: Karst Aquifers' Potential as a Strategic Resource to Compensate for the Impact of Multiannual Droughts

The karst aquifers are an important asset for ADE to manage the water supply of the region thanks to three features: (a) their renewable reserves (annual recharge, estimated at 200 Mm^3/year (Collignon, 2018)), (b) their permanent reserves (water stored underground, estimated at 6,300 Mm^3 (Bensaoula et al., 2019)), and (c) highly productive wells.

How to take the most from these permanent reserves? It is not recommended to mine them. Instead, it is recommended that aquifers be equipped with additional production capacity to cope with multi-year droughts (Stevanovic, 2015) when dams and desalination plants are no longer sufficient. Such an infrastructure would enable managing 50-and even 100-year droughts (as done during 1983–1990—see Fig. 1c).

Currently, two types of water resources are difficult to use in the region: (a) the dams overflow, during years of intense rainfall, and (b) the output of wastewater treatment plants, in winter. The immense storage capacity of the karstic aquifers of the Tlemcen Mountains would make it possible to store part of these resources currently lost to the sea. This would involve setting up an artificial aquifer recharge system in the form of high-flow injection wells (Fig. 1d).

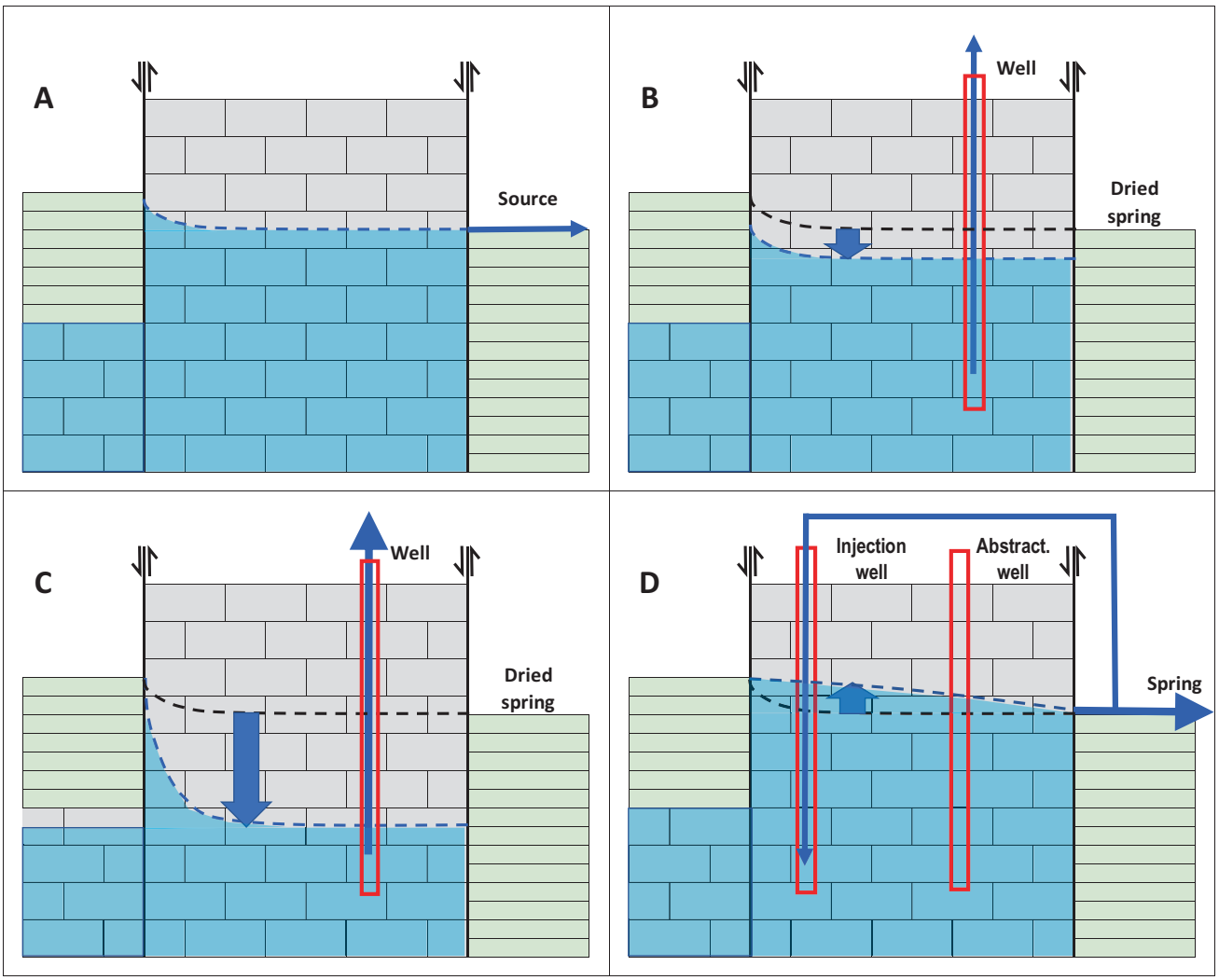

Fig. 1 Progressive intensification of the exploitation of a karst aquifer. **a**—Gravity exploitation of overflow springs. **b**—Summer drawdown of the piezometric level to compensate for the drop in flow from the springs. **c**—Partial emptying of the aquifer to cope with a multi-year drought. **d**—Aquifer recharge during surplus years

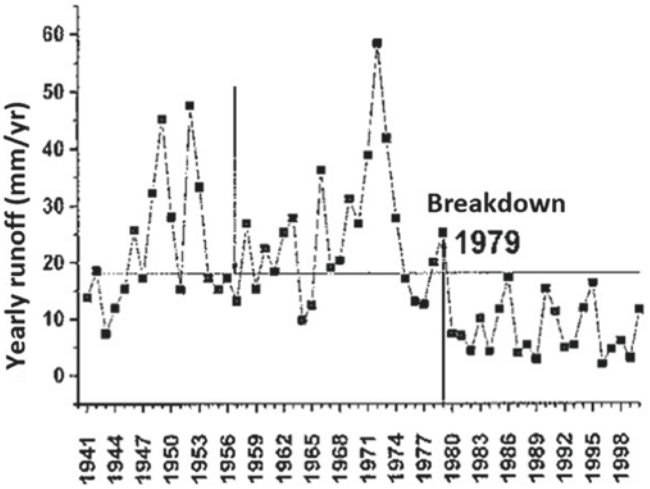

Fig. 2 Beni-bahdel dam annual recharge (Meddi, 2003)

5 Conclusion

Prolonged droughts lasting more than three successive years occur in western Algeria several times per century. Most climate change models conclude that the probability of such events should increase by the end of the century (Zeroual et al., 2017). The karst aquifers constitute a strategic water reservoir suitable to cope with this.

During years of excess rainfall, water resources can be stored in economic conditions and protected from evaporation and eutrophication. They can then be quickly re-mobilized thanks to the very high well productivity, which is a consequence of the intense karstification.

References

ADE. (2019). *Etat des forages*. ADE.

Assaba, M., Laborde, J., & Rezak, S. (2013). Les effets d'une baisse de la pluviométrie sur les volumes regularisables des barrages d'Algérie. RST, Issue LJEE n°21 et 22.

Bensaoula, F. (2007). Etude de la karstification à partir des données de forages: Le cas des monts de Tlemcen (Algérie). *Karstologia*, *49*, 15−24. https://doi.org/10.3406/karst.2007.2596

Bensaoula, F., Collignon, B., & Adjim, M. (2019). Assessment of groundwater resources in the Jurassic Horst (Western Algeria). In *Water Resources in Algeria*. 3, 17. Springer. https://doi.org/10.1007/698_2019_406

Collignon, B. (1986). *Hydrogéologie appliquée des aquifères karstiques des Monts de Tlemcen (thèse de doctorat)*. Univ. Avignon (France)

Collignon, B. (2018). L'aquifère karstique, objet d'études mathématiques ou naturalistes. *Karstologia, Issue, 71*, 53–60.

DRE. (2018). Situation de l'AEP de la wilaya de Tlemcen. s.n.

Ghenim, A. e. M. (2013). Analyse des précipitations dans le Nord-Ouest algérien. *Sécheresse*, *24*, 107–114. https://doi.org/10.7202/1065205ar

Hubert, & Meddi. (2003). Impact de la modification du régime pluviométrique sur les ressources en eau du nord-ouest de l'Algérie. IAHS Publication, *278*.

Stevanovic, Z. (2015). Engineering regulation of karstic spring-flow to improve water resources in critical dry periods. In *Karst aquifers* (pp. 490–522). Springer. https://doi.org/10.1007/978-3-319-12850-4_15

Zeroual, A., Assani, A., & Meddi, M. (2017). Combined analysis of temperature and rainfall variability as they relate to climate indices in northen Northen Algeria over the 1972–2013 period. *Hydrology Research*. https://doi.org/10.2166/nh.2016.244

Springs and Deep Water Wells in Karst: Which is Preferred More Than the Other?

Kamal Taheri, Petar Milanovic, and Chris Groves

Abstract

Digging deep karst wells in many karst regions of the world, including arid and semi-arid regions, to supply emergency water to cities and villages was on the agenda of local planners. In the deep karst of Dinarides, Helenedise, and Taurides, as well as bare and buried karst in areas such as the Zagros in Iran, the deep and highly productive wells have become a standard technology in the water supply. Many karst wells are drilled based on the possibility of reaching the karst waters directly from the karst channel or the buried karst aquifer. Since the purpose of these wells is to supply drinking water, the privacy of karst water sources such as springs is not considered severe. The case studies in this article present the spatial location of karst wells and large karst springs in different areas of Kermanshah province, Western Iran. The main challenge in using these sources is the durability and permanence of karst springs and the overuse of karst water resources in deep wells. These waters are easily extracted by electric pumps and are not considered in the water balance assessments nor the impacts on the entire karst aquifer and spring discharge impacts. This paper discusses the challenges in the sustainability of karst aquifers and spring durability in semi-arid and geosyncline karst regions to address and illustrates the perspective of sustainability conditions and protection of karst water resources in buried karst aquifers and large spring in future outlook.

K. Taheri (✉)
Kermanshah Regional Water Authority, Ministry of Energy, Kermanshah, Iran
e-mail: Taheri.kamal@gmail.com

P. Milanovic
Professor Retired, President of Serbian IAH, Belgrade, Serbia

C. Groves Crawford Hydrology Laboratory, Western Kentucky University, Bowling Green, KY 42101, USA

Keywords

Karst · Water wells · Spring · Sustainability · Spatial analyses · Kermanshah province

1 Introduction

Alluvial aquifers have been exploited and emptied in the last two or three decades due to population growth and the accelerated need to provide water for food security and drinking water supply plans. For this reason, emergency water supply programs targeted karst water resources. Digging deep karst wells in many karst regions of the world, including arid and semi-arid regions, to supply emergency water to cities and villages was on the agenda of local planners. In the deep karst of Dinarides, Helenedise, and Taurides, as well as bare and buried karst in areas such as the Zagros in Iran, the deep and highly productive wells become a standard technology in the water supply. Many karst wells are drilled based on the possibility of reaching the karst waters directly from the karst channel or the buried karst aquifer. Since the purpose of these wells is to supply drinking water, the privacy of karst water sources such as springs is not considered severe. This assumption led to the drying out of various springs or their shortage in discharge in recent years. The main challenge in using these sources is the discharge regime of karst springs and the overuse of karst water resources by deep wells. The deep groundwater is easily extracted by electric pumps and is not considered in the water balance assessments nor the impacts on the entire karst aquifer and spring discharge. This paper discusses the challenges in the sustainability of karst aquifers and spring regime in semi-arid and geosyncline karst regions to address and illustrates the perspective of sustainability conditions and protection of karst water resources in buried karst aquifers and large spring in future outlook.

A. Çiner et al. (eds.), *Recent Research on Environmental Earth Sciences, Geomorphology, Soil Science, Paleoclimate, and Karst*, Advances in Science, Technology & Innovation, https://doi.org/10.1007/978-3-031-42917-0_50

2 Karsto-Geological Setting

Kermanshah province (KP), with an area of 24,998 km2 in western Iran, is one of the typical semi-arid karst areas, about 35% of which is covered by karst formation (Fig. 1). Like in other parts of Iran, an accurate estimate of karst water is not available in this province. However large karst springs and wells drilled in the bare and covered karst are the primary water supply sources to many rural areas and cities such as Paveh, Javanrud, Ravansar, and Sarpol-e Zahab. The danger that has threatened karst water resources in recent years is the attention of local planners and decision-makers to dig karst wells to supply drinking water and ignore the life of springs (Taheri et al., 2016). Even this attitude has gone to fill the reservoir of a dam whose hydrological estimates have not been accurate, and the volume of water evaporation is high.

There are different types of karst (Milanovic, 2004) in KP. Large karst springs have primarily appeared in contact with karstified and non-karstified rocks, called Saraw/Sarab. Karst wells have been drilled on bare karst in some places, such as the hinterlands of Paveh, but in most cases, karst wells have been dug at the end of the fold plunges or karst buried masses. From a hydrogeochemical point of view,

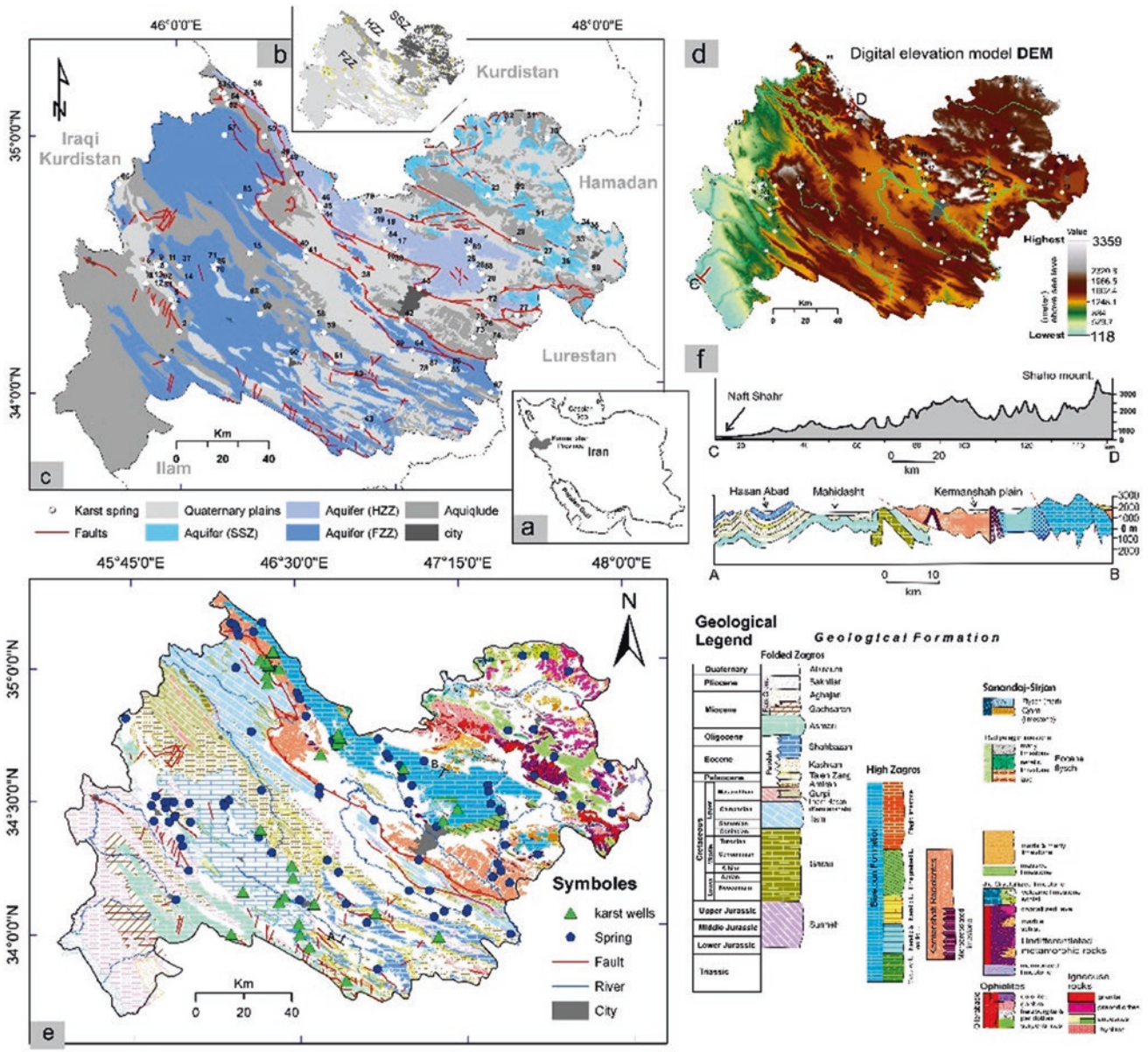

Fig. 1 Kermanshah province in Iran (**a**), Zagros structural zones (**b**), karst and non-karst aquifers (**c**) elevation model (**d**), geological map and springs and karst wells distribution (**c**), and geological cross section (**f**)

mixing alluvial and karst aquifers in many plains of the KP, such as Islamabad, Sarpol-e Zahab, and Ravansar, has been proven (Taheri et al., 2016). In this paper, using the hydrogeochemical study of 95 karst springs and the spatial distribution of 50 karst wells, the answer to the question "which spring and deep water well in karst are preferred more than the other" is discussed.

3 Results

The discharge of 95 springs originating from the KP karst masses was measured every month. The hydrographs highlight the substantial release variability in both time and space domains. A considerable temporal variability of release for a karst spring reflects the active involvement of the conduit system in the aquifer hydrodynamics. However, the moderate and even low temporal variability are unreliable indicators for the absence of conduit system. Table 1 presents the statistical measures of hydrograph temporal variability indicators in relation to the relevant geological formation of groundwater reservoirs. The table shows that the hydrographs had more temporal variability for aquifers originating from Bisetoun formation (BS), followed by the variability of Ilam (IL) and then Asmari-Shahbazan (AS-SB) karst formations. This result is in accordance with the age of geological formations, which means the older the karst formation, the higher the karst development in the subsurface. According to Fig. 1, all deep karst wells in the KP have been drilled in these formations.

Piper diagram shows the distribution of different cations (calcium, magnesium, and potassium plus sodium) and anions (bicarbonate, chloride, and sulfate) in groundwater samples. It indicates the origin of groundwater and the source of soluble salts in it (Fig. 2).

The 95 samples of KP karst springs on the Piper diagram show that most of the hydrochemical facies in the study area are in the Ca-HCO_3 type, except two springs which are Ca-HCO_3-Cl, and Ca-Na-HCO_3 facies. This diagram shows that most of the samples are affected by the dissolution of calcite and dolomite (mainly BS, IL, AS, and AS-SB formations).

4 Discussion

About 50 karst wells have been drilled in KP. These wells are exploited in the outer part of karst spring buffers. These wells do not have tangible and immediate effects on the springs. However, some deep wells, licensed as agricultural wells, are fed by karst water by penetrating the covered karst aquifer. Figure 3 shows these types of drilled wells in KP. In case 2, the mixed waters (alluvial and karst) are mainly exploited, and the karst water balance is practically ignored. These types of wells severely affect the sustainability of springs and karst aquifers. The essential requirements and challenges of managing karst springs and wells in areas such as KP can be described as follows:

(i) The protection zone for karst springs has not been evaluated and designed. In addition, the location of deep wells in the catchment area of springs may cause them to dry out.
(ii) The springs act as alarms for climate change and fluctuations in the volume of karst reservoirs. Therefore, springs protection can effectively monitor the water crisis and manage the karst reservoirs.
(iii) The over-exploitation of wells that have been dug in the alluvial overburden and practically extracting karst water under the name of agricultural wells is the main threat to the life of the springs.
(iv) Lack of laws and regulations with sufficient enforcement to prevent unauthorized drilling in karst aquifers and the absence of quantitative and qualitative

Table 1 The statistical measures of hydrograph temporal variability indicators in relation to the karst geological formations

Temporal variability indicator	Statistical measures	BS	IL	AS	AS-SB
Q_{max}/Q_{min} (−)	Count	25	37	24	8
	Maximum	∞	∞	∞	∞
	Minimum	26.88	6.85	4.98	7.83
	Average	1001.92	558.79	143.24	108.25
Q_{CV} (−)	Count	25	37	24	8
	Maximum	3.4	2.46	2.49	1.52
	Minimum	0.61	0.31	0.19	0.46
	Average	1.48	1	0.82	0.85

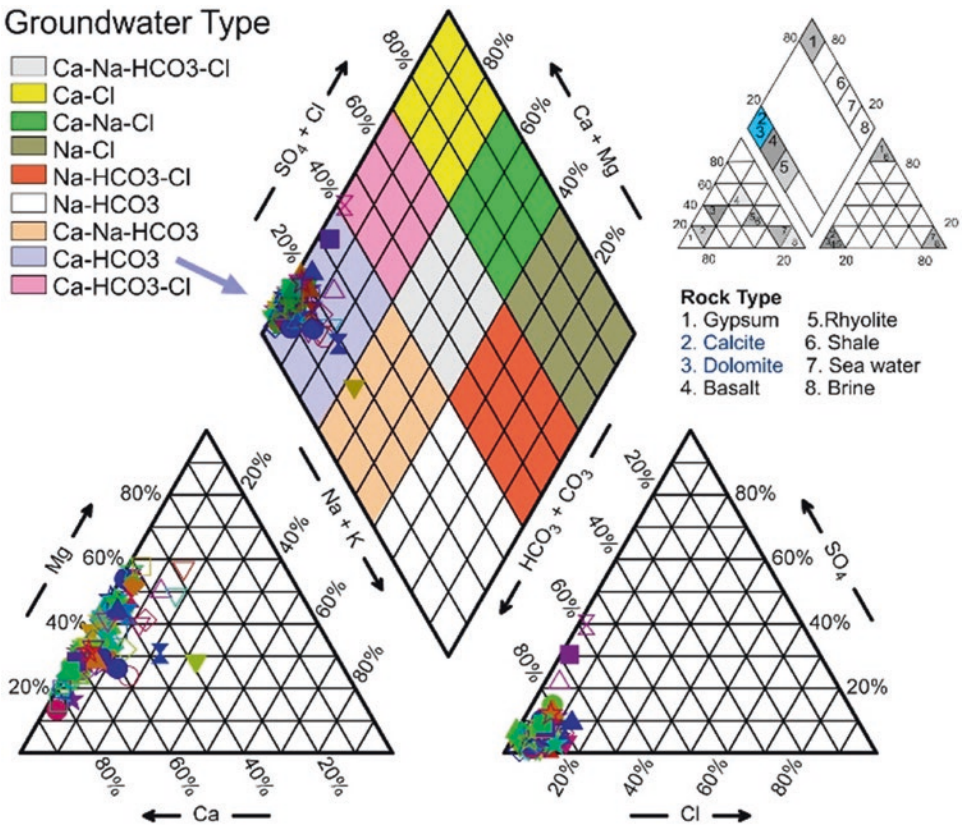

Fig. 2 Piper plot of the studied samples in Kermanshah province springs. Groundwater types are categorized according to Deutsch (1997)

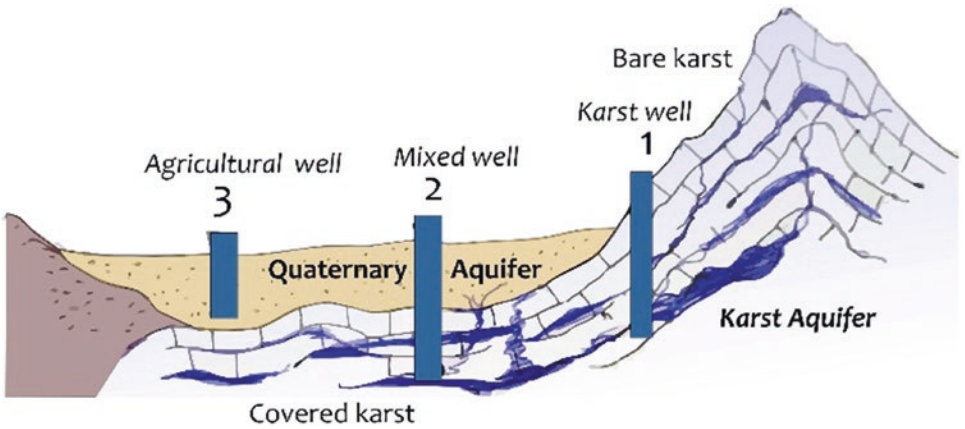

Fig. 3 Different types of deep wells in Kermanshah province

monitoring networks of karst waters is one of the most critical management weaknesses in semi-arid karst areas such as KP.

(V) In formal statistics, only wells drilled in the bare karst are considered karstic wells. Therefore, alluvial wells that have penetrated covered karst aquifers are not considered in any karst water resources assessments.

Although karst wells make up less than 1% of the KP total wells, they are crucial in supplying water to cities and villages in different parts of the region. The study results show that their spatial distribution and recharge sources are the same, and according to the abovementioned, the sustainability of springs is preferable to digging deep wells.

5 Conclusions

Karst deep wells in KP are mostly drilled in the central, northwest, and southwest areas. Although these wells are negligible compared to alluvial wells (less than 1%), their importance in supplying drinking water to the target areas is

vital. Without proper legislation, many alluvial wells extract karst water by increasing the drilling depth, especially in covered karst areas. However, due to the uncertain number of wells, the volumetric values of water abstraction cannot be calculated. Still, the results of hydrogeochemistry observations, especially in the Islamabad-e Gharb, can be seen as the effects of drilling wells on springs drying out.

Supplying water from karst springs is like spending on a bank card without knowing the rest of the money and is an example of unsustainability. In KP, karst springs are drying out, and with the current trend of exploiting mixed aquifers, karst wells will decrease their discharge soon enough. Suppose we want to include the sustainability of water resources in future scenarios. In that case, we must plan based on the hydrogeological potential of the karst springs, but if we want to act only on resolving the water crisis, karst wells will be the best option. However, there is no denying that the situation cannot be resilient to subsequent problems and that planning must be based on the sustainability of karst water resources. Therefore, in the sustainability overview, it is preferable to use karst springs rather than digging deep karst wells.

References

Deutsch, W. J. (1997). *Groundwater geochemistry: Fundamentals and application to contamination*. CRC.

Milanovic, P. (2004). *Water resources engineering in karst*. CRC Press.

Taheri, K., Taheri, M., & Parise, M. (2016). Impact of intensive groundwater exploitation on an unprotected covered karst aquifer: A case study in Kermanshah province, western Iran. *Environmental Earth Sciences, 75*(17), 1–16.

Hawraman Summer Camps: The Last Legacy of Water Scarcity Adaptation in the Western Zagros Karst Territory

Aziz Mostafaei, Kamal Taheri, Mario Parise, Sayed Mukhtar Hashemi, and Pouria Khaledi

Abstract

For several thousand years, the inhabitants of Hawraman Karstic region in Western Iran have adapted to the changing conditions of karst water. These summer pastures perched on the high karsts are always located not far from small sources of water, which often dry up at the end of the summer. Three conventional methods for supplying water to the Hawraman karst plateau and the adjacent mountains have been commonly used for several millenniums. The first method is gathering water from trapped ice and snow in the shafts at an altitude above 2000 m. In this instance, springs water and rivers base flow are used by gardens. The second method is to dig an artificial well in the epikarst in the plateau land of the karst territory of Makwan and Atashgah Karst Mountains. This method allows the margins of karst springs in the warm season to use wild animals and to carry water for livestock on the excavated dug wells. The water and melted snow are directed to these wells during the cold seasons of the year. The third method is constructing a small artificial lake (Gemi) that stores similar to ponds in karst high plateau depressions. This paper presents a conceptual model of human-karst interaction in the Western Zagros by drawing the time movements of Kurdish herders and their spatial territory in the karst regions of Hawraman.

Keywords

Hawraman · Zagros · Kurdish herders · Karst water scarcity · Environmental adaptation · Sustainability

1 Introduction

Karst lands can experience water scarcity in certain geographical circumstances. Water shortages are most pronounced as water demands increase in rural settlements. In such situations, instead of putting too much pressure on karst water resources and the overuse of natural springs, a lifestyle can be adapted to cater to water scarcity conditions. This adaptation is still expected after thousands of years in the karst areas of Hawraman in Iranian Kurdistan and Eastern Iraqi Kurdistan. The Kurdish herds drive the cattle to altitudes where sufficient vegetation grows to feed them. These summer pastures perched on the high karsts are always located not far from small sources of water, which often dry up at the end of the summer (Maire, 1990; Watson, 1964). In this paper, by introducing summer camps (which are locally called Hawars) on the World Heritage Site of Hawraman/Uramanat (HAUR), the three approaches of water supply methods at high karst levels are discussed.

2 Socio-geological Setting and Concepts

The inhabitants of Hawraman karstic region of Iran, which is part of the Central Zagros Mountains and situated in the provinces of Kurdistan (KUP) and Kermanshah (KRP), have adapted to the changing conditions of karst water over the millennia (Fig. 1). There is a traditional agro-pastoral social system in Hawraman. Thus, the local economy relies on agriculture (orchads) and livestock, which can be considered the continuation of post-Neolithic lifestyles

A. Mostafaei · P. Khaledi
Cultural Heritage, Tourism and Handicrafts Organization of Kermanshah Province, Paveh Office, Paveh, Iran

K. Taheri (✉)
Kermanshah Regional Water Authority, Ministry of Energy, Kermanshah, Iran
e-mail: taheri.kamal@gmail.com

M. Parise
University Aldo Moro, Bari, Italy

S. M. Hashemi Land and Water Policy Council, Sanandaj Chamber of Commerce, Industries, Mines and Agriculture, Kurdistan, Iran

A. Çiner et al. (eds.), *Recent Research on Environmental Earth Sciences, Geomorphology, Soil Science, Paleoclimate, and Karst*, Advances in Science, Technology & Innovation, https://doi.org/10.1007/978-3-031-42917-0_51

in the Zagros Mountains (Tehrani et al., 2018). This is a sort of semi-nomads pattern. They usually move vertically going from their permanent settlements (i.e., villages) at the base of the karst plateaus around 1500−2000 m altitude a.s.l. to their summer camps (*Hawarga* or *Hawar* in the Kurdish language) in the high mountains (Ghorbani et al., 2008; Ramezani & Ariyana, 2021). The region by Zhawaro (Zhaverud) and Takht, in KUP, and Lahun in KRP, along with parts of the Jaff area (Leileh River Valley, in KRP), was registered in 2021 as Cultural Landscape of Hawraman/Uramanat as the World Heritage Site based on criteria (iii) and (v) (https://whc.unesco.org/en/list/1647/).

Three conventional methods for supplying water to the Hawraman karst plateau and the adjacent mountains have been commonly used for several thousand years. The first is to gather water from trapped ice and snow patches in the shafts at altitudes above 2000 m a.s.l. The second method is digging an artificial well recharge in the epikarst in the plateau land of the karst territory of Makwan and Atashgah Karst Mountains. In the first case, with the onset of the warm season (after the first 45 days of spring or at the beginning of May), these communities move to higher karst altitude by performing special rituals such as *Kumsay* (*Miraw* in the second type). After the warm season, they return with their livestock to lower altitudes settings or *Garmsir*. Water is supplied using high-altitude ice and melting snow of karst doline and shafts during the day (Taheri & Hashemi, 2011). At this time, springs, water, and river base flows are used by gardens. The second method is to leave the margins of karst springs in the warm season to use wild animals and to carry water for livestock on the excavated dug wells. These shallow and deep wells (close to 50 m), excavated by hand, are drilled in the epikarst until they reach the bedrock. The water and melted snow are directed to these wells during the cold seasons of the year. The third method is constructing an artificial small lake or *Gemi,* which stores water similar to ponds in karst high plateau depressions.

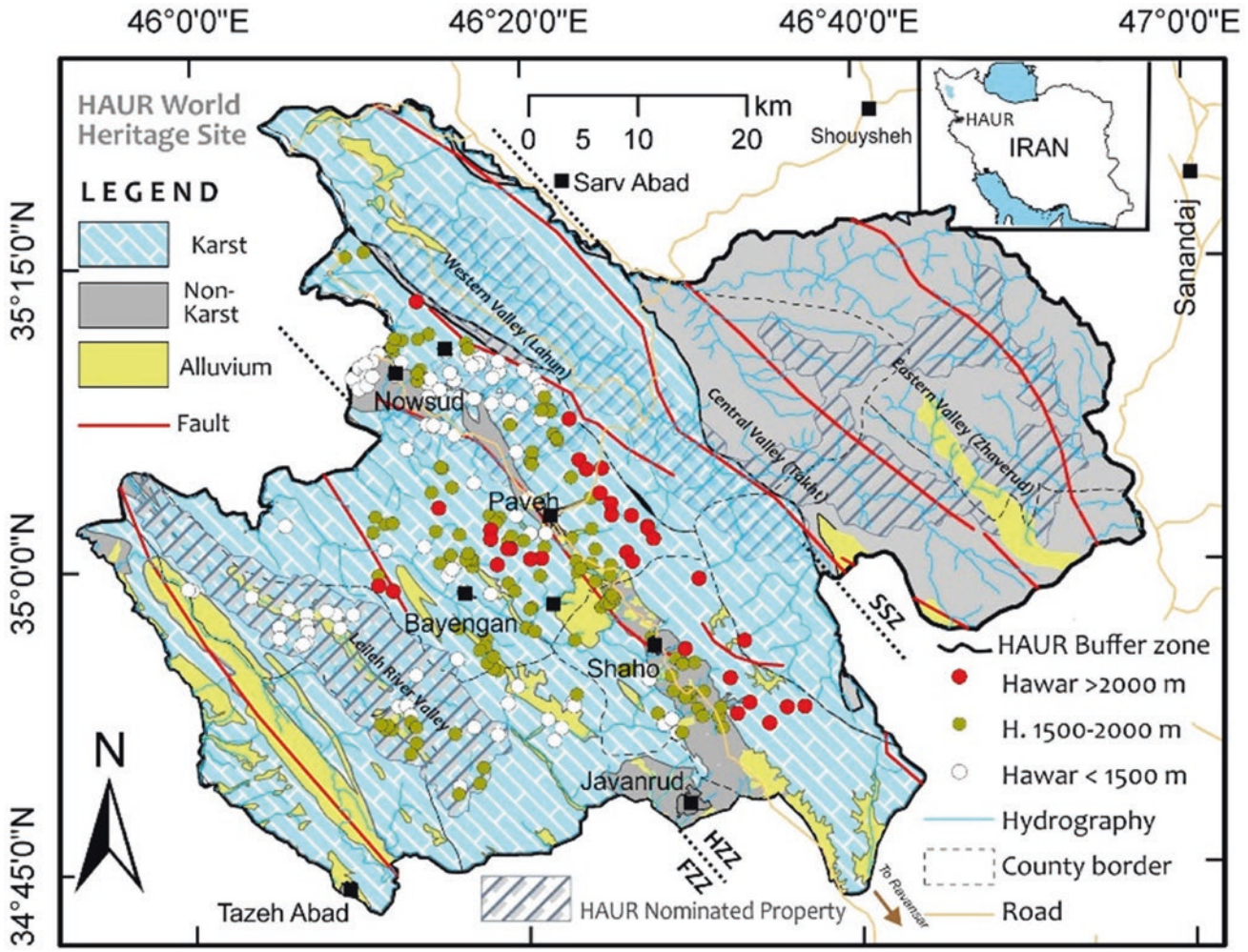

Fig. 1 Geographically extent of Hawraman/Uramanat, karst distribution, and summer camps locations. FZZ: Folded Zagros Zone, HZZ: High Zagros, and SSZ: Sanandaj-Sirjan zone

3 Ethno-Morphotectonic Boundaries and Results

There are more than 150 summer camps (*hawars*) in the study area. Table 1 shows the most famous Hawars in Kermanshah province, mainly supplying their required water by snow melting. Some of these Hawars are still active. The distribution of temporary camps depends on the economic situation of the residents. This distribution follows the pattern of ethnographical (linguistics), tectonic, and livelihood patterns (horticulture-livestock-agriculture) and can be considered an ethno-morphotectonic paradigm. The people of Hawraman use these hawars in areas above 2000 m a.s.l, and Hawrami Kurdish dialect (Guarani) is their language. Their livelihood depends on livestock and horticulture. Their migration is just a vertical pattern. This migration saves water from springs and rivers for gardens inside the village. The water supply is mainly by snow-melt type in the hawars at altitudes higher than 2,000 m a.s.l. Usually, male members of the communities descend in shafts and relatively deep doline to raise ice and frozen snow for consumption. This area is geologically located in the Higher Zagros zone.

At lower altitudes, the number of hawars increases, and the Zardoei tribe and Jaff people use these altitude camps. The Zardoei tribe, who have lived in the Bayengan region, used these two last methods to meet their water, food, and livestock needs in the karst heights. Their dialect is *Sorani* Kurdish, and their livelihood is based on livestock and agriculture. Their type of water supply is Gemi or artificial lake, springs and epikarst dug wells and mainly corresponds to the Folded Zagros Zone. Figure 1 shows the geological map and ethno-morphotectonic boundaries, while Fig. 2 shows the distribution of the camps at different altitudes of the Shahu and Makwan mountains and the abovementioned conceptual method.

4 Discussion

The Hawrami herder people and Jaff and Zardoei nomads have lived in the Takht, Lahun, Liele River Valley, and Zhawaro and use these triple methods to meet their water and livestock needs in the karst heights. Water consumption is saved for three purposes: (1) to irrigate orchards and fruit gardens, (2) for environmental use, and (3) for livestock feeding without the cost of maintaining fodder or collecting plants in summer.

Until nowadays, these Hawars (summer camps) have remained in the study area. However, due to modernization pressures and lifestyle, there has been a disregard for traditional adaptive management methods, and the agro-pastoral transhumance lifestyle has been abandoned. As a result, the region's pastures are leased to non-native herders. Without an Integrated Natural Resources Management Plan, significant damage will be done to this ancient legacy of Hawar settlement patterns. In the not-too-distant future, the last legacy of active camps will be abandoned. With the excessive water consumption, serious water supply challenges in the karst areas of HAUR will be apparent. Population growth and drought and the tendency to effortlessly live in cities disrupt adaptations to millennia of patterns of water scarcity (Fleury, 2009; Parise, 2010).

Table 1 The main Shahu camps (*Hawar*) in Kermanshah province water supply is mainly by ice-snow melting, S: Spring, Elevation (m.a.s.l)

Name	Village	Elevation	Temporal uses	In use	Semi-active	Abandoned
Dalani	Nodesheh	2319		1, 3		
Chalasra	Hadjij	1568			1, S	
Gawl	Hadjij	2019			1, S	
Hwargaw Baram	Paveh	2445				1
Se Mela	Paveh	2921		1		
Shrola	Paveh	2419			1	
Mishyaw	Shemsher	2752			1, S	
Khorila	Shemsher	2793			1.S	
Tlakor	Qouri Qaleh	2078				1
Sanaw	Shabankareh	2419				1
Kasnazan	Shabankareh	2462				1
Pirkhdr	Shabankareh	2441				1
Hamroe	Shabankareh	2119				1
Kosaqawi	Shabankareh	2121				1
Pyaz Dol	Noryab	3054		1		

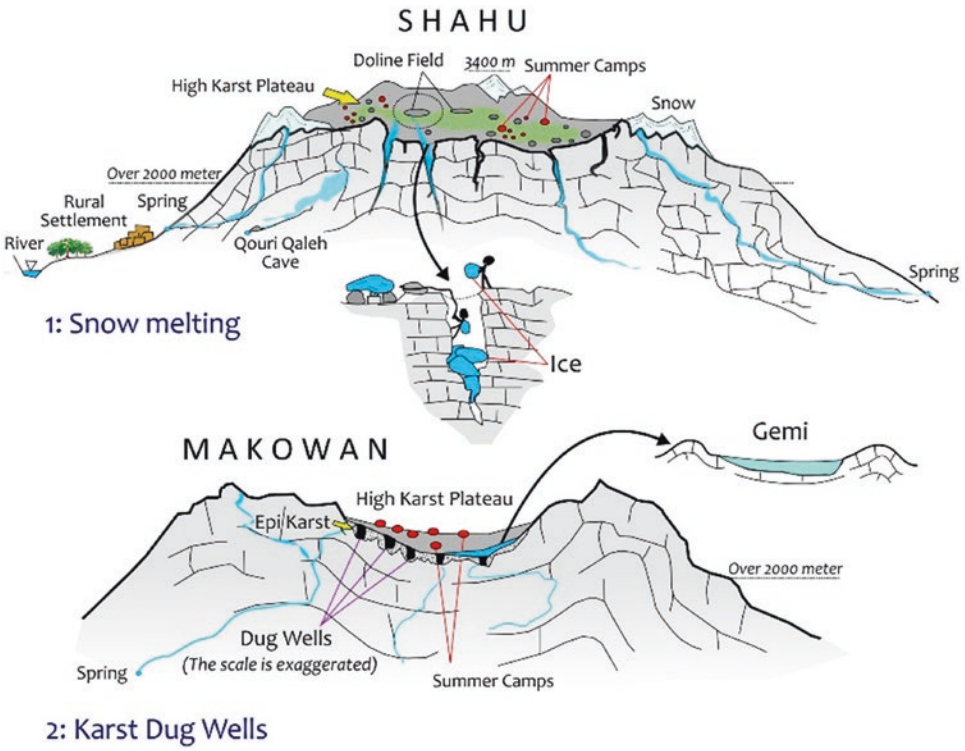

Fig. 2 The conceptual models of human-karst interaction in the HAUR, western Zagros

5 Concluding Remarks

Adaptive management in karst areas is the best way to stand sustainable practices in these fragile areas. The Hawraman/Awramanat World Heritage Site in Western Iran is a prime example of adapting to water scarcity situations, which has been continuously practiced for thousands of years. Currently, climate change, especially drought, has reduced snowfall. Thus the overuse of the ecological capacity of karst areas has caused these areas to be at risk of pollution and deforestation. The conservation of this World Cultural Heritage depends on adopting national and local laws and land change monitoring systems. That should be on the agenda of federal and regional managers and planners.

References

Fleury, S. (2009). *Land use policy and practice on karst terrains*. Springer.

Ghorbani, M. S., Mahmudi, F. A., Yamani, M., & Moghimi, E. (2008). The role of quaternary climate changes on the geomorphic evolution of karst sinkhole. *Physical Geography Research Quarterly, 74*, 1–16. (In Persian).

https://whc.unesco.org/en/list/1647/

Maire, R. (1990). The high karsts of the Kermanshah chain (*Zagros-Iran*), In *La haute montagne calcaire (karsts. Cavités. Remplissage. Quaternaire. Paléoclimats)* (pp. 219–248). Karstologia-Mémoire. Presses Universitaires de Bordeaux.

Parise, M. (2010). Hazards in karst. In O. Bonacci (Ed.), *Proceedings of the International Conference* "*Sustainability of the karst environment*", *IHP-UNESCO*, *Series on Groundwater* (no. 2, pp. 155–162).

Ramezani, H., & Ariyana, S. (2021). Vertical Transhumance at Hawraman, Kurdistan and its implications for neolithic settlement patterns at western zagros. *Bulletin of Miho Museum*, *21*, 1−12.

Taheri, K., & Hashemi, M. (2011). Kurdish karst literature and resources use in the awramanat karst lands of western Zagros, Iran. In *Asian Trans-Disciplinary Karst Conference*.

Tehrani, N., Mashkour, M., & Biglari, F. (2018). Ethnoarchaeological studies in the naw village and the Asparez valley, an attempt to identify seasonal migration patterns and environmental exploitation in prehistoric Hawraman, presented in the first national congress on archaeology of Hawraman: Archaeological salvage excavations at the Darian Dam reservoir. Faculty of Humanities and Social Sciences, University of Kurdistan.

Watson, R. A. (1964). The snow sellers of Mangalat, Iran. *Anthropos*, (H. 5./6), 904–910.

Human-Karst Landscape Interactions and the Anthropo-Karstosphere: Toward a Nexus of Geoethics, Groundwater, and a Sustainable Society

Kamal Taheri and Chris Groves

Abstract

The Earth's karst systems, with all their components (hydrology, human impacts, biodiversity, geodiversity, economic resources, and cultural heritage), could be called the karstosphere. Where human effects can disrupt aspects of the sustainability of karst environments, such a system could be called the anthropo-karstosphere. There are places where the natural environment has been severely affected by, for example, land use change, deep drilling in buried karst aquifers and groundwater mining, destruction of karst landscapes, depletion of karst aquifers, and drying out of karst springs. However, neither simple, one-dimensional scenarios nor multi-dimensional decisions can guarantee conservation plans and protect karst resources without a fundamental, moral understanding of the importance of these resources and the engagement of local communities. Considering the potential effects of climate change, human impacts, increased demand for karst resources (including water, soil, and biodiversity), and disruption of natural karst systems, sustainability paradigms based on responsible management should be integrated by geoethics and the local society's responsibility. In this study, the sustainability of local communities is based on karst resource management, and the perspective of geoethics is taken into consideration. Based on a conceptual model, sustainable extraction of groundwater, ethical views on the utilization and protection of karst aquifers, and patterns of social behavior in various karstosphere settings are discussed with examples from Iran. As expressed in this study, the intellectual framework and communication regarding factors affecting the karstosphere can be considered a basis for establishing a nexus of geoethics, groundwater, and sustainable society.

Keywords

Karstosphere · Groundwater · Geoethics · Sustainable society · Responsible integrated water resources management

1 Introduction

Growing problems and challenges of water resource utilization and their close relationships with human behavior and societal sustainability issues have led to the development of a new discipline focused on multi-dimensional, integrated water resource management methods. The emerging practice of Responsible Integrated Water Resources Management is a reliable, holistic approach to considering the interaction of water and society. The Earth's karst systems, with all their components (hydrology, human impacts, biodiversity, geodiversity, economic resources, and cultural heritage), could be called the karstosphere. This name renews an old term (Andreychouk et al., 2009; Maruashvili, 1970) that, with the complex conditions and fragility of karst systems in the face of climate change and increased carbon dioxide emissions, can serve as a broad term for encompassing the scope of responsible, integrated karst resources management.

Human impacts can disrupt aspects of the sustainability of karst environments. Such a system could be called the anthropo-karstosphere (Fig. 1). In some places, the domain has been severely affected by land use change, deep drilling in buried karst aquifers, and groundwater mining (Karimi &

K. Taheri (✉)
Kermanshah Regional Water Authority, Kermanshah, Iran
e-mail: taheri.kamal@gmail.com

C. Groves
Crawford Hydrology Laboratory, Western Kentucky University, Bowling Green, KY 42101, USA

A. Çiner et al. (eds.), *Recent Research on Environmental Earth Sciences, Geomorphology, Soil Science, Paleoclimate, and Karst*, Advances in Science, Technology & Innovation, https://doi.org/10.1007/978-3-031-42917-0_52

Taheri, 2010; Taheri et al., 2015), destruction of karst landscapes, depletion of karst aquifers, and drying out of karst springs (Taheri et al., 2016). Furthermore, careless management in such systems can lead to the extinction of rare species, the collapse of cultural settings, and damage to both human heritage and human health. In this study, the sustainability of local communities is based on karst resource management, and the perspective of geoethics is taken into consideration. Based on a conceptual model, sustainable extraction of groundwater, ethical views on the utilization and protection of karst aquifers, and patterns of social behavior (economic, agricultural, and ideological) in various karstosphere settings are discussed with examples from Iran.

2 Are Karstosphere Resources a Societal-Defined Concept?

An essential and infrastructural question in karst resource management is the definition of the boundaries of the karstosphere and the coordination between people's perception of the karst concepts and their various resource needs. It must be acknowledged that the karstosphere is not yet understood as an independent, non-commodity entity in many arid and semi-arid regions of the world. The moral knowledge of karst resources and the observance of ethical principles can inform and strengthen the enforcement of the laws that protect these resources.

A great variety of dimensions can characterize karst systems and ways we can think of protecting them. These may include complete water balances, allocation of resources based on dynamic conditions, determining the protection areas of springs, promoting caves and karst social concepts, protecting speleogenetic base flows, maintaining balances between karst water and ecosystems, protecting karst water quality, passing related laws to protect karst, and defining the intrinsic and social values of biodiversity in karst. There are spiritual dimensions. We can trace signs of respect for water and nature. Even karst has its spiritual relevance traced back to ancient religious texts (karst features are specifical mentioned in both the Qur'an and the bible) and the ethical and moral values-based spiritual teachings of all faiths, creating a convergence of the "spiritual world". In the social dimension, the right question is not simply about what resources, such as water, are available for us to utilize. Still, the social needs of those in the karstosphere must remain the same as those of their ancestors. Such requirements are more mental, sensory, moral, and behavioral than quantitative. Many residents of karst regions do not think about what is desirable, undesirable, and advisable for protecting their karstosphere. Still, they expect the responsible authorities to preserve their shared karst resources or geoendowments (Bohle, 2021). This expectation contrasts a one-dimensional management framework based only on technical knowledge with shared management based on multiple social aspects. Adaptive control, which sees human–environment relations beyond rigid law

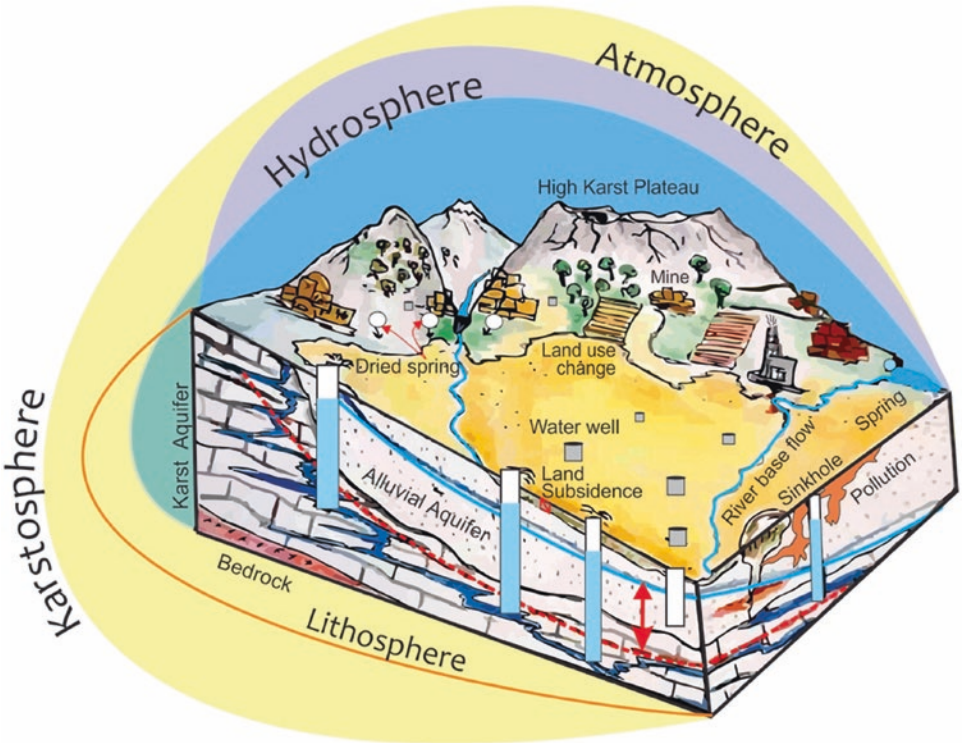

Fig. 1 A small-scale example of an anthropo-karstosphere in a semi-arid area

and regulation, must inevitably expand the basic concepts of the karstosphere in the target community to better understand behaviors and ethical norms. This approach is shown in the conceptual model of Fig. 1.

3 Anthropo-Karstosphere Examples and Results

Along with industrial growth and the expansion of urbanization, a technological paradox is emerging between humans and the karstosphere. This means that, in a way, as people get less connected to the natural world, the understanding of the need for karst protection and the direct connection to karst resources can decrease, while the extraction of karst waters and the degradation of the karst environment are increasing. An example that occurred in different karst areas of Iran residents of a village used several karst springs for water supply. Myths inspired the springs, and some were sacred places, but with the development of deep well drilling technology, deep wells could reach karst groundwater very easily and supply it to the village through piping. This ease of consumption dried out the springs, and consideration of the moral and doctrinal grounds for their protection faded away. Even the new generation of locals forgot that one day there was a spring because the speed of land use change in karst areas is so high that significant changes can be seen in single decades, or sometimes even year to year.

Economic needs such as agricultural development for food security, tourism, raw materials for construction, energy supply, and infrastructure development are examples of social resources needed to sustain communities. In addition to these economic aspects, cultural perspectives are associated with social responsibility. With the help of traditional management methods, myths and symbols, have a profit-free nature and aesthetic or recreational regard to karst heritage. In these cases, karst protection is essential in preserving cultural and religious contexts. Cultural diversity and doctrinal differences can vary in how ethical aspects of karst conservation are expressed. Although the difference in moral teachings can coexist without necessarily creating conflict, economic conflicts of interest can create challenging situations in fragile areas such as karst landscapes. In this state, politics comes into play and seeks to resolve social disputes by enacting laws and regulations. The most crucial work that politicians can do to protect karst resources is to prevent unprofessional interference in land use changes in the karstosphere and try to resolve disputes by building institutional capacity and facilitating science-based laws and regulations.

Purely economic thinking without considering the moral aspects and legal requirements to protect karst bio-geo-endowments is profitable in the short term. However, the lack of recognition of the connection between groundwater in karst with moral conditions and the lack of a sustainable social development program practically exposes the karstosphere to various environmental hazards such as sinkhole and subsidence (Taheri et al., 2019, 2021), water pollution (Taheri et al., 2017) and aquifer depletion through karst water mining.

There is a fundamental, common theme in the teachings of all divine religions to preserve natural resources and blessings of God. Perhaps the most important reference to karst can be seen in religious texts in the Holy Qur'an, where it is written, "And when Moses asked for water for his people, We said: Smite with thy staff the *rock*. And there gushed out from there twelve springs (so that) each tribe knew their drinking place. Eat and drink of that which Allah hath provided, and do not act corruptly, making mischief in the Earth (Pickthall, 2005)." Scholars consider this to be the limestone springs of Ayun Musa in Egypt (Ata et al., 2021). In many parts of Iran, especially in the Central Zagros and the Kurdish regions, until a few years ago, there were still sacred springs, caves, and ancient trees in karst lands that were respected by the people and associated with religious myths and beliefs. This belief has protected these places for thousands of years. Caves and springs are mentioned throughout the bible. In 2 Chronicles 32:30, for example, "It was Hezekiah who blocked the upper outlet of the Gihon spring and channeled the water down to the west side of the City of David" to protect Jerusalem in preparation for an expected siege by the Assyrians. This spring and the waterways through which its waters flow are parts of a natural karst flow system developed in carbonate rocks beneath the city (Gill, 1991). Caves also feature prominently in Hindu and Buddhist traditions.

Climate change is integral to the inherent nature of arid and semi-arid lands. In the karstosphere, which is driven by water and snow, drought can cause adverse events. Drought reduces the dynamic reserves of karst aquifers and the drying out springs by dropping the snow regime. In such a case, groundwater sustainability is seriously endangered—adaptation is the only cure for karst protection against climate change. The teachings of integrated water resources management (IWRM) can lead to the resilience of karst ecosystems and geosystems when targeted in relation to human behavior and moral responsibility.

Water allocation is another issue that can be unfair in the face of groundwater ethics—for example, allocating water to the owner(s) who dug the well earlier instead of the neighbor makes it impossible for the neighbor's owner to drill the well due to locating in water well buffer zones or reduced numerical amounts of planned water in the water budget documents of regional water authorities. Such discrepancies can even negate the laws of water

fair distribution in Iran, which considers water to be public wealth or Anfal (Majidipour et al., 2021). This attitude towards water allocation and water privacy in Iran in the last two decades has led to the expansion of illegal wells and over-exploitation, which can result in land subsidence, groundwater mining, and, ultimately, sinkhole formation (Taheri et al., 2021).

4 Discussion

In recent years, attention to the inanimate environment and geological objects or non-living goods by ethical and moral rules has led to the emergence of the field of geoethics (Abrunhosa et al., 2020; Aragão, 2021; Bohle, 2021). Today, the capitalist system seeks more profit with more production. The effects of climate change and global warming, as much as they did earlier in the collapse of civilizations, have also caused changes in the karstosphere that affect its overall function, with the difference that the self-regulating nature of geological systems can mitigate these effects. In different geological periods, no agent has been able to affect the whole environment (with its various spheres) as much as humankind. In the Anthropocene, groundwater, the world's largest extracted raw material (Foster & Loucks, 2006), puts increasing pressure on natural groundwater and karst systems due to overexploitation. In many parts of the world, these aquifers are hydraulically interconnected. The peak of the groundwater revolution in arid and semi-arid regions such as Iran is the beginning of emptying karst aquifers. The start ends with the destruction of the karstosphere.

The teachings of hydrogeoethics make human beings aware of moral principles. Inducing water as not a commodity but as a geo-endowment can help people also try to appreciate the aesthetic, spiritual, and religious values of karst and groundwater. According to the nexus concept in this paper, if any of the components of Fig. 2 are ignored, the sustainability of the karstosphere may be endangered, or it will face negative impacts such as water pollution, land subsidence, drying springs out, and falling groundwater levels. A sustainable society in the face of karst and groundwater is achieved when the link between moral teachings, law, tradition, and the relationship between humans and karst can be balanced. To do this, ethnographical studies should measure the main factors motivating people to protect

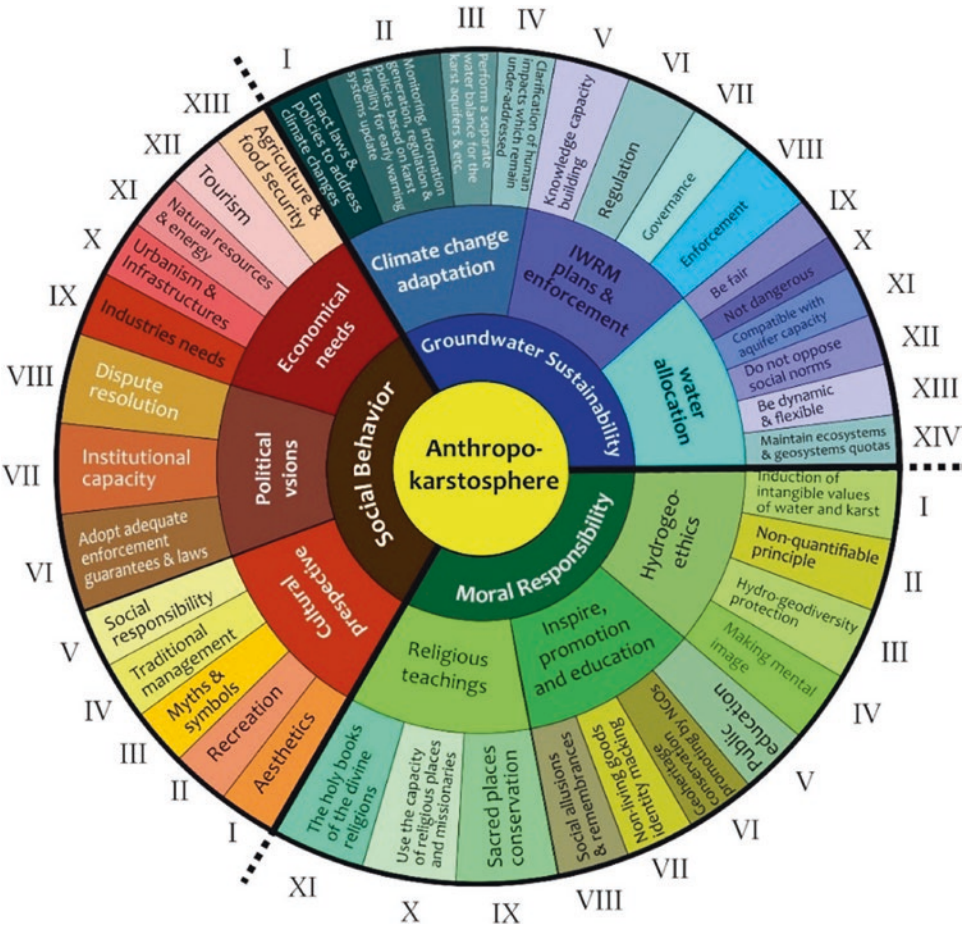

Fig. 2 The conceptual model of the nexus of geoethics, groundwater, and sustainable society

Table 1 Correspondence between main karst media, social behavior, groundwater sustainability, moral responsibility, and relational values

Karst media	Social behavior	Groundwater sustainability	Moral responsibility
Caves	I, II, III, XII	VI, VII, IX, X, XIV	I, III, IV, VI, VII, VIII, IX, X, XI
Springs	I, II, III, IV, V, VII, VIII, X, XI, XII, XIII	II, III, V, VI, VII, XII, XIV	I, II, III, V, IX, X, XI
Karst landscapes	I, II, III, XI, XIII	V, XIV	I, VI, VII, VIII, IX
World heritage sites in karst territories	I, II, III, IV, V, XI, XII	IV, VII, X, XIV	I, III, IV, VII, VIII, IX, XI
Anthropogenic karst sinkholes	V. VI. IX, X, XI, XIII	I, II, III, IV, VII, X, XI, XII, XIV	IV, V
Dams and reservoirs	II, VIII, IX, XI, XII, XIII	II, VIII, XII, XIV	–
Covered karst aquifers	VI, VII, XIII	I, II, III, V, VI, VII, VIII, IX, X, XI, XIV	I, II, III, IV, V, XI
Karst land degradation	I, II, IV, VIII	V, X, XI, XII, XIII,	I, III, VII, VIII, X
Biodiversity and deforestation	I, II, IV, VII, X, XI, XII, XIII	I, V, VI, X, XIV	I, IV, IX, XI,
Intangible heritage values	I, III, XII	II, VI, XIII, XIV	I, IV, V, VII, VIII, IX, X, XI

groundwater and karst based on their ethical themes and social responsibilities. Then, based on the proposed conceptual model (Fig. 2), the main components of karst sustainability are extracted. For more clarity, based on the criteria of Fig. 2, ten cases of karst media are evaluated with this model (Table 1).

5 Conclusions

Based on the conceptual model of Fig. 2, ten different karst environments in Iran were evaluated (Table 1). There are many caves in Iran, and some, like Ali Sadr, are world-famous. However, archaeological caves such as Karaftu are very little known. Every year, several caves in Iran are destroyed for treasure hunting, damaging their sedimentological and archaeological evidence. Demonstration caves are also exposed to increased carbon dioxide emissions and posess the potential to beassociated due to many tourists.

In some cases, cave management in Iran can incompletely consider social responsibility and geoethics rules. After the caves, karst springs have been viewed more than other karst phenomena in Iran. Large springs such as Sasan, Bel, and Ravansar in Fars and Kermanshah provinces are sources of myth and aesthetics, as well as water supply needs and economic development through tourism. These phenomena in the karstosphere are closely related to social responsibility, groundwater sustainability, and social behavior. According to the conceptual model in the nexus of hydrogeoethics, social behavior, and groundwater sustainability, springs are the main manifestations of karstosphere sustainability, and their changes are highly susceptible to the disruption of anthropo-karstosphere.

The presence of karst substrate in the UNESCO World Heritage Sites increases the sensitivity of this heritage's protection. The cultural landscapes of Hawraman/Uramanat, Persepolis, Takht-e Soleyman, Pasargadae, and Bisotun are on the World Heritage List that is located in karst. The cultural, social, and moral significance of these sites is greater than the aspects of groundwater sustainability. However, in Persepolis, groundwater mining is the main threat to land subsidence and the destruction of these heritages.

Increasing rates of groundwater consumption in the last three decades, with disregard for karstosphere characteristics and the fragile nature of karst landscapes, have led to sinkholes forming in several parts of Iran, such as Hamadan and Yazd, Fars, and Kerman provinces. Anthropogenic karst sinkholes are the most prominent symbol of the rupture of the relationship between social responsibility, groundwater unsustainability, and lack of attention to hydrogeoethics.

Most of Iran's reservoir dams are built in karst areas. Lar Dam is a clear global example of not recognizing karst behavior. These structures have been more attractive to the public in terms of people's hopes for water use in agriculture or drinking, and many related social and moral issues have not been considered with adequate care. In this study model, dams have the lowest convergence between social behavior, groundwater sustainability, and hydrogeoethics.

Covered karst aquifers are the most defenseless karstosphere heritage in Iran. Not only are there no laws to protect them, but they are not even considered in water balance studies. For nearly two decades, the water management system in Iran was under the supervision of the private sector. It has intensified the process of emptying these aquifers in the absence of adequate care. In addition to land subsidence, it can cause harmful effects such as water quality degradation and the triggering of sinkholes. Biodiversity in karst areas is closely tied to the health of forests. Changing the use of forest lands in many areas of the Zagros Mountains in Iran, for example, has reduced biodiversity and deforestation, which will significantly impact the volume of karst water reserves in the coming decades by changing the rates of infiltration of water into karst aquifers. The legislative and ethical aspects of karstosphere conservation primarily influence this aspect. Intangible heritage in karst, especially in the Zagros Mountains of Iran, is so abundant that it could be the subject of an international conference. Customs, life at the high karst plateaus, the *Hawars/havars* in the Kurdish regions, and the Kurdish and Lor tribal lifestyles are full of aesthetic aspects, symbols, myths, and tourist attractions. It can be maintained in the karstosphere by maintaining human-environmental interaction and promoting hydrogeoethtics with social responsibility.

Based on what has been said, karst springs, covered karst aquifers, caves, and the World Heritage Sites located in karst areas are among the karst objects that most urgently require consideration and application hydrogeoethics and attention to groundwater sustainability and the promotion of social responsibility to protect them. Therefore, inspiring and promoting geoethics and taking responsibility for educational programs at all levels of society can significantly impact social sustainability and public welfare based on valuing karst heritage while preserving the karstosphere.

References

Abrunhosa, M., Chambel, A., Peppoloni, S., & Chaminé, H. I. (2020, May). Advances in geoethics and groundwater management: Theory and practice for a sustainable development. In *Proceedings of the 1st Congress on Geoethics and Groundwater Management (GEOETH&GWM'20), Porto, Portugal* (pp. 18–22).

Andreychouk, V., Dublyansky, Y., Ezhov, Y., & Lysenin, G. (2009). *Karst in the earth's crust: Its distribution and principal types*. University of Silesia/Ukrainian Academy of Sciences/Tavrichesky National University-Ukrainian Institute of Speleology and Karstology.

Aragão, A. (2021). Relational value as an argument to protect geological and hydrogeologic goods. In *Advances in Geoethics and Groundwater Management: Theory and Practice for a Sustainable Development* (pp. 3–7). Springer.

Bohle, M. (2021). Geoethics for operating in the human Niche. In *Advances in Geoethics and Groundwater Management: Theory and Practice for a Sustainable Development* (pp. 23–26). Springer.

El Ata, A. S. A., Nabawy, B. S., & Badran, O. M. (2021). Integration of shallow geoelectrical investigations for delineating the hidden water springs, case study: Ayun Mousa, Northern Gulf of Suez, Egypt. *Environmental Technology & Innovation, 22*, 101499.

Foster, S., & Loucks, D. P. (2006). Non-renewable groundwater resources. A guidebook on socially sustainable management for water policy makers. *IHP series on groundwater*, (10).

Gill, D. (1991). Subterranean waterworks of biblical Jerusalem: Adaptation of a karst system. *Science, 254*(5037), 1467–1471.

Karimi, H., & Taheri, K. (2010). Hazards and mechanism of sinkholes on Kabudar Ahang and Famenin plains of Hamadan, Iran. *Natural Hazards, 55*(2), 481–499.

Majidipour, F., Najafi, S. M. B., Taheri, K., Fathollahi, J., & Missimer, T. M. (2021). Index-based groundwater sustainability assessment in the socio-economic context: A case study in the western Iran. *Environmental Management, 67*(4), 648–666.

Maruashvili, L. I. (1970). Karstosfera, yeyo razmery i otnoshenie k drugim sferam (Karstosphere, its dimensions and relations with other spheres). *Soobshch. AN GSSR, 57*(2), 357–360. (In Russian).

Pickthall, M. (2005). *The Quran translated*. ICSFP.

Taheri, K., Gutiérrez, F., Mohseni, H., Raeisi, E., & Taheri, M. (2015). Sinkhole susceptibility mapping using the analytical hierarchy process (AHP) and magnitude–frequency relationships: A case study in Hamadan province, Iran. *Geomorphology, 234*, 64–79.

Taheri, K., Taheri, M., & Parise, M. (2016). Impact of intensive groundwater exploitation on an unprotected covered karst aquifer: A case study in Kermanshah province, western Iran. *Environmental Earth Sciences, 75*(17), 1–16.

Taheri, K., Missimer, T. M., Mohseni, H., Fidelibus, M. D., Fathollahy, M., & Taheri, M. (2021). Enhancing spatial prediction of sinkhole susceptibility by mixed waters geochemistry evaluation: Application of ROC and GIS. *Environmental Earth Sciences, 80*(14), 1–28.

Taheri, K., Taheri, M., & Komail, M. S. (2017). Sin-DRASTIC: A modified vulnerability mapping method for alluvial aquifer hosted by karst in the north of Hamadan province, west of Iran. In *EuroKarst 2016*, *Neuchâtel* (pp. 255–271). Springer.

Taheri, K., Shahabi, H., Chapi, K., Shirzadi, A., Gutiérrez, F., & Khosravi, K. (2019). Sinkhole susceptibility mapping: A comparison between bayes-based machine learning algorithms. *Land Degradation & Development*, *30*(7), 730–745. T.

Present-Day Rates of Processes in NW Dinaric Karst

Mitja Prelovšek

Abstract

Karst areas are generally dominated by dissolution, but other fluvial and denudational processes, like mechanical erosion in channels and mass wasting, can also be critical and accompany the pivotal dissolution process. When measuring present-day rates of karst geomorphic processes, the qualitative approach provides objective insight into the rates of karst evolution, enables comparison of rates between each other and with other geomorphic environments, and indicates a rough estimate of the age of karst phenomena. Especially over the last decade, improvement of methodology for measurement of dissolution rates < 0.5 μm/a, measurement in different environmental settings, and a vast number of measurement sites improved our understanding of the NW Dinaric karst evolution. The paper evaluates measured surface and underground dissolution rates, mechanical erosion rates, calcite precipitation rates from percolation water and cave streams, and freshwater bio-dissolution in surface waters. The highest rates for calcite precipitation from percolation water that might exceed 1 mm/a in extreme settings have been found. On the other hand, maximal mechanical erosion rates caused by attrition, bio-dissolution rates in surface waters, and dissolution denudation rates are one order of magnitude lower. In contrast, dissolution and calcite precipitation rates by cave streams are usually two orders of magnitude lower. Site-specific comparison between measured rates provides insight into local geomorphic phenomena' evolution. To some extent, comparing rates provides plausible mechanisms for some crucial landform formations, e.g., karst valleys by bio-dissolution and poljes by combining underground and surface dissolution.

Keywords

Dissolution rates · Calcite precipitation rates · Cave · MEM · Limestone tablets

1 Introduction

Karst is a type of landscape controlled by underground dissolution and drainage. Although it was initially recognized in carbonates, it is characteristic of other well-soluble rocks, like gypsum and halite. Dissolution occurs when undersaturated water chemically reacts with soluble bedrock at the surface or/and underground along permeable structural discontinuities. It results in dissolution denudation. However, despite being crucial, dissolution is far from being the only geomorphic process affecting karst surface or underground; i.e., at steep soluble slopes, mass wasting might exceed the dissolution rate by orders of magnitude, and glaciers have substantially modified high plateaus composed of soluble rocks. Once disintegrated, mechanically weathered soluble material can be considerably eroded by running water and transported from the catchment area as bedload or suspended load with a relatively insignificant role of dissolution. Even in some caves, fluvial erosional features prove at the least partial effect of fluvial transport, i.e., abrasion. On the other hand, mass wasting and mechanical denudation can be neglected at leveled karst areas. Furthermore, dissolution can be a dominant exogenic process.

Quantifying geomorphic processes is an objective approach to understanding Earth's dynamics and might provide an improved understanding and comparison of different geomorphic processes. Despite enhanced quantification stimulated by process geomorphology during the last half of the century, the rate of multiple processes is rarely studied, even on small scales. Surface denudation research

M. Prelovšek (✉)
Karst Research Institute ZRC SAZU, 6230 Postojna, Slovenia
e-mail: mitja.prelovsek@zrc-sazu.si

A. Çiner et al. (eds.), *Recent Research on Environmental Earth Sciences, Geomorphology, Soil Science, Paleoclimate, and Karst*, Advances in Science, Technology & Innovation, https://doi.org/10.1007/978-3-031-42917-0_53

dominates karst areas and provides a global comparison of rates. However, in the NW Dinaric karst, measuring processes in different environmental settings offers an excellent opportunity to compare rates. This is also a goal of this paper—to present measured rates and controlling factors. Since the systematic evaluation of all essential geomorphic processes was not achieved and the overview is far from complete, this paper can be considered the first step to compare rates at least at the level of magnitude.

2 Methodology

This paper evaluates some already published fieldwork output supplemented by unpublished measurements. Three principal methods have been used to address the processes' rates: hydrochemical measurement (catchment-scale dissolution denudation rates), micro (erosion) meter (MEM), and limestone tablets. Details for each method with accuracy can be seen in Prelovšek (2012). All presented rates result from several years of monitoring (in some more important even more than a decade) and include extreme hydrological situations; shorter measurement periods are indicated. While hydrochemical measurement and MEM represent real on-site dissolution rates, limestone tablets represent a reliable quantitative estimate of dissolution and calcite precipitation rate where MEM is no longer possible due to low rates (<10 μm/a). To interpret measured rates, complementary interdisciplinary-connected hydrochemical (PHREEQC calculation; Parkhurst & Appello, 2013), hydrological (hydrograph evaluation of hydrographs), cave micro-climatological (CO_2 monitoring), and biological (Mulec & Prelovšek, 2015) methods have been used.

3 Results

3.1 Dissolution Rates

Dissolution is a chemical process where ions of minerals are transferred into the water (a solvent) by solvation. While surface dissolution can be found in nearly all at least partly soluble rocks, e.g., marls, underground dissolution and geological discontinuities characterize karstic geomorphic systems and strongly define karst underground's ability to transfer surface water through the underground.

Surface dissolution encompasses the dissolution of the surface bedrock and dissolution in soil and underlying epikarst zone. It directly contributes to the denudation (lowering) of the surface and is usually responsible for the majority of the catchment's dissolved load defined at spring (Gunn, 1986). The main factors controlling karst denudation rates are the precipitation amount and underground CO_2 partial pressure. Global observations based on hydrochemical calculations show rates between 4 and 35 μm/a (bare karst, Svalbald; Krawczyk, 2008) or 10 and 40 μm/a (SW Iran; Sepahvand et al., in press) and 90 and 100 μm/a characteristic for Alpine karst (Gams, 1966) with Dinaric karst close to the highest values (60–70 μm/a; Gams, 1966).

Although **dissolution in caves** seems obvious, since at least initiation of caves depends on dissolution, it is not as common due to (over)saturated water, even in big sinking allogenic streams like in the Škocjan Caves (Blatnik et al., 2020). The main driver for temporal variation of dissolution rates along the allogenic stream was found to be discharge (Blatnik et al., 2020; Gunn, 1986), while in caves with autogenic recharge underground ventilation, CO_2 outgassing and water saturation can be more important (Prelovšek, 2009, 2012). The highest dissolution rate (between 35.7 and 77.4 μm/a) has been recorded in a cave fed by a low-gradient allogenic stream with vegetated surface drainage where carbonates have been already dissolved and leached from the soil and underlying bedrock (Prelovšek, 2012). The upward decrease is expected due to less frequent flooding (and exposure time). In contrast, the downstream exponential decrease is connected with increased CO_2 outgassing and decreased CO_2 production rate in the cave sediment (Covington et al., 2013). In most 85 measurement sites where dissolution has been measured over an 8-month-long period, dissolution rates are much lower and usually amount to several μm/a (Prelovšek, 2012). In the Škocjan Caves, dissolution rates are minimal (up to 0.2 μm/a; Blatnik et al., 2020) and limited to periods of high discharge (+109 m^3/s), which happens on average 2-times per year for several hours. Despite being fed by an allogenic stream, but with an important share of water from autogenic recharge, a slightly higher dissolution rate has been measured in the Postojna Cave (0.6 μm/a; Prelovšek, 2012). In the Križna Cave, where autogenic recharge prevails, the highest dissolution rates are 0.2 μm/a (Prelovšek, 2012). Dissolution has been measured in Alpine and Dinaric shafts in the vadose zone. In a typical Alpine cave (Rene Pit, Kanin Plateau, Slovenia), limestone tablets have been used to measure dissolution rates at the bottom of shafts and in the hydrologically active vadose meander. In contrast, 0.2–0.5 μm/a have been measured in the upper 600 m deep sequence shafts, vadose meander 1,100 m below the entrance (2,257 m a.s.l.) shows for a magnitude of higher values (6.6 μm/a). A vertical cave located in the Dinaric karst (Slovak Pit, Croatia; 359 days of measurement in 2015–2016) shows similar dissolution rates (0.0–0.3 μm/a) 130–555 m below the entrance (1,520 m a.s.l.) with the trend of downward dissolution rate increase.

3.2 Calcite Precipitation in Caves

Despite being the same chemical process, site-specific calcite precipitation due to (dripping) percolation water in vadose conditions can be distinguished from calcite precipitation found in bigger water bodies (cave streams) in (epi) phreatic conditions due to different precipitation locations, discharge, and outgassing CO_2 rate. **Precipitation rates in vadose zones** by percolation water have been measured in the Škocjan Caves, where one of the highest calcite deposition rates can be observed regionally. At four measurement sites, rates of 140 ± 80, 293 ± 80, 421 ± 60 and 722 ± 130 µm/a have been observed during 2019–2021. Nearby the fifth measurement site with evidently the highest rate, where rates were measured only during 155 days of 2021, exhibits a 1.8-times higher rate than the highest rate among the four mentioned suggesting rates at the fifth site of about 1,300 µm/a.

Calcite precipitation rates in (epi)phreatic zone have been detected, especially in extensive passages with big cross-sections (Prelovšek, 2012). For example, in the Križna Cave, an epi-phreatic cave with typical discharge at 0.4 m^3/s and maximum above 10.8 m^3/s, calcite precipitation from the cave stream prevails over dissolution with net precipitation rates between 27 µm/a (the 10th lake) and 81 µm/a (rapids below the 1st lake) during the 2006–2018 monitoring period. These are rather extreme calcite precipitation rates, and several µm/a, e.g., 2.4 µm/a in the Škocjan Caves, where water is oversaturated already during average discharge (Blatnik et al., 2020), are more common. The calcite precipitation rate in the Postojna-Planina Cave System amounts to 1 µm/a (Prelovšek, 2012).

3.3 Biodissolution Rates in Surface Water

Although most of the total dissolved load is based on biological CO_2-enhanced dissolution, since CO_2 derives from biological activity, direct dissolution (etching) occurs in surface waters. Freshwater bio-dissolution has been observed at springs and surface rivers with carbonate bedrock (Prelovšek, 2012). Rates have been measured using limestone tablets in settings where the chemical dissolution rate is known or insignificant. Biodissolution rates of 49.2 µm/a have been measured in NW Dinaric karst (Mulec & Prelovšek, 2015) with an indication that at some other sites, up to 150 µm/a (Prelovšek, 2012) of bio-dissolution might be expected.

3.4 Mechanical Erosion (Attrition, Abrasion) Rates in Caves

Due to differences in dissolution rates between allochems or sparry calcite and matrix or cement, mechanical and hydraulic erosion can not be fully distinguished from dissolution. However, especially caves of the contact karst are frequently affected by bed load and suspended sediment. In the Škocjan Caves, where the dissolution rate by the cave stream was as low as 0.2 µm/a, mechanical erosion by the cave stream was measured by MEM at five places visually affected by attrition and abrasion by bedload and suspended sediment. The highest rates were found at sites with attrition where siliciclastic pebbles are hitting a bedrock (from 40 to 160 µm/a) and much lower rates (about 20 µm/a) for surfaces abraded by rotating bedload, often resulting in a pothole. A measurement site that lacks evident abrasion and where the rate is too high for dissolution suggests abrasion by a suspended material of 5 µm/a.

4 Discussion

Rates of measured processes are summarized in Fig. 1. The highest rates and the highest absolute variation have been found for calcite precipitation from percolation water where the rate can exceed 1 mm/a. An order of magnitude lower rate is characteristic of dissolutional denudation rate at the surface, mechanical erosion, and bio-dissolution in surface water. Although the highest dissolution rate in caves can be compared to the dissolutional denudation rate at the surface, moderate mechanical erosion (attrition), and bio-dissolution in surface water, dissolution rates in caves are usually an additional order of magnitude lower. High (spatial) variability of rates makes a clear distinction between rates of processes impossible. While the initiation of cave passages can be fast, a negative feedback loop between dissolution rates and underground CO_2 outgassing in big ventilated caves hinders further dissolutional enlargement of passages close to a water table. The introduction of fluvial sediment into the cave passage may complement and surpass dissolution and manifest in a 90-meters-deep underground vadose meander over millions of years, as observed in the Škocjan Caves. Here, some extreme rates of opposite processes (calcite precipitation and mechanical erosion) are manifested in small areas. Biodissolution rates in surface waters can be compared with the highest mechanical erosion rates. Both can be higher than the

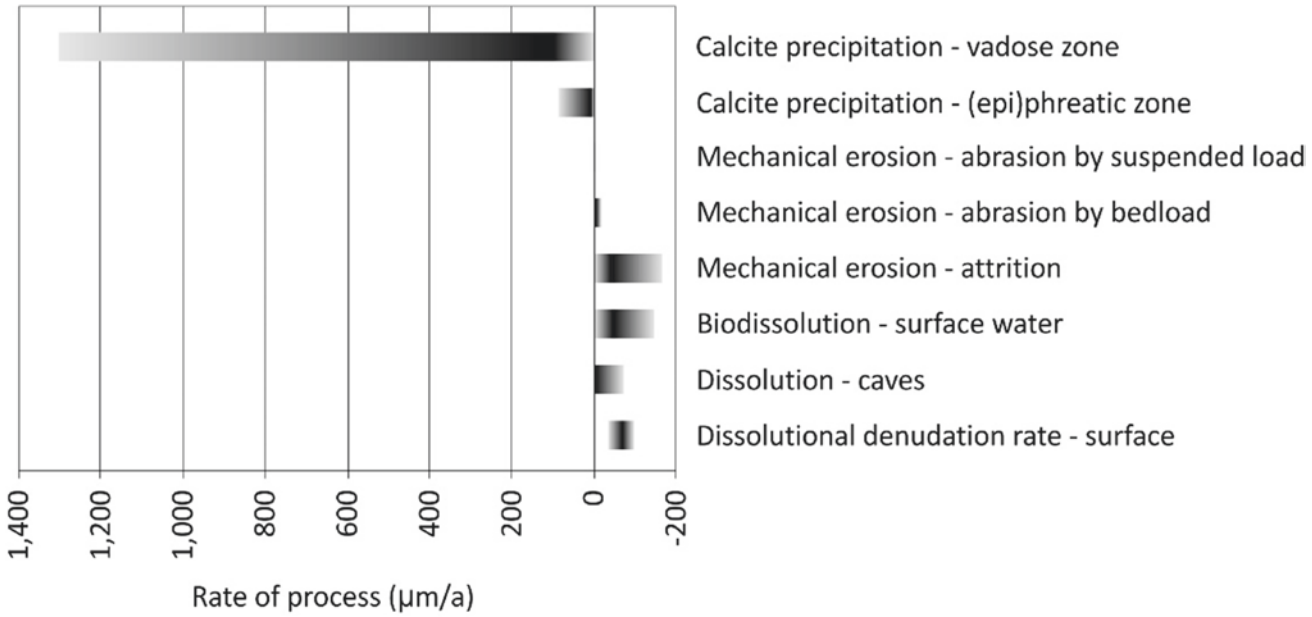

Fig. 1 Comparison of rates of some geomorphic processes found in the area of NW Dinaric karst. Shades of grey represent average and maximal rates. Dissolution and erosion are represented as negative values

dissolutional denudation rate at the surface, resulting in channel incision.

On the other hand, bio-dissolution and mechanical erosion can be absent or lower in several geomorphic settings, which prevents channel incision. Dissolution rates are generally so small that several hundreds of thousands of years are usually needed to form a passable passage. An order of magnitude lower dissolution rates than the surface's dissolutional denudation rate partly explains the formation of broad enclosed occasionally flooded flat depressions (poljes) upstream of swallow holes/caves. It is somehow surprising that calcite precipitation from cave streams at several measurement sites exceeds the dissolution rate, which should, in longer terms, result in complete filling of the cave passage. However, the calcite precipitation rate and thickness of precipitated calcite suggest important changes at the boundary between Holocene and Pleistocene with a tendency toward weaker (if any) calcite precipitation and more intensive dissolution during cold climates.

5 Conclusions

Measured rates indicate a variation of rates across multiple orders of magnitude. Despite the high variation of processes observed at the karst surface and underground, measured local rates of different processes and rates of the same process between measurement sites provide a better understanding of the karst evolution and provide essential quantitative information on the genesis of landforms. While some rates are very site-specific and high spatial differences are expected (e.g., calcite precipitation by percolation water, attrition), others are spatially less heterogenous (e.g., dissolution at the surface and in the underground, calcite precipitation in (epi)phreatic conditions). Despite measurement at several measurement sites, rates of bio-dissolution in surface water on a regional and international scale are the most uncertain.

References

Blatnik, M., Culver, D. C., Gabrovšek, F., Knez, M., Kogovšek, B., Kogovšek, J., Liu, H., Mayaud, C., Mihevc, A., Mulec, J., Aljančič, M., Otoničar, B., Petrič, M., Pipan, T., Prelovšek, M., Ravbar, N., Shaw, T. R., Slabe, T., Šebela, S., & Zupan Hajna, N. (2020). *Karstology in the classical karst*. Springer.

Covington, M. D., Prelovšek, M., & Gabrovšek, F. (2013). Influence of CO_2 dynamics on the longitudinal variation of incision rates in soluble bedrock channels: Feedback mechanisms. *Geomorphology, 186*, 85–95.

Gams, I. (1966). Faktorji in dinamika korozije na karbonatnih kameninah slovenskega dinarskega in alpskega krasa. *Geografski Vestnik, 38*, 11–68.

Gunn, J. (1986). Solute processes and karst landforms. In S. T. Trudgill (Ed.), *Solute processes* (pp. 363–437). John Willey & Sons.

Krawczyk, W. E. (2008). The range of chemical denudation rates on Svalbard. In *Geophysical Research Abstracts 10*. EGU General Assembly 2008.

Mulec, J., & Prelovšek, M. (2015). Freshwater biodissolution rates of limestone in the temperate climate of the Dinaric karst in Slovenia. *Geomorphology, 228*, 787–795.

Parkhurst, D. L., & Appelo, C. A. J. (2013). Description of input and examples for PHREEQC (version 3)–a computer program for

speciation, batch-reaction, one-dimensional transport, and inverse geochemical calculations. *U.S. Geological Survey Techniques and Methods*, *6*(A43).

Prelovšek, M. (2012). *The dynamics of the present-day speleogenetic processes in the stream caves of Slovenia*. ZRC Publishing.

Prelovšek, M. (2009). Influence of meteorology on speleothem deposition: Example from Križna jama, Slovenia. In W. B. White (Ed.), *Proceedings of the 15th International Congress of Speleology, Kerrville, Texas, July 19–26, 2009, Vol. 1, Symposia Part 1* (pp. 1643–1649). International Union of Speleology.

Sepahvand, A., Prelovšek, M., Nazari Samani, A. A., & Wasson, R. J. (2021). Solute transport and solutional denudation rate of carbonate karst in the semi-arid Zagros region (southwestern Iran). *Journal of Cave and Karst Studies*. in press.

Morphological and Hydrogeological Features of Sinkholes in Coastal Settings

Isabella Serena Liso, Stefano Margiotta, and Mario Parise

Abstract

The coastlines of Apulia (SE Italy) are intensely interested in the development of sinkhole processes related to the carbonated nature of the rocks, the generally low elevation, and the hydrogeological conditions of the coastal groundwater of this peninsula. Sinkholes are the main geohazard in the region, and particularly along the coasts, they represent the leading cause of economic losses to the tourist industry. In this contribution, we discuss the main events in southern Apulia, pointing to the geological and hydrogeological characteristics leading to sinkhole formation.

Keywords

Karst · Hydrogeology · Coastal groundwater · Sinkholes · Apulia

1 Introduction

In many areas of the world, coastal areas, both as high rock cliffs or low coastal plains, are interested in the development of sinkhole phenomena, mainly related to karst processes and their combination with marine erosion and mixing of fresh and saltwater (Ford & Williams, 2007; Gutierrez et al., 2014; Parise, 2019; Sauro, 2003; Waltham et al., 2005). However, beyond the danger posed to local inhabitants and human structures, sinkhole formation may reduce the environmental appeal for tourists in the affected areas, with significant losses to the local economy (Brinkmann & Parise, 2012). In this contribution, we examine the Apulian coastlines (SE Italy), characterized by the extensive presence of sinkholes (Delle Rose et al., 2004; Festa et al., 2012; Prete et al., 2010).

2 Geological and Hydrogeological Setting

Apulia is an elongated peninsula with about 900 km of coastlines in a mostly carbonate setting made of Cretaceous limestone bedrock, partly covered by Oligo-Miocene and Plio-Pleistocene calcarenites (Doglioni et al., 1994; Pieri et al., 1997). Based upon the elevation of the MIS 5.5 shoreline markers, Lambeck et al. (Lambeck et al., 2004) pointed out a generally stable situation for Apulia with the highest value of local uplift, at sites along the Adriatic and Jonian coasts, of 0.08 ± 0.11 mm yr^{-1}. In addition, there are marshlands and wetland areas at many coastal locations, bounded on the outer side by dunes (Mastronuzzi & Sansò, 2002). They determine the formation of interesting and marvelous naturalistic sites, many of which have been declared Sites of Community Importance (SIC) according to the European Commission Habitats Directive (Boenzi et al., 2006; Delle Rose & Parise, 2002; Margiotta & Parise, 2019). As regards the hydrogeological coastal setting, many karst springs are present, most of which as submarine springs, identified through thermal camera surveys (Cotecchia, 2014; Liso & Parise, 2020). The diffuse presence of springs testifies to the great importance of karst aquifers, which are heavily threatened by seawater intrusion (Cotecchia, 2014; Masciopinto et al., 2017).

I. S. Liso · M. Parise (✉)
Dipartimento Di Scienze Della Terra E Geoambientali, University Aldo Moro, Bari, Italy
e-mail: mario.parise@uniba.it

S. Margiotta
University of Salento, Lecce, Italy

M. Parise Institute of Research for Geo-Hydrological Protection, National Research Council, Rome, Italy

A. Çiner et al. (eds.), *Recent Research on Environmental Earth Sciences, Geomorphology, Soil Science, Paleoclimate, and Karst*, Advances in Science, Technology & Innovation, https://doi.org/10.1007/978-3-031-42917-0_54

3 Results

In the last decades, many events of sinkholes have been registered along the Apulian coastal zone (Table 1), mainly in correspondence with low rock cliffs or beaches. These events have inevitably posed a risk to human society, given the high tourist vocation of the area. Among the most affected sites on the Adriatic coast, the Casalabate site shows small-size sinkholes that occurred both in the vicinity of the beach and offshore, threatening several houses in this small town, mostly frequented during the touristic season. Over the carbonate karstified bedrock, the presence of thin layers of marsh deposits with high compressibility is at the origin of the many episodes of cover suffusion sinkholes (Gutierrez et al., 2014; Parise, 2019) registered in the town since the 1990s (Margiotta et al., 2012).

A few km SE, again on the Adriatic coast, the Acquatina basin is part of the reclamation works realized to gain agricultural land and convey water from the marshlands to the sea. These remediation activities were made during the first decades of the last century, ending after World War II. Local stratigraphy consists of Cretaceous limestone bedrock, overlain by less permeable Miocene deposits, determining the condition of confined aquifer within the limestones. Due to discontinuity systems in the Miocene succession, groundwater from the coastal karst aquifer rises upward and originates springs; further, in the upwelling, it mixes with other waters from more shallow aquifers in the Plio-Pleistocene deposits. This water flows within the basin and undermines the cover deposits by internal erosion, triggering the development of suffusion sinkholes. As a result, the cover behaves as a ductile or loose granular material, settling gradually and originating the circular depressions from 1 to a few meters wide. The process, observed since 2006 is still ongoing, thanks to the availability of high-quality aerial photographs, and, in time, brought to the formation of several tens of sinkholes with increasing diameter and coalescing features. A similar situation was probably at the origin of the Cesine marshlands, some km to the south. The formation has been interpreted as being related to several coalescing and evolving sinkholes, partly controlled by the geological and structural features of the area (Delle Rose & Parise, 2002) (Fig. 1).

Other sinkholes have been documented as collapses along the Jonian coast (Torre Castiglione, Alliste, spunnulate, etc.), mainly near the shoreline as the product of failures in the cave ceilings, with hyperkarst processes likely deriving from the mixing of fresh and sea waters (Basso et al., 2013; Bruno et al., 2008).

Table 1 Chronology of main documented sinkhole events along the Apulian coastlines

Date	Location	Type of sinkhole
1980	Torre Castiglione	Collapse
1992	Torre Inserraglio–Sant'Isidoro	Collapse
1993/01/06	Casalabate	Cover suffosion
1994/01/01	Casalabate	Cover suffosion
1997/08/20	Casalabate	Cover collapse
2000/05/15–19	Casalabate	Cover collapse (?)
2004/02	Marina di Alliste	Collapse
2004/11/17	Casalabate	Cover collapse
2006–present	Acquatina	Suffosion
2009	Torre Castiglione	Collapse
2010/03/02	Casalabate	Cover collapse
2010/11/06	Casalabate	Cover suffosion
2011/03/10	Casalabate	Cover collapse (?)
2019/09	Spunnulata La Pajara	Collapse (enlargement)
Before June 2020	Porto Ligno	Collapse

4 Discussion

In Apulia, a mostly carbonate region, the presence of impervious or low-permeability deposits covering the limestone karstified bedrock is often at the origin of the development of sinkholes along the coasts, with severe damage to the tourist activities and losses to the local economy. Deepening on this the knowledge about the mechanisms of sinkhole formation is crucial to mitigate the related risk (Parise & Gunn, 2007; Parise et al., 2015) and better understanding of the modality of groundwater flow in relation to the many springs located along the coastlines. This knowledge gain is needed since large sinkholes have been documented offshore (Taviani et al., 2012) to further testify to the relevance of these phenomena in the region and, generally, in the Adriatic area.

Fig. 1 Multi-temporal evolution of sinkholes in the Acquatina basin (google earth)

References

Basso, A., Bruno, E., Parise, M., & Pepe, M. (2013). Morphometric analysis of sinkholes in a karst coastal area of southern Apulia (Italy). *Environment and Earth Science, 70*(6), 2545–2559.

Boenzi, F., Caldara, M., Pennetta, L., & Simone, O. (2006). Environmental aspects related to the physical evolution of some wetlands along the Adriatic coast of Apulia (southern Italy): A review. *Journal of Coastal Research, 39*, 170–175.

Brinkmann, R., & Parise, M. (2012). Karst environments: Problems, management, human impacts, and sustainability. *Journal of Cave and Karst Studies, 74*(2), 135–136.

Bruno, E., Calcaterra, D., & Parise, M. (2008). Development and morphometry of sinkholes in coastal plains of Apulia, southern Italy. Preliminary sinkhole susceptibility assessment. *Engineering Geology, 99*, 198–209.

Cotecchia, V. (2014). Le acque sotterranee e l'intrusione marina in Puglia: dalla ricerca all'emergenza nella salvaguardia della risorsa. Memorie Descrittive della Carta geologica d'Italia, *92*, 416.

Del Prete, S., Iovine, G., Parise, M., & Santo, A. (2010). Origin and distribution of different types of sinkholes in the plain areas of southern Italy. *Geodinamica Acta, 23*(1/3), 113–127.

Delle Rose, M., & Parise, M. (2002). Karst subsidence in south-central Apulia, Italy. *International Journal of Speleology, 31*(1/4), 181–199.

Delle Rose, M., Federico, A., & Parise, M. (2004). Sinkhole genesis and evolution in Apulia, and their interrelations with the anthropogenic environment. *NHESS, 4*, 747–755.

Doglioni, C., Mongelli, F., & Pieri, P. (1994). The Puglia uplift (SE Italy): An anomaly in the foreland of the Apenninic subduction due to buckling of a thick continental lithosphere. *Tectonics, 13*, 1309–1321.

Festa, V., Fiore, A., Parise, M., & Siniscalchi, A. (2012). Sinkhole evolution in the Apulian karst of southern Italy: A case study, with some considerations on sinkhole hazards. *Journal of Cave and Karst Studies, 74*(2), 137–147.

Ford, D. C., & Williams, P. (2007). *Karst hydrogeology and geomorphology*. Wiley & Sons.

Gutierrez, F., Parise, M., De Waele, J., & Jourde, H. (2014). A review on natural and human-induced geohazards and impacts in karst. *Earth Science Reviews, 138*, 61–88.

Lambeck, K., Antonioli, F., Purcell, A., & Silenzi, S. (2004). Sea level change along the Italian coast for the past 10,000 years. *Quaternary Science Reviews, 23*, 1567–1598.

Liso, I. S., & Parise, M. (2020). Apulian karst springs: A review. *International Journal of Environmental Science and Technology, 8*, 63–83.

Margiotta, S., & Parise, M. (2019). Hydraulic and geomorphological hazards at wetland geosites along the eastern coast of Salento (SE Italy). *Geoheritage, 11*, 1655–1666.

Margiotta, S., Negri, S., Parise, M., & Valloni, R. (2012). Mapping the susceptibility to sinkholes in coastal areas, based on stratigraphy, geomorphology and geophysics. *Natural Hazards, 62*(2), 657–676.

Masciopinto, C., Liso, I. S., Caputo, M. C., & De Carlo, L. (2017). An integrated approach based on numerical modelling and geophysical survey to map groundwater salinity in fractured coastal aquifer. *Water, 9*, 875.

Mastronuzzi, G., & Sansò, P. (2002). Holocene coastal dune development and environmental changes in Apulia (southern Italy). *Sedimentary Geology, 150*, 139–152.

Parise, M., & Gunn, J. (Eds.). (2007). *Natural and anthropogenic hazards in karst areas: Recognition analysis and mitigation*. Geological Society London, sp. publ. 279.

Parise, M. (2019). Sinkholes. In W. B. White, D. C. Culver, & T. Pipan (Eds.), *Encyclopedia of caves* (3rd ed., pp. 934–942). Academic Press, Elsevier.

Parise, M., Ravbar, N., Živanovic, V., Mikszewski, A., Kresic, N., Mádl-Szo ˝nyi, J., & Kukuric, N. (2015). Hazards in karst and managing water resources quality. In Z. Stevanovic (Ed.), *Karst*

Aquifers–Characterization and Engineering (pp. 601–687). Springer.

Pieri, P., Festa, V., Moretti, M., & Tropeano, M. (1997). Quaternary tectonic of the Murge area (Apulian foreland-southern Italy). *Annali Di Geofisica, 40*(5), 1395–1404.

Sauro, U. (2003). Dolines and sinkholes: Aspects of evolution and problems of classification. *Acta Carsol, 32*(2), 41–52.

Taviani, M., Angeletti, L., Campiani, E., Ceregato, A., Foglini, F., Maselli, V., Morsilli, M., Parise, M., & Trincardi, F. (2012). Drowned karst landscapes offshore the Apulian margin (Southern Adriatic sea, Italy). *Journal of Cave and Karst Studies, 74*(2), 197–212.

Waltham, T., Bell, F., & Culshaw, M. (2005). *Sinkholes and subsidence*. Springer.

Geophysical Investigation of Recently Formed Collapse in Latvia

Pēteris Džeriņš, Jānis Karušs, and Jurijs Ješkins

Abstract

In December 2020, a sinkhole appeared in Latvia, nearby Skaistkalne's vicinity, where active karst processes occur. It is the most active karst region in Latvia, with an average density of approximately 13 sinkholes per km^2 (Paukstys & Narbutas Paukstys B., & Narbutas V. (1996). Gypsum karst of the baltic republics. International Journal of Speleology, 25. 10.5028/1827-806X.25.3.21). This region is in the southern part of Latvia (on the border with Lithuania), and it is part of the Gypsum Karst Region of the Baltic States that continues south and is well pronounced in the territory of Lithuania. However, this recent collapse formed more than 6 km from the officially known karst area (SGS Ministry of Environmental Protection and Regional Development. (1997). State geological survey. Karst area map of Latvia, scale 1:200 000 (in text: SGS 1997).). UAV was used to prepare the Digital Elevation Model (DEM) of the surrounding area to evaluate the collapse's volume precisely. In addition, the Electrical Resistivity Tomography (ERT) method was used to investigate ground conditions under the collapse. Results show a low-resistivity zone under the collapse at 30 m depth, which coincides with the boundary between clastic sediments on top and carbonate sediments (dolomites) at the bottom. The results of this study could be used to understand the origin of this sinkhole better and subsequently used to assess possible karst risk outside the officially known karst area of Latvia.

Keywords

Sinkhole formation · Carbonate karst · Geophysics · Electrical resistivity tomography

1 Introduction

Karst processes in Latvia are related to carbonate rocks or gypsum dissolution. The present climate does not favor the evolution of the karst process in carbonates. Therefore currently, only the active gypsum karst process takes place. However, paleokarst features have been reported in carbonate rocks in Latvia, nearby Daugava valley. These features are mostly filled with secondary material—sand, clay, or dolomite powder. In some areas, surface features of karst processes such as sinkholes, karst shafts, land subsidence, lakes, and dolines are present (Paukstys, Narbutas 1996).

The relevant sinkhole is formed approximately 200 m from the coast of the Memele river, which is known to recharge from the karst aquifer (Delina et al., 2012). The geological section here consists of Quaternary and Upper Devonian sediments. The upper 8 m are formed by glacial till and sandy gravel, followed by a 24 m thick Upper Devonian marlstone and sandstone layer. Below carbonatic Devonian sediments are found—mostly dolomite with marl, gypsum, and dolomitic marl interlayers.

This study aims to investigate the geological setting of the nearby area surrounding the recent collapse and to understand its origin better.

2 Materials and Methods

The cause of the collapse was investigated using Electrical Resistivity Tomography (ERT) frequently applied to a shallow subsurface investigations (Drahor, 2019; Karušs et al., 2021; Lamsters et al., 2020). ERT survey was carried out using a multichannel Syscal Pro Switch (IRIS Instruments)

P. Džeriņš (✉) · J. Karušs · J. Ješkins
Faculty of Geography and Earth Sciences, University of Latvia, Jelgavas Str. 1, Riga LV-1004, Latvia
e-mail: peteris.dzerins@lu.lv

A. Çiner et al. (eds.), *Recent Research on Environmental Earth Sciences, Geomorphology, Soil Science, Paleoclimate, and Karst*, Advances in Science, Technology & Innovation, https://doi.org/10.1007/978-3-031-42917-0_55

device. Measurements were performed using 72 stainless steel electrodes and Wenner and Dipole–dipole electrode configurations. Data were gathered using two different electrode spacings—1 and 2 m. Results were visualized by combining separate profiles into a 3D resistivity model. ERT data processing was done using RES2DINV and RES3DINV (Geotomo Software). In addition, aerial photographs of the surrounding area were taken from unmanned aerial vehicle (UAV) and used to produce an orthophoto map and DEM.

3 Results

The collapse area is 72 m^2, and the approximate volume is 134 m^3 based on a Digital Elevation Model (DEM). ERT results show a low-resistivity zone under the collapse that is traceable until the maximum Depth of Investigation (DOI), which is 27 m, and possibly continues deeper (see Fig. 1). DOI coincides with the geological boundary between Devonian clastic sediments (sandstone, marlstone) on top and Devonian more carbonatic sediments (dolomite) at the bottom. A high resistivity zone directly below the ground surface is interpreted as Quaternary sediments (glacial till, sand, gravel), which typically have high resistivity values, followed by a thick low resistivity layer corresponding to Upper Devonian clastic sediments. In the ERT profile, at approximately 20 m depth, the resistivity increases again, which is interpreted as the boundary between Upper Devonian clastic and carbonatic sediments. However, under the collapse, at 25 m depth, depression of low resistivity in the surrounding higher resistivity layer was found. It could be explained by the downward movement of the overlaying low-resistivity material.

Results show that dissolution processes must have introduced the origin of the collapse in carbonate layers, followed by the upwards progression of the void in overlaying clastic sediments.

4 Discussion

To map karst risk zones for geotechnical purposes, some relationship between geological setting, underground void size, and sinkhole formation risk can be used. Waltham's (2016) estimations show that the stable thickness of rock cover above the underground void for gypsum and weak limestone should be approximately the same as the width of the cavity itself. Although our investigations don't provide insight into the size of the underground cavity, the limiting factor for vertical dimension usually is the thickness of dolomite and gypsum layers (here, less than ten continuous meters). Comparably thick Devonian cover over this void (24 m) suggests that such a relationship between void size and stable rock cover might not be appropriate in this geological setting. Instead, the authors hypothesize that relative proximity to the Memele river significantly impacts underground dissolution processes and subsequent formation of the collapse. However, this should be further investigated using, for example, hydrogeological methods.

As this is ongoing research, for a better understanding of the geological setting under the collapse, ERT measurements could be complemented with other geophysical methods, such as seismics. In continuation of this study, it is planned to use the seismic reflection method to specify boundaries between layers—seismic data could be used to improve the ERT model.

Since UAV was used to capture sinkhole dimensions soon after its formation, repeated measurements over a more extended period could be taken to visualize slope development over time.

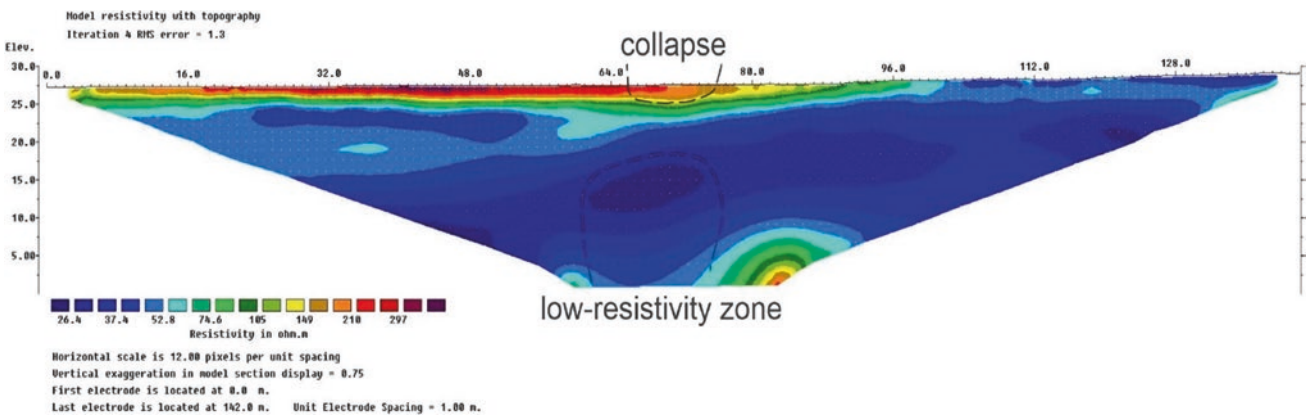

Fig. 1 ERT profile along the collapse. This profile was performed using Wenner electrode array and 2 m electrode spacing

5 Conclusions

A recently formed sinkhole outside of an active karst area of Latvia was investigated using UAV and ERT measurements to understand its origin better. Based on photogrammetry results, the collapse area is 72 m^2, and the approximate volume is 134 m^3.

ERT results show a low-resistivity zone up to 27 m depth (limited by DOI) that most probably continues deeper. This suggests that dissolution processes must have introduced the origin of the collapse in carbonate layers, followed by the upwards progression of the void in overlaying clastic sediments. However, additional geophysical investigations are planned in this location. For example, a different ERT profile should be performed with broader electrode spacing to reach DOI, where the extent of the low-resistivity zone in the vertical dimension could be seen. Also, additional geophysical methods (for example, seismic reflection) could be used to improve the ERT model.

Acknowledgements This work was financially supported by the performance-based funding of the University of Latvia within the "Climate change and sustainable use of natural resources" project.

References

Delina, A., Babre, A., Popovs, K., & Sennikovs, J. (2012). Effects of karst processes on surface water and groundwater hydrology at Skaistkalne Vicinity, Latvia. *Hydrology Research, 43*(4), 445–459.

Drahor, M. G. (2019). Identification of gypsum karstification using an electrical resistivity tomography technique: The case-study of the Sivas gypsum karst area (Turkey). *Engineering Geology, 252*, 78–98.

Karušs, J., Lamsters, K., Poršņovs, D., Zandersons, V., & Ješkins, J. (2021). Geophysical mapping of residual pollution at the remediated Inčukalns acid tar lagoon, Latvia. *Estonian Journal of Earth Sciences, 70*(3), 140–151.

Lamsters, K., Karušs, J., Stūrmane, A., Ješkins, J., & Džeriņš, P. (2020). Mapping of large-scale diapir structures at the paleo-ice tongue bed in western Latvia from geophysical investigations and borehole data. *Quaternary International*. https://doi.org/10.1016/j.quaint.2020.12.003.

Paukstys B., & Narbutas V. (1996). Gypsum karst of the baltic republics. *International Journal of Speleology*, *25*. https://doi.org/10.5028/1827-806X.25.3.21

Ministry of Environmental Protection and Regional Development. (1997). State geological survey. Karst area map of Latvia, scale 1:200 000 (in text: SGS 1997).

Waltham, T. (2016). Control the drainage: The gospel accorded to sinkholes. *Quarterly Journal of Engineering Geology and Hydrogeology*, *49*.

Karst Phenomenon in Gypsum and Interference with Quarry Activity: Examples from Monferrato Area (NW Italy)

Chiara Caselle and Sabrina Maria Rita Bonetto

Abstract

Investigating karst systems in gypsum and anhydrite terrains is essential in minimizing risks connected with the presence of civil infrastructures (e.g., underground quarries). However, if not carefully evaluated, the interference between karst systems and quarry activity may evolve in risk scenarios for the stability of underground tunnels, causing collapses of karst caves, slop instabilities, subsidence phenomena on the surface, and modification of the hydrogeological setting of the area. This article describes the features of gypsum quarries in the Monferrato area of Piedmont (NW Italy), aiming to highlight the main risks connected with karst circulation in evaporite terrains.

Keywords

Karst · Gypsum · Quarries

1 Introduction

The development of the karst phenomenon is usually related to the presence of rocks with high solubility in water. However, even if the most studied karst circuits are developed in carbonate rocks (e.g., limestones and dolomite), important karst morphologies can also be recognized in sandstones or evaporite terrains (e.g., salt beds, gypsum, or anhydrite). In particular, due to the bedrock's higher solubility and lower mechanical strength, karst in evaporite rocks presents some peculiarities, such as the higher probability of occurrence of surface morphologies (e.g., sinkholes) (Gutiérrez et al., 2008, 2014; Parise, 2019).

Large volumes of evaporite rocks are also an essential resource for quarry exploitation. Consequently, the excavation operations may interfere with the karst circuits, creating unexpected risk scenarios. Without careful management, these scenarios may cause severe damage not only to the quarry site but also to the safety and environmental sustainability of the surrounding area (Ramon et al., 2021).

Detailed knowledge of local karst circulation features is, therefore, fundamental for risk minimization and prevention. For this reason, the present study proposes a review of the typical features of the karst phenomenon in the Monferrato area (Piedmont–NW, Italy). This area hosts big volumes of gypsum that are interested in active and relict karst circulation and have been the object of diffuse exploitation by open air and underground quarries for several decades, representing one of the main production areas of gypsum in Italy.

2 Geological Framework and Orebody Exploitation

Monferrato area of Piedmont (NW Italy) hosts large volumes of evaporite rocks that may be attributed to the Messinian Salinity Crisis. This paleo-oceanographic event involved the Mediterranean area at the end of the Miocene.

Figure 1 shows the location of the main bodies of evaporite rocks in Monferrato. In most outcrops, the rocks are organized in depositional cycles consisting of gypsum beds (up to 15 m of thickness) and marl layers (with thickness between a few decimeters and a few meters). The sequence is usually regular and presents high lateral continuity. Gypsum may have different features in different cycles. In particular, the lower cycles typically consist of beds of selenitic gypsum with big crystals of up to several decimeters. However, the most recent cycles usually consist of

C. Caselle (✉) · S. M. R. Bonetto
Earth Science Department, Università Degli Studi Di Torino, Torino, Italy
e-mail: chiara.caselle@unito.it

A. Çiner et al. (eds.), *Recent Research on Environmental Earth Sciences, Geomorphology, Soil Science, Paleoclimate, and Karst*, Advances in Science, Technology & Innovation, https://doi.org/10.1007/978-3-031-42917-0_56

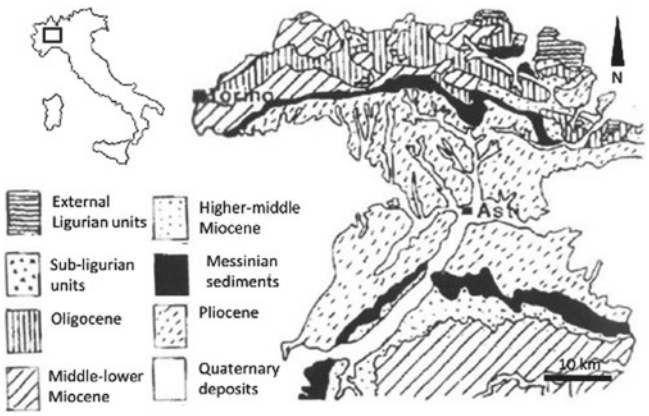

Fig. 1 Geological sketch of the Monferrato area (Oggeri et al., 2006)

fine-grained gypsum (with a grain size of a few millimeters) with a marl matrix representing between 5 and 20% of the volume of the rock (Dela Pierre et al., 2003).

The western outcrops in the area show different features: gypsum is included in a chaotic deposit, with rock blocks of various nature and sizes in a marl-clayey matrix. Following the most recent interpretations, the deposition of this chaotic body is related to the action of complex regional-scale landslide phenomena that brought to the re-deposition of the evaporitic succession and older sediments (Dela Pierre et al., 2003).

The gypsum exploitation in the Monferrato area is active in 5 quarry sites (including two open pitches and three underground quarries). In the eastern regions, the gypsum beds' regularity and high lateral continuity assure large, easily predictable, and continuous orebodies. Where gypsum sediments lay within the chaotic body, on the other hand, the orebodies are more unpredictable. The most productive ones are usually located in correspondence with the most significant blocks with the lower proportion of the matrix.

3 Features of Karst Phenomenon in the Monferrato Area

In the Monferrato area (as in most geological frameworks), the Messinian gypsum sediments are upper and lower, confined by impermeable rocks (marly-clayey deposits). Despite that, sub-vertical discontinuity surfaces often allow preferential flow paths for meteoric water and deep-rising fluids. The progressive dissolution of gypsum then guarantees the hydric connection between downflowing and uprising water. Depending on the stratigraphic and structural features of the specific site, the gypsum dissolution may evolve in different ways.

In the more continuous evaporite successions (eastern part of Monferrato), if the gypsum body is well intact and only crossed by a few well-localized fractures, gypsum dissolution starts along the fracture surfaces. Then it concentrates along the sub-horizontal stratigraphic contacts between gypsum and marl. Then, with the progressive enlargement of these initial conduits, the karst circuit evolves, occupying the entire volume of rock. It maintains, however, an organization driven by the presence of caves and conduits where water concentrates while the surrounding rock is intact. In this framework, the resulting circuits may be very complex and deep (Banzato et al., 2017; Bonetto et al., 2008; Vigna et al., 2017).

However, despite a similar stratigraphic situation at some sites, the evaporitic body may be characterized by diffuse micro-cracking and fracturing. Consequently, the karst circulation will be organized along several interconnected micro-conduits and cracks. The resulting karst aquifer is highly connected and develops a water table behaving similarly to the phreatic surfaces of porous aquifers (Vigna et al., 2017).

Eventually, in the chaotic body (in the western part of Monferrato), several randomly oriented sedimentary discontinuities between the different blocks favor the water flow, which can more easily penetrate the rock body. In addition, these initial sedimentary discontinuities may be enlarged through water dissolution, creating a karst circuit that is usually directly related to the ground surface.

4 Risks Related to the Interference Between Karst Phenomenon and Quarry Activity and Possible Mitigation Strategies

Without careful geological monitoring, the interaction between quarry activity and karst circulation may cause severe risk scenarios, especially for underground quarries that often require the de-watering of tunnels through pumping operations (Hutchinson et al., 2002; Parise, 2010, 2012; Sunwoo et al., 2010). In the presence of highly connected karst aquifers, this may bring an acceleration of the water flow in the karst conduits that, changing the equilibrium of the karst circuit, causes an acceleration of rock dissolution. However, one of the main risks is related to the unpredictability of karst

Fig. 2 **a** Example of collapse in an underground tunnel of a gypsum quarry. **b** Example of sinkhole developed on the surface (Bonetto et al., 2008) **c**—application of GPR in identifying karst caves in gypsum (Caselle et al., 2020)

morphologies. As shown in Fig. 2a, the intersection of unexpected conduits or caves during the excavation may cause a fall of material or water inrushes in the underground drifts, as reported, for example, by Golian et al. (2021). This may provoke a lowering of the static level of surface aquifers, with repercussions on the productivity of springs and wells in the surrounding area. In some cases, the set of these phenomena may bring an upward propagation of the dissolution up to the coverage units and the ground surface, causing collapses, subsidence phenomena, and slop instabilities (Fig. 2b).

Hence, one of the most important objectives for mitigating risk in this framework is the identification of karst conduits and caves behind the excavation faces. For this purpose, indirect geophysical methods are often successfully used. In particular, good results were recently obtained with GPR (Ground Penetrating Radar) (Caselle et al., 2020). Starting from an "a priori" knowledge of the hydrogeological conditions and karst framework, this instrument was successfully used for the identification of the presence of karst conduits, cavities, and open fractures and the determination of their filling (water, air, or marl) in underground gypsum quarries of Monferrato (Fig. 2c).

References

Banzato, C., Vigna, B., Fiorucci, A., De Waele, J. (2017). Hypogene gypsum caves in piedmont (N-Italy). In A. Klimchouk, A. N. Palmer, J. De Waele, A. S. Auler, P. Audra (Eds.), *Hypogene Karst Regions and Caves of the World* (pp. 211–224). Springer International Publishing. ISBN 978–3–319–53347–6.

Bonetto, S., Fiorucci, A., Fornaro, M., & Vigna, B. (2008). Subsidence hazards connected to quarrying activities in a karst area: The case of the Moncalvo sinkhole event (Piedmont, NW Italy). *Estonian Journal of Earth Sciences, 57*, 125. https://doi.org/10.3176/earth.2008.3.01

Caselle, C., Bonetto, S., Comina, C., & Stocco, S. (2020). GPR surveys for the prevention of karst risk in underground gypsum quarries. *Tunnelling and Underground Space Technology, 95*, 103137. https://doi.org/10.1016/j.tust.2019.103137

Dela Pierre, F., Piana, F., Fioraso, G., Boano, P., Bicchi, E., Forno, M. G., Violanti, D., Balestro, G., Clari, P., D'atri, A., De Luca, D., Morelli, M., Ruffini, R. (2003). Note Illustrative della Carta geologica d'Italia alla scala 1:50.000; Foglio 157 Trino. Settore Studi e ricerche Geologiche–Sistema Informativo Prevenzione Rischi-ARPA, Litografia Geda, Nichelino.

Golian, M., Teshnizi, E. S., Parise, M., Terzić, J., Milanović, S., Vakanjac, V. R., Mahdad, M., Abbasi, M., Taghikhani, H., & Saadat, H. (2021). A new analytical method for determination of discharge duration in tunnels subjected to groundwater inrush. *Bulletin of Engineering Geology and the Environment, 80*, 3293–3313. https://doi.org/10.1007/s10064-021-02140-6

Gutiérrez, F., Guerrero, J., & Lucha, P. (2008). A genetic classification of sinkholes illustrated from evaporite paleokarst exposures in Spain. *Environmental Geology, 53*, 993–1006. https://doi.org/10.1007/s00254-007-0727-5

Gutiérrez, F., Parise, M., De Waele, J., & Jourde, H. (2014). A review on natural and human-induced geohazards and impacts in karst. *Earth-Science Reviews, 138*, 61–88. https://doi.org/10.1016/j.earscirev.2014.08.002

Hutchinson, D. J., Phillips, C., & Cascante, G. (2002). Risk considerations for crown pillar stability assessment for mine closure planning. *Geotechnical and Geological Engineering, 20*, 41–64. https://doi.org/10.1023/A:1013852722768

Oggeri, C., Bonetto, S., & Fornaro, M. (2006) Geo-surveying for safe underground mining in gypsum deposit in Monferrato basin (Italy). In *Conference MPES,Mine Planning and Equipment Selection* (vol. 1, pp. 382−387).

Parise, M. (2012). A present risk from past activities: Sinkhole occurrence above underground quarries. *Carbonates and Evaporites, 27*, 109–118. https://doi.org/10.1007/s13146-012-0088-3

Parise, M. (2019). Sinkholes. In W. B. White, D.C. Culver, T. Pipan (Eds.), *Encyclopedia of Caves* (3rd ed., pp. 934–942). Academic Press, Elsevier.

Parise, M. (2010). The impacts of quarrying in the Apulian karst (Italy). In B. Andreo, F. Carrasco, J. J. Durán, J. W. LaMoreaux (Eds.), *Advances in Research in Karst Media* (pp. 441–447). *Environmental Earth Sciences*. Springer. ISBN 978–3–642–12486–0

Ramon, A., Caselle, C., Bonetto, S. M. R, Costanzo, D., & Alonso, E. E. (2021). Effect of microstructure and relative humidity on strength and creep of gypsum. *Rock Mech Rock Eng*. https://doi.org/10.1007/s00603-021-02510-2

Sunwoo, C., Song, W.-K., & Ryu, D.-W. (2010). A case study of subsidence over an abandoned underground limestone mine. *Geosystem Engineering, 13*, 147–152. https://doi.org/10.1080/12269328.2010.10541322

Vigna, B., D'Angeli, I., Fiorucci, A., Waele, J.D. (2017). Hydrogeological flow in gypsum karst areas: Some examples from northern Italy and main circulation models. *International Journal of Speleology*, *46*, https://doi.org/10.5038/1827-806X.46.2.2095</p>

Impact of Geological Fracturing on the Development of Karst Networks in the Western Region of the City of Jijel—Northeastern Algeria

Mustapha Tekkouk, Riad Benzaid, and Chahra Yellas

Abstract

On the northeastern edge of Algeria, on the national road RN 43 connecting the cities of Jijel and Béjaia, we carried out work on fracturing carbonate formations. We tried to link the effect of this fracturing to the development of karstification in this western coastal part of the Jijel region. In addition to the interest shown in the study of the fracturing of limestone formations and its role in the development of the karstification of places, we must point out the geotechnical interest linked to the knowledge of these faults, as during winter, the RN 43 is often rendered impracticable because of falling boulders, landslides and other mass movements. The hydrogeological side is also of interest because until now, the water potential of the karstic reservoirs of this Mediterranean region is not known and even less identified, and the populations of the villages established in these places suffer from a crucial lack of this precious liquid which is undoubtedly buried in large quantitiesa few tens of meters under their feet. This work aims to show the impact of the geological fracturing observed in the field on the development of karst networks identified in the western region of the city of Jijel (northeastern Algeria). The surveys and measurements of the fracturing we carried out along the studied section made it possible to identify different families of faults and main tectonic axes. The measurements carried out in the field and the study of the seismo-tectonic map gave the same results where, for each of the two methods used, the main faults and tectonic axes that emerge are: north-east–southwest, north-west–south-east, east–west, and north–south.

Keywords

Limestone formations · Fracturing · Rock falls · Karstification · Water reserves

1 Introduction

Taking advantage of the effects of tectonics and fracturing, in particular, the phenomena of erosion, corrosion, and dissolution linked to precipitation, year after year, promote the degradation of soils, loose soils, and the karstification of carbonate formations in the west of the city of Jijel (North-East of Algeria). To highlight the impact of fracturing on the development of the morphology and karst networks of the region, we will first proceed with a geological synthesis of the places. Then, the study of the region's fracturing will follow a morphological and speleological approach. Finally, some figures and images of the site will be presented to illustrate the studied phenomenon's effects.

2 Geological Context

As part of "Petite Kabylia", the region studied fits into the eastern part of the Maghrebids, the southern branch of the Alpine chain of the eastern Mediterranean. Structured in thrust sheets, the four geological domains characterizing this northeastern part of the Alpine chain of Algeria are the kabyle base, the limestone (or kabyle ridge), the flysch domain, and the tellien domain. Along the section called "Aftis-Falaises" where the carbonate formations of the tellian domain abound, the Eastern Babors extend from west to east and from north to south of the Mediterranean (Obert, 1981). From south to north, three large units emerge, Babors, Drâa el Arbaa-Erraguène, and Brek. These three large units are divided into subunits (Fig. 1).

M. Tekkouk · R. Benzaid (✉) · C. Yellas
Geological Engineering Laboratory (LGG), Jijel University, Jijel, Algeria
e-mail: r_benzaid@univ-jijel.dz

A. Çiner et al. (eds.), *Recent Research on Environmental Earth Sciences, Geomorphology, Soil Science, Paleoclimate, and Karst*, Advances in Science, Technology & Innovation, https://doi.org/10.1007/978-3-031-42917-0_57

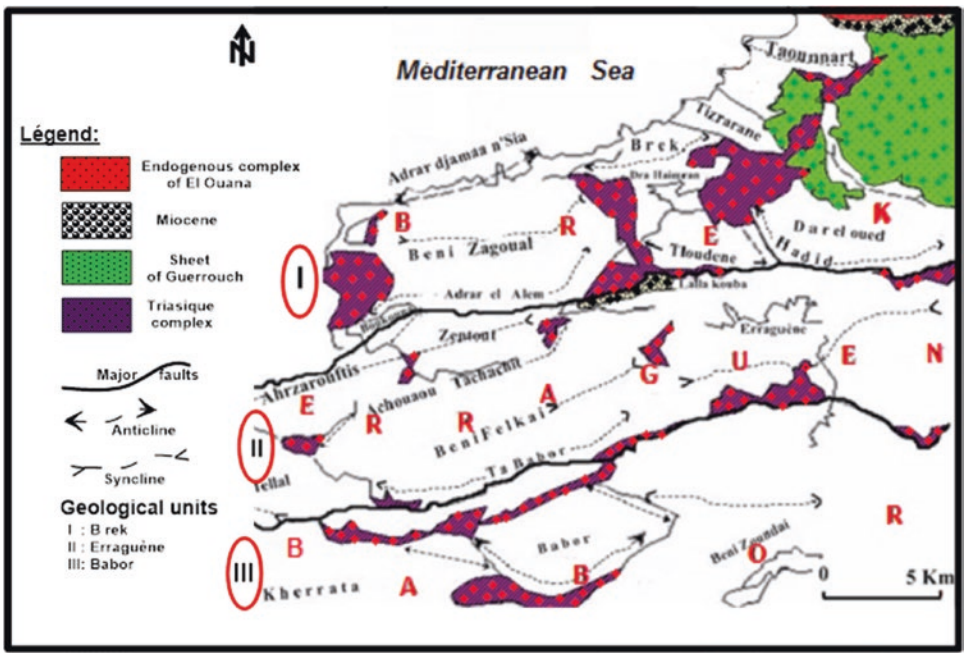

Fig. 1 Oriental Babor units and subunits (Obert, 1981)

3 Fracturing

The surveys and measurements of the fracturing carried out along the studied section made it possible to identify different families of faults and main tectonic axes represented in Fig. 2 (Yellas, 2021; Yellas et al., 2021).

Based on the seismotectonic map of northeastern Algeria proposed by Harbi et al. (Harbi et al., 2003), Tekkouk (Tekkouk, 2019) presents four major fault systems in Jijel-Béjaia oriented: northeast-southwest, north-west-south-east, east–west, and north–south.

4 Karst Forms of the Region

During his speleological research in the region of Jebel[1] Brek and the surrounding regions, Biberent (Birebent, 1948) wrote, "…. *where the cavities could allow the study of the circulation of underground water, therefore the knowledge of the excavated cavities, fossils or active and the rules of the digging of these cavities in the same region, the same grounds, and the same conditions as in Jebel Brek*". It should be noted that Biberent's work remains the only research carried out to date in the studied region.

It is in this spirit that the research carried out by Biberent (Birebent, 1948) in the region of Ziama Mansouriah concerned the following places: Jebel Brek and its annex, Jebel Hamra; the surrounding valleys; the massifs in the east; the massifs in the south; the more distant massifs. In his descriptive report of the places prospected, Birebent (Birebent, 1948) provided numerous details and precisions relating to caves and other forms of karstic dissolution. In what follows, we take up some of the diagrams established by the author, which perfectly illustrate the karstic forms (Figs. 3 and 4) found in the region studied.

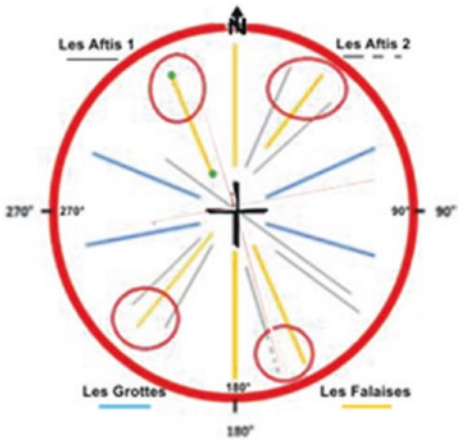

Fig. 2 Fracture families of the studied sites (Yellas, 2021; Yellas et al., 2021)

[1] Jebel: Mountain in Arabic.

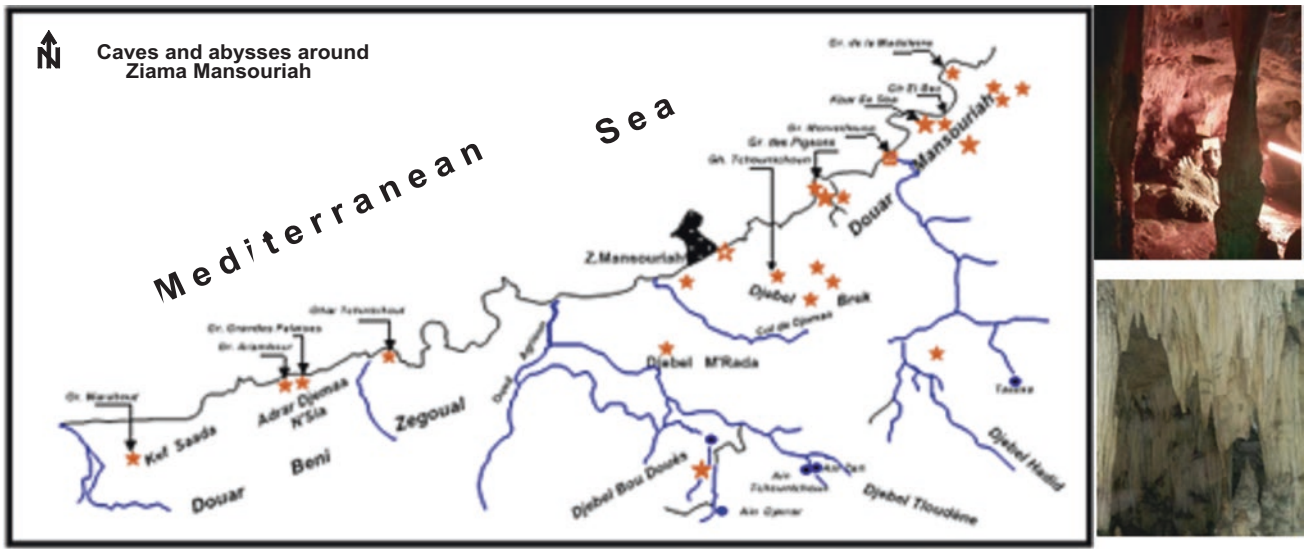

Fig. 3 Caves and abysses around Ziama Mansouriah (Birebent, 1948)

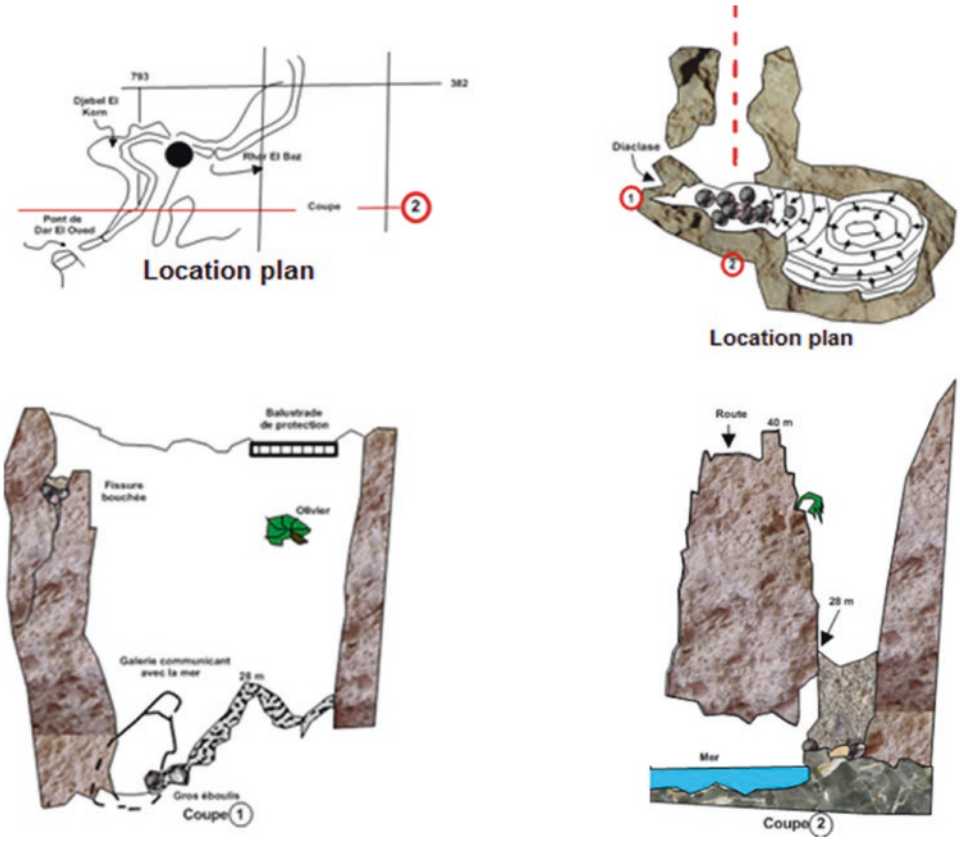

Fig. 4 Aven and sea cave at Kbeur-Es-Sba (Tekkouk, 2019)

5 Conclusion

In his introduction to the speleological study of Jebel Brek and the surrounding areas, Birebent (1946/47) wrote: "*Lambert, the geologist-not the Abbot-had found ghosts of holes at the top of Jebel Brek, plugged holes. He had concluded that the water had circulated well before his birth in this whole region and that it still buried itself there on stormy days*". We have voluntarily taken up this passage because we believe that in a few words, Birebent has demonstrated the role played by rainwater, which falls annually

and in large quantities in the region, and is taking advantage of the fracturing of massive burrows deep. The two critical elements of the inventory studied here are well-identified. By studying the fracturing of massifs, we supported the author's comments and identified the different families of faults that plague the region. The measurements carried out in the field and the study of the seismo-tectonic map gave the same results where, for each of the two methods used, the main faults and tectonic axes that emerge are: north-east-southwest, northwest-southeast, east–west, and north–south. The limestone formations of the region, thus fractured, have not ceased since the dawn of time to receive the abundant rainwater, which, through their work, has given the morphologies and other karstic forms of the Jijel cornice.

References

Birebent, J. (1948). Explorations souterraines en Algérie. Campagne 1946–1947-Extrait des annales de spéléologie–Tome III-1948–Fascicule 2–3, 153p (1946/47).

Harbi, A., Maouche, S., & Benhallou, H. (2003). Re-appraisal of seismicity and seismotectonics in the northeastern Algeria part II: 20th century seismicity and seismotectonics analysis. *Journal of Seismology, 7*(2), 221–234. https://doi.org/10.1023/A:1023571316216

Obert, D. (1981). Etude géologique des Babors orientaux (Domaine tellien, Algérie) Thèse d'Etat –Université Pierre et Marie Curie-Paris 6, 635p.

Tekkouk, M. (2019). *Étude hydrogéologique et géotechnique de deux sites de barrage de l'Algérie nord-orientale. Cas des sites de Tabellout et de Kissir de la région de Jijel*. Doctoral thesis, University of Jijel, Algeria.

Yellas, C. (2021). *Evaluation de l'aléa lié aux éboulements rocheux et du risque associé-Cas de la route national RN43 reliant Jijel à Béjaia (Nord Est Algérien)*. Université de Jijel, Algerie. In French.

Yellas, C., Benzaid, R., & Tekkouk, M. (2021). Application of classification systems for the assessment of rock mass stability-case of national road 43, Jijel, Algeria. *Arabian Journal of Geosciences, 14*, 203. https://doi.org/10.1007/s12517-021-06537-1